발 간 등 록 번 호
11-1543000-000780-01

질환 동물 모델을 이용한 농업바이오 분야의 CRO 구축

Development of CRO for Bio-Agriculture using Animal Disease Model

(주) 바이오톡스텍

농 림 축 산 식 품 부

제 출 문

농림축산식품부 장관 귀하

이 보고서를 “질환 동물 모델을 이용한 농업바이오 분야의 CRO 구축” 과제의 보고서로 제출합니다.

2014 년 12 월 31 일

주관연구기관명 : (주) 바이오톡스텍
주관연구책임자 : 강 종 구
협동연구기관명 : 서울대학교
협동연구책임자 : 성 제 경
연 구 원 : 이 한 웅
협동연구기관명 : 부산대학교
협동연구책임자 : 최 영 환
위탁연구기관명 : 성균관대학교

요 약 문

Ⅰ. 제 목

질환 동물 모델을 이용한 농업바이오 분야의 CRO 구축
(Development of CRO for Bio-Agriculture using Animal Disease Model)

Ⅱ. 연구개발의 목적 및 필요성

본 기술개발사업의 목표는 10대 질환을 중심으로 특정고유질환 동물모델을 개발하고, 우수한 천연물 후보물질을 발굴하여 효력을 평가하고, 이를 대상으로한 비임상시험 (GLP)을 수행함으로서, 후보물질의 안전성 및 유효성을 입증함과 동시에 전문적인 연구개발지식과 농업바이오 분야에서의 R&D 사업의 수익을 지속적으로 창출할 수 있는 모델을 제시하고, 독립적인 R&D 컨설팅 CRO를 법인화하는데 있다.

본 연구의 필요성은
첫째, CRO는 신물질을 개발하는 기업의 최고 파트너로서, 기업의 비용 절감, 전문적 노하우에 바탕을 둔 가격경쟁력 및 효율적인 전임상·임상 진행을 통한 개발기간의 단축을 위하여 제약, 화학, 화장품, 식품회사 등의 CRO 이용은 폭발적으로 증가하였으며 2010년도 세계 시장 규모는 240억 달러에 이르고 있다. 따라서 CRO의 역량은 국가 R&D사업의 성패를 좌우할 뿐 아니라 국가 경쟁력의 원천 분야이다. 농업 바이오산업은 생명공학을 필두로 하는 첨단기술 개발로 시장 규모가 넓고 분야가 다양화된 연 평균 18%의 경제성장을 보이는 국가경쟁력의 원천 분야로서, 신약소재에서 기능성 식품, GMO, 천연화장품까지 확대되어 후보물질이나 신기술을 상품화하는 글로벌 농업 CRO 출현을 필요로 한다. 또한, 농업 바이오 전문가인프라 구축과 전문 비임상 CRO 및 임상 CRO를 연계시키고, 농업 바이오산업 분야의 특성화된 전문 컨설팅 서비스를 제공하는 농업 바이오 CRO 법인을 설립할 필요가 있다.
둘째, 최근 생명과학분야의 눈부신 발전과 함께 생명과학과 관련된 다양한 연구가 진행되고 있다. 분자적 수준의 연구 성과가 사람에게 적용되기 위해서 가장 중요한 연구 인프라는 실험동물을 이용한 동물 실험 분야이다. 국내에서도 의약품, 화학물질 등의 많은 신물질이 개발되어 약효검증, 독성 및 안전성 평가 등 비임상 실험의 수효 및 빈도가 폭발적으로 증가되었으며, 이와 관련한 실험동물의 수요 또한 급속하게 증가되고 있으며, 특히 유전자 변형이 가능한 마우스의 사용량이 최근 전 세계적으로 증가될 뿐 아니라 국내에서도 증가하고 있는 추세이다. 국내 주요 연구과제에서도 마우스를 이용한 인프라 구축사업은 국가중점 육성 분야의 개별 세부 사업 목표 달성을 위해서도 매우 중요하게 다루어져야 할 것으로 사료되나 국내 인프라는 매우 취약한 상황이기 때문에 관련 연구가 매우 절실히 필요하다.

셋째, 세계적인 천연물의약산업의 활성화, 생명자원에 대한 보호주의 확산 및 지적 재산권 협약 등으로 외국 자원 또는 기술의 도입은 점차 어려워지고 있으며, 이러한 기술을 도입할 경우에는 막대한 royalty를 지불해야 한다. 우리나라에는 옛날부터 한의학이 발달되었으나, 한약재로부터 생리활성을 탐색한 후 식의약품, 보건식품 또는 식품첨가제의 개발에 관한 연구는 유럽연합이나 미국 등의 선진국에 비해 오히려 뒤지고 있다. 최근 들어 생약제를 이용한 식품보조제나 건강식품의 개발에 의한 생물산업이 활성화되고 있는데, 이에 부응하기 위하여 식물로부터 얻은 천연물 신약 후보물질의 산업화는 농가의 소득작물 개발에 필연적인 과제로 부각되고 있다.

이상의 내용을 종합해 볼 때, 농업바이오분야 R&D 사업을 원활히 수행할 민간 CRO 기관의 인프라가 부족하므로 허가 당국 및 정부기관의 긴밀하며 적극적인 협조를 통해 부족한 CRO 기관의 육성이 무엇보다 절실히 필요하다고 판단된다. 더불어 본 기술개발사업에서 10대 질환을 중심으로 고유질환동물모델을 개발하고, 우수한 천연물 후보물질을 발굴하여, 이를 대상으로한 비임상시험을 수행함으로서, 안전성 및 유효성을 입증함과 동시에 전문적인 연구개발지식과 농업바이오 분야에서의 R&D 사업의 수익을 지속적으로 창출할 수 있는 모델을 제시하고자한다.

Ⅲ. 연구개발 내용 및 범위

1. 1차년도

(1) 제 1세부

① 자초추출물에 대한 비임상시험 연구
조제물분석시험, 단회투여독성시험 (설치류), 최대내성 용량시험 (비설치류), 2주 용량결정시험 및 4주 반복투여독성시험(설치류/비설치류), 유전독성시험인 복귀돌연변이시험, 염색체이상시험 및 소핵시험, 국소독성시험으로서 피부자극시험 및 안점막자극시험, 항원성시험

② CRO운용 관련 SOP 제정

(2) 제 1협동

주요 5대 질환의 모델동물 개발

① 심순환모델동물 개발: ASC-2 GEM

② 암모델동물 개발: Ei24 GEM

③ 대사성질환 모델동물 개발: ATF-3 GEM

(3) 제 2협동

① 항암 효능 천연물 후보물질 개발

② α-Iso-cubebenol의 대량분리 방법 확립 / 패혈증 치료효과 조사

③ Gomisin J의 혈관이완작용 및 이의 분자생물학적 기전 규명 / 고혈압 실험동물 모델 개발 및 Gomisin J의 항고혈압 효과 규명

2. 2차년도

(1) 제 1세부

① 자초추출물에 대한 비임상시험 연구 계속 진행
분석법개발 및 validation (설치류/비설치류), 4주 반복투여독성시험(설치류/비설치류), 독성동태시험 (설치류)

② Gomisin J에 대한 비임상시험 연구
분석법개발 및 validation (설치류/비설치류)

③ EC-18에 대한 비임상시험 연구
4주 반복투여독성시험(설치류/비설치류), 항암효능시험, 관절염 효능시험, 안전성약리시험(중추신경계)

④ 농업바이오 CRO를 위한 인프라 구축

(2) 제 1협동

주요 5대 질환의 모델동물 개발

① 신경계 질환모델동물 개발: DMI-1, GX2 GEM

② 암, 심순환, 대사성 질환동물모델의 질환관련 특성 분석 표준화 기반 구축 및 분석

(3) 제 2협동

① 항암 효능 후보물질: 지치 추출물 대량 확보

② α-Iso-cubebenol의 대량분리 / 패혈증 치료효과 조사

③ Gomisin J의 항고혈압 효과 및 기전 규명

3. 3차년도

(1) 제 1세부

① 개발후보물질 사업성 판단

② α-Iso-cubebenol에 대한 비임상시험 연구
단회경구독성시험 (설치류), 피부자극시험 (비설치류), 안점막자극시험 (비설치류)

③ Gomisin J에 대한 비임상시험 연구
분석법 validation (설치류)

④ EC-18에 대한 비임상시험 연구
수태능 및 초기배 발생독성시험 (설치류)

⑤ 농업 CRO 기반구축을 위한 전문가 육성 세미나 개최

⑥ 농업 바이오 CRO 구축, 산학연과 MOU 체결

(2) 제 1협동

① ASC-2 (심순환), Ei24 (암질환), UQCRB (대사성질환) 마우스의 질환특성 분석연구

② 신약후보물질 1종의 유효성 평가 연구 : 종양 억제 유효성 평가

(3) 제 2협동

① α-Iso-cubebenol의 대량분리

② 제 2협동에 자초 추출물과 α-Iso-cubebenol 공급 : 종양 억제 유효성 평가 사용

③ 오미자 성분의 효능 검증

Ⅳ. 연구개발결과

1. 1차년도

(1) 제 1세부

① 자초추출물에 대한 비임상시험 연구

조제물분석시험, 단회투여독성시험 (설치류), 최대내성 용량시험 (비설치류), 유전독성시험인 복귀돌연변이시험, 염색체이상시험 및 소핵시험, 항원성시험

: 특이사항 없음.

국소독성시험으로서 피부자극시험 및 안점막자극시험

: 홍반의 관찰은 불가능하였지만 부종이 확인되었기 때문에 토끼의 피부에 대한 자극성이 있는 것으로 판단

: 토끼의 안점막에 대해서 '자극물'로 판단

② CRO운용 관련 SOP를 제정 완료

(2) 제 1협동

주요 5대 질환의 모델동물 개발

① 심순환모델동물 개발: ASC-2 KO 마우스 확보 및 생산 (확장성 심근병증)

② 암모델동물 개발: Ei24 GEM 개발 완료 (간암)

③ 대사성질환 모델동물 개발: ATF-3 GEM (인슐린 저항성 관련 모델 가능성 확인)

(3) 제 2협동

① 항암 효능 천연물 후보물질 개발 : 지치(*L. erythrorhizon*)로부터 항암효능 추출물 확보

② 오미자로부터 α-Iso-cubebenol의 대량분리 방법 확립 / 패혈증 치료효과 조사 완료

③ Gomisin J의 혈관이완작용 및 이의 분자생물학적 기전 규명 / 고혈압 실험동물 모델 개발 및 Gomisin J의 항고혈압 효과 규명 완료

2. 2차년도

(1) 제 1세부

① 자초추출물에 대한 비임상시험 연구 계속 진행

분석법개발 및 validation (설치류/비설치류)

: 개발 완료.

2주반복 및 4주 반복투여독성시험 (설치류)

: 본 시험물질의 무독성량 (NOAEL)은 암수 모두 400 mg/kg/day로 판단

4주 반복 경구투여 독성시험, 2주 회복시험 및 독성동태시험 (비설치류)

: 암•수 300 mg/kg/day 용량에서 구토, 설사 및 체중 또는 체중 증가 감소 등의 변화가 관찰되어 암•수 비글견에 대한 무독성량 (NOAEL)은 100 mg/kg/day으로 판단

② Gomisin J에 대한 비임상시험 연구

분석법개발 및 validation (설치류/비설치류)

: 개발 완료.

③ EC-18에 대한 비임상시험 연구

13주 반복투여독성시험(설치류)

: 암•수 무독성량(NOAEL) : ≥2000 mg/kg

4주 반복투여독성시험(비설치류)

: 무독성량(NOAEL) : ≥2000 mg/kg

13주 반복투여독성시험(비설치류)

: 무독성량(NOAEL) : ≥2000 mg/kg

안전성약리시험(중추신경계)

: EC-18은 500, 1,000 및 2,000 mg/kg 용량에서 중추신경계에 미치는 영향이 없는 것으로 판단

항암효능시험

: EC-18은 종양의 성장을 억제하는 효과가 없는 것으로 판단

관절염 효능시험

: EC-18은 125, 500 및 2,000 mg/kg 용량에서 관절염증상을 개선시키는 효능이 있는 것으로 판단

④ 농업바이오 분야 R&D 사업을 원활히 수행할 타 기관과의 전문가 인프라 구축 진행

(2) 제 1협동

주요 5대 질환의 모델동물 개발

① 신경계 질환모델동물 개발: DMI-1, GX2 GEM 완료 (뇌 신경 질환)

② 암, 심순환 질환동물모델의 질환관련 특성 분석 표준화 기반 구축 및 분석 실시 완료

(3) 제 2협동

① 항암 효능 후보물질: 지치 추출물 대량 확보 및 제 1세부에 전달 완료

② 오미자로부터 α-Iso-cubebenol의 대량분리 / 패혈증 치료효과 조사 완료

③ Gomisin J의 항고혈압 효과 및 기전 규명: 혈관 세포 nitric oxide 생성 및 혈관 세포 산소유리기 생성에 미치는 작용 규명 완료 / 고혈압 동물모델 예방 효과 확인

3. 3차년도

(1) 제 1세부

① 개발후보물질 사업성 판단

: 자초추출물, EC-18, Gomisin J, α-Iso-cubebenol에 대한 사업성 판단 완료

② α-Iso-cubebenol에 대한 비임상시험 연구

단회경구독성시험 (설치류)

: 개략의 치사량은 암수 모두 2,000 mg/kg을 상회하는 것으로 판단

피부자극시험 (비설치류)

: 토끼의 피부에 대해서 '중등도 자극성'이 있는 물질로 판단

안점막자극시험 (비설치류)

: 토끼의 안에 대해서 자극성이 없는 것으로 판단

③ Gomisin J에 대한 비임상시험 연구

분석법 validation (설치류)

: 개발 완료.

④ EC-18에 대한 비임상시험 연구

수태능 및 초기배 발생독성시험 (설치류)

: 시험진행 중

⑤ 농업 CRO 기반구축을 위한 전문가 육성 세미나 개최
: 2014년 11월 20일(목) 실시
: 발표연사-충북대 김대중교수, 부산대 황대연교수, ㈜바이오톡스텍 강종구대표이사, 서울대 성제경교수, 부산대 최영환교수
⑥ 농업 바이오 CRO 구축, 산학연과 MOU 체결

(2) 제 1협동
① ASC-2 (심순환), Ei24 (암질환), UQCRB (대사성질환) 마우스의 질환특성 분석연구
② 신약후보물질 1종의 유효성 평가 연구 : 종양 억제 유효성 평가 진행 중

(3) 제 2협동
① α-Iso-cubebenol의 대량분리: 1차년도에 확립한 방법을 반복적으로 수행하여 3차 연도까지 325 g 확보
② 제 1세부에 자초 추출물과 α-Iso-cubebenol 공급 : 종양 억제 유효성 평가 사용
③ 오미자 성분의 효능 작용기전 규명

Ⅴ. 연구성과 및 성과활용 계획

○ 농업바이오분야 R&D 사업을 원활히 수행할 민간 CRO 기관의 인프라를 구축, 10대 질환을 중심으로 발굴된 우수한 천연물 후보물질을 대상으로 비임상시험을 수행함으로서, 후보물질의 안전성 및 유효성을 평가 가능하며, 동시에 전문적인 연구개발지식과 농업바이오 분야에서의 R&D 사업의 수익을 지속적으로 창출할 수 있는 모델을 제시할 수 있으리라 기대된다.

○ 국내 질환모델 동물의 개발단계 수준을 넘어서 의약품 평가에 효율성이 높은 질환모델 동물자원을 발굴함으로써 국내 질환모델 동물자원의 활용성을 높이고 국내 신약 개발 및 독성 연구에 지원 가능할 것으로 기대된다.

○ 면역조절 물질이 향후 패혈증 치료제 개발에 필요한 후보물질로 제공될 수 있음을 규명한 결과를 국내외에 특허화하여 지적 재산권을 확보하고, 오미자 유래 gomisin J의 고혈압 예방 및 치료 후보물질 발굴로 제약회사에 licensing out함으로써 의약품 개발에 응용 가능하며, 자초 유래 항암성분을 동물모델에서 효능을 검증하여 천연물 후보물질로서 제공할 수 있으리라 기대된다. 또한 면역조절 물질을 이용한 패혈증 치료제 개발을 주도하여 미래의 패혈증을 포함한 감염질환 치료제 개발 분야를 선도할 수 있을 것으로 기대된다.

SUMMARY

Ⅰ. Title

Development of CRO for Bio-Agriculture using Animal Disease Model

Ⅱ. Purpose and Importance of Research and Development

The goal of the technology development project is to develop a disease-specific animal model focusing the 10 major diseases, to discover fine natural productcandidates and to evaluate their efficacy. Furthermore, we conduct non-clinical studies (GLP) with them to validate the safety and efficacy of the candidates and thus present a model that ensures profitable R&D business in the Bio-agriculture sector and to provide specialized R&D knowledge and to incorporate an independent R&D consulting CRO.

The purposes of this research project are as follows.
First, as the best partner for companies that develop a new compound, the utilization of CRO has been increased exponentially with cut down cost with a competitive price based on professional expertise and shorteneddevelopment time through efficient preclinical stage. In 2010, the global market size has reached 240 billion US dollars. Thus, the capacity of the CRO sector influences not only national R&D projects, it is also an important national competitive field. Bio-Agriculture industry leading to an advanced biotechnology development has a broad market and the fieldis diversified. As a source area of national competitiveness with an average annual growth of 18%, the emergence of global agricultural CRO is needed to commercialize new technologies or candidate substances expanded from new drug material, functional food, GMO to natural cosmetics.
Furthermore, it is necessary to establish an Bio-Agriculture CRO firm that ensures experts in agricultural biotechnology, links specialized preclinical CRO and clinical CRO and provides professional consulting services specialized in Bio-Agriculture industry.

Secondly, a variety of research related to life sciences has been in progress with the remarkable development in the life sciences lately. The most important research infrastructure in order to apply molecular level research to human is animal testing using experimental animals.
Non-clinical studies on efficacy, toxicity and safety assessment have increased

explosively in number and frequency while a number of new compounds have been developed domestically, such as pharmaceuticals, chemicals, etc. The demand of experimental animals in this regard also increased rapidly and in particular, the trend is that the use of transgenic mice is increased worldwide as well as domestically. Infrastructure projects using mice should be in great consideration in domestic major researches toward a goal of fostering individual specific projects of national key areas. However, domestic infrastructure is in a very vulnerable situation and thus related research is needed desperately.

Thirdly, the introduction of foreign resources or technology is becoming increasingly difficultdue to activation of natural product industry worldwide, spreading protectionism for life resources and intellectual property rights agreements, etc., and once introduced this technology has to pay a huge royalty. Chinese medicine has been developed from the old days in the country, and domestic researches fall behind the advanced countries such as the European Union and the United States on the development of the food and drug, health foods or food additives after exploring physiological activity from medicinal plants. The bioindustry has been activated by the development of food supplements and health foods using herbal remedy in recent years. Consequently, the industrialization of natural product medicine candidates derived from plants is emerging as the inevitable challenges in the development of farm economic crops.

To sum up, it is deemed to be imminent to foster inadequate CRO above all through a close and active cooperation of the permitting authorities and government agencies due to the lack of infrastructure of private CRO to smoothly perform R&D projects in the Bio-Agriculture industry. Furthermore, this biotechnology development project focuses on developing a disease-specific animal model on the basis of the 10 major diseases and performing non-clinical studies on fine natural product candidates. At the same time, the goal is to propose a model that can continue to generate consistently specialized knowledge about R&D and revenues from the R&D projects in Bio-Agriculture sector as well as to validate the safety and efficacy of the candidates.

Ⅲ. Contents and Scope of Research and Development

1. The first year

(1) The first details

① Non-clinical studies on Gromwell Water Fraction

Analysis of dosing formulation, single dose toxicity study (Rodents), maximum tolerated dose finding study (Non-rodents), 2-week DRF study, 4-week

repeated dose toxicity study (Rodents/Non-rodents), genetic toxicity studies including reverse mutation study, chromosomal aberration study and micronucleus study, and local toxicity studies including skin irritation and eye irritation studies and antigenicity study

② Enactment of CRO management-related SOPs

(2) The first collaboration

Development of Animal Disease Model of the 5 Major Diseases

① Development of Animal Cardiovascular Model : ASC-2 GEM

② Development of Animal Cancer Model : Ei24 GEM

③ Development of Animal Metabolic Disease Model : ATF-3 GEM

(3) The second collaboration

① Development of Natural Anti-Cancer Product Candidates

② Establishment of Large Scale Separation Method of α-Iso-cubebenol/ Therapeutic Research of Sepsis

③ Study on Vasorelaxant Action of Gomisin J and Molecular Biological Mechanism/ Development of Animal Hypertension Model and Study of Antihypertensive Effects of Gomisin J

2. The second year

(1) The first details

① Non-clinical studies continued on Gromwell Water Fraction

Development and validation of analytical method (Rodents/Non-rodents), 4-week repeated dose toxicity study (Rodents/Non-rodents), toxicokinetics (Rodents)

② Non-clinical studies on Gomisin J

Development and validation of analytical method (Rodents/Non-rodents)

③ Non-clinical studies on EC-18

4-week repeated dose toxicity study (Rodents/Non-rodents), anticancer efficacy test, arthritis efficacy test, safety pharmacology test (central nervous system)

④ Infrastructure for CRO for Bio-Agriculture

(2) The first collaboration

Development of Animal Disease Model of the 5 Major Diseases

① Development of Animal Neurological Disease Model : DMI-1, GX2 GEM

② Foundation and analysis based on the standardized disease-specific analysis of Animal Model for cancer, cardiovascular and metabolic diseases

(3) The second collaboration

① Anti-Cancer Product Candidates: Large supply of Gromwell Extracts

② Large Scale Separation of α-Iso-cubebenol/ Therapeutic Research of Sepsis

③ Study of Antihypertensive Effects and Mechanism of Gomisin J

3. The third year

(1) The first details

① Determination of profitability of candidate compounds in development

② Non-clinical studies on α-Iso-cubebenol

Single dose toxicity study (Rodents), skin irritation study (Non-rodents), eye irritation study (Non-rodents)

③ Non-clinical studies on Gomisin J

Validation of analytical method (Rodents)

④ Non-clinical studies on EC-18

Fertility and early embryonic toxicity studies (Rodents)

⑤ Experts training seminars held for CRO infrastructure for Bio-Agriculture

⑥ CRO infrastructure for Bio-Agriculture, signing MOU with industries and academics

(2) The first collaboration

① ASC-2 (cardiovascular disease), Ei24 (cancer), UQCRB (metabolic disease) Disease-specific analysis in mice

② Assessment of efficacy of one kind of new substance candidates: Tumor suppression efficacy assessment

(3) The second collaboration

① Large Scale Separation of α-Iso-cubebenol

② Supply of Gromwell Water Fraction in the second collaboration and α-Iso-cubebenol: Use of tumor suppression efficacy assessment

③ Assessment of efficacy action mechanism of Schisandra chinensis ingredients

Ⅳ. Research Results

1. The first year

(1) The first details

① Non-clinical studies on Gromwell Water Fraction

Analysis of dosing formulation, single dose toxicity study (Rodents), maximum tolerated dose finding study (Non-rodents), genetic toxicity studies including reverse mutation study, chromosomal aberration study and micronucleus study and antigenicity study:

No significant remark

Local toxicity studies including skin irritation and eye irritation studies: Observation of erythema was impossible, but edema was confirmed. Therefore, it was determined that there was skin irritation on the rabbit skin:

It was determined to be 'Irritant' on the ocular mucous membrane of the rabbit.

② Completion of enactment of CRO management-related SOPs

(2) The first collaboration

Development of Animal Disease Model of the 5 Major Diseases

① Development of Animal Model for neurological disease:
Acquisition and production of ASC-2 KO mice (dilated cardiomyopathy)

② Development of Animal Cancer Model:
Completion of Ei24 GEM development (liver cancer)

③ Development of Animal Model for metabolic disease:
ATF-3 GEM (verification of potential insulin resistance-related model)

(3) The second collaboration

① Development of Natural Anti-Cancer Product Candidates:
Anti-Cancer extracts obtained from L. *erythrorhizon*

② Establishment of Large Scale Separation Method of α-Iso-cubebenol from Schisandra chinensis/ Completion of Therapeutic Research of Sepsis

③ Study on Vasorelaxant Action of Gomisin J and Molecular Biological Mechanism/ Completion of Development of Animal Hypertension Model and Study of Antihypertensive Effects of Gomisin J

2. The second year

(1) The first details

① Non-clinical studies continued on Gromwell Water Fraction
Development and validation of analytical method (Rodents/Non-rodents):
Development completion
2-week and 4-week repeated dose toxicity studies (Rodents):
The NOAEL of the test substance was considered to be 400 mg/kg/day for both sexes.
4-week repeated dose toxicity study, 2-week recovery study and toxicokinetics (Non-rodents):
Vomiting, diarrhea and change in body weight or decrease of weight gain were observed in males and females at a dose of 300 mg/kg/day. Therefore, the NOAEL of the test substance was considered to be 100 mg/kg/day for beagle dogs of both sexes.

② Non-clinical studies on Gomisin J
Development and validation of analytical method (Rodents/Non-rodents):
Development completion

③ Non-clinical studies on EC-18
13-week repeated dose toxicity study (Rodents):
NOAEL for both sexes: =2000 mg/kg
4-week repeated dose toxicity study (Non-rodents):
NOAEL: ≥2000 mg/kg
13-week repeated dose toxicity study (Non-rodents):

NOAEL: ≥2000 mg/kgsa

Safety pharmacology test (central nervous system):

It was determined that there was no effect of EC-18 on the central nervous system at doses of 500, 1,000 and 2,000 mg/kg.

Anticancer efficacy test:

It was determined that there was no suppressing effect of EC-18 on the growth of tumors Arthritis efficacy test:

It was determined that there was improving effect of EC-18 on arthritis symptoms at doses of 125, 500 and 2,000 mg/kg.

④ Experts infrastructure in progress in other organizations that will perform smoothly R&Dprojects for Bio-Agriculture

(2) The first collaboration

Development of Animal Disease Model of the 5 Major Diseases

① Development of Animal Model for neurological disease:
Completion of DMI-1, GX2 GEM (brain neurological disease)

② Completion of foundation and analysis based on the standardized disease-specific analysis of Animal Model for cancer, cardiovascular and metabolic diseases

(3) The second collaboration

① Anti-Cancer Product Candidates:
Large supply of Gromwell Extracts and completion of delivery to the first details

② Large Scale Separation of α-Iso-cubebenol from Schisandra chinensis/
Completion of Therapeutic Research of Septicemia

③ Study on Antihypertensive Effects of Gomisin J and Mechanism:
Production of nitric oxide in vascular cells and completion of investigation of the effect on the production of oxygen free radicals in vascular cells/ verification of preventive effects of animal hypertension model

3. The third year

(1) The first details

① Determination of profitability of candidate compounds in development:
Completion of determination of profitability regarding Gromwell Water Fraction, EC-18, Gomisin J and α-Iso-cubebenol

② Non-clinical studies on α-Iso-cubebenol
Single oral toxicity study (Rodents):
The approximate lethal dose was considered to be more than 2,000 mg/kgfor both sexes.
Skin irritation study (Non-rodents):
It was determined to be 'Moderately irritant' on the rabbit skin.
Eye irritation study (Non-rodents):

It was determined that there was no eye irritation in rabbits.

③ Non-clinical studies on Gomisin J
Validation of analytical method (Rodents): Development completion

④ Non-clinical studies on EC-18
Fertility and early embryonic toxicity studies (Rodents): Studies in progress

⑤ Experts training seminars held for CRO infrastructure for Bio-Agriculture:
Conducted in November 20th, 2014 (Thursday)
Speakers-*Prof.* Dae Jung Kim (Chungbuk National University), *Prof.* Dae Youn Hwang (Pusan National University), CEO Jong Koo Kang (Biotoxtech Co., Ltd.), *Prof.* Je Kyung Seong (Seoul National University), *Prof.* Young Whan Choi (Pusan National University)

⑥ CRO infrastructure for Bio-Agriculture, signing MOU with industries and academics

(2) The first collaboration

① ASC-2 (cardiovascular disease), Ei24 (cancer), UQCRB (metabolic disease)
Disease-specific analysis in mice

② Assessment of efficacy of one kind of new substance candidates:
Tumor suppression efficacy assessment in progress

(3) The second collaboration

① Large Scale Separation of α-Iso-cubebenol:
325 g obtained by repeatedly performing the method established in the first year until the third year

② Supply of Gromwell Water Fraction in the first details and α-Iso-cubebenol:
Use of tumor suppression efficacy assessment

③ Assessment of efficacy action mechanism of Schisandra chinensis ingredients

Ⅴ. Research Result and Application of Result

○ A model that is able to generate consistently specialized knowledge and revenues from the R&D projects in Bio-Agriculture sectorat the same time is expected to be proposed. The model will be evaluated by conducting non-clinical studies on fine natural product candidates chosen for the 10 major diseases for the safety and efficacy of the candidates in an infrastructure built for the private CRO institutions that will smoothly perform R&D projects for Bio-Agriculture.

○ It is expected to support the development of new drugs and toxicity studies improving the utilization of animal resources for domestic animal disease models by discovering animal resources for Animal Disease Models with high efficiency in pharmaceutical assessment beyond the development stage of domestic animal disease model.

○ Based on the result of investigation on immunoregulatory substance that may be provided as a candidate substance for the future development of therapeutic agent for sepsis, a patent is to be obtained to secure intellectual property rights and Schisandra chinensis origin (Schisandrae Fructus-derived) gomisin J as a candidate substance for the prevention and treatment of hypertension is to be licensed out in pharmaceutical companies to be used in drug development. Gromwell Water-derived anticancer ingredient is expected to be presented as one of natural product candidateswith the efficacy validation in animal model. It is also expected to lead the development of sepsis therapies using immunomodulatory substances with the development of therapeutic agents for infectious diseases including future sepsis.

CONTENTS

목 차

제 1 장 연구개발과제의 개요

제1절. 연구개발의 목표

본 기술개발사업의 목표는 10대 질환을 중심으로 특정고유질환 동물모델을 개발하고, 우수한 천연물 후보물질을 발굴하여 효력을 평가하고, 이를 대상으로한 비임상시험 (GLP)을 수행함으로서, 후보물질의 안전성 및 유효성을 입증함과 동시에 전문적인 연구개발지식과 농업바이오 분야에서의 R&D 사업의 수익을 지속적으로 창출할 수 있는 모델을 제시하고, 추후 독립적인 R&D 컨설팅 CRO를 법인화 하고자 한다.

세부 및 협동과제별 목표는 다음과 같다.

- 제 1세부. 농업바이오 분야의 CRO 비임상시험 연구: 후보물질 (천연물)을 대상으로 비임상시험 (GLP)을 진행하여 후보물질의 안전성을 평가한다.
- 제 1협동. 질환 동물 모델 개발 및 효력시험 연구: 신약평가를 위한 국내 5대 질환의 모델동물 개발과 이를 이용한 효력시험을 실시한다.
- 제 2협동. 천연물 신약후보물질의 개발 및 효력시험 연구: 오미자로부터 패혈증에 효능이 있는 신물질인 α-iso-cubebenol, 심혈관질환 효능을 가진 gomisin J 및 항암 효능을 가진 성분을 다량 분리하여 in vivo 작용기작을 규명하여 천연물 신약 후보물질을 개발한다.

<연구개발의 최종 목표>

제2절. 연구개발의 필요성 및 연구 범위

1. 제 1세부

농업바이오 분야의 Contract Research Organization (CRO) 비임상시험 연구

가. 연구개발의 필요성

㈜바이오톡스텍은 의약품, 식품, 화학물질, 화장품 등 신물질을 탐색하고 개발하는 과정에서 요구되는 광범위한 연구개발 용역을 제공하는 전문성을 갖춘 연구개발서비스기관이다. CRO산업은 바이오산업의 핵심 인프라산업으로 바이오산업과 함께 고성장하고 있는 추세로, 최근 CRO산업은 단순한 연구서비스 제공을 지양하여 초기 물질 연구에서, 비임상시험, 임상시험, 분석시험, 임상데이터 관리, 컨설팅, 영업, 마케팅지원 사업(CSO)까지 다양화되고 있다.

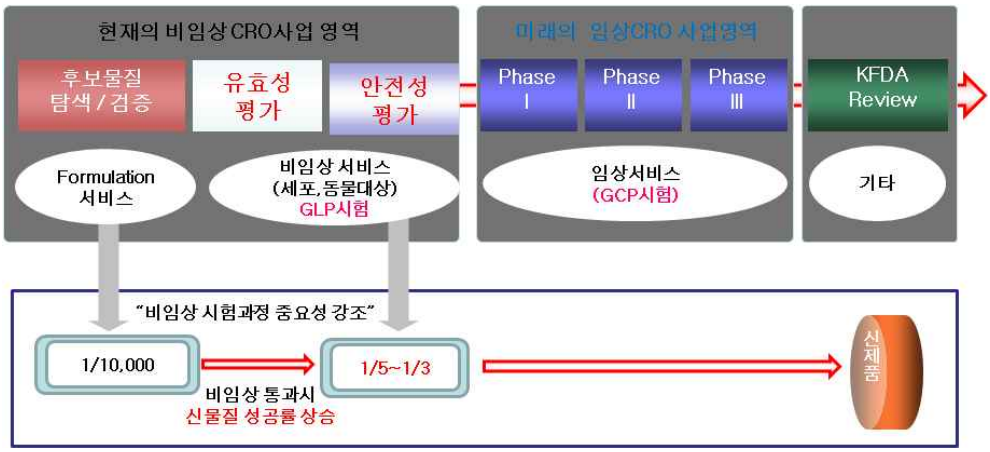

<(주)바이오톡스텍의 사업영역>

(주)바이오톡스텍은 3개 허가 당국 (식품의약품안전청, 국립환경과학원 및 농촌진흥청)으로부터 전항목 GLP 시험인증을 보유하고 있다.

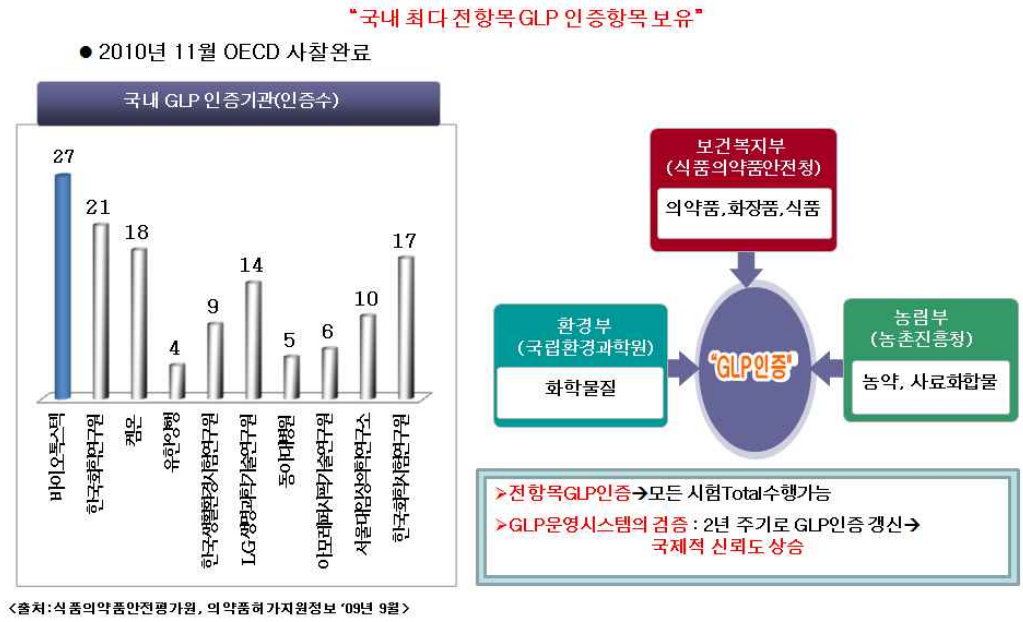

<(주)바이오톡스텍의 우수한 기반 인프라 소개>

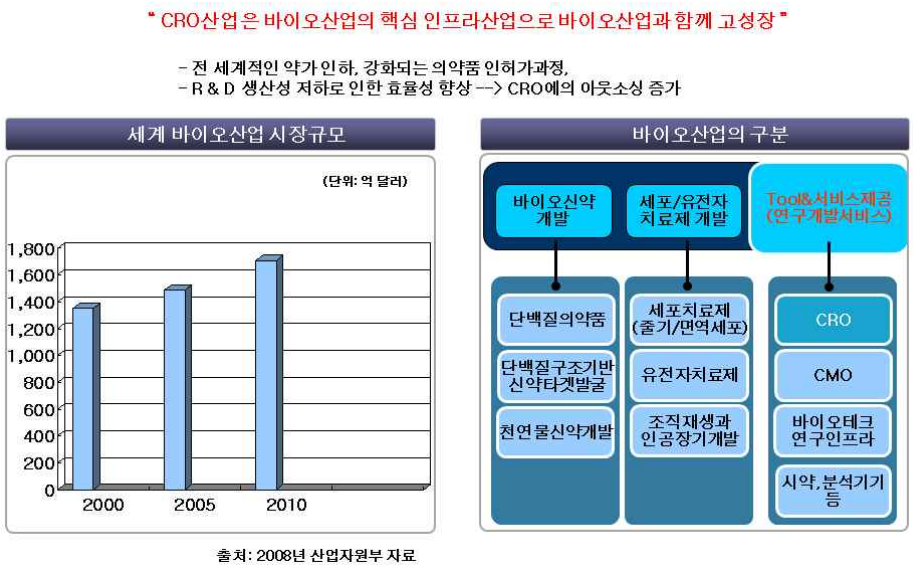

< CRO 산업>

GLP시험기관에서 실시하는 시험운영기준 및 해당 시험가이드라인을 준수하며, 시험의 신뢰성을 보증하기 위해 아래와 같은 연구추진 전략 및 체계로 본 과제를 수행한다.

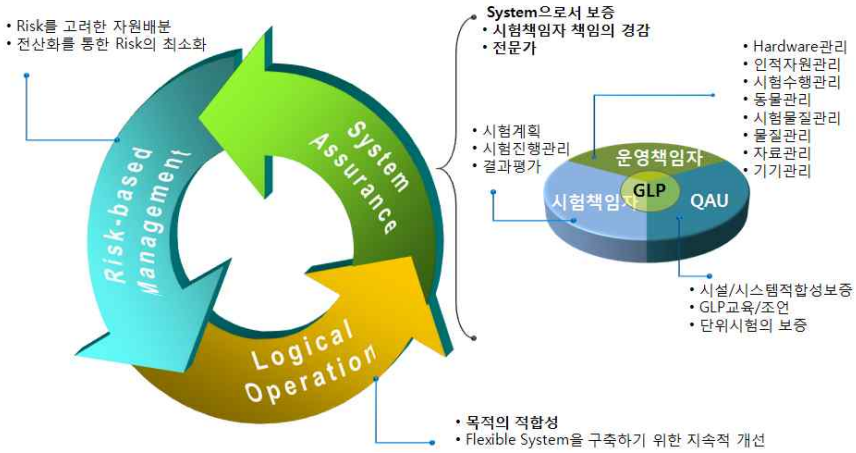

<GLP 운영 policy>

이러한 GLP 시험기관에서 실시하는 시험운영기준 및 해당 시험가이드라인을 준수하며, 유전자재조합옥수수 등 농업바이오 분야 국가연구개발과제를 다수 수행한 경험을 바탕으로 우수한 연구결과를 도출할 수 있다고 판단된다.

농업 바이오 산업은 생명공학을 필두로 하는 첨단기술 개발로 시장 규모가 넓고 분야가 다양화된 연 평균 18%의 경제성장을 보이는 국가경쟁력의 원천 분야로서, 신약소재에서 기능성 식품, GMO, 천연화장품까지 확대되어 후보물질이나 신기술을 상품화하는 글로벌 농업 CRO 출현을 필요로 한다.

또한, 농업 바이오 전문가인프라 구축과 전문 비임상 CRO 및 임상 CRO를 연계시키고, 농업 바이오 산업 분야의 특성화된 전문 컨설팅 서비스를 제공하는 농업 바이오 CRO 법인을 설립할 필요가 있다.

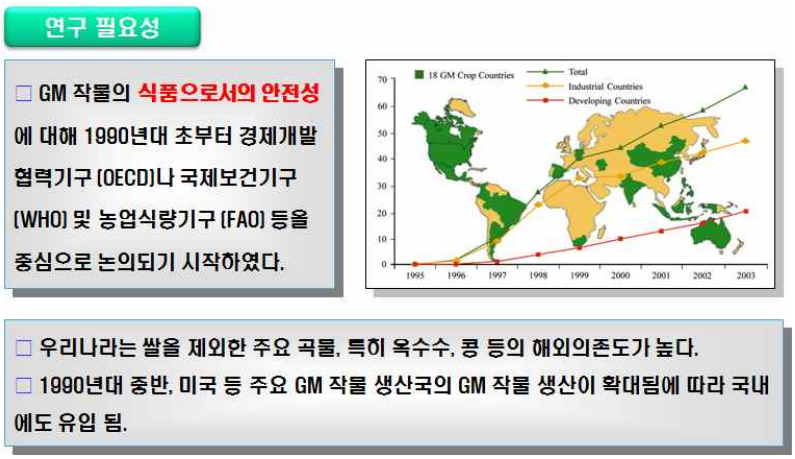

이러한 CRO 법인 설립을 위해 1,2년차에 산학연계 프로그램을 통해 우수 인력을 확보하였고, 내부 인원에 대한 전문성을 강화하기 위해 정기적인 교육 및 훈련을 실시하며, 국내외 전문가 초빙 세미나 및 전문 교육 프로그램 지원을 통해 농업 바이오 분야의 전문 CRO로서의 입지를 구축하였다. 3년차 이후에는 주관기업 내에 농업 바이오 R&D 컨설팅 전담부서를 구성하여 본 과제로부터 도출된 우수한 결과를 보인 국산 농산물 후보물

질에 대한 IND 신청자료를 파일링하고, R&D 컨설팅 네트워크 구축을 지원을 실시하며, 독립적인 R&D 컨설팅 CRO 법인을 설립하였다.

농업전문 국가기관과 농업전문 CRO 간의 MOU를 체결하여 국가기관에서 주관하는 주요 사업의 신약후보물질이 발굴되면 농업전문 CRO에서 컨설팅을 한다. 농업전문 CRO는 농업바이오분야에 저명한 학계와 우수실험실을 갖춘 비임상 및 임상 시험 전문기관과의 인프라를 구축하고 유지한다. 이러한 시스템을 이용하여 농업바이오분야의 우수한 신약후보물질의 효력 및 안전성 검증에서부터 상품화까지 컨설팅 역할을 수행함으로써 차별화된 농업전문 CRO 역할을 수행한다.

(1) CRO의 역할 및 국내외의 현황

(가) CRO란? 계약연구기관으로 신약개발에 필요한 비임상, 임상시험 및 기타 제반 업무를 계약을 통하여 위탁 수행하는 전문대행 기관으로 신약 개발의 대부분의 과정을 CRO가 대행함. 따라서 CRO의 역량은 국가 R&D사업의 성패를 좌우할 뿐 아니라 국가 경쟁력의 원천 분야이다.

(나) CRO는 신물질을 개발하는 기업의 최고 파트너로서, 기업의 비용 절감, 전문적 노하우에 바탕을 둔 가격경쟁력 및 효율적인 전임상·임상 진행을 통한 개발기간의 단축을 위하여 제약, 화학, 화장품, 식품회사 등의 CRO 이용은 폭발적으로 증가하였으며 2010년도 세계 시장 규모는 240억 달러에 이르고 있다. 한 예로서 미국 화이자 "비아그라"의 개발비 50% 이상을 CRO 사업자에게 아웃소싱, 신약개발기간을 7년에서 4년으로 단축한다.

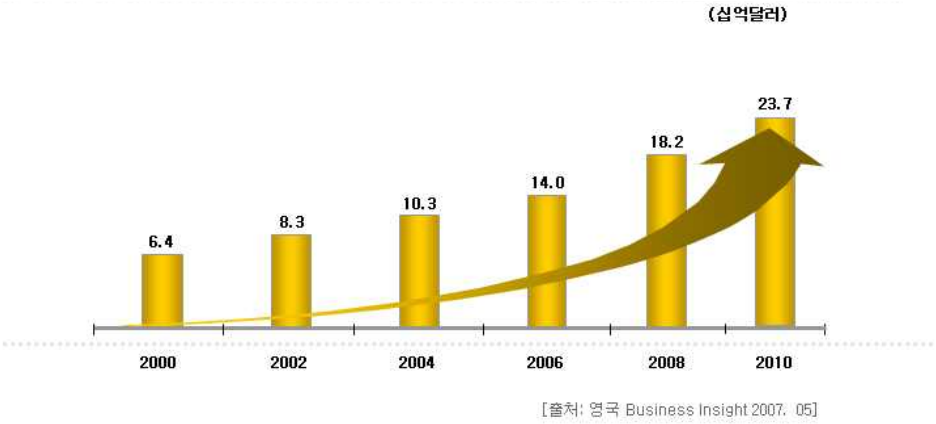

<세계 CRO 시장의 규모>

(다) 선진국 및 중국 등 개발도상국에서는 바이오산업 및 신약개발 활성화를 위하여 자국의 CRO 산업보호 및 육성정책으로 신물질 도입에 대한 무역장벽 강화와 인·허가에 대한 규제를 강화하고, 자국에서 상품화 할 신물질에 대해 자국 CRO 이용을 권장한다.

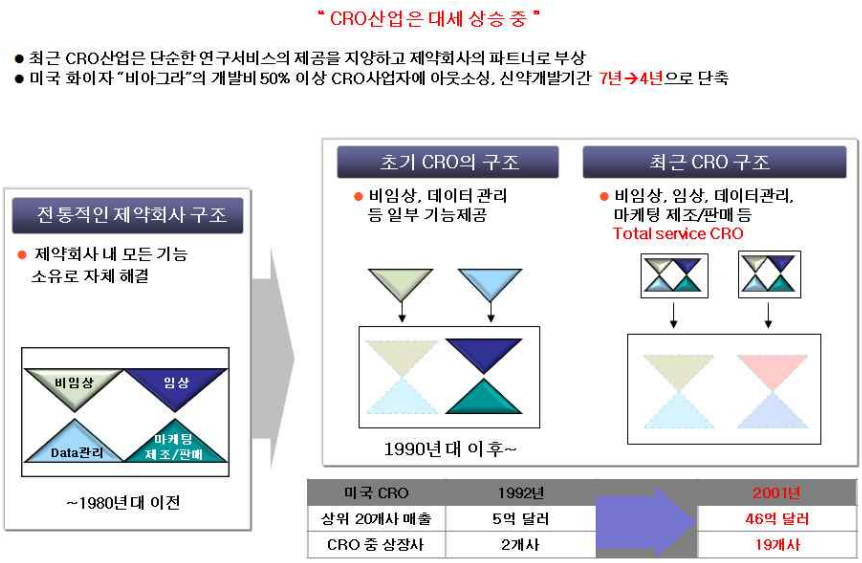

<CRO 산업의 흐름>

(라) 현재 국내의 대표적 비임상 CRO는 바이오톡스텍, 켐온, 메드빌 등이 있고, 정부출연 연구소인 안전성평가연구소 (KIT)가 있다. CRO의 비지니스는 글로발화되어 Covance, PPD, Charles River등의 CRO 년간 매출액은 2조원을 넘고 있으나, 국내 시장 규모는 극히 열악하여 100억을 넘는 국내 CRO는 바이오톡스텍, 안전성평가연구소의 2곳으로 가장 육성해야할 미래 성장 동력 분야이다.

(2) CRO의 육성에 대한 정부의 정책

(가) 글로벌 신약개발 경쟁력을 위하여 교육과학기술부, 보건복지부, 지식경제부 3개 부처 공동으로 2011년부터 2019년까지 정부 6,000억원, 민간 6,000억원 규모의 총사업 1.2 조원을 투입하는 "범부처 전주기 신약개발 사업" 계획안을 마련했다.

(나) [신성장동력 프로젝트] 중 2018년까지 세계 5대 생명공학·의료기기 산업 강국을 목표로 첨단의료복합단지조성, CRO·CMO등 관련서비스 육성, 전문인력 양성, 해외시장진출기반 조성 등을 통해 인프라 구축 예정이다.

(다) [지식경제부] 바이오시밀러 사업화 촉진과 함께 신약개발의 상업화 단계(비임상, 임상)를 집중 지원해 바이오스타제품 개발 및 글로벌 성공사례를 창출할 계획이다.

(라) [농림수산식품부] 농림수산식품과학기술 5개년 종합계획 발표 中

- 기업의 연구활동을 촉진하는 연구환경을 조성할 계획.
  : 국가 R&D 참여기업의 연구비 중에서 현금 부담을 완화하는 등의 국가연구비 운영제도를 개선할 예정.
- 고가의 장비구매와 고급인력 확보가 필요한 첨단기술도 쉽게 접근할 수 있도록 다양한 형태의 기술서비스 조직(CRO, CMO)을 육성할 예정.
- 상기와 같은 CRO 육성책과는 별도로 아직도 국가 R&D사업은 글로벌 신약개발이라는 목표하에 해외 CRO 이용을 권장하고, 국내 CRO에는 다른 정산시스템을 적용하므로써 해외 CRO의 국내 점유율은 폭발적로 증가되고 있는 상황이며, 어렵게 기반을 다진 국내 민간 CRO 산업의 경쟁력 및 생태계는 더욱 약화되어 생존에 위협을 받고 있는 상황임.

(3) 국내 비임상 CRO의 특성

(가) GLP 시험의 특징은 장치산업의 형태로 초기 엄청난 시설 및 장비투자가 요구되는 반면, 오랜 투자 회수기간이 소요되는 사업이며, GLP 규정에 따른 validation된 일정 규모 이상의 공간을 사용하고, 고비용의 연구기기를 사용하는 등의 임대료, 감가상각비용이 높다.

(나) 같은 공정으로 line화된 제조업과는 달리 매 시험마다 개별공정이 필요하고, 1년 내내 항온항습, 실험실 내부 청정도·조도·소음 유지 등 시설유지비가 높고 연구개발이 축이 되는 기술서비스 분야로서 많은 연구 인력과 고도의 기술력을 가진 전문가가 필요하여 인건비 의존도가 극히 높다.

(다) 또한 시험을 위한 실험, 기술, 고도로 숙련된 각 분야의 전문가가 필요하며 시대 흐름에 맞는 시험기술 이해와 습득이 필요하고 바이오의약품과 바이오시밀러의 새로운 시장의 등장에 적응하기 위한 훈련프로그램과 SOP의 지속적인 업그레이드도 필요하다.

(라) 따라서 무엇보다 국내 GLP 비임상 CRO 기관과 허가 당국 및 정부기관의 긴밀한 협조 및 적극적인 육성을 통해 부족한 인프라 구축이 절실히 필요하다.

나. 연구 목표 및 범위

(1) 조제물분석시험

① 시험목적

본 시험은 HPLC를 이용하여 조제물의 농도분석법 보증을 위한 validation 및 안정성을 확인하기 위해 실시한다.

② 분석법

시스템 적합성 (System suitability), 직선성 (Linearity), 특이성 (Specificity), 일내 재현

성 (Intra-day), Autosampler 내에서의 안정성 (Stability in autosampler), 균질성 (Homogeneity), 안정성 (Stability) 및 QC(Quality Control)를 실시한다.

(2) 단회투여독성시험 (설치류)

① 시험목적

암·수 랫드를 이용하여 단회 경구투여시 나타나는 독성반응을 관찰하고, 개략의 치사량을 구하기 위하여 실시한다.

② 관찰 및 검사법

일반증상관찰, 사망관찰, 체중측정, 부검 및 조직병리학적 검사 (필요시)를 실시한다.

(3) 최대내성 용량시험 (비설치류)

① 시험목적

암·수 비글견을 이용하여 일정한 간격으로 용량을 증가하여 단회 경구투여하고, 나타나는 독성반응을 질적·양적으로 평가하기 위하여 실시한다.

② 관찰 및 검사법

일반증상관찰, 사망관찰, 체중측정, 부검 및 조직병리학적 검사 (필요시)를 실시한다.

(4) 2주 용량결정시험 (설치류)

① 시험목적

암·수 랫드를 이용하여 2주간 반복 경구투여시 나타나는 독성반응을 평가하고, 4주 반복투여 독성시험의 용량설정 근거자료로 이용하기 위하여 실시한다.

② 관찰 및 검사법

일반증상 관찰, 빈사 및 사망동물의 처리, 체중측정, 사료섭취량 측정, 혈액학적 검사, 혈액생화학적 검사, 부검, 장기중량 측정 및 조직병리학적 검사를 실시한다.

(5) 2주 용량결정시험 (비설치류)

① 목적

암·수 비글견을 이용하여 2주간 반복 경구투여 시 나타나는 독성 반응을 평가하고, 4주 반복투여 독성시험의 용량설정 근거자료로 이용하기 위하여 실시한다.

② 관찰 및 검사법

일반증상 관찰, 빈사 및 사망동물의 처리, 체중측정, 사료섭취량 측정, 혈액학적 검사, 혈액생화학적 검사, 부검, 장기중량 측정 및 조직병리학적 검사를 실시한다.

(6) 4주 반복투여독성시험, 회복시험, TK시험 (설치류)

① 목적

암·수 랫드를 이용하여 4주간 반복 경구투여시 나타나는 독성반응과 안전성을 평가하기 위하여 실시한다.

② 관찰 및 검사법

일반증상 관찰, 빈사 및 사망동물의 처리, 체중측정, 사료섭취량 측정, 혈액학적 검사, 혈액생화학적 검사, 부검, 장기중량 측정, 조직병리학적 검사 및 TK시험을 실시한다.

(7) 4주 반복투여독성시험, 회복시험, TK시험 (비설치류)

① 목적

암·수 비글견을 이용하여 4주간 반복 경구투여시 나타나는 독성반응과 안전성을 평가하기 위하여 실시한다.

② 관찰 및 검사법

일반증상 관찰, 빈사 및 사망동물의 처리, 체중측정, 사료섭취량 측정, 혈액학적 검사, 혈액생화학적 검사, 부검, 장기중량 측정, 조직병리학적 검사 및 TK시험을 실시한다.

(8) 복귀돌연변이시험

① 목적

살모넬라균 (Salmonella typhimurium) TA98, TA100, TA1535, TA1537및 대장균 (Escherichiacoli) WP2uvrA(pKM101)의 5균주를 이용하여 유전자돌연변이유발성의 유무를 검색한다.

② 용량설정시험 및 본시험을 실시한다.

(9) 염색체이상시험

① 목적

포유류배양세포인 Chinese Hamster Lung(CHL/IU) 배양세포를 이용하여, 염색체손상을 형태의 변화와 염색체수의 변화로 구분하여 유전학적으로 평가하는 것을 목적으로 한다.

② 세포증식억제시험 및 본시험을 실시한다.

(10) 소핵시험

① 목적

설치류를 이용하여 생체내에서의 마우스골수세포에 있어서 소핵유발유무를 평가하는 것을 목적으로 한다.

② 용량설정시험 및 본시험을 실시한다.

(11) 출생전, 후 모체기능시험(랫드)

① 시험목적

본 시험은 랫드를 이용하여 수컷은 교배전부터 부검시까지, 암컷은 교배전부터 착상시기까지 투여하여, 수태능 및 초기배발생에 미치는 독성변화를 관찰하고, 그 안전성을 평가하기 위해서 실시한다.

② 관찰 및 검사방법

일반증상관찰, 빈사 및 사망동물의 처리, 체중측정, 사료섭취량측정, 암컷의 성주기 관찰, 교배 및 교배성적산출, 착상률 및 배자사망률, 부검, 장기중량 측정, 조직병리학적 검사 및 정자검사를 실시한다.

(12) 배·태자 발생독성시험 (랫드)

① 시험목적

본 시험은 임신한 랫드에 배자의 착상시기부터 경구개가 폐쇄되는 시기 (임신 7 ~ 17일)까지 경구투여하여 모동물 및 배 • 태자의 발생에 미치는 독성 변화를 관찰하고, 그 안전성을 평가하기 위해서 실시한다.

② 관찰 및 검사

일반증상 관찰, 빈사 및 사망동물의 처리, 체중측정, 사료섭취량 측정, 부검, 장기중량 측정, 조직병리학적 검사, 제왕절개, 태자의 체중 및 태반중량의 측정, 태자의 외표 검사 및 태반 관찰, 태자의 내부장기 검사 및 태자의 골격 검사를 실시한다.

(13) 배태자 발생독성시험 (토끼)

① 시험목적

본 시험은 임신한 토끼에 배자의 착상시기부터 경구개가 폐쇄되는 시기 (임신 6 ~ 18일)까지 경구투여하여 모동물 및 배 • 태자의 발생에 미치는 독성변화를 관찰하고, 그 안전

성을 평가하기 위해서 실시한다.

② 관찰 및 검사

일반증상 관찰, 빈사 및 사망동물의 처리, 체중측정, 사료섭취량 측정, 부검, 장기중량 측정, 조직병리학적 검사, 제왕절개, 태자의 체중 및 태반중량의 측정, 태자의 외표 검사 및 태반 관찰, 태자의 내부장기 검사 및 태자의 골격 검사를 실시한다.

(14) 피부자극시험

① 시험목적

토끼의 피부에 1회 처치한 후, 피부자극성/부식성의 유무 및 그 정도를 평가하기 위해 실시한다.

② 관찰 및 검사

일반증상 관찰, 체중측정, 피부반응의 평가, P.I.I. 산출 및 피부자극성의 분류 및 피부 부식성의 판정을 실시한다.

(15) 안점막자극시험

① 시험목적

토끼의 안점막에 1회 처치한 후, 안자극성/부식성의 유무 및 그 정도를 평가하기 위해 실시한다.

② 관찰 및 검사

일반증상 관찰, 체중측정, 안구병변의 관찰 및 안자극성의 평가를 실시한다.

(16) 항원성시험

① 시험목적

기니픽의 면역계에 작용하여 나타나는 이상면역 반응을 검색하기 위해, 아나필락시스 쇼크 반응시험 (Active Systemic Anaphylaxis, ASA) 및 동종 수동 피부 아나필락시스 반응시험 (Passive Cutaneous Anaphylaxis, PCA)을 실시한다.

② 관찰 및 검사

일반증상 관찰, 체중측정, 청색반점의 직경 (장경과 단경의 평균)이 5 mm이상이면 양성으로 하고, 양성을 나타내는 가장 마지막 혈청희석배수 (최대희석배수)를 그 혈청의 최종 역가 (항체가)로 정하여 수동 피부 아나필락시스 반응을 판정한다.

2. 제 1협동

질환 동물 모델 개발 및 효력시험 연구

가. 연구개발의 필요성

본 연구과제의 최종목표는 농업 바이오 전문가인프라 구축과 전문 비 임상 CRO 및 임상 CRO를 연계시키고, 농업 바이오 산업 분야의 특성화된 전문 컨설팅 서비스를 제공하는 농업 바이오 CRO 법인을 설립하기 위하여 자체적인 질환모델동물 개발과 이를 통한 천연물 유래 신약 후보 물질의 유효성 및 효력 평가 실험에 있다. 최근 생명과학분야의 눈부신 발전과 함께 교내에서도 의생명과학과 관련된 다양한 연구가 진행되고 있음. 분자적 수준의 연구 성과가 사람에게 적용되기 위해서 가장 중요한 연구 인프라는 실험동물을 이용한 동물 실험 분야이다.

국내에서도 의약품, 화학물질 등의 많은 신물질이 개발되어 약효검증, 독성 및 안전성 평

가 등 비임상 실험의 수효 및 빈도가 폭발적으로 증가되었으며, 이와 관련한 실험동물의 수요 또한 급속하게 증가되고 있으며, 특히 유전자 변형이 가능한 마우스의 사용량이 최근 전 세계적으로 증가될 뿐 아니라 국내에서도 증가하고 있는 추세이다. Pubmed를 이용한 분석에 의하면 2007년 전 세계에서 출간된 SCI 논문 중에서 마우스를 이용한 논문은 7.18%이고, 이중 Cell, Nature, Science 등 high profile journal (CNS 계열 논문)은 21.5%를 차지함. 즉, 마우스를 이용한 연구결과가 좋은 논문에 발표될 확률이 매우 크다는 사실을 보여준다.

국내 주요 연구과제에서도 마우스를 이용한 인프라 구축사업은 국가중점 육성 분야의 개별 세부 사업 목표 달성을 위해서도 매우 중요하게 다루어져야 할 것으로 사료되나 국내 인프라는 매우 취약한 상황이다. 최근 생물자원 법에서도 생물자원의 수집, 보관, 활용 기회 확대를 목표로 하는 범국가적 관리 시스템 구축을 준비 중이나 국가 차원의 모델동물 현황 조사 및 데이터베이스 구축을 포함한 대비책이 이루어 지지 않고 있는 실정임. 생물자원 세부분야는 리소스센터 구축 및 체계적 관리를, 인적 세부분야는 인재육성 시스템 구축을 명시하고 있다.

(1) 경제적 측면

KNOCKOUTS MODEL THE 100 BEST-SELLING DRUGS — WILL THEY MODEL THE NEXT 100?

Brian P. Zambrowicz and Arthur T. Sands

Table 5 | **Best-selling drugs and KO-mouse phenotype: menopause, metabolism and hypertension***

Drug target	Drug name (utility)	2001 Sales‡	Mouse phenotype
Estrogen receptor	Premarin (menopause/ osteoporosis) Evista Nolvadex (breast)	$2,074.0 $665.0 $630.0	Reproductive defects, reduced bone mineral density.
Probably farnesyl diphosphate synthase	Fosamax (osteoporosis) Aredia (hypercalcemia)	$1,760.0 $752.0	Embryonic lethal; heterozygous males have increased bone mineral density.
Unknown target, perhaps ACC2	Glucophage (diabetes)	$2,049.0	Anti-diabetic effects seen in ACC2 knockouts.
Insulin	Humulin/insulin (diabetes) Humalog	$1,061.0 $628.0	No phenotype for KO of insulin I or insulin II; insulin-receptor-KO mice display hyperglycemia, ketoacidosis, increased triglyceride levels and fatty livers; 10% of heterzygotes develop diabetes.
PPAR-γ	Avandia (diabetes)	$1,018.0	Increased insulin sensitivity in heterozygotes; embryonic lethal homozygotes.
Lipases	Xenical (obesity)	$570.0	PLRP2 , decreased fat absorption, carboxyl ester lipase reduced dietary cholesterol ester absorption.

<갱년기와 골다공증, 당뇨, 대사와 비만의 치료 약물들에 사용되는 knockout (KO) 마우스 표현형과 best-selling 약물 사이의 관계>

(가) 국내 in vivo animal 분야의 기술보유현황을 볼 때 암질환, 대사성질환, 면역질환, 심혈관질환 별로 아주 초기단계의 induced model 만을 보유하고 있으며 전문적인 약효평가모델이나 약리 연구모델을 보유하고 있지 못한 것으로 나타났으며, 일부 기업에서는 의약품의 in vivo animal 평가에 사용되는 모델을 구체적이고 현실적으로 갖추고 있으나 일부의 모델에 국한되어 있고 타기관의 기술 수요자가 활용할 수 없다는 점에서 역량이 높다고 판단되어 지지 않다.

(나) 대개의 경우 유전적 동물 모델은 확보하지 못하고 있는데 이는 동물의 보존, 형질유지 등의 기초기술을 갖고 있지 못하기 때문이며, 또한 실제로 동물을 사육할 수 있는 시설자체도 미비하다는 것을 반영하고 있다.

(다) 기업 및 학계에서 신약개발역량강화를 위해 약리/약효 in vivo animal 분야에 대해서는 상당히 포괄적인 요구가 있는데, 국내현황을 고려하여 우선확보가 필요한 질환모델동물에 대한 재평가 필요성이 있다.

(라) 신약개발 기업 또는 연구자들이 필요로 하는 질환모델동물을 파악하고 이들이 이용할 수 있는 질환모델동물을 이용한 신약개발기반을 구축하여 제공함으로서 국내의 신약개발 역량을 강화하고 막대한 비용을 투자하고 있는 신약개발 관련 사업의 성공가능성을 향상시키고자 한다.

(마) 국내의 기업과 학계의 약리/약효 수요를 감당하기 위해서는 암 질환, 당뇨 질환 등 수요가 많은 부분의 국내역량을 세밀히 분석하여 기반구축과 역량강화가 필요할 것으로 분석되고 있다.

(바) 가장 많은 비용이 소요되는 단계인 임상시험에서의 결과를 효과적으로 예측할 수 있는 적절한 시스템 즉, 동물모델의 개발과 선택이 필요하다.

(2) 사회적 측면

(가) 인간유전자지도가 확보된 이후 개체 수준 (organismic level)에서의 유전자 기능 규명이 포스트 게놈 시대의 선결 과제이다. 이는 세포수준과 하등동물 (선충, 초파리, 개구리 등)에서 기능이 규명되거나 프로테오믹스, 유전체 연구를 통해 발굴된 질병 관련 유전자의 경우, 사람에 적용하기 전에 반드시 마우스 개체수준에서의 기능 확인 및 질병모델 확보가 필수적 과제이다.

(나) 효용이 검증된 질환모델동물은 질병에 대한 원인규명 뿐만 아니라 인간 질병을 구현함으로써 직접적으로 의약품평가에 새로운 접근 방향을 제시할 수 있다. 미국 NIH의 Roadmap에서도 실험실 연구가 임상 또는 산업화로 결실을 맺기 위해서는 전임상 연구를 할 수 있는 질환모델을 이용하여 Translational Research를 하여야 한다고 강조하고 있으며, 효용이 검증된 질환모델동물은 질병에 대한 원인규명 뿐만 아니라 인간 질병을 구현함으로써 직접적으로 의약품평가에 새로운 접근 방향을 제시할 수 있다.

(다) 타 연구는 특정단백질 또는 유전자가 인간질병 유발 (암, 신경질환, 심혈관계 질환, 감염성질환 등)의 원인이라는 것까지 밝히는 것이 한계이지만 질환모델동물을 사용한 연구는 in vivo에서 그 결과를 실제적으로 증명할 수 있다. 생명현상을 밝히는데 사용된 질환모델동물은 그 현상을 직접적으로 인간의 질병현상에 적용되어 질환모델을 얻게 되고 이를 토대로 의학 및 약리학, 그리고 이를 기반으로 하는 산업에 직접으로 사용될 수 있다.

(라) 신약개발에 있어서 질환모델동물을 이용한 약효, 독성 및 약동력학 평가는 신약후보물질의 개발 성공가능성을 평가하기 위하여 필수적으로 요구되고 있으며, FDA를 비롯한 허

가기관에서는 임상시험 승인 전에 동물실험 결과의 제출을 요구하고 있다. 질환모델동물을 이용한 전 임상 평가는 막대한 비용이 드는 임상시험에서의 성공 가능성을 예측할 수 있는 가장 좋은 방법이므로 적절한 질환모델동물의 선정 및 이를 이용한 평가는 필수적이다.

(마) 인간 및 마우스 유전체의 정보가 확보됨에 따라 이를 활용하여 마우스 개체 수준에서의 유전자 기능이 확인되고 있으며 이를 통해 유용한 질환모델동물의 확보가 이루어지고 있으므로 향후 의약품 개발에 있어서 질환모델동물의 활용도는 더 높아질 것으로 예상이다.

(바) 국내의 제약업체들은 규모가 작고 연구개발에 투자할 수 있는 여력이 많지 않아 자체적으로 질환모델동물을 이용하여 신약 후보물질을 평가할 수 있는 기반을 구축하는 데 현실적인 어려움이 있다. 국내 의약품 산업은 대형제약사를 비롯하여 의약품 산업의 Value chain 중 승인·마케팅에 역량이 집중되어 있으며 '원료물질개발-신약선정-신약개발' 단계의 역량이 부족한 실정이다.

(사) 지금까지 국내외에서 마우스 사육 시설과 유지 능력의 미비로 인한 귀중한 질환모델동물의 손실이 막대함. 1970년대에 일본에서 한탄 바이러스의 오염으로 수명의 인명손실이 있었으며 그 후 시설과 유지비의 확충으로 질환모델동물의 연구가 활성화됨. 국내에서도 열악한 여건 하에서 질환모델동물을 연구하던 과학자들이 간염, 한탄, 센다이 바이러스 등에 의한 피해로 연구의 중단 사태까지 이르게 된다.

(3) 기술적 측면

(가) 인간유전체기능은 유전적, 생리학적 및 행동학적으로 인간과 매우 유사한 마우스를 모델동물로 이용하여 생체 기능을 발견함으로써 완성될 것이다. 마우스유전체 염기서열 초안이 발표(Nature 2002년 12월)됨에 따라, GEM(유전자변형마우스, Genetically Engineered Mice)의 개발과 분석을 통한 인간유전체의 기능 연구가 가속화된다.

(나) 유전자의 모든 정보는 전 세계가 공유하고 있어 기능이 규명되지 않은 유전자는 실질적 효용이 없는 자료에 불과, 유전자의 기능 규명을 위한 마우스의 제작 및 분석은 생물학 및 의학 등 제반 분야에 큰 파급 효과를 불러온다. 질환 치료후보물질은 질환모델동물 실험을 통해 검증하는 것이 가장 중요하다.

(다) GEM 이용 연구의 필요성에 대한 설문조사 결과: 생명과학 전문가의 95%가 필요하다고 응답하였고,(*별첨) 발굴한 유전자의 가치는 최종적으로 GEM개발을 통한 생체 내 기능 규명을 통해 검정되며, 개발한 질환모델마우스는 후보신약의 효능검정에 필수자원이다.

(라) 살아 있는 시약 마우스의 장점

- 기술적 측면 : 형질전환 마우스의 생산에 필요한 노하우와 지식이 이미 축적.
- 경제적 측면 : 포유류 중 대량 번식 및 유지 관리가 가능한 유일한 동물.
- 실험적 측면 : 사람의 질병은 마우스에서도 일어남. 마우스가 지니고 있는 생식능력, 수명 등의 생리학적 특성으로 인해 포유동물 중 사람의 질병 원인규명을 위한 연구에 가장 적합한 생명체로 규정.
- 유방암 치료제 Herceptin의 예: in vitro에서 유방암 세포의 증식을 억제하여 FDA승인을 받은 약이 개발이 되었으나(1998년), 유방암의 억제에는 탁월한 효과가 있으나,

몇 년 후 이 약을 투여 받은 환자들이 심장병에 걸리는 부작용이 있었음(28%의 환자가 심장병 발병). 마우스에서 Herceptin의 target인 Her2 유전자를 결손 시킨 마우스는 심장병에 걸림. 만약 Her2를 결손 시킨 마우스의 표현형을 먼저 알았더라면, 장기간 이 약을 투여하면 엄청남 부작용이 있었음을 미리 인지 했을 것 임. 현재 소송 진행 중. 따라서 마우스(포유류)가 아닌 다른 모델 생명체 혹은 세포주에서의 연구는 사람에게 직접 응용이 가능한 고부가 가치의 연구 결과를 도출하기 위한 효율적인 시스템이 아님.

연구 대상 (재료) / 평가 항목	초파리 & *C. elegans*	세포주 연구	마우스 연구	영장류
유전자 기능	가능	가능	가능	미약
유전자 발현양상	가능	부분적 가능	가능	미약
유전자 과발현	가능	가능	가능	부분적 가능
유전자 결손	가능	가능	가능	불가능
전체염기서열해독	완결	완결	완결	거의완결
유전자 과발현/결손에 의한 조직/세포의 연구	가능	불가능	가능	불가능
사람 유전자와 유사성	유전자 상의 상동성은 있으나, 염기서열상의 유사성은 떨어짐	인간 세포주 (비정상)	95% 상동/ 사람의유전자99% 마우스에도 존재	99% 상동
일반 병원에서의 검사항목	불가능	불가능	대부분 가능	가능
질병의 단서제공	미약	미약	결정적 단서제공	미약
신약개발 시의 잠재적 문제 단서제공	미약	미약	결정적 단서제공	미약
동물실험에 대한 규제(Law)	없음	없음	미약	엄격
논문의 Quantity and Quality	전통적으로 강했으나, 약화추세	양적(뛰어남) 질적(떨어짐)	질적/양적 뛰어남	미약
파급효과 (타연구자의 참여 유도)	미약	미약	뛰어남	검증 안됨

<인간의 질병 모델로서의 유전자 변형마우스 (GEM Models for Human Disease)의 가치>

(마) 사람의 질병을 모델링하기 위해 필요했던 기술적인 측면이 마우스에서 거의 확립되어 응용단계에 접어듦. 인간의 다양한 유전병과 대사질환을 모델링하기 위한 기술로서, 특정 유전자의 과발현 혹은 결손 마우스, ENU mutant 마우스, Exon-trap 마우스, siRNA 마우스 등이 확립됨. 이들의 표현형을 통해 유전자의 이상 (결손 또는 과발현)이 나타낼 수 있는 사람의 질병에 대한 가장 직접적인 단서를 찾을 수 있다.

(바) 국내에서는 많은 연구진에 의해 암과 관련된 유전자에 대한 형질전환 마우스들이 제작되었으나 항암제 효능 확인을 위한 국가적인 체계적 관리와 확보가 집중화되어 있지 않

다. 우선적으로 국외 및 국내의 항암제 개발의 경향을 파악하고 이용 가능한 동물모델에 대한 네트워크화가 필요하지만 현재 국내에서는 원활히 이루어지고 있지 않는다. 향후 국내 표적항암제에 대한 개발 현황 및 앞으로 동향에 맞는 동물모델의 확보가 시급함. 또한 현재 국내에서 사용되는 orthotopic 모델, 전이 모델의 제작에 있어서 결과의 신뢰성 및 재현성 확보를 위해 마우스 모델 확립에 대한 표준화가 필요하다.

(사) GEM을 포함한 실험동물의 주요시장은 유전자 기능 규명 및 신약개발의 후보물질 발굴 및 약효, 독성 평가와 같은 임상시험을 대신하는데 주로 이용되고 있다.

① 2009년 질환모델동물 설문에 의하면 많은 기관이 기초연구와 치료제 개발에 질환모델동물을 사용하고 있는 것으로 조사됨

② 질환모델동물의 주 사용처는 생명과학기초연구가 60%, 질병치료제 개발이 50%, 질병진단지표개발 20%, 기타 10% 순으로 조사됨. (*별첨)

나. 연구 목표 및 범위

(1) Ei24 질환동물모델을 이용한 자초추출물 유효성 평가

(가) 연구 목적

제1협동(서울대학교) Ei24 질환동물 모델을 이용한 제2협동(부산대학교) 신약후보물질(자초추출물, α-iso-cubebenol)의 항암 효능시험을 평가하는데 목적이 있음.

(나) 연구 방법

① 투여경로: 복강투여

② 부형제: Olive oil (양성대조군: 생리식염수)

③ 시험물질 투여농도: 0.1, 10mg/kg

④ 투여기간: 6개월, 2번/일주일

⑤ 투여군 구성

	음성대조군	시험군 1	시험군 2	양성대조군
투여물질	Olive oil	자초추출물 (Olive oil)	자초추출물 (Olive oil)	Cyclophosphamide (PBS용액)
투여농도	원액	0.1mg/kg	10mg/kg	20mg/kg

⑥ 시험 결과

혈액 검사(ALP, AST, ALT 등), 간 조직 염색 (H&E, PCNA), 간 조직 면역염색 (p53, CDK1,2, cyclin D1)

DEN을 투여한 Ei24 KO 마우스(암컷, 수컷)를 활용해 자초 추출물의 유효성을 평가함. 실험군은 크게 4군으로, 음성대조군(Olive oil), 자초추출물 0.1mg/kg, 자초추출물 10mg/kg, 양성 대조군(Cyclophosphamide)으로 나누어 복강 투여함. 생후 3개월 령에 투여를 시작하여 6개월 동안 일주일에 2번 투여함. 투여하는 동안 몸무게를 측정함. 실험 종료 후 샘플링은 혈액 샘플과 간 조직을 샘플링 함. 혈액에서는 ALP, AST, ALT 등을 측정하고, 간 조직에서는 PCNA, p53, CDK1,2, cyclin D1 등을 면역 염색하여 세포 증식 능력을 측정함.

3. 제 2협동

천연물 신약후보물질의 개발 및 효력시험 연구

가. 연구개발의 필요성

(1) 세계적인 천연물의약산업의 활성화, 생명자원에 대한 보호주의 확산 및 지적 재산권 협약 등으로 외국 자원 또는 기술의 도입은 점차 어려워지고 있으며, 이러한 기술을 도입할 경우에는 막대한 royalty를 지불해야 한다. 우리나라에는 옛날부터 한의학이 발달되었으나, 한약재로부터 생리활성을 탐색한 후 식의약품, 보건식품 또는 식품첨가제의 개발에 관한 연구는 유럽연합이나 미국 등의 선진국에 비해 오히려 뒤지고 있다.

또한 많은 연구기관에서 투자를 하여 좋은 결과를 얻었으나 대부분 연구비의 지원이 단회성으로 연구가 종결되므로 좋은 연구결과를 얻더라도 연구의 결과를 활용할 수 있는 후속 연구가 미비한 상황이다.

최근 들어 생약제를 이용한 식품보조제나 건강식품의 개발에 의한 생물산업이 활성화되고 있는데, 이에 부응하기 위하여 식물로부터 얻은 천연물 신약 후보물질의 산업화는 농가의 소득작물 개발에 필연적인 과제로 부각되고 있다.

(2) 한국사회 식생활의 서구화는 비만과 더불어 허혈성 질환의 발병률을 더욱 높이고 있으며, 의료기술의 발전으로 생명이 연장되어 고령화 사회로 접어들면서 허혈성 질환에 고통을 받는 인구가 더욱더 증가하고 있으며, 나아가 삶의 질을 평가하는 데에 있어서 건강하게 노후를 보내고자 하는 허혈성 질환의 극복은 현 사회문화의 흐름 속에 비추어 볼 때 결코 간과할 수 없는 질병이다.

고혈압에 대한 효과적이면서도 실용적인 치료법 개발은 21세기 생명과학 및 생명공학 시대에 있어서 고부가가치 산업으로 등장할 것이 확실시 되고 있는 현 시점에서 약용작물을 기초로 한 고혈압을 예방 및 치료하기 위한 신물질의 발굴은 매우 중요하다.

(가) 국내의 경우 학계와 산업계에서 고지혈증 관련 의약품 및 기능성 식품에 대한 연구가 광범위하게 이루어지는 상태는 아니지만 경북대학교 박용복 교수팀, LG화학 중앙연구소, 한국화약 중앙연구소, 제일제당 중앙연구소, 한국생명공학연구원 지질대사연구실에서 활발히 진행되고 있으나 천연물을 소재로 한 연구는 거의 전무하다.

(나) 1998년에 이미 심혈관계질환 치료제의 시장은 460억불로 전체 의약품시장의 18%를

점유하였고, 세계 상위 100대 처방약 중에서 심장순환계 약물은 20여개에 이르렀으며, 현재는 세계 제약시장에서 심혈관계약물들이 최고의 매출액을 기록하고 있다. 특히 혈중콜레스테롤 강하제인 스타틴계열 약물의 2001년 세계 시장은 무려 191억 달러로서 주로 Merck사의 Zocor(simvastatin)와 Pfizer의 Lipitor (atorvastatin)가 주도했다. 심혈관계약물 시장은 크게 성장되었으나, 다른 질환들에 비하여 환자의 수가 많고, 기존 의약품에 대한 불만족도가 높으므로 새로운 약물에 대한 기대도가 크다. 예를 들면 스타틴계열의 약물을 장기간 복용 시 근골격계에 대한 부작용, 신경독성 등의 치명적인 부작용이 있다. 그러나 이러한 부작용의 위험 보다 혈중콜레스테롤 농도를 낮추는 혜택에 상대적으로 큰 비중을 두어 스타틴계열의 약물 사용은 증가하고 있다. 따라서 기존 약물의 한계를 극복하는 새로운 심혈관계 치료물질의 개발은 그 경제적 효과가 클 것이다.

(다) Gomisin A는 혈관내피세포에서 혈관이완성 물질을 생성/분비하여 혈관근을 이완시키는 작용을 나타내었을 뿐만 아니라, gomisin A는 직접적으로 혈관평활근을 이완시킴으로서 혈관근 이완을 유도하는 것을 확인하였다. 또한, gomisin A가 angiotensin II에 의하여 고혈압이 유도된 흰쥐에서 현저한 항고혈압 효과가 있음을 실험을 통해 확인하였다.

(라) 최근, 본 연구진들은 gomisin J가 혈관 평활근을 이완시킬 수 있음을 증명하였을 뿐만 아니라, gomisin J의 혈관이완작용 강도는 gomisin A의 강도보다 3배 정도 더 강함을 알 수 있었다. 이를 통하여 gomisin J가 gomisin A보다 더 높은 약리학적 효능을 가지고 있으며 또한, 더 높은 부가가치를 창출할 것으로 사료된다.

이에, 본 연구에서는 흰쥐 대동맥 및 사람의 혈관근을 이용하여 gomisin J의 혈관이완작용과 작용기전을 규명하고자 하고, 더 나아가 다양한 형태의 고혈압 실험동물 모델에서 gomisin J의 항고혈압 작용 및 작용 기전을 규명하고자 한다.

(3) 만성염증은 암, 심혈관질환, 신경장애, 대사장애 합병증, 뼈 근육 및 골격질환, 당뇨합병증 및 만성질환 염증을 유발하기 때문에 모든 병의 근원인 염증의 예방 또는 치료방법이 절실히 요구되고 있음.

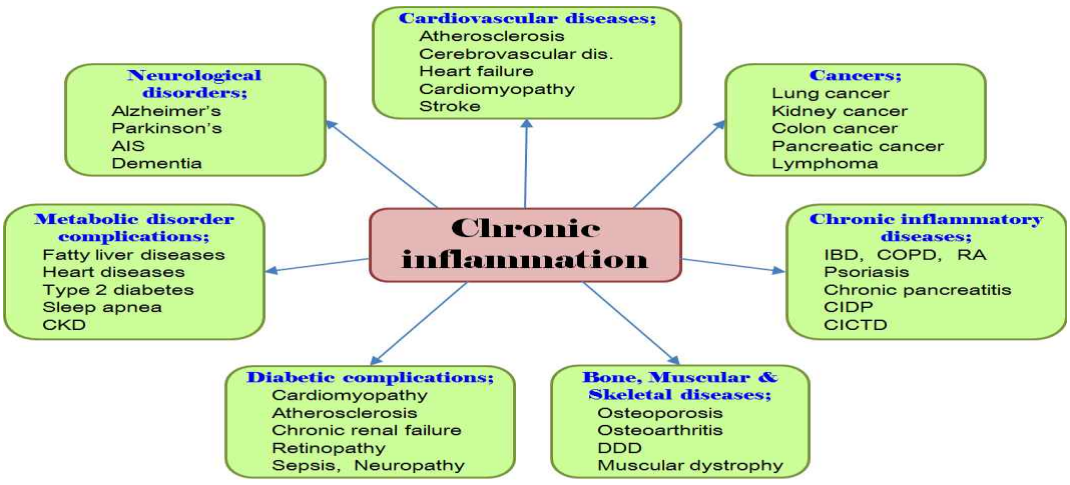

<만성염증에 의한 병유발>

(가) 패혈증은 생체에 침입한 박테리아 및 곰팡이 등의 병원균에 의해 염증성 사이토카인을 포함한 염증 매개 물질의 과도한 분비로 인해 전신적인 염증 반응이 유도되어 궁극적으로 조직 및 장기 손상, 백혈구 세포의 기능 상실이 유발되어 감염균에 대한 방어 능력이 마비되는 심각한 급성 감염성 염증 질환이다. 패혈증은 다양한 종류의 염증면역세포, 즉 대식세포, 단핵구, 호중구 등의 과도한 활성으로 야기되는 것으로 전형적인 급성 염증 질환임. 이들 면역 세포들은 정상적으로는 외부의 감염균을 제거하는 생체 방어 역할을 담당하지만, 패혈증 환경에서는 과도하게 활성화되어 오히려 생체에 해로운 각종 염증성 사이토카인이나 염증성 매개체를 생성하여 그 증상을 빠른 시간 내에 악화시켜 조절 불능 상태로 빠지게 하여 생체 중요 기관 및 장기들의 이상을 초래하여 전신적인 쇼크 및 사망에 이르게 하다.

(나) 패혈증의 역학적인 측면에서 보면 미국에서 연간 700,000명이 발병하는 것으로 알려져 있으며 발병률이 매년 1%이상 증가하고 있음. 한편, 패혈증 발병환자의 약 30-50%가 사망하며, severe sepsis의 경우 약 70% 이상이 사망하는 것으로 알려졌다.

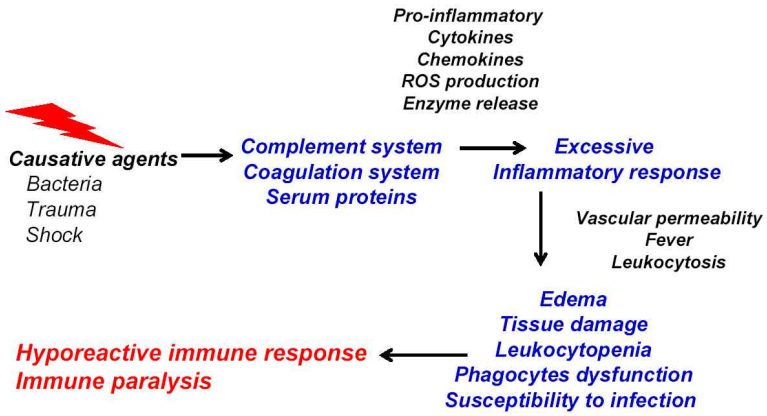

Immune responses during sepsis

패혈증은 박테리아 또는 비브리오균의 감염으로 빈번히 그리고 집단적으로 발생할 가능성이 커서 지역 사회적으로 문제가 큰 것임. 패혈증을 유발하는 원인은 항상 우리 주위에 존재하며, 한번 발생하면 급격하게 빠른 속도로 진전되기 때문에 응급으로 처치되는 경우가 많음. 또한 각종 외상, 교통사고 및 암과 같은 각종 질환 치료과정에서 진단된 본래의 질병보다는 궁극적으로는 2차적으로 박테리아 감염으로 인한 패혈증에 의한 사망률을 감소시키기 위해서 본 연구는 매우 필수적이다.

(다) 중환자에게서 빈번하게 발생하는 패혈증은 나날이 증가하며 사망률도 증가 추세에 있음. 국내외 패혈증 환자의 증가추세로 볼 때 막대한 경제적 손실을 막기 위해서는 패혈증 치료제 개발 연구가 필수적임. 성공적인 패혈증 치료제 개발 연구는 현재까지 1차적인 치료목적으로 사용되고 있는 막대한 양의 항생제 사용과 그럼에도 불구하고 줄지 않는 사망률을 줄이기 위해 응급치료로 사용되는 각종 보조 치료약과 인력동원에 따른 손실을 막을 수 있음. 아울러, 패혈증 치료제 개발은 선진국에 비해 처져 있는 우리의 의약업계의 생산성 향상과 기술력 증진에 크게 기여하여 경제적 및 산업적 가치를 향상시킬 수 있다.

(라) 국제적으로 패혈증 치료제 개발에 필요한 연구가 매우 활발히 진행되고 있으며, 특히 염증 반응을 제어할 수 있는 면역 조절 물질들에 의한 패혈증 치료제 개발 분야가 각광을 받고 있음. 하지만, 아직까지 뚜렷한 면역 조절을 통한 패혈증 치료제의 개발은 이뤄지지 않고 있다. 현재까지 패혈증 치료제 개발의 문제점은 효과적인 면역 조절제가 없고, 면역 세포활성 조절제의 분리 정제가 어려우며, 염증 반응 조절제의 개발 및 생체내의 자연적인 방어 시스템을 이용한 패혈증 치료제의 개발을 요구하고 있음.현재 사용되고 있는 패혈증 치료제의 대부분이 항생제로서 패혈증의 치료효과를 향상시키는데 이미 문제점을 드러내고 있으므로 신 개념의 면역 활성 물질들에 의한 패혈증 치료효과 연구는 이 분야의 새로운 전기를 제공할 수 있을 것으로 기대된다.

(마) 따라서 패혈증 치료효과에 대한 본 연구팀의 연구주제는 임상적인 응용이 절실히 요구되고 있는 분야이므로 패혈증 병리적 관련성에 대한 연구와 신약개발을 위한 정보의 발굴이라는 매우 중요한 영역에 대한 연구라고 볼 수 있으며 꼭 수행되어야만 할 필요성이 있다. 또한 암을 극복할 수 있는 다양한 방법이 제시되고 있으나 암 사망률은 28.1%로서 3명의 사망자 중에 1명이 암으로 사망하고 있으며, 그 중에서 위암, 폐암, 대장암 및 간암이 50% 이상 차지하고 있어서 매우 심각하다.

이상의 내용을 종합해 볼 때, 농업바이오분야 R&D 사업을 원활히 수행할 민간 CRO 기관의 인프라가 부족하므로 허가 당국 및 정부기관의 긴밀하며 적극적인 협조를 통해 부족한 CRO 기관의 육성이 무엇보다 절실히 필요하다고 판단된다. 더불어 본 기술개발사업에서 10대 질환을 중심으로 고유질환동물모델을 개발하고, 우수한 천연물 후보물질을 발굴하여, 이를 대상으로한 비임상시험을 수행함으로서, 안전성 및 유효성을 입증함과 동시에 전문적인 연구개발지식과 농업바이오 분야에서의 R&D 사업의 수익을 지속적으로 창출할 수 있는 모델을 제시하고자한다.

나. 연구 목표 및 범위

세부연구목표: 효능성분의 다량 분리 및 패혈증과 고혈압 작용기전 규명

제 2 장 국내외 기술개발 현황

1절. 제 1세부. 농업바이오 분야의 CRO 비임상시험 연구

CRO는 신물질을 개발하는 기업의 최고 파트너로서, 기업의 비용 절감, 전문적 노하우에 바탕을 둔 가격경쟁력 및 효율적인 비임상·임상 진행을 통한 개발기간의 단축을 위하여 제약, 화학, 화장품, 식품회사 등의 CRO 이용은 폭발적으로 증가하였으며 2010년도 세계 시장 규모는 240억 달러에 이르고 있다. 한 예로서 미국 화이자 "비아그라"의 개발비 50% 이상을 CRO 사업자에게 아웃소싱하여 신약개발기간을 7년에서 4년으로 단축한 예가 있다.

1. CRO 시장현황

세계 CRO 시장은 신흥국가의 성장과 함께, 2009년 금융위기에서 점차 회복세에 들어서고 있다. CRO 세계 시장은 2010년 214.2억 달러로 추정되며, CAGR('10~'17) 10.5%로 향후 고성장 전망되며, 2000년대 후반 금융위기를 극복하고, 미래 고성장을 이어가려는 움직임이 보이며, 신흥시장에 대한 공략이 활발히 이루어지고 있다. 의약 및 생명공학 기업의 거대 수요가 예상되며, 이에 따라 CRO 시장은 미래 고 성장이 예견된다. 또한 전체 CRO 시장에서 미국이 차지하는 비중은 2010년 53.4%이며 향후 미국 외 시장의 점진적 변화가 예상되며, 인도, 중국, 동유럽 국가의 저비용 CRO 시장은 신흥국가의 CRO 시장 점유를 증가시키는 중요요인이 되지만, 신흥시장마다의 각기 다른 임상관련 관련 법규가 성장을 저해할 가능성이 있다.

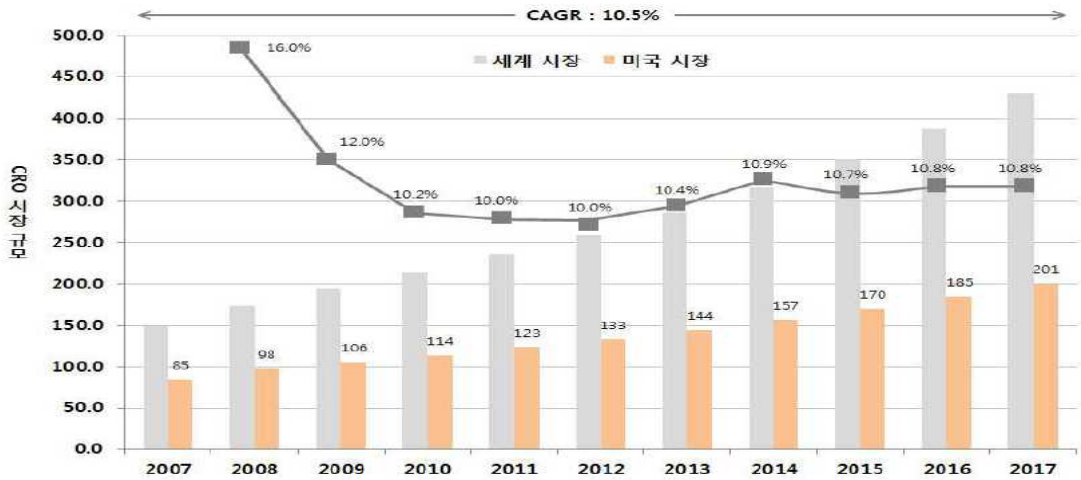

<글로벌 CRO 시장 규모(단위 : 억 달러, %)>

해외 CRO 산업은 미국, 유럽 등 선진국에서 1970년대 niche service 모델을 시작으로 도입기를 거쳐 1980년대부터 서비스 영역확대와 더불어 1990년대에 full service model을 바탕으로 본격적인 성장기를 이룬 바 있다. 2002년부터 연평균 14%의 성장을 유지하는 성숙기 상황이었으나 2009년 이후부터 선진국(미국, 유럽)의 CRO outsourcing 시장이 아시아(인도, 중국 등)로 이동함에 따라 선진국 해외 CRO시장은

위축기에 접어들 것으로 예상되는 반면, 아시아의 임상 CRO outsourcing 시장은 지속적으로 성장할 것으로 예측된다. GlobalData의 시장예측자료에 의하면 향후 5년간(2012년~2017년) CAGR 8.5%의 CRO 시장을 예상하고 있다.

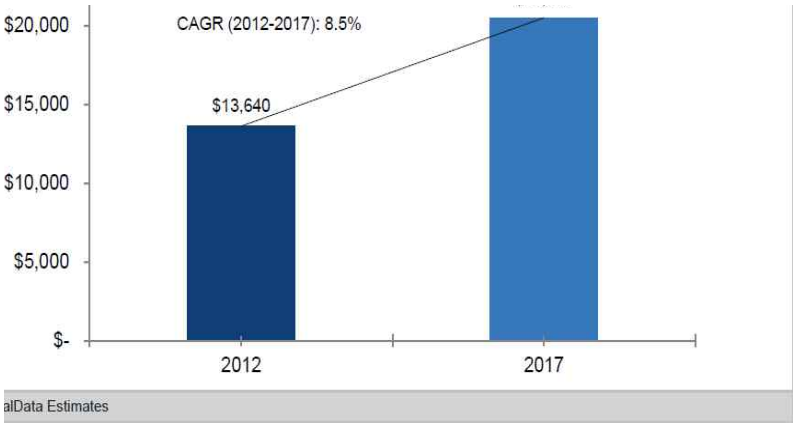

< CRO 시장 전망, Global Market Forecasts, '12~'17(USD Bil.)>

세계 R&D 투자의 증가는 CRO들의 성장을 동반하며, 가격경쟁력을 갖춘 신흥시장의 성장이 예상되는데, CRO 시장의 성장은 R&D 투자의 증가를 넘어서고 있으며, 이는 기업의 R&D에 CRO의 비중이 높아지고 있음을 의미한다. CRO의 성장에서 신흥시장의 성장은 단기적으로는 가격 경쟁으로 낮은 수익에 직면하고 있지만, 장기적 관점에서 규모의 증가로 인한 수익증대가 전망되고 있다.

기업의 R&D 투자는 수익에 근거하여 증가하며, 주요 블록버스터 의약품의 만료로 인한 대기업의 수익감소에도 불구하고 기업은 파이프라인 강화를 위한 R&D 투자를 지속적으로 증가할 전망이며, 지역적으로 북아메리카의 R&D 투자는 2010년 전 세계의 약 50%를 차지하고 있으며, 향후에도 세계 R&D 투자의 절반정도를 차지할 것으로 예상하지만, 가격경쟁력에서 우위에 있는 아시아・태평양 지역의 급격한 성장이 함께 예상된다.

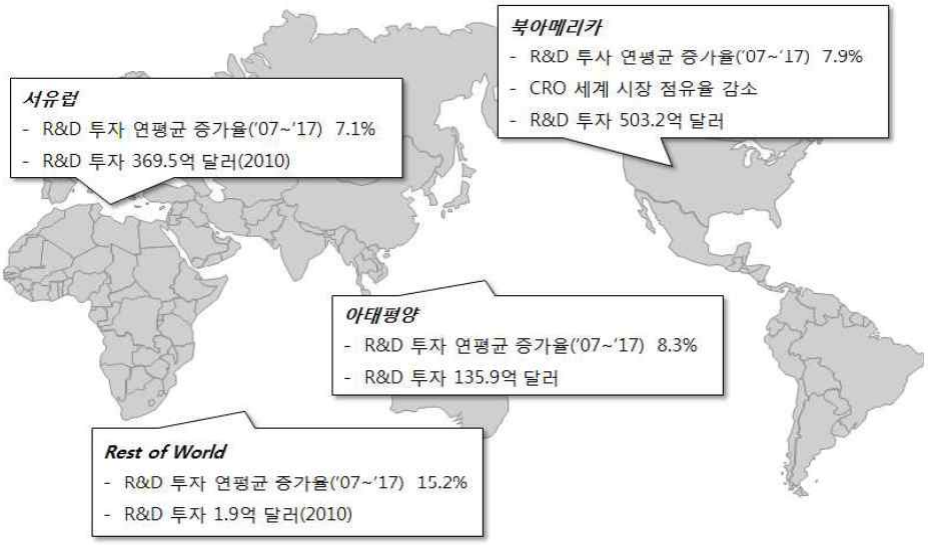

<세계 CRO 부문 R&D 투자 성장 전망>

임상시험의 증가는 CRO 시장의 성장을 예견하고 있으며, 북아메리카 지역에서 활발한 임상시험이 수행하고 있으며, 2011년 세계 임상시험은 7만3천여건이 이루어졌으며, 2017년 9만건을 넘어설 것으로 전망되며, 이중 임상 1상(24%), 임상 2상(28%)의 진행 건수가 가장 많았으며, 파이프라인 Drug 역시 2007년 1,301건에서 2011년 1,380건으로 증가한다.

특히, 아시아 신흥시장 및 동아시아 지역의 성장이 세계 시장 평균 8%의 두배에 상당하는 15.8%의 성장률을 보이고 있으며, 기존 아시아 임상시험 중점 지역이 과거의 임상 2~3상 중심의 싱가포르에서 인적, 시장 규모등의 중심이 되는 한국, 대만 및 신흥 시장인 베트남 등으로 임상 시험을 수행하기 위한 중요한 대상이 되고 있다.

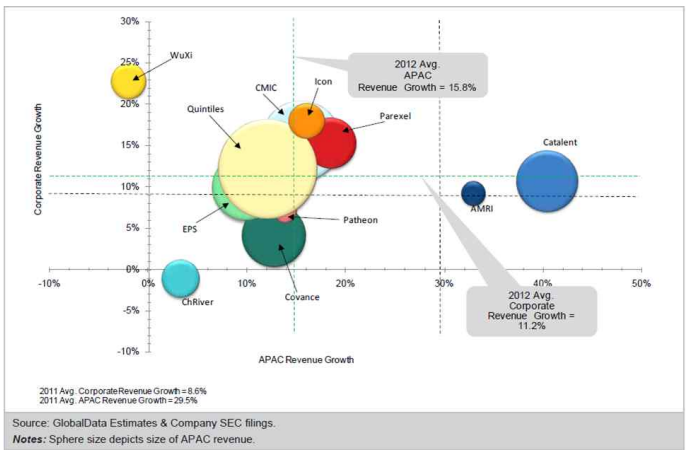

< 아시아 지역에서의 수익 및 기업간 협력, APCA Landscaoe Assessment, 1012>

세계 시장의 임상시험의 증가는 자연스럽게 CRO 수요의 증가를 의미하며, 시장 규모 성장을 유발하고 지역적 규모로 볼 때, 2011년 북아메리카지역에서 전세계 55.3%,유럽에서 25.3%의 임상시험이 진행되었으며, 이외 앞서 언급된 중국, 인도, 라틴아메리카 지역의 임상시험이 눈에 띄게 증가 한다.

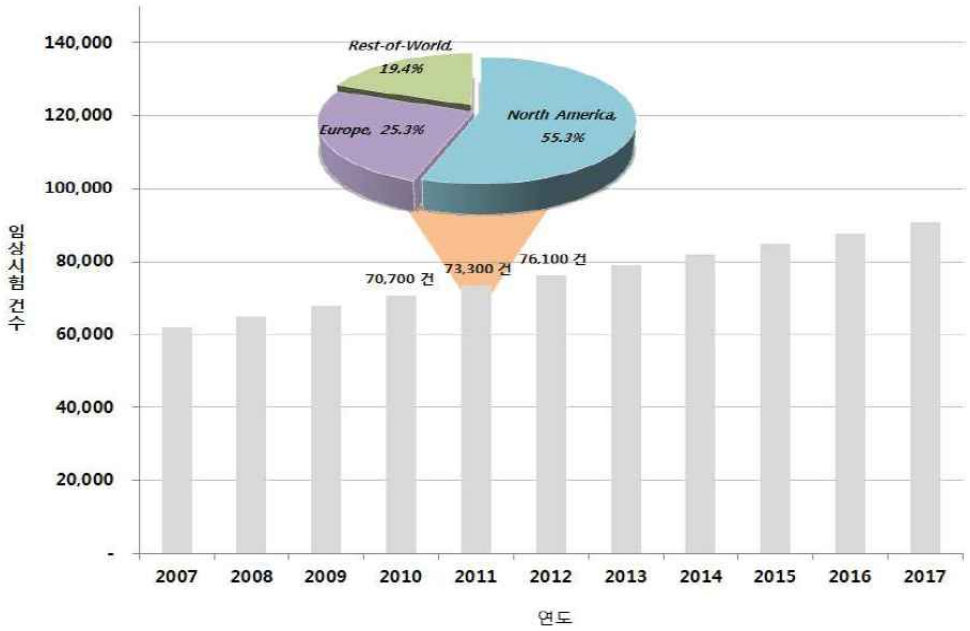

<세계 임상시험 건수 예측>

유럽의 CRO 시장은 2018년 607억 달러 규모에 이를 것으로 예상한다.(출처 : 프로스트 설리반) 유럽에서 임상연구기관(CRO) 시장은 프로스트 & 설리반의 분석에 따르면, 2011~2018년 기간동안 115.4억 달러에서 607억 달러 규모로 성장할 것이며 전략적 아웃소싱 파트너십과 전략적 장기 계약을 통해 제약 및 생명공학기업을 선도하기 위한 CRO 시장이 강화될 것이다.

중국 계약연구기관(CRO) 산업 보고서, 2012-2013(출처: Research In China)에 따르면, 글로벌 CRO 시장의 7~10% 정도가 중국에서 진행되고 있는데, 중국의 CRO 시장은 유럽과 미국의 산업에 비해 훨씬 후에 진행되었고, 현재 중소규모가 대부분으로 500여개의 CRO가 있다. 전체 글로벌 CRO의 10% 미만을 차지하지만 2011년 중국의 CRO 시장은 약 25억 위안(4,500억 원) 규모로 중국의 CRO 시장에 투자 시작하는 외국 기업에 대한 경쟁으로 낮은 비용, 인적 자원을 사용할 수 있어 퀸타일즈, Covance, PPD, CRL 및 ICON등 글로벌 유명 CRO 업체 모두 최근 중국에 투자하여 중국과 아시아시장에 활동하고 있다.

해외 임상의 경우, 초기 2010~2011년의 해외 임상 준비 시기 및 Market Promotion 시기로 매출이 일부 발생이 되기는 하나 미미할 것으로 예상되며, 초기 도입시기인 2012~2014년까지는 전 세계 대상이 아닌 일본의 CRO 시장을 타겟으로 점유율을 예상하였으나 추후 전 세계 CRO 시장으로 확대될 것으로 예상된다.

일본 PMDA 발표에 따르면 일본의 CRO 시장은 2012년 1조 7천억 원 규모로 확대될 것으로 예상되며 현재 일본의 asian study 비중이 5%를 차지하고 있는데, 이중 asian study가 가능한 국가는 한국, 대만, 홍콩, 일본순으로 일본의 asian study 5% 비중을 4개국이 분할해서 진행한다고 가정할 경우, 2012~2013년까지 한국 CRO의 outsourcing 점유율은 1.25%로 예측되고 있고, 2014년의 경우는 아시아 4개국 중 임상시험 성장률 등을 고려하여 우리나라의 점유율이 2%로 상승할 것으로 전망하고 있다. 또한, 해외 매출과 관련하여 일본 CRO 산업의 위탁수주를 받을 경우 2012년 기준 일본 CRO 시장규모 예상액 1조 7천억 원을 기준으로 일본 임상 CRO 점유율에 따라서 예상 매출액을 산정하였을 때 2012~2014년까지 일본으로부터 총 688억 원 규모의 수주가 예상된다.

2. 비임상 CRO 국내외 시장현황

국내 비임상 CRO의 전체 시장규모는 1,000 억원을 상회하는 것으로 추정되며 이중 국내시장은 500 억원, 해외 CRO 부분은 600 억원 이상으로 최근 정부차원의 국내 바이오산업의 연구개발비에 대한 전폭적 지원 및 CRO사업에 지급하는 위탁관리지원비가 증가되고 있으며, 한·미, 한·EU FTA의 본격 실시 및 EU REACH 등 전 세계 제약 및 화학물질 관리 규정의 강화로 국내외 시험·분석 서비스 시장은 지속적인 성장(연간 6~8% 성장) 전망한다.

(단위 : 백만원)

년도	2013 년	2014년	2016년
세계 시장 규모*	609,000	677,100	825,000
한국 시장 규모**	139,671	165,790	233,592

<국내외 비임상 시험 시장 규모>

* 세계시장규모의 경우, GBI Research(2011.3)와 Frost&Sullivan(2011.6) 비임상시험분야 시장전망보고서를 절충한 수치임

**국내 비임상시장의 경우, '11년 시장규모(99,130백만원)를 기준으로 최근 5년간의 연평균성장률(CAGR) 18.7%을 적용하여 추정한 수치임(국내의약품개발 R&D 투자비용중 10.2%가 비임상시험에 소요된다고 가정하여 국내시장규모 추정 Frost & Sullivan, 2012).

또한 일부 신약개발 제약회사들의 미국 FDA 시판허가를 위해 전략적으로 외국 CRO업체를 통한 시험을 제외하고는 국내 대다수 바이오벤처회사는 국내 CRO 업체를 이용하고 있어 시장의 규모는 더욱 성장하고 있다.

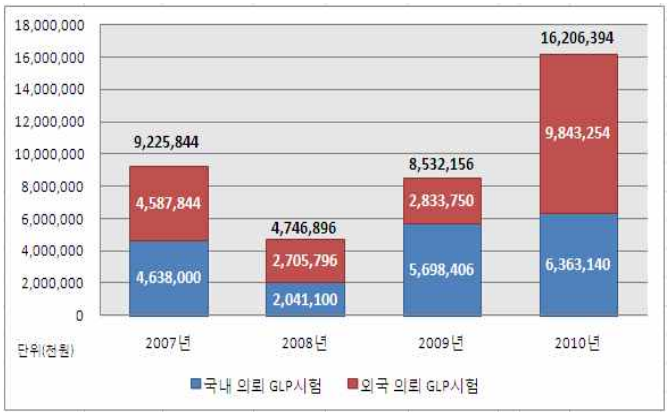

< GLP시험 의뢰를 위해 국내 제약업체(30개 기관)가 국내·외 시험기관에 투자한 금액>

전 세계 비임상시험 시장 및 제약산업과의 동반성장관련 전 세계 500대 기업의 신약개발 R&D 예산 123조 원('09)의 7% 수준인 8.6조 원을 비임상시험에 투자하고 있는 것으로 추정된다.

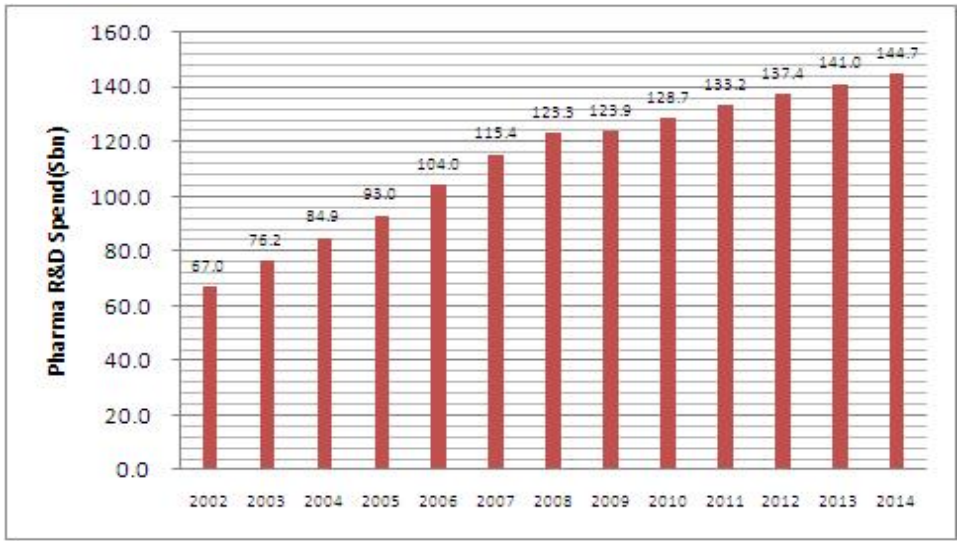

< 전 세계 500대 기업의 R&D 지출현황>

(단위 : 백만달러, %)

개발단계 조사항목	선도 물질	후보 물질	비임상	IND	임상1	임상2	임상3	NDA	총계
단계별 소요비용 (투자비율)	73 (8)	146 (17)	62 (7)		128 (15)	185 (21)	235 (27)	44 (5)	873 (100)

<신약개발 전체 투자비용 중 비임상시험 단계 투자 비율>

국내 비임상 CRO관련 기업의 국제경쟁력 핵심기반을 확보하기 위해 글로벌 기준에 부합하는 비임상관 자료 관리시스템을 구축하고, CRO 프로젝트의 효율적인 관리를 통해서 프로젝트 수행의 생산성 및 효성을 극대화하고 글로벌 CRO 수준으로 성장한다.

선진국 및 중국 등 개발도상국에서는 바이오산업 및 신약개발 활성화를 위하여 자국의 CRO 산업보호 및 육성정책으로 신물질 도입에 대한 무역장벽 강화와 인·허가에 대한 규제를 강화하고, 자국에서 상품화할 신물질에 대해 자국 CRO 이용을 권장하고 있는 실정이다.

3. 농업 CRO 현황

농업생명자원은 미래를 지탱하는 무궁한 가치의 미래자원이자 발전가능성이 높은 거대 시장으로 국가연구 사업중 비임상시험에 진입하는 물질은 10%에 내외이며 특히 농업생명 과학 분야에서 비임상 CRO의 활용은 아직 극히 초기 단계이다.

국제 무역환경은 데이터가 없으면 시장도 없기에 우수한 농생명소재가 개발되더라도 이에 대한 안전성 데이터가 확보되지 못한다면 이들의 제품화는 물론 글로벌 상품화, 수출입이 불가능하므로 이를 위한 전문 농업 CRO구축이 필요하다. 국내 비임상 CRO는 선진국에 뒤지지 않는 기술력, 빠른 대응력을 통한 개발기간 단축, 높은 가격경쟁력 등의 장점이 있으며, 고난위도의 의약품 시장에서 경험한 높은 기술력으로 농업 분야 안전성 평가 자료의 국제적 활용에는 전혀 문제가 없다.

연구과제의 최종목표는 농업 바이오 전문가인프라 구축과 전문 비임상 CRO 및 임상 CRO를 연계시키고, 농업 바이오 산업 분야의 특성화된 전문 컨설팅 서비스를 제공하는 농업 바이오 CRO 법인의 기초를 마련하는데 있다.

이러한 CRO 법인 설립을 위해 산학연계 프로그램을 통해 우수 인력을 확보하고, 내부 인원에 대한 전문성을 강화하기 위해 정기적인 교육 및 훈련을 실시하며, 국내외 전문가 초빙 세미나 및 전문 교육 프로그램 지원을 통해 농업 바이오 분야의 전문 CRO로서의 입지를 구축한다. 이후에 주관기업 내에 농업 바이오 R&D 컨설팅 전담부서를 구성하여 본 과제로부터 도출된 우수한 결과를 보인 국산 농산물 후보물질에 대한 IND 신청자료를 파일링하고, R&D 컨설팅 네트워크 구축을 지원한다.

농업전문 국가기관과 농업전문 CRO 간의 MOU를 체결하여 국가기관에서 주관하는 주요 사업의 신약후보물질이 발굴되면 농업전문 CRO에서 컨설팅을 한다. 농업전문 CRO는 농업바이오분야에 저명한 학계와 우수실험실을 갖춘 비임상 및 임상 시험 전문기관과의 인프라를 구축하고 유지한다. 이러한 시스템을 이용하여 농업바이오분야의 우수한 신약후보물질의 효력 및 안전성 검증에서부터 상품화까지 컨설팅 역할을 수행함으로써 차별화된 농업전문 CRO 역할을 수행할 수 있을 것으로 판단한다.

2절. 제 1협동. 질환 동물 모델 개발 및 효력시험 연구

1. 신약 개발 연구 대상 질환

가. 국내 학계의 신약 개발 연구 대상 질환

한국응용약물학회 회원 및 대한약학회 대의원 389명을 대상으로 설문조사를 실시함. (설문조사 기관 : 이즈마인드사, 설문조사 기간 : 2008. 9. 1-9, 17)

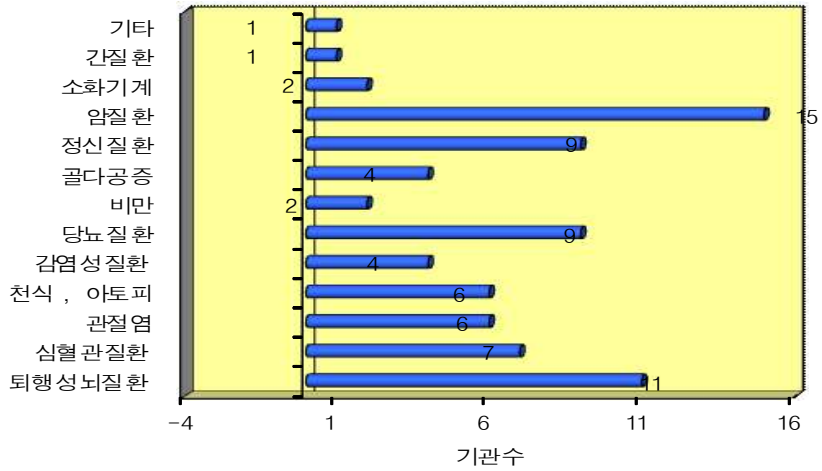

<국내 학계의 신약개발연구 대상 질환>

(1) 질환별 분석한 결과 암질환이 가장 많은 15개 기관으로 조사되었으며, 퇴행성뇌질환 11개 기관, 당뇨질환 9개 기관, 정신질환 9개 기관, 심혈관질환 7개 기관, 관절염 6개 기관, 천식/아토피 6개 기관 순으로 나타난다.

(2) 향후의 개발양상은 암질환, 퇴행성뇌질환, 당뇨질환이 계속 강한 것으로 조사되었으며, 심혈관질환의 수요가 일부 증가할 것으로 분석된다.

나. 국내 제약기업의 신약개발연구 대상 질환

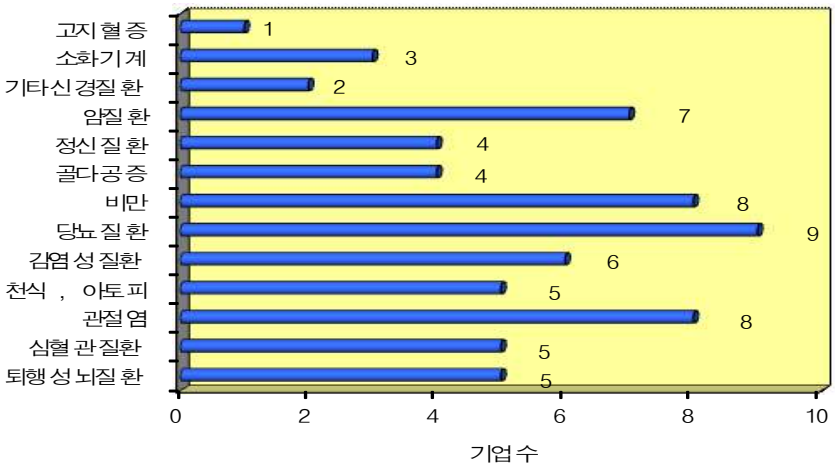

<국내 제약기업의 신약개발연구 대상 질환>

(1) 질환별 분석한 결과 당뇨질환이 가장 많은 9개 기관으로 조사되었으며, 관절염 8개 기관, 비만 8개 기관, 암질환 7개 기관, 감염성질환 6개 기관, 천식/아토피 5개 기관, 심혈관질환 5개 기관, 퇴행성뇌질환 5개 기관 순으로 나타나다.

(2) 향후의 개발양상은 당뇨질환, 관절염, 비만, 암질환 치료제가 퇴행성뇌질환, 계속 강한 것으로 조사되었으며, 비만의 수요가 일부 증가한 것이 특이사항으로 분석된다.

다. 향후 3년간 신약개발연구 대상 질환

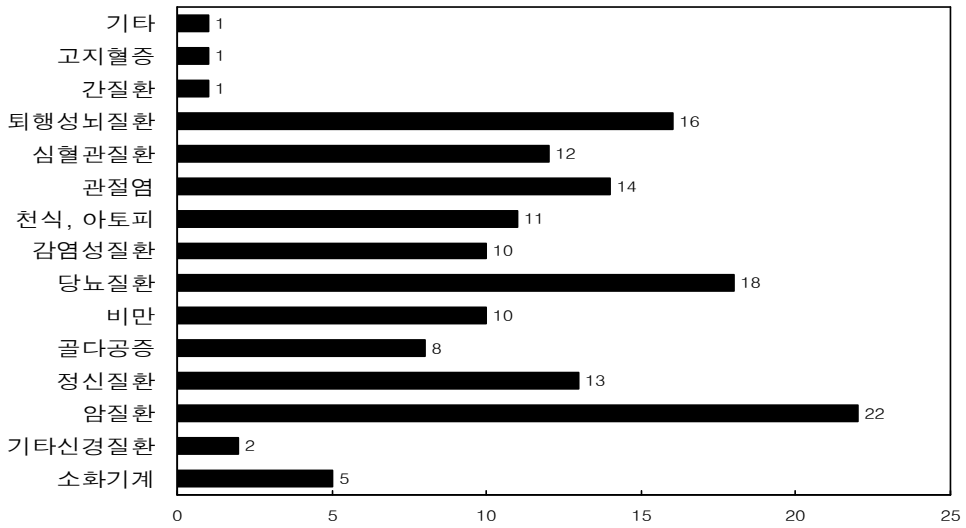

<향후 3년간 신약개발연구 대상 질환>

(1) 암질환과 당뇨질환의 경우는 각각 22건과 18건으로 최근의 개발경향이 그대로 이어져 가장 높은 비중을 차지하고 있음. 최근 현황에서 4위를 차지한 퇴행성뇌질환이 16건으로 3위를 차지하여 비중이 강화될 것으로 예측되고 있으며 관절염의 경우도 14건으로 나타나 상당한 비중을 차지할 것으로 관찰되고 있음. 이어서 정신질환 13건, 심혈관질환 12건, 천식/아토피 11건 등으로 나타나 감염성질환의 수요가 적어질 것으로 판단되고 있다.

(2) 국내의 기업과 학계의 약리/약효 수요를 간당하기 위해서는 암질환, 당뇨질환 등 수요가 많은 부분의 국내역량을 세밀히 분석하여 기반구축과 역량강화가 필요할 것으로 분석되고 있다.

2. 질환 모델 마우스 기술 개발 현황

가. 질환 모델 마우스 사용 현황

(1) 현재 국내에는 한국화학연구소 안전성센터, 바이오톡스텍 등 국제실험동물관리인증협회(AAALA)의 인증을 받았다.

(2) 국내 질환모델마우스 수요는 바이오산업 증가와 함께 증가하고 있으며, 연간 수 요는 500만 마리 이상으로 추정되고 있다. 그 중 80~90% 정도가 마우스 등 쥐 종류이고, 쥐 종류와

기니피그, 토끼 등을 합치면 99% 이상을 차지하고 있다.

(3) 최근 개선되고 있기는 하나 국내에서는 공급, 가격 때문에 일반 동물이 바이오실험에 상당량 사용되고 있는 것으로 파악되고 있다. 그러나 일반 동물은 사육환경에서 오는 동물품질의 한계로 인하여 실험결과의 신뢰도에 문제가 생길 수 있으며, 더나가 생산물의 품질에도 영향을 미칠 수 있는 중요한 문제이다.

(4) 국내에서는 한국생명공학연구원이 1992년 국제실험동물과학협의회 (ICLAS; International Council Laboratory Animal Science)에 실험동물품종유지기관으로 등록한 이래 각종 실험동물을 계통유지, 보존하고 연구기관에 분양하고 있으며, ICLAS monitoring subcenter로 국제적인 실험동물 품질 검정기관으로 활동하고 있다.

나. 질환 모델 마우스 제작 현황

(1) 국내에는 현재 10여개 정도의 연구실만이모델마우스 제작 경험이 있으며, 이 중. 2마리 이상의 연간 KO 제작 능력을 확보하고 있는 연구실은 7곳에 불과하다.

(2) 국내 연구자에 의해서 개발된 질환모델마우스는 연구자의 전공분야에 따라 암, 노화, 뇌과학, 심혈관질환, 대사질환 등의 분야에 분포하고 있다.

총 생산 실적	유전자 과발현(TG) 질환모델마우스	130 종(누적)
	유전자 적중(KO) 질환모델마우스	20 종(누적)

<국내 주요 질환모델마우스 퍼실리티의 생산 능력(2008년)>

3. 국내외 질환별 연구현황

가. 암질환

(1) 암 치료는 외과수술, 방사선요법, 화학요법, 생물요법의 단독 혹은 병용치료에 응용되고 있으나 완벽한 치료법은 없는 상태임. 따라서, 거의 모든 다국적 제약회사들이 이 분야에 집중적인 연구를 진행하고 있음.

(2) 임상실험 전 적절한 동물모델을 이용한 생체 실험은 시간과 비용을 절감할 수 있게 해주고 직접적인 인체 투여에 있어서 발생할 수 있는 부작용 등의 위험 요소들을 미리 예측, 관찰할 수 있는 기회를 제공한다. 국내에서도 최근 새로운 항암제 개발이 활발히 이루어지고 있으며 효과적인 항암 효능평가 동물 모델의 확보 및 활용은 개발에 투입되는 비용의 감소와 개발 기간을 앞당길 수 있을 것이다.

(3) 미국의 국립암연구소(NCI) 를 비롯한 많은 제약회사에서는 화학물질에 의해 유도된 종양마우스 모델, 종양이식 모델 등을 이용하여 항암제 효능 평가를 해왔으나 최근에는 유전자 변형 마우스들 도 사용되고 있으며, 유전자 변형 마우스는 암이 빠르게 발생하며 생체 내 다양한 부분에서 동시 다발적으로 암이 발생하는 특성이 있으며, 특정 조직이나 특정 발생 단계에 있어서 원하는 유전자를 발현시키거나 억제할 수 있어 종양이 보다 인체 조건과 비슷한 환경에서 발생할 수 있도록 한다.

(4) 표적항암제가 성공률이 높고 신약으로 개발될 수 있었던 배경에는 표적으로 하는 유전자

가 선택적으로 활성화되어 있는 동물들을 제작할 수 있었던 기술적 기반이나 확보할 수 있는 네트워크가 형성되어 있었고 이러한 시스템을 활용할 수 있는 인력이 확보되어 있었기 때문이다.

(5) 누드 마우스를 사용하여 사람의 암 세포주 또는 종양조직을 이식하는 마우스 모델과 마우스로부터 유래한 암세포주 또는 암 조직을 이식하는 syngeneic 마우스 모델 등의 xenograft 모델은 다양한 종류의 암 모델을 확립할 수 있고 단기간에 다양한 항암의 효능평가를 할 수 있어 미국 국립암염구소에서도 항암제 효능 확인에 널리 사용되고 있으며 국내에서도 많은 기관에 기반 기술이 확립되어 있다.

(6) 전이, 즉 종양이 원래의 위치를 이탈하여 혈류를 통해 다른 장기를 침범하는 현상이 암으로 인한 사망원인의 90% 이상을 차지하는 현실에 맞춰 혈관 신생 및 전이 억제를 위한 암 모델이 각광받고 있다.

(7) 유전자 변형 마우스, 화학물질의 투여에 의한 암 모델 마우스와 사람의 종양조직을 이식한 누드 마우스 등으로 암의 발생원인 규명 및 새로운 치료제의 약효를 시험할 수 있었고, xenograft 모델의 경우 비교적 쉽게 많은 종류의 항암제 효능을 시험할 수 있지만 종양의 발생하는 환경에서 암과 미세 환경과의 상호작용이 없는 단점이 있다. 또한, 국내에서는 많은 연구진에 의해 암과 관련된 유전자에 대한 형질전환 마우스들이 제작되었으나 항암제 효능 확인을 위한 국가적인 체계적 관리와 확보가 집중화되어 있지 않는다.

(8) 최근 과학기술의 발달로 대량의 후보물질 도출과 in vitro 스크리닝이 가능해져 다양한 후보신약을 시험할 수 있는 폭넓은 in vivo 항암시험계가 요구되며, 암환자에서 사망의 주원인이 되는 전이와 혈관신생을 악성 암의 특징으로서 최근 이를 억제할 수 있는 많은 신약후보물질이 개발되고 있어 국내에서도 전이 및 혈관신생 억제제의 효능 확인이 가능한 다양한 암 모델의 확보가 필요하다.

(9) 전 세계적으로 RNA chip, 프로테오믹스와 같은 과학기술의 발달로 대량의 표적유전자들이 빠르게 발굴되고 이에 대한 Molecular Targeted Therapy (MTT)를 위한 치료제들이 개발됨에 따라 이들의 효과를 임상시험에서 예측할 수 있는 다양한 동물모델이 필요하다. 또한 국내에서도 최근 새로운 항암제 개발이 활발히 이루어지고 있으며 효과적인 항암 효능평가 동물모델의 확보 및 활용은 개발에 투입되는 비용의 감소와 개발 기간을 앞당길 수 있을 것이다.

나. 치매

(1) 중추신경계 질환의 세계시장규모는 772억 달러로 전세계 치료제 시장의 17% 이르며, 전년도 대비 13%로 빠르게 성장하고 있음.뇌신경 치료제의 세부질환별 시장 규모는 통증, 우울증, 정신분열증, 진정제, 편두통 치료제, 다발성 경화증, 파킨슨병, 비만, 알츠하이머병 순서로 형성되었고, 최근 국가차원에서 천연물센터 등을 통해 다량의 후보물질이 도출되고 있으며, 이를 통한 퇴행성 뇌질환의 효능 실험을 위한 실험체계가 요구되고 있다.

(2) 뇌질환에 대한 효능 연구를 위해서 많은 동물 모델이 사용되고 있으며, 각 질환별 동물 모델이 많이 알려져 있으며, 대부분 임상실험에서 실패하는 경우는 동물실험에서 약효의 검증을 단기간에만 진행하거나 행동학적 변화 양상의 확인, 중추신경에서 유발되는 신경세포 재생과의 상관관계 확인을 유도하지 않은 경우가 대부분이다.

(3) 퇴행성 뇌질환을 효과적으로 개선시키거나 진행을 억제시킬 수 있는 신약개발을 위해서는

질환모델동물을 이용한 행동학적 변화 양상, 형태적 변화 양상, 내인성 신경세포재생 등에 대한 체계적 검증 시스템의 확립이 무엇보다 필요하다.

다. 심혈관질환

심혈관 질환 특히 동맥경화증의 경우 질환의 발병에 따른 주요 관련 유전자를 기반으로 한 모델동물이 많이 개발되어 있다.

라. 당뇨

(1) 평균수명 증가와 생활수준이 향상으로 열량의 과잉섭취와 운동부족, 스트레스 등에 의해 당뇨병, 고혈압, 고지혈증, 비만, 중풍, 심혈관질환, 지방간 및 전신 동맥경화증의 발생이 폭발적으로 증가하는 추세이며, 이러한 비만 및 제2형 당뇨를 포함하는 만성 대사 질환 군을 통틀어 대사성증후군 이란 말로 표현하고 있음. 대사증후군 발생 원인의 중심에는 비만과 인슐린 저항성(제2형 당뇨병)이 있다. 현재 미국에서는 만성성인병 치료에 드는 비용이 HMO (Health Maintenance Organization) 전체 비용의 30%를 차지한다.

(2) 비만과 당뇨는 multigenetic disease로 인정되고 있는 만큼 발병 원인이 다양하기 때문에 병인을 이해하기 위해서 단독 연구를 통해 병인이나 치료법 개발을 할 수 없으며 다양한 병인의 분자적 해석에 기반을 둔 약제들이 개발되고 있으며 이러한 질환 치료제의 개발에 질환모델동물의 개발이 필수적인 핵심요소이다. 또한 모델동물에서 일어나는 변화를 정확하게 분석하여 in vitro 연구에서 한계에 다다른 분자기전을 in vivo에서 밝혀 향후 대사성 질환의 병인 규명 및 치료제 개발 등에 활용할 수 있다.

(3) 국내는 물론 전 세계적으로 폭발적으로 증가하고 있는 대사성질환은 경제적 및 사회적인 막대한 손실을 초래하고 있을 뿐만 아니라 국가적으로 해결되어야할 시급한 과제임. 운동부족과 과도한 영양분 섭취로 인하여 체내에는 영양분이 축적되어 복부비만이 발생하고 지방세포에서는 기능 이상이 초래되면서 고지혈증, 고혈압 및 당뇨병 등과 같은 증상이 나타나게 된다. 제1형 당뇨병 모델동물, 제2형 당뇨병 모델동물, 당뇨병/비만 모델동물, 유전자 변형 당뇨병/비만 모델동물 등 다양한 병태 양상의 비만, 당뇨 질환 모델동물이 확립되어 이용되고 있으나 비만, 당뇨병 모델동물이라고 하더라고 췌장의 병태와 인슐린 저항서이 모델동물에 따라서 다양한 양상을 보이고 있다.

(4) 당뇨병의 주요 질환 양태는 혈관 합병증을 동반하는 다양한 당뇨병성 신증, 망막증, 신경증과 같은 합병증이 주요 원인이나 이러한 합병증 치료제 개발의 적절한 모델동물의 확보가 이루어 지지 않고 있다.당뇨병과 비만의 치료 지표가 고혈당, 비만 의외에도 다양한 생리적 생화학적 지표가 있는데 모델동물을 활용하여 신약의 효능을 검색하고 작용기전을 유추해 볼 수 있는 다양한 형태의 지표를 확보하여 연구할 수 있는 기술 축적이 부족하다.

(5) 현재 국내에 도입되어 활용 중인 비만, 당뇨 모델동물은 주로 Leptin mutation 및 Leptin receptor mutation에 기인한 ob, db 마우스가 주로 사용되고 있으나 이러한 모델동물의 비만과 당뇨 병인은 사람에서 주로 발병되는 비만, 당뇨, 병인과 차이가 많아서 사람 질환 유전자를 대상으로 하는 신약개발의 효능 스크리닝에 적당하지 않은 경우가 있다.

마 . 면역계 질환

(1) 류마티스 관절염은 병인 또는 발병 기전에 대하여 잘 알려져 있지 않을 뿐만 아니라 치료가 어려운 난치병이어서 심각한 사회적 경제적 문제를 일으키는 요인으로, 류마티스 관절염 및 골관절염 등의 질병의 악화를 지연시키고 증상을 완화시키는 다양한 약물이 사용되고 있지만 이에 대한 치료제는 극히 제한적이다. 또한 새로운 치료제 개발을 위해서는 동물을 대상으로 관절염을 재현해야 하지만 결론적으로 사람과 동일한 병변을 재현하는 모델은 현재까지 없다.

(2) 동물모델로는 1977년 Andrew Kan 박사 등에 의해 처음으로 확립된 콜라겐 유도 관절염 모델이 가장 널리 사용되는 자가면역성 관절염 모델로, 관절염 모델로는 크게 Adjuvant arthritis, Collagen induced arthritis, Zymosan induced arthritis, Immune complex arthritis, Streptococcal cell wall arthritis 모델 등 항원 또는 항체를 주사하는 모델들이 있고 최근 개발된 형질전환 마우스 hTNF, K/BxN TCR 마우스 등이 사용되기도 한다. 또한 다양한 평가시험계가 확충되어 있지 않아 각 시험계의 비교를 통한 장단점 파악이 되지 않는다.

(3) 국내의 경우 국외에서 사용되는 다양한 모델이 확보되어 있지 않음. 새롭게 발굴되고 있는 분자 타겟을 이용한 유전자 변형 마우스 모델 확충이 필요하다.

4. 연구개발결과의 기대성과

국내 질환모델동물의 개발단계 수준을 넘어서 의약품 평가에 효율성이 높은 질환모델동물자원을 발굴함으로서 국내 질환모델동물자원의 활용성을 높이고 국내 신약개발 및 독성연구에 지원 가능할 것으로 기대된다. 또한 의약품 평가에 활용이 높을 것으로 예상되는 질환모델동물에 대해 개발자와 협의하여 농립수산식품부에서 수탁 관리하고 지속적인 계통관리와 품질관리를 통해 자원화 한다.

<별첨 1>

유전자변형마우스(GEM) 이용 연구에 대한 설문조사

2004년 12월 9일
한국분자세포생물학회 마우스유전체분과

1. 우리나라의 생명-의과학 연구에 GEM을 이용한 연구가 필요하다고 생각하십니까?

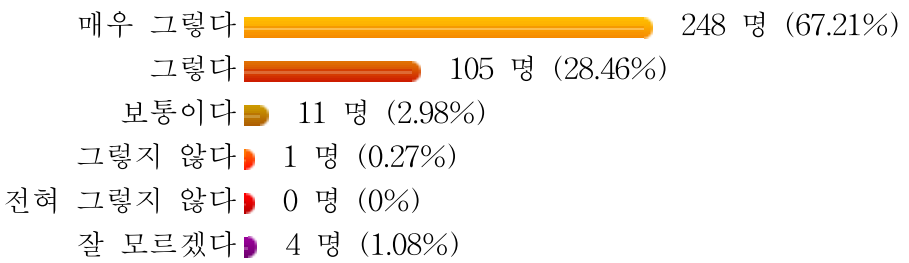

2. 현재 우리나라에서 GEM을 이용한 연구가 용이하다고 생각하십니까?

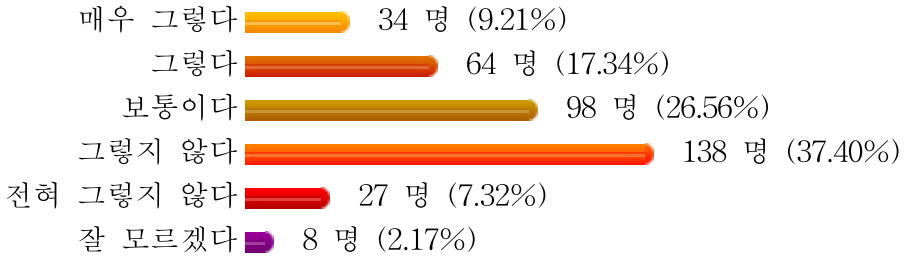

3. 현재 국가 및 기관단체의 GEM 인프라 구축에 대한 지원이 적절하다고 생각하십니까?

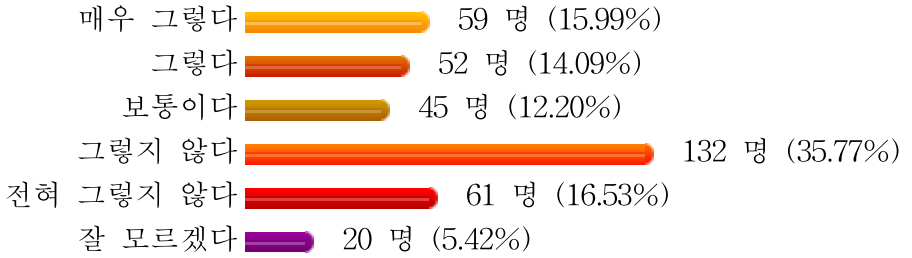

※ 2009년 국가질환모델동물자원 관리시스템 구축관련 모델동물 설문조사로 10개 문항에 대해 서울대학교, 안전성평가연구소, 국립독성과학원 등 27개 기관을 대상으로 실시

3절. 제 2협동. 천연물 신약후보물질의 개발 및 효력시험 연구

세계적인 천연물의약산업의 활성화, 생명자원에 대한 보호주의 확산 및 지적 재산권 협약 등으로 외국 자원 또는 기술의 도입은 점차 어려워지고 있으며, 이러한 기술을 도입할 경우에는 막대한 royalty를 지불해야 한다.

우리나라에는 옛날부터 한의학이 발달되었으나, 한약재로부터 생리활성을 탐색한 후 식의약품, 보건식품 또는 식품첨가제의 개발에 관한 연구는 유럽연합이나 미국 등의 선진국에 비해 오히려 뒤지고 있다. 또한 많은 연구기관에서 투자를 하여 좋은 결과를 얻었으나 대부분 연구비의 지원이 단회성으로 연구가 종결되므로 좋은 연구결과를 얻더라도 연구의 결과를 활용할 수 있는 후속 연구가 미비한 상황이다. 최근 들어 생약제를 이용한 식품보조제나 건강식품의 개발에 의한 생물산업이 활성화되고 있는데, 이에 부응하기 위하여 식물로부터 얻은 천연물 신약 후보물질의 산업화는 농가의 소득작물 개발에 필연적인 과제로 부각되고 있다.

한국사회 식생활의 서구화는 비만과 더불어 허혈성 질환의 발병률을 더욱 높이고 있으며, 의료기술의 발전으로 생명이 연장되어 고령화 사회로 접어들면서 허혈성 질환에 고통을 받는 인구가 더욱더 증가하고 있으며, 나아가 삶의 질을 평가하는 데에 있어서 건강하게 노후를 보내고자 하는 허혈성 질환의 극복은 현 사회문화의 흐름 속에 비추어 볼 때 결코 간과할 수 없는 질병이다.

1. 고혈압 연구

고혈압에 대한 효과적이면서도 실용적인 치료법 개발은 21세기 생명과학 및 생명공학 시대에 있어서 고부가가치 산업으로 등장할 것이 확실시 되고 있는 현 시점에서 약용작물을 기초로 한 고혈압을 예방 및 치료하기 위한 신물질의 발굴은 매우 중요하다.

가. 국내의 경우 학계와 산업계에서 고지혈증 관련 의약품 및 기능성 식품에 대한 연구가 광범위하게 이루어지는 상태는 아니지만 경북대학교 박용복 교수팀, LG화학 중앙연구소, 한국화약 중앙연구소, 제일제당 중앙연구소, 한국생명공학연구원 지질대사연구실에서 활발히 진행되고 있으나 천연물을 소재로 한 연구는 거의 전무하다.

나. 1998년에 이미 심혈관계질환 치료제의 시장은 460억불로 전체 의약품시장의 18%를 점유하였고, 세계 상위 100대 처방약 중에서 심장순환계 약물은 20여개에 이르렀으며, 현재는 세계 제약시장에서 심혈관계약물들이 최고의 매출액을 기록하고 있다. 특히 혈중콜레스테롤 강하제인 스타틴계열 약물의 2001년 세계 시장은 무려 191억 달러로서 주로 Merck사의 Zocor(simvastatin)와 Pfizer의 Lipitor (atorvastatin)가 주도했다. 심혈관계약물 시장은 크게 성장되었으나, 다른 질환들에 비하여 환자의 수가 많고, 기존 의약품에 대한 불만족도가 높으므로 새로운 약물에 대한 기대도가 크다. 예를 들면 스타틴계열의 약물을 장기간 복용 시 근골격계에 대한 부작용, 신경독성 등의 치명적인 부작용이 있다. 그러나 이러한 부작용의 위험보다 혈중콜레스테롤 농도를 낮추는 혜택에 상대적으로 큰 비중을 두어 스타틴계열의 약물사용은 증가하고 있다. 따라서 기존약물의 한계를 극복하는 새로운 심혈

관계 치료물질의 개발발은 그 경제적 효과가 클 것이다.

다. 본 연구진의 선행 연구결과에 의하면, gomisin A는 혈관내피세포에서 혈관이완성 물질을 생성/분비하여 혈관근을 이완시키는 작용을 나타내었을 뿐만 아니라, gomisin A는 직접적으로 혈관평활근을 이완시킴으로서 혈관근 이완을 유도하는 것을 확인하였다.
또한, gomisin A가 angiotensin II에 의하여 고혈압이 유도된 흰쥐에서 현저한 항고혈압 효과가 있음을 실험을 통해 확인하였다.

라. 최근, 본 연구진들은 gomisin J가 혈관 평활근을 이완시킬 수 있음을 증명하였을 뿐만 아니라, gomisin J의 혈관이완작용 강도는 gomisin A의 강도보다 3배 정도 더 강함을 알 수 있었다. 이를 통하여 gomisin J가 gomisin A보다 더 높은 약리학적 효능을 가지고 있으며 또한, 더 높은 부가가치를 창출할 것으로 사료된다.

마. 이에, 본 연구에서는 흰쥐 대동맥 및 사람의 혈관근을 이용하여 gomisin J의 혈관이완작용과 작용기전을 규명하고자 하고, 더 나아가 다양한 형태의 고혈압 실험동물 모델에서 gomisin J의 항고혈압 작용 및 작용 기전을 규명하고자 한다.

2. 패혈증 연구

만성염증은 암, 심혈관질환, 신경장애, 대사장애 합병증, 뼈 근육 및 골격질환, 당뇨합병증 및 만성질환 염증을 유발하기 때문에 모든 병의 근원인 염증의 예방 또는 치료방법이 절실히 요구되고 있다.

가. 패혈증은 생체에 침입한 박테리아 및 곰팡이 등의 병원균에 의해 염증성 사이토카인을 포함한 염증 매개 물질의 과도한 분비로 인해 전신적인 염증 반응이 유도되어 궁극적으로 조직 및 장기 손상, 백혈구 세포의 기능 상실이 유발되어 감염균에 대한 방어 능력이 마비되는 심각한 급성 감염성 염증 질환이다.

나. 패혈증은 다양한 종류의 염증면역세포, 즉 대식세포, 단핵구, 호중구 등의 과도한 활성으로 야기되는 것으로 전형적인 급성 염증 질환임. 이들 면역 세포들은 정상적으로는 외부의 감염균을 제거하는 생체 방어 역할을 담당하지만, 패혈증 환경에서는 과도하게 활성화되어 오히려 생체에 해로운 각종 염증성 사이토카인이나 염증성 매개체를 생성하여 그 증상을 빠른 시간 내에 악화시켜 조절 불능 상태로 빠지게 하여 생체 중요 기관 및 장기들의 이상을 초래하여 전신적인 쇼크 및 사망에 이르게 한다.

다. 패혈증의 역학적인 측면에서 보면 미국에서 연간 700,000명이 발병하는 것으로 알려져 있으며 발병률이 매년 1%이상 증가하고 있음. 한편, 패혈증 발병환자의 약 30-50%가 사망하며, severe sepsis의 경우 약 70% 이상이 사망하는 것으로 알려진다.

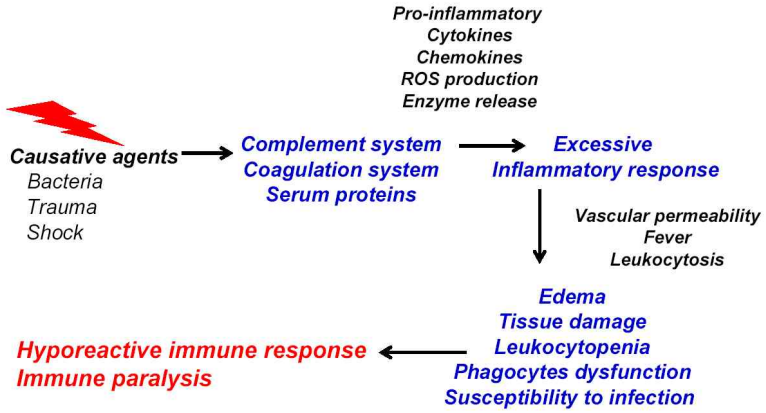

<Immune responses during sepsis>

라. 패혈증은 박테리아 또는 비브리오균의 감염으로 빈번히 그리고 집단적으로 발생할 가능성이 커서 지역 사회적으로 문제가 큰 것임. 패혈증을 유발하는 원인은 항상 우리 주위에 존재하며, 한번 발생하면 급격하게 빠른 속도로 진전되기 때문에 응급으로 처치되는 경우가 많음. 또한 각종 외상, 교통사고 및 암과 같은 각종 질환 치료과정에서 진단된 본래의 질병보다는 궁극적으로는 2차적으로 박테리아 감염으로 인한 패혈증에 의한 사망률을 감소시키기 위해서 본 연구는 매우 필수적이다.

마. 중환자에게서 빈번하게 발생하는 패혈증은 나날이 증가하며 사망률도 증가 추세에 있음. 국내외 패혈증 환자의 증가추세로 볼 때 막대한 경제적 손실을 막기 위해서는 패혈증 치료제 개발 연구가 필수적임. 성공적인 패혈증 치료제 개발 연구는 현재까지 1차적인 치료목적으로 사용되고 있는 막대한 양의 항생제 사용과 그럼에도 불구하고 줄지 않는 사망률을 줄이기 위해 응급치료로 사용되는 각종 보조 치료약과 인력동원에 따른 손실을 막을 수 있음. 아울러, 패혈증 치료제 개발은 선진국에 비해 처져 있는 우리의 의약업계의 생산성 향상과 기술력 증진에 크게 기여하여 경제적 및 산업적 가치를 향상시킬 수 있다.

바. 국제적으로 패혈증 치료제 개발에 필요한 연구가 매우 활발히 진행되고 있으며, 특히 염증 반응을 제어할 수 있는 면역 조절 물질들에 의한 패혈증 치료제 개발 분야가 각광을 받고 있음. 하지만, 아직까지 뚜렷한 면역 조절을 통한 패혈증 치료제의 개발은 이뤄지지 않고 있다.

사. 현재까지 패혈증 치료제 개발의 문제점은 효과적인 면역 조절제가 없고, 면역 세포 활성 조절제의 분리 정제가 어려우며, 염증 반응 조절제의 개발 및 생체내의 자연적인 방어 시스템을 이용한 패혈증 치료제의 개발을 요구하고 있으며, 현재 사용되고 있는 패혈증 치료제의 대부분이 항생제로서 패혈증의 치료효과를 향상시키는 데 이미 문제점을 드러내고 있으므로 신 개념의 면역 활성 물질들에 의한 패혈증 치료 효과 연구는 이 분야의 새로운 전기를 제공할 수 있을 것으로 기대된다.

아. 따라서 패혈증 치료효과에 대한 본 연구팀의 연구주제는 임상적인 응용이 절실히 요구되

고 있는 분야이므로 패혈증 병리적 관련성에 대한 연구와 신약개발을 위한 정보의 발굴이라는 매우 중요한 영역에 대한 연구라고 볼 수 있으며 꼭 수행되어야만 할 필요성이 있다. 또한 암을 극복할 수 있는 다양한 방법이 제시되고 있으나 암 사망률은 28.1%로서 3명의 사망자 중에 1명이 암으로 사망하고 있으며, 그 중에서 위암, 폐암, 대장암 및 간암이 50% 이상 차지하고 있어서 매우 심각하다.

제 3 장 연구개발수행 내용 및 결과

1절. 제 1세부. 농업바이오 분야의 CRO 비임상시험 연구

천연물 후보물질인 자초추출물, Gomisin J를 대상으로 비임상시험과 분석법 개발을 수행하였으며 EC-18(녹용성분), α-iso-cubebenol을 대상으로 비임상시험을 수행하였다.

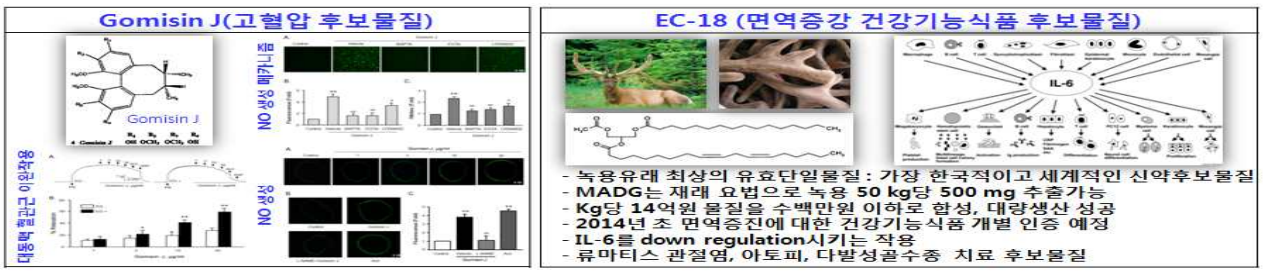

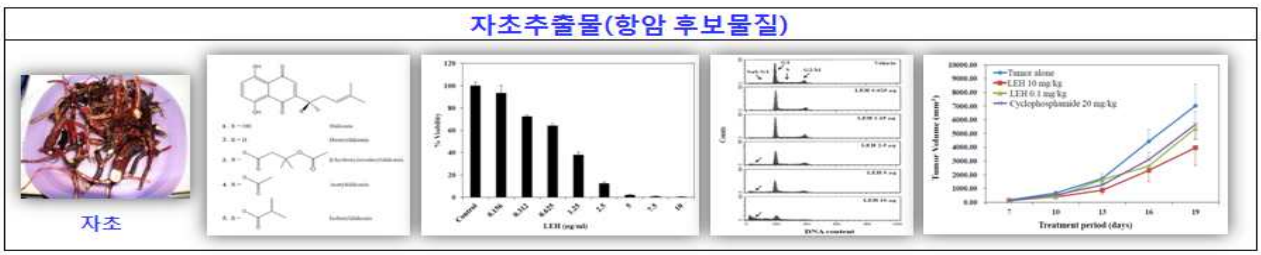

시험물질	항목	내용
1. 자초추출물	성상	검정색 (진한 붉은 색)의 점액
	성분	Shikonin; Deoxyshikonin; Acetylshikonin; β-hydroxyisovalerylshikonin; Isobutylshikonin 함유
2. Gomisin J	성상	점성이 있는 갈색 고체
	구조	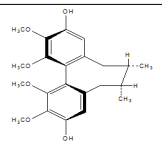
	분자식 및 분자량	$C_{22}H_{28}O_6$, 388.4541
3. EC-18	성상	무색의 액체
	성분	1-Palmitoyl-2-Linoleoyl-3-acetylglyceride
	구조	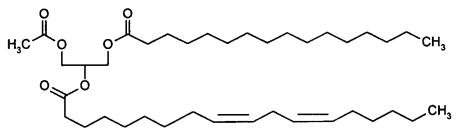
	분자식 및 분자량	$C_{39}H_{70}O_6$, 634.99
4. α-iso-cubebenol	성상	투명한 노란색 점액
	분자식 및 분자량	$C_{15}H_{24}O$, 220.18
	구조	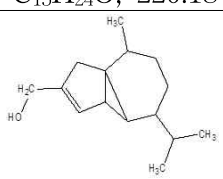

1. 비임상시험 요약(자초추출물, 알파아이소쿠베베놀, EC-18, Gomisin J)

구분	시험종류	시험명	수행기관	시험요약
자초추출물	단회	자초추출물의 랫드를 이용한 단회 경구투여 독성시험	바이오톡스텍	• 암수 랫드에서 개략적인 치사량이 2,000 mg/kg을 상회함.
		자초추출물의 비글견을 이용한 단회 경구투여 용량증가 독성시험	바이오톡스텍	• 암수 비글견에서 최대내성용량(MTD)이 2,000 mg/kg으로 판단됨.
	유전	자초추출물의 세균을 이용한 복귀돌연변이시험	바이오톡스텍	• 유전자돌연변이 유발성이 없음.
		자초추출물의 포유류 배양세포를 이용한 염색체이상시험	바이오톡스텍	• 염색체이상을 유발하는 것으로 판단됨.
		자초추출물의 마우스를 이용한 소핵시험	바이오톡스텍	• 마우스골수세포의 소핵유발에 영향을 미치지 않음.
	국소	자초추출물의 토끼를 이용한 피부자극시험	바이오톡스텍	• 홍반은 관찰되지 않았으나, 부종이 확인되어 토끼의 피부에 대한 자극성이 있는 것으로 판단됨.
		자초추출물의 토끼를 이용한 안점막자극시험	바이오톡스텍	• 토끼의 안점막에 대해서 '자극물'로 판단
	항원성	자초추출물의 기니픽을 이용한 항원성 평가	바이오톡스텍	• 동종 수동 피부 아나필락시스 반응시험 및 아나필락시스 쇼크 반응시험에서 음성의 결과가 나타나, 항원성이 없는 물질로 판단됨.
	반복	자초추출물의 랫드를 이용한 2주반복 경구투여 및 용량결정(DRF)시험	바이오톡스텍	• 수컷 300 mg/kg/day 투여군 및 암컷 1,000 mg/kg/day 투여군에서 사망동물이 관찰되었고, 암수 1,000 및 300 mg/kg/day 투여군의 일반증상, 체중, 사료섭취량, 부검소견 및 조직병리학적 검사에서 독성학적인 변화가 관찰됨. 따라서, 4주 반복투여 독성시험을 25, 100 및 400 mg/kg/day으로 제안함.
		자초추출물의 랫드를 이용한 4주 반복 경구투여 독성시험 및 2주 회복시험	바이오톡스텍	• 암수 25, 100 및 400 mg/kg/day 투여군에서 시험물질의 투여와 관련하여 독성학적으로 의미있는 변화가 관찰되지 않음. 따라서, 본 시험물질의 무독성량 (NOAEL)은을 암수 모두에서 400 mg/kg/day로 판단함.
		자초추출물의 랫드를 이용한 4주 반복 경구투여 독성동태시험	바이오톡스텍	• AUClast : 310.06-4595.75ng·hr/mL, Cmax : 35.40-400.00ng/mL, Tmax : 0.50-3.00hr, t1/2 : 5.48-43.29hr • 고용량군에서 AUClast와 투여28일의 고용량군에서 Cmax를 제외하고 수컷이 암컷보다 더 높은 경향을 나타냈지만, 그 차이가 작기 때문에 성차는 없다고 판단함.

구분	시험 종류	시험명	수행기관	시험요약
	반복	자초추출물의 비글견을 이용한 2주 반복 경구투여 용량결정시험	바이오톡스텍	•2주간의 DRF 시험 결과를 바탕으로 4주 반복투여 독성시험의 용량을 300, 100 및 30 mg/kg/day으로 선정함.
		자초추출물의 비글견을 이용한 4주 반복 경구투여 독성시험, 2주 회복시험 및 독성동태시험	바이오톡스텍	• 암•수 300 mg/kg/day 용량에서 구토, 설사 및 체중 증가 감소 등의 변화가 관찰되어 암•수 비글견에 대한 무독성량 (NOAEL)은 100 mg/kg/day으로 판단함.
	조제물 분석	자초추출물의 조제물 중 Acetylshikonin의 농도분석법 중 validation 및 안정성 확인시험	바이오톡스텍	• 부록 참조
	분석검증	LC/MS/MS를 이용한 랫드 혈장 중acetylshikonin의 분석법 Validation	SBB	• 부록 참조
		LC/MS/MS를 이용한 비글견 혈장 중acetylshikonin의 분석법 Validation	SBB	• 부록 참조
	농도 분석	자초추출물의 랫드를 이용한 4주 반복 경구투여 독성동태시험에서 채취된 랫드 혈장 중 아세틸시코닌의 농도 측정	SBB	• 부록 참조
		자초추출물의 비글견을 이용한 4주 반복 경구투여 독성시험, 2주회복시험 및 독성동태시험에서 채취된 비글견 혈장 중 아세틸시코닌의 농도 측정	SBB	• 부록 참조
	분석법개발	LC/MS/MS를 이용한 랫드 혈장 중 Acetylshikonin의 Method development	SBB	• 부록 참조
		LC/MS/MS를 이용한 비결견 혈장 중 Acetylshikonin의 Method development	SBB	• 부록 참조
		LC/MS/MS를 이용한 랫드 혈장 중 Acetylshikonin의 검량선 확인 시험	SBB	• 부록 참조
		LC/MS/MS를 이용한 랫드 혈장 중 Acetylshikonin의 검량선 확인 시험	SBB	• 부록 참조
		LC/MS/MS를 이용한 랫드 및 비글견 혈장중 Acetylshikonin의 분석법 개발	SBB	• 부록 참조
알파아이소쿠	유전	α-iso-cubebenol의 마우스를 이용한 소핵시험	바이오톡스텍	• 마우스 골수세포의 소핵유발에 영향을 미치지 않음.
		α-iso-cubebenol의 세균을 이용한 복귀돌연변이시험	바이오톡스텍	• 유전자돌연변이 유발성을 나타내지 않음.
		α-iso-cubebenol의 포유류 배양세포를 이용한 염색체이상시험	바이오톡스텍	• 염색체이상을 유발하는 것으로 판단됨.

구분	시험종류	시험명	수행기관	시험요약
알파아이소쿠베베놀	단회	α-iso-cubebenol의 Sprague-Dawley 랫드를 이용한 단회 경구투여 독성시험	바이오톡스텍	• 개략의 치사량은 암수 모두 2,000 mg/kg을 상회하는 것으로 판단됨.
	국소	α-iso-cubebenol의 토끼를 이용한 피부자극시험	바이오톡스텍	• 토끼의 피부에 대해서 '중등도 자극성'이 있는 물질로 판단됨.
		α-iso-cubebenol의 토끼를 이용한 안점막자극시험	바이오톡스텍	• 토끼의 안점막에 대해서 자극성을 유발하지 않음.
	분석법 개발	LC/MS/MS법을 이용한 랫드 및 비글견 혈장중 α-isocubebenol 분석법 개발 및 검증	바이오톡스텍	• 부록 참조
EC 18	반복	EC-18의 랫드를 이용한 13주 반복 경구투여 독성시험	바이오톡스텍	• 암 • 수 무독성량(NOAEL) : ≥ 2000 mg/kg
		EC-18의 비글견을 이용한 4주 반복 경구투여 독성시험 및 2주 회복시험	바이오톡스텍	• 암 • 수 무독성량(NOAEL) : ≥ 2000 mg/kg
		EC-18의 비글견을 이용한 13주 반복 경구투여 독성시험, 4주 회복시험 및 독성동태시험	바이오톡스텍	• 암 • 수 무독성량(NOAEL) : ≥ 2000 mg/kg
	중추신경계	EC-18의 단회 경구투여에 의한 랫드의 중추신경계에 미치는 영향 평가시험	바이오톡스텍	• EC-18은 500, 1,000 및 2,000 mg/kg 용량에서 중추신경계에 영향을 미치지 않는 것으로 판단됨.
	효능	EC-18의 누드마우스에 이식된 인체 유래의 골수암 세포주 RPMI 8226에 대한 항암시험	바이오톡스텍	• EC-18은 종양의 성장을 억제하는 효과가 없는 것으로 확인됨.
		EC-18의 collagen으로 유발된 DBA/1J 마우스의 관절염에 대한 효능시험	바이오톡스텍	• EC-18은 125, 500 및 2,000 mg/kg 용량에서 관절염 증상을 개선시키는 효능이 있는 것으로 판단
	생식	EC-18의 랫드를 이용한 경구투여 배태자 발생독성시험	바이오톡스텍	• 부록 참조
		EC-18의 랫드를 이용한 경구투여 수태능 및 초기배 발생독성시험	바이오톡스텍	시험이 진행 중에 있음.
		EC-18의 랫드를 이용한 출생전후 모체기능 시험	바이오톡스텍	시험이 진행 중에 있음.
고미신 J	분석법 개발	LC/MS/MS법을 이용한 랫드 및 비글견 혈장중 Gomisin J의 분석법 개발	바이오톡스텍	• 부록 참조
	분석법 개발	LC/MS/MS를 이용한 랫드 혈장 중 Gomisin J의 분석법 Validation	바이오톡스텍	• 부록 참조
	분석법 개발	LC/MS/MS를 이용한 랫드 및 비글 혈장 중 Gomisin J의 분석법 개발을 위한 타당성 시험	바이오톡스텍	• 부록 참조

2. 확보된 후보물질을 대상으로 비임상시험과 SOP 제정을 통한 안전성평가

가. 시험실시의 개요

(1) Good Laboratory Practices

모든 시험은 다음의 Good Laboratory Practices를 준수하였다.

-“비임상시험관리기준”

식품의약품안전청 고시 제2009-183호 (2009년 12월 22일)와 제2012-121호 (2012년12월 18일) 및 식품의약품안전처 고시 제2013-40호 (2013년 4월 5일)

-“Good Laboratory Practice for Nonclinical Laboratory Studies”(21CFR58, revised as of April 1, 2012)

(2) 시험기준

모든 시험은 다음의 시험기준에 근거하여 실시하였다.

-“의약품등의독성시험기준”

식품의약품안전청 고시 제2009-116호 (2009년 8월 24일), 2012-86호 (2012년 8월 24일) 및 식품의약품안전처 고시 제2013-121호 (2013년4월5일)

-“생체시료분석법 Validation 해설서” (식품의약품안전청, 2010년)

-“Guidance for Industry: Bioanalytical Method Validation” (Food and Drug Administration, May 2001)

-“Guideline on bioanalytical method validation” (European Medicines Agency, July 2011)

(3) 동물윤리

본 연구에서 동물이 사용된 시험의 경우, 동물보호법 (제정 1991년 5월 31일 법률제4379호, 전부개정 2011년 8월 4일 법률 제10995호)에 근거한 ㈜바이오톡스텍의 동물실험윤리위원회에 의해 승인되었다.

(4) 수의학적 관리

본 연구에서 동물이 사용된 시험의 경우, 동물보호법 및 실험동물의 관리와 사용에 관한 지침에 따라 실험동물의 극심한 통증 및 고통 등을 예방하기 위한 안락사가 포함된 수의학적 관리를 시험책임자, 수의사 및 시험의뢰자와 협의 하에 실행하였다.

나. 자초추출물을 대상으로 한 비임상시험

(1) 자초추출물의 조제물 중 Acetylshikonin 의 농도 분석법 validation 및 안정성 확인 시험

본 시험은 HPLC를 이용하여 시험물질인 자초추출물의 조제물 중 Acetylshikonin 의 농도 분석법 보증을 위한 validation 및 안정성을 확인하기 위해 실시하였다.

분석결과 QC 시료를 6회 반복 측정한 피크면적 및 retention time의 정밀성은 판정기준을 모두 만족하였다. 표준용액 5 ~ 100 μg/mL 농도의 범위에서 측정한 직선성은 상관계수와 정확성의 판정기준을 모두 만족하였다. 표준물질은 분석에 충분한 형상을 나타내었으며, 이동상, 희석용매 및 부형제가 표준물질의 피크에 영향을 주는 성분은 검출되지 않았다. 일내재현성의 결과 10 mg/mL 및 400 mg/mL농도의 조제물 중 Acetylshikonin의 정확성 및 정밀성은 판정기준을 모두 만족하였다. 표준원액을 실온 4 시간 및 냉장조

건 (2.8 ~ 4.1°C) 에서 7 일간 보관 후 안정성을 확인한 결과 정확성 및 정밀성은 판정기준을 모두 만족하였다. 10 mg/mL 및 400 mg/mL 농도의 조제물을 Autosampler내에서 20 시간동안 안정성을 확인한 결과 Acetylshikonin의 초기농도에 대한 변동율 및 정밀성은 판정기준을 모두 만족하였다. 10 mg/mL 및 400 mg/mL 농도의 조제물에서 상층, 중층 및 하층의 균질성을 확인한 결과 Acetylshikonin의 정확성 및정밀성은 판정기준을 모두 만족하였다. 10 mg/mL 및 400 mg/mL 농도의 조제물을 실온에서 4시간 및 냉장조건 (2.8 ~ 4.1°C) 에서 7 일간 방치 후 안정성을 확인한 결과 Acetylshikonin의 조제직후 초기농도에 대한 변동율 및 정밀성은 판정기준을 모두 만족하였다. QC시료 20 μg/mL의 농도에서 정확성 및 정밀성은 판정기준을 모두 만족하였다.

이상의 결과로부터 자초추출물의 조제물 중Acetylshikonin 의 농도 분석을 위한 본 분석법은 적합하며, 10 mg/mL 및 400 mg/mL 농도의 조제물은 실온 4시간 및 냉장7 일간 안정한 것으로 확인되었다.

(2) 자초추출물의 랫드를 이용한 단회 경구투여 독성시험

본 시험은 시험물질인 자초추출물을 Sprague-Dawley계 암수 6주령 랫드에 단회 경구투여시 나타나는 독성을 평가하고, 개략의 치사량을 구하기 위하여 실시하였다. 군구성은 시험물질 500, 1,000 및 2,000 mg/kg의 용량 및 대조군 (corn oil)의 4군으로 하고, 암수 각각 5 마리씩 단회 경구투여 하였다. 투여 후 14일 동안, 일반증상의 관찰 및 체중측정을 실시하고, 관찰기간 종료 시에 안락사시켜 부검하였다.

암수 500, 1,000 및 2,000 mg/kg 투여군에서 사망례는 관찰되지 않았다. 일반증상에서 시험물질에 의한 영향으로 유연 (salivation), 연변(soft stool), 하복부오염 (soiled perineal region), 설사 (diarrhea), 약물혼입변 (compound colored stool), 착색뇨 (chromaturia), 사료섭취량 감소(decrease in food intake) 및 변량 감소 (decrease of fecal volume)가 관찰되었다.

체중변화에서 수컷은 투여 후 14일까지 대조군과 비교시 감소 혹은 증가억제가 (-1.7 ~ -22.0%) 관찰되었고, 암컷은 투여 후 14일까지 대조군과 비교시 증가억제가 (-0.3 ~ -13.3%) 관찰되었다. 또한 부검에서 시험물질 투여에 의한 영향은 인정되지 않았다.

본 시험의 조건 하에서 자초추출물을 랫드에 단회 경구투여한 결과, 개략의 치사량은 암수 모두 2,000 mg/kg을 상회하는 것으로 판단된다.

(3) 자초추출물의 랫드를 이용한 2주 반복 경구투여 용량결정시험

본 시험은 자초추출물을Sprague-Dawley계 암수 랫드에 2주간 반복 경구 투여시에 대한 독성을 평가하고, 4주 반복투여 독성시험의 용량설정 근거자료로 이용하기 위하여 실시하였다.

시험물질은 100, 300 및 1,000 mg/kg의 3개 용량으로 암수 각 군당 5마리에 2주간 반복 경구 투여하였다. 또한, 대조군 (corn oil)을 설정하여 군당 5마리에 2주간 반복 경구 투여하였다.

관찰기간 동안 일반증상관찰, 체중측정 및 사료섭취량 측정을 실시하였고, 관찰기간 종료 후 혈액 및 혈액생화학적 검사, 장기의 중량, 부검 시 육안적 검사 및 조직병리학적 검사를 수행하였다.

암컷 1,000 mg/kg 투여군에서 투여 11일에 2마리, 수컷 300 mg/kg 투여군에서 투여 14일에 1마리가 사망하였다. 1,000 mg/kg 투여군에서 연갈색의 착색뇨, 흑색 및 적색의 시

험물질색변, 불규칙호흡, 점액변, 입모, 피모착색, 입주위오염, 투여 전 및 후의 유연, 사료섭취량 감소, 호흡곤란, 체온저하, 변량감소, 복부팽만, 300 mg/kg 투여군에서 흑색 및 자색의 시험물질색변, 점액변, 투여 전 및 후의 유연, 착색뇨, 입모, 100 mg/kg 투여군에서 흑색의 시험물질색변, 투여 전 및 후의 유연, 입모가 관찰되었다. 체중에 있어서 암수 300 및 1,000 mg/kg 투여군에서 체중감소가 관찰되었다. 사료섭취량에 있어서 암수 300 및 1,000 mg/kg 투여군에서 투여 1주에 사료섭취량 감소가 관찰되었다. 암수 시험물질 투여군에서 혈액학적, 혈액생화학적 변화 및 장기중량 검사에서 시험물질에 의한 변화로 판단되는 결과는 없었다.

부검소견에서 생존동물의 경우, 암수 1,000 mg/kg 투여군의 신장에서 양측성 암적색 변색 소견, 수컷 1,000 mg/kg 투여군의 비장 및 흉선에서 소형화 소견이 관찰되었고, 사망동물의 경우, 수컷 300 mg/kg 투여군 및 암컷 1,000 mg/kg 투여군에서 비장 및 흉선의 소형화 소견이 관찰되었다.

조직병리학적 검사에서 생존동물의 경우, 암수 300 및 1,000 mg/kg 투여군의 위의 전위에서 과각화를 동반한 편평상피 증식 및 미란/궤양, 신장에서 피질의 세뇨관 상피에 적갈색 색소의 존재가 관찰되었고, 사망동물의 경우, 수컷 300 mg/kg 투여군 및 암컷 1,000 mg/kg 투여군의 위의 전위에서 미란/궤양, 과각화를 동반한 편평상피 증식, 암컷 1,000 mg/kg 투여군의 신장 피질의 세뇨관 상피에 적갈색 색소 존재 및 호염기성 세뇨관을 동반한 단세포 괴사가 관찰되었다.

이상으로 본 시험 조건하에서 자초추출물에 대한 암수 랫드에 2주간 반복 경구 투여 한 결과, 암수 1,000 및 300 mg/kg 투여군에서 일반증상, 체중, 사료섭취량, 부검소견 및 조직병리학적 검사에서 독성학적인 변화가 관찰되었다. 따라서, 4주 반복투여 독성시험의 고용량은 300 mg/kg으로 설정해야 될 것으로 판단된다.

(4) 자초추출물의 랫드를 이용한 4주 반복 경구투여 독성시험 및 2주 회복시험

본 시험은 자초추출물을Sprague-Dawley (Crl:CD(SD))계 암수 랫드에 4주간 반복 경구 투여시에 대한 안전성을 평가하고, 2주간의 회복군을 설정하여 독성변화의 가역성 여부를 확인하기 위하여 실시하였다.

군구성은 시험물질 25, 100 및 400 mg/kg/day의 3개의 용량과 대조군 (corn oil)의 1군으로 하고, 군당 암수 각 10마리에 4주간 경구 투여하였다. 또한, 대조군 및 400 mg/kg/day의 용량군에는 암수 각 5마리씩 추가하여 독성의 가역성을 평가하기 위해 2주간의 회복기간을 두었다.

관찰기간 동안 일반증상관찰, 체중측정, 사료섭취량 측정, 안과학적 검사 및 뇨검사를 실시하였고, 관찰기간 종료 후 혈액 및 혈액생화학적 검사, 장기의 중량, 부검 시 육안적 검사 및 조직병리학적 검사를 수행하였다.

수컷 25 mg/kg/day 투여군에서 투여3일에 1마리의 사망례가 관찰되었다. 사망동물은 부검소견 및 조직병리학적 검사 결과, 폐의 변색 및 폐렴 및 충혈이 관찰되었으며, 고용량군에서 관찰되지 않은 소견들로 우발적인 것으로 판단된다.

일반증상, 체중, 사료섭취량, 안과학적 검사, 혈액 및 혈액생화학적 검사 및 장기중량에 있어서, 암수 시험물질 25, 100 및 400 mg/kg/day 투여군에서 시험물질 투여에 기인한 독성변화는 관찰되지 않았다.

암수 100 및 400 mg/kg/day 투여군에서 뇨단백의 증가 경향, 케톤체, 빌리루빈의 검출,

잠혈의 출현은 시험물질의 특성인 색소에 의한 비특이적인 반응으로서 신장의 암적색 변색 및 조직병리학적 변화에서 신장내 세뇨관의 변화가 없이 적갈색 색소만 관찰되었기에 독성학적으로 의미있는 변화는 아닌 것으로 판단되었다.

이상으로 본 시험 조건하에서 자초추출물에 대한 암수 랫드에 4주간 반복 경구 투여 한 결과, 무독성량 (NOAEL)은 암수 모두 400 mg/kg/day로 판단된다.

(5) 자초추출물의 비글견을 이용한 단회 경구투여 용량증가 독성시험

본 시험은 암수 각 2마리의 비글견에 시험물질인 자초추출물의 500, 1,000 및 2,000mg/kg을 4일 간격으로 용량을 증가하여 단회 경구투여 시 나타나는 독성반응을 평가하기 위하여 실시하였다.

실험기간 중, 암수 모두에서 사망동물은 발생하지 않았다. 시험물질 500투여 후, 수컷은 약 2 및 4시간, 암컷은 약 20분, 1, 4 및 6 시간에 설사증상이 관찰되었다. 1,000투여 후, 수컷은 약 1, 2 및 6시간, 암컷은 약 4시간에 설사증상이 관찰되었으며, 수컷에서는 추가로 25분 및 6시간에 구토증상이 관찰되었다. 2,000투여 후, 수컷은 약 30분, 1, 2 및 4시간, 암컷은 약 25분, 2, 4 및 6시간에 설사증상이 관찰되었으며, 투여 다음날에도 1/2례에서 설사 증상이 관찰되었다. 또한, 추가로 구토 증상이 수컷은 약 4시간, 암컷은 약25분에 1회씩 관찰되었다. 그리고, 설사에는 시험물질이 혼입되었다. 그 외, 체중 및 부검에서는 이상변화는 관찰되지 않았다.

이상의 결과에 의해, 모든 용량에서 관찰된 설사 증상은 시험물질의 투여에 의한 것으로 인정되었으나, 용량의존성이 없고, 체중 및 부검에서도 연관된 변화가 관찰되지 않아, 독성학적 의미는 미약한 것으로 판단되었다. 따라서, 본 시험조건 하에 암수 비글견에 대한 최대내성용량 (MTD)은 2,000mg/kg으로 판단된다.

(6) 자초추출물의 비글견을 이용한 2주 반복 경구투여 용량결정시험

본 시험은 군당 암수 각 2 마리의 비글견을 이용하여 시험물질인 자초추출물을 0(대조군), 100, 300 및 500 mg/kg의 용량으로 2주간 반복 경구투여 시 나타나는 독성반응을 평가하고, 4주 반복투여 독성시험에서 용량설정의 근거자료로 이용하기 위해 실시하였다.

실험기간 중 암수 모두에서 사망례는 발생하지 않았으나, 모든 시험물질 투여군에서 설사 또는 연변 증상이 거의 지속적으로 관찰되고, 구토 증상이 산발적으로 관찰되었으며, 500 mg/kg 투여군에서는 추가로 유연 증상이 거의 지속적으로 관찰되었다. 이러한 연변, 설사, 구토 및 유연 등의 증상은 시험물질의 투여에 의한 변화로 사료되나, 체중, 혈액 및 조직병리학적 검사에서 연관된 변화가 관찰되지 않아 독성학적 의미는 미약한 것으로 판단된다.

혈액생화학적 검사에서는 암수 모든 시험물질 투여군에서 총빌리루빈(T-Bili)이 용량의존적으로 증가하는 경향이 관찰되었다. 그러나, 다른 연관된 항목이나 조직병리학적 변화가 관찰되지 않아, 이는 시험물질의 색상에 의한 변화로 예측되며, 독성학적 의미는 없는 것으로 판단된다.

그 외, 체중, 사료섭취량, 뇨검사, 혈액학적 검사, 장기중량, 부검 및 조직병리학적 검사에서는 시험물질에 의한 변화가 관찰되지 않았다.

이상의 결과에 의해, 4주 반복투여 독성시험에서는 고용량을 300 mg/kg/day으로 설정하고, 100 및 30 mg/kg/day을 중 및 저용량으로 설정하는 것을 추천한다.

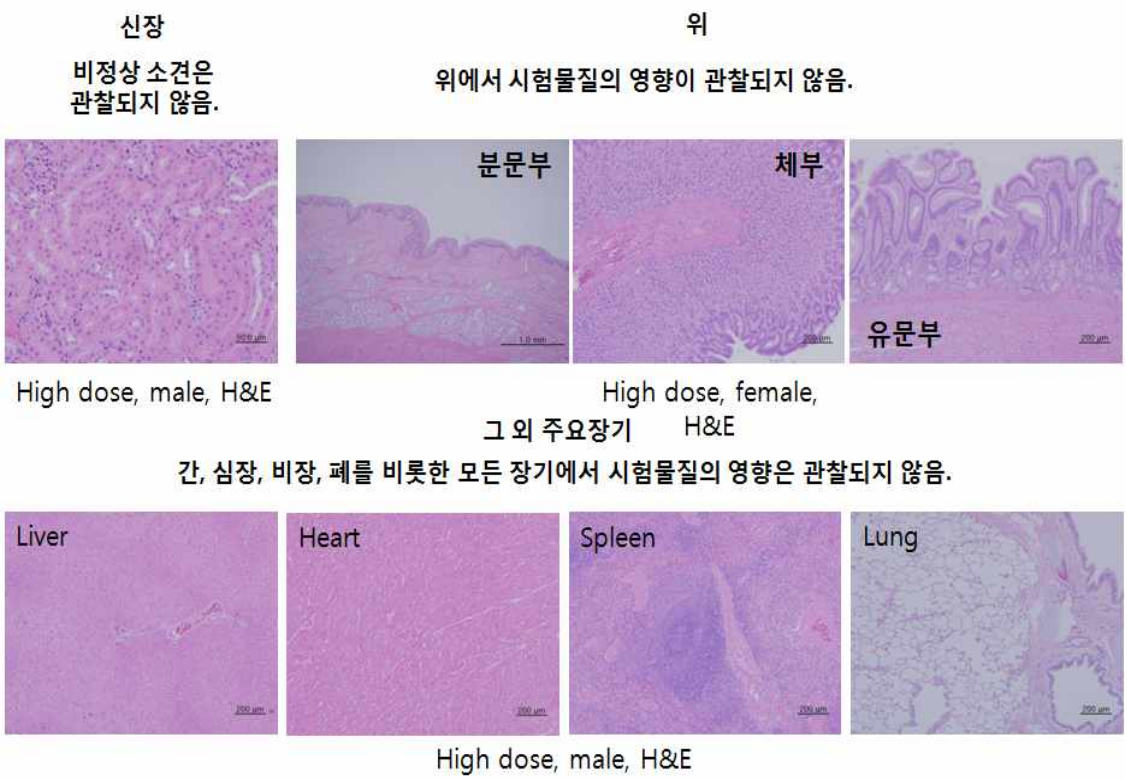

(7) 자초추출물의 비글견을 이용한 4주 반복 경구투여 독성시험, 2주 회복시험 및 독성동태시험

본 시험은 군당 암·수 3마리의 비글견을 이용하여 시험물질인 자초추출물을 30, 100 및 300 mg/kg/day의 용량으로 4주간 반복 경구투여 시 나타나는 독성반응과 그 안전성을 평가하고, 대조군과 고용량군에 암·수 각 2마리씩 2주간 회복군을 설정하여 독성변화의 가역성 여부를 확인하며, 독성동태시험을 통해 약물 전신노출도를 평가하기 위하여 실시하였다.

실험기간 중, 암·수 모두에서 사망동물은 발생하지 않았으나, 투여기간 중 모든 시험물질 투여군에서 유연, 구토, 연변 및 설사 등 소화계통 증상이 용량의존적으로 관찰되었고, 암·수 300 mg/kg/day 투여군에서 체중 또는 체중 증가의 감소가 관찰되었다. 그 외, 사료섭취량, 안과학적 검사, 심전도 검사, 뇨 검사, 혈액학적 및 혈액생화학적 검사, 장기중량, 부검 및 조직병리학적 검사에서는 시험물질의 투여에 의한 이상 변화는 관찰되지 않았다.

또한, 독성동태시험에서 시험물질의 전신노출도 (AUClast, Cmax)는 투여 첫날 (Day 1)에는 투여용량 증가에 따른 변화가 거의 없었으나, 투여 28일째에는 암·수 모두 투여용량 증가에 따라 전신노출도가 증가하였으며, 투여 첫날에 비해 AUClast가 수컷에서는 4.2 ~ 10.3배 및 암컷에서는 저용량군을 제외하고 3.2 ~ 3.7배 높게 나타났다. 또한, 암·수 간에 성별 차이는 없었으나, 100 및 300 mg/kg/day 투여군에서 반복투여에 따라 18 ~ 31%의 축적현상이 관찰되었다.

이상의 결과에 의해, 본 시험조건 하에 암·수 300 mg/kg/day 용량에서 구토, 설사 및 체중 또는 체중 증가 감소 등의 변화가 관찰되어 암·수 비글견에 대한 무독성량 (NOAEL)은 100 mg/kg/day으로 판단된다.

(8) 자초추출물의 세균을 이용한 복귀돌연변이시험

시험물질 자초추출물의 유전자돌연변이 유발성을 히스티딘 요구성 살모넬라균 (TA98, TA100, TA1535 및 TA1537 균주) 및 트립토판 요구성 대장균 (WP2uvrA(pKM101) 균주)을 이용하여 대사활성화비존재하 및 존재하의 경우에 대해 각각 검토하였다.

본시험의 최고용량을 설정하기 위해, 5,000 μg/plate을 최고용량으로 하고, 이하 공비 4로 1,250, 313, 78.1, 19.5 및 4.88 μg/plate의 용량으로 용량설정시험을 실시한 결과, 시험물질에 의한 생육저해가 대사활성화비존재하의 TA98 균주는 78.1 μg/plate 이상, TA100, TA1535 및 TA1537 균주는 19.5 μg/plate 이상, 대사활성화비존재하의 WP2uvrA(pKM101) 균주, 대사활성화존재하의 TA100, 및 TA1537 균주의 1,250 μg/plate 이상에서 관찰되었다. 대사활성화존재하의 TA98, TA1535 및 WP2uvrA(pKM101) 균주에서는 생육저해가 관찰되지 않았다.

시험물질의 침전은 대사활성화비존재하 및 존재하의 1,250 μg/plate 이상에서 관찰되었지만, 복귀콜로니수 계측에는 영향이 없었다. 따라서, 본시험의 용량은 아래와 같이 설정하였다.

균주명	S9 mix	본시험의 용량 (μg/plate)
TA98	-	78.1, 39.1, 19.5, 9.77, 4.88, 2.44
TA100, TA1535, TA1537	-	19.5, 9.77, 4.88, 2.44, 1.22, 0.610
WP2*uvrA*(pKM101)	-	1,250, 625, 313, 156, 78.1, 39.1
TA98, TA1535, WP2*uvrA*(pKM101)	+	5,000, 2,500, 1,250, 625, 313
TA100, TA1537	+	1,250, 625, 313, 156, 78.1, 39.1

(9) 자초추출물의 포유류 배양세포를 이용한 염색체이상시험

시험물질 자초추출물의 염색체이상 유발성 유무를 검토하기 위하여 Chinese Hamster Lung (CHL/IU) 배양세포를 이용하여 염색체이상시험을 실시하였다. 본시험의 최고용량을 설정하기 위해, 5,000 μg/mL을 최고용량으로 하고, 2,500, 1,000, 500, 250, 100, 50, 10 및 5 μg/mL으로 세포증식억제시험을 실시하였다. 그 결과, 단시간처리법의 대사활성화비존재하 및 존재하, 연속처리법의 대사활성화비존재하의 모든 처리계열에서 세포독성이 관찰되었다. 50% 세포증식억제 용량 (Inhibition concentration 50%: IC50)을 산출한 결과, 단시간처리법의 대사활성화비존재하는 4.9 μg/mL, 존재하는 83.1 μg/mL, 연속처리법의 대사활성화비존재하는 6.5 μg/mL이었다.

시험물질의 침전은 단시간처리법의 대사활성화비존재하 및 연속처리법의 대사활성화비존재하의 500 μg/mL 이상, 단시간처리법의 대사활성화존재하의 250 μg/mL 이상에서 관찰되었다.

따라서 본시험의 용량은 아래와 같이 설정하였다. 또한, 각각의 처리 계열에 음성대조군 및 양성대조군을 설정하였다.

계열	S9 mix	본시험의 용량 (μg/mL)
단시간처리법	-	5.00, 2.50, 1.25, 0.625
	+	84.0, 42.0, 21.0, 10.5
연속처리법	-	7.00, 3.50, 1.75, 0.875

본시험의 결과, 단시간처리법의 대사활성화존재하의 42.0 μg/mL의 용량에서 구조이상을 가진 세포의 출현빈도는 16.0%로, 음성대조군 (0%)과 비교하여 통계학적으로 유의하게 증가하였고, 용량의존성도 확인되었다.

단시간처리법의 대사활성화비존재하에서는 염색체이상을 가진 세포의 출현빈도는 5% 미만으로 염색체이상 유발작용은 확인되지 않았으며, 음성대조군과 비교시 통계학적인 유의성도 관찰되지 않았다.

각 처리계열의 양성대조군에서는 구조이상을 가진 세포의 출현빈도가 10% 이상으로 음성대조군과 비교시 통계학적으로 유의하게 증가되었다.

이상의 결과로부터 본 시험조건하에서 자초추출물은 염색체이상을 유발하는 것으로 판단된다.

(10) 자초추출물의 마우스를 이용한 소핵시험

시험물질 자초추출물의 마우스 골수세포에 대한 소핵유발 유무를 평가하기 위하여 수컷 ICR 마우스를 이용하여 단회 경구투여 하여 검토하였다.

본시험의 최고용량을 설정하기 위해, 2,000 mg/kg을 최고용량으로 하고, 이하 공비 2로 1,000, 500, 250 및 125 mg/kg으로 용량설정시험을 실시한 결과, 모든 용량에서 시험물질에 의한 사망동물은 관찰되지 않았다.

따라서, 본시험의 최고용량은 2,000 mg/kg으로 하고 이하 공비 2로 2용량 (1,000 및 500 mg/kg)의 시험물질군을 설정하였다. 또한, 음성대조군에는 corn oil, 양성대조군에는 MMC를 설정하였다.

검체제작설정시험에서는 용량설정시험에서 설정된 최고용량 (2,000 mg/kg)을 투여하고, 투여 후 24, 48 및 72시간에 골수를 채취하여 소핵유발빈도를 관찰한 결과, 모든 관찰시간대에서 소핵유발빈도는 증가되지 않았다. 따라서 일반적으로 사용되는 투여 후 24시간을 본시험의 골수채취시간으로 설정하였다.

시험물질군에서는 다염성적혈구 (Polychromatic erythrocyte, PCE) 중 소핵다염성적혈구 (Micronucleated polychromatic erythrocyte, MNPCE)의 출현빈도는 음성대조군과 비교하여 유의한 증가는 관찰되지 않았다. 또한, 총 적혈구에 대한 다염성적혈구의 비율도 음성대조군과 비교시 유의한 차이는 없었다.

양성대조군에서는 다염성적혈구 중 소핵다염성적혈구의 출현빈도가 음성대조군에 비해 유의하게 증가하였다. 총 적혈구에 대한 다염성적혈구의 비율은 음성대조군과 비교하여 유의한 차이는 관찰되지 않았다.

이상의 결과로부터 자초추출물은 본 시험의 조건하에서 마우스 골수세포의 소핵유발에 영향을 미치지 않는 것으로 판단된다.

(11) 자초추출물의 토끼를 이용한 피부자극시험

시험물질 자초추출물의 피부자극시험을 11주령의 수컷 NZW 토끼 6마리를 사용해서 검토하였다.

토끼의 경배부위에 좌·우 각 2부위, 합 4부위의 투여부위를 설정하고, 그 중 2부위를 비찰과부위, 그 외 2부위를 찰과부위로 하였다. 시험물질원액 0.5 mL를 각각의 비찰과 및 찰과부위의 시험물질투여부위에 적용하여 24시간 폐색첩포하였다. 투여 후 24, 48 및 72시간에 'Draize의 피부반응 평가표1)'에 따라서 피부반응을 평가하였다.

시험물질투여부위의 비찰과 및 찰과부위에서 투여 후 24, 48 및 72시간에 평점 4의 부종

이 6마리 모두에서 관찰되었다. 홍반은 시험물질의 심한 피부착색으로 인하여 관찰이 불가능 하였다. 따라서, 1차피부자극지수 (Primary Skin Irritation Index, P.I.I.)는 산출 할 수 없었으며, 피부자극성의 분류도 할 수 없었다. 무처치대조부위의 비찰과 및 찰과부위에서는 모든 관찰시간에 홍반 및 부종등의 피부반응은 모든 동물에서 관찰되지 않았다. 관찰기간 중, 모든 동물에서 일반증상 및 체중에 이상은 확인되지 않았다.

이상의 결과로부터, 본 시험 조건하에서 시험물질 자초추출물은 홍반의 관찰은 불가능 하였지만 부종이 확인되었기 때문에 토끼의 피부에 대한 자극성이 있는 것으로 판단된다.

(12) 자초추출물의 토끼를 이용한 안점막자극시험

시험물질 자초추출물의 안점막자극시험을 11주령의 수컷 NZW 토끼 9마리를 사용해서 검토하였다.

비세안군은 토끼 6마리의 우안 결막낭 내에 시험물질원액 0.1 mL를 투여하고, 투여 1, 2, 3, 4 및 7일에 각막, 홍채 및 결막등의 안구병변을 관찰하였다. 세안군은 3마리의 토끼를 추가로 사용해서 비세안군과 동일하게 투여하고, 투여 30초 후에 세척한 후 세안효과를 확인하였다. 'Draize의 안구병변의 등급1)'에 따라서 시험물질의 안점막자극을 평가하고, Guillot의 '안점막자극 평가표2)'를 참조해서 안점막자극의 정도를 분류하였다. 또한, 비세안군은 투여 7일에 안자극성이 확인되었기 때문에 3일간격으로 투여 13일까지 관찰을 계속하였다. 비세안군에서는 시험물질투여 1일 이후의 관찰에서 결막발적 (평점 1 ~ 2), 결막부종 (평점 1 ~ 3) 및 배출물 (평점 1 ~ 2)이 관찰되었다. 이러한 자극반응은 투여 13일에 모든 동물에서 소실되었다. 비세안군의 급성안자극지수 (Index of Acute Ocular Irritation, I.A.O.I.)는 '12.7'로 최종평가는 '자극물'로 분류되었다. 세안군에서는 시험물질투여 1일 이후의 관찰에서 결막발적 (평점 1), 결막부종 (평점 1) 및 배출물 (평점 1)이 관찰되었다. 이러한 자극반응 중 배출물은 투여 2일에, 결막발적 및 결막부종은 투여 7일에 모든 동물에서 소실되었다. 세안군의 I.A.O.I.는 '6.0'이었다. 비세안군과 비교하면 I.A.O.I. 및 안자극성의 소실시간에서 차이가 있으므로 안자극성에 대한 세안효과가 확인되었다. 관찰기간 중, 각군의 모든 동물에서 일반증상 및 체중에 이상은 확인되지 않았다. 이상의 결과로부터, 본 시험 조건하에서 시험물질 자초추출물는 토끼의 안점막에 대해서 '자극물'로 판단된다. 또한, 안자극성에 대한 세안효과가 확인되었다.

(13) 자초추출물의 기니픽을 이용한 항원성 평가 (아나필락시스 쇼크 반응시험 및 동종 수동 피부 아나필락시스 반응시험)

시험물질 자초추출물의 이상면역반응을 검색하기 위하여 Hartley계 기니픽을 이용하여 음성대조군 (0 mg/kg), 저용량군 (25 mg/kg), 고용량군 (200 mg/kg), 혼합투여군 (200 mg/kg-FCA) 및 양성대조군 (OVA 5 mg/kg-FCA)의 합 5군을 설정하여 항원성을 평가하였다. 음성대조군, 저용량군 및 고용량군은 감작항원량을 약 2주간 총 6회 경구투여하고, 혼합투여군 및 양성대조군은 동물의 등부에 약 2주간 총 3회 피하투여하여 감작시켰다. 동종 수동 피부 아나필락시스 반응시험 (Passive Cutaneous Anaphylaxis, PCA)은 최종감작 12일째에 안와정맥총으로부터 채혈하여 항혈청을 분리하고, 감작된 기니픽의 항혈청을 10배에서 5120배까지 연속배수 희석하여 최종감작 13일째에 항혈청 1개당 2마리의 감작되지 않은 기니픽의 등부위에 피내투여하여 수동감작시켰다. 4시간 후 2% evans blue와 혼합한 야기 항원량을 후지정맥으로 투여하고, 약 30분 후에 등부위 피부

를 박리하여 피부반응을 관찰하였다. 아나필락시스 쇼크 반응시험 (Active Systemic Anaphylaxis, ASA)은 최종감작 14일째에 야기 항원량을 감작된 기니픽의 후지정맥에 투여하여 약 30분간 아나필락시스 쇼크반응 유·무를 관찰하였다. 그 결과, 동종 수동 피부 아나필락시스 반응시험에서는 음성대조군, 저용량군, 고용량군 및 혼합투여군에서 희석배수 10배에서 5120배까지 모든 동물에서 음성반응이 관찰되었다. 양성대조군에서는 최대희석배수 5120배까지 양성반응이 관찰되었다. 아나필락시스 쇼크반응 시험에서는 음성대조군, 저용량군, 고용량군 및 혼합투여군에서 아나필락시스 쇼크반응은 관찰되지 않았다. 양성대조군에서는, 모든 동물에서 호흡곤란 (Dyspnea), 경련 (Convulsion) 및 횡와 (Side position)등의 전형적인 아나필락시스 쇼크반응이 관찰되다가 5분 이내에 '사망 (Death)' 하였다. 관찰기간 중, 각 군의 일반증상 및 체중에 대해서 이상은 확인되지 않았다. 이상의 결과로부터, 본 시험 조건하에서 시험물질 자초추출물은 동종 수동 피부 아나필락시스 반응시험 및 아나필락시스 쇼크 반응시험에서 음성반응이 관찰되어, 항원성이 없는 물질로 판단된다.

(14) 자초추출물의 랫드를 이용한 4주 반복 경구투여 독성동태시험

본 시험은 암수 Sprague-Dawley 랫드를 이용하여 자초추출물을 4주간 반복 경구투여 시 시험물질의 전신노출도를 모니터링하기 위하여 실시하였다.

군구성은 시험물질 25, 100 및 400 mg/kg/day의 3개의 용량과 대조군 (corn oil)의 1군으로 하고, 시험물질 투여군은 군당 암수 각 6마리, 대조군은 군당 암수 각 3마리에 4주간 반복 경구 투여하였다.

관찰기간 동안 일반증상관찰, 체중측정을 실시하였고, 투여 개시일 (Day 1) 및 투여 28일에 시간대별로 경정맥 채혈하여 독성동태학적 분석을 실시하였다.

투여개시일 및 투여 28일에 아세틸시코닌의 AUClast 및 Cmax는 투여 용량이 증가함에 따라 증가하는 경향을 나타내었다. 투여개시일의 고용량군에서 AUClast와 투여 28일의 고용량군에서 Cmax를 제외하고 수컷이 암컷보다 더 높은 경향을 나타냈지만, 그 차이가 작기 때문에 성차는 없다고 판단했다. 모든 시험물질 투여군에서 반복투여의 영향이 있었고, 투여 28일의 AUClast 및 Cmax는 투여개시일 보다 더 높게 나타내었다. Tmax는 0.50 ~ 3.00 시간 및 t1/2는 5.48 ~ 43.29 시간으로 나타났다.

(15) LC/MS/MS를 이용한 랫드 혈장 중 acetylshikonin의 분석법 Validation

본 시험에서는 Liquid Chromatography/Tandem Mass Spectrometry (이하 LC/MS/MS)를 이용하여 랫드 혈장 중 acetylshikonin의 분석방법에 대한 유효성 검증 (이하 validation)을 실시하였다.

랫드 혈장 중 acetylshikonin의 농도 측정을 위해 emodin을 내부표준물질로 사용하였으며, 안정화된 랫드 혈장 55 μL (랫드 혈장 50 μL에 해당함)에 들어있는acetylshikonin을

2-Mercaptoethanol로 유도체화 시킨 다음 acetylshikonin derivatized 및 내부표준물질을 cyclohexane으로 추출한 후 재용해용액으로 재용해하여 LC/MS/MS로측정하였다.

아래 표에 validation 항목 및 결과를 요약하였으며, 본 기관에서 확인한 분석방법은 랫드 혈장 중 acetylshikonin의 농도 측정에 적용 가능하다고 판단된다.

Sex	Group / Dose (mg/kg)	Phase	Toxicokinetic parameters			
			AUC_{last} (ng·hr/mL)	C_{max} (ng/mL)	T_{max} (hr)	$t_{1/2}$ (hr)
Male	G2 /	Day 1	376.79	41.80	0.50	7.42
	25	Day 28	722.05	60.90	3.00	15.60
	G3 /	Day 1	1,042.90	123.00	0.50	11.49
	100	Day 28	2,018.40	146.00	3.00	14.24
	G4 /	Day 1	1,198.80	145.00	0.50	43.29
	400	Day 28	5,008.25	360.00	0.50	14.42
Female	G2 /	Day 1	310.06	35.40	0.50	5.48
	25	Day 28	580.33	53.10	3.00	24.76
	G3 /	Day 1	710.13	55.40	0.50	11.05
	100	Day 28	1,677.03	127.00	1.00	13.85
	G4 /	Day 1	1,410.68	106.00	0.50	-
	400	Day 28	4,595.75	400.00	3.00	14.99

-: $t_{1/2}$ was not calculated because of less than 3 points for calculation.

Validation items	Classifications	Results	
Stability in plasma	Initial sample (15 and 750 ng/mL)	Accuracy	96.1% and 92.8%
		Precision	5.6% and 2.9%
	Short-term temperature stability (on ice, 0.5 hr)	Accuracy	91.1% and 102.4%
		Precision	6.0% and 1.0%
	Short-term temperature stability (on ice, 1 hr)	Accuracy	94.7% and 98.3%
		Precision	6.1% and 2.3%
	Short-term temperature stability (room temp. after derivatization) (22.9 ~ 24.1 °C, 1 hr)	Accuracy	89.1% and 94.2%
		Precision	4.8% and 2.9%
	Initial sample (15 and 750 ng/mL)	Accuracy	103.7% and 94.8%
		Precision	13.8% and 11.5%
	Long-term stability (-77.3 to -59.3°C, 5 days)	Accuracy	91.8% and 83.6%
		Precision	5.1% and 7.1%
	Long-term stability (-77.3to -59.3°C, 7 days)	Accuracy	110.9% and 86.0%
		Precision	19.1% and 3.0%
	Long-term stability (-77.3to -59.3°C, 14 days)	Accuracy	105.1% and 98.3%
		Precision	6.4% and 7.4%
	Long-term stability (-77.3to -59.3°C, 32 days)	Accuracy	87.6% and 88.7%
		Precision	6.7% and 0.8%
	Freeze /thaw cycle stability	Accuracy	106.0% and 89.7%

	(1 cycle)	Precision	7.6% and 12.6%
	Initial sample	Accuracy	119.1% and 116.8%
	(15 and 750 ng/mL)	Precision	12.4% and 9.4%
	Post preparative stability	Accuracy	94.4% and 83.4%
	(10°C, 24 hrs)	Precision	28.7% and 8.3%
	Post preparative stability	Accuracy	100.9% and 87.8%
	(10°C, 48 hrs)	Precision	27.9% and 6.9%

Validation items	Classifications		Results
Stock solution Stability	Acetylshikonin		
	Room temperature (22.2 to 24.2 °C, 2 hrs)	Residual ratio	101.8%
	Refrigeration (3.2 to 7.5°C, 20 days)	Residual ratio	91.8%
	Emodin		
	Room temperature (22.2 to 24.2 °C, 2 hrs)	Residual ratio	111.8%
	Refrigeration (3.2 to 7.5°C, 20 days)	Residual ratio	99.7%

(16) LC/MS/MS를 이용한 비글견혈장 중 acetylshikonin의 분석법 Validation

본 시험에서는 Liquid Chromatography/Tandem Mass Spectrometry (이하 LC/MS/MS)를 이용하여 비글견 혈장 중 acetylshikonin의 분석방법에 대한 유효성 검증 (이하 validation)을 실시하였다.

비글견 혈장 중 acetylshikonin의 농도 측정을 위해 emodin을 내부표준물질로 사용하였으며, 안정화된 비글견 혈장 55 μL (비글견 혈장 50 μL에 해당함)에 들어있는 acetylshikonin을 2-Mercaptoethanol로 유도체화 시킨 다음 acetylshikonin derivatized 및 내부표준물질을 cyclohexane으로 추출한 후 재용해용액으로 재용해하여 LC/MS/MS로 측정하였다.

아래 표에 validation 항목 및 결과를 요약하였으며, 본 기관에서 확인한 분석방법은 비글견 혈장 중 acetylshikonin의 농도 측정에 적용 가능하다고 판단된다.

Validation items	Classifications	Results	
Carryover effect	Acetylshikonin	0.0% to 4.3%	
	Emodin	0.0%	
Selectivity	Acetylshikonin	No interfering peak	
	Emodin	No interfering peak	
Matrix effect	Acetylshikonin	Accuracy	90.9%
	(5 ng/mL)	Precision	24.5%

Linearity of calibration curve and quantification range	5 to 1,000 ng/mL, $1/X^2$	Correlation coefficient	0.9927 to 0.9990
	LLOQ (5 ng/mL)	Accuracy	94.0% to 101.4%
	Other concentrations (10 to 1,000 ng/mL)	Accuracy	80.0% to 117.3%
Intra-assay	LLOQ	Accuracy	122.3%
	(5 ng/mL)	Precision	4.5%
	Low, Mid and High	Accuracy	118.0%, 116.5% and 99.1%
	(15, 300 and 750 ng/mL)	Precision	5.4%, 11.0% and 5.6%
Inter-assay	LLOQ	Accuracy	106.8%
	(5 ng/mL)	Precision	12.0%
	Low, Mid and High	Accuracy	109.8%, 104.0% and 91.2%
	(15, 300 and 750 ng/mL)	Precision	8.2%, 9.7% and 6.8%
Dilution reproducibility	10-fold dilution	Accuracy	103.5%
		Precision	4.0%

Validation items	Classifications	Results	
Stability in plasma	Initial sample	Accuracy	96.9% and 86.9%
	(15 and 750 ng/mL)	Precision	6.0% and 2.8%
	Short-term temperature stability	Accuracy	97.1% and 84.7%
	(on ice, 2 hr)	Precision	4.6% and 3.4%
	Post preparative stability	Accuracy	109.8% and 103.7%
	(10°C, 47 hrs)	Precision	8.3% and 3.1%
	Post preparative stability	Accuracy	119.3% and 106.3%
	(10°C, 71 hrs)	Precision	3.9% and 2.8%
	Freeze/thaw cycle stability	Accuracy	98.0% and 94.5%
	(1 cycle)	Precision	11.2% and 1.1%
	Long-term stability	Accuracy	116.9% and 104.1%
	(-74.2 to -66.1°C, 14 days)	Precision	3.7% and 5.9%
	Long-term stability	Accuracy	117.6% and 117.4%
	(-74.2 to -66.1°C, 42 days)	Precision	7.2% and 7.4%

(17) 자초추출물의 랫드를 이용한 4주 반복 경구투여 독성동태시험에서 채취된 랫드 혈장 중 아세틸시코닌의 농도 측정

본 시험에서는 자초추출물의 4주 반복 경구 투여에 따른 전신노출도를 확인하기 위해, 독성동태시험에서 채취된 랫드 혈장 중 지표성분인 아세틸시코닌의 농도를 LC/MS/MS로 측정하여 독성동태학적 파라미터를 산출하였다.

랫드 혈장 중 아세틸시코닌의 농도 측정을 위해 emodin을 내부표준물질로 사용하였으며, 안정화된 랫드 혈장 55 µL (랫드 혈장 50 µL에 해당함)에 들어 있는 아세틸시코닌을 2-Mercaptoethanol로 유도체화 시킨 다음 아세틸시코닌 유도체 및 내부표준물질을 cyclohexane으로 추출한 후 재용해용액으로 용해하여 LC/MS/MS로 측정하였다.
정량 대상인 모든 TK 검체 (투여개시일 (Day 1) 및 투여 28일 (Day 28)의 300개)는 시험법 검증에서 확인한 안정성 조건 [초저온 냉동 (관리범위: -80°C ~ -60°C)에서 32일 이내 및 냉•해동 과정 (초저온 냉동/빙냉 상태(on ice)) 1회 이내]에서 전처리하여 측정하였다. 검체의 정량은 품질관리 시료에 대한 판정기준에 따라 실시되었으며, 모든 결과가 판정기준을 만족함에 따라 아세틸시코닌의 정량 결과는 신뢰할 수 있다고 판단된다.
투여개시일 및 투여 28일에 아세틸시코닌의 AUClast 및 Cmax는 투여 용량이 증가함에 따라 증가하는 경향을 나타내었다. 투여개시일의 고용량군에서 AUClast와 투여 28일의 고용량군에서 Cmax를 제외하고 수컷이 암컷보다 더 높은 경향을 나타냈지만, 그 차이가 작기 때문에 성차는 없다고 판단했다. 모든 시험물질 투여군에서 반복투여의 영향이 있었고, 투여 28일의 AUClast 및 Cmax는 투여개시일 보다 더 높게 나타내었다. Tmax는 0.50 ~ 3.00 시간 및 t1/2는 5.48 ~ 43.29 시간으로 나타났다.

Sex	Group / Dose (mg/kg)	Phase	Toxicokinetic parameters			
			AUC_{last} (ng·hr/mL)	C_{max} (ng/mL)	T_{max} (hr)	$t_{1/2}$ (hr)
Male	G2 /	Day 1	376.79	41.80	0.50	7.42
	25	Day 28	722.05	60.90	3.00	15.60
	G3 /	Day 1	1,042.90	123.00	0.50	11.49
	100	Day 28	2,018.40	146.00	3.00	14.24
	G4 /	Day 1	1,198.80	145.00	0.50	43.29
	400	Day 28	5,008.25	360.00	0.50	14.42
Female	G2 /	Day 1	310.06	35.40	0.50	5.48
	25	Day 28	580.33	53.10	3.00	24.76
	G3 /	Day 1	710.13	55.40	0.50	11.05
	100	Day 28	1,677.03	127.00	1.00	13.85
	G4 /	Day 1	1,410.68	106.00	0.50	-
	400	Day 28	4,595.75	400.00	3.00	14.99

-: $t_{1/2}$ was not calculated because of less than 3 points for calculation.

(18) 자초추출물의 비글견을 이용한 4 주 반복 경구투여 독성시험, 2 주 회복시험 및 독성동태시험"에서 채취된 비글견 혈장 중 아세틸시코닌의 농도 측정

본 시험에서는 자초추출물 4 주 반복 경구 투여에 따른 전신노출도를 확인하기 위해, 독성동태시험에서 채취된 비글견 혈장 중 지표성분인 아세틸시코닌의 농도를 LC/MS/MS로 측정하여 독성동태학적 파라미터를 산출하였다.
비글견 혈장 중 아세틸시코닌의 농도 측정을 위해 emodin을 내부표준물질로 사용하였으

며, 안정화된 비글견 혈장 55 µL (비글견 혈장 50 µL에 해당함)에 들어 있는 아세틸시코닌을 2-Mercaptoethanol로 유도체화 시킨 다음 아세틸시코닌 유도체 및 내부표준물질을 cyclohexane으로 추출한 후 재용해용액으로 용해하여 LC/MS/MS로 측정하였다.

정량 대상인 모든 TK 검체 (투여개시일 (Day 1) 및 투여 28 일 (Day 28)의 372 개)는 유효성 검증에서 확인한 안정성 조건 [초저온 냉동 (관리범위: -80°C ~ -60°C)에서 42 일 이내 및 냉•해동 과정 (초저온 냉동/on ice) 1 회 이내]에서 전처리하여 측정하였다. 검체의 정량은 품질관리 시료에 대한 판정기준에 따라 실시되었으며, 모든 결과가 판정기준을 만족함에 따라 아세틸시코닌의 정량 결과는 신뢰할 수 있다고 판단된다. 투여 28 일에 아세틸시코닌의 AUClast 및 Cmax 는 용량 증가에 따라 증가하는 경향을 나타내었으나, 투여개시일에는 증가 경향은 없었다. 투여개시일에 AUClast 는 암컷이 수컷보다 저용량군은 5.1 배 및 고용량군은 2.6 배 더 높은 경향을 각각 나타내었지만 성차는 없었고, Cmax 는 암컷이 수컷보다 1.9 배 더 높은 경향을 나타내었다. 투여 28 일의 AUClast 와 Cmax 는 투여개시일의 암컷 저용량군을 제외한 모든 시험물질 투여군에서 더 높은 경향을 나타내어, 반복투여의 영향이 있었다. Tmax 는 0.25 ~ 4.00 시간 및 t1/2 는 1.63 ~ 31.06 시간으로 나타났다.

(19) LC/MS/MS를 이용한 랫드 혈장 중 Acetylshikonin의 Method Development

LC/MS/MS를 이용한 랫드 혈장 중 Acetylshikonin의 유도체화 방법을 이용한 분석법 개발을 위하여 감도, 직선성 및 안정성 확인을 실시하였다.

(가) Acetylshikonin의 유도체화 방법으로 25 ~ 1,000 ng/mL의 정량범위에서 랫드 혈장 중 Acetylshikonin의 직선성을 확인하였고, 10ng/mL의 농도를 검출할 수 있을 것으로 예상되어 10 ~ 2,000 ng/mL의 정량범위에서 직선성 확인 예정임.

(나) 랫드 혈장 중 Acetylshikonin의 직선성 재확인 후 재현성 확인 예정임.

(다) 랫드 혈장 중 Acetylshikonin의 실온안정성이 좋지 않은 것으로 확인하였고, 유도체 반응 직전까지 냉장 조건이 유지되도록 on ice 상태에서 조제해야 할 것으로 판단됨.

Sex	Group / Dose (mg/kg)	Phase	Toxicokinetic parameters			
			AUC_{last} (ng·hr/mL)	C_{max} (ng/mL)	T_{max} (hr)	$t_{1/2}$ (hr)
Male	G2	Day 1	98.06	31.33	0.67	2.49
	30	Day 28	413.06	42.37	1.50	11.51
	G3	Day 1	260.32	37.50	0.75	5.25
	100	Day 28	1202.06	88.17	0.83	12.74
	G4	Day 1	138.46	37.40	1.00	4.91
	300	Day 28	1427.68	142.67	1.67	12.46
Female	G2	Day 1	502.42	60.70	3.33	6.90
	30	Day 28	452.89	44.67	2.33	16.31
	G3	Day 1	356.48	43.80	1.58	8.77
	100	Day 28	1156.48	82.07	2.25	15.11
	G4	Day 1	361.67	56.20	1.08	6.93
	300	Day 28	1330.31	120.10	1.50	17.17

(라) 분석법 개발 중 Acetylshikonin과 내부표준물질 (Emodin)의 피크면적 변화 (감소)를 확인

함.

→ Acetylshikonin과 내부표준물질의 피크면적 비슷한 비율로 감소하여 피크면적비 변화가 크지 않은 것을 미루어 볼때 Acetylshikonin의 유도체 반응에서 나타나는 Acetylshikonin 이외의 반응물에 의한 mass 오염에서 기인된 것으로 판단되어 valco valve 사용 조건 검토 예정임.

→ Acetylshikonin과 내부표준물질 (Emodin)의 표준원액 및 표준용액을 새로 조제하여 안정성 확인 예정임.

(마) 예비 시험 (B12624)의 검체시료를 측정하여 랫드 혈장 중 Acetylshikonin의 정량범위가 적합한지 확인 예정임.

(20) LC/MS/MS를 이용한 비글견 혈장 중 Acetylshikonin의 Method Development

본 시험은 LC/MS/MS를 이용한 비글견 혈장 중 2-Mercaptoethanol로 Acetylshikonin을 유도체화하여 분석하는 조건을 검토하기 위하여 실시하였다.

(가) 2-Mercaptoethanol을 사용한 Acetylshikonin의 유도체화 방법에서 비글견 혈장 중 10 ~ 500 ng/mL의 정량범위에서 Acetylshikonin 유도체의 직선성을 확인하였다.

(나) 2-Mercaptoethanol의 몰농도를 낮출수록 Acetylshikonin의 유도체화가 증가하는 것을 확인하였다.

(다) 추출용매 (Ethylacetate, Tert-butylmethylether,Hexane,Cyclohexane)에서 Acetylshikonin 유도체 및 Emodin의 추출율이 서로 다른 양상으로 나타나는 것으로 확인하였고, 최저정량한계농도를 낮추기 위해 Acetylshikonin 유도체의 추출율이 가장 높은 Cyclohexane으로 추출하는 것이 적절하다고 판단한다.

따라서, 2-Mercaptoethanol의 몰농도를 2 M에서 0.5 M로 변경하여 비글견 혈장 중 5 ~ 500 ng/mL의 정량범위로 Acetylshikonin 유도체의 직선성을 확인할 수 있을 것으로 예상된다. 해당 조건으로 예비 시험 (B12616P)의 검체를 측정하여 비글견 혈장 중 Acetylshikonin 유도체의 정량범위가 적합한지 확인 예정입니다.

(21) LC/MS/MS를 이용한 랫드 혈장 중 Acetylshikonin의 검량선 확인 시험

본 시험은 시험물질을 10 mg/kg 및 1,000 mg/kg으로 투여한 예비 검체에서 Acetylshikonin의 농도 측정 결과로 랫드 혈장 중 Acetylshikonin의 적합한 정량 범위를 확인하기 위하여 실시하였다.

“LC/MS/MS를 이용한 랫드 혈장 중 Acetylshikonin의 유도체화 방법을 이용한 분석법 개발 (시험번호: S12065)”에서 확인한 조건으로 예비 검체에서 Acetylshikonin의 농도를 측정하였고, 품질관리 시료의 판정기준을 만족하지 못하였기 때문에 검체의 Acetylshikonin의 측정 농도는 유효하다고 판단하기에는 어려울 것으로 사료되지만 다음과 같이 평가하였다.

(가) 시험물질을 10 mg/kg으로 투여한 경우에는 Acetylshikonin이 투여 후 0.5 ~ 1 시간에 최고 농도 (22.48 ~ 30.93 ng/mL)로 검출된 후, 투여 후 8시간 (최저정량한계농도: 10 ng/mL)까지 감소되는 양상으로 검출되었다.

(나) 시험물질을 1,000 mg/kg으로 투여한 경우에는 Acetylshikonin이 투여 후 0.5 시간에 최고 농도 (2,000 ~ 2,500 ng/mL)로 검출된 후, 투여 후 8시간 (농도: 380 ~ 600 ng/mL)까지 감소되는 양상으로 검출되었다.

따라서, 랫드 독성동태시험의 예정된 투여 용량인 25 mg/kg, 100 mg/kg 및 400

mg/kg으로 시험물질을 투여하였을 때 랫드 혈장 중 Acetylshikonin의 정량 범위인 10 ~ 2,000 ng/mL에서 검출 가능할 것으로 예상된다. 그러나, 랫드 혈장 중 Acetylshikonin의 정량 범위인 10 ~ 2,000 ng/mL에서 직선성 및 재현성이 향상된 보다 확고한 분석법을 위하여 추가적인 분석법 검토가 필요할 것으로 판단된다.

(22) LC/MS/MS를 이용한 비글견 혈장 중 Acetylshikonin의 검량선 확인 시험

본 시험은 시험물질을 10 mg/kg 및 1,000 mg/kg으로 투여한 예비 검체에서 Acetylshikonin의 농도 측정 결과로 랫드 혈장 중 Acetylshikonin의 적합한 정량 범위를 확인하기 위하여 실시하였다.

"LC/MS/MS를 이용한 비글견 혈장 중 Acetylshikonin의 유도체화 방법을 이용한 분석법 개발 (시험번호: S12066)"에서 확인한 조건으로 예비 검체에서 Acetylshikonin의 농도를 측정하였고, 다음과 같이 평가하였다.

(가) 시험물질을 10 mg/kg으로 투여한 경우에는 Acetylshikonin 유도체가 투여 후 0.25 ~ 1 시간에 최고 농도 (3.804 ~ 6.567 ng/mL)로 검출된 후, 투여 후 6 시간 (최저정량한계농도: 2 ng/mL)까지 감소되는 양상으로 검출되었고, 투여 후 10 시간 이후에는 최저정량한계농도 미만으로 검출되었다.

(나) 시험물질을 1,000 mg/kg으로 투여한 경우에는 Acetylshikonin 유도체가 투여 후 0.5 ~ 2 시간에 최고 농도 (29.21 ~ 35.40 ng/mL)로 검출된 후, 투여 후 24 시간 (농도: 3.793 ~ 4.409 ng/mL)까지 감소되는 양상으로 검출되었다.

비글견 독성동태시험의 투여 용량이 아직 예정되지 않았기 때문에 비글견 혈장 중 Acetylshikonin의 정량 범위는 투여 용량 확정 후 검토할 수 있을 것으로 판단된다.

(23) 자초추출물의 설치류 4주 반복투여독성시험의 조제물 중 Acetylshikonin의 농도분석

본 시험에서는 자초추출물의 4주 반복 경구 투여에 따른 전신 노출도를 확인하기 위해, 독성동태시험에서 채취된 랫드 혈장 중 지료성분인 아세틸시코닌의 농도를 LC/MS/MS로 측정하여 독성동태학적 파라미터를 산출하였다.

정량대상인 모든 TK 검체는 유효성 검증에서 확인된 안정성 조건 [초저온 냉동(관리범위: -80℃ ~ -60℃)에서 32일 이내 및 냉·해동 과정(초저온 냉동/빙냉 상태(on ice)) 1회 이내] 에서 전처리하여 측정하였다. 검체의 정량은 품질관리 시료에 대한 판정기준에 따라 실시되었으며, 모든 결과가 판정기준을 만족함에 따라 아세틸시코닌의 정량 결과는 신뢰할 수 있다고 판단된다.

투여개시일(Day 1) 및 투여 28일(Day 28)에 아세틸시코닌의 AUC_{last} 및 C_{max} 는 용량 증가에 따라 증가하는 경향을 나타내었다. 투여개시일의 고용량군에 AUC_{last}와 투여 28일(Day 28)의 고용량군에서 C_{max}를 제외하고 수컷이 암컷보다 더 높은 경향을 나타냈지만, 그 차이가 작기 때문에 성차는 없다고 판단했다. 모든 시험물질 투여군에서 반복투여의 영향이 있었고, 투여 28일(Day 28)의 AUC_{last} 및 C_{max}는 투여개시일(Day 1)보다 더 높게 나타냈었다. T_{max}는 0.50 ~ 3.00 시간 및 $t_{1/2}$는 5.48 ~ 43.29 시간으로 나타났다.

(24) LC/MS/MS를 이용한 랫드 및 비글견 혈장중 Acetylshikonin의 validation

(가) LC/MS/MS를 이용한 랫드 혈장중 Acetylshikonin의 분석방법에 대한 validation: LC/MS/MS를 이용한 랫드 혈장중 Acetylshikonin의 분석방법에 대한 validation을 실시하였다. Carryover effect, 특이성, Matrix effect, 직선정, 일내재현성, 일간재현성 및 희석재현성을 검토한 결과 모두 판정기준을 만족하여 해당 분석방법은 유효한 것

으로 판단된다.

아울러 랫드 혈장 중 acetylshikonin은 on ice에서 1시간 이내로 방치하는 경우, 초저온 냉동(관리범위: -80℃ ~ -60℃)에서 32일 이내로 보관하는 경우, 냉·해동과정(초저온 냉동/on ice)을 1회 실시하는 경우 및 전처리를 마친 후 축정하는 경우에도 안정성이 있음을 확인하였다. 또한, 표준물질 및 내부표준물질 표준원액은 실온에서 2시간 이내로 방치하거나 냉장(관리범위: 2 ~ 8℃)에서 20일 이내에 보관한 경우에도 안정성이 있음을 확인하였다. 따라서, 랫드 혈장 중 acetylshikonin의 분석방법은 검체의 농도 분석 시험에 적용할 수 있다고 판단된다.

(나) LC/MS/MS를 이용한 비글견 혈장중 Acetylshikonin의 분석방법에 대한 validation: LC/MS/MS를 이용한 비글견 혈장중 Acetylshikonin의 분석방벙에 대한 validation을 실시하엿다. Carryover effect, 특이성, Matrix effect, 직선성, 일간재현성, 일내재현성 및 희석재현성을 검토한 결과 모두 판정기준을 만족하여 해당 분석방법은 유효한 것으로 판단된다.

아울러 비글견 혈장 중 acetylshikonin은 on ice에서 2시간 이내로 방치하는 경우, 초저온 냉동(관리범위: -80℃ ~ -60℃)에서 42일 이내로 보관하는 경우, 냉·해동과정(초저온 냉동/on ice)을 1회 이내로 실시하는 경우 및 전처리를 마친 후 71시간 이내에 측정하는 경우에도 안전성이 있음을 확인하였다. 따라서, 비글견 혈장 중 acetylshikonin의 분석방법은 검체의 농도 분석 시험에 적용할 수 있다고 판단된다.

다. α-iso-cubebenol을 대상으로 한 비임상시험

(1) α-iso-cubebenol의 마우스를 이용한 소핵시험

시험물질 α-iso-cubebenol의 마우스 골수세포에 대한 소핵유발 유무를 평가하기 위하여 ICR 마우스를 이용하여 단회 경구투여하여 검토하였다.

소핵시험의 투여용량은 3용량(437, 219 및 109 mg/kg)으로 설정하였다. 또한, 음성대조군 및 양성대조군을 설정하였다.

시험기간 동안, 시험물질 투여로 인한 일반증상 및 사망동물은 관찰되지 않았고, 시험물질군의 체중도 음성대조군과비교시 유의성 있는 변화는 관찰되지 않았다.

소핵시험의 결과, 시험물질군에서는 다염성적혈구(Polychromatic erythrocyte, PCE) 중 소핵다염성적혈구 (Micronucleated polychromatic erythrocyte, MNPCE)의 출현빈도가 음성대조군과 비교하여 유의한 증가는 관찰되지 않았다. 또한, 총적혈구에 대한 다염성적혈구의 비율도 음성대조군과 비교시 유의한 차이는 관찰되지 않았다.

양성대조군에서는 다염성적혈구 중 소핵다염성적혈구의 출현빈도가 음성대조군에 비해 현저하게 증가하였고, 총적혈구에 대한 다염성적혈구의 비율은 음성대조군과 비교시 유의한 차이는 관찰되지 않았다.

이상의 결과로부터 α-iso-cubebenol은 본 시험의 조건하에서 마우스 골수세포의 소핵유발에 영향을 미치지 않는 것으로 판단하였다.

(2) α-iso-cubebenol의 세균을 이용한 복귀돌연변이시험

시험물질 α-iso-cubebenol의 유전자돌연변이 유발성을 히스티딘 요구성인 살모넬라균(TA98, TA100, TA1535 및 TA1537 균주)과 트립토판 요구성인 대장균(WP2uvrA(pKM101) 균주)을 이용하여 대사활성화비존재하 및 존재하의 경우에 대해 각

각 검토하였다.

본시험의 최고용량을 설정하기 위해, 5,000 μg/plate를 최고용량으로 하고, 이하 공비 4로 1,250, 313, 78.1, 19.5 및 4.88 μg/plate으로 용량설정시험을 실시한 결과, 시험물질에 의한 생육저해가 대사활성화비존재하의 TA98균주는 313 μg/plate 이상, TA100, TA1535 및 TA1537균주는 19.5 μg/plate 이상, 대사활성화존재하의 TA98, TA100, TA1535 및 TA1537균주는313 μg/plate 이상에서 관찰되었다. WP2uvrA(pKM101)균주는 대사활성화 유무에 관계없이 생육저해는 관찰되지 않았다.

따라서, 본시험의 용량은 아래와 같이 설정하였다. 또한, 음성대조군 및 양성대조군을 설정하였다.

균주명	S9 mix	본시험의 용량 (μg/plate)
TA98	-	313, 156, 78.1, 39.1, 19.5, 9.77
TA100, TA1535, TA1537	-	19.5, 9.77, 4.88, 2.44, 1.22, 0.610
TA98, TA100, TA1535, TA1537	+	313, 156, 78.1, 39.1, 19.5, 9.77
WP2*uvrA*(pKM101)	-/+	5,000, 2,500, 1,250, 625, 313

본시험의 결과, 시험물질군에서는 대사활성화 유무에 관계없이 각 균주의 모든 용량에 대해서 복귀변이콜로니수는 부형제대조군의 2배를 초과하지 않았고, 용량의존적인 증가도 관찰되지 않았다.

각 균주에 대한 양성대조군의 복귀변이콜로니수는 음성대조군과 비교하여 2배 이상 확실하게 증가하였다.

이상의 결과로부터, 본 시험조건에서 시험물질 α-iso-cubebenol의 유전자돌연변이 유발성은 없는 것으로 판단된다.

(3) α-iso-cubebenol의 포유류 배양세포를 이용한 염색체이상시험

시험물질 α-iso-cubebenol의 염색체이상 유발성을 포유류 배양세포주 (Chinese Hamster Lung (CHL/IU) cell line)를 사용하여 검토하였다.

본시험의 최고용량을 설정하기 위해, 5,000 μg/mL을 최고용량으로 하고, 이하 2,500, 1,000, 500, 250, 100, 50, 10 및 5 μg/mL의 용량으로 세포증식억제시험을 실시한 결과, 단시간처리법의 대사활성화 비존재하 및 존재하, 연속처리법의 대사활성화 비존재하에서 세포독성이 관찰되어, 50% 세포증식억제용량 (Inhibition concentration 50%: IC50)을 산출한 결과, 단시간처리법의 대사활성화 비존재 하에서는 29.5 μg/mL, 대사활성화 존재하에서는 167.0 μg/mL, 연속처리법의 대사활성화 비존재 하에서는 28.0 μg/mL이었다.

따라서 , 본시험의 용량은 아래와 같이 설정하였다. 단시간처리법의 대사활성화 비존재하 및 연속처리법의 대사활성화 비존재 하에서는 IC 50 근처에서 급격한 세포독성이 관찰되었기 때문에 200 개의 분열중기상 세포를 관찰할 수 있는 3용량을 확보하기 위해 이하 공비 2로 4용량의 용량의 시험물질군을 설정하였다. 또한 , 각각의 처리계열에 대해 음성대조군 및 양성대조군을 설정하였다.

계열	S9 mix	본시험의 용량 (μg/plate)
단시간처리법	-	30.0, 15.0, 7.50, 3.75, 1.88
	+	170, 85.0, 42.5, 21.3
연속처리법	-	28.0, 14.0, 7.00, 3.50, 1.75

본시험의 결과 , 단시간처리법의 대사활성화비존재 하 및 존재 하, 연속처리법의 대사활성화비존재하의 모든 처리계열에서 염색체이상을 가진 세포의 출현빈도는 5% 미만으로 염색체이상 유발 작용은 확인되지 않았으며, 음성대조군과 비교하여 통계학적으로 유의한 차이도 관찰되지 않았다.

각 처리계열의 양성대조군에서는 구조이상을 가진 세포의 출현빈도가 음성대조군과 비교시 통계학적 유의 하게 증가되었다.

이상의 결과로부터 본 시험조건 하에서 시험물질인 α-iso-cubebenol은 염색체이상을 유발하지 않는 것으로 판단된다.

(4) α-iso-cubebenol의 Sprague-Dawley 랫드를 이용한 단회 경구투여 독성시험

본 시험은 시험물질인 α-iso-cubebenol을 Sprague-Dawley계 암수 6주령 랫드에 단회 경구투여시 나타나는 독성을 평가하고, 개략의 치사량을 구하기 위하여 실시하였다.

군구성은 시험물질 2,000 및 1,500 mg/kg의 용량 및 대조군(corn oil)의 3군으로 하고, 암수 각각 5 마리씩 단회 경구투여 하였다. 투여 후 14일 동안, 일반증상의 관찰 및 체중측정을 실시하였고, 관찰기간 종료 시에 안락사시켜 부검하였다.

암수 1,500 및 2,000 mg/kg 투여군에서 사망례는 관찰되지 않았다. 일반증상에서는 암수 1,500 mg/kg 투여군에서 투여당일 또는 투여 후 1일에 유연 또는 점액변이 관찰되었고, 암수 2,000 mg/kg 투여군에서 투여당일 또는 투여 후 1일에 유연, 점액변, 보행이상 또는 하복부의 오염이 관찰되었으나, 투여 후 2일부터는 일반증상의 이상은 관찰되지 않았다. 체중 및 부검에서 시험물질 투여에 의한 영향은 인정되지 않았다.

본 시험의 조건 하에서 α-iso-cubebenol을 랫드에 단회 경구투여한 결과, 개략의 치사량은 암수 모두 2,000 mg/kg을 상회하는 것으로 판단된다.

(5) α-iso-cubebenol의 토끼를 이용한 피부자극시험

시험물질 α-iso-cubebenol의 피부자극시험을 11주령의 수컷 NZW 토끼 6마리를 사용해서 검토하였다.

토끼의 경배부위에 좌우 각 2부위, 합 4부위의 투여부위를 설정하고, 그 중 2부위를 비찰과부위, 그 외 2부위를 찰과부위로 하였다. 시험물질원액 0.5 mL를 각각의 비찰과 및 찰과부위의 시험물질투여부위에 적용하여 24시간 폐색첩포하였다. 투여 후 24, 48 및 72시간에 'Draize의 피부반응 평가표1)'에 따라서 피부반응을 평가하고, 투여 후 24 및 72시간에 대한 1차피부자극지수(Primary Skin Irritation Index, P.I.I.)를 구하여 피부자극성을 판정하였다.

시험물질투여부위의 비찰과 및 찰과부위에서 투여 후 24시간에 모든 동물에서 홍반(평점 3)이, 투여 후 48 및 72시간에는 모든 동물에서 홍반(평점 2)이 관찰되었다. 시험물질의 1차피부자극지수(P.I.I.)는 '2.5'로, 자극정도는 '중등도 자극성(Moderately irritant)'으로 분류되었다.

무처치대조부위의 비찰과 및 찰과부위에서는 모든 관찰시간에 홍반 및 부종등의 피부반응은 모든 동물에서 관찰되지 않았다.

관찰기간 중, 모든 동물에서 일반증상 및 체중에 이상은 확인되지 않았다.

이상의 결과로부터, 본 시험 조건하에서 시험물질 α-iso-cubebenol은 토끼의 피부에 대해서 '중등도 자극성'이 있는 물질로 판단된다.

(6) α-iso-cubebenol의 토끼를 이용한 안점막자극시험

시험물질 α-iso-cubebenol의 안자극시험을 11주령의 수컷 NZW 토끼 9마리를 사용해서 검토하였다.

비세안군은 토끼 6마리의 우안 결막낭 내에 시험물질원액 0.1 mL를 투여하고, 투여 1, 2, 3, 4 및 7일에 각막, 홍채 및 결막 등의 안구병변을 관찰하였다. 세안군은 별도의 3마리의 토끼를 사용해서 비세안군과 동일하게 투여하고, 투여 30초 후에 세안한 후, 세안효과를 확인하였다. 'Draize의 안구병변의 등급1)'에 따라서 시험물질의 안점막자극을 평가하고, Guillot의 '안점막자극 평가표2)'를 참조해서 안점막자극의 정도를 분류하였다.

비세안군에서 시험물질의 투여 1, 2, 3, 4 및 7일에 각막, 홍채 및 결막 등의 안구병변은 모든 동물에서 관찰되지 않았다. 비세안군의 I.A.O.I. (Index of Acute Ocular Irritation)는 '0'으로, 자극정도는 '무자극물'로 분류되었다.

세안군에서는 모든 관찰시간에 안구병변은 모든 동물에서 관찰되지 않았다.

관찰기간 중, 각 군의 모든 동물에서 일반증상 및 체중에 이상은 확인되지 않았다.

이상의 결과로부터, α-iso-cubebenol은 토끼의 안에 대해서 자극성이 없는 것으로 판단된다.

(7) LC/MS/MS법을 이용한 랫드 및 비글견 혈장중 α-iso-cubebenol 분석법 개발 및 검증

이 연구의 목적은 랫드와 비글견 혈장에서 α-iso-cubebenol 정량을 위한 생체시료분석법을 개발하는데 있다. 이 연구에서 최우선 순위로 있는 것은 측정하고자 하는 물질이 앞서 보고된 "LC/MS/MS를 이용한 랫드 및 비글견 혈장중 α-iso-cubebenol의 분석법 개발을 위한 타당성시험 (Study No. S12076/S12077)"에서 electrospray ionization (ESI) 및 atmospheric pressure chemical ionization (APCI)에 의한 이온화가 되지 않았기 때문에 유도체화를 하여 이온화될 수 있는 조건을 개발하는 것이었다.

측정물질 α-iso-cubebenol의 구조로 부터 hydroxyl group과 화학적으로 반응성 있는 3-nitrophthalic anhydride (NPA)를 유도체화 시약으로 사용하였다. 유도체화 반응 요소에 대해 최적화를 수행하였고 α-iso-cubebenol-NPA를 negative mode에서 multiple reaction monitoring 방법을 이용하여 최적화 하였다. 내부표준물질은 mefenamic acid로서 유도체화 없이 사용하였다.

분석컬럼은 XBridge Shield RP18 column (2.1 mm ×50 mm, 3.5 μm, Waters, USA)으로 40oC 의 온도조건에서 사용하였다. 이동상 A는 0.1% formic acid, 이동상 B는 0.1% formic acid in acetonitile로 B가 65% (35/65, v/v) 로 유지되도록 isocratic 조건으로 하였다. 유속은0.4 mL/min으로 하였다. Mass spectrometer는 negative ESI mode로 수행하였다.

랫드 및 비글견 혈장시료는 n-hexane/ethanol (97:3, v/v) 용매로 추출하고 40oC 온도조건의 질소 기류하에서 증발건조 시켰다. 유도체화 완료후에 유도체화 용액을 건조시켰다. 건조후 남은 잔사에 메탄올과 산성 버퍼를 첨가하여 재용해하고, 산성조건 하에서 n-hexane/ethanol (97:3, v/v)용매로 추출하였다. 유기용매 상층액을 40oC 온도조건의 질소기류하에서 증발건조 시켰다. 남은 잔사는 이동상(A:B, 35:80, v/v)으로 재용해하고, LC/MS/MS에 5 μL 주입하였다.

LC조건과 전처리 조건을 최적화 후에 생체시료분석법의 부분 밸리데이션을 수행하였다. 랫드와 비글견 혈장중 검량선은 10~2000ng/mL 정량범위에서 양호한 직선성을 나타내었

다. 그러나 품질관리시료를 이용한 배치내 재현성 시험에서는 정확성과 정밀성이 시험기준을 만족시키지는 못했다. 이 시험방법에서 재현성이 좋지 않은 것은 유도체화 방법이 양호하지 않다는 것과 적절한 내부표준물질로 유도체화를 시키는 것이 필요하다고 생각되었다.

내부표준물질 후보는 구조적으로 hydroxyl group이 있고, α-iso-cubebenol-NPA와 유사한 소수성을 지닌 물질이 필요하다고 판단되어 1-pentadecanol을 내부표준물질로 선택하여 유도체화하는 것으로 선택하였다. 내부표준물질을 이용하여 유도체화 조건을 확인하는 것으로 진행하고 있으나, 적절한 내부표준물질의 합성이 불가능하여 차선의 물질로서 선정이 필요할 수 있다. 또한 Taget 분석 물질의 물질특성으로 인해 전반적 물질 분석의 분석법 개발 및 검증에 어려움이 있어 추후 변경 될 수 있다.

라. EC-18을 대상으로 한 비임상시험

(1) EC-18의 랫드를 이용한 13주 반복 경구투여 독성시험

본 시험은 EC-18을 Sprague-Dawley (Crl:CD(SD))계 암수 랫드에 13주간 반복 경구투여시 나타나는 독성반응과 그 안전성을 평가하기 위하여 실시하였다.

시험물질은 500, 1,000 및 2,000 mg/kg/day의 3개 용량으로 군당 암수 각 10마리에 13주간 경구투여하였다. 또한, 부형제 (Olive oil)를 투여하는 대조군을 설정하여 군당 10마리에 13주간 경구 투여하였다.

관찰기간 동안 일반증상관찰, 체중측정, 사료섭취량 측정, 안과학적 검사 및 뇨검사를 실시하였고, 관찰기간 종료 후 혈액 및 혈액생화학적 검사, 장기의 중량, 부검 시 육안적 검사 및 조직병리학적 검사를 수행하였다.

관찰기간 동안, 암수 시험물질 투여군 모두에서 일반증상에서의 이상 및 사망례는 관찰되지 않았다.

체중, 사료섭취량, 안과학적 검사, 뇨검사, 혈액학적 검사, 혈액생화학적 검사, 장기중량, 부검소견 및 조직병리학적 검사에 있어서, 암수 시험물질 투여군에서 시험물질 투여에 기인한 독성학적인 변화는 관찰되지 않았다.

본 시험 조건하에서 EC-18을 500, 1,000 및 2,000 mg/kg/day로 암수 랫드에 13주간 반복 경구투여한 결과, 독성학적으로 의미 있는 변화가 관찰되지 않았기에 무독성량(NOAEL)은 암수 모두 2,000 mg/kg/day를 상회하는 것으로 판단한다.

(2) EC-18의 비글견을 이용한 13주 반복 경구투여 독성시험, 4주 회복시험 및 독성동태시험

본 시험은 군당 암수 각 3 마리의 비글견을 이용하여 시험물질인 EC-18을 0 (대조군), 500, 1,000 및2,000 mg/kg/day의 용량으로 13주간 반복 경구투여 시 나타나는 독성반응과 그 안전성을 평가하고, 대조군과 고용량군에 암수 각 군당 2마리씩 4주간의 회복군을 설정하여 독성변화의 가역성 여부를 확인하였으며, 독성동태시험을 통해 약물의 전신노출도를 평가하기 위하여 실시하였다

실험기간 중, 암수 모두에서 사망동물은 발생하지 않았으며, 암수 모든 시험물질투여군에서 시험물질에 의한 회백변이 용량의존적으로 빈번하게 관찰된 것을 제외하고, 시험물질의 투여에 의한 이상증상은 관찰되지 않았다. 그 외, 체중, 사료섭취량, 안검사, 심전도검사, 뇨검사, 혈액학적 및 혈액생화학적 검사, 장기중량, 부검 및 조직병리학적 검사에

서 이상 변화는 관찰되지 않았다.

투여 13주 (투여 91일)에 실시한 독성동태시험에서 EC-18의 전신노출도 (AUClast, Cmax)는 암수 모두 비례적이지는 않지만 용량의 증가에 따라 증가하였으나, 암컷 2,000 mg/kg/day 투여군에서는 1,000 mg/kg/day 투여군과 유사하였으며, 500 및 1,000 mg/kg/day 투여군에서는 암컷이 수컷보다 전신노출도가 높은 경향을 보였다. 그 외, 반복투여에 의한 축적현상은 없는 것으로 판단되며, Tmax는 개체에 따라 1~2시간 또는 8~12시간으로 나타났다.

이상의 결과에 의해, 본 시험조건 하에 암수 비글견에 대한 무독성량 (NOAEL)은 2,000 mg/kg/day를 상회하는 것으로 판단된다.

(3) EC-18의 비글견을 이용한 13주 반복 경구투여 독성시험, 4주 회복시험 및 독성동태시험

본 시험은 군당 암수 각 3 마리의 비글견을 이용하여 시험물질인 EC-18을 0 (대조군), 500, 1,000 및2,000 mg/kg/day의 용량으로 13주간 반복 경구투여 시 나타나는 독성반응과 그 안전성을 평가하고, 대조군과 고용량군에 암수 각 군당 2마리씩 4주간의 회복군을 설정하여 독성변화의 가역성 여부를 확인하였으며, 독성동태시험을 통해 약물의 전신노출도를 평가하기 위하여 실시하였다

실험기간 중, 암수 모두에서 사망동물은 발생하지 않았으며, 암수 모든 시험물질투여군에서 시험물질에 의한 회백변이 용량의존적으로 빈번하게 관찰된 것을 제외하고, 시험물질의 투여에 의한 이상증상은 관찰되지 않았다. 그 외, 체중, 사료섭취량, 안검사, 심전도검사, 뇨검사, 혈액학적 및 혈액생화학적 검사, 장기중량, 부검 및 조직병리학적 검사에서 이상 변화는 관찰되지 않았다.

투여 13주 (투여 91일)에 실시한 독성동태시험에서 EC-18의 전신노출도 (AUClast, Cmax)는 암수 모두 비례적이지는 않지만 용량의 증가에 따라 증가하였으나, 암컷 2,000 mg/kg/day 투여군에서는 1,000 mg/kg/day 투여군과 유사하였으며, 500 및 1,000 mg/kg/day 투여군에서는 암컷이 수컷보다 전신노출도가 높은 경향을 보였다. 그 외, 반복투여에 의한 축적현상은 없는 것으로 판단되며, Tmax는 개체에 따라 1~2시간 또는 8~12시간으로 나타났다.

이상의 결과에 의해, 본 시험조건 하에 암수 비글견에 대한 무독성량 (NOAEL)은 2,000 mg/kg/day를 상회하는 것으로 판단된다.

(4) EC-18의 단회 경구투여에 의한 랫드의 중추신경계에 미치는 영향 평가시험

본 시험은 6 주령의 수컷 Sprague-Dawley 랫드에 시험물질인 EC-18을 단회 경구투여하였고, 기능관찰시험 (Functional observational battery, FOB)을 실시하여 중추신경계에 미치는 영향을 평가하였다.

군구성은 대조군과 500, 1,000 및 2,000 mg/kg 용량의 시험물질투여군의 총 4 군으로 설정하여 각 군당 8 마리씩 투여하였고, 대조군은 부형제인 olive oil을 투여하였다.

기능관찰시험의 home cage 내에서의 관찰, open field 내에서의 관찰, hand held 하에서의 관찰, 감각•운동기능검사 및 체온측정은 투여 전 (pre), 투여 후 0.5, 1, 3, 6 및 24 시간째에 실시하였다.

500, 1,000 및 2,000 mg/kg 용량의 시험물질투여군은 기능관찰시험의 모든 parameters에서 시험물질의 투여에 의한 변화는 관찰되지 않았다.

결론적으로 랫드를 이용한 단회 경구투여에서, 시험물질인 EC-18은 500, 1,000 및 2,000

mg/kg 용량에서 중추신경계에 미치는 영향이 없는 것으로 판단된다.

<Functional observational battery, FOB>

(5) EC-18의 누드마우스에 이식된 인체 유래의 골수암 세포주 RPMI 8226에 대한 항암시험

본 시험은 인체 유래의 골수암 세포주인 RPMI 8226 세포가 이식된 수컷 누드마우스에 시험물질인 EC-18 을 경구투여 한 후 종양의 성장 억제 효과를 평가하고자 실시하였다. 군구성은 음성대조군, 125, 500 및 2,000 mg/kg 용량의 시험물질투여군 및 120 mg/kg 용량의 양성대조군으로 각 군당 10 마리씩 총 5 군으로 설정하였다.음성대조군은 부형제인 olive oil 을, 시험물질투여군은 EC-18 을, 양성대조군은 젬시타빈(Gemcitabine)을 1 일 1 회, 5 주간, 총 32 회 위내에 강제투여하였고, 투여 후 33 일째까지 관찰하였다.

관찰기간 동안 매일 1 회 일반증상을 관찰하였고, 동물의 체중 및 종양의 부피는 주 2 회 측정하였다. 관찰기간 종료 일에 종양을 적출하여 종양의 중량을 측정하였다. 종양의 부피측정에서, 500 mg/kg 용량의 시험물질투여군의 일부 측정시점에서 음성대조군과 비교하여 유의하게 억제 되었으나, 125 및 2,000 mg/kg 용량에서는 모든 측정시점에서 통계학적으로 유의한 차이를 나타내지 않았다.

종양의 중량측정에서, 125, 500 및 2,000 mg/kg 용량의 시험물질투여군은 음성대조군과 비교하여 통계학적으로 유의한 차이를 나타내지 않았다.

양성대조군의 종양의 부피는 일부 측정시점에서 음성대조군과 비교하여 유의 ($p<0.05$)하게 억제되었고, 종양의 중량은 음성대조군과 비교하여 작게 측정되는 경향을 나타냈다.

일반증상관찰 및 체중측정 결과, 모든 투여군에서 각 물질의 투여에 의한 이상소견 및 사망례는 관찰되지 않았다.

결론적으로, 누드마우스에 이식된 인체 유래의 골수암 세포주인 RPMI 8226 에 대한 항암효능시험에서, 시험물질인 EC-18 은 종양의 성장을 억제하는 효과가 없는 것으로 판단된다.

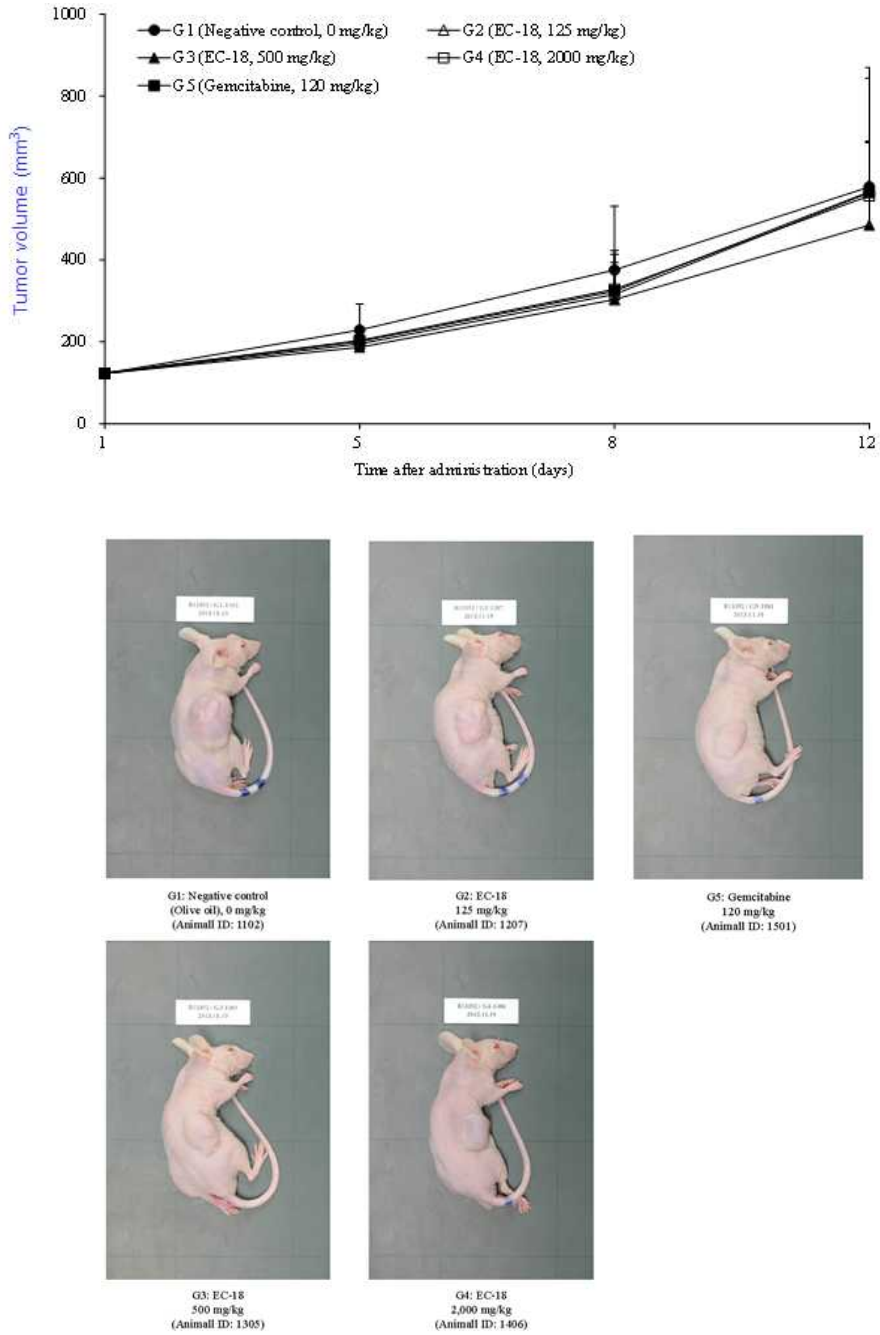

Photograph 1. Photograph of RPMI 8226 tumor-bearing nude mice at the end of obserbation period

G3: EC-18

500 mg/kg

G4: EC-18

2,000 mg/kg

G5: Gemcitabine

120 mg/kg

Photograph 2. Photograph of tumors removed from RPMI 8226 tumor-bearing nude mice at the end of observation

(6) EC-18의 collagen으로 유발된 DBA/1J 마우스의 관절염에 대한 효능시험

본 시험은 수컷 DBA/1J 마우스에 bovine type II collagen을 투여하여 관절염을 유발한 후, 시험물질인 EC-18을 반복 경구투여하여 관절염에 대한 개선효능을 평가하고자 실시하였다. 동시에 양성대조물질1인 레미케미드는 반복 복강투여하고, 양성대조물질2인 메토트렉세이트를 반복 경구투여하여 비교하였다.

군구성은 정상대조군, 음성대조군, 125, 500 및 2,000 mg/kg 용량의 시험물질투여군, 20 mg/kg 용량의 양성대조군1 및 2.5 mg/kg 용량의 양성대조군2의 총 7군으로 각 군당 10마리씩 설정하였다.

정상대조군 및 음성대조군은 부형제1인 olive oil을, 125, 500 및 2,000 mg/kg 용량의 시험물질투여군은 EC-18을, 양성대조군1은 remicade를, 양성대조군2는 methotrexate를 1일1회, 5주간, 총 35 회 양성대조군1은 복강투여를, 그 외 나머지 투여군은 위내에 강제투여하였다.

정상대조군으로 사용하기 위하여 관절염을 유발하지 않은 동물을 제외한 모든 동물은 bovine type II collagen과 complete Freund's adjuvant 또는 incomplete Freund's adjuvant를 유화한 emulsion으로 총 2 회 immunization하여 관절염을 유발하였다.

관찰기간 동안 매일 1회 일반증상 관찰, 주1회 체중측정, 주2회 육안적 관절염지수 평가 및 주2회 발등두께 측정을 실시하였다. 조직적출일에 채취한 혈청에서 interleukin-6 및 anti-type II collagen IgG의 농도를 측정하였고, 양쪽 뒷다리의 무릎관절을 적출하여 관절염 증상에 대한 조직병리학적 검사를 실시하였다.

정상대조군과 비교하여 음성대조군은 관절염 평가항목인 육안적 관절염지수, 발등두께, 혈중 interleukin-6 (IL-6) 및 anti-type II collagen (anti-CII) IgG 농도 및 조직병리학적 관절염점수가 유의하게 증가하여 관절염 모델이 확립된 것으로 확인되었다.

125 mg/kg 용량의 시험물질투여군은 발등두께, 조직병리학적 관절염점수 및 혈중 IL-6, anti-CII IgG 농도는 음성대조군과 비교하여 유의한 차이는 나타나지 않았으나, 감소하는 경향을 나타냈고, 가장 중요한 평가항목인 육안적 관절염지수에서 음성대조군과 비교하여 유의하게 감소하였다.

500 및 2,000 mg/kg 용량의 시험물질투여군은 발등두께, 조직병리학적 관절염점수 및 혈중 Anti-CII IgG의 농도는 음성대조군과 비교하여 유의한 차이는 나타나지 않았으나, 감소하는 경향을 나타냈고, 육안적 관절염 지수와 혈중 IL-6 농도에서 음성대조군과 비교하여 유의하게 감소하였다.

20 mg/kg 용량의 양성대조군1 및 2.5 mg/kg 용량의 양성대조군2는 발등두께, 조직병리학적 관절염점수 및 혈중 anti-CII IgG의 농도는 음성대조군과 비교하여 유의한 차이는 나타나지 않았으나, 감소하는 경향을 나타내었고, 가장 중요한 평가항목인 육안적 관절염 지수와 혈중 IL-6 농도에서 음성대조군과 비교하여 유의하게 감소하였다.

결론적으로, 본 시험에서 DBA/1J 마우스에 bovine type II collagen으로 유발된 관절염에 대하여 시험물질인 EC-18은 125, 500 및 2,000 mg/kg 용량에서 관절염증상을 개선시키는 효능이 있는 것으로 판단된다.

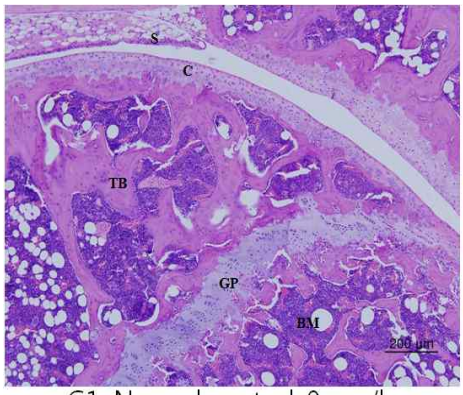

G1: Normal control, 0 mg/kg

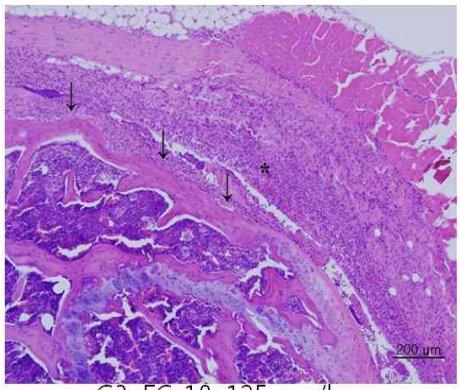

G3: EC-18, 125 mg/kg

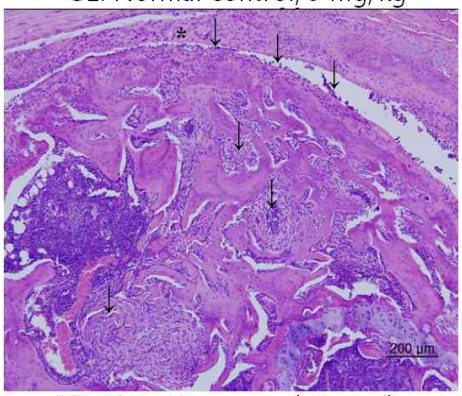

G2: Negative control, 0 mg/kg

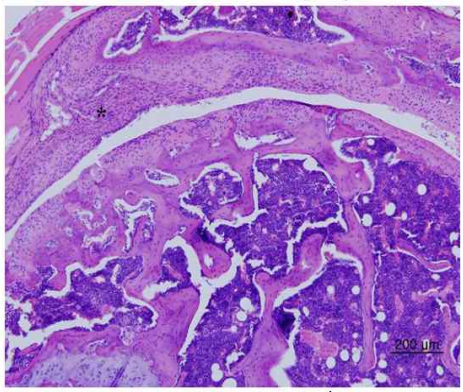

G4: EC-18, 500 mg/kg

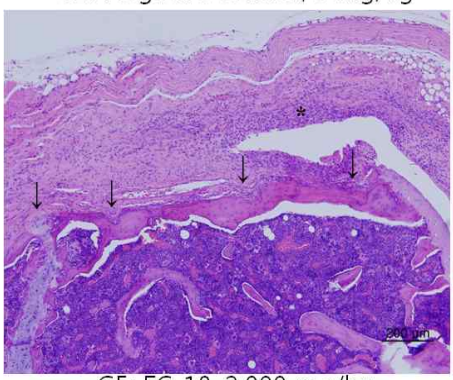

G5: EC-18, 2,000 mg/kg

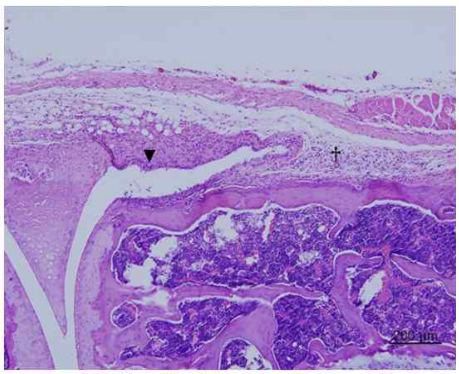

G7: Methotrexate, 2.5 mg/kg

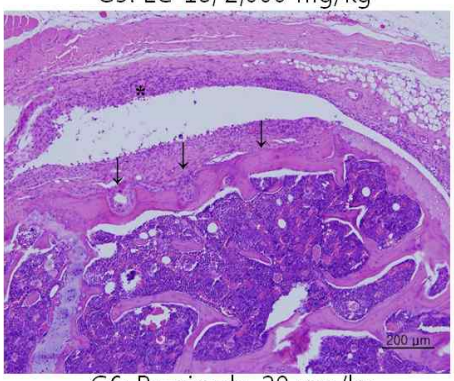

G6: Remicade, 20 mg/kg

S: synovial membrane,

C: cartilage, TB: trabecular bone,

GP: growth plate, BM: bone marrow

Arrow (↓: Articular cartilage destruction and bone erosion, Star (*): Pannus

Arrow head (▼: hyperplasia of the synovial membrane, Cross(†): polymorphonuclear cell infiltration

Representative Observation of Arthritic Severity (H&E stain, × 100)

(7) EC-18의 랫드를 이용한 경구투여 배태자 발생독성시험

본 시험은 임신한 Sprague-Dawley 랫드를 이용하여 시험물질인 EC-18을 착상부터 경구개가 폐쇄되는 시기 (임신 7 ~ 17 일)까지 경구투여하여 임신모체 및 배·태자의 발생에 미치는 영향을 관찰하고, 그 안전성을 평가하기 위해서 실시하였다.

관찰기간 중, 암수 모든 시험군에서 사망례는 관찰되지 않았으며, 일반증상, 체중, 사료섭취량, 장기중량 및 부검 등 검사에서도 시험물질에 의한 영향은 관찰되지 않았다. 또한, 제왕절개 성적, 생존태자의 체중 및 태반중량, 외표, 내장, 골격 및 골화도 등의 검사에서도 시험물질에 의한 영향으로 판단되는 변화는 관찰되지 않았다. , 본 시험 조건하에 임신모체 및 배•태자의 발생에 대한 무독성량 (NOAEL)은 2,000 mg/kg으로 판단된다.

(8) EC-18의 랫드를 이용한 경구투여 수태능 및 초기배 발생독성시험

암수 Sprague-Dawley 랫드를 EC-18를 수컷은 교배 전 4주부터 부검 시까지, 암 컷은 교배 전 2주부터 착상 시기까지 경구투여하여 수태능 초기배 , 그 안전성을 평가하기 위하여 실시하였으며, 수컷 7주령부터 9주간(약 62일), 암컷 8주령부터 7 일까지(약 28 ~ 37일) 경구투여(투여용량, 대조군, 500, 1,000 및 2,000 mg/kg/day) 하였다.

암컷 대조군과 500 및 2,000 mg/kg/day 투여군에서 1례씩 , 수컷에서 이상증상은 관찰되지 않았다. 체중은 암수 체중변화는 대조군 및 시험물질투여군에서 용량의존적인 변화가 관찰되지 않았으며, 사료섭취량에서도 대조군 및 시험물질투여군에서 용량의존적인 변화가 관찰되지 않았다. 또한 교배성적면에서 군당 22마리의 수컷과 암컷을 교배시켜 본 결과 대조군과 저, 중 및 고용량군에서 용량의존적인 차이는 관찰되지 않았다.(교미율(%) 각각 95.5, 100, 100 및 100이고 수컷 및 암컷의 수태율(%)은 각각 100, 100, 100 및 100, 군평균 교배기간(일)은 각각 2.7, 2.2, 1.7 및 1.8일). 착상률 및 배자사망률은 임신 15일 제왕절개 결과, 대조군과 저, 중 및 고용량군에서 용량의존적인 차이는 관찰되지 않았다. (착상률(%) 각각 84.4, 80.7, 85.1 및 82.7, 배자사망률(%) 각각 4.2, 4.2, 7.2 및 4.7)

마. Gomisin J를 대상으로 한 비임상시험

(1) LC/MS/MS를 이용한 랫드 및 비글견 혈장 중 Gomisin J의 분석법 개발

랫드와 비글견 혈장중에서 gomisin J와 내부표준물질인 glimepiride는 액-액 추출법으로 추출하고 LC/MS/MS로 측정하였다. 랫드 및 비글견 혈장중 gomisin J의 측정은 2~1,000 ng/mL의 검량범위에서 양호한 직선성을 보였다. 랫드 혈장중 최저정량한계에서 일내정밀성 및 정확성은 5.5% 및 101.7%이었고, 그 이외 농도에서는 일내 정밀성은 2.7% ~ 6.6%이었고, 정확성은 92.8% ~ 94.0%이었다. 비글견 혈장중 최저정량한계에서는 일내 정밀성 및 정확성은 6.7% 및 84.8% 이었고, 그 이외 농도에서는 일내 정밀성은 3.0% ~ 14.6% 이었고, 정확성은 102.1% ~ 103.7%이었다.

생체시료분석에 관한 상세사항은 하기에 나타내었다.

상기의 결과는 랫드와 비글견 혈장중 gomisin J에 대해 개발된 생체시료분석법은 경량범이 2 ~ 1,000 ng/mL에서 양호한 직선성과 재현성 있는 결과를 나타내었음을 확인하였다. 따라서 개발된 생체시료분석법은 벨리데이션 시험에 적용할 수 있다.

LC/MS/MS	Prominence, API4000 (No. 7)
LC column	PRODIGY ODS-3, 2 mm i.d. × 50 mm, 5 μm Phenomenex Inc.
Column temperature	40°C
Mobile Phase	Mobile phase A: 10 mM ammonium formate in 0.1% formic acid Mobile phase B: Methanol Isocratic 70%B
Flow rate	0.3 mL/min
Retantion Time	Gomisin J: approximately 1.4 min
	Glimepiride: approximately 2.1 min
Injection volume	10 μL
Ionization Mode	SRM positive ionization mode
Monitor ions	Gomisin J: *m/z* 389 to 287
	Glimepiride: *m/z* 492 to 352
Calibration Range	2 to 1,000 ng/mL
Weighting Factor	1/X
Internal Standard	Glimepiride
Biological Matrix	Rat and beagle dog plasma
Anticoagulant	Heparin Sodium
Sampling Volume	50 μL
Pretreatment Method	Liquid-liquid extraction

(2) LC/MS/MS를 이용한 랫드 혈장 중 Gomisin J의 분석법 Validation

본 시험에서는 Liquid Chromatography/Tandem Mass Spectrometry (이하 LC/MS/MS)를 이용하여 랫드 혈장 중 Gomisin J의 분석방법에 대한 유효성 검증 (이하 validation)을 실시하였다.

랫드 혈장 중 Gomisin J의 농도 측정을 위해 Glimepiride 를 내부표준물질로 사용하였으며, 랫드 혈장 50 μL로부터 Gomisin J와 내부표준물질을 tert-butyl methyl ether로 추출한 후 LC/MS/MS로 측정하였다.

아래 표에 validation 항목 및 결과를 요약하였으며, 본 기관에서 확인한 분석방법은 랫드 혈장 중 Gomisin J의 농도 측정에 적용 가능하다고 판단된다.

Validation items	Classifications	Results	
Carryover effect	Gomisin J	No carryover effect	
	Glimepiride	No carryover effect	
Selectivity	Gomisin J	No interfering peak	
	Glimepiride	No interfering peak	
Matrix effect	Gomisin J	Matrix effect	59.0% and 71.7%
	(6 and 800 ng/mL)	Precision	1.5% and 4.4%
	Glimepiride	Matrix effect	92.9%
	(60 ng/mL)	Precision	0.9%
Recovery	Gomisin J	Recovery	48.9%, 63.1% and 57.7%
	(6, 80 and 800 ng/mL)	Precision	12.7%
	Glimepiride (60 ng/mL)	Recovery	7.2%
Linearity of	Gomisin J 2 to 1000 ng/mL, 1/X	Correlation	0.9970 to 0.9999

calibration curve and quantification range			coefficient	
		LLOQ (2 ng/mL)	Accuracy	94.0% to 119.8%
		Other concentrations (5 to 1000 ng/mL)	Accuracy	88.2% to 112.3%
Intra-assay	Gomisin J	LLOQ	Accuracy	99.4%
		(2 ng/mL)	Precision	5.9%
		Low, Mid and High	Accuracy	97.6%, 87.1% and 91.1%
		(6, 80 and 800 ng/mL)	Precision	1.9%, 2.5% and 4.1%
Inter-assay	Gomisin J	LLOQ	Accuracy	99.0%
		(2 ng/mL)	Precision	8.9%
		Low, Mid and High	Accuracy	94.2%,92.2% and 93.7%
		(6, 80 and 800 ng/mL)	Precision	5.2%, 5.7% and 4.4%
Dilution reproducibility	Gomisin J	2-fold dilution	Accuracy	97.2%
		(1500 ng/mL)	Precision	2.8%
Stability in plasma	Gomisin J	Initial sample	Accuracy	97.6% and 91.1%
		(6 and 800 ng/mL)	Precision	1.9% and 4.1%
		Short-term temperature stability	Accuracy	102.4% and 93.6%
		(21.4 to 23.2°C, 4 hrs)	Precision	14.3% and 7.6%
		Long-term stability	Accuracy	88.8% and 95.4%
		(-72.2 to -60.9°C, 35 days)	Precision	7.0% and 3.6%
		Long-term stability	Accuracy	102.4% and 93.6%
		(-72.2 to -60.9°C,38 days)	Precision	14.3% and 7.6%
		Freeze /thawcycle stability	Accuracy	92.5% and 99.0%
		(5 cycles)	Precision	3.4% and 3.3%
		Processed sample in autosampler	Accuracy	112.5% and 114.4%
		(10°C, 27.5 hrs)	Precision	4.7% and 2.3%
Stability in stock solution	Gomisin J	Initial sample	Precision	9.3%
		Room temperature	Residual	100.3%
		(20.4 to 22.8°C, 6 hrs)	Precision	10.2%
		Refrigeration	Residual	90.1%
		(4.0 to 4.9°C, 34 days)	Precision	14.5%
	Glimepiride	Initial sample	Precision	9.8%

		Room temperature (20.4 to 22.8°C, 6 hrs)	Residual	103.8%
			Precision	8.8%
		Refrigeration (4.0 to 4.9°C, 34 days)	Residual	114.7%
			Precision	4.6%
Stability in working solution	Gomisin J	Initial sample	Precision	9.3%
		Room temperature (20.4 to 22.8°C, 6 hrs)	Residual	101.0%
			Precision	5.9%
		Refrigeration (4.0 to 4.9°C, 34 days)	Residual	92.3%
			Precision	5.3%
	Glimepiride	Initial sample	Precision	9.8%
		Room temperature (20.4 to 22.8°C, 6 hrs)	Residual	94.4%
			Precision	11.5%
		Refrigeration (4.0 to 4.9°C, 34 days)	Residual	85.5%
			Precision	12.7%

(3) LC/MS/MS를 이용한 랫드 및 비글견 혈장중 Gomisin J의 분석법 개발을 위한 타당성 시험

랫드와 비글견 혈장에서 gomisin J에 대한 생체시료분석법 개발의 타당성을 확인하였다. Gomisin J와 내부표준물질로서 사용된 sildenail 의 MS/MS이온화 및 LC 용출조건에 대한 분석법 최적화를 실시하였다. 분석조건의 상세사항은 아래표에 정리하였다.

LC/MS/MS	Prominence, API4000 (No. 7)
LC column	PRODIGY ODS-3, 2 mm i.d. × 50 mm, 5 μm
Column temperature	40°C
Mobile Phase	Mobile phase A: Water Mobile phase B: Methanol Isocratic mode, 70%B
Flow rate	0.2 mL/min
Retention Time	Gomisin J: approximately 2.2 min
	Sildenafil: approximately 1.9 min
Injection volume	10 μL
Ionization Mode	SRM positive ionization mode
Monitor ions	Gomisin J: *m/z* 389 to 357, 389 to 325, 389 to 287, 389 to 227
	Sildenafil: *m/z*: 475 to 283, 475 to 100, 475 to 58

최적화 조건에서 LC/MS/MS 장치로 2.5 pg의 gomisin J를 측정하였다. 측정된 2.5 pg의 양은 랫드와 비글 혈장량을 20 μL 샘플링하여 전처리한 시료 100 μL 중 10 μL를 주입하였을 때 회수율과 생체시료영향을 배제의 경우로 산정시 1.25 ng/mL로 예상되었다. 따라서 생체시료분석법 개발은 최적화된 LC/MS/MS조건에 따라 실시될 수 있다.

2절. 제1협동. 질환 동물 개발 및 효력시험 연구

1. 연구내용

가. 질환모델동물개발 : 주요 5대 질환의 모델동물을 개발하여 질환 관련 특성을 분석하고, 신약 유효성을 테스트 할 수 있는 질병 관련 인자들을 확인하여 모델동물로서 유효한 사용 가능성을 연구하였다.

(1) 심순환 질환 모델동물 개발 : ASC-2 GEM 마우스 개발

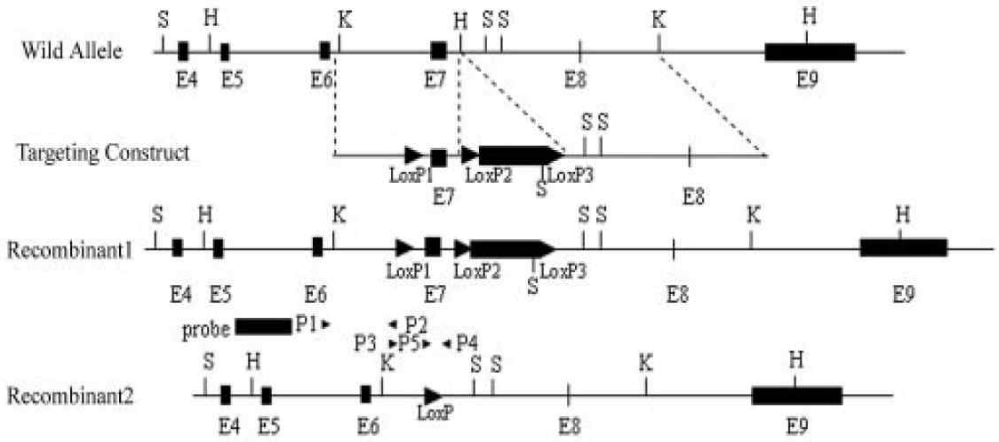

<Disruption of mouse Asc-2 gene>

(가) Germ-line mutation에 의한 Asc-2의 결핍은 심장을 포함한 다양한 organ에서 문제를 일으킴. Germ-line mutation에 의한 Asc-2의 결핍은 마우스에서 embryonic lethality를 유발함. Germ-line Asc-2 결핍에 의한 embryonic lethality를 피하고, 성체에서만 심장 특이적으로 Asc-2를 제거하기 위해서 alpha-MHC-Cre transgenic 마우스를 이용해 Asc-2f/f:alpha-MHC-Cre TG의 genotype을 갖는 마우스를 만듦으로써 심장질환 모델 마우스를 생산

(나) 심장질환의 생체 내 연구를 가능하게 하는 심장질환동물모델의 유의성 있는 개체수를 확보하고 ASC-2 GEM 마우스에서 나타나는 확장성 심근병증을 정밀진단함. 사람의 병증과 비교를 통해 인간질환 동물모델로서의 가치를 판단한다.

(2) 암 질환 모델동물 개발 : Ei24 GEM 마우스 개발

(가) 생체 내에서 Ei24가 암발생의 억제에 관여하는지의 여부를 관찰하기 위해서는 GEM 모델의 확립이 절실하다.

(나) 당시 유전자 결손 마우스를 대량으로 생산하기 위해 International Gene Trap Consortium (IGTC)이 결성되어 Gene Trap된 내량의 ES cell colne들을 확보하였다.

(다) Ei24 유전자가 결손된 마우스를 제작하기 위해서 Ei24 gene trap ES cell을 분양받았으며, 이를 사용하여 Ei24 KO 마우스를 생산였으며, Ei-24의 결손은 Embryonic lethality를 유발함을 발견하였다.

(3) 대사성질환 동물모델 개발 : ATF-3 GEM 마우스 개발

생체 내에서 ATF3에 의한 대사질환 표현형을 보이는 모델동물을 개발하기 위하여 Vector

를 구축하고 cloning, construction의 과정을 거쳐 ATF3 GEM 마우스 제작하고 제작된 ATF3 GEM 마우스 모델에 대사성질환유도를 위해 고지방식이로 비만을 유도하여 대사질환 특성에 대한 연구를 진행하였다.

(4) 뇌신경질환 동물모델 개발 : DM-1, GX2 GEM 마우스 개발

(가) RIKEN 및 IKMC Banking resource에서 targeted ES cell line 확보 및 blastcyst injection. DM-1, GX2 GEM의 targeted ES의 GLT(Germline trasmission) 후 chimera를 생산한 뒤 GEM 마우스의 genotyping을 하여 GEM 마우스를 대량 생산하였다.

(나) 제작된 DM-1, GX2 GEM 마우스에서 신경계질환 특성에 대한 연구를 진행하였다.

나. 모델동물 활용 천연물 유래 신약 후보 물질 유효성 검증

세부 과제에서 개발된 모델동물을 이용하여 본 과제내의 타 연구팀에서 확보한 천연물 유래 신약 후보 3종의 질환관련 치료제로서의 유효성을 검토하였다.

다. 연구내용 변경

본 과제의 3차년도 진행후 과제 계속 평가에서 평가 위원들의 의견을 종합하여 연구내용을 다음과 같이 변경하였다.

(1) 본 과제에서 개발된 모델동물 중 한종에 대하여 집중적으로 모델동물의 표현형 및 질환 관련 특성을 분석 : Ei-24 활용 종양 발생 억제 연구 진행 (2) 본 과제에서 개발된 모델동물 중 모델동물의 표현형 및 질환 관련 특성이 분석된 1종을 대상으로 천연물 유래 신약 후보의 질환관련 치료제로서의 유효성을 검토

2. 연구방법

가. 질환동물모델

(1) 심순환질환 동물모델 : ASC-2 GEM 마우스 개발

① ASC-2 GEM의 vector 제작

② ASC-2 GEM의 targeted ES 확보

③ ASC-2 GEM targeted ES의 blastocyst injection

④ ASC-2 GEM targeted ES의 GLT (Germline transmission)

⑤ ASC-2 GEM targeted ES의 chimera 생산

⑥ ASC-2 GEM genotype 및 대량 생산

(2) 암질환 동물모델

① Ei24 GEM의 vector 제작

② Ei24 GEM의 targeted ES 확보

③ Ei24 GEM targeted ES의 blastocyst injection

④ Ei24 GEM targeted ES의 GLT (Germline transmission)

⑤ Ei24 GEM targeted ES의 chimera 생산

⑥ Ei24 GEM genotype 및 대량 생산

(3) 대사성질환 동물모델

① ATF-3 GEM의 vector 제작

② ATF-3 GEM의 targeted ES 확보
③ ATF-3 GEM targeted ES의 blastocyst injection
④ ATF-3 GEM targeted ES의 GLT (Germline transmission)
⑤ ATF-3 GEM targeted ES의 chimera 생산
⑥ ATF-3 GEM genotype 및 대량 생산

(4) 뇌신경질환 동물모델
① DMI-1, GX2 (뇌신경질환) GEM의 vector 제작
② DMI-1, GX2 (뇌신경질환) GEM의 targeted ES 확보
③ DMI-1, GX2 (뇌신경질환) GEM의 targeted ES의 blastocyst injection
④ DMI-1, GX2 (뇌신경질환) GEM의 targeted ES의 GLT(Germline transmission)
⑤ DMI-1, GX2 (뇌신경질환) GEM의 targeted ES의 chimera 생산
⑥ DMI-1, GX2 (뇌신경질환) GEM의 genotype 및 대량 생산

(5) GEM의 genotype 및 대량 생산
① Genotyping : 마우스의 꼬리를 0.5~1cm정도 잘라 DirectPCR lysis solution을 첨가하여 60℃에서 O/N으로 녹인 후에 13,000rpm에서 30초간 centrifuge하여 상등액을 취해 PCR을 실시
② Mass Production and Breeding : heterozygote를 선발하여 hetxhet 교배 방식으로 homozygote KO 마우스와 wild type control 마우스를 선발

나. 신약개발 유효성 평가를 위한 질환관련 특성 분석

(1) 심순환질환 동물모델
① 조직처리 : 심장 및 혈관을 적출하여 formalin 고정 후 파라핀에 포매하여 H&E 염색을 통하여 조직병리학적 변화를 관찰
② H&E 염색 : paraffin 처리된 slide를 xylene 7분간 염색함. 염색된 슬라이드를 alcohol 100%, 90%, 80%, 70% 순서대로 7분씩 처리함. 그 후에 tap water로 10분간 washing하고 다시 D.W.로 washing함. filter paper로 여과한 헤마톡실린으로 3분 염색한 후 tap water로 10분간 washing함. 다시 D.W.로 washing해준 후 eosin 5분 염색한 후 alcohol 80, 90, 95, 100% 순으로 2회씩 dipping하여 탈색함. 마지막으로 xylene을 처리하여 투명하게 만들어 주는데 처음엔 한번 담그기만 하고, 2,3,4,5번째는 7분씩 담가둠.

(2) 암질환 동물모델
① 조직병리 : 조직을 적출하여 formalin 고정 후 파라핀에 포매하여 H&E 염색을 통하여 조직병리학적 변화를 관찰
② H&E 염색 : paraffin 처리된 slide를 xylene 7분간 염색함. 염색된 슬라이드를 alcohol 100%, 90%, 80%, 70% 순서대로 7분씩 처리함. 그 후에 tap water로 10분간 washing하고 다시 D.W.로 washing함. filter paper로 여과한 헤마톡실린으로 3분 염색한 후 tap water로 10분간 washing함. 다시 D.W.로 washing해준 후 eosin 5분 염색한 후 alcohol 80, 90, 95, 100% 순으로 2회씩 dipping하여 탈색함. 마지막으로 xylene을 처리하여 투명하게 만들어 주는데 처음엔 한번 담그기만 하고, 2,3,4,5번째는 7분씩 담가둠.
③ 세포증식능 검색 : Ei24이 과발현된 cell line을 nude mouse에 injection하여 tumor growth를 parental tumor cell과 비교함. 7일, 14일 경과 후 종양의 크기와 무게를 측정하

여 Ei24이 세포 증식능에 미치는 영향을 연구함.

④ 발암물질 감수성 검색(DEN) : Ei24 GEM 마우스에 DEN(예시)을 처리하여 발암 감수성에 대한 유의한 차이가 있는 지를 검색하여 종양모델동물로서의 유효성 가치를 평가함.

(3) 대사성질환 동물모델

① 체중증가, 지방량 측정 : 각 주령마다 몸무게와 비만의 척도인 지방과 간의 무게를 측정함. 지방의 무게는 부고환에 붙어있는 지방의 무게(epididymal fat)를, 간 조직의 무게는 간의 전체 무게를 측정함. 측정된 무게를 몸무게로 나눠서 실제로 몸무게 증가량에 비례하여 증가된 지방과 간 조직의 무게를 확인 함.

② 지방조직검사 : 적출된 지방 조직을 파라핀 포매 후 HE 염색을 하여 지방조직의 크기, 수를 조사하여 지방조직의 증식 정도를 파악함.

③ 혈당, GTT : 대조군과 KO 마우스의 혈액을 채취하여 혈청 화학 분석을 통해 중성지방과 콜레스테롤 수치를 분석, leptin, adiponectin, level 분석 glucose tolerance test 를 실시함으로 비만 정도를 확인함.

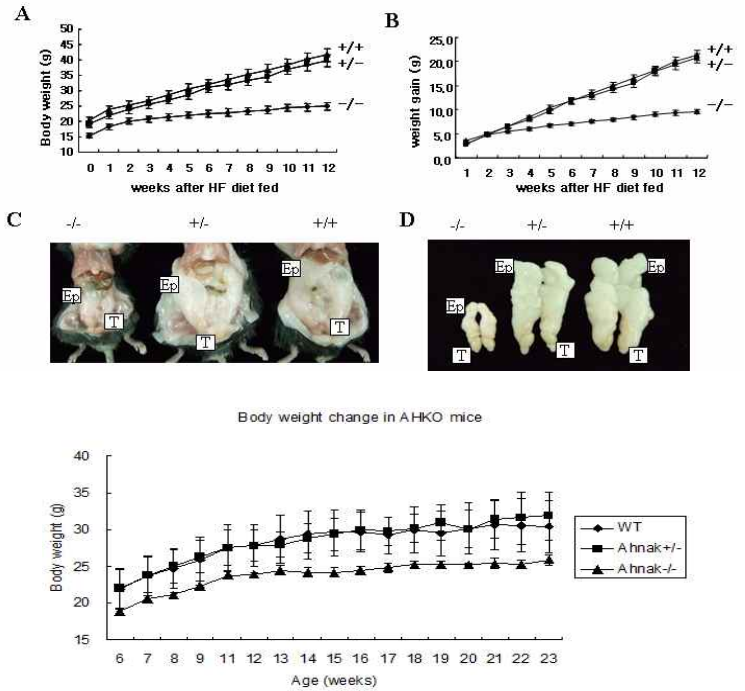

<체중증가, 지방량 측정>

(4) 뇌신경질환 동물모델

① 조직처리 : 조직을 적출하여 formalin 고정 후 파라핀에 포매하여 H&E 염색을 통하여 조직병리학적 변화를 관찰

② H&E 염색 : paraffin 처리된 slide를 xylene 7분간 염색함. 염색된 슬라이드를 alcohol 100%, 90%, 80%, 70% 순서대로 7분씩 처리함. 그 후에 tap water로 10분간 washing하고 다시 D.W.로 washing함. filter paper로 여과한 헤마톡실린으로 3분 염색한 후 tap water로 10분간 washing함. 다시 D.W.로 washing해준 후 eosin 5분 염색한 후 alcohol 80, 90, 95, 100% 순으로 2회씩 dipping하여 탈색함. 마지막으로 xylene을 처리하여 투명하게 만들어 주는데 처음엔 한번 담그기만 하고, 2,3,4,5번째는 7분씩 담가둠.

③ Hippocampuse의 세포 증식능 검색 : 각 조직에서 유전자의 발현을 확인하여 뇌와 근육에서 특이적으로 유전자가 과다 발현됨을 확인함. 생산된 이들 마우스의 행동적 이상을 관찰하기 위하여 Water Mazing을 실시하여 정상 마우스와 형질전환 마우스에서 Escape Latancy, Distance를 SMAT-DL 프로그램을 이용하여 확인함.

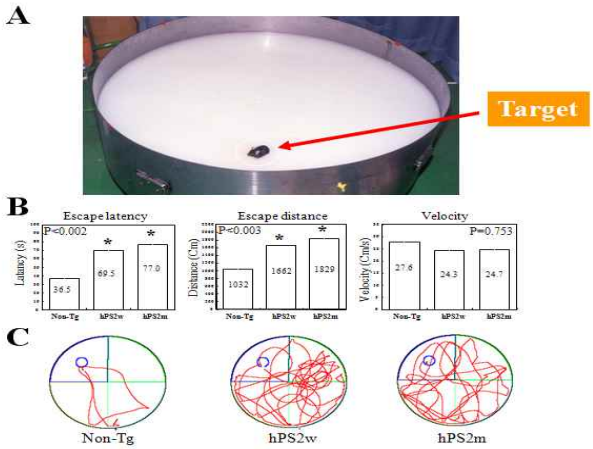

<치매모델동물의 행동학적 시험결과>

3. 연구결과

가. 질활동물모델 개발

(1) 심순환 질환 모델동물 개발 : ASC-2 GEM 마우스 개발

① Classical ASC-2 KO 마우스는 발생단계 중 embryo의 심장형성 과정에서 defect가 발생함에 따라 homozygote KO 마우스는 embryonic lethality를 나타냄. 따라서 ASC-2의 defect로 인한 심장질환의 발생 가능성을 예상할 수 있지만, 심장질환 연구에 성체인 homozygote KO 마우스의 사용이 불가능했기 때문에 동물모델로는 부적합하다.

② ASC-2 KO 마우스의 embryonic lethality를 극복하고, 심장질환에서 ASC-2의 역할을 연구하기 위해서 ASC-2 Dominant Negative (DN)를 발현시킴으로써 KO 마우스를 mimic하는 전략을 마련함. ASC-2의 DN은 normal ASC-2와 nuclear hormone receptor의 결합을 저해함으로써 본래의 기능을 억제하지만 lethality는 관찰되지 않았다.

③ ASC-2의 DN1 TG 마우스는 heart에서 DN1을 발현하며, 확장성 심근병증으로 진단되는 심장질환을 보인다.

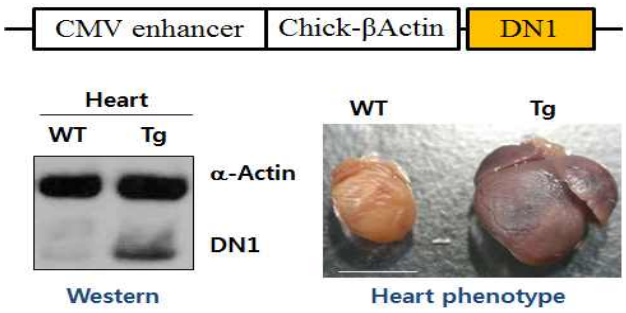

<DN1 TG 마우스의 생산>

④ 심장질환 중 확장성 심근병증은 환자 10만명 중 40여명이 걸리는 매우 흔한 질병으로, 이 중 약 40%의 환자가 가족력을 보임. 확장성 심근병증은 RRAR이나 RAR과 같은 nuclear hormone receptor가 knockout 되면 유발되는 것이 알려져 있는데, ASC-2가 이런 nuclear hormone receptor와 결합하여 기능을 조절할 수 있었으나 심장질환은 혈관 및 복잡한 생리작용의 이상으로도 나타날 수 있는 만큼, whole body에서 DN1이 발현되는 TG의 특성상 타 장기이상에 의한 영향을 고려하지 않을 수 없음. 이에 추가적으로 conditional ASC-2 마우스를 이용하여 심장특이적인 KO 마우스를 생산함으로써 본 심장병증을 정밀진단하고 동물모델로 정립하였다.

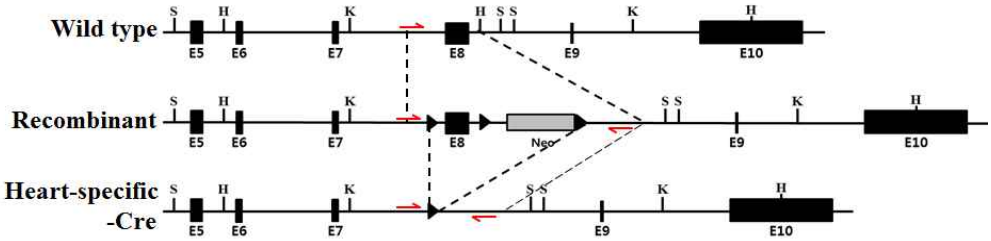

<Conditional ASC-2 KO 마우스를 이용한 심장특이적인 ASC-2 KO 마우스 제작>

⑤ Conditional ASC-2 마우스에서 심장 특이적으로 유전자를 적중시키기 위해서 심장에서만 Cre를 발현시키는 α-MHC-Cre 마우스와 교배함으로써 심장특이적인 ASC-2 KO 마우스를 확보할 수 있었다.

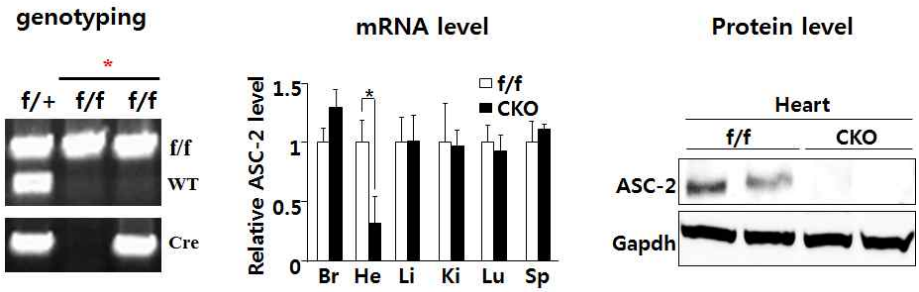

<심장특이적인 ASC-2 KO 마우스의 생산>

⑥ 이 마우스들은 심순환질환모델로서 분석하여 유의성 있는 결과를 도출할 수 있는 수준의 개체수 확보와 연령대 유지를 위해서 유전학적 교배계획과 사육을 진행하였음. 본 과정에 최소 9개월에서 12개월의 기간이 소요되었다.

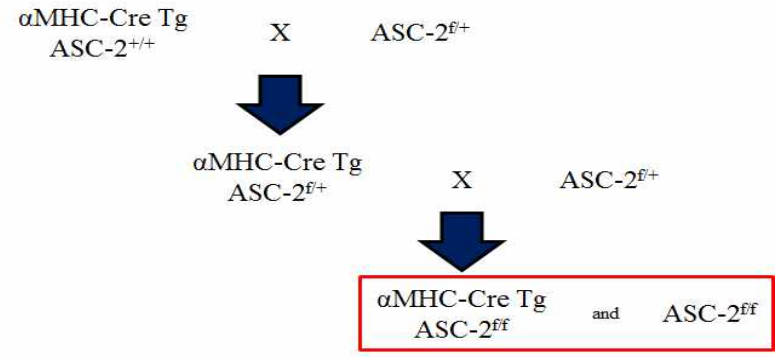

<심장특이적인 ASC-2 KO 마우스의 생산을 위한 mating scheme>

⑦ 확보된 마우스 중 3개월령에서부터 12개월령까지의 마우스를 분석에 이용하여 ASC-2 KO 마우스에서 나타나는 확장성 심근병증을 진단하였음. 심장 특이적으로 ASC-2의 결손이 일어날 경우, 3개월령부터 8개월령까지 premature death가 일어남을 관찰할 수 있었다.

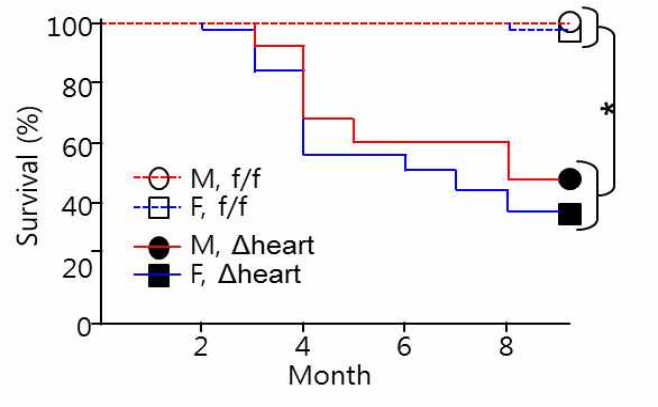

<심장 특이적 ASC-2 결손 마우스(Δheart)의 survival rate>

⑧ Premature death가 발생한 마우스의 심장은 정상에 비해 2배가량 커져있고, 절편조직염색에서 심벽의 두께가 얇아진 것이 확인됨. 이는 사람의 확장성심근병증과 매우 유사하다.

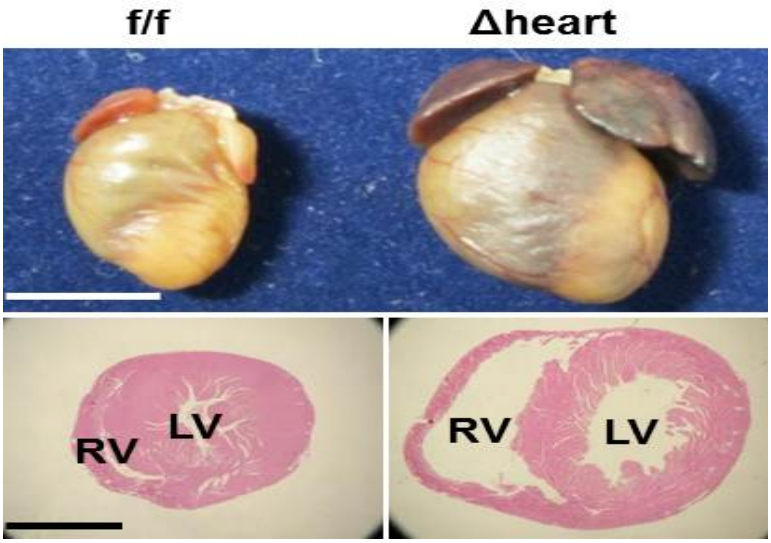

<Premature death가 발생한 심장 특이적 ASC-2 결손 마우스(Δheart)의 확장된 심장 및 절편조직염색>

⑨ 절편조직의 trichrome 염색 결과, 심장 내 damage에 의한 fibrosis가 초래되어 있음을 확인함. 심장 내 fibrosis는 약 5개월령의 마우스에서 관찰되었으며, 이후 ASC-2가 어떤 mechanism을 통해서 심장병을 유발하는지 밝히기 위해서 확보된 마우스들에서도 추가적인 병리관찰이 필요하다.

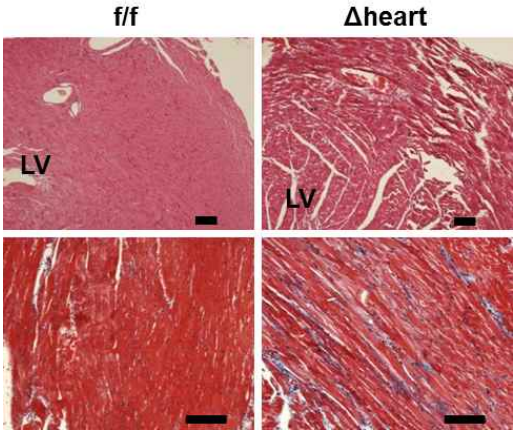

<심장 특이적 ASC-2 결손 마우스의 확장된 심장의 절편조직염색>

⑩ 해당 연구기간 동안 기 확보된 ASC-2 conditional KO 마우스를 이용하여, 심순환질환 모델로서 가치를 판단하기 위한 연구를 진행하였음. 국내 심순환질환 전문가와의 공동 연구를 통해 심장 특이적으로 ASC-2를 KO 시킨 마우스에서 나타나는 표현형을 정밀 분석하였다.

⑪ Echocardiography를 이용하여 심장특이적 ASC-2 결손이 DCM을 유발함을 심장기능이 직접적으로 조절됨을 보임. f/f (WT)에 비해 ASC-2가 한 allele만 제거되어도 심장병이 유발됨을 확인할 수 있었고, 두 allele가 모두 사라졌을 때 증상이 더욱 심해진다.

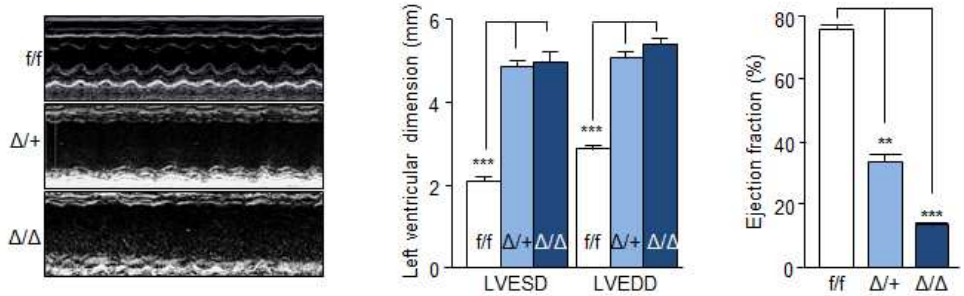

<Echocardiography>

⑫ 투사전자현미경(TEM)을 이용한 심근세포 분석 결과로 ASC-2가 결손 되면 mitochondria의 모양과(왼쪽 그림) mitochondrial DNA 양에 이상이 생김을 알 수 있다.

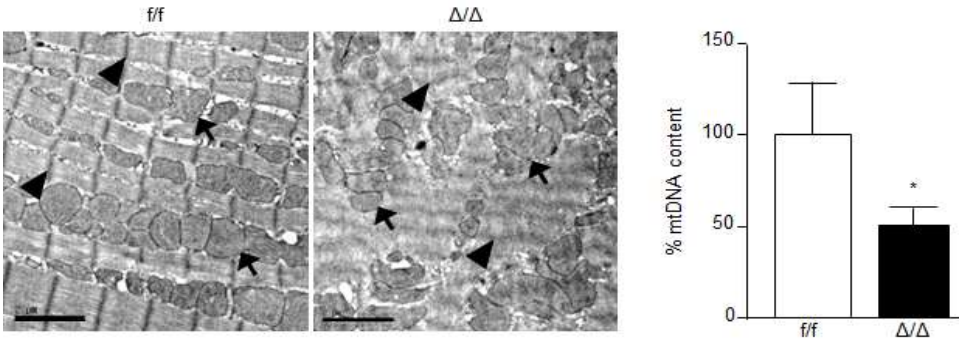

<투사전자현미경(TEM)을 이용한 심근세포 분석>

⑬ 심장의 mitochondrial RNA를 분석한 결과 ASC-2유전자가 하나라도 결손 되면 WT에 비해 그 양이 감소하며, 두개의 ASC-2가 모두 제거되면 더욱 증상이 심해짐을 알 수 있다.

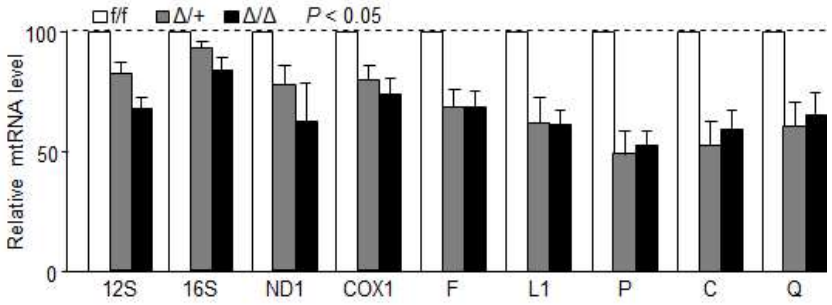

<심장의 mitochondrial RNA분석>

⑭ nuclear receptor 중 하나인 PPARδ 결손이 확장성 심근병증을 유발함. ASC-2가 이러한 receptor와 결합을 하므로 PPARδ의 타깃을 보기로 함. ASC-2결손 마우스의 심장에서 PPARδ 타깃인 Mcpt1, Cd36, Fatp1, Pdk4, 그리고 Ucp3 등이 감소함. 따라서 심장 특이적 ASC-2결손 마우스는 PPARδ의 활성화를 못 시켜 확장성 심근병증이 유발됨을 밝혔다.

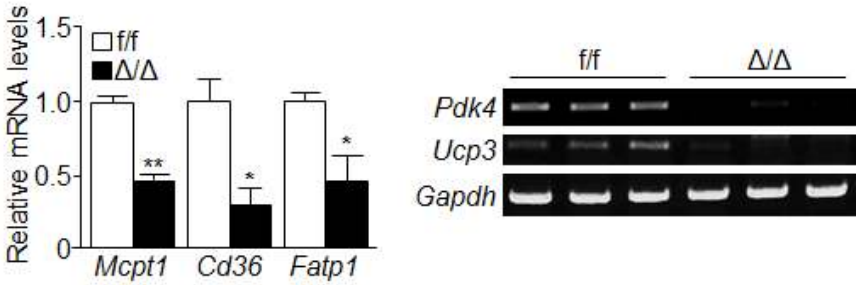

<ASC-2결손에 따른 PPARδ의 활성 저하>

⑮ 사람에서 또한 ASC-2가 확장성 심근병증과 연관이 있는지 조사하기 위해 특발성 심근병증 환자 50명에게서 얻은 DNA를 이용해 ASC-2의 변이를 조사함. 50명 중 5명에게서 3가지 종류의 변이가 확인됨. 이러한 변이는 아미노산의 변이를 유발한다.

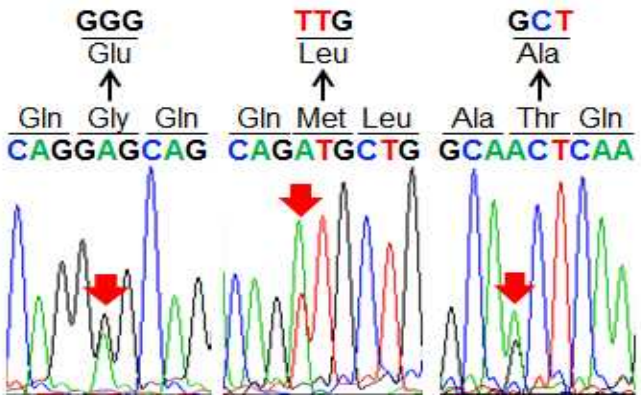

사람의 ASC-2 유전자에서 발견된 3가지 종류의 DNA 서열 변이

⑯ 변이가 일어난 부분에 대한 종간의 서열 분석을 통해 3개 중 2가지 종류의 변이가 사람에서부터 제브라피시까지 보존이 됨을 확인하였으며 703번과 1176번 아미노산은 종 간 매우 잘 보존되어 있으며, 766번은 한 종류의 원숭이에서 자연적인 변화가 있음을 확인하였다.

```
                          703          766                1176
Homo sapiens              QMMGPQGQVLLQQ--QM-SGQMLPQQGP---GPSPLSAT-
Pan troglodytes           QMMGPQGQVLLQQ--QM-SGQMLPQQGP---GPSPLSAT-
Macaca mulatta            QMMGPQGQVLLQQ--QM-SGQLLPQQGP---GPSPLSAT-
Callithrix jacchus        QMMGPQGQVLLQQ--QM-SGQMLPQQGP---GPSPLSAT-
Canis lupus               QMMGPQGQVLLQQ--QI-SGQMLPQQGP---GPSPLSAT-
Rattus norvegicus         QMMGPQGQVLLQQ--QM-SGQMLPQQGP---GPSPLSAT-
Mus musculus              QMMGPQGQVLLQQ--QM-SGQMLPQQGP---GPSPLSAT-
Danio rerio               QMMPPQG--------QMGQQQMTPQQHP---VPHQTGAS-
```

<사람에서부터 제브라피시에 걸친 ASC-2의 아미노산 서열 분석>

⑰ 이러한 변이가 PPARδ의 활성에 영향을 주는지 luciferase 분석을 통해 규명하고자 함. luciferase 분석 결과 703번과 1176번 아미노산이 변이가 일어났을 때 정상과 766에 비해 현저히 낮은 PPARδ 활성을 보임을 확인하였다. 따라서 마우스뿐만 아니라 사람에서도 ASC-2가 확장성 심근병증 유발에 관여할 수 있음을 보였다.

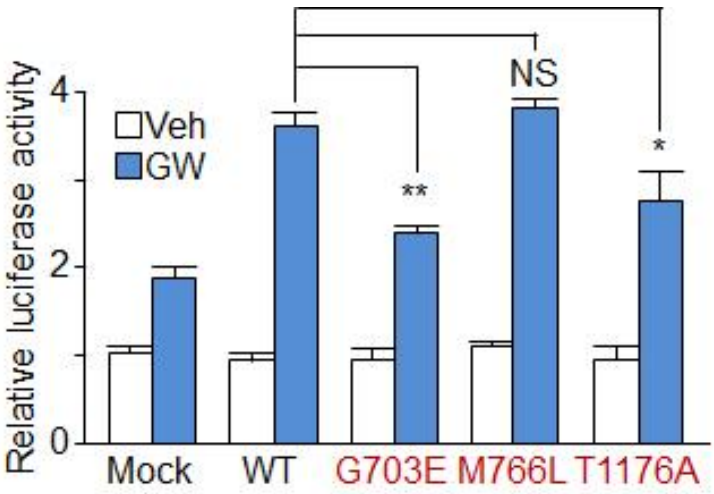

<ASC-2의 아미노산 변이에 따른 PPARδ 활성도의 변화>

(2) 암질환 모델동물 개발 : Ei24 GEM 마우스 개발

① Ei24가 E2F1의 target임을 밝히고 tumor suppressor로써의 기능을 제시함. 또한 암의 전이과정에 필요한 성질인 세포의 migration과 invasiveness, Epithelial - mesenchymal transition (EMT) 등을 억제하는 것을 확인함으로써 Ei24가 암발생 및 전이 과정에 관여할 수 있음을 확인하였다.

② Ei24가 포함된 생체 내 발암 기전을 분석하여 암질환 동물모델로 확립하기 위해서 Ei24 gene trap ES cell을 확보하고 Ei24 KO 마우스를 생산하였다.

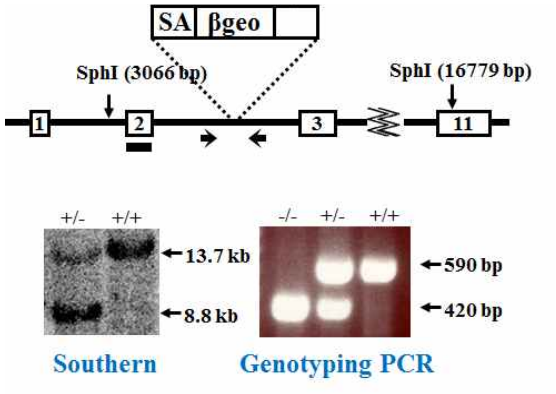

<Ei24 KO 마우스 생산>

③ Ei24의 결손은 embryonic lethality를 유발함. 이로 인해서 암 연구를 위한 성체 homozygote의 확보가 어려웠음. 이후 Ei24+/- 마우스의 조직에서 Ei24 발현의 haplo-insufficient를 확인하고 암질환 동물모델의 생산을 위해서 Ei24 heterozygote 마우스를 이용하였다.

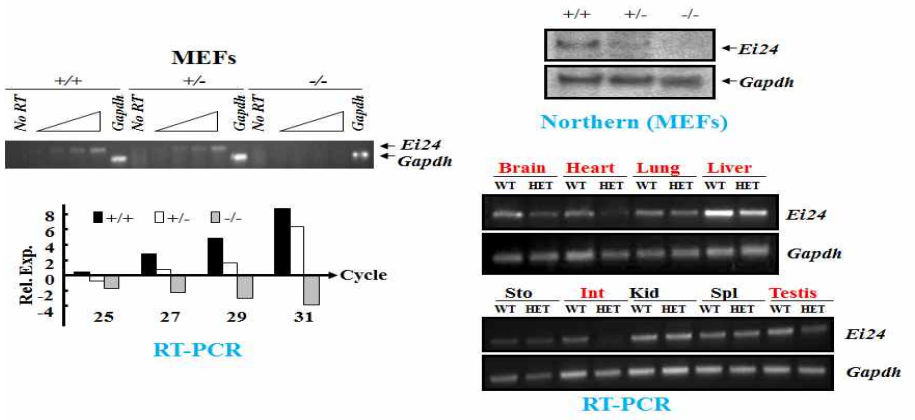

<Haplo-insufficient Expression of Ei24 in Ei24+/- Mouse Tissues>

④ Ei24+/- 마우스의 조직들을 H&E염색하여 관찰한 결과, 주요 장기들에서 염증반응이 증가되어 있음. Ei24가 염증반응에 관여함. 위암 및 간암의 경우 많은 경우 염증반응으로 인해 발생하였다.

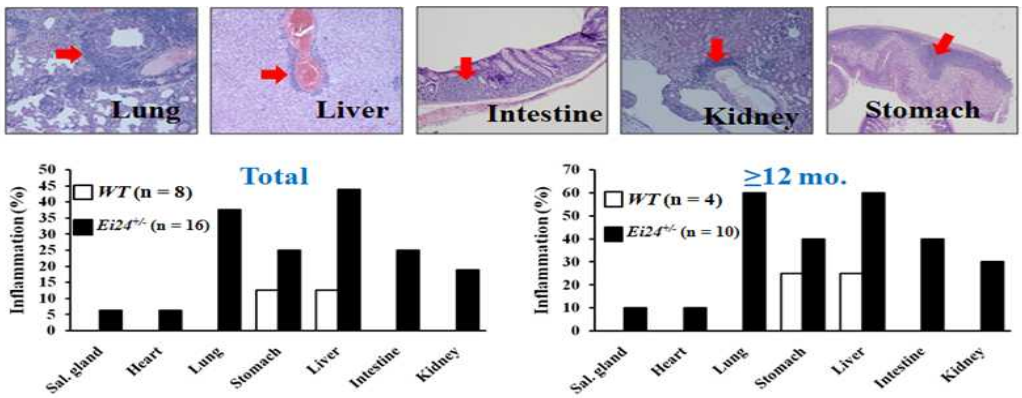

<Ei24+/- 마우스 조직의 비정상적 Chronic Inflammation>

⑤ 간암 연구 및 치료제 개발을 위한 동물모델 개발의 필요성이 부각됨에 따라 Ei24+/- (Het) 마우스를 간암 동물모델로 확립하기 위해서 Het (Ei24+/-) 마우스에 Diethylnitrosamine (DEN)을 처리하여 hepatocellular carcinoma (HCC)를 유도함. 대조군 WT 마우스에 비해 Het (Ei24+/-) 마우스에서 HCC의 발생이 증가하므로 간암 동물모델로서의 분석 필요성을 보였다.

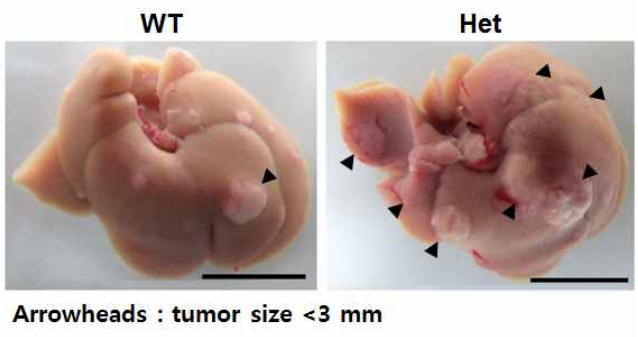

<Ei24+/-(Het) 마우스에 DEN을 처리>

⑥ DEN을 처리한 후 damaged liver의 lesion을 H&E염색하여 분석한 결과, Ei24+/- (Het) 마우스에서 hepatocellular carcinoma (HCC)의 증가와 함께 hepatocellular adenoma (HCA)도 증가하였으며 유의성 검사 및 추가적인 DEN-induced HCC의 분석이 필요하다.

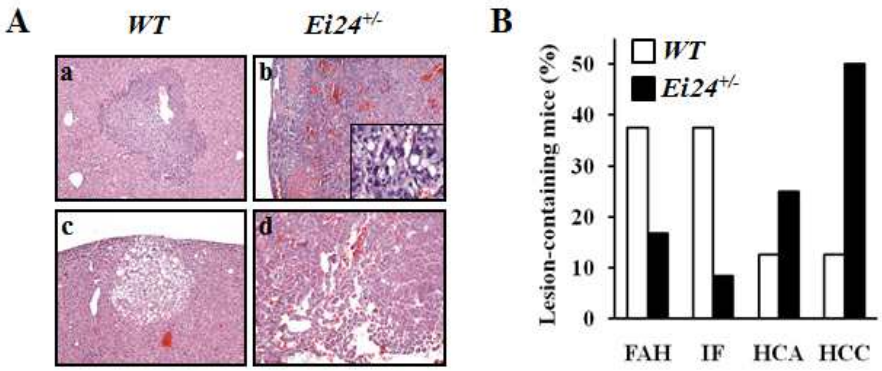

<HCC가 유발된 Ei24+/- 마우스의 간 절편조직염색과 lesion 분석>

⑦ WT과 Ei24+/- 마우스에 각각 DEN을 처리한 후 30주와 50주에 tumor formation을 분석하여, genotype에 따른 tumor 발생의 유의성을 분석하였다.

Weeks after DEN inj.	Ei24 genotype	Body weight (g)	Liver weight (g)	Liver to body weight ratio (%)	Tumor No.	Max tumor size (mm)
30	+/+ (n = 7)	40.57 ± 6.21	1.90 ± 0.33	4.67 ± 0.42	7.14 ± 8.01	2.14 ± 1.57
	+/- (n = 7)	43.98 ± 4.41	2.82 ± 1.19	6.36 ± 2.51	22.14 ± 20.78	6.43 ± 4.76
	p	n.s.	n.s.	n.s.	n.s.	< 0.05
50	+/+ (n = 5)	42.03 ± 4.73	2.33 ± 0.97	5.40 ± 1.66	18.00 ± 10.89	6.00 ± 1.58
	+/- (n = 8)	35.62 ± 5.18	4.12 ± 0.97	11.71 ± 2.95	95.57 ± 43.83	16.00 ± 7.43
	P	< 0.05	< 0.01	< 0.005	< 0.005	< 0.05

<DEN-induced HCC formation in wild-type and Ei24+/- mice>

⑧ Ei24 TG마우스와 genetic 모델을 이용하여 Ei24가 암 질환을 억제하는지 살펴보기로 하였다.

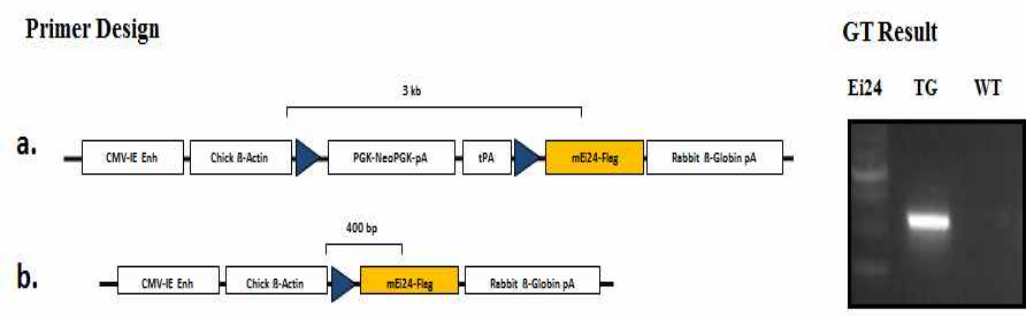

<Ei24 TG마우스 제작 및 Genotyping 결과>

⑨ MMTV-PyMT 마우스와 교배를 통해 Ei24가 breast tumorigenesis를 억제함을 증명하였다.

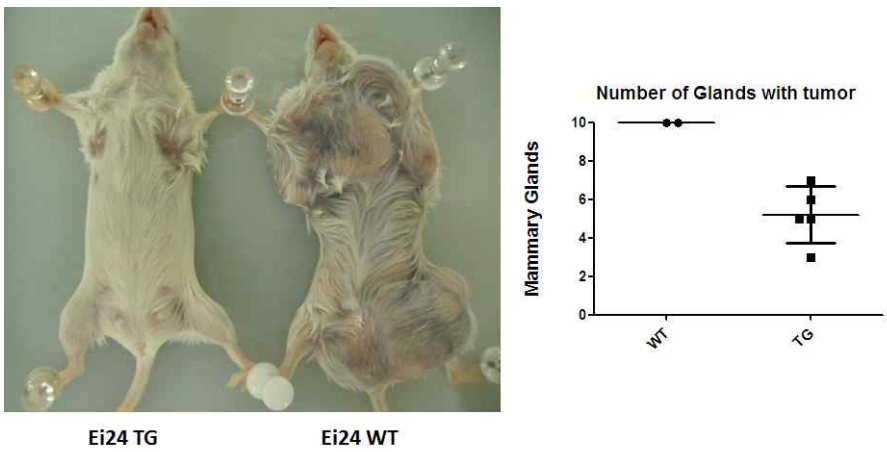

<MMTV-PyMT 마우스와 교배>

⑩ Mammary gland specific cre를 이용하여 breast에 Ei24를 과발현 시킨 마우스와 breast cancer model인 MMTV-PyMT 모델과의 교배를 통하여 Ei24의 breast에서의 과발현은 breast tumor를 상당히 감소시키는 것을 확인하였다.

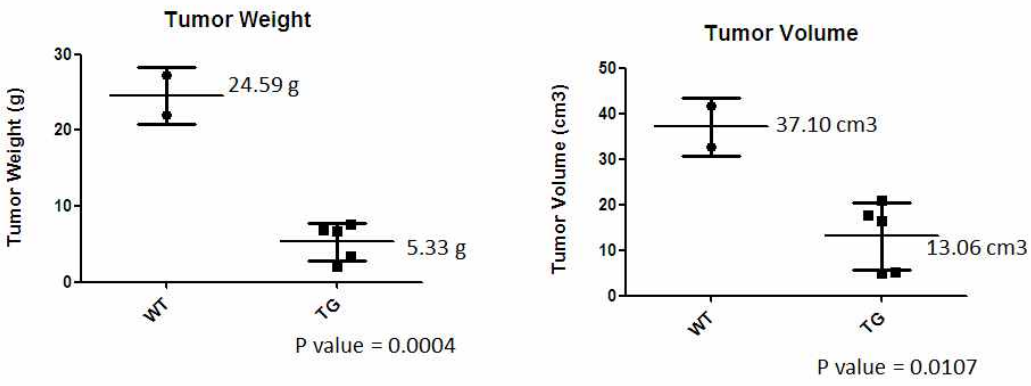

<WT, TG 마우스의 Tumor weight, volume>

⑪ MMTV-PyMT로 유도된 breast tumor는 대략 120일 정도 시간이 지나면 lung으로 metastasis가 되고 Ei24의 breast에 과발현으로 인해 breast cancer의 lung metastasis가 현저히 감소함을 알 수 있다.

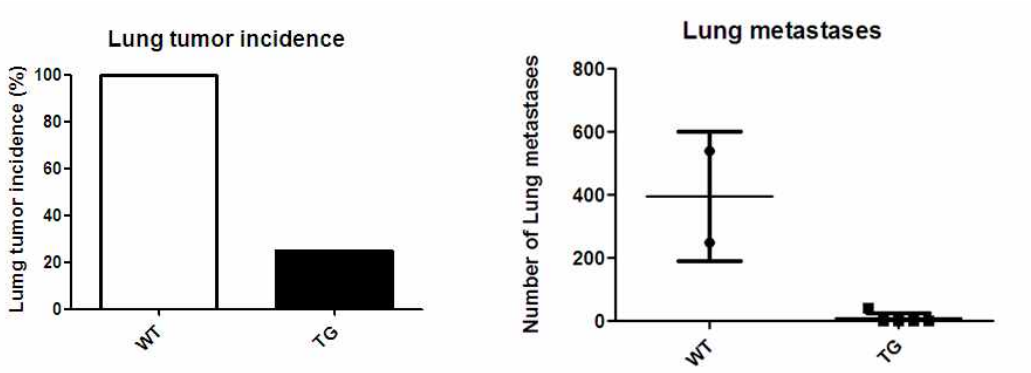

<MMTV-PyMT로 유도된 breast tumor에서 lung으로의 metastasis>

⑫ 세포의 운동성 조절은 암 세포가 전이를 하는데에 있어서 가장 기본적이지만 필수적인 요인이므로 Ei24의 발현 조절이 세포의 운동성에 대한 영향을 알아보기 위해 boyden chamber를 이용하여 세포의 운동성을 조사하였다. Ei24의 발현은 human과 mouse의 세포의 운동성을 저하시키고 Ei24의 발현 저하는 오히려 세포의 운동성을 증가 시킴켰으며, 세포의 운동성 조절에 가장 필수적인 세포 골격의 변화를 앞서 구축한 stable cell line들을 이용하여 조사함. Ei24의 발현 저하는 세포의 골격을 좀 더 세포가 이동하기 수월한 방향으로 변화시켜서 운동성을 조절하는 것을 확인하엿다.

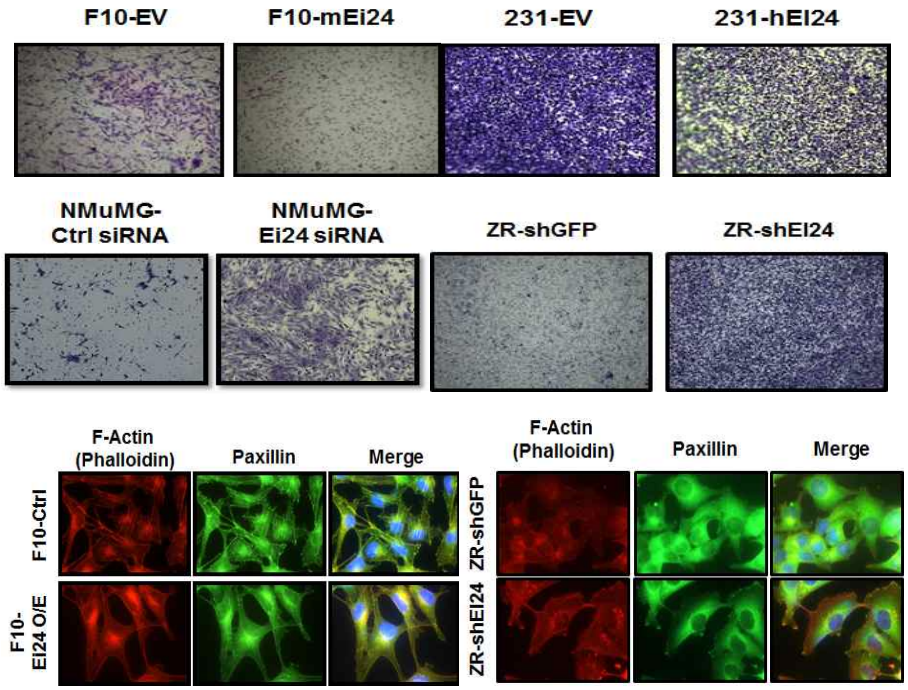

< EI24에 의한 세포 운동성 조절 및 세포 골격 변화>

⑬ 암의 전이에 필요조건인 세포간의 communication의 조절 여부를 확인하기 위해 hanging drop culture를 통해 cell-cell interaction을 조사하였다. Ei24의 발현 저하는 세포 간의 interaction을 감소시켜 세포들을 자유로운 상태로 변화시키는 것을 확인함. Ei24 발현 저하 세포는 주변의 ECM들과의 interaction을 증가시켜 세포의 운동성, 암의 전이에 더 유리하게 만드는 것을 알 수 있었다.

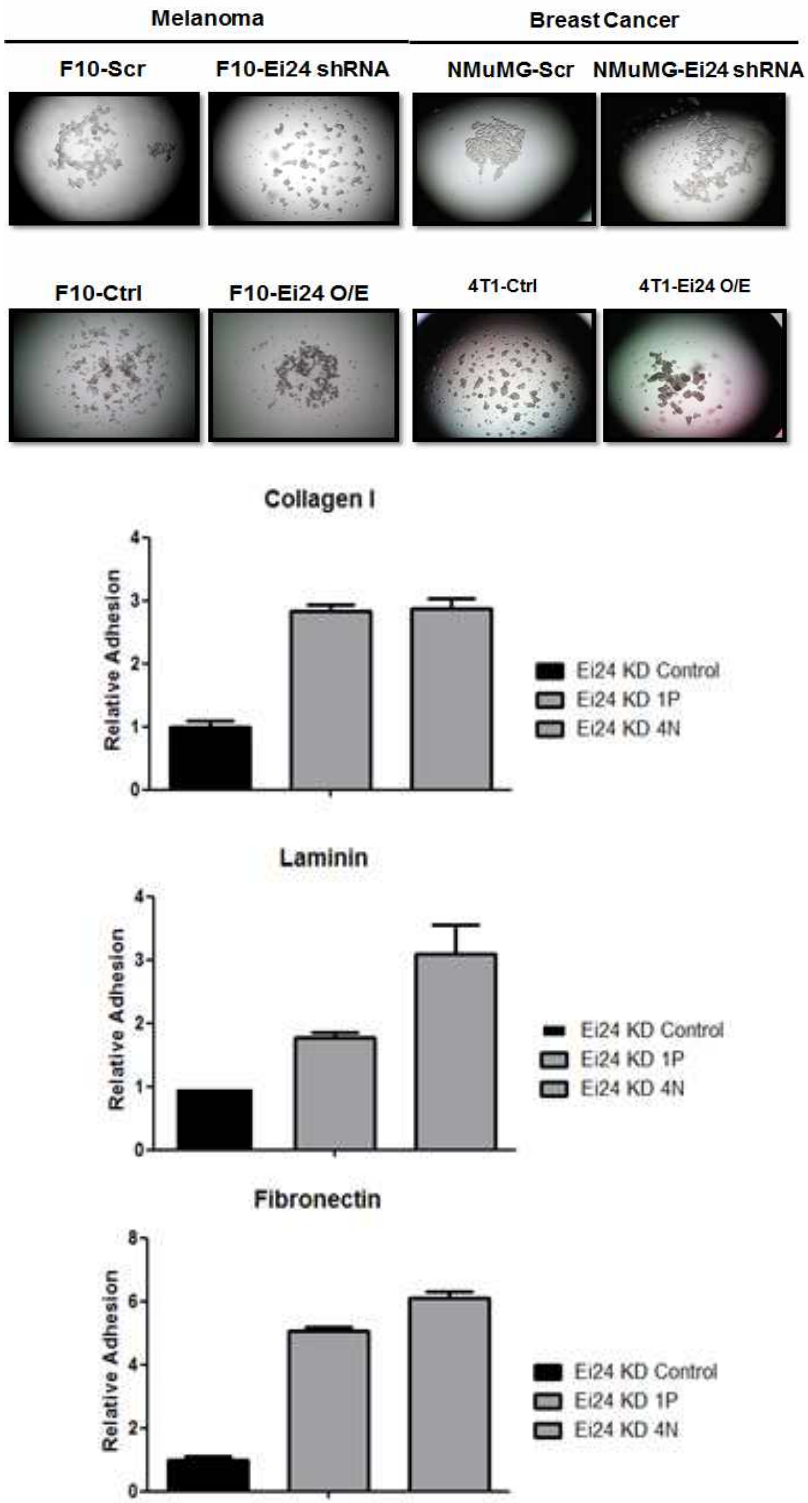

<EI24에 의한 adhesion 조절>

⑭ EI24가 암의 전이를 조절하는 데 있어 세포의 골격 구조의 변화, 세포 간의 interaction, 세포와 ECM과의 adhesion 조절은 Epithelial to Mesenchymal Transition (EMT)의 전형적인 표현형임. Ei24에 의한 EMT의 조절을 연구하고자 epithelial type의 cancer cell을 이용하여 Ei24에 의한 EMT 여부를 확인하였고, Cellular, biochemical data 모두 EI24에 의한 epithelial 세포의 mesenchymal 세포로의 전환이 일어난다는 것을 증명하고 있으며, EMT에서 가장 중요한 cadherin switch의 여부는 사람 환자에서도 그 경향성이 있음을 확인하였다.

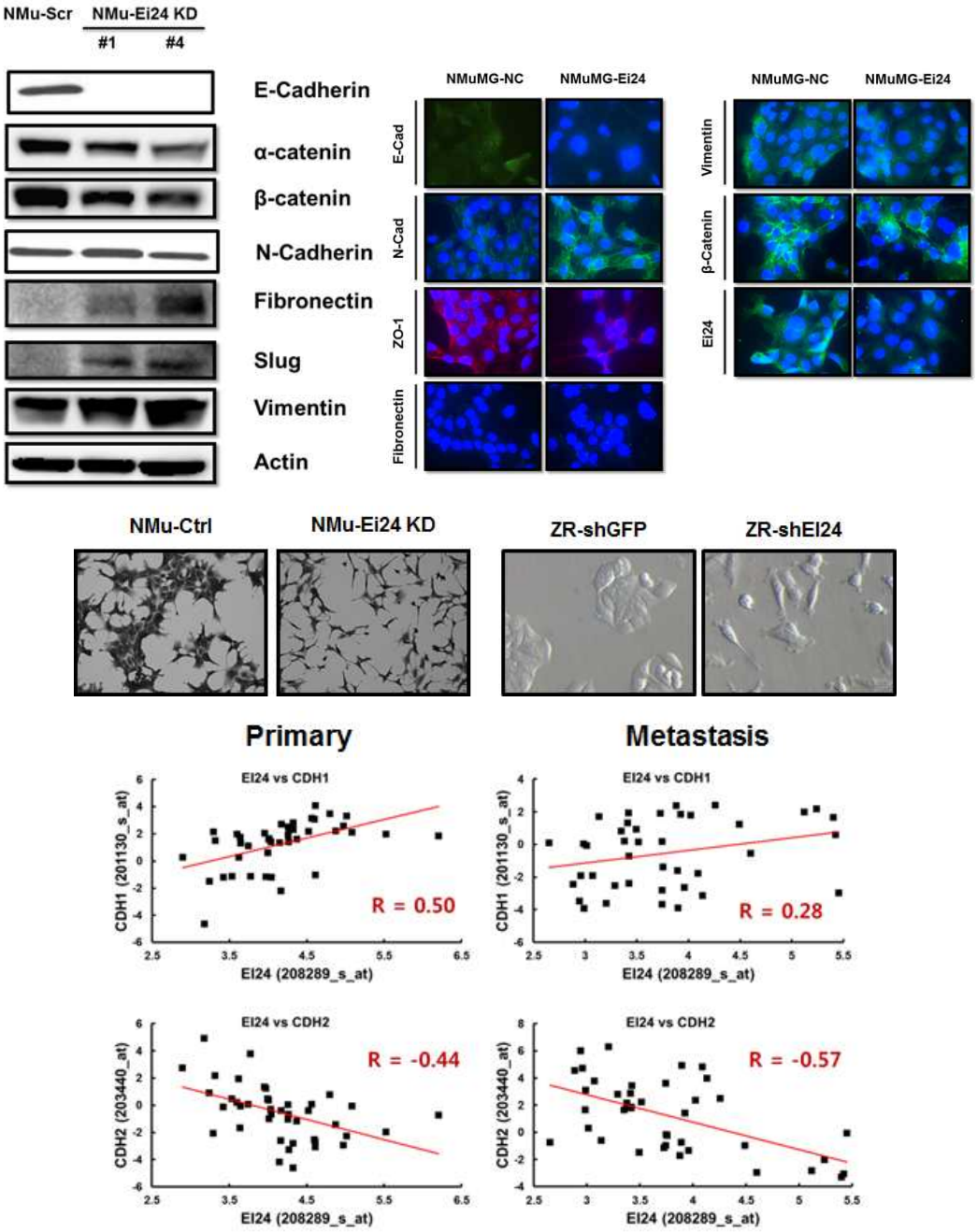

<EI24에 의한 EMT 조절>

⑮ EMT로 수반되는 EI24의 암 전이에 대한 조절은 암 세포가 침윤력(invasiveness)을 갖게 하고, Anoikis에 대한 저항성을 지니게 한다.

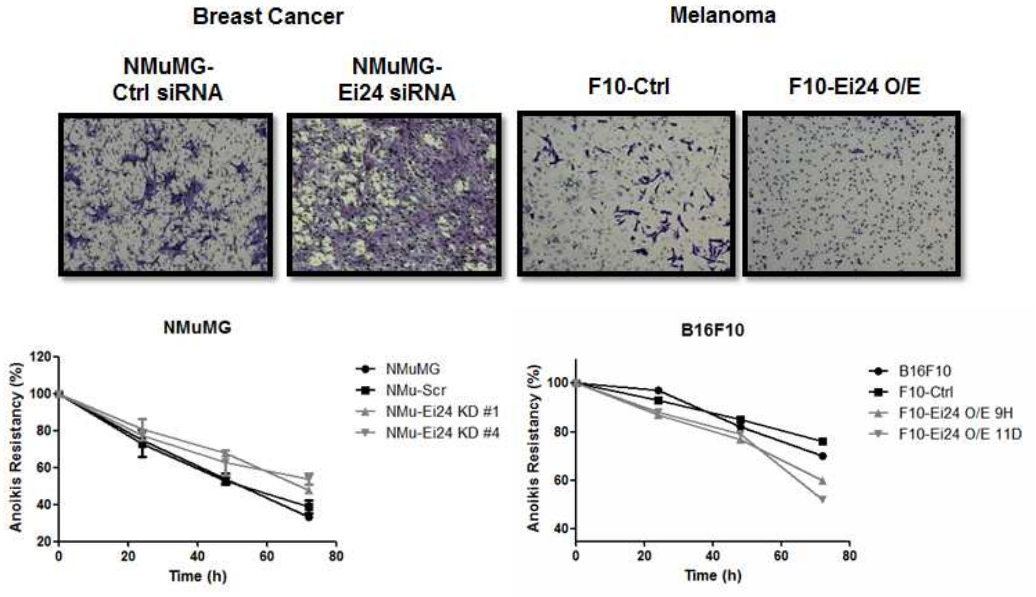

<EI24의 EMT 조절>

⑯ EI24 유전자를 발현 조절하여 수행한 microarry결과 EI24는 NF-kB 신호전달과정에 밀접한 연관이 있음을 알 수 있었음. luciferase결과 EI24는 NF-kB 활성을 억제하는 것으로 관찰됨. EI24는 NF-kB의 구성 요소인 p65의 핵으로의 이동을 억제함. 염증반응과 관련된 사이토카인의 발현을 조절하는 것으로 관찰되었다.

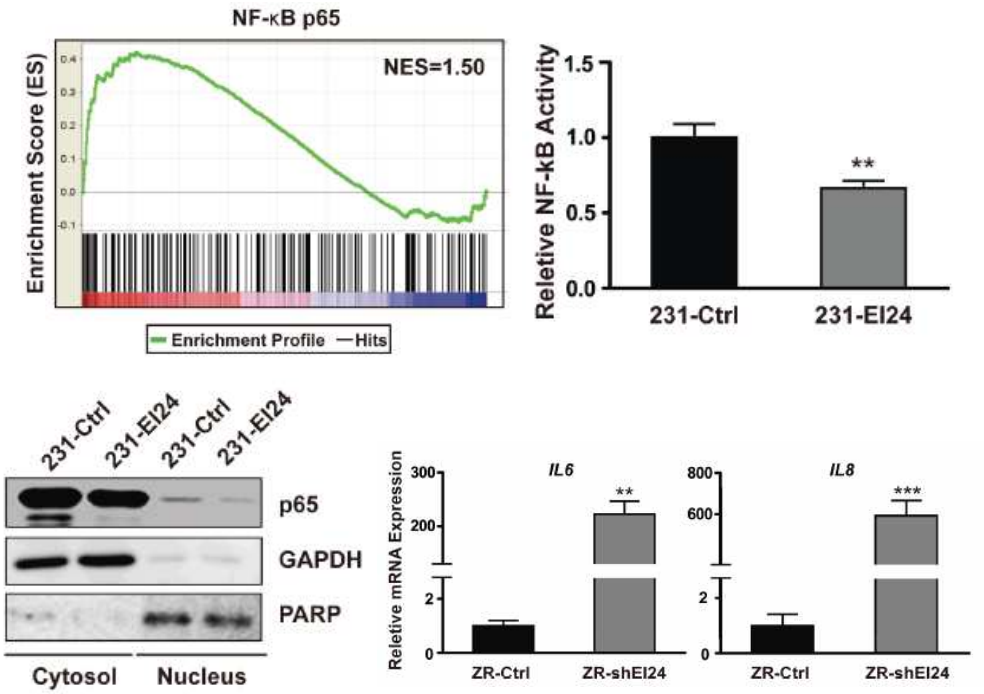

<EI24의 NF-kB 신호조절>

⑰ EI24는 TNFα complex I의 구성요소인 TRAF2/5와 protein binding을 함을 관찰함. TNFα를 매개로하는 NF-kB의 활성을 조절하였다.

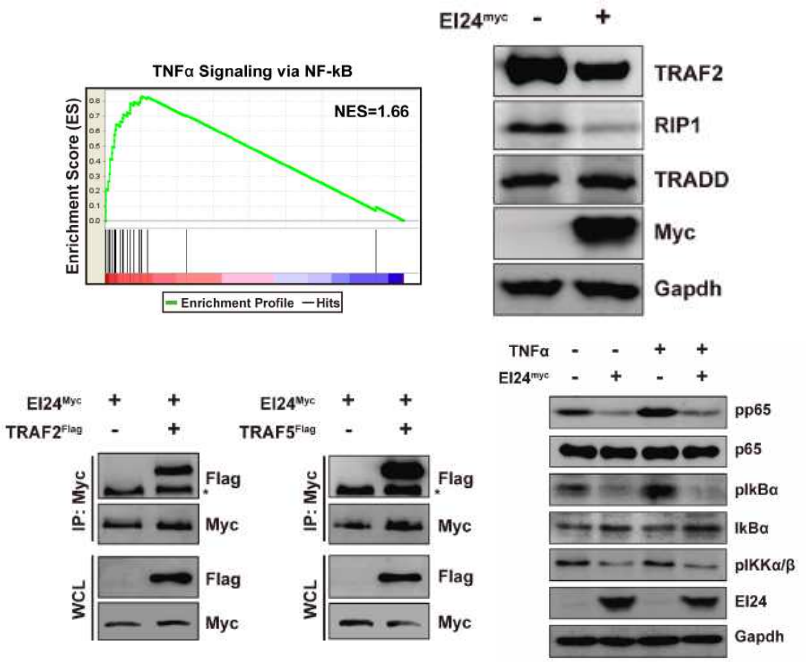

<TNFα complex I의 조절을 통해 NF-kB의 활성을 조절하는 EI24>

⑱ Cellular data와 Biochemical data들을 토대로 실제 생체 내에서 EI24의 암 전이의 역할을 규명하기 위해 syngeneic mouse model 시스템을 이용함. EI24의 과발현은 malignant 한 세포의 전이성을 현저히 감소, EI24의 발현 저하는 암 세포의 전이를 생체 내에서도 촉진하였다.

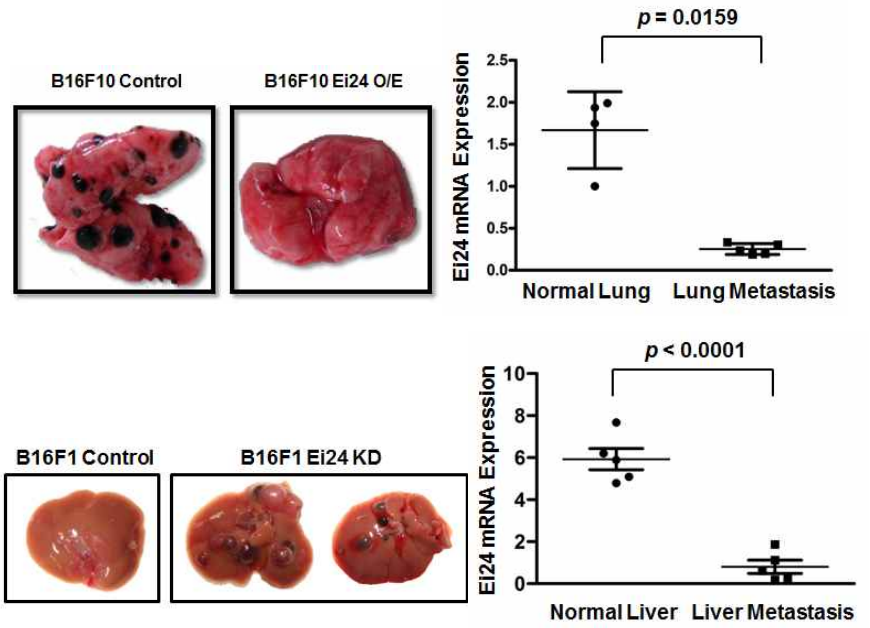

<in vivo 모델에서 EI24에 의한 암 전이 조절>

⑲ EI24의 발현은 정상 혹은 낮은 grade의 암보다 전이 암에서 현저히 감소되는 것으로 관찰됨. EI24의 발현이 적은 전이암환자의 예후가 좋지 않음을 관찰함. EI24가 TRAF2를 통한 NF-kB를 조절함을 밝혔고, 환자수준에서도 밀접한 관련이 있음을 관찰함. 전이암 환자 중 낮은 EI24와 높은 TRAF2의 발현을 보이는 환자들이 반대의 경우보다 좋지않은 예후를 보였다.

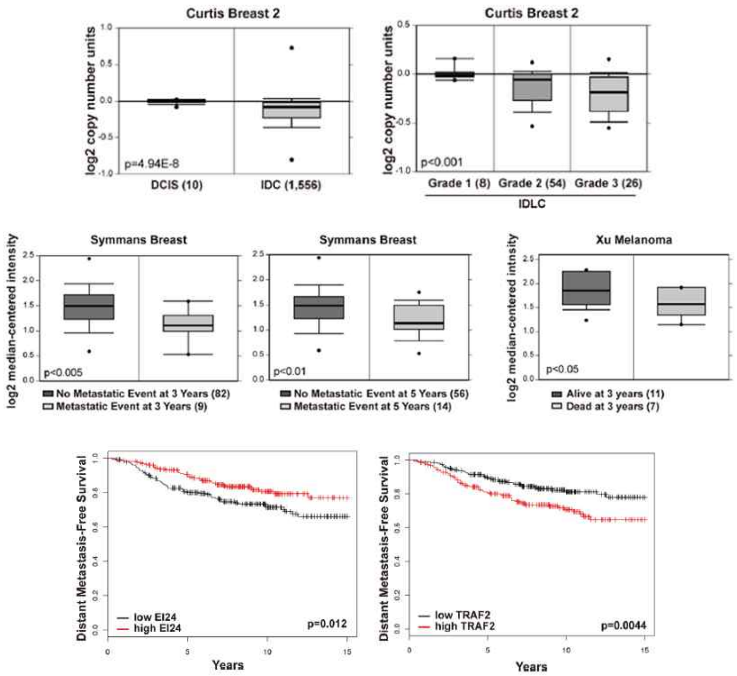

<in silico 분석을 통한 clinical 수준에서 EI24의 암전이에서의 역할 규명>

⑳ EI24 존재하에서 Complex I 구성 물질인 TRAF2/5는 EI24에 의해 lysosomal degradation이 되어 complex I이 붕괴되어 신호전달을 못하지만 EI24가 발현 저하되면 TRAF2/5등이 안정화되고 TNFa에 의한 신호전달이 constitutive하게 활성화되어 외부 신호를 RIP1의 K63 Ub를 통한 scaffold 작용으로 IKK complex를 통해 p65의 활성화를 이끌어 내어 transcription factor로 작용하게 하였다. IL-6, IL-8등의 염증 반응과 관련된 사이토카인들의 분비가 촉진되며 암전이를 촉진하게 되었다.

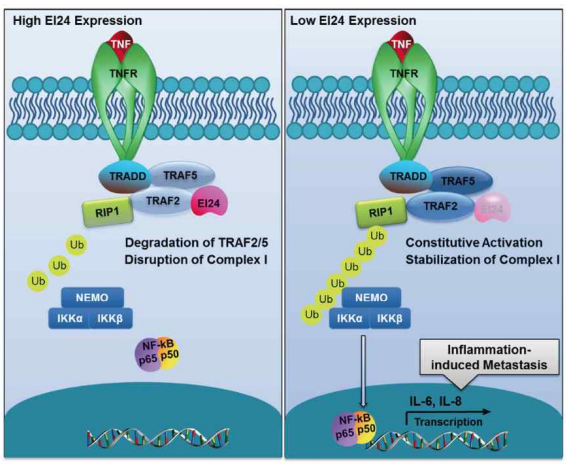

<EI24에 의한 NF-kB 활성화 조절을 통한 암 전이 조절 모델>

(3) 대사성질환 모델동물 개발 : ATF-3 GEM 마우스 개발

① 생체 내에서 ATF3 에 의한 대사질환 표현형을 보이는 모델동물을 개발하기 위하여 Vector 구축하고 cloning, construction의 과정을 거쳐 ATF3 GEM제작을 하였다.

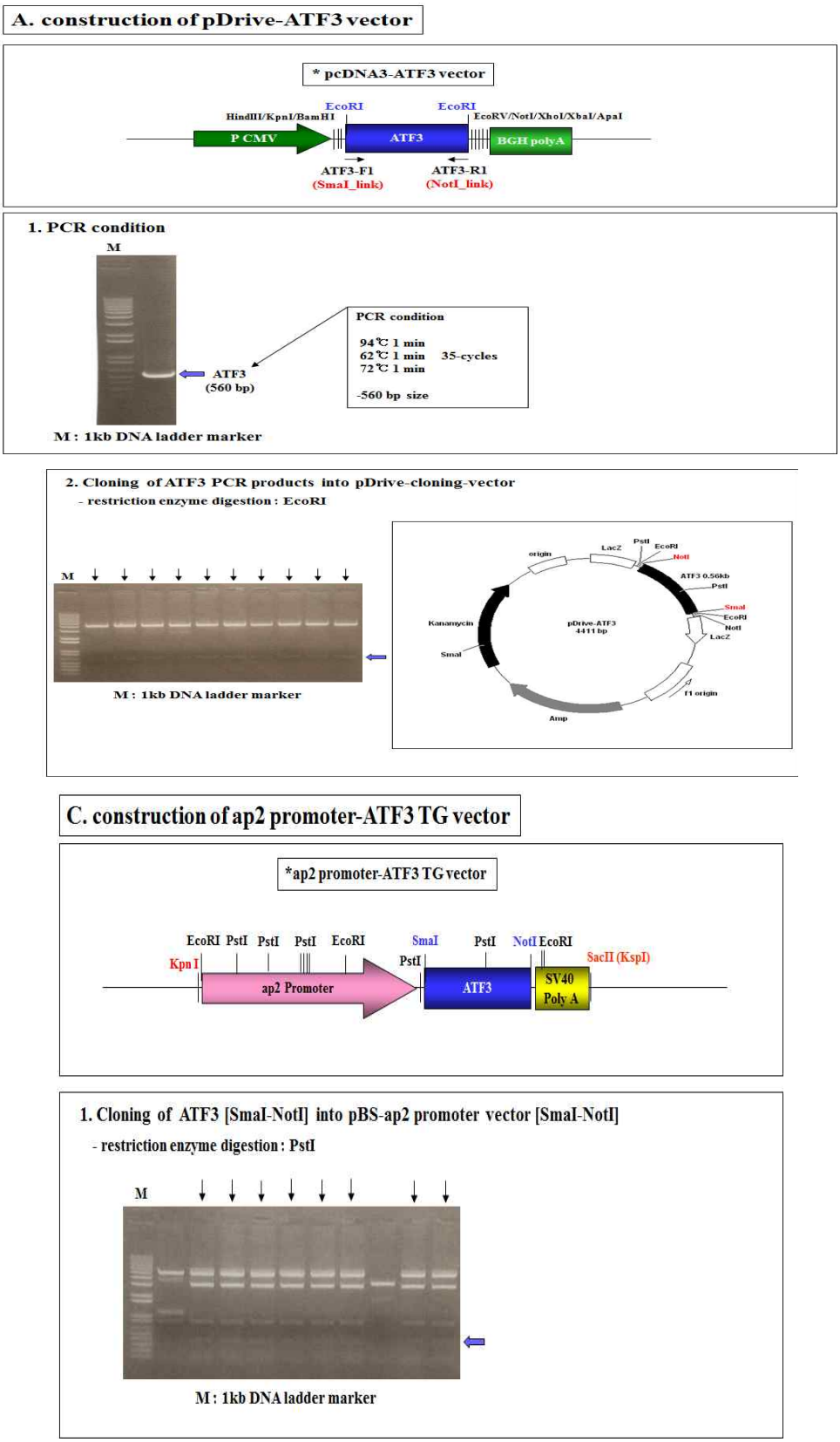

<ATF3 vector contsruction, cloning>

② 대사성질환유도를 위해 고지방식이로 비만을 유도한 뒤 체중변화는 큰 차이가 없었으며 IPGTT의 반응성에는 차이를 보임. 지방조직의 변화는 유의미한 차이를 보이고 있지 않았다.

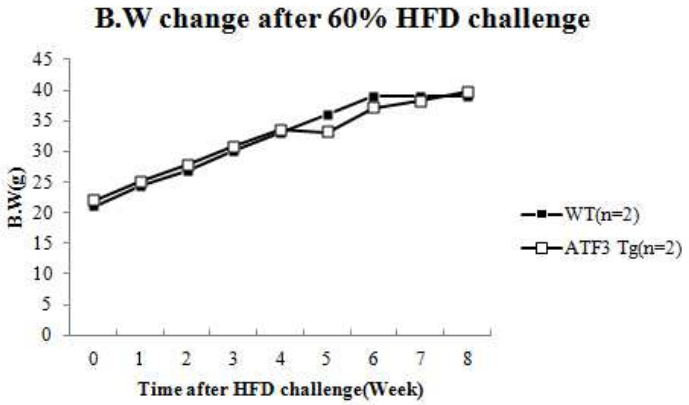

<HFD challenge 후 Body weight변화>

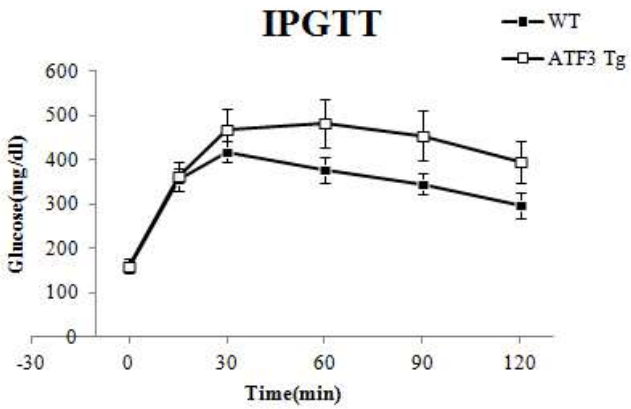

<ATF3 Tg 마우스의 IPGTT>

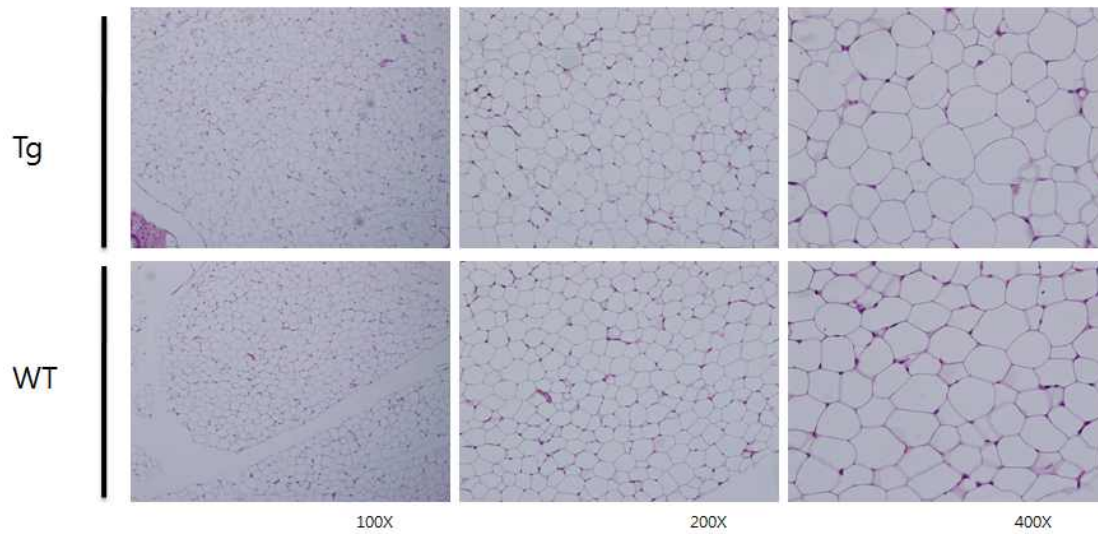

<ATF3 Tg, WT 마우스의 Adipose tissue staining>

③ ATF3 GEM은 비만 특이적 특성 변화는 크지 않지만 인슐린 저항성과 관련된 모델동물로서의 발전 가능성은 있는 것으로 사료된다. 2차년도 연계 연구에서는 지방간 중심의 대사질환 특성을 좀 더 연구할 필요가 있을 것으로 사료된다.

④ 현재 다른 유전자를 대상으로 대사질환 모델 개발 가능성 여부를 타진 중에 있음. UQCRB 유전자를 타겟으로 knock-out mouse를 제작하기 위하여 targeted ES cell 확보와 blastocyst injection을 할 계획이다.

(4) 뇌신경질환 동물모델 개발 : GX2, DM-1 GEM 마우스 개발

① RIKEN 및 IKMC Banking resource에서 targeted ES cell line 확보 및 blastcyst injection.

② Germline transmisstion test중에 있다.

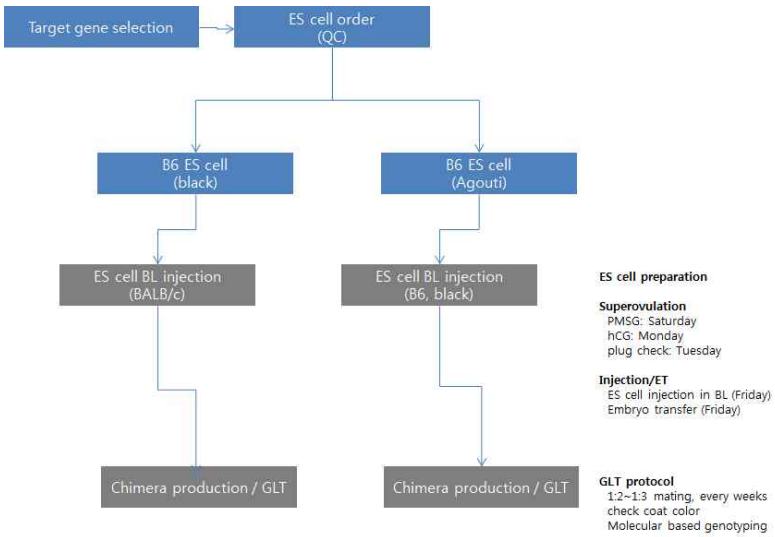

<DM-1, GX2 GEM 마우스 개발 scheme>

<DM-1, GX2 GEM 마우스 Germline transmission test>

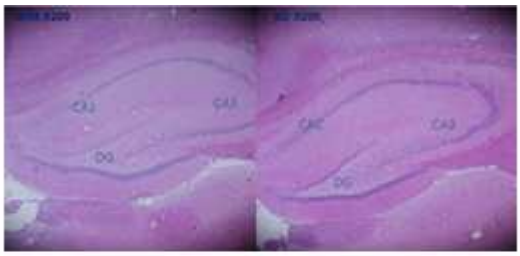

Hippocampus(HE stain)

신경증식능 소실확인: : Ki-67 IH stain

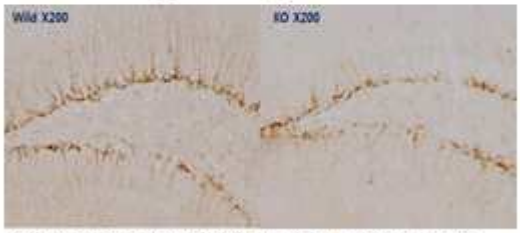

신경세포 재생능력 소실 : DCX stain

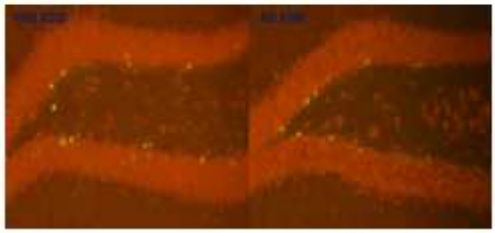

BrdU/NeuN doble stain

나. 개발된 질환모델동물을 이용한 신약후보물질의 유효성 검증

(Ei24 GEM 활용 신약 후보 물질 유효성 평가 (진행중))

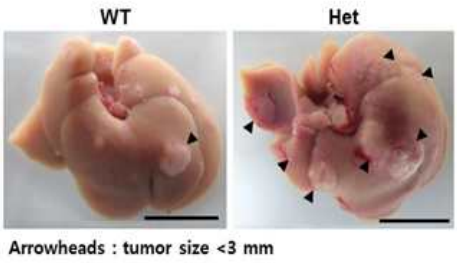

Ei24+/-(Het) 마우스에 DEN을 처리

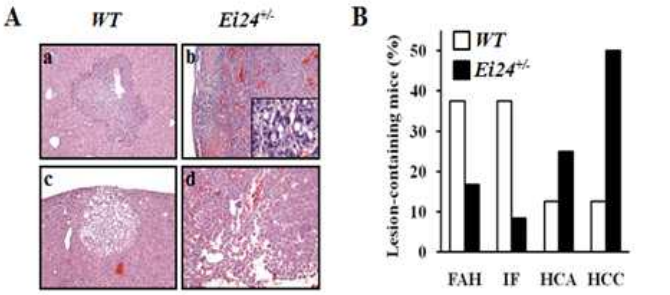

HCC가 유발된 Ei24+/- 마우스의 간 절편조직염색과 lesion 분석

다. 개발된 실험동물모델에 대한 보완사항 점검

제1협동 과제에서 개발한 모델동물의 신약후보 검색 유효성에 적합한 지를 판단하기 위하여 전문자 집단을 활용한 모델동물의 자원으로서의 가치를 검증 받는다.

성명	소속	분야
황대연	부산대학교	신경질환모델동물
이호	국립암센터	암질환모델동물
이영재	가천의대	심순환질환모델동물
엄홍덕	원자력의학원	암질환모델동물
오승현	국립암센터	암질환모델동물
최철수	가천의대	대사질환모델동물

3절. 제2협동. 천연물 질환, 패혈증 및 항암 효능 천연물 신약후보물질개발

1. 오미자로부터 패혈증에 효능을 가진 α-iso-cubebenol의 대량 분리

가. 오미자로부터 α-iso-cubebenol의 대량추출

(1) α-iso-cubebenol이 다량 함유된 분획 추출

DI 66.22 g을 충진한 25 cm × 3.0 cm의 칼럼에 오미자 헥산 추출물 12.29 g을 loading 한 다음 pretanol 50, 75, 95%와 chloroform 및 hexane을 순차적으로 가하여 eluting하였다 (방법 A와 B의 반복). 방법 A와 B에서 Pretanol의 농도는 물질을 분리하는 효과가 없을 것으로 판단되었다.

따라서 pretanol의 농도를 95%로 고정하고, chloroform 및 hexane으로 eluting한 결과 pretanol의 동도를 나누어서 실험한 결과와 유사하였다 (방법 C). Pretanol을 대체할 수 있는 acetone 및 methano의 효과를 검증하기 위하여 방법 C에서 acetone으로 대체한 결과 α-iso-cubebenol을 함유하는 분획을 얻을 수 없었다. 따라서 적당한 방법을 95%의 pretanol을 이용하면 α-iso-cubebenol이 함유된 분획을 얻을 수 있었다 (방법 D).

분리 함량을 높이기 위하여 DI 267.27 g을 충진한 35 cm × 5.5 cm의 칼럼에 오미자 헥산 추출물 55.13 g을 loading 한 다음 95%의 pretanol, chloroform 및 hexane으로 순차 추출한 결과 방법 C와 유사한 결과를 얻었으므로 하나의 칼럼에 추출물 약 55 g을 loading할 수 있는 좋은 방법이 확립되었다 (방법 E와 F).

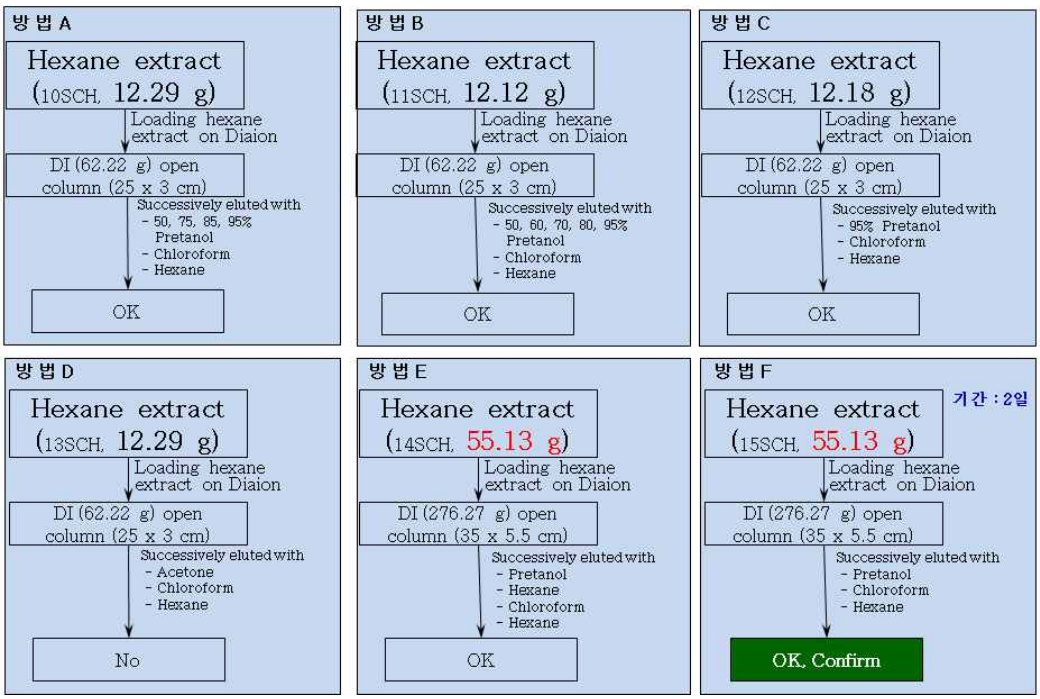

그림 2-1. DI를 이용한 α-iso-Cubebenol이 다량 함유된 분획방법 확립

(2) 방법 2-2. α-iso-cubebenol의 다량 순수분리

1차 년도와 동일한 방법을 이용하였는데 그 방법은 다음과 같이 수행되었다. DI 칼럼을 이용하여 α-iso-cubebenol이 다량 함유된 방법이 개발되었으므로, 이를 근거로 하여 α

-iso-cubebenol의 순수분리 방법의 개발이 필요하다.

DI 칼럼으로부터 얻은 1번 분획 14SCH1 7.3036 g을 100 cm × 3.0 cm의 sephadex 칼럼에 loading 한 후 MeOH로 eluting 한 결과 거의 분리되지 않았기 때문에 분획물 7.6551 g (14SCH1IB)을 얻었다. 14SCH1IB 분획물을 실리카겔로 충진한 60 cm × 5.0 cm의 칼럼에 loading하여 dichloromethane, dichloromethane과 acetone의 혼합용액을 순차적으로 가하여 순수분리한 α-iso-cubebenol 272.3 mg과 α-iso-cubebenol이 함유된 분획물 (14SCH1IBIL-IM) 436.6 mg을 얻었다. 14SCH1IBIL-IM 436.6 mg을 다시 실리카겔 컬럼하여 55.3 mg의 순수물질을 얻어 6일 동안에 방법 F-1으로부터 328.5 mg의 순수분리한 α-iso-cubebenol을 얻었다 (그림 2-2, 2-3, 2-4).

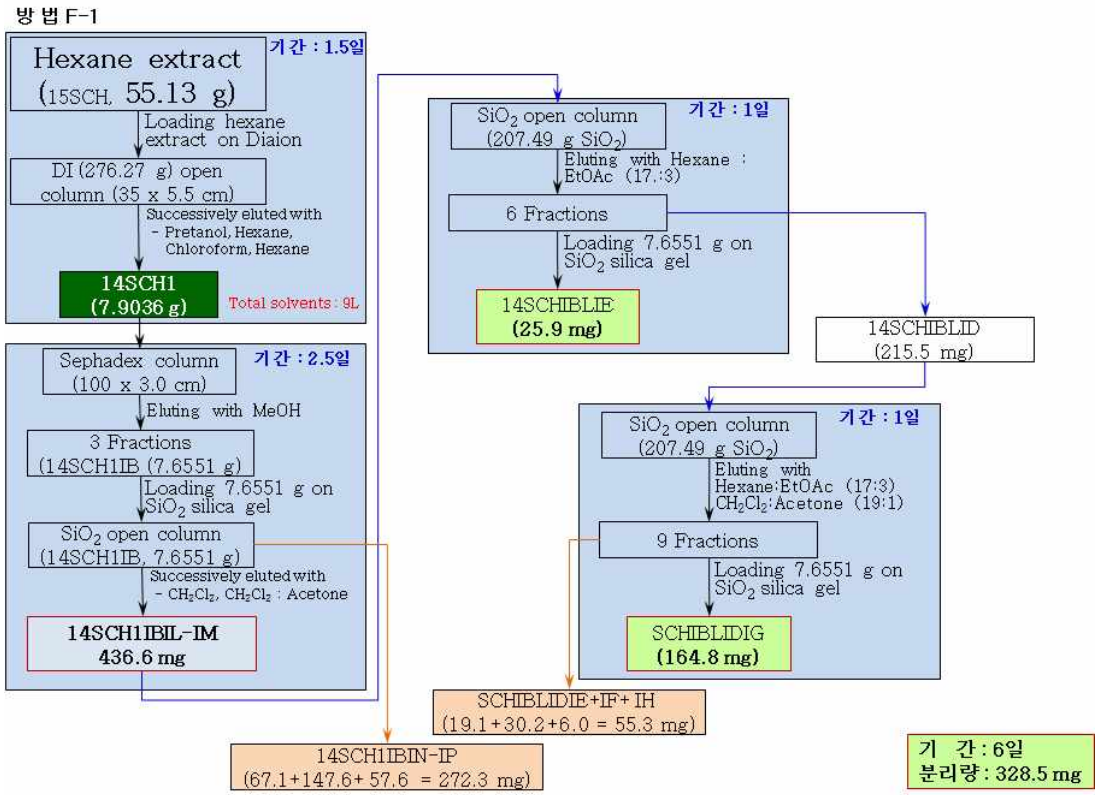

그림 2-2. α-iso-Cubebenol이 다량 함유된 분획으로부터 순수분리 방법

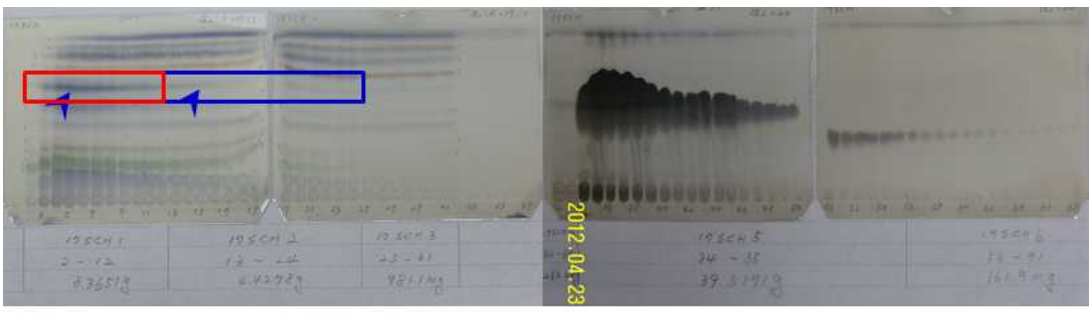

그림 2-3. α-iso-Cubebenol이 다량 함유된 TLC profile

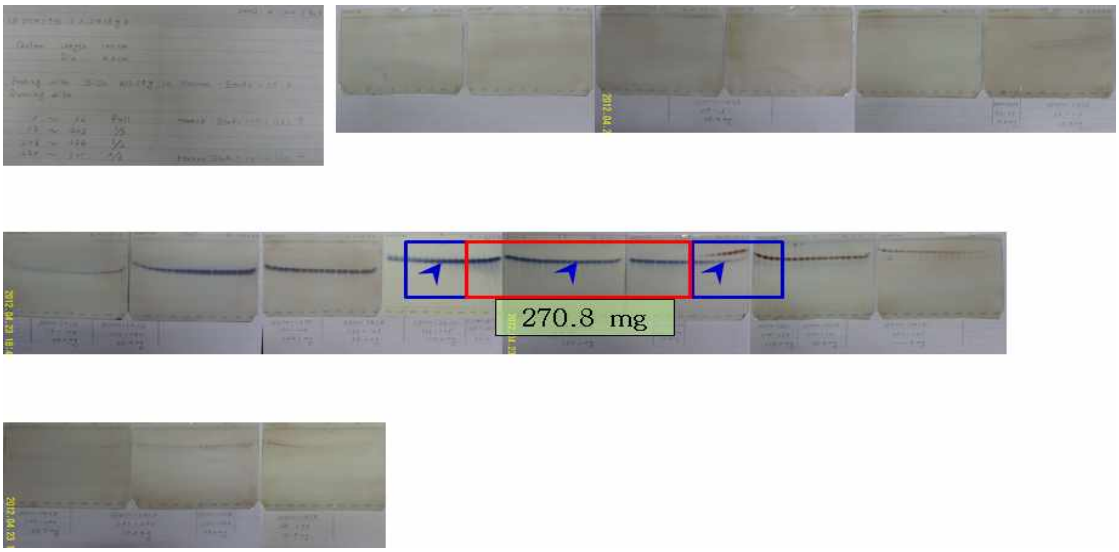

그림 2-4. α-iso-Cubebenol이 다량 분리된 TLC profile

따라서 이러한 방법을 이용하여 2차연도에는 97% 이상의 순도를 가진 α-iso-cubebenol 약 10 g을 순수분리하였으며, 약 5 g은 제 1세부과제 책임자에게 물질을 전달하여 현재 전임상 실험 중에 있다.

2. 지치로부터 항암 효능 추출물의 대량 확보

가. 지치 추출물의 함량 평가

지치 추출물의 함량은 1년차와 동일하게 HPLC 분석법을 이용하여 지치 추출물 중 5종의 shikonin 유도체의 함량을 측정하였다. HPLC 분석 조건은 Agilent/HP 1100 series HPLC-DAD 시스템, 칼럼은 Luna C18 column (150 mm × 3.0 mm, ID 5 μm), 용매조건은 1.0 ml/min의 조건에서 methanol - acetonitrile gradient를 이용하여 분석하였다. 그 결과 5종의 시코닌 유도체들의 상관값이 모두 0.99900-0.99987로서 분석조건을 얻었다.

나. 항암 효능 물질로 공급된 지치 추출물의 구조 및 HPLC 결과

5종의 순수분리한 성분은 GC-MS, ^{1}H-NMR and ^{13}C NMR spectral 분석을 통하여 Shikonin (**1**), Deoxyshikonin (**2**), β-Hydroxyisovalerylshikonin (**3**), Acetylshikonin (**4**) and Isobutyrylshikonin (**5**)임을 밝혔다. 순수분리한 5종의 shikon 유도체는 분석이 확립된 HPLC로서 확인한 결과 98% 이상의 순도를 나타내었다.

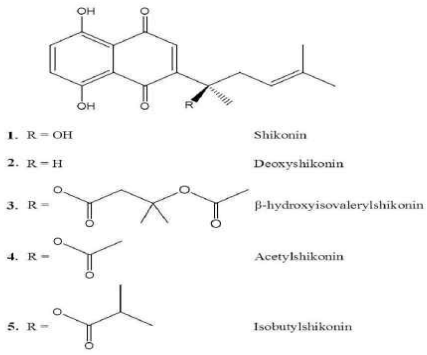

Fig. 1. Chemical structures of shikonin derivatives isolated from LEH extract.

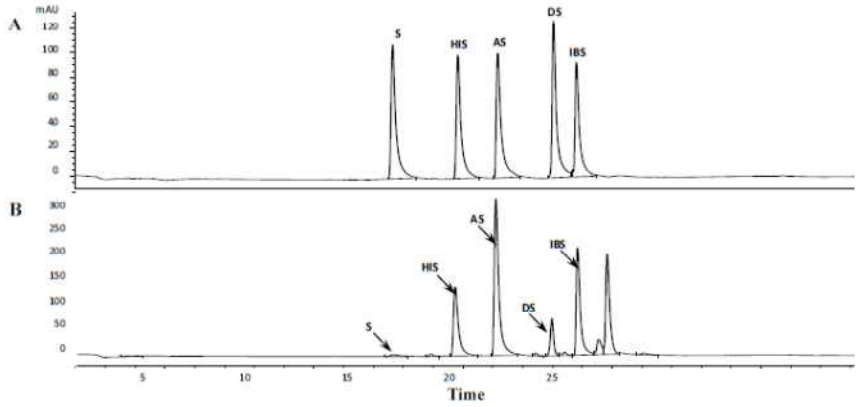

Fig. 2. A typical HPLC chromatogram of pure compounds (A) and hexane extract (B) from the roots of LE using a Luna C18 (2) column (Phenomenx, 150×3mm, 5μm particle size) fitted to to an Agilent 1100 series. S, shikonin; DS, deoxyshikonin; AS, acetylshikonin; HIS, β-hydroxyisovalerylshikonin; IBS, isobutylshikonin. Acquisition wavelength: 520 nm.

다. 지치 추출물의 주요 성분 함량

지치 시코닌 유도체를 HPLC를 이용하여 분석한 결과, 항암 활성을 나타내는 추출물의 주요 성분은 acetylshikonin 23.24%, isobutylshikonin 18.62% 및 β-hydroxyisovalerylshikonin 15.07%였으며, 그 외에도 deoxyshikonin은 3.82% shikonin은 1.85%로서 소량 함유되어 있었다.

Table 1. Contents of naphthoquinone derivatives in hexane extract of *L. erythrorhizon*.

Napthoquinones	Concentrations (%)
Shikonin	1.85 ± 0.06
Deoxyshikonin	3.82 ± 0.05
Acetylshikonin	23.34 ± 0.41
β-hydroxyisovalerylshikonin	15.07 ± 0.51
Isobutylshikonin	18.62 ± 0.36

3. Gomisin J의 혈관이완작용 규명

가.흰쥐 대동맥 혈관근에 대한 Gomisin J의 이완작용을 규명

Gomisin J는 혈관 내피세포 의존성과 비의존성 이완작용을 나타내었고, 내피세포 의존성 이 작용이 비의존성 이완작용에 비하여 더 강함을 나타냄(Fig. 1)

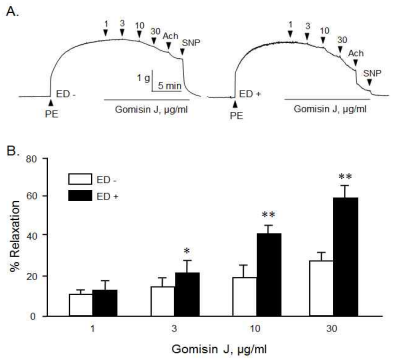

Fig. 1. Gomisin J-induced relaxation in aortic rings without endothelium (ED-) or with endothelium (ED+). (A) Representative tracings show the vasorelaxant effects of GJ (1 - .30 μ g/ml) in phenylephrine (PE, 10^{-5} M)-precontracted aortic rings. Ach, 10^{-6} M acetylcholine; SNP, 10^{-7} M sodium nitroprusside. (B) Quantitative data of GJ-induced vasorelaxation in ED− (n=5) or ED+group (n=6). Data were expressed as means±SEM. *Pb0.05, **P<0.01 vs. corresponding value in ED−group.

나. Gomisin J와 Gomisin A의 혈관이완작용 강도 비교

Gomisin J에 의한 혈관근 이완작용이 Gomisin A의 작용보다 더 강함이 증명되었음(Fig. 2).

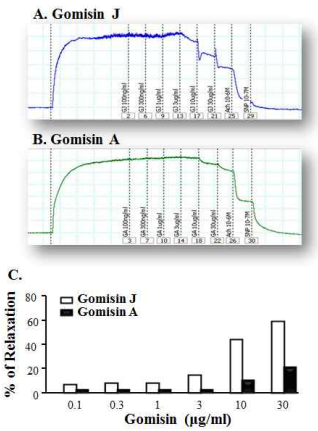

Fig. 2. Pharmacological characterization of gomisin J-induced vasorelaxation. GJ-induced relaxation was significantly attenuated when the endothelium (ED)-intact specimens were exposed to NG-nitro-L-argininemethyl ester (L-NAME, 10^{-4} M), but remained unaffected by indomethacin (INDO, 10^{-5} M) and tetraethylammonium (TEA, 10^{-3} M). (A) Representative tracings. (B) Quantitative data were expressed as means±SEM from 5 experiments. *P<0.05, **P<0.01 vs. corresponding control value.

다. Gomisin J의 혈관근 이완작용 기전 규명

(1) 흰쥐 대동맥 혈관근 이완작용 기전 규명. 혈관 내피세포 존재시 nitric oxide (NO) 생성 저해제인 L-NAME에 의해서 Gomisin J의 혈관 이완작용이 억제되었음. 하지만, cyclooxygenase 억제제인 indomethacin (INDO)과 K 통로 억제제인 tetraethylammonium (TEA)에 의하여서는 영향을 받지 아니하였음. 따라서, Gomisin J의 혈관이완작용이 혈관내피세포에서 생성되는 NO 생성과 연관이 있음을 확인하였음 (Fig. 3).

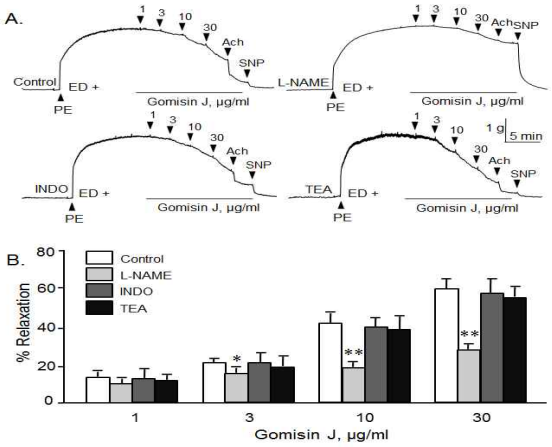

Fig. 3. Gomisin J-induced NO production in aortic tissues. Aortic tissues were treated with GJ (1 - 30 μg/ml) for 30 min, and then NO production was measured by DAF-FM using a fluorescent microscope. (A) Representative photographs from 4 independent experiments. (B) Representative photographs for GJ-induced NO production in aortic tissues in the presence of L-NAME (10^{-4} M). Acetylcholine (Ach, 10^{-6} M) was used as a positive control. (C) Quantitative data was expressed as ratio of control value, and data were represented as means±SEM from 4 experiments. $^{**}P<0.01$ vs. control; $^{\#\#}P<0.01$ vs. vehicle.

(2) Gomisin J와 NO 생성과의 연관성을 확인하기 위하여, 흰쥐 대동맥 혈관근을 이용하여 Gomisin J에 의한 NO 생성을 확인한 결과, Gomisin J의 농도 의존적으로 NO의 생성이 증가함을 확인하였고, 이 역시 NO 생성 저해제인 L-NAME에 의해 억제됨을 확인함 (Fig. 4).

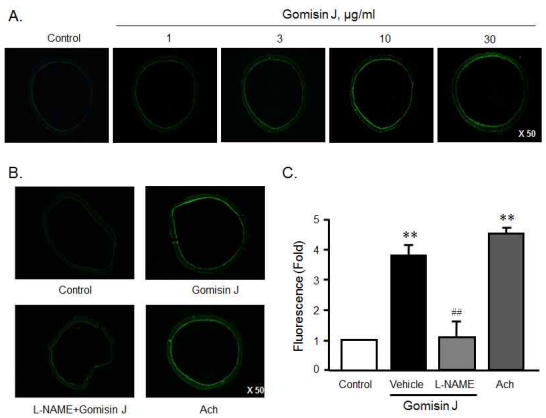

Fig. 4. Gomisin J-induced NO production in HCAEC. Cells were treated with GJ (0.1 - ″3 μ

g/ml) for 30 min, and then NO production was measured by DAF-FM. (A) Representative photographs from 4 independent experiments. (B) Representative photographs for GJ-induced NO production in HCAEC in the presence of L-NAME (10−4 M). Acetylcholine (Ach, 10−6 M) was used as a positive control. (C) Quantitative data were expressed as ratio to the control, and data were represented as means±SEM from 4 experiments. $^{**}P<0.01$ vs. control; $^{\#\#}P<0.01$ vs. vehicle.

(3) 혈관내피세포를 이용하여 Gomisin J에 의한 NO 생성을 확인한 결과, Gomisin J의 농도 의존적으로 NO의 생성이 증가하였고, 이 역시 NO 생성 저해제인 L-NAME에 의해 억제됨을 확인하였음(Fig. 5).

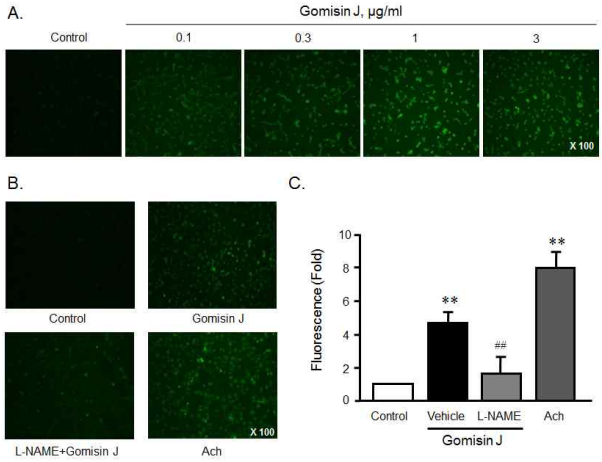

Fig. 5. Gomisin J-induced NO production in HCAEC. Cells were treated with GJ (0.1 - 3 μg/ml) for 30 min, and then NO production was measured by DAF-FM. (A) Representative photographs from 4 independent experiments. (B) Representative photographs for GJ-induced NO production in HCAEC in the presence of L-NAME (10^{-4} M). Acetylcholine (Ach, 10^{-6} M) was used as a positive control. (C) Quantitative data were expressed as ratio to the control, and data were represented as means±SEM from 4 experiments. $^{**}P<0.01$ vs. control; $^{\#\#}P<0.01$ vs. vehicle.

(4) Gomisin J에 의한 NO 생성의 메카니즘을 확인한 결과, Ca^{2+}과 PI3K/Akt와 관련이 있음을 확인함(Fig. 6).

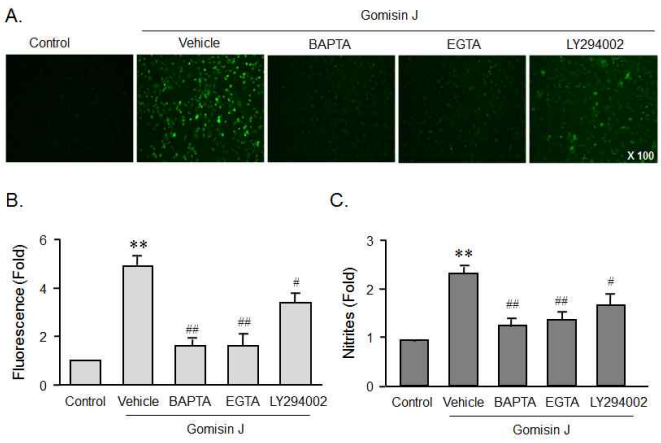

Fig. 6. Effects of calcium chelators and an Akt inhibitor on both NO production and eNOS activity in

HCAEC. (A) Representative photographs for GJ (1 μg/ml)-induced NO production in HCAEC, and its inhibition by various inhibitors including BAPTA-AM (2×10^{-5} M), EGTA (10−3 M), and LY294002 (10^{-5} M). (B) Quantitative data of NO production were expressed as ratio to the control value, and represented as means±SEM from 5 experiments. $^{**}P<0.01$ vs. control; $^{\#}P<0.05$, $^{\#\#}P<0.01$ vs. vehicle. (C) The activity of eNOS as measured by L-NAME-inhibitable nitrite production was expressed as ratios to the control value, and was represented as means±SEM from 5 experiments. $^{**}P<0.01$ vs. control; $^{\#}P<0.05$, $^{\#\#}P<0.01$ vs. vehicle.

(5) Gomisin J가 eNOS translocation과 eNOS phosphorylation을 유도하였고, 이러한 Gomisin J에 의한 eNOS phosphorylation은 Ca^{2+}과 PI3K/Akt 저해제에 의해 억제됨을 확인하였으며, 특히 Ca^{2+} 저해제에 의해 강력히 억제됨을 확인함(그림 7).

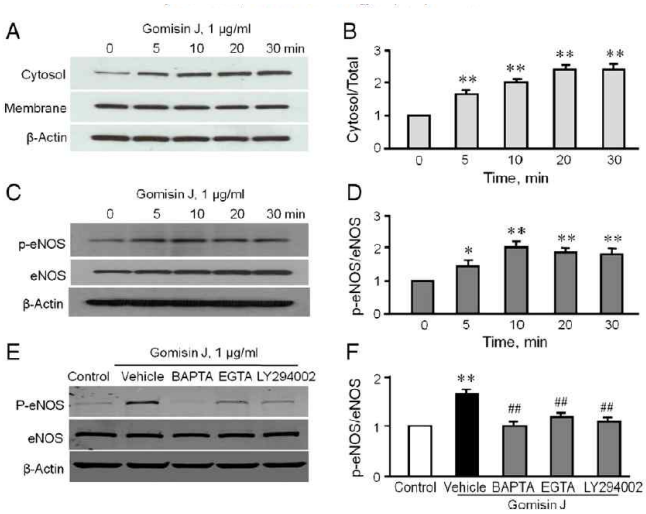

Fig. 7. Effects of gomisin J on cytosolic translocation and phosphorylation of eNOS in HCAEC. (A), (C) and (E) show representative blots for the time-course effects of GJ (1 μg/ml) on eNOS translocation, phosphorylation at Ser^{1177}, and its inhibition by calcium chelators (BAPTA-AM, 2×10^{-5} M; EGTA, 10^{-3} M) and a PI3K/Akt inhibitor (LY294002, 10^{-5} M), respectively. (B), (D), and (F) show respective quantification data. Datawere expressed as ratio of cytosolic eNOS/total eNOS (cytosolic eNOS+membrane eNOS) and phosphorylated eNOS/eNOS, and represented as means±SEM of 4-6 experiments. $^{*}P<0.05$, $^{**}P<0.01$ vs. corresponding control. $^{\#\#}P<0.01$ vs. vehicle.

(6) Gomisin J에 의한 혈관이완작용 기전을 규명하기 위하여 세포내 calcium 농도와 Akt phosphorylation을 측정한 결과, 세포내 calcium 농도가 Gomisin J에 의해서 농도 의존적으로 증가함을 확인하였고, Akt phosphorylation 또한 시간 의존적으로 증가함을 확인하였음. 하지만 Gomisin J에 의해 증가한 NO와 calcium은 5분 내에 빠르게 증가한 반면, Akt phosphorylation은 20분 이후에 증가함을 확인함(Fig. 8).

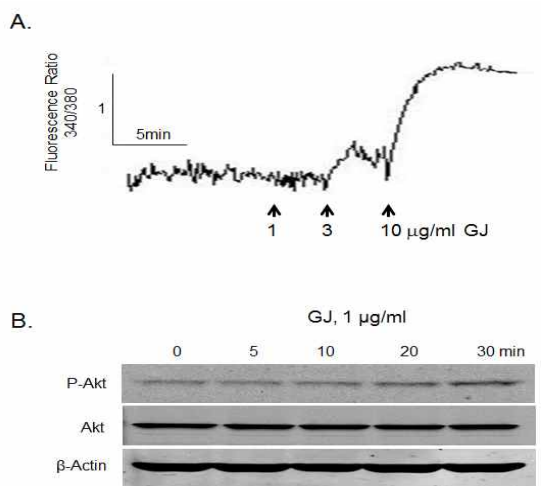

Fig. 8. Effects of gomisin J on intracellular calcium levels and Akt phosphorylation. (A) Representative tracing for the dose-response effects of GJ on intracellular calcium (n=5). HCAEC were incubated with the calcium indicator dye Fura 2-AM and then treated with GJ (0.1, 1 and 3 μg/ml). Cellular fluorescence was measured in fluorescence spectrophotometer. (B) Time-course effects of GJ (1 μg/ml) on the levels of p-Akt and total Akt in HCAEC treated with GJ for the indicated time. Representative photographs from 5 independent experiments.

라. 이러한 연구결과를 바탕으로 Gomisin J가 혈관 이완작용을 가지고 있으며, 이는 Ca^{2+} 경로를 통해 eNOS가 활성화시키고, 결과적으로 NO를 많이 생성하게 되어 혈관을 이완시킴을 밝혔다.

마. 1차연도의 연구결과를 근거로 Gomisin J를 고혈압 위험성 혹은 고혈압 환자에게 투여시 예방 혹은 치료효과가 있을 것으로 예측됨. 따라서, 2차연도의 연구에서 다양한 방법으로 고혈압이 유도된 마우스를 이용하여 Gomisin J의 고혈압 예방 혹은 치료효과를 밝히고자 하였다.

4. Gomisin J의 항고혈압 작용기작 규명

가. 혈관 세포 nitric oxide 생성에 대한 Gomisin J (GJ)의 작용 규명

Gomisin J의 농도에 따라 NO의 생성량이 증가하며 (A), Angiotensin II (Ang II)에 의해 감소되었던 NO의 생성량이 GJ에 의해 다시 회복되는 것을 나타내고 있음(B).

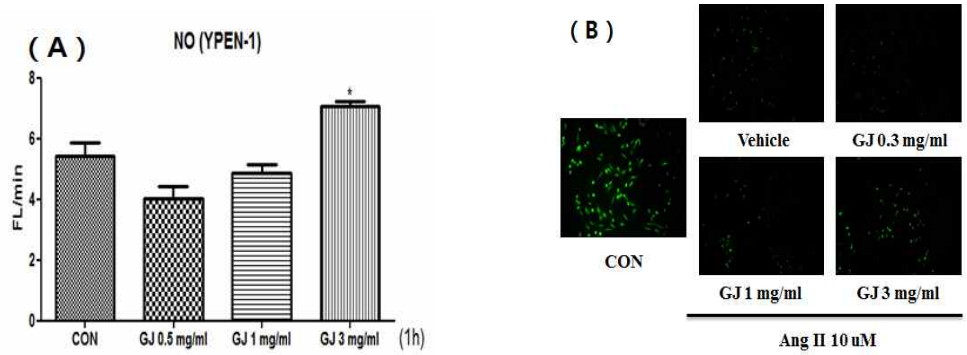

나. 혈관 세포 산소유리기 생성에 대한 Gomisin J (GJ)의 작용 규명

Angiotensin II에 의해 생성되는 산소 유리기인 ROS가 Gomisin J에 의해 농도 의존적으로 감소하는 것을 확인하였다.(C) 고혈압 동물 모델의 대동맥에서의 활성산소를 확인해 보았을 때 Angiotensin II를 투여한 고혈압 동물 모델에서는 활성 산소인 ROS가 증가 한 것dl 증명되었고, Gomisin J를 투여한 군에서는 ROS가 감소되는 것을 확인하였다.(D)

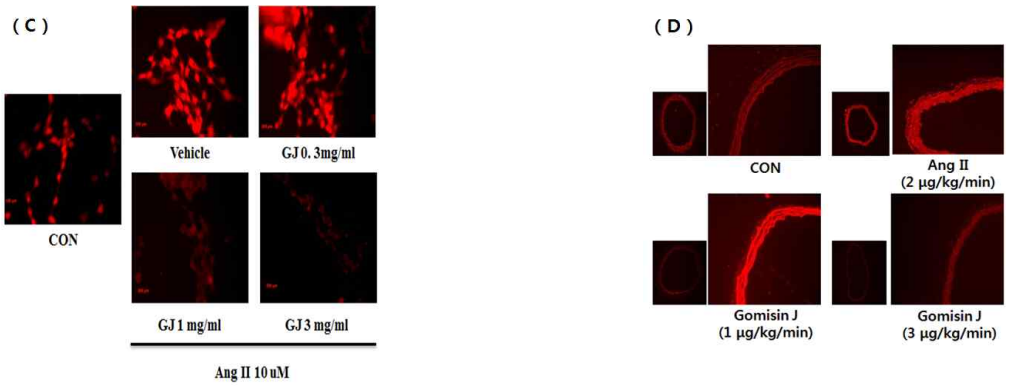

다. 고혈압 동물모델 개발 및 Gomisin J의 고혈압 예방효과

Angiotensin II를 1 μg/kg/min 용량으로 마우스에 투여 시, 투여 1주 후부터 혈압이 증가하였으나 통계학적인 유의성은 관찰되지 아니하였다. Angiotensin II를 2 μg/kg/min 용량으로 마우스에 투여 시, 투여 4일 후부터 혈압이 증가되었고, 투여 후 6일에 최고치에 도달 후 2주간 높은 혈압이 유지되었음. 따라서, Gomisin J의 고혈압 예방효과 혹은 치료효과를 관찰하기에 적합한 고혈압 모델로 생각된다.

Gomisin J를 1 μg/kg/min와 3 μg/kg/min의 두 가지 용량을 이용하여 실험하였음. 대조군에서는 angiotensin II 투여 후 3일부터 혈압이 증가하기 시작하였으나, Gomisin J 1 μg/kg/min과3 μg/kg/min를 투여한 군에서는 angiotensin II에 의한 혈압의 증가가 현저히 억제되었다.

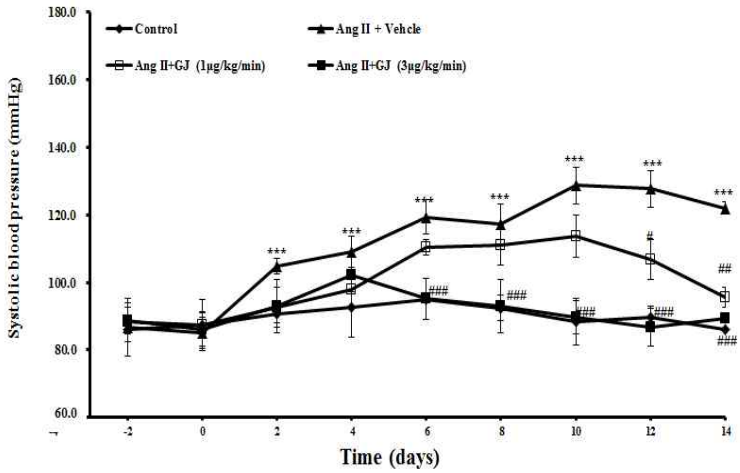

라. Gomisin J와 타 약물들과의 효능 비교

Angiotensin II receptor blocker인 Losartan 3 ㎍/kg/min 과 Gomisin A 3㎍/kg/min 군과 보다 더 좋은 혈압 감소 효과를 나타내는 본 연구 결과로 보아 Gomisin J가 고혈압 예방 약물로서의 가치가 높을 것으로 예상된다.

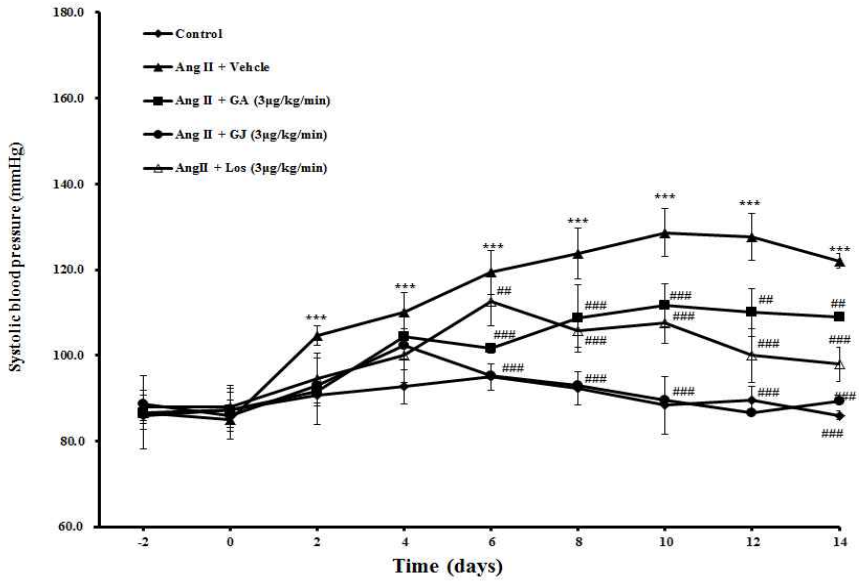

5. α-iso-cubebenol의 패혈증 치료효과

가. α-iso-cubebenol의 패혈증 효과

오미자 유래 신기능 물질인 α-iso-cubebenol에 의해서 패혈증 치료효과가 유도되는 지를 조사하기 위해, 사람 패혈증을 가장 mimic하는 것으로 알려진 CLP (Cecal Ligation & Puncture) 모델을 확립하여 이용하였음. CLP 모델을 만들면 severity에 따라서 정도의 차이가 있지만, 일반적으로 1-2일 사이에 높은 비율로 마우스의 생존율이 감소하게 됨. 확립된 CLP 패혈증 동물모델에서 α-iso-cubebenol 주입에 의한 치료효과를 조사하기 위해, CLP 모델을 만든 2시간 후에 최초로 두 용량 (5 mg/kg 및 15 mg/kg)의 α-iso-cubebenol을 피하로 주사하였음. 이어서 12시간 간격으로 총 4회 주사하고 마우스의 생존율을 총 10일간 관찰하였음. 그 결과, 5 mg/kg 및 15 mg/kg α-iso-cubebenol의 주입에 의해 매우 효과적으로 마우스 생존율이 증가함을 관찰하였음. 이 결과는 α-iso-cubebenol이 패혈증 치료효과를 가짐을 의미한다.

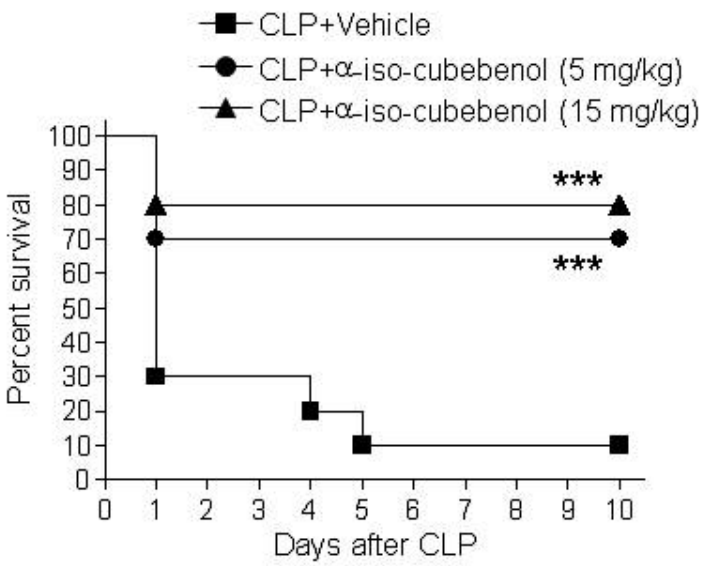

Fig. α-Iso-cubebenol protects against CLP-induced mortality. Several doses (0, 5, 15 mg/kg) of α-iso-cubebenol were injectedsubcutaneously four times into CLP mice at 2, 14, 26, and38 post-CLP. ***P<0.001 compared to vehicle control by ANOVA, Sample size: n = 10 mice/group.

나. α-Iso-cubebenol과 항생제의 조합적 사용에 의한 패혈증 치료효과 조사

임상적으로 패혈증 환자를 치료하기 위해서는 항생제를 사용하고 있음. 병원에서 실제로 패혈증 환자들에게 사용하는 항생제인 Gentamycin 및 Cephalosporin을 주입한 경우에 severe sepsis CLP 모델에서 약간 (약 20%)의 치료효과가 관찰되었음. 한편, severe sepsis CLP 모델에서 α-iso-cubebenol 주입에 의해서도 약 50%의 마우스 생존율 증강 효과가 관찰되었음. α-iso-cubebenol을 2종의 항생제와 병용 주사한 경우에는 약 80%의 마우스 생존율 증강효과가 유도되었음. 이 결과는 α-iso-cubebenol을 항생제와 병용 투여한 경우에 항생제 단독 사용에 의해 유도되는 치료효과를 매우 효과적으로 개선할 수 있음을 의미함. 임상적으로 패혈증 환자들에게 항생제와 병용 사용함으로써 패혈증 치료 효과를 획기적으로 높일 수 있음을 의미함.

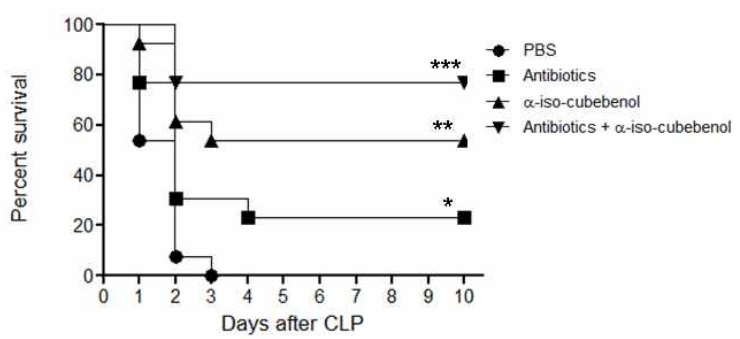

Fig. 2. α-Iso-cubebenol additively protects against CLP-induced mortality in the presence ofantibiotics. Vehicle (0.8% DMSO in PBS) or α-iso-cubebenol (15 mg/kg)was administrated 2and 14 after CLP. The mice were scarified 24 h after surgery and the lungs stainedhematoxylin and eosin (magnification, × 100) *P<0.05, **P<0.01, ***P<0.001 compared to vehicle control by ANOVA, sample size: n=15 mice/group.

다. α-Iso-cubebenol에 의한 패혈증 모델에서의 주요 주요장기 손상 제어 효과 조사

패혈증에 수반되어 주요 장기등의 손상이 초래됨. Spleen 및 thymus등의 장기에서는 면역세포의 사멸을 통한 기능 마비가 초래되어 multiple organ failure의 원인을 제공할 수 있음. CLP 패혈증 동물모델에서 spleen 및 thymus에서의 면역세포 사멸 정도를 TUNEL assay법으로 조사하였음. 그 결과, CLP 유발 24시간 후에 spleen 및 thymus에서 면역세포의 사멸이 매우 높게 유발됨을 확인하였음. 이러한 CLP 모델에 α-iso-cubebenol을 CLP 모델을 만들고 2시간 후에 최초로 피하로 주사하고 이어서 12시간 간격으로 1회 추가 주사한 경우에는 spleen 및 thymus에서 TUNEL positive 세포의 수가 현저히 감소함을 확인하였음. 이 결과는, α-iso-cubebenol 주입에 의해 CLP 패혈증 동물모델에서 면역세포 사멸 저해효과를 통해 패혈증 치료효과가 유도될 수 있음을 의미함.

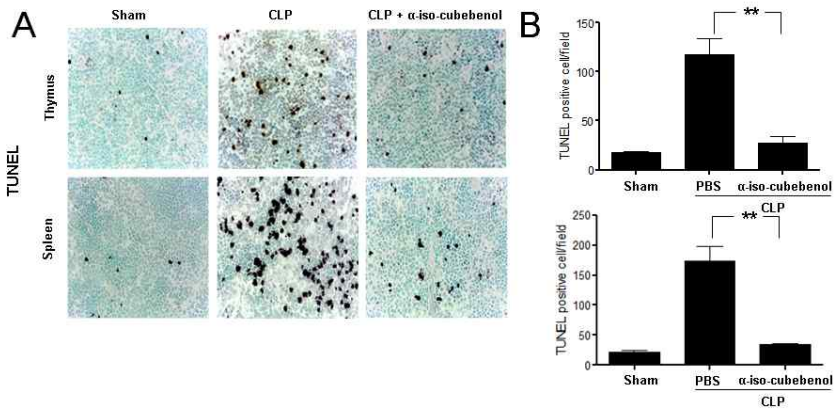

Fig. 3. α-Iso-cubebenol protects against widespread CLP-induced leukocyte apoptosis. (A) vehicle (0.8% DMSO in PBS) or α-iso-cubebenol (15 mg/kg) was injected two times intoCLP mice 2 and 14 h post-CLP. The spleen and the thymuswere collected 24 h after sham, CLP plus vehicle, or CLP plus α-iso-cubebenol administration, and use for a TUNEL assay. (B) TUNEL-positive cells from the spleensof mice described in (A) were quantified. Data are expressed as the mean ± SEM(n=8). **P<0.01, significantly different from the CLP alone control. Data are representative ofeight mice per group (A).

라. α-Iso-cubebenol에 의한 패혈증 모델에서의 caspase-3 활성 저해 효과 조사

패혈증에 수반되어 면역세포의 사멸은 주로 caspase-3의 활성화를 통해서 매개되는 것으로 알려져 있음. CLP 패혈증 동물모델에서 spleen 및 thymus에서의 caspase-3의 활성화 여부를 activated caspase-3에 대한 항체를 이용하여 immunohistochemistry법으로 조사하였음. 그 결과, CLP 유발 24시간 후에 spleen 및 thymus에서 caspase-3의 활성화가 유발됨을 확인하였음. 이러한 CLP 모델에 α-iso-cubebenol을 CLP 모델을 만들고 2시간 후에 최초로 피하로 주사하고 이어서 12시간 간격으로 1회 추가 주사한 경우에는 spleen 및 thymus에서 caspase-3 활성화가 현저히 저해됨을 확인하였음. 이 결과는, α-iso-cubebenol 주입에 의해 CLP 패혈증 동물모델에서 면역세포 사멸 저해효과가 caspase-3 활성화 저해를 통해 유도될 수 있음을 의미하다.

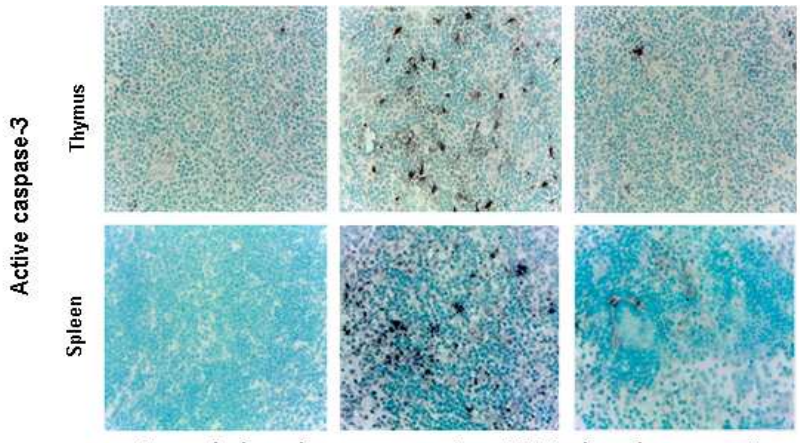

Fig. 4. α-Iso-cubebenol protects against CLP-induced caspase-3 activation. Vehicle (0.8% DMSO in PBS) or α-iso-cubebenol (15 mg/kg) was injected two times into CLP mice 2 and 14 h post-CLP. The spleens and thymus from the micedescribed above were subjected to immunohistochemistry with cleaved-caspase-3 antibody (magnificatio, × 100). Data are representative of eight mice per group.

마. α-Iso-cubebenol에 의한 패혈증 모델에서의 bactericidal 활성 조사

오미자 유래 신기능 물질인 α-iso-cubebenol에 의해서 패혈증 치료효과가 유도되었기에, CLP (Cecal Ligation & Puncture) 모델에서, α-iso-cubebenol 주입에 의해 복강 내 박테리아 수가 조절되는 지를 조사하였음. CLP 모델을 만든 후 2, 14시간에 각각 15mg/kg의 α-iso-cubebenol을 마우스에 주입하고 CLP 모델을 만든 지 24시간 후에 peritoneal fluid를 수확하여 peritoneal fluid에 존재하는 bacteria 수를 계수하였음. 그 결과, sham에서는 bacteria가 거의 관찰되지 않았으나, CLP 모델에서는 많은 수의 bacteria가 관찰되었음. CLP 모델에 α-iso-cubebenol을 주입한 군에서는 CLP 단독군에 비해서 현저히 bacteria 수가 줄어들어 있음을 관찰하였음. 동일모델에서 blood를 채혈하고 blood내에 존재하는 bacteria 수를 계수하였을 때에도 유사하게 α-iso-cubebenol 주입에 의해서 bacteria 수가 급격히 줄어듦을 확인하였음. 이 결과는 CLP 패혈증 동물 모델에서 α-iso-cubebenol 주입에 의해 bactericidal activity가 현저히 증가함을 의미한다.

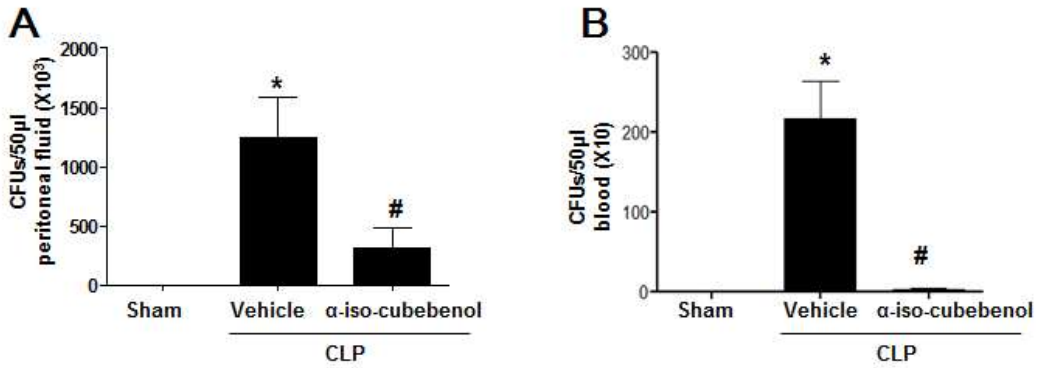

α-Iso-cubebenol stimulates bactericidal activity. (A, B) Vehicle (0.8% DMSO in PBS) or α-iso-cubebenol (15 mg/kg) was injected two times into CLP mice 2 and 14 h post-CLP. Peritoneal lavage fluid (A), or peripheral blood (B) collected 24 h after sham operation, CLP, or CLP plus α-iso-cubebenol administration was cultured overnight on blood-agar base plates at 37°C, and CFUs were determined. Data are expressed as the mean ± SEM; n = 8. *, $P < 0.05$, compared with the value obtained from the sham control (A, B); #, $P < 0.05$, significantly different from the CLP alone control (A, B).

바. α-Iso-cubebenol에 의한 항원탐식 활성 및 반응성 산소 생성 조절 효과 조사

α-iso-cubebenol에 의해서 패혈증 동물모델에서 bactericidal 활성이 증가함을 관찰한바, bactericidal activity 매개에 중요한 기능을 담당하는 항원탐식능 및 반응성 산소 생성에 α-iso-cubebenol이 미치는 영향을 조사하였음. Raw264.7 세포주에 FITC-dextran을 첨가하고 이어서 다양한 농도의 α-iso-cubebenol을 처리하였음. Raw264.7 세포내로 탐식된 FITC-dextran의 양을 Flow cytometer를 이용하여 측정한 결과, α-iso-cubebenol 처리에 의해 농도-의존적으로 FITC-dextran의 항원 탐식이 증가됨을 관찰하였음. 이 결과는 α-iso-cubebenol이 대식구 세포의 항원탐식능을 촉진할 수 있음을 의미함. 한편, 사람 호중구 세포를 대상으로 α-iso-cubebenol 처리에 의해 생성되는 superoxide anion의 양을 cytochrome c reduction assay법으로 측정한 결과, α-iso-cubebenol 처리에 의해 매우 효과적으로 superoxide anion 생성이 촉진됨을 관찰하였음. 이러한 결과는 α-iso-cubebenol에 의해 대식구 및 호중구에서 항원탐식능 증가 및 superoxide anion 생성 촉진을 통해 궁극적으로 bactericidal activity를 증가시킬 수 있음을 의미한다.

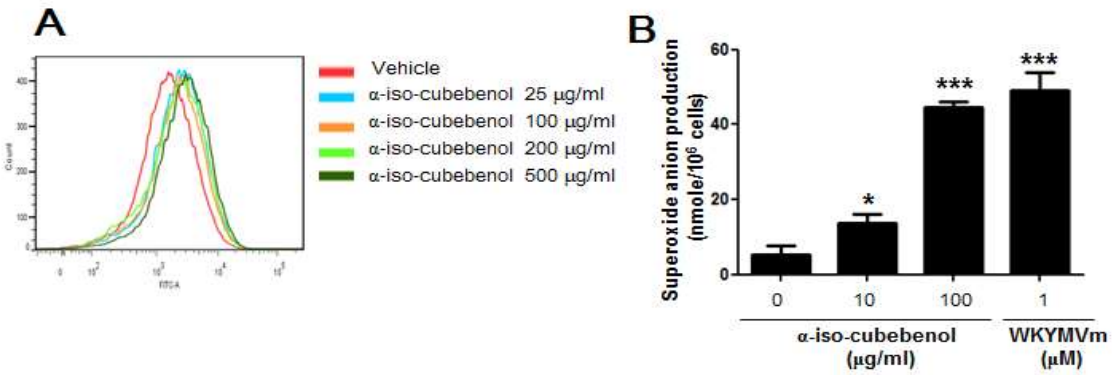

α-Iso-cubebenol stimulates phagocytic activity and superoxide anion production. (A) Raw 264.7 cells (2×10^5) were resuspended in 100 μl PBS and preincubated with or without α-iso-cubebenol for 30 min. Then the cells were further incubated with FITC-dextran (1 mg/ml) at 37°C for 30 min. After fixing the cells, phagocytic uptake was analyzed on a flow cytometer. The result is representative of three independent experiments. (B) Freshly isolated human neutrophils were stimulated with vehicle (0.1% DMSO in PBS) or α-iso-cubebenol (10 or 100 μg/ml) for 5 min. The amount of superoxide anions produced from neutrophils was measured using a cytochrome c reduction assay. Data are expressed as the mean ± SEM; n = 8. *, *P<0.05; ***P<0.001 compared to the vehicle control (B).

사. α-Iso-cubebenol에 의한 패혈증 모델에서의 염증성 사이토카인 생성 저해 효과 조사

패혈증에 수반되는 주요 염증반응은 염증성 사이토카인 생성을 통해 매개될 수 있음. CLP 패혈증 동물모델에서 α-iso-cubebenol 주입 여부에 따른 염증성 사이토카인의 생성 조절 효과를 조사하기 위해, CLP 모델 확립 후 2시간 및 14시간에 α-iso-cubebenol (15mg/kg)을 주입하고 CLP 모델 확립 24시간 후에 peritoneal fluid를 취해, peritoneal fluid에 존재하는 IL-1β 및 IL-6의 양을 측정하였음. 그 결과, CLP 모델 확립에 의해 peritoneal fluid내에서의 IL-1β 및 IL-6의 양이 현저히 증가하였으며, α-iso-cubebenol 주입군에서는 이들 염증성 사이토카인의 생성이 매우 효과적으로 저해됨을 관찰하였음.

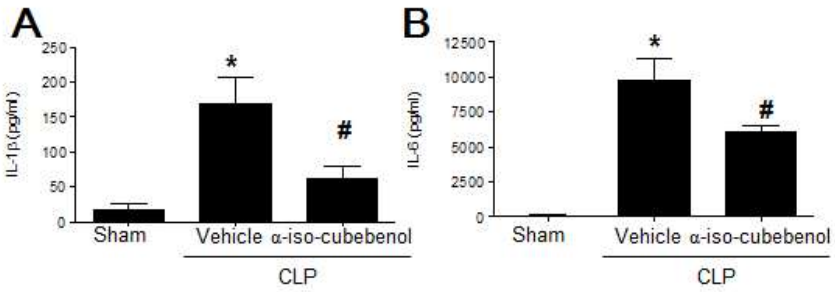

Effects of α-iso-cubebenol on CLP- induced cytokine production. (A-B) Vehicle (0.8% DMSO in PBS) or α-iso-cubebenol (15 mg/kg) was injected two times into CLP mice at 2 and 14 h post-CLP. Separate groups of animals were subjected to sham, CLP plus vehicle, or CLP plus α-iso-cubebenol treatment. Peritoneal fluids were collected at 24 h after CLP. Cytokine levels in the peritoneal fluid were determined by ELISA analysis. Panels A, B display results for IL-1β and IL-6 respectively. Data are expressed as the mean ± SEM (n = 8). *, $P < 0.05$, compared with the value obtained from the sham (A, B) control; #, $P < 0.05$, significantly different from the CLP alone (A, B) control.

아. α-Iso-cubebenol에 의한 LPS-유도 염증성 사이토카인 생성 저해 효과 조사

CLP 패혈증 모델에서 α-iso-cubebenol 주입에 의해 염증성 사이토카인 생성 저해효과를 관찰한 바, LPS 자극에 의해 생성되는 염증성 사이토카인 생성에 α-iso-cubebenol이 영향을 주는 지를 조사하였음. 이를 위해, mouse splenocyte를 분리하고 분리된 mouse splenocyte에 LPS 단독 및 LPS + α-iso-cubebenol를 처리하고 4시간 배양후에 생성되는 사이토카인의 양을 측정하였음. 그 결과, mouse splenocyte에서 LPS에 의해 생성되는 IL-1β, IL-6 및 IFN-γ의 생성이 α-iso-cubebenol에 의해 매우 효과적으로 감소함을 관찰하였음. 이 결과는, α-iso-cubebenol에 의해 LPS에 의한 염증 반응이 저해될 수 있음을 의미한다.

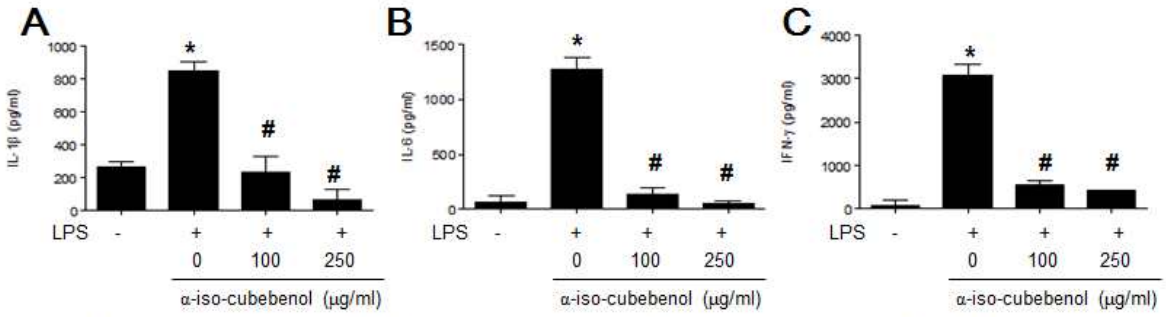

Effects of α-iso-cubebenol on LPS-induced cytokine production. (A-C) Mouse splenocytes were stimulated with PBS or LPS (100 ng/ml). After 15 min, cells were subsequently stimulated with vehicle (0.1% DMSO in PBS) or α-iso-cubebenol (100 or 250 mg/ml) for 4 h. IL-1β (A), IL-6 (B), and IFN-γ (C) levels were measured by ELISA. Data are expressed as the mean ± SEM (n = 8). *, $P < 0.05$, compared with the value obtained from the not treated (A-C) control; #, $P < 0.05$, significantly different from the LPS alone (A-C) control.

자. α-Iso-cubebenol에 의한 호중구 세포에서의 칼슘이온 조절 효과 규명

α-iso-cubebenol에 의해 사람 호중구 세포의 활성이 조절되는 지를 조사하기 위해, 대표적인 세포 활성화 신호인 세포 내 칼슘이온의 변화를 측정하였음. 먼저 다양한 농도의 α-iso-cubebenol를 호중구에 처리한 결과, 1-200μg/ml의 α-iso-cubebenol에 의해서 농도-의존적으로 호중구내의 칼슘이온의 증가가 유도됨을 관찰하였음. α-iso-cubebenol에 의한 호중구에서의 칼슘이온 증가에 관련된 작용기전을 규명하기 위해, PLC 저해제인 U-73122를 처리하여 조사하였음. 그 결과, α-iso-cubebenol에 의한 호중구내에서의 칼슘

이온 증가는 U-73122에 의해서 거의 완전히 저해됨을 관찰하였음. U-73122의 inactive analogue인 U-73343에 의해서는 α-iso-cubebenol에 의한 칼슘증가가 영향을 받지 않았음. 이 결과는 α-iso-cubebenol에 의한 호중구에서의 칼슘이온 증가는 PLC활성화를 통해서 매개됨을 의미함. 세포막에 존재하는 다양한 종류의 칼슘이온 채널에 의한 칼슘이온 증가 가능성을 조사하기 위해, diltiazem, SK&F 및 nifedifine을 전처리하고 α-iso-cubebenol에 의한 칼슘이온 증가가 영향을 받는지 조사하였음. α-iso-cubebenol에 의한 칼슘이온 증가는 이들 칼슘이온 채널 저해제에 의해서는 전혀 영향을 받지 않았음. 이 결과를 종합하면, α-iso-cubebenol에 의한 호중구에서의 칼슘이온 증가는 PLC 활성화를 통한 세포 내 칼슘이온 유리를 통해서 매개될 수 있음을 의미한다.

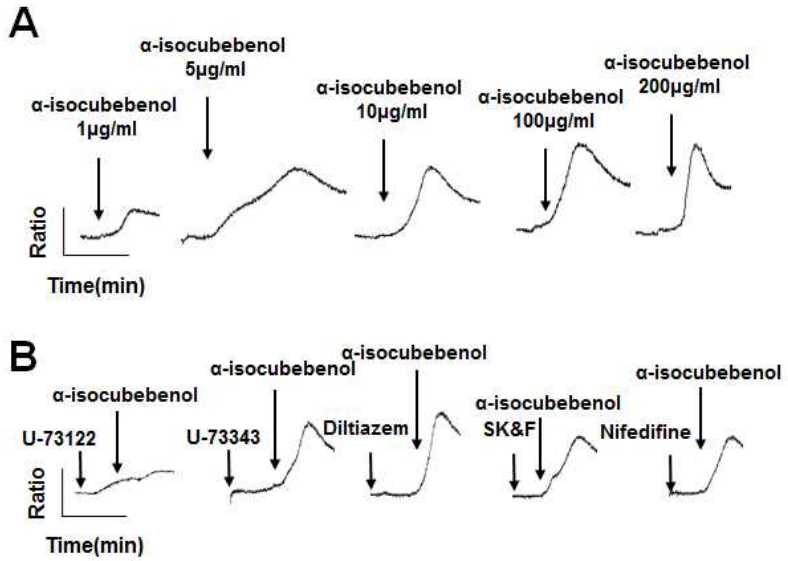

α-Iso-cubebenol stimulates $[Ca^{2+}]_i$ release in human neutrophils. Human neutrophils were stimulated with various concentrations (1, 5, 10, 50, 100, or 200 μg/ml) of α-iso-cubebenol (A). Human neutrophils were preincubated with U-73122 (5 μM), U-73343 (5 μM), diltiazem (10 μM), SK&F (10 μM), or nifedifine (1 μM), and then stimulated with α-iso-cubebenol (10 μg/ml) (B). The relative $[Ca^{2+}]_i$ are expressed as fluorescence ratios. The data represents three independent experiments (A and B).

차. α-Iso-cubebenol에 의한 호중구 세포에서의 탈과립 활성 조절 효과 조사

α-iso-cubebenol에 의해 사람 호중구 세포에서 탈과립 활성이 조절되는 지를 조사하였음. 이를 위해, 건강한 성인으로부터 분리한 사람 호중구에 다양한 농도의 α-iso-cubebenol을 처리하고 생성되는 β-hexosaminidase의 활성을 측정하였음. 그 결과, 50-100μg/ml의 α-iso-cubebenol에 의해 효과적으로 탈과립 활성이 증가됨을 관찰하였음. 이 결과는 α-iso-cubebenol에 의해서 호중구의 탈과립 활성 증강을 통해 과립내의 다양한 효소의 유리를 촉진할 수 있음을 의미한다.

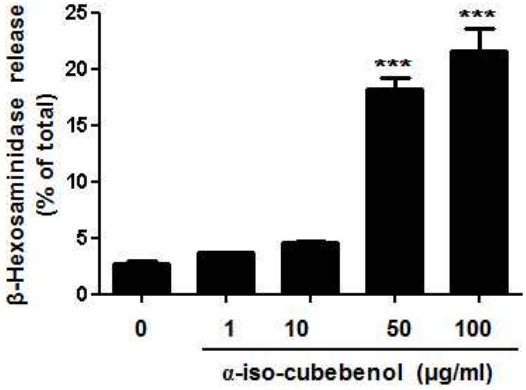

α-Iso-cubebenol stimulates degranulation activity in human neutrophils. Various concentrations (0, 1, 10, 50, or 100 μg/ml) of α-iso-cubebenol were administered to human neutrophils. The α-iso-cubebenol-induced secretion of β-hexosaminidase was determined. Data are expressed as mean ± S.E.; n = 8. ***P<0.001, compared with the value obtained from the untreated control.

카. α-Iso-cubebenol에 의한 호중구 세포의 이동성 조절 효과 조사

α-iso-cubebenol에 의해 사람 호중구 세포의 이동성이 조절되는 지를 boyden chamber를 이용하여 조사하였음. 다양한 농도의 α-iso-cubebenol을 처리한 결과 1-100μg/ml의 α-iso-cubebenol에 의해서 효과적으로 호중구 세포의 이동성을 촉진함을 관찰하였음. 이러한 α-iso-cubebenol에 의한 호중구 세포의 이동성 증강은 기존에 보고된 WKYMVm에 의한 호중구 이동성 조절 효과에 버금갈 정도로 매우 높은 활성임을 관찰하였음. 한편, 대표적인 호중구 이동성 조절 활성 조절 수용체인 CXCR2가 α-iso-cubebenol에 의한 호중구 이동성 조절에 관여하는지를 CXCR2 antagonist인 SB225002를 처리하여 조사하였음. 그 결과, α-iso-cubebenol에 의한 호중구 세포의 이동성 증강은 SB225002에 의해 완전히 저해됨을 관찰하였음. 이 결과는 α-iso-cubebenol에 의한 호중구 세포의 이동성 증강이 CXCR2를 통해서 매개될 수 있음을 의미한다.

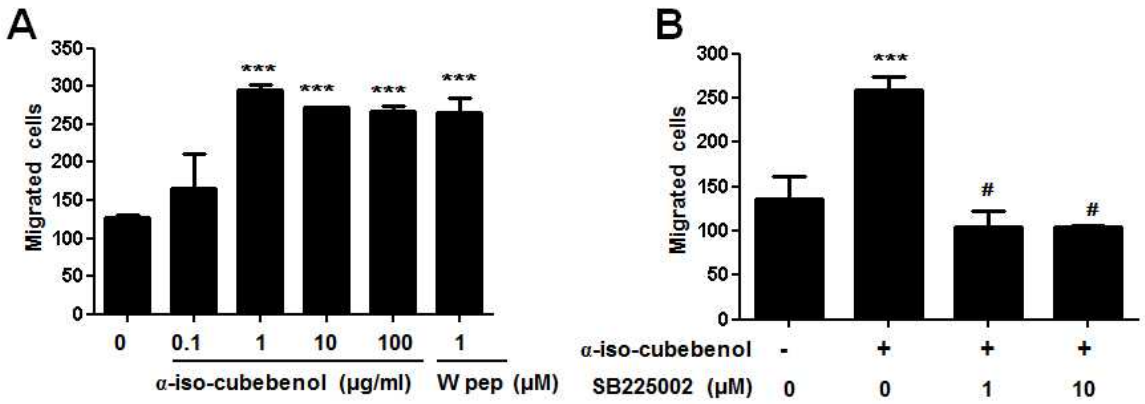

α-Iso-cubebenol stimulates neutrophil chemotaxis via CXCR2. Human neutrophils (1×10^6 cells/ml of serum-free RPMI) were added to the upper wells of a 96-well chemotaxis chamber, and migration across a 3-μm pore size polycarbonate membrane was assessed after 1.5-h of incubation at 37°C. Various concentrations (0, 0.1, 1, 10, or 100 μg/ml) of α-iso-cubebenol or 1 μM WKYMVm were used for chemotaxis assay (A). Vehicle or two different concentrations (1 or 10 μM) of SB225002 pretreated cells were subjected to chemotaxis assay with 10 μg/ml of α-iso-cubebenol (B). The number of migrated cells was determined by counting in a high-power field (400×). Data are presented as mean ± S.E. of three independent experiments performed in duplicate. ***P<0.001, compared with the value obtained from the untreated control. #, P < 0.05, significantly different from the α-iso-cubebenol alone control (B).

타. -Iso-cubebenol에 의한 패혈증 치료효과에서의 CXCR2의 기능 조사

α-iso-cubebenol에 의한 패혈증 치료효과가 CXCR2를 통해서 매개되는 지를 조사하기 위해, CLP 패혈증 동물모델에서 α-iso-cubebenol 주입에 의해 증가된 생존율이 CXCR2 antagonist인 SB225002 주입에 의해 영향을 받는지를 조사하였음. 그 결과, α-iso-cubebenol 주입에 의해 증가한 마우스 생존율이 SB225002 주입군에서는 거의 완전히 저해됨을 관찰하였음. 이 결과는 α-iso-cubebenol에 의한 CLP 패혈증 동물 모델에서의 마우스 생존율 증강 및 패혈증 치료효과가 CXCR2를 통해서 매개될 수 있음을 의미한다.

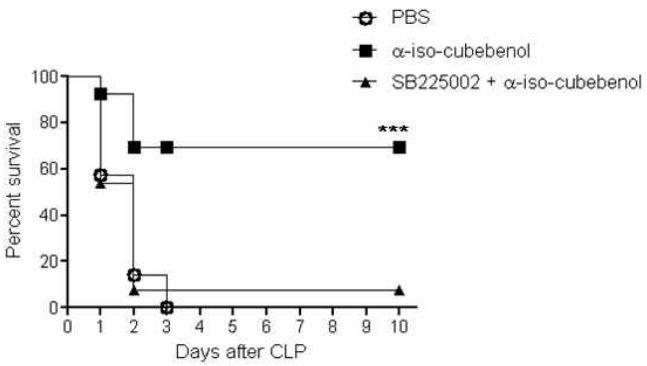

Role of CXCR2 on α-iso-cubebenol-induced protection against CLP-induced mortality. Vehicle (0.8% DMSO in PBS), α-iso-cubebenol (15 mg/kg), or SB225002 (15mg/kg) plus α-iso-cubebenol (15 mg/kg) were injected subcutaneously four times into CLP mice at 2, 14, 26, and 38 h post-CLP. Sample size: n = 9-10 mice/group. ***P<0.001 compared to the vehicle control by ANOVA.

6. α-Iso-cubebenol의 신경세포 보호 효과 검증

가. 세포 생존율 검사(Cell viability assay)

자극제에 의해 유도된 신경세포 사멸에 대한 알파-이소-쿠베베놀의 세포보호 효과를 검증하기 위하여, 다음과 같이 신경 세포 생존율 검사를 수행하였다. 마우스의 해마(Hippocampal) HT22 세포 및 인간 신경모세포종(Human neuroblastoma) SH-SY5Y 세포에 알파-이소-쿠베베놀을 24시간 처리한 후, 알파-이소-쿠베베놀이 각 신경세포에 유해성이 없음을 확인하였다. 그 후, 각 세포에 알파-이소-쿠베베놀을 각각 0, 5, 10 및 20 μM 농도로 12시간 처리하였다. 마우스의 해마 HT22 세포에는 신경 세포 손상을 유발하는 자극제(stimulator)로써 5 μM 농도의 글루타메이트(glutamate) 12시간 처리하였고, 인간 신경모세포종(Human neuroblastoma) SH-SY5Y 세포에는 150 μM 농도의 6-하이드록시도파민(6-hydroxydopamine, 6-OHDA)을 24시간 처리하였다.

그 후, 각각이 처리된 세포를 $4x10^4$ cells/well의 농도로 24-웰 플레이트에 넣어 배양하고, MTT 용액(50g/ml)를 각 웰에 첨가하였다. 각각의 플레이트를 5% CO_2 대기에 4시간 동안 및 37℃에서 배양한 후, 상층액은 제거하였다. 생존한 세포에서 형성된 포르마잔 크리스탈(Formazan crystals)을 다이메틸설폭시화물(dimethylsulfoxide, DMSO)에 용해 을 이용하여 가용화(solubilized)하였다. 각 웰의 흡광도(absorbance)를 마이크로 플레이트 리더(Wallace, Boston, MA, USA)를 이용하여 570 nm에서 측정하였다. 그 결과를 그림 1 및

2에 나타내었다. 그림 1에 나타낸 바와 같이, 알파-이소-쿠베베놀의 처리 농도가 증가함에 따라, 6-OHDA가 처리된 인간 신경모세포종 SH-SY5Y 세포 생존율이 증가함을 확인하였다. 따라서 알파-이소-쿠베베놀은 농도 의존적으로 신경세포를 보호하는 효과를 가짐을 확인하였고, 특히 알파-이소-쿠베베놀의 처리 농도가 20 μM 이상인 경우부터 생존률이 현저히 상승하는 것을 확인할 수 있었다.

그림 2에 나타낸 바와 같이, 알파-이소-쿠베베놀이 처리된 마우스의 해마 HT22 세포와 비교하였을 때, 글루타메이트에 의해 자극된 마우스의 해마 HT22 세포는 53.1% 만이 생존하나, 알파-이소-쿠베베놀의 처리 농도가 증가함에 따라, 세포의 생존량이 증가하는 것을 확인하였다. 따라서 알파-이소-쿠베베놀이 농도 의존적으로 뇌의 해마세포도 보호하는 효과를 가짐을 확인하였고, 특히 알파-이소-쿠베베놀의 처리 농도가 10 μM 이상인 경우부터 생존률이 현저히 상승하는 것을 확인할 수 있었다. 따라서, 알파-이소-쿠베베놀이 농도 의존적으로 손상된 신경세포의 생존율을 증가시킴을 확인하였다.

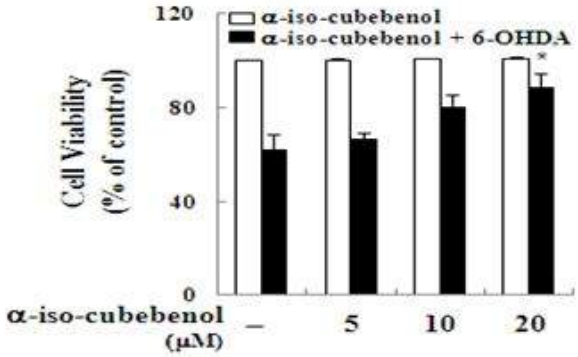

그림 1. 인간 신경모세포종 SH-SY5Y 세포에 알파-이소-쿠베베놀을 처리하고 6-OHDA로 자극한 후 MTT 검정을 통하여 세포 생존률 측정 값. 그래프의 세로축은 세포의 생존률을 대조군에 대한 상대값으로 나타낸 것이고, 가로축은 알파-이소-쿠베베놀의 처리량을 나타내는 것임

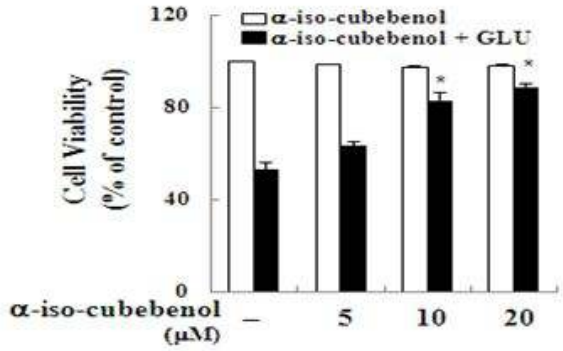

그림 2. 마우스의 해마 HT22 세포에 알파-이소-쿠베베놀을 처리하고 글루타메이트(GLU)로 자극한 후 MTT 검정을 통하여 세포 생존률의 측정 값. 그래프의 세로축은 세포의 생존률을 대조군에 대한 상대값으로 나타낸 것이고, 가로축은 알파-이소-쿠베베놀의 처리량을 나타내는 것임.

나. 젖산탈수소효소(Lactate dehydrogenase, LDH) 분비 검사

자극제에 의해 유도된 신경 세포 사멸에 대한 알파-이소-쿠베베놀의 세포보호 효과를 검증하기 위하여, 다음과 같이 LDH 분비 검사를 수행하였다. 세포외 LDH 활성은 세포독

성 진단 키트를 이용하여 제조사의 프로토콜에 따라 분광광도법을 실시하여 측정하였다. 마우스의 해마 HT22 세포 및 인간 신경모세포종 SH-SY5Y를 96 웰 플레이트에 각각 접종한 후, 각 세포에 알파-이소-쿠베베놀을 5 내지 20 μM 농도로 12시간 처리하였다. 세포에 마우스의 해마 HT22 세포에는 신경 세포 손상을 유발하는 자극제로서 5 μM 농도의 글루타메이트를 12시간 처리하였고, 인간 신경모세포종 SH-SY5Y 세포에는 150 μM 농도의 6-OHDA를 24시간 처리하였다. 그 후, 상등액을 각 웰에서 추출한 뒤, 촉매 용액을 웰에 첨가한 뒤 실온에서 30분 동안 배양하였다. 각 웰의 흡광도는 마이크로플레이트 리더(Wallace, Boston, MA, USA)를 이용하여 490 nm로 측정하였다. 그 결과를 그림 3 및 그림 4에 나타내었다. 그림 3에 나타낸 바와 같이, 알파-이소-쿠베베놀 처리 농도가 증가함에 따라, 6-OHDA로 자극된 인간 신경모세포종 SH-SY5Y 세포의 젖산탈수소효소 분비가 유의적으로 저해되었음을 확인하였다. 특히, 알파-이소-쿠베베놀의 처리 농도가 20 μM 이상인 경우부터 젖산탈수소효소 분비가 유의적으로 저해되는 것을 확인할 수 있었다. 그림 4에 나타낸 바와 같이, 알파-이소-쿠베베놀 처리 농도가 증가함에 따라, 글루타메이트로 자극된 마우스의 해마 HT22 세포의 젖산탈수소효소 분비가 유의적으로 저해되었음을 확인하였다. 특히, 알파-이소-쿠베베놀의 처리 농도가 10 μM 이상인 경우부터 젖산탈수소효소 분비가 유의적으로 저해되는 것을 확인할 수 있었다. 따라서, 알파-이소-쿠베베놀은 손상된 신경세포의 젖산탈수소효소의 분비를 저해하여 세포 독성으로부터 신경세포를 보호함을 확인하였다.

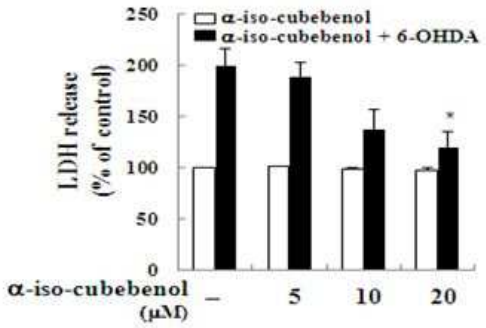

그림 3. 인간 신경모세포종 SH-SY5Y 세포에 알파-이소-쿠베베놀을 처리하고 6-OHDA로 자극한 후 젖산탈수소효소(Lactate dehydrogenase, LDH) 분비를 확인한 그래프로, 그래프의 세로축은 LDH 분비량을 대조군에 대한 상대값으로 나타낸 것이고, 가로축은 알파-이소-쿠베베놀의 처리량을 나타냄

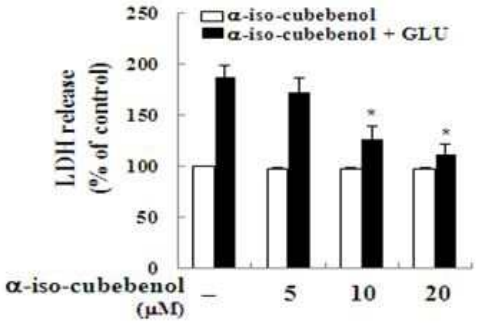

그림 4. 마우스의 해마 HT22 세포에 알파-이소-쿠베베놀을 처리하고 글루타메이트 (GLU)로 자극한 후 젖산탈수소효소(Lactate dehydrogenase, LDH) 분비를 확인한 그래프로, 그래프의 세로축은 LDH 분비량을 대조군에 대한 상대값으로 나타낸 것이고, 가로축은 알파-이소-쿠베베놀의 처리량을 나타냄.

다. 세포내의 ROS 및 칼슘 측정

자극제에 의해 유도된 신경 세포 사멸에 대한 알파-이소-쿠베베놀의 세포보호 효과를 검증하기 위하여, 다음과 같이 세포내의 ROS 및 칼슘을 측정하였다. 세포내의 ROS 및 칼슘 수준을 평가하기 위하여, 마우스의 해마 HT22 세포 및 인간 신경모세포종 SH-SY5Y를 96 웰 플레이트에 각각 접종한 후, 각 세포에 알파-이소-쿠베베놀을 0, 5, 10 및 20 μM 농도로 12시간 처리하였다. 각 세포에 마우스의 해마 HT22 세포에는 5 μM 농도의 글루타메이트를 12시간 처리하였고, 인간 신경모세포종 SH-SY5Y 세포에는 150 μM 농도의 6-OHDA를 24시간 처리하였다. 그 후, 각 세포에 ROS-민감한 형광 지표인 CM-H2DCFDA 또는 Ca^{2+}민감한 형광 지표인 Fluo 4-AM을 5% CO_2하에 1시간동안 37℃에서 처리하였다. 각 세포를 수득하고, PBS로 3회 세척하였다. 형광강도(fluorescence intensity)는 유세포분석기로 488 nm의 여기 파장(excitation wavelength) 및 525 nm의 방사 파장(emission wavelength)으로 측정하였다. 데이터 분석은 CXP software 2.0(Beckman Coulter)을 이용하여 수행하였다. 그 결과를 그림 5 및 그림 8에 나타내었다. 그림 5 및 그림 6에 나타낸 바와 같이, 알파-이소-쿠베베놀의 처리 농도가 증가함에 따라, 6-OHDA로 자극된 인간 신경모세포종 SH-SY5Y 세포내의 ROS 및 칼슘의 축적이 감소됨을 확인하였다. 특히, 알파-이소-쿠베베놀의 처리 농도가 20 μM 이상인 경우부터 ROS 및 칼슘의 축적이 현저히 감소하는 것을 확인할 수 있었다. 그림 7 및 그림 8에 나타낸 바와 같이, 알파-이소-쿠베베놀처리 농도가 증가함에 따라, 글루타메이트로 자극된 마우스의 해마 HT22 세포내의 ROS 및 칼슘의 축적이 감소됨을 확인하였다. 특히, 알파-이소-쿠베베놀의 처리 농도가 20 μM 이상인 경우부터 ROS 및 칼슘의 축적이 현저히 감소하는 것을 확인할 수 있었다. 따라서, 알파-이소-쿠베베놀은 신경세포의 세포내의 ROS 및 칼슘의 축적을 감소시켜 신경보호능을 가짐을 확인하였다.

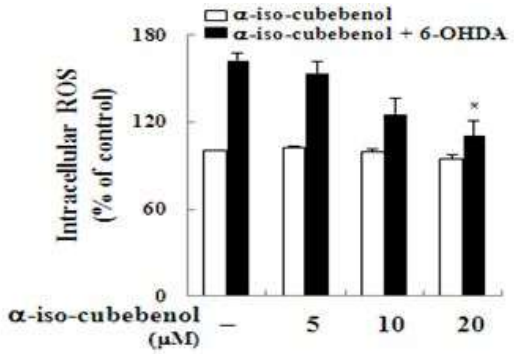

그림 5. 인간 신경모세포종 SH-SY5Y 세포에 알파-이소-쿠베베놀을 처리하고 6-OHDA로 자극한 후 세포 내 ROS를 측정한 값을 나타낸 그래프로, 그래프의 세로축은 ROS 분비량을 대조군에 대한 상대값으로 나타낸 것이고, 가로축은 알파-이소-쿠베베놀의 처리량을 나타냄.

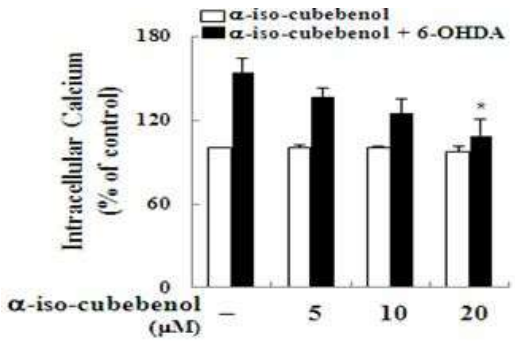

그림 6. 인간 신경모세포종 SH-SY5Y 세포에 알파-이소-쿠베베놀을 처리하고 6-OHDA로 자극한 후 세포내 칼슘을 측정한 값을 나타낸 그래프로, 그래프의 세로축은 세포내 칼슘을 대조군에 대한 상대값으로 나타낸 것이고, 가로축은 알파-이소-쿠베베놀의 처리량을 나타냄.

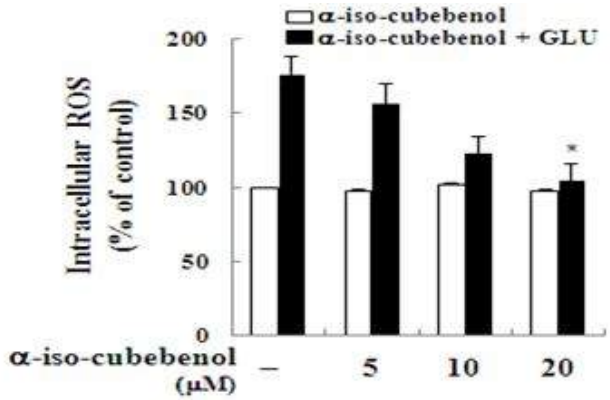

그림 7. 마우스의 해마 HT22 세포에 알파-이소-쿠베베놀을 처리하고 글루타메이트(GLU)로 자극한 후 세포내 ROS를 측정한 값을 나타낸 그래프로, 그래프의 세로축은 ROS 분비량을 대조군에 대한 상대값으로 나타낸 것이고, 가로축은 알파-이소-쿠베베놀의 처리량을 나타냄.

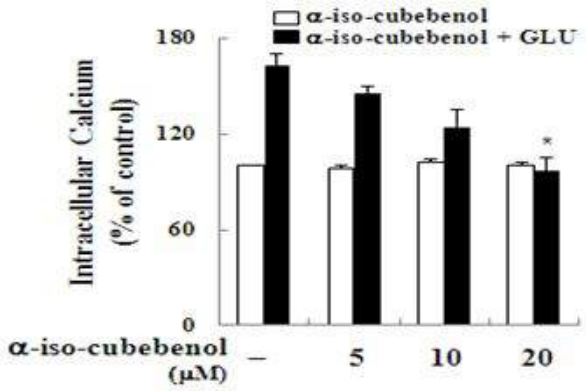

그림 8은 마우스의 해마 HT22 세포에 알파-이소-쿠베베놀을 처리하고 글루타메이트(GLU)로 자극한 후 세포내 칼슘을 측정한 값을 나타낸 그래프로, 그래프의 세로축은 세포내 칼슘을 대조군에 대한 상대값으로 나타낸 것이고, 가로축은 알파-이소-쿠베베놀의 처리량을 나타냄.

라. 자극제에 의해 유도된 sub-G1 분율(fraction) 및 아폽토시스 세포 사멸(apoptotic cell death)에 대한 알파-이소-쿠베베놀의 신경세포 보호 효과 검증

(1) Sub-G1 분석

자극제에 의해 유도된 sub-G1 분율 및 아폽토시스 세포 사멸에 대한 알파-이소-쿠베베놀의 세포보호 효과를 검증하기 위하여, 다음과 같이 Sub-G1 분율을 측정하였다. 마우스의 해마 HT22 세포 및 인간 신경모세포종 SH-SY5Y를 96 웰 플레이트에 각각 접종한 후, 각 세포에 알파-이소-쿠베베놀을 12시간 처리하였다. 그 후, 마우스의 해마 HT22 세포에는 5 μM 농도의 글루타메이트를 12시간 처리하였고, 인간 신경모세포종 SH-SY5Y 세포에는 150 μM 농도의 6-OHDA를 24시간 처리하였다. 그 후, 각 세포를 800 rpm에서 3분 원심분리하여 수득하고, PBS로 2회 세척한 뒤, 75% 에탄올로 하루 종일 두어 고정시켰다. 세포계수 분석을 실시하기 전에, 고정된 세포를 PBS로 세척하고, 최종농도 50 μg/ml인 프로피디움 요오드화물(propidium iodide)을 암조건에 10분간 처리하여 배양하였다. 아폽토시스(apoptosis)의 비율은 CXP software 2.0 (Beckman Coulter)로 측정한 sub-G1 피크의 백분율로 계산되었다.

인간 신경모세포종 SH-SY5Y 세포를 6-OHDA로 자극하였을 때, 대조군에 비해 sub-G1 분율이 증가하고, 유도된 사멸 세포의 증가함을 확인하였다. 그러나, 알파-이소-쿠베베놀을 전처리한 후, 6-OHDA 로 자극된 인간 신경모세포종 SH-SY5Y 세포에서의 아폽토시스는 감소함을 확인하였다. 그림 10에 나타낸 바와 같이, 마우스의 해마 HT22 세포를 글루타메이트로 자극하였을 때, 대조군에 비해 sub-G1 분율이 증가하고, 사멸 세포가 증가함을 확인하였다. 그러나, 알파-이소-쿠베베놀을 전처리한 후, 글루타메이트로 자극된 마우스의 해마 HT22 세포에서의 아폽토시스는 감소함을 확인하였다. 따라서, 6-OHDA 또는 글루타메이트로 유도되는 아폽토시스 세포 사멸에 대하여 신경 세포의 보호 효과가 있음을 확인하였다.

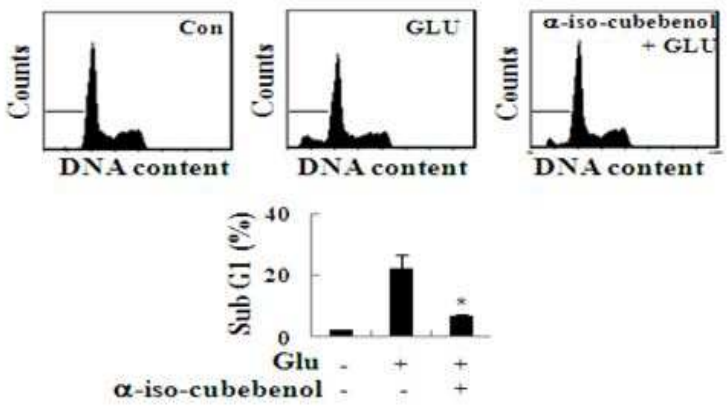

그림 9. 마우스의 해마 HT22 세포에 알파-이소-쿠베베놀을 처리하고 글루타메이트로 자극한 후 유세포 분석을 통하여 Sub-G1 분율 피크를 측정한 값. Con은 대조군을 나타내고, CLU 는 글루타메이트만 처리한 군, α-iso-cubebenol+GLU는 알파-이소-쿠베베놀을 처리 후 글루타메이트를 처리한 군을 나타냄.

(2) DNA 분절 검정을 통한 아폽토시스 세포 사멸 측정

자극제에 의해 유도된 sub-G1 분율 및 아폽토시스 세포 사멸에 대한 알파-이소-쿠베베놀의 세포보호 효과를 검증하기 위하여, 다음과 같이 TUNEL 분석을 수행하였다. 마우스의 해마 HT22 세포 및 인간 신경모세포종 SH-SY5Y를 96 웰 플레이트에 각각 접종

한 후, 각 세포에 알파-이소-쿠베베놀을 12시간 처리하였다. 그 후, 마우스의 해마 HT22 세포에는 5 μM 농도의 글루타메이트를 12시간 처리하였고, 인간 신경모세포종 SH-SY5Y 세포에는 150 μM 농도의 6-OHDA를 24시간 처리하였다. 그 후, 세포는 APO-BrdUTM TUNEL 분석 키트 (Invitrogen, San Diego, CA, USA)를 이용하여 제조사의 프로토콜에 따라 TUNEL 분석하여 측정하였다. 유세포 분석기(플루오레세인이소티오시안산염 시약, 488 nm 여기 및 520 nm의 방출)를 이용하여 수행하였다. 데이터 분석은 CXP 2.0(Beckman Coulter)를 이용하여 수행하였다. TUNEL 염색된 세포는 세포괴사 신호 케스케이드(cascades)에 의해 야기되는 핵 DNA 분절을 나타낸다. 그 결과를 그림 10 및 그림 11에 나타내었다.

그림 10에 나타낸 바와 같이, 알파-이소-쿠베베놀을 처리하지 않고 6-OHDA로 자극된 인간 신경모세포종 SH-SY5Y 세포에서는 DNA 분절된 TUNEL-염색된 세포의 수가 5.5%에서 28.1%로 증가함을 확인하였으나, 알파-이소-쿠베베놀을 처리한 경우, 6-OHDA 자극의 효과를 억제시킴을 확인하였다.

그림 11에 나타낸 바와 같이, 글루타메이트로 자극된 마우스의 해마 HT22 세포에서 DNA 분절은 유의적으로 증가됨을 확인하였으나, 알파-이소-쿠베베놀을 전처리한 후, 글루타메이트로 자극된 마우스의 해마 HT22 세포에서의 DNA 분절은 일반적인 수준임을 확인하였다. 따라서, 알파-이소-쿠베베놀은 손상된 신경세포의 DNA가 분절되는 것을 방지함으로써 손상된 신경세포의 세포사멸을 방지하여, 신경세포를 보호하는 효과를 가짐을 확인하였다.

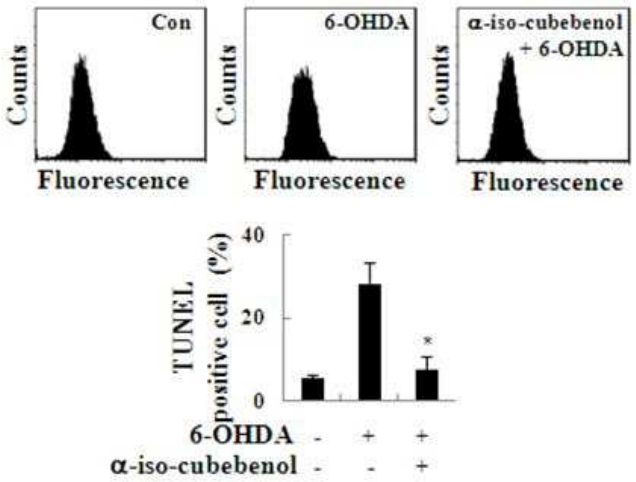

그림 10. 인간 신경모세포종 SH-SY5Y 세포에 알파-이소-쿠베베놀을 처리하고 6-OHDA로 자극한 후 TUNEL 분석한 값을 나타낸 그림. Con은 대조군을 나타내고, 6-OHDA는 6-OHDA 만 처리한 군, α-iso-cubebenol+6-OHDA는 알파-이소-쿠베베놀을 처리 후 6-OHDA를 처리한 군을 나타냄.

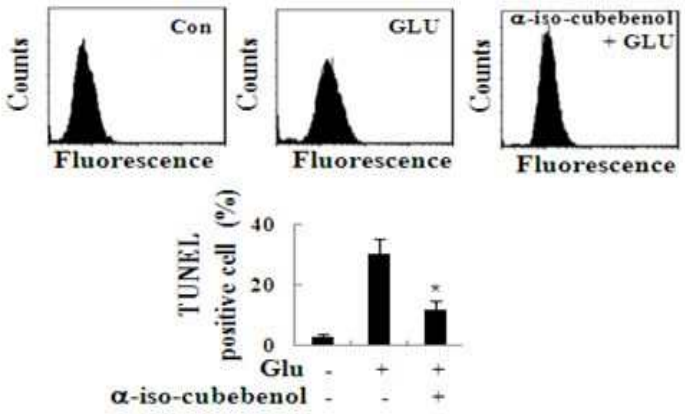

그림 11. 마우스의 해마 HT22 세포에 알파-이소-쿠베베놀을 처리하고 글루타메이트로 자극한 후 TUNEL 분석한 값. Con은 대조군을 나타내고, CLU 는 글루타메이트만 처리한 군, α-iso-cubebenol+GLU는 알파-이소-쿠베베놀을 처리 후 글루타메이트를 처리한 군을 나타냄.

마. 자극제에 의해 유도된 미토콘드리아 세포막 전위(mitochondrial membrane potential, MMP, Δψm) 분열 및 미토콘드리아 AIF 수준에 대한 알파-이소-쿠베베놀의 효과

(1) 미토콘드리아 세포막 전위(MMP, Δψm)의 검정

미토콘드리아의 손상을 확인하기 위하여, 다음과 같은 실험을 수행하여 분자 프로브 JC-1을 이용하여 미토콘드리아 세포막 전위를 확인하였다. 마우스의 해마 HT22 세포 및 인간 신경모세포종 SH-SY5Y를 96 웰 플레이트에 각각 접종한 후, 각 세포에 알파-이소-쿠베베놀을 20 μM 농도로 12시간 처리하였다. 각 세포에 마우스의 해마 HT22 세포에는 신경 세포 손상을 유발하는 자극제로서 5 μM 농도의 글루타메이트를 인간 신경모세포종 SH-SY5Y 세포에는 150 μM 농도의 6-OHDA를 각 0, 4, 8, 12, 16 및 24시간 처리하였다. 그 후, 각 세포의 미토콘드리아 세포막 전위는 친유성기 양이온 프로브(lipophilic cationic probe) JC-1(5,5′, 6,6′-tetrachloro-1,1′, 3,3′-tetraethylbenzimidazolcarbocyanineiodide)로 이루어진 J-화합체(J-aggregate)를 이용하여 유세포 분석기로 분석하였다. 세포를 JC-1으로 염색한 후, CXP software 2.0 (Beckman Coulter)을 이용하여 subsequent 유세포 분석기를 이용하여 분석하였다. 완전한(intact) 미토콘드리아 세포막 전위(△ψm)를 나타내는 JC-1 붉은 형광(fluorescence)은 488 nm에서 여기되었고, 방출은 613 ± 20 nm 밴드 패스 필터(band pass filter)를 이용하여 검출하였다. 각 샘플마다 10,000개의 세포를 획득하고, 유세포 분석기로 분석하였다. 데이터는 분석된 세포 개체의 형광 강도(fluorescence intensity)를 이용하여 분석하였다. 그 결과를 그림 12 및 그림 13에 나타내었다. 그림 12에 나타낸 바와 같이, 6-OHDA로 자극된 인간 신경모세포종 SH-SY5Y 세포에서는 미토콘드리아 세포막 전위가 낮아지거나, 붕괴(collapse)되었음을 확인하였다. 그러나, 알파-이소-쿠베베놀을 전처리한 6-OHDA로 자극된 인간 신경모세포종 SH-SY5Y세포에서는 미토콘드리아 세포막 전위가 낮아지거나, 붕괴되는 것이 억제되었음을 확인하였다. 그림 13에 나타낸 바와 같이, 글루타메이트로 자극된 마우스의 해마 HT22 세포에서 미토콘드리아 세포막 전위 감소를 나타내는 초록 형광-양성 세포의 비율이 증가한 것을 확인하였다. 그러나, 알파-이소-쿠베베놀을 전처리한 뒤 글루타메이트로 자극된 마우스의 해마 HT22 세포에서는 초록

형광-양성 세포가 복구됨을 확인하였다. 따라서, 알파-이소-쿠베베놀은 손상된 신경세포에서 미토콘드리아 세포막 전위가 감소되어 사멸되는 것을 방지함을 확인하였다.

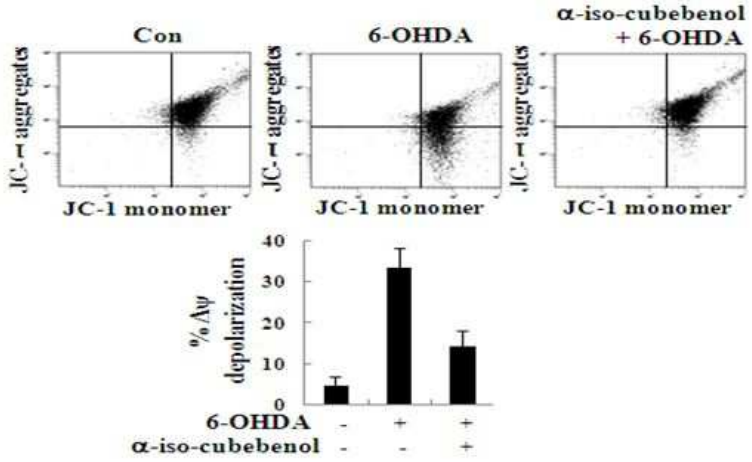

그림 12. 인간 신경모세포종 SH-SY5Y 세포에 알파-이소-쿠베베놀을 처리하고 6-OHDA로 자극한 후 유세포 분석을 통하여 JC-1을 측정한 값을 나타냄. Con은 대조군을 나타내고, 6-OHDA는 6-OHDA 만 처리한 군, α-iso-cubebenol+6-OHDA는 알파-이소-쿠베베놀을 처리 후 6-OHDA를 처리한 군을 나타냄.

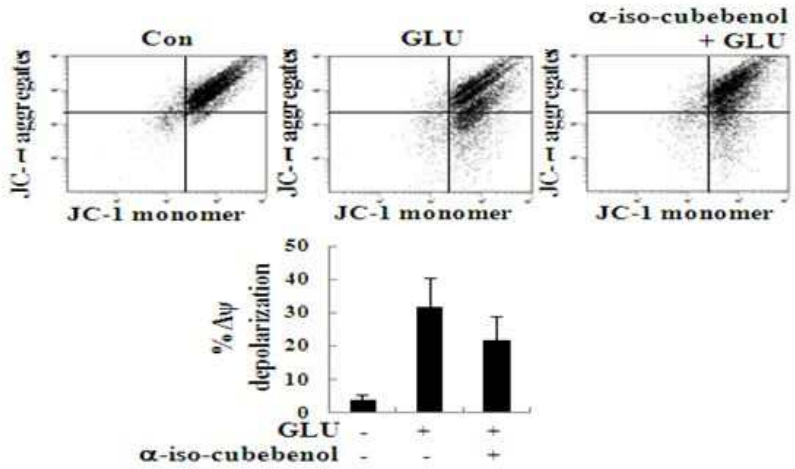

그림 13. 마우스의 해마 HT22 세포에 알파-이소-쿠베베놀을 처리하고 글루타메이트로 자극한 후 유세포 분석을 통하여 JC-1을 측정한 값을 나타낸 그림. Con은 대조군을 나타내고, CLU 는 글루타메이트만 처리한 군, α-iso-cubebenol+GLU는 알파-이소-쿠베베놀을 처리 후 글루타메이트를 처리한 군을 나타냄.

(2) AIF 단백질 수준 측정

자극제가 AIF 단백질의 미토콘드리아 분포(mitochondrial localization)를 달라지게 하므로, 알파-이소-쿠베베놀이 AIF의 전위(translocation)를 조절하는지를 알아보기 위하여, 미토콘드리아, 세포기질 및 핵의 AIF 단백질 수준을 다음과 같이 측정였다. 마우스의 해마 HT22 세포 및 인간 신경모세포종 SH-SY5Y를 96 웰 플레이트에 각각 접종한 후, 각 세포에 알파-이소-쿠베베놀을 20 μM 농도로 12시간 처리하였다. 마우스의 해마 HT22 세포에는 5 μM 농도의 글루타메이트를, 인간 신경모세포종 SH-SY5Y 세포에는

150 μM 농도의 6-OHDA를 각 0, 4, 8, 12, 16 및 24시간처리하였다. 그 후, 세포기질(cytosol), 핵 및 미토콘드리아는 핵 추출 키트를 이용하여 제조사의 프로토콜에 따라 추출되었다. 세포 용해물(lysates)의 단백질 함량은 Bradford reagent (Bio-Rad)를 이용하여 측정하였다. 각 샘플의 단백질은 SDS-polyacrylamide gel electrophoresis (SDS-PAGE)에 의해 분해되었으며, 폴리비닐리덴 디플루오라이드(polyvinylidenedifluoride, PVDF) 막에 이입시키고, 적절한 항체에 노출시켰다. 각 항체에 노출된 단백질은 호스래디시(horseradish) 퍼옥시다제-공역된(peroxidase-conjugated) 항-래빗 혹은 항-마우스 이차항체를 이용하여 증가된 화학발광 검출 시스템(enhanced chemiluminescence detection system)(Amersham Biosciences, Piscataway, NJ, USA)을 이용하여 시각화하였다. 그림은 ImageQuant 350 analyzer (Amersham Biosciences)을 이용하여 얻었다. 그 결과를 그림 14 및 그림 15에 나타내었다.

그림 14에 나타낸 바와 같이, 알파-이소-쿠베베놀을 전처리한 후, 6-OHDA로 자극된 인간 신경모세포종 SH-SY5Y 세포에서는 미토콘드리아로부터 AIF의 방출이 억제되고, 미토콘드리아에서 AIF의 발현이 유지됨을 확인하였다. 그림 15에 나타낸 바와 같이, 글루타메이트로 자극된 마우스의 해마 HT22 세포에서 미토콘드리아 AIF 수준이 감소되었으나, 세포 기질 및 핵의 AIF 수준은 증가됨을 확인하였다. 알파-이소-쿠베베놀을 전처리한 후, 글루타메이트로 자극된 마우스의 해마 HT22 세포에서의 AIF 단백질 수준은 반대로, 미토콘드리아 AIF 수준이 증가되었고, 세포 기질 및 핵의 AIF 수준은 감소됨을 확인하였다. 따라서, 알파-이소-쿠베베놀을 처리 시, 미토콘드리아에서 AIF의 방출을 억제시켜, 6-OHDA 및 글루타메이트 자극제에 의한 미토콘드리아의 기능 장애를 방지하여, 인간 신경모세포종 SH-SY5Y 세포 및 마우스의 해마 HT22 세포를 보호함을 확인하였다.

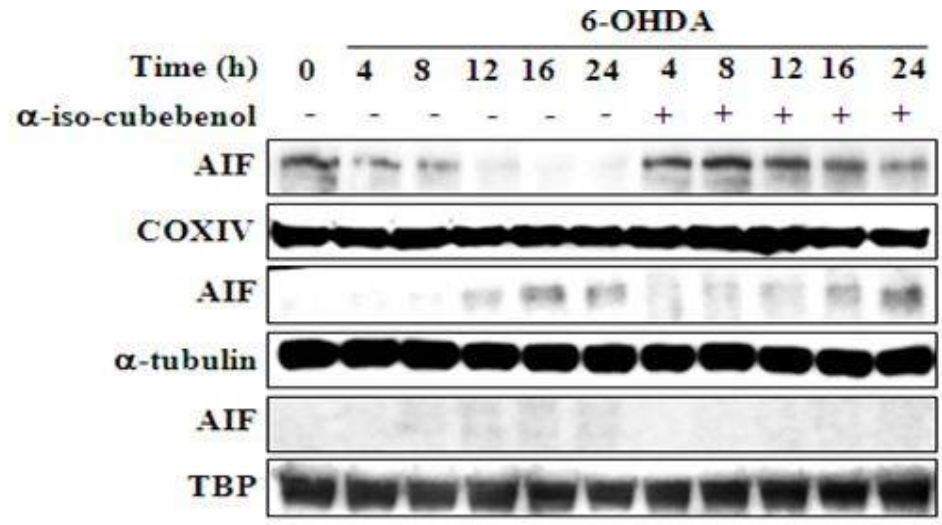

그림 14. 인간 신경모세포종 SH-SY5Y 세포에 알파-이소-쿠베베놀을 처리하고 6-OHDA로 자극한 후 웨스턴 블랏을 통하여 AIF의 발현을 측정한 값을 나타냄.

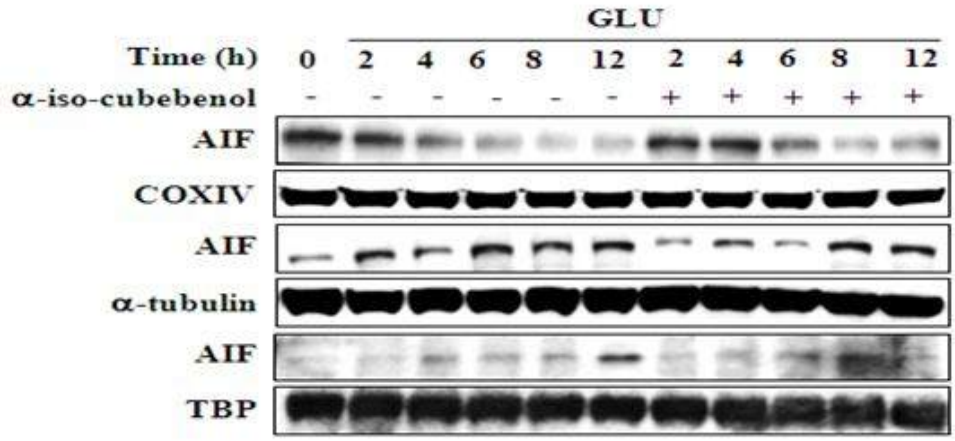

그림 15. 마우스의 해마 HT22 세포에 알파-이소-쿠베베놀을 처리하고 글루타메이트로 자극한 후 웨스턴 블랏을 통하여 AIF의 발현을 측정한 값을 나타냄.

바. 자극제에 의해 유도된 ERK, JNK 및 p38를 포함하는 MAPKs 인산화에 대한 알파-이소-쿠베베놀의 억제 효과

ERK, JNK 및 p38을 포함하는 MAPKs는 뉴런의 플라크(neuronal plaque) 발생에 대한 주요 조절자이기 때문에, 신경 질환(neurodegenerative diseases)의 과정을 나타낼 것으로 여겨지므로, 알파-이소-쿠베베놀이 자극제에 의해 유도된 MAPKs의 인산화 반응을 감소시키는지 알아보기 위하여, 다음과 같이 웨스턴 블랏을 수행하였다. 마우스의 해마 HT22 세포 및 인간 신경모세포종 SH-SY5Y를 96 웰 플레이트에 각각 접종한 후, 각 세포에 알파-이소-쿠베베놀을 20 μM 농도로 12시간 처리하였다. 마우스의 해마 HT22 세포에는 5 μM 농도의 글루타메이트를, 인간 신경모세포종 SH-SY5Y 세포에는 5 μM 농도의 6-OHDA를 0, 4, 8, 12, 16, 및 24시간 처리하여 배양하였다. 그 후, 각 세포들을 수득하여 ERK, JNK 및 p38을 포함하는 MAPKs에 대한 인산화-특이 항체를 이용하여 웨스턴 블랏을 실험 3의 2) 방법과 동일하게 수행하였다. 그 결과를 드림 17 및 그림 18에 나타내었다.

그림 17에 나타낸 바와 같이, 알파-이소-쿠베베놀을 전처리한 후, 6-OHDA로 자극된 인간 신경모세포종 SH-SY5Y 세포에서의 ERK의 인산화 강도 및 기간이 감소되었고, JNK 및 p38의 인산화 반응도 억제됨을 확인하였다.

그림 18에 나타낸 바와 같이, 알파-이소-쿠베베놀을 전처리한 후, 글루타메이트로 자극된 마우스의 해마 HT22 세포에서 ERK의 인산화 반응 강도 및 기간이 감소되었고, JNK 및 p38의 인산화 반응도 억제됨을 확인하였다. 따라서, 알파-이소-쿠베베놀이 자극제에 의해 유도된 ERK, JNK 및 p38을 포함하는 MAPKs의 인산화 반응을 감소시킴으로써 세포의 염증성 반응을 억제하는 방법으로 신경세포를 보호함을 확인하였다.

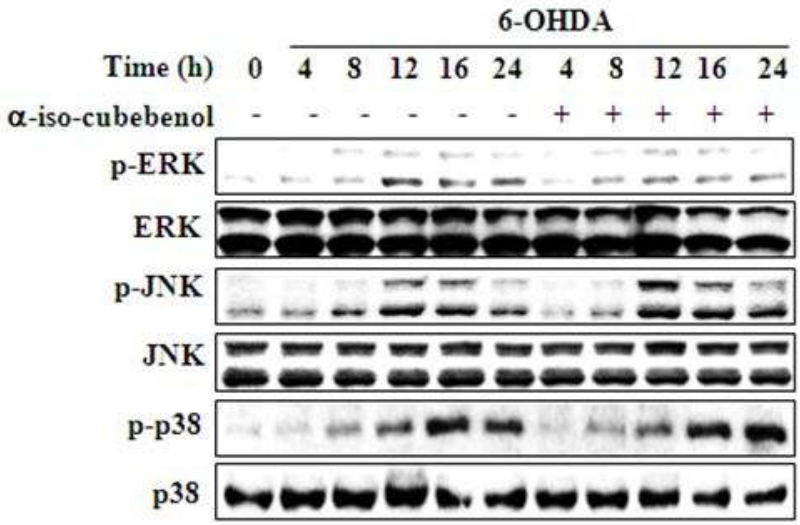

그림 16. 인간 신경모세포종 SH-SY5Y 세포에 알파-이소-쿠베베놀을 처리하고 6-OHDA로 자극한 후 웨스턴 블랏을 통하여 ERK, JNK 및 p38을 포함하는 MAPKs의 발현 수준을 측정한 것을 나타냄.

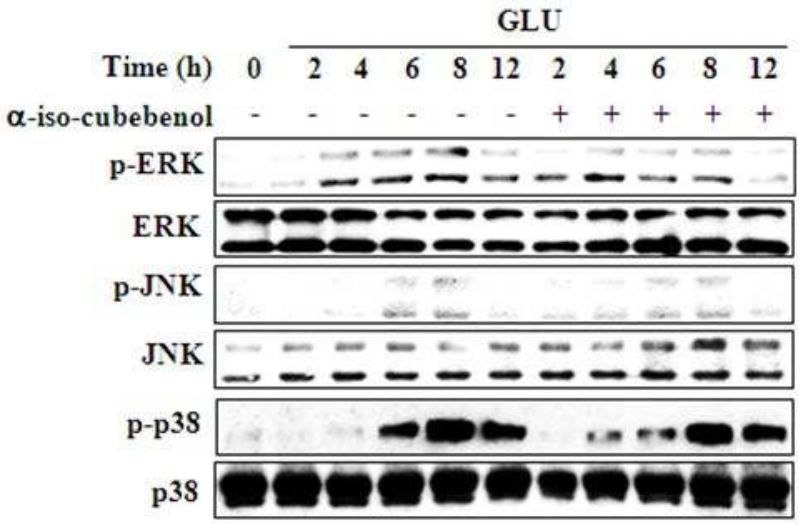

그림 17. 마우스의 해마 HT22 세포에 알파-이소-쿠베베놀을 처리하고 글루타메이트로 자극한 후 웨스턴 블랏을 통하여 ERK, JNK 및 p38을 포함하는 MAPKs의 발현 수준을 측정한 것을 나타냄.

사. 신경세포에서 HO-1 및 NQO 1 발현을 조절하는 PKA/CREB/Nrf-2의 활성을 유도하는 알파-이소-쿠베베놀의 효과

(1) PKA 및 CREB 인산화 반응 활성에 대한 알파-이소-쿠베베놀의 효과

PKA 및 CREB 인산화 반응 활성에 대한 알파-이소-쿠베베놀의 효과를 알아보기 위하여, 다음과 같이 웨스턴 블랏을 수행하였다. 마우스의 해마 HT22 세포 및 인간 신경모세포종 SH-SY5Y에 알파-이소-쿠베베놀을 0 내지 20 μM 처리한 후 웨스턴 블랏을 실험 3의 2) 방법과 동일하게 수행하여, PKA, PKB, CREB, Nrf-2 및 TBP의 인산화반응 및 활성을 측정하였다. PKA 및 PKB 신호 경로는 신경 세포 생존에 주요 역할을 하는 것이 밝혀져 있고, PKA 및 PKB는 다양한 신경독성에 대항하는 신경보호 효과와 대한 주요 전사 인자인 CREB 및 Nrf-2의 활성을 조절과 관련되어 있음이 알려져 있다. 웨스

턴 블랏 결과를 그림 19 및 그림 20에 나타내었다.

그림 18에 나타낸 바와 같이, 인간 신경모세포종 SH-SY5Y에 알파-이소-쿠베베놀을 처리 시, 농도 의존적으로 PKA 및 PKB의 인산화를 유도함을 확인하였다. 또한, CREB 인산화반응 및 Nrf-2의 핵 전좌(translocation)를 유도함을 확인하였다. 그림 19에 나타낸 바와 같이, 마우스의 해마 HT22 세포에 알파-이소-쿠베베놀을 처리하면 PKA 및 CREB의 인산화 반응을 유의적으로 유도함을 확인하였다. 또한, 알파-이소-쿠베베놀을 4시간 처리하였을 때, Nrf-2 핵 축적이 유의적으로 증가됨을 확인하였으며, Nrf-2 핵 내 이동은 알파-이소-쿠베베놀의 농도의존적으로 유도됨을 확인하였다.

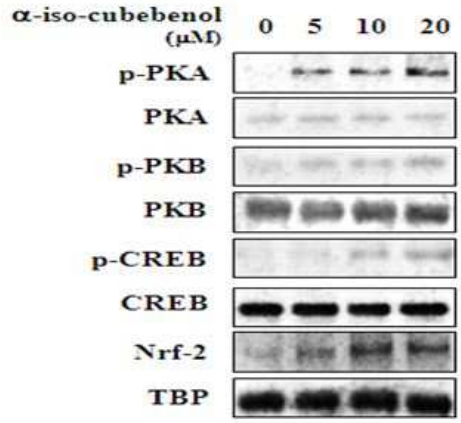

그림 18. 인간 신경모세포종 SH-SY5Y 세포에 알파-이소-쿠베베놀을 처리하고 6-OHDA로 자극한 후 웨스턴 블랏을 통해 p-PKA, PKA, p-CREB 및 CREB의 발현, Nrf-2 핵 분포를 측정한 것을 나타냄.

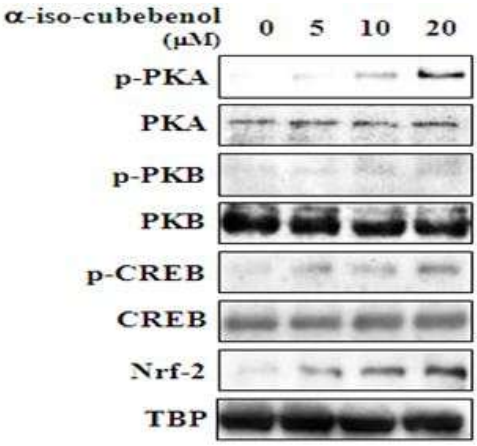

그림 19. 마우스의 해마 HT22 세포에 알파-이소-쿠베베놀을 처리하고 글루타메이트로 자극한 후 웨스턴 블랏을 통해 p-PKA, PKA, p-CREB 및 CREB의 발현, Nrf-2 핵 분포를 측정한 것을 나타냄.

(2) 일시적 주입 및 듀얼 루시퍼라제 검정(dual luciferase assay)

전사 활성을 확인하기 위하여, CREB 및 Nrf-2 각 반응 요소에 의해 유도되는 루시퍼라제 유전자를 포함하는 CRE 및 ARE-LUC 플라스미드 DNAs를 마우스의 해마 HT22 세포 및 인간 신경모세포종 SH-SY5Y 세포에 도입하였다. 마우스의 해마 HT22 세포 및 인간 신경모세포종 SH-SY5Y 세포에 FuGENE-HD 시약을 이용하여 제조사의 프로토콜에 따라 CRE 및 ARE-리포터 플라스미드 또는 HO-1 프로모터 리포터 플라스미드를 포함하여 주입하였다. 레닐라 루시퍼라아제(Renilla luciferase) 컨트롤 플라스미드인

pRL-CMV는 주입 효율에 대한 내부 컨트롤(internal control)로서 보조-주입(co-transfected)되었다. 주입된 세포에 알파-이소-쿠베베놀을 0, 5, 10 및 20μM 농도로 처리하였다. 그 후, 루시퍼라아제 활성은 듀얼-루시퍼라아제 분석 키트를 이용하여 제조사의 프로토콜에 따라 분석되었다. 발광(Luminescence)은 발광측정기(microplate luminometer)(Wallac 1420)로 측정하였다. 그 결과를 그림 21 및 그림 22에 나타내었다. 그림 20에 나타낸 바와 같이, 이입된 인간 신경모세포종 SH-SY5Y 세포에 알파-이소-쿠베베놀을 전처리한 것은 CREB 및 Nrf2 프로모터 활성에서 5.2- 및 4.6-폴드(fold) 상승을 유도하였으며, 루시퍼라제 활성은 알파-이소-쿠베베놀의 농도의존적으로 증가함을 확인하였다. 특히, 알파-이소-쿠베베놀은 10 μM 농도로 처리된 경우 그 효과가 현저히 상승하는 것을 확인 하였다. 그림 21에 나타낸 바와 같이, 마우스의 해마 HT22 세포에서 루시퍼라제 활성은 알파-이소-쿠베베놀의 농도의존적으로 증가함을 확인하였다. 특히, 알파-이소-쿠베베놀은 10 μM 농도로 처리된 경우 그 효과가 현저히 상승하는 것을 확인 하였다.

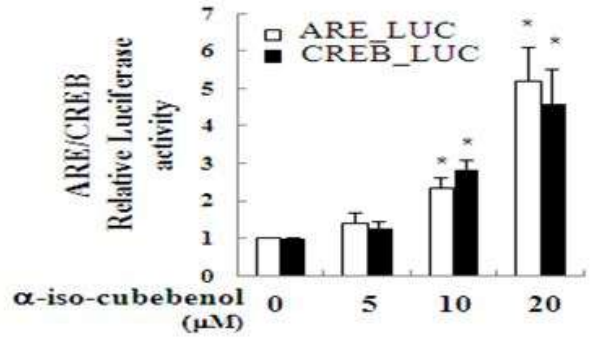

그림 20. 인간 신경모세포종 SH-SY5Y 세포에 알파-이소-쿠베베놀을 처리하고 6-OHDA로 자극한 후 듀얼-루시퍼라제(ARE/CREB Relative Luciferse) 활성을 측정한 값을 나타냄.

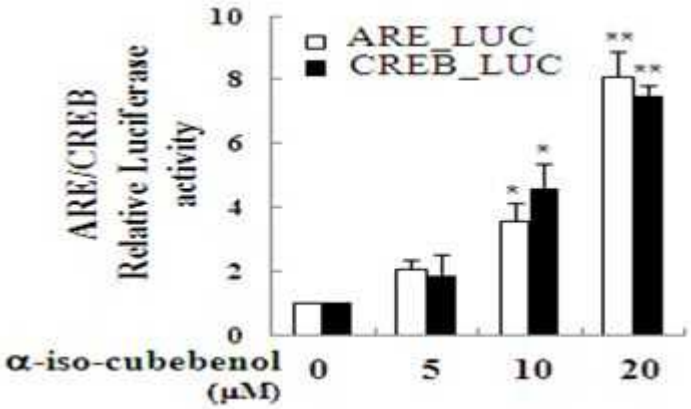

그림 21. 마우스의 해마 HT22 세포에 알파-이소-쿠베베놀을 처리하고 글루타메이트로 자극한 후 듀얼-루시퍼라제(ARE/CREB Relative Luciferse) 활성을 측정한 값을 나타냄.

(3) HO-1 및 NQO1 단백질 발현과 HO-1 프로모터 활성 측정

Nrf-2 및 CREB 전사촉진(transactivation)은 HO-1 및 NQO1 단백질을 포함하는 ARE-관련된 산화방지 유전자의 발현과 관련되었음을 확인; HO-1 및 NQO1 단백질 발현에 대한 알파-이소-쿠베베놀의 효과 확인; 및 HO-1 프로모터 활성을 확인하기 위하여, 다

음과 같은 실험을 수행하였다. 마우스의 해마 HT22 세포 및 인간 신경모세포종 SH-SY5Y에 알파-이소-쿠베베놀을 각각 0, 5, 10 및 20 μM 농도로 12시간 처리한 후, 웨스턴 블랏을 실험 4의 2) 방법과 동일하게 수행하였다. 그 결과를 그림 23 내지 그림 26에 나타내었다.

그림 22 및 그림 23에 나타낸 바와 같이, 알파-이소-쿠베베놀 농도 의존적으로 처리한 인간 신경모세포종 SH-SY5Y 세포에서는 50 μM 농도에서부터 HO-1 및 NQO1 단백질의 발현 수준이 증가하였고, 특히 10 μM 이상부터 그 효과가 현저히 우수함을 확인하였다. 또한, HO-1 프로모터 활성도 알파-이소-쿠베베놀 농도 의존적으로 증가함을 확인하였다.

그림 23 및 그림 24에 나타낸 바와 같이, 알파-이소-쿠베베놀 농도 의존적으로 처리한 마우스의 해마 HT22 세포에서는 5 μM 농도에서부터 HO-1 및 NQO1 단백질의 발현 수준이 증가함을 확인하였고, 특히 20 μM에서 그 농도가 현저히 증가하는 것을 확인하였다. 또한, HO-1 프로모터 활성도 알파-이소-쿠베베놀 농도 의존적으로 증가함을 확인하였다.

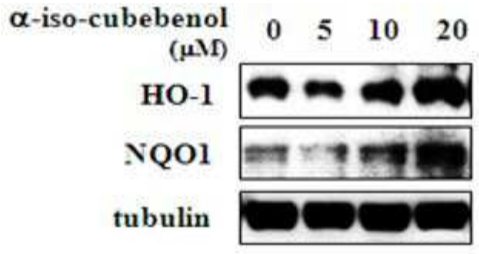

그림 22. 인간 신경모세포종 SH-SY5Y 세포에 알파-이소-쿠베베놀을 처리하고 6-OHDA로 자극한 후 웨스턴 블랏을 통해 HO-1 및 NQO-1 발현을 측정한 것을 나타냄.

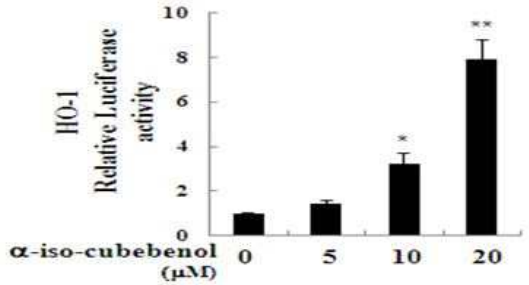

그림 23. 인간 신경모세포종 SH-SY5Y 세포에 알파-이소-쿠베베놀을 처리하고 6-OHDA로 자극한 후 HO-1 프로모터-루시퍼라제 활성을 측정한 값을 나타냄.

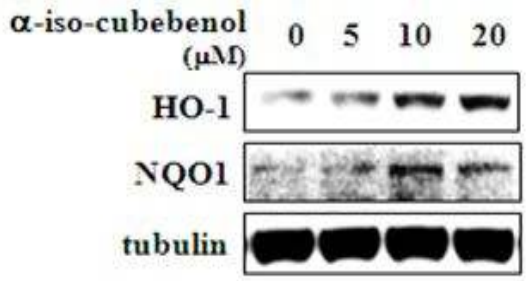

그림 24. 마우스의 해마 HT22 세포에 알파-이소-쿠베베놀을 처리하고 글루타메이트로 자극한 후 웨스턴 블랏을 통해 HO-1 및 NQO-1 발현을 측정한 것을 나타냄.

아. 자극제에 의해 유도된 신경 세포에서 알파-이소-쿠베베놀의 항-아폽토시스 특성과 관련된 CREB 및 Nrf-2

CREB/Nrf-2-관련된 단계 II 해독/산화방지(phase II detoxifying/antioxidant)효소 신호 경로를 통해 발생된 알파-이소-쿠베베놀의 산화방지 및 신경보호 작용 효과를 확인하기 위하여, 다음과 같이 CREB 및 Nrf-2 siRNA를 이용하여 실험을 수행하였다. Small interfering RNA (siRNA)를 포함한 세포의 주입은 X-treme GENE siRNA Transfection Reagent (Roche Applied Science)을 이용하여 제조사의 프로토콜에 따라 수행하였다. 상업적으로 구입할 수 있는 마우스 CREB- 및 Nrf-2-specific siRNAs (Santa Cruz, Heidelberg, Germany)와 음성대조군 siRNAs (Santa Cruz)이 주입하기 위해 사용되었다. 간단하게, X-treme GENE siRNA Transfection Reagent (10 μl)를 각 2 μg siRNA이 포함된 100 μl 무혈청 배지(serum-free medium)에 첨가한 후, 실온에서 20분간 배양하였다. 그 후, 마우스의 해마 HT22 세포 및 인간 신경모세포종 SH-SY5Y를 96 웰 플레이트에 각각 접종한 후, 각 세포에 알파-이소-쿠베베놀을 20 μM 농도로 12시간 처리하였다. 세포에 마우스의 해마 HT22 세포에 글루타메이트를 12시간 처리하였고, 인간 신경모세포종 SH-SY5Y 세포에는 6-OHDA를 24시간 처리하였다. 유전자 사일런싱(Gene silencing)은 웨스턴 블랏으로 48시간 후에 측정하였다.

또한, 각 실험 1의 2) 방법과 동일하게 LDH 분비 검사하여, 그 결과를 그림 26 및 그림 27에 나타내었다. 또한, 실험2의 2) 방법과 동일하게 TUNEL 분석을 실시하여, 그 결과를 그림 26 및 그림 29에 나타내었다. 그림 26 및 그림 27에 나타낸 바와 같이, CREB 및 Nrf2 siRNAs를 이입한 세포는 CREB 및 Nrf2 단백질 발현 수준을 억제시킴을 확인하였다. 또한, 알파-이소-쿠베베놀을 처리하였을 때, 대조군 siRNA이 이입된 인간 신경모세포종 SH-SY5Y 세포에 대한 6-OHDA의 사멸이 억제됨을 확인하였으나, CREB 및 Nrf2 siRNAs를 이입한 SH-SY5Y 세포에서는 그 효과가 적음을 확인하였다.

그림 28 및 그림 29에 나타낸 바와 같이, CREB 및 Nrf2 siRNAs를 이입한 세포는 CREB 및 Nrf2 단백질 발현 수준을 억제시킴을 확인하였다. 또한, 알파-이소-쿠베베놀을 처리하였을 때 CREB 및 Nrf2 siRNA가 이입된 세포를 제외하고 글루타메이트로 자극된 아폽토시스 세포 사멸은 알파-이소-쿠베베놀 처리 시 억제되었음을 확인하였다. 따라서, 알파-이소-쿠베베놀은 신경보호작용 효과를 나타내고, CREB/Nrf2의 신호 경로의 활성에 의해 6-OHDA 및 글루타메이트 자극에 의한 신경 세포 사멸을 효과적으로 억제함을 확인하였다.

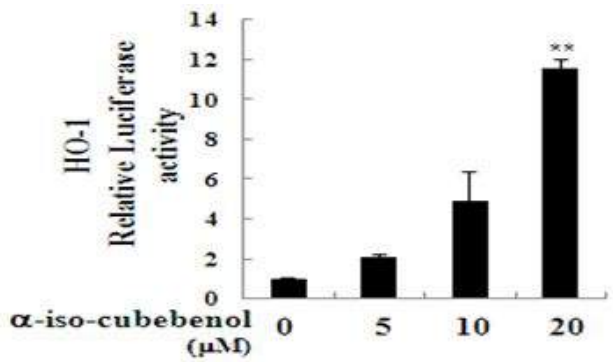

그림 25. 마우스의 해마 HT22 세포에 알파-이소-쿠베베놀을 처리하고 글루타메이트로 자극한 후 HO-1 프로모터-루시퍼라제 활성을 측정한 값을 나타냄.

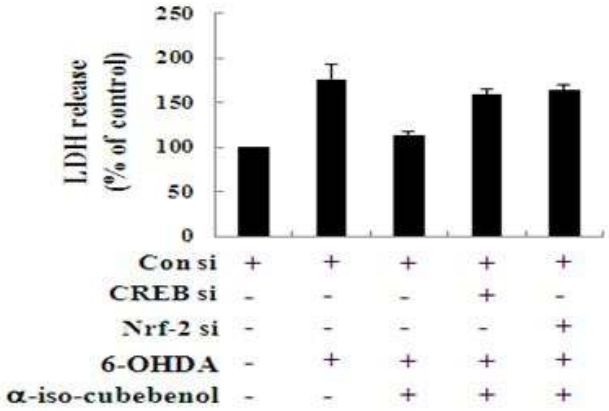

그림 26. 인간 신경모세포종 SH-SY5Y 세포에 CREB 및 Nrf-2 siRNA를 이입한 후, 알파-이소-쿠베베놀을 처리하고 6-OHDA로 자극하고, 젖산탈수소효소(Lactate dehydrogenase, LDH) 분비 검사한 값을 나타냄.

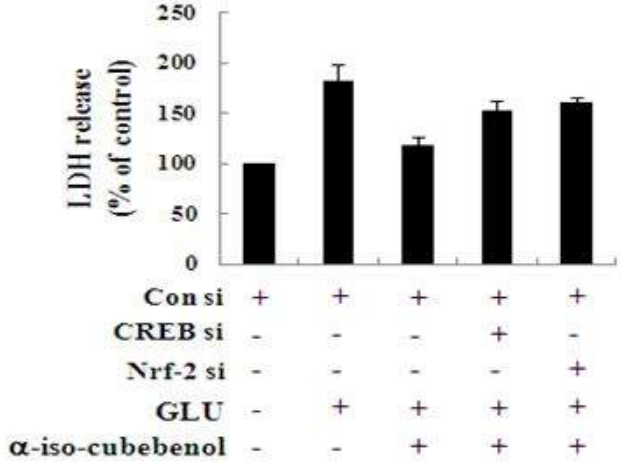

그림 27은 마우스의 해마 HT22 세포에 CREB 및 Nrf-2 siRNA를 이입한 후, 알파-이소-쿠베베놀을 처리하고 글루타메이트로 자극하고, 젖산탈수소효소(Lactate dehydrogenase, LDH) 분비 검사한 값을 나타냄.

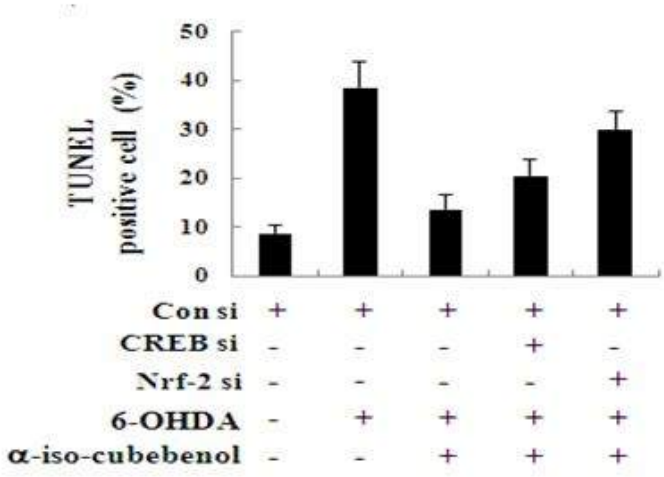

그림 28, 인간 신경모세포종 SH-SY5Y 세포에 CREB 및 Nrf-2 siRNA를 이입한 후, 알파-이소-쿠베베놀을 처리하고 6-OHDA로 자극하고, TUNEL 검사한 값을 나타냄.

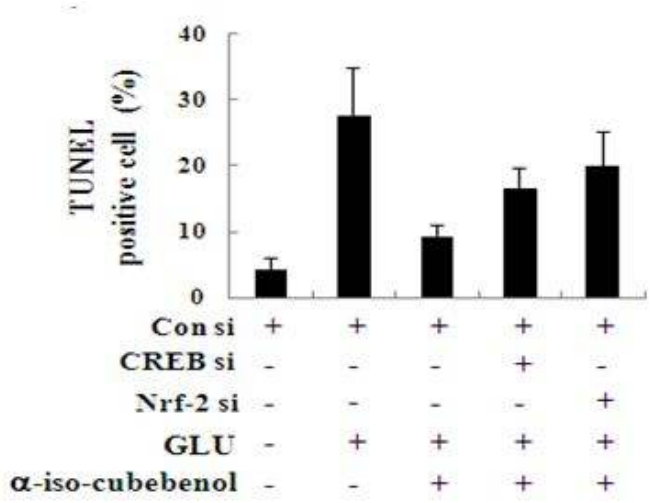

그림 29. 마우스의 해마 HT22 세포에 CREB 및 Nrf-2 siRNA를 이입한 후, 알파-이소-쿠베베놀을 처리하고 글루타메이트로 자극하고, TUNEL 검사한 값을 나타냄.

제 4 장 목표달성도 및 관련분야에의 기여도

1절. 연차별 연구개발의 목표달성도 및 내용

본 기술개발사업의 목표는 10대 질환을 중심으로 특정고유질환 동물모델을 개발하고, 우수한 천연물 후보물질을 발굴하여 효력을 평가하고, 이를 대상으로 한 비임상시험 (GLP)을 수행함으로서, 후보물질의 안전성 및 유효성을 입증함과 동시에 전문적인 연구개발지식과 농업바이오 분야에서의 R&D 사업의 수익을 지속적으로 창출할 수 있는 모델을 제시하고자한다.

CRO산업은 바이오산업의 핵심 인프라산업으로 바이오산업과 함께 고성장하고 있는 추세로, 최근 CRO산업은 단순한 연구서비스 제공을 지양하여 초기 물질 연구에서, 비임상시험, 임상시험, 분석시험, 임상데이터 관리, 컨설팅, 영업, 마케팅지원 사업(CSO)까지 다양화되고 있다.
농업 바이오 산업은 생명공학을 필두로 하는 첨단기술 개발로 시장 규모가 넓고 분야가 다양화된 연 평균 18%의 성장을 보이는 국가경쟁력의 원천 분야로서, 신약소재에서 기능성 식품, GMO, 천연화장품까지 확대되어 후보물질이나 신기술을 상품화하는 글로벌 농업 CRO 출현을 필요로 한다.
본 연구과제의 최종목표는 농업 바이오 전문가인프라 구축과 전문 비임상 CRO 및 임상 CRO를 연계시키고, 농업 바이오 산업 분야의 특성화된 전문 컨설팅 서비스를 제공하는 농업 바이오 CRO 법인을 설립하는데 있다.

이러한 CRO 법인 설립을 위해 1, 2년차에 산학연계 프로그램을 통해 우수 인력을 확보하고, 내부 인원에 대한 전문성을 강화하기 위해 정기적인 교육 및 훈련을 실시하며, 국내외 전문가 초빙 세미나 및 전문 교육 프로그램 지원을 통해 농업 바이오 분야의 전문 CRO로서의 입지를 구축한다. 3년차 이후에는 주관기업 내에 농업 바이오 R&D 컨설팅 전담부서를 구성하여 본 과제로부터 도출된 우수한 결과를 보인 국산 농산물 후보물질에 대한 IND 신청자료를 파일링하고, R&D 컨설팅 네트워크 구축을 지원한다. 추후 독립적인 R&D 컨설팅 CRO 법인을 설립한다.

농업전문 국가기관과 농업전문 CRO 간의 MOU를 체결하여 국가기관에서 주관하는 주요 사업의 신약후보물질이 발굴되면 농업전문 CRO에서 컨설팅을 한다. 농업전문 CRO는 농업바이오분야에 저명한 학계와 우수실험실을 갖춘 비임상 및 임상 시험 전문기관과의 인프라를 구축하고 유지한다. 이러한 시스템을 이용하여 농업바이오분야의 우수한 신약후보물질의 효력 및 안전성 검증에서부터 상품화까지 컨설팅 역할을 수행함으로써 차별화된 농업전문 CRO 역할을 수행한다.

구분 (연도)	세부과제명	세부연구목표	달성도 (%)	연구개발 수행내용
1차 년도 (2012)	제 1세부 농업바이오 분야의 CRO 비임상시험 연구	○ 확보된 후보물질을 대상으로 비임상시험 실시	100%	○ 조제물분석
			100%	○ 자초추출물 단회투여독성(설치류/비설치류) 2주용량설정시험 (설치류/비설치류) 단회경구투여독성 (설치류,비설치류) 4주반복 투여독성 및 회복시험 (설치류, 비설치류)
			100%	○ 자초추출물 국소독성(피부, 안점막) 및 항원성
			100%	○ 자초추출물 유전독성(복귀돌연변이, 염색체이상, 소핵시험)
			100%	○ 자초추출물 LC/MS/MS를 이용한 랫드 및 비글견 중 acetylshikonin 분석법개발 및 검량선 확인시험 (설치류, 비설치류)
	제 1협동 질환 동물 모델 개발 및 효력시험 연구	심순환모델동물 ASC-2 GEM 개발	100%	○ ASC-2 (심순환) GEM의 vector 제작 ○ ASC-2 (심순환) GEM의 targeted ES 확보 ○ ASC-2 (심순환) GEM 의 targeted ES의 blastocyst injection ○ ASC-2 (심순환) GEM의 targeted ES의 GLT (Germline transmission) ○ ASC-2 (심순환) GEM의 targeted ES의 chimera 생산 ○ ASC-2 (심순환) GEM의 genotype 및 대량 생산

구분 (연도)	세부과제명	세부연구목표	달성도 (%)	연구개발 수행내용
1차 년도 (2012)	제 1협동 질환 동물 모델 개발 및 효력시험 연구	암모델동물 Ei24 GEM 개발	100%	○ Ei24 (암) GEM의 vector 제작 ○ Ei24 (암) GEM의 targeted ES 확보 ○ Ei24 (암) GEM 의 targeted ES의 blastocyst injection ○ Ei24 (암)GEM의 targeted ES의 GLT (Germline transmission) ○ Ei24 (암) GEM의 targeted ES의 chimera 생산 ○ Ei24 (암) GEM의 genotype 및 대량 생산
		대사성질환 모델동물 ATF-3 GEM 개발	100%	○ ATF-3 (대사)GEM의 vector 제작 ○ ATF-3 (대사) GEM의 targeted ES 확보 ○ ATF-3 (대사) GEM 의 targeted ES의 blastocyst injection ○ ATF-3 (대사) GEM의 targeted ES의 GLT (Germline transmission) ○ EATF-3 (대사) GEM의 targeted ES의 chimera 생산 ○ ATF-3 (대사) GEM의 genotype 및 대량 생산
	제 2협동 천연물 신약후보물질의 개발 및 효력시험 연구	○ 항암 효능 지치 지치의 대량 추출	100%	○ 전임상 실험에 필요하 추출물 제공
		○ α-iso-cubebenol의 대량 분리법 확립	100%	○ 다양한 방법으로 추출 효율 3배 이상 향상 ○ 용매 절약 및 순수분리 기간 단축
		○ Gomisin J의 혈관이완작용 및 이의 분자생물학적 기전을 규명, 다양한 형태의 고혈압 실험동물 모델 개발 및 이에 대한 gomisin J의 항고혈압 효과를 규명한다.	100%	○ Gomisin J의 혈관이완작용 규명 ○ Gomisin J와 Gomisin A의 혈관이완작용 강도 비교 ○ Gomisin J에 의한 혈관이완작용에 있어서 혈관 내피세포와의 관련성 규명 ○ Gomisin J의 혈관이완작용 기전에 규명
		○ 오미자 유래 신기능 물질의 동물모델에서의 패혈증 치료효과	100%	○ CLP 모델에서의 신기능 물질에 의한 패혈증 치료효과 조사 ○ Antibiotics 주입 모델에서의 신기능 물질의 패혈증 치료효과 조사 ○ 신기능 물질에 의한 주요 장기 손상 저해 효과 조사

구분 (연도)	세부과제명	세부연구목표	달성도 (%)	연구개발 수행내용
2차 년도 (2013)	제 1세부 농업바이오 분야의 CRO 비임상시험 연구	○ 확보된 후보물질을 대상으로 비임상시험 실시	100%	○ 자초추출물 4반복투여독성시험, 독성동태시험(설치류) acetylshikonin 분석법개발 및 validation(설치류)
			100%	○ Gomisin J 분석법 Validation(설치류)
			100%	○ EC-18 13반복투여(설치류/비설치류) 4반복투여독성(비설치류) 항암효능시험 관절염 효능시험 안전성약리시험 (중추신경계)
	제 1협동 질환 동물 모델 개발 및 효력시험 연구	세부연구목표 신경계 질환모델동물 DMI-1, GX2 GEM 개발	100%	- DMI-1, GX2 (뇌신경질환) GEM의 vector 제작 - DMI-1, GX2 (뇌신경질환) GEM의 targeted ES 확보 - DMI-1, GX2 (뇌신경질환) GEM의 targeted ES의 blastocyst injection - DMI-1, GX2 (뇌신경질환) GEM의 targeted ES의 GLT(Germline transmission) - DMI-1, GX2 (뇌신경질환) GEM의 targeted ES의 chimera 생산 - DMI-1, GX2 (뇌신경질환) GEM의 genotype 및 대량 생산
		암, 심순환, 대사성 질환동물모델의 질환 관련 특성 분석 표준화 기반 구축 및 분석	100%	- 종양 발생 검색 : 조직병리, 세포증식능 검색, 발암물질 감수성 검색(DEN) - 심순환 질한 특성 검색 : 심장 및 혈관의 조직학적 검사 - 대사성질환 특성 검색: 체중증가, 지방량 측정, 지방조직검사, 혈당, GTT - 신경계질환 검색 : 조직검사, Hippocampus의 세포 증식능 검색
	제 2협동 천연물 신약후보물질의 개발 및 효력시험 연구	• α-iso-Cubebenol의 대량분리	100%	- 1차년도에 확립한 방법을 반복적으로 수행하여 3차연도까지 3차연도까지 25 g 확보
		• 제 1세부에 자초추출물과 α-iso-cubebenol 공급	100%	- 항암 효능을 가진 자초 추출물 공급 - 97% 이상 순도를 가진 α-iso-cubebenol의 순수분리 - GC-MS를 이용한 순도확인
		• 오미자 성분의 효능 검증	100%	- 효능성분의 작용 기전 규명

구분 (연도)	세부과제명	세부연구목표	달성도 (%)	연구개발 수행내용
3차 년도 (2014)	제 1세부 농업바이오 분야의 CRO 비임상시험 연구	후보물질을 대상으로 비임상 시험 진행	100%	○ 개발후보물질 사업성 판단 (EC-18, 자초추출물, Gomisin J, α-Iso-cubebenol)
			100%	○ α-Iso-cubebenol 단회경구투여독성(설치류) 피부자극시험 (비설치류) 안점막자극시험 (비설치류)
			100%	○ Gomisin J 분석법 Validation(설치류)
			100%	○ EC-18 배태자 발생독성시험(설치류) 수태능 및 초기배 발생독성시험(설치류)
		농업 CRO 기반구축을 위한 전문가 육성 세미나 개최	100%	2014년 11월 20일 외부 전문가, 제1세부, 제1협동, 제2협동 과제책임자가 기능성 식품 및 의약품 개발에 대한 특강, 개발한 질환모델 소개
		농업 바이오 CRO 구축,산학연과 MOU 체결	100%	- 농림수산식품기술기획 평가원과 MOU 체결 - 세종벤쳐 파트너스와 연계하여 컨설팅 조직 구축
	제 1협동 질환 동물 모델 개발 및 효력시험 연구	신약후보물질의 종양, 심순환, 대사성, 신경계 질환 유효성 평가를 위한 질환동물모델 개발	100%	- ASC-2 (심순환), Ei24 (암질환), UQCRB (대사성질환), 마우스의 질환 특성 분석 연구
		암 질환동물모델을 이용한 신약후보물질 1종의 유효성 평가 (2차년 종료후 과제평가에 따른 수정사항)	100%	- 종양 발생 검색 : 조직병리, 세포 증식능 검색, 발암물질 감수성 검색 (DEN) 모델에서 종양억제 유효성 평가
	제 2협동 천연물 신약후보물질의 개발 및 효력시험 연구	• α-iso-Cubebenol의 대량분리	100%	- 1차년도에 확립한 방법을 반복적으로 수행하여 3차연도까지 25 g 확보
		• 제 2 협동에 자초 추출물과 α-iso-cubebenol 공급	100%	- 항암 효능을 가진 자초 추출물 공급 - 97% 이상 순도를 가진 α-iso-cubebenol의 순수분리 - GC-MS를 이용한 순도확인
		• 오미자 성분의 효능 검증	100%	- 효능성분의 작용 기전 규명

2절. 관련분야에의 기여도

1. 제 1세부. 농업바이오 분야의 CRO 비임상시험 연구

○ 농업바이오분야 R&D 사업을 원활히 수행할 민간 CRO 기관의 인프라를 구축한다.

○ 10대 질환을 중심으로 발굴된 우수한 천연물 후보물질을 대상으로 비임상시험을 수행함으로서, 후보물질의 안전성 및 유효성에 대한 평가가 가능하게 되었다

○ 동시에 전문적인 연구개발지식과 농업바이오 분야에서의 R&D 사업의 수익을 지속적으로 창출할 수 있는 모델을 제시할 수 있으리라 기대된다.

2. 제 1협동. 질환 동물 모델 개발 및 효력시험 연구

○ 국내 질환모델동물의 개발단계 수준을 넘어서 의약품 평가에 효율성이 높은 질환모델동물자원을 발굴함으로써 국내 질환모델동물자원의 활용성을 높이고 국내 신약개발 및 독성연구에 지원 가능할 것으로 기대된다.

○ 개발된 4개 질환에 대한 동물모델을 대상으로 후보 물질의 효력 시험연구(유효성)에 활용 가능할 것으로 기대된다(학계, 산업계 활용 가능).

○ 개발된 질환모델동물을 이용한 신약 후보 물질의 산업화를 위해서는 마우스 계통 유지 및 대량 생산이 필요하며 이를 위해서는 계통 유지 및 대량생산에 필요한 시설 및 재원의 지원이 필요함. 모델동물 개발자와 협의하여 농림수산식품부에서 수탁 관리하고 지속적인 계통관리와 품질관리를 통해 산업화 가능할 것으로 기대된다.

3. 제 2협동. 천연물 신약후보물질의 개발 및 효력시험 연구

○ 지적 재산권의 확보:
- 면역조절 물질이 향후 패혈증 치료제 개발에 필요한 후보물질로 제공될 수 있음을 규명한 결과를 국내외에 특허화하여 지적 재산권을 확보하고 향후, 이를 글로벌 제약회사에 licensing out함으로써 의약품 개발에 응용하도록 한다.
- 오미자 유래 gomisin J의 고혈압 예방 및 치료 후보물질 발굴로 제약회사에 licensing out함으로써 의약품 개발에 응용하도록 한다.
- 자초 유래 항암성분을 동물모델에서 효능을 검증하여 천연물 후보물질로서 제공한다.

○ 면역조절 물질에 의한 생리활성 반응의 조절 및 생리활성 반응과 염증반응과의 상호관련성에 대한 확인으로 염증반응과 감염질환 연구에 새로운 계기를 마련할 수 있을 것으로 기대된다.

○ 면역조절 물질을 다른 질병 치료제 개발에 응용할 수 있는 좋은 예를 제시할 수 있을 것임.

○ 면역조절 물질을 이용한 패혈증 치료제 개발을 주도하여 패혈증을 포함한 감염질환 치료제 개발 분야를 선도할 수 있을 것으로 기대됨.

○ 면역조절 물질을 이용한 패혈증 치료제 개발 연구의 초석을 제공함으로 인하여 국내 신약개발 역량을 향상시킬 것으로 기대됨.

○ 연구에 참여한 연구원들이 패혈증 및 감염질환에 관련된 다양한 연구 경험을 쌓을 수 있게 되어 우수한 연구 인력을 양성하여 향후 관련 Bio 산업 발전에 기여할 수 있을 것으로 기대됨.

구분	최종목표	목표달성도 및 기여도
고혈압 효능 천연물 신약 후보물질 개발	천연물 후보물질 1종	- 기존에 고혈압 치료제로 사용되고 있는 Losartan보다 효과 높은 성분 발굴 - 천연물을 이용한 고혈압 치료 소재 발굴 방법 확립
패혈증 치료제 후보물질 개발	물질개발 수 (1개)	- 오미자로부터 패혈증에 효과가 있는 성분의 패혈증 기작을 구명하여 패혈증 치료제 후보물질 1종 발굴 - 효능성분의 염증성 사이토카인인, Th1 사이토카인의 영향규명 - 패혈증 치료제 개발을 위한 효능연구 시스템 확립 - 특히 천연물 후보물질인 α-iso-cubebenol은 단백질 의 발현 및 신경전달의 조절을 통해서 신경세포 보호하고, 신경질환을 개선, 치료 또는 예방하는 효과가 높고, 천연물로써 안정성이 높기 때문에 다양한 분야에 활용가능한 성분으로 증명됨
항암 효능 천연물 후보물질 개발	천연물 후보물질 1종	- 항암 효능을 가진 복합 추출물의 효능을 검증하였으며, 추출물로부터 효능성분을 순수분리하여 효능성분의 함량 표준화로 천연물 후보물질 1종 발굴 - 효능성분의 순수분리 방법 확립 - 효능성분의 함량분석을 통한 추출물의 표준화

제 5 장 연구개발 성과 및 성과활용 계획

제 1절. 농업바이오 분야의 CRO 구축

사 업 자 등 록 증

(법인사업자)

등록번호 : 264-81-12657

법인명(단체명) : 주식회사 세종벤처파트너스

대 표 자 : 류준걸, 강종구

(각 자 대 표)

개 업 년 월 일 : 2013년 03월 13일 법인등록번호 : 110111-5088665

사업장 소재지 : 서울특별시 서초구 법원로1길 22 (서초동,영진빌딩2층)

본 점 소 재 지 : 서울특별시 서초구 법원로1길 22 (서초동,영진빌딩2층)

사 업 의 종 류 : 업태 금융업 종목 창업투자

교 부 사 유 : 신규

사업자단위과세 적용사업자 여부 : 여( ) 부(v)

전자세금계산서 전용메일주소 :

2013 년 03 월 22 일

서초 세무서장

3본부 1연구소

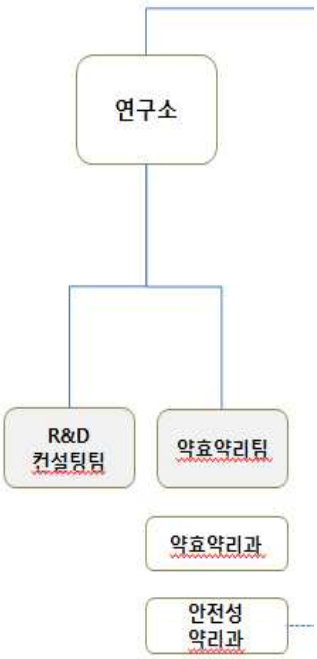

<조직도>

제 2절. 계획 대비 연구성과

(단위 : 건수)

구분		특허		신약후보물질			SOP 개발	논문	
		출원	등록	후보물질 검증	IND 제출	상품화		SCI	비SCI
1차년도	목표						제정	2	
	성과	2		1				3	
2차년도	목표	1		1				3	2
	성과	3		1				1	2
3차년도	목표	1		2	(1)			3	3
	성과	2	1			1		4	2
4차년도	목표		1	2					(2)
5차년도	목표		1			(1)			
계	목표	2	2	3	(1)	(1)		8	5
	성과	7	1	4		1		8	4(2)

**4차년도(2014년) 비SCI 논문 투고중 "Dose escalating single and repeated dose oral toxicity studies of Lithospermumerythrorhizonextract in dogs"*
"Acute and 28-day subchronic toxicity studies of Lithospermum erythrorhizon extract, in Sprague-Dawley rats"

제 3절. 주요 연구성과 세부내용

1. 주요 연구성과

가. 후보물질의 비임상 시험 실시 및 산업화

(1) 10대 질환을 중심으로 발굴된 천연물 후보물질을 대상으로 비임상독성시험(일반독성, 유전독성, 특수독성시험 등) 수행하였다.

(2) 또한, 농업바이오 분야의 개발후보 물질의 독성시험을 통한 안전성 검증과 관절염, 항암시험 등의 유효성 평가 시행을 통해 전문적 연구개발 지식 및 R&D 사업의 수익을 지속적으로 창출할 수 있는 모델 제시하였으며,

(3) 후보물질 검증에서 효능이 입증되고 독성이 없는 것으로 인정된 후보물질의 경우, 건강기능식품 및 천연물신약에 대한 IND 신청자료로 제출하고 시험결과에서 경쟁력 확보시 상품화 진행 예정중이다.

■ 후보물질의 비임상 시험 실시 및 산업화 • 10대 질환을 중심으로 발굴된 천연물 후보물질(1차년도 자초추출물)을 대상으로 비임상 독성시험 (일반독성 (단회 및 반복, 설치류 및 비설치류), 유전독성, 특수독성시험 등) 수행.	
• 농업바이오분야의 개발후보물질의 안전성 및 유효성 평가와 동시에 전문적인 연구개발 지식과 R&D 사업의 수익을 지속적으로 창출할 수 있는 모델 제시함.	• 후보물질 검증에서 효능이 입증되고 독성이 없는 것으로 인정된 후보물질의 경우, 건강기능식품 및 천연물신약에 대한IND 신청 자료로 제출하고 시험결과에서 경쟁력 확보 시 상품화 진행 예정.

나. 농업바이오분야 전문 CRO 법인화 추진

(1) 농업바이오분야 R&D 사업을 원활히 수행할 타 기관과의 전문가 인프라 구축완료 하였으며,

(2) 본 주관기관은 바이오 전 분야(농업분야 포함)의 전문 CRO로서 바이오산업 분야의 특성화된 전문 컨설팅 서비스를 이미 제공하고 있으며, 본 과제의 목표로 정한 법인화를 추진하여 현재 '세종벤처파트너스'를 설립하였으며, 현재 사업을 다각화하여 농업CRO로서의 기업의 역량을 강화하기 위하여, 우수 신약 item 개발, 유망 벤처 발굴 및 육성 등의 역할을 수행하는 조직을 구성하여 운영중이다.

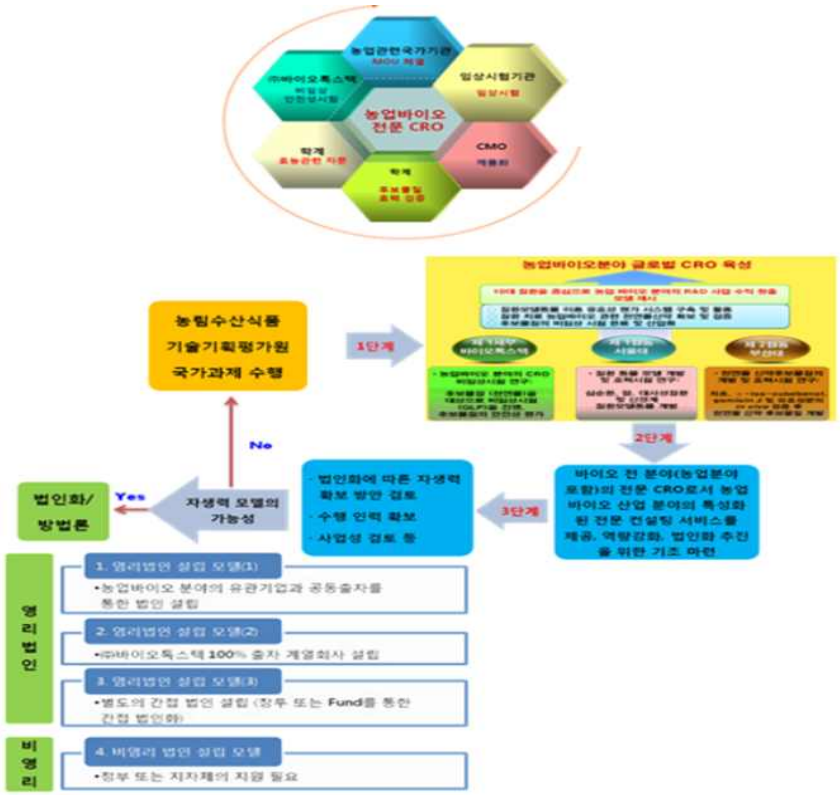

2. 특허/논문 성과

가. 논문 성과

게재연도	논문명	저자			학술지명	Vol. (No.)	국내외 구분	SCI 구분
		주저자	교신저자	공동저자				
2012	Gomisin J from Schisandra chinensis induces vascular relaxation via activation of endothelial nitric oxide synthase	박지영	김치대	최영환, 윤정욱, 배진웅, 서교원, 이승진, 박소연	Vascular Pharmacology	57	국외	SCI
2012	Antihypertensive effect of gomisin A from Schisandra chinensis on angiotensin II-induced hypertension via preservation of nitric oxide bioavailability	박지영	최영환	윤정욱, 배진웅, 서교원, 이승진, 박소연, 홍기완, 김치대	Hypertension Research	35	국외	SCI
2012	Therapeutic effects of α-iso-cubebenol, a natural compound isolated from the Schisandra chinensis fruit, against sepsis.	이성규	최영환, 배외식	김상두, 국민수, 이하영, 박준성, 박영훈, 강점순	Biochem Biophys Res Commun	427	국외	SCI
2013	Role of CXCR2 on the immune modulating activity of α-iso-cubebenol a natural compound isolated from the Schisandra chinensis fruit.	정영수, 이성균	최영환, 배외식	옥창엽, 조은정, 박준성	Biochem Biophys Res Commun	431	국외	SCI
2013	EI24 regulates epithelial-to-mesenchymal transition and tumor	최정민 Sushil Devkota	이한웅	성영훈	Oncotarget	4(12)	국외	SCI
2013	Proteomic analysis of liver in miniature pigs according to developmental stages using two-dimensional electrophoresis and matrix-assisted later desorption/ionization-time of flight mass spectrometry	이순신	성제경	오재진 김일용 염혜정 염수청 황승용	Lab Anim Res	29(3)	국내	비SCI
2014	α-Iso-cubebenol inhibits inflammation-mediated neurotoxicity and amyloid beta 1-42 fibril-induced microglial activation	박선영	최영환, 배외식	박태경, 이상준	J. of Pharmacy and Pharmacology	66(1)	국외	SCI

게재연도	논문명	저자			학술지명	Vol. (No.)	국내외 구분	SCI구분
		주저자	교신저자	공동저자				
2014	Involvement of activation of the Nrf2/ARE pathway in protection against 6-OHDA-induced SH-SY5Y cell death by a-iso-cubebenol	박선영	최영환,	김도연, 강종구, 박근태	NeuroToxicology	44	국외	SCI
2014	Identification of the responsible proteins for increased selenium bioavailability in the brain of transgenic rats overexpressing selenoprotein M	김요나 구준서	성제경 황대연	김일용 김지은 곽문화 고준 심선보 홍진태	International J. of Mol. Med.	34	국외	SCI
2014	Perturbation of NCOA6 Leads to Dilated Cardiomyopathy	노재일	이한웅 강석민	정철호 성영훈 이지현 오재원 이범섭 이종은 고용송 김덕경 박찬배 이지현 이재운	Cell Reports	8	국외	SCI
2014	Proteomic analysis of domestic pig pancreas during development using two-dimensional electrophoresis and matrix-assisted laser desorption/ionization -time of flight mass spectrometry	안지예	성제경	김일용 오새진 황혜숙 이순신 김요나 신재훈 윤여성	Lab Anim Res	30(2)	국내	비SCI
2014	Proteomic analysis of pancreas in miniature pigs according to developmental stages using two-dimensional electrophoresis and matrix-assisted laser desorption/ ionization -time of flight mass spectromet	이순신	성제경	김일용 오새진 염혜정 염수청 황승용	Lab Anim Res	30(1)	국내	비SCI

나. 특허 성과

출원된 특허의 경우				
출원연도	특허명	출원인	출원국	출원번호
2012.08.28	알파—이소—쿠베베놀을 유효성분으로 포함하는 감염성 및 염증성 질환의 예방 또는 치료용 조성물	부산대 산학협력단, 성균관대 산학협력단	대한민국	10-2012-0094114
2012.08.10	지치 추출물을 유효성분으로 포함하는 암의 예방 또는 치료용 약학적 조성물	부산대학교 산학협력단	PCT	PCT/KR2012/006359
2013.12.31	오미자로부터 알파-이소-쿠베베놀을 대량으로 분리하는 방법	부산대학교 산학협력단	대한민국	10-2013-0168998
2013.11.07	고미신 J를 유효성분으로 포함하는 고혈압의 예방 또는 치료용 조성물	부산대학교 산학협력단	대한민국	10-2013-0134646
2013.0101	전 알파-이소-쿠베벤 또는 알파-이소-쿠베베놀을 유효성분으로 포함하는 감염성 및 염증성 질환의 예방 또는 치료용 조성물	부산대 산학협력단, 성균관대 산학협력단	PCT	PCT/KR2013/007381
2014.05.12	알파-이소-쿠베베놀을 유효성분으로 포함하는 신경 질환의 예방 또는 치료용 조성물	부산대학교 산학협력단	대한민국	10-2014-0056503
2014.05.12	알파-이소-쿠베베네를 유효성분으로 포함하는 신경 질환의 예방 또는 치료용	최영환 박순영 박근태 김영훈 강종구	대한민국	10-2014-0056508

등록된 특허의 경우				
등록연도	특허명	출원인	출원국	출원번호
2014.07.09	알파—이소—쿠베베놀을 유효성분으로 포함하는 감염성 및 염증성 질환의 예방 또는 치료용 조성물	부산대 산학협력단, 성균관대 산학협력단	대한민국	10-1420010

다. 연구 성과 활용목표 및 결과

(단위 : 건수)

구분		기술실시 (이전)	상품화	정책자료	교육지도	언론홍보	기타
활용건수	목표	1	(1)				1(SOP)
	달성		1			1	1(SOP)

(1) 후보물질 검증

① 자초추출물(Acetylshikonin): 비임상시험 실시,사업성판단(사업화보고서 참조)

Acetylshikonin(자초추출물)에 대한 비임상 시험은 단회, 반복(4주 단회 설치류, 비설치류), 유전, 국소, 항원성 시험을 진행하였으며, 개략의 치사량, 최대내성용량을 2,000mg/kg이상으로 설정, 유전독성시험(복귀돌연변이, 염색체이상)에서는 음성, 소핵시

험에서는 소핵유발에 영향을 미치지 않는 것으로 판단되었다. 또한 항원성 음성, 피부 자극 및 안점막 자극 시험에서는 자극성이 있는 것으로 판단됨

② EC-18: 사업성판단(사업화보고서 참조)

EC-18에 대한 비임상 시험은 단회, 반복(4주 설치류, 비설치류, 13주 설치류), 유전, 생식, 안전성 약리 시험을 진행하였으며, MTD, NOAEL, 2,000mg/kg이상으로 설정, 기타 유전독성 음성, 생식발생, 안전성약리 시험에서 2,000mg/kg 이하에서 특이사항 없었음. 효능시험은 천식, 아토피 및 폐혈증 동물 모델에서 효능입증 하였으며, 건강기능성 식품 등재를 위해 사람을 대상으로 안전성과 유효성 평가를 입증함.

③ Gomisin-J: 사업성판단(사업화보고서 참조)

Gomisin J가 혈관 평활근을 이완시킬 수 있음을 증명하였을 뿐만 아니라, gomisin J의 혈관이완작용 강도는 gomisin A의 강도보다 3배 정도 더 강함을 알 수 있었으며, 이를 통하여 gomisin J가 gomisin A보다 더 높은 약리학적 효능을 가지고 있음.

④ α-iso-cubebenol: 비임상시험 실시(사업화보고서 참조)

(2) 농업 CRO 기반구축을 위한 전문가 육성 Seminar 개최

① 일시 : 2014년 11월 20일(목)

② 장소 : (주)바이오톡스텍 C동 세미나실

③ 발표연사 및 내용

시간	프로그램	
15:00~15:10	인사 및 일정 공지	사회자 등
15:10~15:50	건강기능식품의 유효성/안전성 평가:개요 및 실제	충북대 김대중교수
15:50~16:30	Detection of allergic compounds and evaluation of therapeutic agents using IL-4/Luclferase/ CNS-1 transgenic mice	부산대 황대연교수
16:30~17:00	농업 바이오 분야의 CRO의 역할	㈜바이오톡스텍 강종구대표이사
17:00~17:30	질환 동물 모델 개발 및 효력시험 연구	서울대 성제경교수
17:30~18:00	천연물 후보물질의 개발 및 효력시험 연구	부산대 최영환교수
18:00~	폐회	

(3) 상품화 : EC-18 (PLGA: 1-palmitoyl-2-linoleoyl-3-acetyl-rac-glycerol) 건강기능성 식품 개별인증 획득

① EC-18 (PLGA: 1-palmitoyl-2-linoleoyl-3-acetyl-rac-glycerol)은 녹용 천연물 유래 단일 활성성분으로, 국내 최조 건강기능성 원료로 인증 받았다.

② 녹용은 지난 100여년 이상 대표적인 보양식품으로, 여러가지 작용 중에서 조혈작용이나 면역계에 대한 효능이 입증되어 오랜세월 동안 사용하여 안전성이 입증되었다. 반면 단회, 반복, 소핵, 복귀돌연변이, 염색체이상, 약물동태, 안전성 약리(중추신경, 호흡기계, 심혈관기계) hERG assay, 동위원소를 이용한 약물동태(흡수, 분포, 대사) 시험, 효력시험 등을 바이오톡스텍에서 수행하였을 때, 안전성 또한 입증된 원료이다.

③ 현재 EC-18은 면역력 증진, 관절건강, 피로회복, 중성지방 저하 등 다양한 효능을 기초로 건강기능식품으로 “록피드”를 제조해 국내 종합병원 및 건강기능성 식품으로 판매 중에 있다.

④ 록피드는 현재 판매되고 있는 상품으로서 약 10억원 이상의 연 매출을 올리고 있으며, 면역력 증진, 관절건강, 피로회복, 중성지방 저하 등 다양한 효능을 가지고 있으므로 추후 지속적인 매출액 증대가 있을 것으로 예상함

(4) CRO 운용관련 SOP 제정 : 기밀사항으로 예시만 공개

SOP번호	조직 및 업무분장	제정일자	2012-11-30
SOP/AGR/001	**Organization and Job Descriptions**	개정일자(차수)	(0)

1. 목적

㈜바이오톡스텍 내부 조직으로서 가칭 '농업전문CRO'에서 기획, 실시되는 시험의 신뢰성을 확보하기 위하여 조직의 책임과 권한을 명확히 함.

2. 적용범위

㈜바이오톡스텍 내부 조직으로서 가칭 '농업전문CRO'에서 시험 등을 실행, 유지하는 구성원에 적용한다.

3. 조직의 구성 및 운영

3.1 조직 구성은 추후 확정한다.

3.2 주요 업무에 대한 의결은 "운영위원회"를 통하여 결정하고 운영자의 승인을 받는다.

3.3 각 구성원의 역할, 책임 및 권한은 "업무분장표"에 따르며, "업무분장표"는 운영자의 승인을 받는다.

4. 책임과 권한

4.1 운영자

4.1.1 소속된 개개인이 규정에 명시된 책무를 수행하였음을 확인 한다.

4.1.2 담당자의 자격, 훈련, 경험, 책무분담에 대한 기록의 관리유지를 확인한다.

4.1.3 담당자 별로 그들이 실시해야 하는 책무를 명확히 이해하고 관련된 교육이 실시되고 있는지 확인한다.

4.1.4 기술적으로 타당한 표준작업수순서(SOP, Standard Operating Procedure)가 작성되고 준수되는지를 확인하고, 모든 표준작업수순서의 제정, 개정 및 폐기를 승인한다.

4.1.5 모든 관련 표준작업수순서 파일을 유지토록 한다.

4.2 팀장

4.2.1 팀원의 역할, 책임 및 권한에 대하여 업무 분장표를 작성한다.

4.2.2 팀원의 자격을 평가하고 업무 수행에 대하여 관리 감독한다.

4.2.3 년간 교육 훈련 계획서를 작성하고, 팀원의 자질 향상을 위해 교육을 실시한다.

4.2.4 팀별 업무 목표 및 추진 계획을 설정, 실행한다.

4.2.5 해당 SOP의 제정, 개정 내용을 검토하고, 유지, 관리한다.

4.2.6 시정 및 예방조치 사안에 대하여 계획을 수립하고 실시한다.

4.3 담당자

4.3.1 담당자는 관련된 해당 규정의 조항을 숙지하고 있어야 한다.

4.3.2 담당자는 적절한 표준작업수순서에 따라 업무를 수행하고, 문제 발생시 운영자에게 보고한다.

5. 기록 및 보관

모든 기록의 관리는 ㈜바이오톡스텍 "자료관리(SOP/GER/006)"에 따른다.

(5) 인터비즈(바이오파트너링&투자포럼) 참석

제 1 세부와 제 2협동 공동으로 연차 결과를 InterBizBio-Partering & Investment Forum에 참석하여 결과 홍보 및 기술이전 제약회사 탐색하였다.

제 4절. 성과활용계획

○ 농업바이오신약 후보물질인 자초추출물의 비임상시험 평가 및 사업화

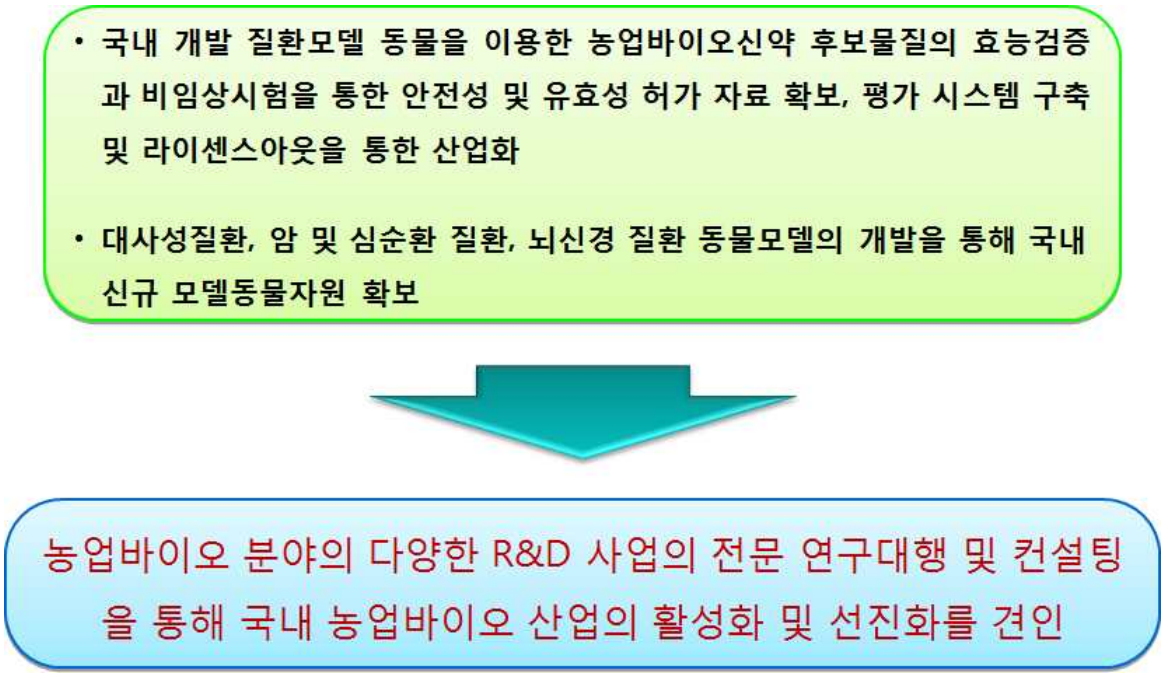

○ 본 연구과제에서 도출된 연구성과는 기술 이전의 효율성을 증대시키기 위하여 주관기업으로 기술이전을 하거나 연구성과 결과에 따라서 일정 지분을 주관연구기관과 공유하게 될 것임. 이러한 기술은 부산대학의 산학협력단과 주관기관인 바이오톡스텍이 기 구축된 인프라를 이용하여 상호협력 또는 개별적으로 기술이전을 추진할 계획임

○ 신약 후보물질의 산업화에 전략

- 천연물 신약 후보물질인 표준화된 자초추출물, α-iso-cubebenol 및 gomisn J 등은 농기평 등의 산업화 연구과제 개발을 위한 추가적인 연구 시도 후 나온 연구결과 또는 현재의 연구결과를 부산대의 산학협력단이나 바이오톡스텍의 인프라를 통하여 기술을 이전할 수 있는 다양한 방법을 강구할 계획임.

- 연구성과의 산업화를 위해서는 국신약개발연구조합에서 시행하고 있는 인터비즈(바이오파트너링&투자포럼) 또는 (사)한국대학기술이전협회 등에 참여하여 기술을 홍보하고, 제약회사와의 미팅을 통하여 기술이전을 위하여 노력할 것임

○ 세부과제별 농기평 연구과제와 연계한 발전 방향

본 연구과제에서 도출된 농업전문 CRO구축, 주요 질환동물 개발 및 고기능성 천연물의 발굴, 순수분리와 함량분석을 통한 표준화 기술은 농산물을 이용한 건강기능성 식품, 천연물 신약 개발 등에 반드시 필요한 분야임.

따라서 본 과제에서 구축한 인프라를 잘 활용하는 것이 무엇보다도 중요하다. 따라서 농기평에서 수행하고 있는 과제 중에서 농업전문 CRO, 질환동물을 이용한 효능 검증 및 추출물의

표준화를 위한 지표성분 발굴과 함량분석이 필요시 위탁기관으로 선정하여 활용하는 것도 농기평의 연구 성공을 위해서 매우 필요한 분야라고 생각됨.

본 연구팀도 연구성과가 단순히 보고서 제출로서 마무리 되는 것이 아니라 농업의 연구기반을 구축하고, 앞으로 농업 연구에 더 큰 도움이 되도록 노력할 것임

본 연구 연구성과 활용의 활성화를 위한 모식도를 다음과 같이 요약할 수 있음

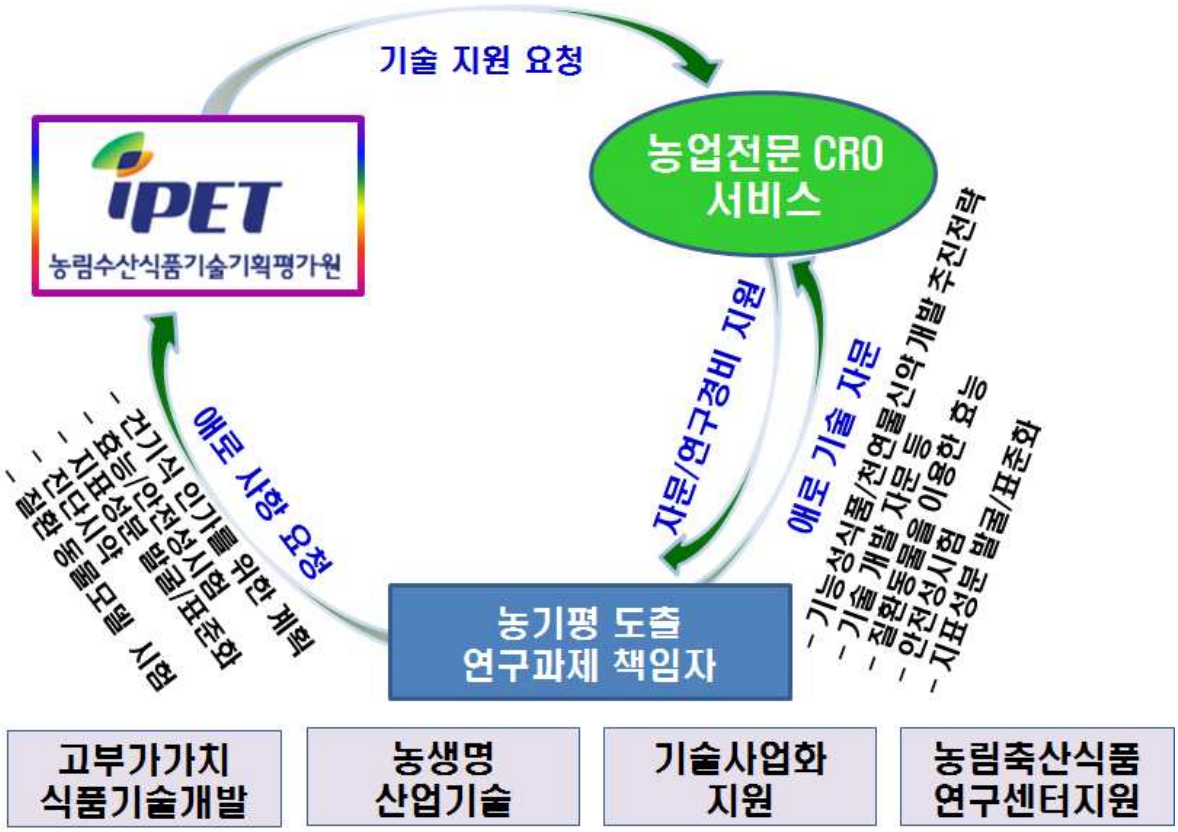

<연구결과 활용을 위한 모식도>

제 6 장 연구개발과정에서 수집한 해외과학기술정보

제 1 절 국외 기술 개발 현황

1. 질환 모델 마우스 관련 연구 현황

가. 질환모델마우스 관련 해외업체 및 산업화 사례

질환모델마우스의 제작 및 판매 관련 주요 업체로는 미국의 찰스리버 (Charles River), 타코닉(Taconic), 할란(Harlan), 영국의 B&K, 일본의 SLC 및 Clea 등으로 조사되었다. 이들 중 미국의 찰스리버사는 질환모델마우스 시장의 50% 이상을 점유할 것으로 예측되며 찰스리버는 비영리기구인 미국의 잭슨 연구실에서 개발된 질환 모델 마우스를 판매한다. 잭슨 연구소(Jackson Laboratory)에는 총 4,000 계통 이상의 마우스를 보유하고 있으며 이 중 질환 모델 마우스는 50~60% 정도이다.

실제로 일본 Clea사에서 개발한 Tg-rasH2 마우스는 기존의 1.5~2년 정도 걸리는 발암성 시험기간을 6개월 이내에 평가할 수 있도록 기간을 단축시켜, 의약품 개발을 위한 발암성 독성평가에 매우 유용하게 쓰이며, 미국 타코닉사에서 개발된 Trp53-deficient (p53+/-) 마우스 역시 의약품 개발을 위한 발암성시험의 평가기간을 단축시켜 주는 장점이 있어 의약품 개발을 위한 독성평가에 산업적으로 많이 활용한다.

일본에서 생산되어 WHO 공인을 받은 Polio Virus Receptor TG 마우스는 매년 20,000마리 이상을 전 세계적으로 공급함. 판매가격은 마리당 10,000엔으로 고부가가치 산업으로서의 가능성을 제시하였다.

질환모델마우스의 가격은 마리당 최소 100~250달러 수준으로 질환모델마우스의 산업적 활용도와 함께 경제적 가치 또한 높은 것으로 판단됨. 1994년 OB 유전자 KO 마우스(비만 마우스)의 경우 미국 Rockefeller 대학의 연구결과가 Amgen 회사에 2,000만 달러에 판매되었다.

나. 해외 기관별 모델마우스 등록된 특허 동향

유전자 변형 질환모델 마우스의 등록특허에 대한 주요 출원인으로는 각각 세 건의 특허등록을 받은 Regeneron(미국), Probiodrug(독일), KMT Hepatech(캐나다), Elan(미국), Aventis(프랑스), University of California(미국) 등 여섯 기관이 있었음. 이들 등록특허 수 상위 주요출원인들의 등록 특허 수 합계는 40건으로, 전체 유효등록특허 96건의 41.7%에 해당한다.

(1) 연도별 등록건수와 등록특허의 출원 연도 경향

<등록특허의 등록연도와 출원 연도의 분포 >

2009년에서 2014년 사이에 등록된 유효특허(96건)의 등록연도와 등록특허가 출원된 연도의 분포한다. 선별된 질환별 모델마우스에 대한 특허는 2010년에 가장 많은 26건이 등록된 이래 해마다 감소하여 연 11건에 머물러 있고, 최근 5년 사이에 등록된 특허들은 가장 많은 15건이 2007년에 출원되었고 이어 2005년과 2002년에 각각 12건씩 출원되었으며, 2007년 이후로는 계속 감소하였다.

출원에서 등록까지 가장 짧게는 약 20개월(미국), 길게 14년의 기간이 걸림(미국). 출원이 가장 많았던 2007년의 경우 미국과 유럽에서 대체로 3~4년의 기간을 거쳐 등록된 것으로 나타난다.

(2) 질환별 출원 경향

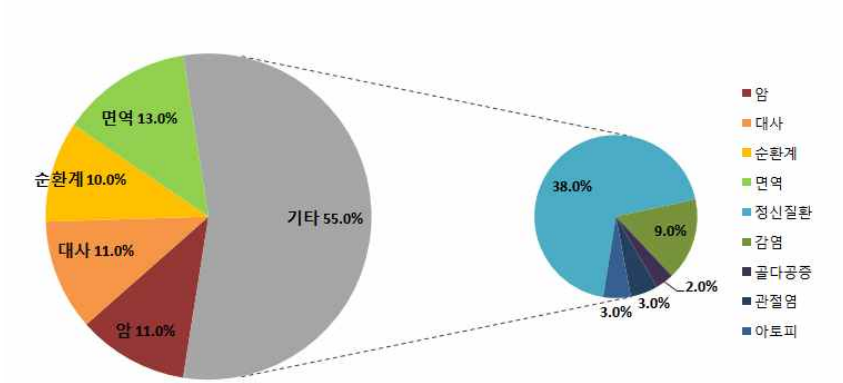

<등록특허의 질환별 경향>

2009년에서 2014년 사이에 등록된 유효특허(96건)의 질환별 출원 경향을 나타내며 (특허의 모델마우스가 둘 이상의 질환에 해당될 경우 각각 한 건으로 포함시킴) 질환 중에서는 정신질환(치매를 동반하는 알츠하이머, 파킨슨, 헌팅턴씨병 등을 포함하는)이 전체에서 38%로 가장 높은 비율을 차지하고 있고 다음으로 면역(13.0%), 대사(11.0%), 암(11.0%)과 순환계 질환(10.0%)이 비슷한 비중으로 등록받았다. 기타질환으로 분류된 골다공증, 관절염, 아토피 등은 매우 낮은 비중을 차지하고 있으며, 질병 기작이 많이 연구되어 있거나 질병 유발 유전자가 알려진 질병일수록 특허출원이 많은 것으로 보인다.

다. in silico 질환모델

국외 in silico ADME 예측기술을 개발/서비스 중인 회사는 아래 표와 같으며, 미국이 최고의 수준으로 대부분 회사를 보유하고 있고 유럽, 캐나다, 일본 국적의 회사도 일부 ADME 관련 서비스를 제공하고 있다.

	Accelrys, Inc. (USA)	Camitro, Cambridge (UK)	Comgenex, Budapest (HU)	Lhasa, Ltd Leeds (UK)	LionBioscience, Inc. (USA)	Simulation plus, Inc. (USA)
홈페이지	www.acceryls.com	www.camitro.com	www.comgenex.com	www.chem.leads.ac.uk/luk/meteor	www.lionbioscience.com	www.simulations-plus.com
프로그램 기능	ADME: 유사약물의 ADME 예측	용해도 예측 모델 ADME: 장흡수도, 혈뇌장벽투과성, CYP 대사(3A4,2D6,2C9)와 CYP 저해도 계산	선도물질 최적화를 위한 ADME/Tox 예측	METERO: 1개의 질의화합물 구조로부터 생체 내 대사 예측	IDEA 흡수 모듈: 투과도와 시간에 따른 흡수도 예측 대사 모듈: 생체이용성 예측	QMPRPlus: 물리화학적 특성계산: 용해도, 투과도, 흡수, 분포 GastroPlus: 위장관에서 용출,이동, 흡수, 생체 이용성와 약물동력학 예측 혈장 단백질 결합력 예측
물리화학적 특성 파라미터	물리화학적 성질들(logP, PSA, 용해도)과 흡수, 혈뇌장벽 투과성 간의 관계식	분자의 표면성질과 정전기적 특성을 이용한 반응에너지 계산	구조-대사의 지식기반 rules 이용	구조-대사의 지식기반 rules 이용	치환기 구조분류를 이용한 지식기반 모델 이용	QMPRPlus: 화합물의 문헌정보와 특성, 신경네트워크, PLS 통계적 툴 이용 GastroPlus: 생체내 반응기작, 흡수, 이동 모델
요구되는 데이터	물리화학적 성질	분자구조	분자구조	분자구조	구조기반흡수모델: 화합물구조 생리학적흡수모델: 화합물구조, 1회투여량, 용해도, caco-2 cell 투과도	화합물 구조, 시간에 따른 생체 내 반응

<대표적인 in silico ADME/PK 예측 관련 회사 및 제품 특성>

(1) In silico 독성 예측모델

in vivo 동물 모델은 시험 비용이 많이 들고 다수의 실험을 동시에 수행하기 어려움. 또한, 인체에서의 유효성을 신뢰할 수 있는 동물 종 선택과 시험 설계 및 결과 해석에 대한 경험 및 임상적 결과를 추론할 수 있는 전문적 지식이 요구되기 때문에, in silico 기술을 이용하여 후보 물질의 독성을 예측하는 연구가 활발하게 수행되고 있다.

회사	프로그램	독성시험	홈페이지
Accelrys	TOPKAT	돌연변이성, 발암성, 토끼 LD_{50}, 토끼 유전체 LOAEL, 발생독성, 피부민감성, 피부자극성	www.accelrys.com
Compudrug	HazardExpert	돌연변이성, 발암성, 약물의초기성, 자극성, 민감성, 면역독성, 신경독성	www.compudrug.com
Lhasa Limited	DEREK	돌연변이성, 발암성, 자극성, 유루(lachrymation), 신경독성, 갑상독성, 약물의초기성, 호흡기와 피부 민감성	www.chem.leeds.ac.uk
Multicase Inc.	M-CASE	발암성, 자극성, 약물의초기성, 최대용량, 단기유전독성, biodegradation	www.multicase.com
SciVision	ToxSYS QSARIS	돌연변이유전독성, 급성독성, 내분비교란물질	www.scivision.com
<in silico 독성예측 시스템>			

국소독성시험 예측모델: 피부자극과 안점막자극 시험 예측을 위해 QSAR 방법이 사용됨.피부자극시험: 주로 페놀류, 하이드록시알콜류, 지방족알콜류 화합물들에 대한 물리화학적 특성(분자궤도 LUMO와 HOMO, 옥탄올과 물분배계수, 분자량, 분자 크기)과 피부자극수치와의 상관관계식을 이용하여 예측하였다. 안점막자극시험: 살리실산, 알콜, 아세테이트, 유기용매 그리고 양이온 계면활성제에 대해 용질-막간의 상호작용을 나타내는 물리화학적 특성과 분자의 편극도, 수소결합 등으로 MES(molar eye store)를 예측하였다.

	BfR-DSS	LHASA (UK)	MultiCASE Inc. (US)	Acceryls Inc. (US)
모델	Expert rules	Structural alerts	QSAR	QSPR/QSAR
모델적용	95% 이상의 순도를 가진 화합물	유기화합물과 금속이 포함된 화합물	작은 분자	유기분자
피부/눈 자극모델	피부와 눈 자극성 유해 화합물들의 구조 정보와 비부식성, 비자 극성 화합물 선정을 위한 물리 화학적 특성 제한값 계산	피부/눈자극성 화합물에 대한 29개의 계산모델	인공지능 모델	다른 구조 군에 분류되어 있는 13개 피부자극성 모델과 15개의 눈자극성 모델
계산결과	피부자극성 R38), 피부부식성 (R34와 R35), 눈자극성 (R36) 와 심각한 눈의 유해 (R41)에 대한 EU 위험 정도	독성을 가지는 화합물의 치환체 정의, 모체 유해 화합물의 문헌 정보	화합물의 피부/눈 자극성 정도 예측	화합물의 피부, 눈 자극성 정도에 따라 분류
<in silico 피부/눈 자극성 예측 시스템>				

유전독성시험 예측모델: 유전독성 유해 화합물의 fragment 존재 여부를 분자 표현자, toxicophore로 나타내어 toxicophore와 유전독성 값의 상관관계식으로 유전독성 정도를 예측함. OSIRIS property explorer(http:// www.organic-chemistry.org/prog/peo/), Lazer(http://www.predictive- toxicology.org/lazer/form.php) 등 유전독성 예측 프로그램이 개발되어 있다.생식발생독성시험: 의약품이 사람의 생식 및 발생과정에 미치는 영향을 분석하기 위한 동물시험이다.

프로그램	홈페이지	모델설명	생식독성 임상종점과 원천 데이터
DEPEK	Lhasa Ltd. http://www.lhasalimited.org	구조적 정보에 따라 예측하는 지식기반 시스템	약물의 초기성과 약물의 초기종점에서 21개 구조적인 정보, 에스트로제닉 활성모델에서 4개의 구조정보, FDA/TERIS로부터 생식발생독성 여부 검색
TOPKAT	Accelrys Inc. http://www.accelrys.com/products/topkat	치환기와 전자 구조 인덱스를 포함하는 많은 독성 데이터 베이스로 부터 개발한 QSAR 모델	
MC4PC	MultiCASE Inc. http://www.multicase.com	작용기를 이용하는 많은 DB로부터 유도된 QSAR 모델	- FDA 약물의 초기성 내에 존재하는 발생독성 유해도 (토끼 1286개 화합물, 래빗 812개 화합물, 마우스 794개 화합물, 포유동물 1409개 화합물) - FDA/TERIS 발생독성 (사람 323개 화합물) - 발생광독 화합물 (마우스 101개 화합물, 토끼 134개 화합물, 래빗 66개 화합물, 사람 119개 화합물, 햄스터 192개 화합물)
PASS	Insitute of Biomedical Chemitsry of the Russian Academy of Medicinal Sicences, Moscow. http://ibmc.p450.ru/PASS	생식발생 독성값이 알려진 화합물로부터 시험물질 간의 구조유사성 계산	생식독성의 30개 이상 임상 종점 예측
HazardExpertPro	CompuDrug Inc. http://www.compudrug.com	분자의 fragment들로부터 약물의 초기성 예측	US EPA에 보고된 유해독성 화합물과 *in vivo* 실험으로 부터 얻어진 독성 분자구조
OSIRIS property explorer	Organic Chemistry Portal http://www.organic-chemistry.org/prog/tox.html	분자의 fragment들로부터 생식발생독성예측	RTECS에 있는 생식독성을 가진 3,370개 화합물의 분석 으로부터 유해분자의 fragments 분류
OECD (Q)SAR Application Toolbox	OECD, Paris http://www.oecd.org/document/23/0,3343,en_2649_34379_33957015_1_1_1_1,00. html	QSAR 모델과 분석경향 제공	
<in silico 생식독성 임상종점 예측 시스템>			

- 면역독성시험 예측모델: EPA에 보고된 유해화합물과 *in vivo* 실험으로부터 얻어진 유해 작용기 정보를 toxicophore로 정의한 지식기반 HazardExpert 프로그램을 이용하여 예측.

(2) In silico 가상 질환모델

최근들어 새롭게 대두되고 있는 시스템 생물학은 생물 시스템의 복잡한 상호작용에 대한 시스템적인 연구를 중심으로 하는 새로운 생물학 분야이며, 생물 시스템의 복잡한 상호작용 결과로 나타나는 신약 후보물질의 약효, 효능, 독성 연구가 활발히 수행되고 있으며, 특히 시스템 생물학을 이용하여 특정 질환모델을 개발하고 이를 신약 후보물질의 평가에 적용함으로 동물실험을 대체할 수 있을 것으로 기대된다. 2007년 Entelos 사는 미국 FDA의 'Critical Path Initiative' 일환으로 간독성 관련 컴퓨터 모델을 개발하고 있으며, 간독성 유발의 기전을 구명하여 효과적으로 간독성 유발여부를 미리 알 수 있는 생체지표를 찾아 결과적으로 신약개발 비용을 절감하고 개발 기간을 단축하고자 한다.

기관/회사	핵심기술	in silico 시험	연구영역
Entelos사 http://www.entelos.com/	미분방정식을 기반으로 다세포/ 조직/장기 네트워크 기능모델	질환이해와 치료를 위한 생물화학적 데이터, 세포, 조직, 장기와 생리기능을 설명하는 역학적 모델	지방세포, 천식, 당뇨병, 비만, 류마티스 관절염 타겟발굴과 타겟선정 후보물질 발굴· 최적화 생물지표 발굴 임상시험디자인·최적화
Iconix	초고속 스크리닝 분자생물학 데이터 마이닝, 인포매틱스	신약후보물질의 부작용과 독성을 예측하기 위하여 화학 유전체 통합	독성예측
Ingenuity	형질변이 경로 데이터베이스	형질변이 데이터로부터 증가된 경로를 정의하기 위하여 대용량 경로, 데이터베이스 계산	타겟발굴
Surromed	초고속 효능검색 분자생물학 데이터 마이닝, 인포매틱스	생물지표를 발굴하기 위하여 작은 유기분자, 단백질, 면역세포모집단 탐색	생물지표 디자인 임상시험 디자인

<시스템 생물학 관련 주요 프로그램 및 특징>

당뇨병 모델: Entelos사의 가상 NOD-마우스 모델은 제1형 당뇨병 발병기전과 치료제에 대한 환자의 반응예측, 다양한 당뇨병 진행과정과 불확실성을 탐색하기 위한 모집단을 만들어 질환에서 가장 중요하게 작용하는 새로운 타겟 발굴. 또한 제2형 당뇨병에 대해서는 개체부터 유전자를 연구대상으로 하는 'Top-down' 방법의 미분방정식을 기반으로 다세포/조직/장기 네트워크 기능모델인 PhysioLab의 가상환자를 이용함. 새로운 당뇨병 치료제의 저혈당 유발 용량을 분석하기 위해 가상환자를 대상으로 임상시험을 수행함.

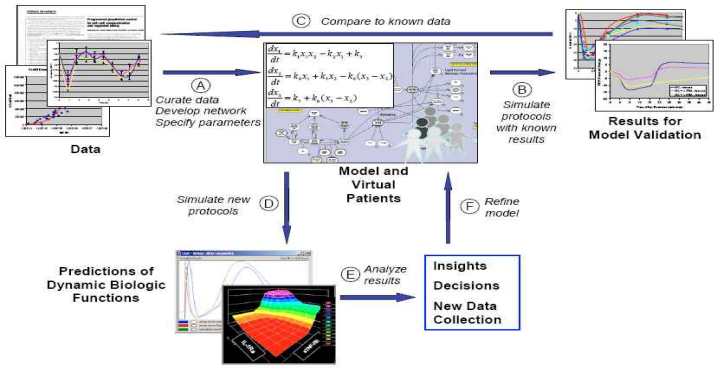

<Entrols사에서 개발한 PhysioLab 시스템 구성>

천식질환 모델: 미국 내에서만 17,000,000명의 환자가 고통 받고 있으며 WHO 보고에 의하면 2020년에는 사망원인 중 3위를 차지할 것으로 예측됨. 천식질환에 대한 in silico 가상 모델은 리간드와 수용체간의 상호작용, 가상 세포, 가상 기도, 그리고 가상환자 모델을 이용하여 연구되고 있다.

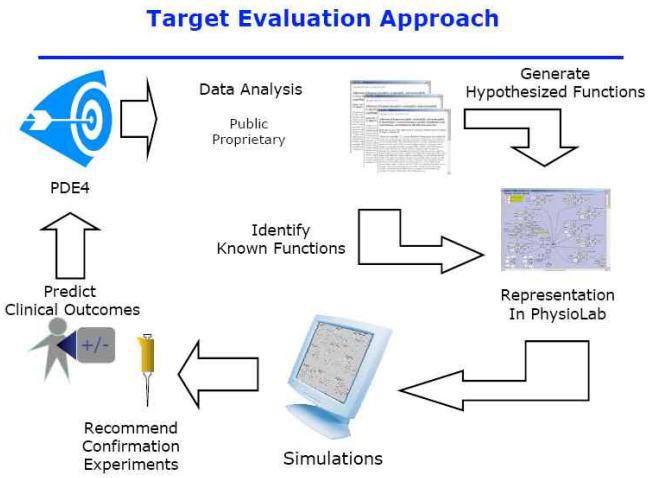

<Entelos사의 천식질환 연구과정>

임상실험 시뮬레이션을 이용한 타겟 선정: Entelos사는 기도구조와 기능, 염증과 염증반응의 수식적 모델과 50개 이상의 PDE4 분자간의 천식 관련 네트워크에 대한 정보 및 인체 내 후보 화합물의 용량에 따른 효과를 예측함으로써 가상 천식환자 임상모델을 개발하였다.

가상약물전달 시스템으로 혈관세포 접착분자 저해제 개발: 혈관세포 접착분자 (vascular cell adhesion molecule 1, VCAM-1)의 인테그린(integrin) 활성부위에 결합하는 α4β1 저해제 4-[N′-(2-methylphenyl)-ureido] phenylacetyl-Leu -ASp-Val)의 알려진 구조정보와 3D pharmacophore model을 이용하여 생리활성 가상검색 결과 IC50 < 1nM인 저해제 후보물질 제안한다.

PDE4를 타겟으로 하는 천식치료제 후보물질 개발: 한국화학연구원과 크리스탈지노믹스(주)는 Phosphodiesterase4(PDE4)와 리간드의 복합체 구조를 기반으로 새로운 화합물을 설계하였고, 의약화학적 구조개선 및 물리화학적 특성규명(용해도, logP 등), 생체 내 효능시험, 약동력학시험, 구토관련 부작용시험 등을 수행하여 부작용이 거의 없으며 안정성이 향상된 후보화합물 PDE4-0423을 개발하였다.

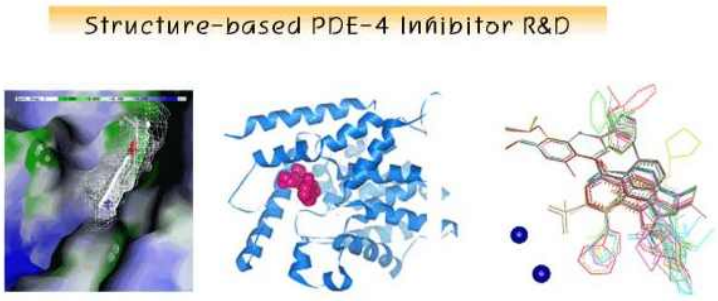

<3D-모델링을 이용한 천식치료제 후보물질설계>

(3) 결론

<신약개발에 필요한 in silico ADME/Tox 예측 모델 및 구축 현황>

ADME/Tox	예측범위	세부범위	예측모델		완성도
Absorption	물리화학적상수	용해도	- 다양한 예측모델 존재 - 예측 정확도 향상이 요구됨		중
		logP	- 다양한 예측모델 존재 - 예측 정확도 높음		상
		logD	- 다양한 예측모델 존재 - 예측 정확도 향상이 요구됨		중
		pKa	- 다양한 예측모델 존재 - 예측 정확도 향상이 요구됨		중
	Permeability	Caco-2 cell	- 관련 실험데이터 부족 - 예측 정확도 향상이 요구됨		하
		MDCK cell	- 관련 실험데이터 부족 - 예측 정확도 향상이 요구됨		하
		인체장흡수	- 관련 실험데이터 부족 - 예측 정확도 향상이 요구됨		하
		BBB	- 관련 실험데이터 부족 - 예측 정확도 향상이 요구됨		하
Distribution	Plasma Protein Binding		- 정량화된 실험데이터 미비로 예측모델 구현이 어려움		하
Metabolism	Phase I reaction	CYP2C, 2D6, 3A4 등	substrate	- 예측 정확도 향상이 요구됨	하
			inhibitor		하
			inducer	- 관련 실험데이터 미비	초기
	Phase II reaction	GST, SULT, UGT 등	substrate	- 모델 미확립	초기
			inhibitor	- 모델 미확립	초기
			inducer	- 모델 미확립	초기
Toxicity	Ames		- 관련 실험데이터 부족 - 예측 정확도 향상이 요구됨		중
	Carcinogenicity		- 관련 실험데이터 부족 - 예측 정확도 향상이 요구됨		중
	HERG inhibition		- 2D/3D QSAR 모델 존재 - 예측 정확도 향상이 요구됨		중
	P-gp		- 관련 실험데이터 부족		하

약물의 흡수와 관련성이 높은 물리화학적상수 logP, logD 및 독성 예측 모델은 정확도가 높은 편이다. 아직까지 예측모델이 개발되지 않았거나 예측 정확도 향상이 요구되는 모델의 경우, in silico 예측모델 개발에 필요한 관련 데이터를 산출하기 위해서 다양한 실험 연구가 뒷받침되어야 한다. 기존에 개발되어 있는 예측 모델을 실제 신약개발에 활용하기 위해, 독성 예측 모델과 cytochrome P450 약물대사 예측 모델의 정확도 개선이 요구된다.

제 2 절 GEM 개발 국제 동향

선진국에서는 후기유전체 프로젝트로 GEM의 중요성을 인식하여 GEM 생산 기반 및 분석을 표준화, 고속화하기 위한 국제적 컨소시움의 형태로 국가집중지원 기구를 설립하였다. GEM 제작 및 연구에는 많은 비용과 시간이 들기 때문에 전 세계적인 자원공유 등의 공조체계 구축이 필수적이다.

국제적 컨소시움에는 제작 목적의 국제GEM컨소시움 (IKMC), 보존분야의 국제마우스자원연합(FIMRe), 아시아 유전자 변형 마우스자원 연합(AMMRA), 표현형분석 분야 국제GEM표현형분석 컨소시엄(IMPC), 정보관리 분야 마우스유전자 DB(MGD), 마우스표현형 DB(MPD), 마우스표현형 데이터 컨소시움 DB(MPDIC)이 있다.

구분	GEM 제작	GEM 보존	GEM 표현형분석	GEM 정보
글로벌	- 국제GEM컨소시움(IKMC)	- 국제마우스자원연합(FIMRe) - 아시아 유전자 변형 마우스 자원 연합(AMMRA)	- 국제 GEM 표현형 분석 컨소시움(IMPC)	- 마우스 유전자DB(MGD) - 마우스 표현형DB(MPD) - 마우스 표현형 데이터컨소시움(MPDIC)
미국	- 미국GEM프로젝트(KOMP)	- 암 모델 마우스 컨소시움(MMHCC) - 지역별마우스거점센터(MMRRC)	- 암 모델 마우스 컨소시움(MMHCC) - 마우스 대사질환 연구센터(MMPC)	- 종양모델마우스(MTB)
캐나다	- 캐나다GEM프로젝트(NorCOMM) - 인간질환모델링 센터(CMHD)	- 캐나다GEM뱅크(CMMR)	- 인간질환모델링센터(CMHD)	
유럽	- 유럽GEM프로젝트(EuCOMM)	- 유럽마우스모델뱅크(EMMA)	- 유럽마우스질환연구소(EUMODIC) - 유럽 마우스 표현형연구연합센터(EUMORPHIA)	- 유럽마우스표현형DB(EuroPhenome) - 마우스정보해석센터(CASIMIR)
일본	BRC(RIKEN)	BRC(RIKEN)	BRC(RIKEN)	BRC(RIKEN)
중국	ChCOMM	ChCOMM	ChCOMM	현재 추진 중
한국	부재	KGEMC(KRIBB)	KGEMC(KRIBB)	KGEMC(KRIBB)

<글로벌 GEM 컨소시엄>

1. IKMC (International Knock-out Mouse Consortium)

가. IKMC 설립목적 및 목표

(1) 세계 주요국은 2008년 GEM 컨소시엄을 구성하여 국제공동프로젝트를 진행하여 연구 성과를 공유하고 GEM을 통한 유전자 기능해석 및 특허확보 경쟁을 가속화 하고 있다. IKMC는 기존 KOMP, NorCOMM, EUCOMM의 연합으로 2004년부터 2010년까지 생산된 GEM제작 정보를 공유하는 1세대 글로벌 GEM 컨소시움이며, IKMC는 미국, 캐나다, 유럽 중심의 컨소시움으로 GEM 대량생산과 기본 분석 플랫폼 표준화를 목표로 2008년 설립되었다.

(2) IKMC 조직

① KOMP : Knockout Mouse Project

② NorCOMM : North American Conditional Mouse Mutagenesis project

③ EuCOMM : European Conditional Mouse Mutagenesis project

④ TIGM : Texas A&M Institute for Genomic Medicine

미국 중심의 KOMP와 TIGM 캐나다 중심의 NorCOMM, 유럽중심의 EUCOMM의 연합 컨소시엄으로 GEM 생산 및 표현형 분석연구의 선도적 역할을 수행중이다.

Total Genes	KOMP		EUCOMM	NorCOMM	TIGM
	CSD	Regenerron			
Project goal	5,000	3,500	8,000	500	-
Vectors generated	6,415	4,951	6,258	797	-
Vectors available	5,871	3,326	6,258	797	-
ES cells generated	4,072	2,807	4,765	397	-
ES cells available	3,768	1,757	4,765	397	10,689
Mutant mice generated	259	283	489	3	43
Mutant mice available	259	179	489	3	43

<IKMC의 Gene Progress 구축현황>

(3) 주요활동

IKMC는 GEM제작 공유 및 각 가입 기관별 관리 유통을 수행하고 있으며 24,645개의 ES cell lines중 15,586개의 단백질을 코딩한다.

나. 국제마우스자원연합 (FIMRe)

(1) FIMRe 가입 기관

① 북아메리카: The Jackson Laboratory, 3개의 Mouse Mutant Resource Regional Center (MMRRC), Mouse Models of Human Cancer Consortium (MMHCC), Canadian Mouse Consortium (CMC), Canadian Mouse Mutant Repository (CMMR)

② 유럽: European Mouse Mutant Archive (EMMA) (이탈리아, 프랑스, 영국 2곳, 스웨덴, 포르투갈, 독일 등 7곳)

③ 일본: RIKEN BioResource Center, Center for Animal Resources and Development (CARD)

④ 호주: Australian Phenomics Facility (APF)

(2) FIMRe의 설립목적

① 마우스 수탁 및 자원기관의 협력 활동: 가치 있는 유전적으로 동정된 마우스와 배아줄기세포의 저장 및 보존, 유전적으로 동정된 마우스와 배아줄기세포에 대한 연구용 요구 충족한다.

② 모든 국제 마우스자원기관에 있는 마우스에 대한 일정한 수준의 고품질의 건강한 상태 표준화 구축한다.

③ 유전학적 보증 및 유전배경 및 변이에 대한 quality control 제공한다.

④ 동결보존자원을 이용할 수 있도록 이용자의 능력을 향상시키기 위한 자원훈련 제공.

다. 아시아 유전자 변형 마우스자원 연합 (AMMRA)

(1) AMMRA 가입 기관

① 한국: 한국생명공학연구원(KRIBB)

② 일본: RIKEN BioResource Center, Center for Animal Resources and Development, 구마모토대학

③ 중국: National Resource Center for Mutant Mice, Shanghai Institute of Biological Sciences, Nanjing Center for Model Organisms, Beijing Institute. Laboratory Animal Science(BLARC)

④ 싱가포르: Biological Resource Center

⑤ 타이완: National Laboratory Animal Center

(2) AMMRA 설립목적

① 아시아 지역에서의 유전자변형마우스의 개발을 촉진하고 생산된 마우스 자원에 대한 접근을 용이하게 한다.

② 유전체기능을 분석하기 위한 마우스모델의 사용을 촉진하고 최종적으로는 인간의 건강을 향상시키는 것을 목적으로 두고 있다.

라. IMPC (International Mouse Phenotyping Consortium)

(1) IMPC 설립목적 및 목표

① IMPC는 GEM제작 결과 생산된 GEM의 특성을 분석하여 인간 유전자의 기능을 연구하기 위해 설립된 마우스 표현형분석을 공유 국제 컨소시엄으로 Phase Ⅰ('11~'16년)과 PhaseⅡ('16~'21년)의 각각 5년의 기간 동안 1단계 4,000라인과 2단계 12,750마우스 라인에 대하여 표현형분석 실시예정이다.

② GEM의 phenotype 정보를 제공하고 궁극적으로 포유류의 유전자 기능을 확인할 수 있는 시스템을 확립하는 목표를 가지며, Primary phenotyping과 mouse production에 대한 세계적 컨소시움을 형성 최종적으로 20,000 mutant mouse line에 대한 테스트를 한다. 또한 phenotyping에 대한 각 연구기관 전문가 등의 네트워크를 공고화 하여 인간의 질병 연구

에 있어서 마우스 모델을 이용 가능하게 확립한다. 데이터를 중앙에 집중화 하고 구축된 자료는 제한 없이 이용이 가능하도록 무료개방 한다.

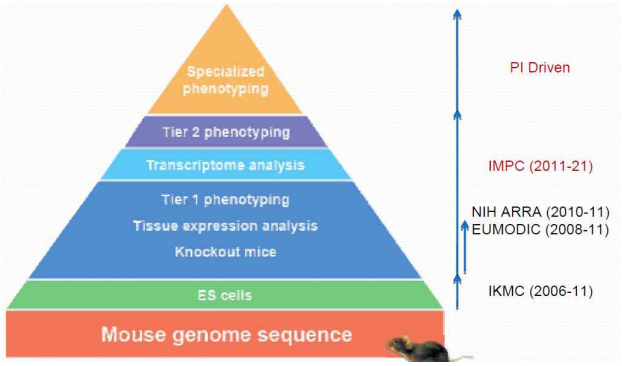

<IMPC의 비전>

(2) IMPC 조직

2단계 글로벌 컨소시움이 IMPC는 각 분야별 수집된 표현형을 중앙 데이터 센터를 통해 데이터 질과 표준화 및 분석을 수행한다.

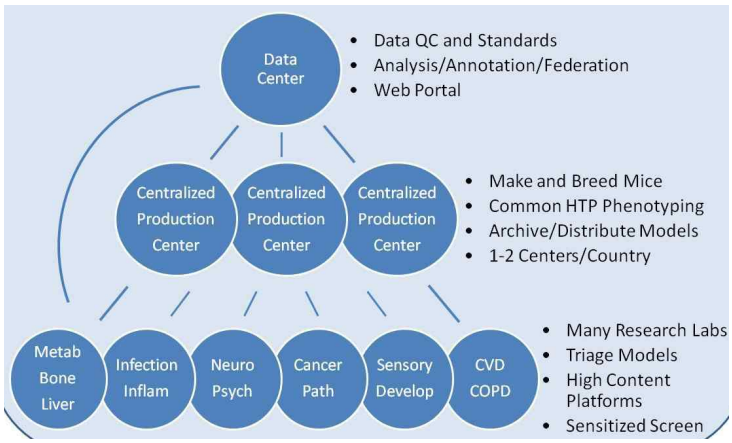

<IMPC의 조직 체계도>

(3) 주요활동

IMPC는 궁극적으로 유전자 기능을 확인하는데 초점을 두고 2단계(Phase)로 사업을 구성하고, 데이터 이용 시 무료이용, 제한 없는 이용을 추진하고 있으며 사업을 통해 얻게 되는 지적재산권에 대한 정의는 현재 명확히 정리되어 있지는 않는다. Phase 1 (2011~2016): EUMODIC 과 같은 존재하는 프로그램을 완수를 목표로 데이터를 중앙 집중화 하고 생산을 표준화 하며, 4,000개의 타겟 유전자의 표현형을 분석한다.

마. KOMP (Knock-Out Mouse Project)

(1) KOMP 설립목적 및 목표

① 미국국립보건원 주도의 Knockout-mouse 프로젝트는 IKMC의 일원으로 Conditional 제

작 및 null KO 마우스 생산을 위해 형성된 국가주도 GEM 프로젝트이다.

② 국립보건원 19개 기관(Office of AIDS Research 포함)에서 주도하고 있으며, 유전자가 결손된 마우스의 배아줄기세포(ES cell, Embryonic Stem cell)를 일반 연구자에게 공급하여 연구 및 연구 지원함을 목적으로 한다.

③ 8,500개의 유전자가 적중 파괴된 ES cell 생산, 궁극적으로 마우스 전체 유전자에 대한 Knockout ES cell 및 마우스의 생산 등을 목표를 가진다.

④ KOMP (knockout mouse project)는 1단계는 2011년 종료를 앞두고 프로젝트를 통해 수집된 자원을 바탕으로 한 KOMP2 (Knockout Mouse Phenotyping 2) 프로젝트가 2011년 시작. KOMP2는 유전적으로 비슷하거나 유사성을 가진 근친 종 탐색, monoclonal 항체개발, 유전자 결손 또는 비활성화된 KO 동물 개발, 신규 유전자를 위한 형질전환 동물모델 개발 등을 목표로 한다.

(2) KOMP 조직

KOMP는 NIH 19개 기관의 지원 지도 아래 GEM 생산과 데이터 조정, 저장, 연구, 지원, 평가 등으로 세분화된 구성 체계를 갖추어 마우스 제작에서부터 수집관리 분양까지 전주기적 과정을 수행하고 있으며, 생산은 산학협력의 Children's Hospital Oakland Research Institute (CHORI), Welcome Trust Sanger Institute, Univ. of California at Davis와 글로벌제약사인 Regeneron Pharmaceuticals, Inc. 2개의 그룹으로 구성된다. KOMP는 KOMP 데이터조정센터(KOMP DCC, KOMP Data Coordination Center)인 Jackson Laboratory를 중심으로 유전자의 수집, 보존, 표준화작업을 수행하고 있다. 데이터의 저장은 캘리포니아 소재 CHORI (Children's Hospital Oakland Research Institute)와 캘리포니아 대학(California at Davis) 두 기관에서 담당하고 있으며, 연구그룹으로 펜실베니아대학, 마운트 사이나이 병원(Mount Sinai Hospital)의 Samuel Lunenfeld 연구소가 있으며, 연구그룹에서는 C57BL/6 ES cell line를 통해 생산 및 효율성 증대를 위한 방법을 연구한다. KOMP의 모든 과정은 패널별로 전문 컨설턴트를 통해(KOMP research network) 각 구성원의 진도를 평가하고 있다.

(3) 주요활동

주요 활동분야로는 C57BL/6 마우스를 중심으로 reporter 유전자를 이용한 null allele의 생산, 상용화되지 못한 knockout mouse의 생산 및 공급, High throughput 생산을 위한 C57BL/6 ES cell의 공급 및 효율성 증대, Data coordination center 운용 등을 하고 있다.

바. EUCOMM (European Conditional Mouse Mutagenesis Program)

(1) 설립목적 및 목표

① EU FP5 보건의료 사업 분야의 일환으로 유럽 질환모델 마우스 개발프로그램 EUCOMM 사업이 실행되었으며, 사업 결과로 제작된 GEM 자원은 IKMC를 통해 미국, 캐나다와 공유하고 있다. C57BL/6N ES cell에서 conditional gene trapping과 gene targeting 방법을 사용하여 20,000 개의 재조합된 유전자 리스트를 작성하기 위한 프로그램으로 이 데이터를 이용해 전 세계적으로 분포되어 있는 320종류의 유전자 재조합 마우스를 만들고 DB를 구축하였다.

② 마우스를 통한 인간 유전자 확인, 인체 모든 유전자의 GEM 제작, 제작한 GEM의 표현형 분석 기반 구축, GEM을 활용한 질환모델구축을 목적을 가진다.

③ 5,000 종의 변이유전자 gene trap ES cell 제작, 8,000 종의 targeted ES cell 제작, 320 종의 GEM 제작, 20 종의 Cre-TG 제작, Vector, ES cell 및 GEM의 보존과 분양을 목표로 하고 있다.

(2) EUCOMM 조직

EUCOMM은 마우스 유전자 기능해석을 위한 GEM 제작과 분석으로 인체 질환 원인의 분자적 수준의 통합적 이해를 위한 인프라성 마우스 종합 프로그램이며, 영국, 프랑스, 독일 등 총 13개 나라가 참여하고 있다.

<EUCOMM 거점센터>

(3) 주요활동

① 2008년 기준 EUCOMM에서는 약 198개의 ES cell과 650개의 EUMODIC 프로그램을 운영한바 있다.

② Gene Trapping에는 Universitat의 벡터를 이용하고 있으며, Gene Targeting 방법은 웰컴트러스트생거 연구소(Wellcome trust Sanger institute)의 벡터를 이용하여 GEM을 제작한다.

또한, Gene Trapping: Unicarsitat을 통해 생산된 벡터는 Helmholts institute Munich를 통해 clone picking과 cell culture 후 charite를 통한 splinkerette PCR, 웰컴트러스트생거 연구소의 시퀀싱을 거쳐 Helmholtz Munich 연구소의 제작의 단계로 진행되며, Gene Targeting: 웰컴트러스트생거 연구소의 벡터생산, 생거 연구소 및 Helmholtz Munich 연구소의 ES 세포주 생산을 통해 웰컴트러스트생거, MRC Harwell, ICS Straßburg, CNR Monterotondo, Helmholtz Munich의 GEM 제작단계로 진행된다.

제 7 장 연구시설·장비 현황

해당사항 없음

제 8 장 참고문헌

1. Adachi T et al. (2002) Twenty-six week carcinogenicity study of ampicillin in CB6F1-Tg rasH2 mice. J Toxicol Sci. 27(3):147-63.
2. Alden C et al. (2002) Application of genetically altered models as replacement for the lifetime mouse bioassay in pharmaceutical development. Toxicol Pathol. 30(1):135-8.
3. Ashby J et al. (2001)Expectations for transgenic rodent cancer bioassay models. Toxicol Pathol. 29 Suppl:177-82.
4. Battershill JM and Fielder RJ et al. (1998) Mouse-specific carcinogens: an assessment of hazard and significance for validation of short-term carcinogenicity bioassays in transgenic mice. Hum Exp Toxicol. 17(4):193-205. Review.
5. Brian P. Zambrowicz & Arthur T. Sands. Knockouts model the 100 best-selling drugs－will they model the next 100?. 2003. Nat Rev Drug Discov 2 (1): 38 - 51
6. Blain PG et al. (2003) Committee on Carcinogenicity of Chemicals in Food, Consumer Products and theEnvironment. Statement on ILSI/HESI research programme on alternative cancer models. Toxicol Pathol. 31(2):254-7.
7. Box RJ and Spielmann H et al. (2005) Use of the dog as non-rodent test species in the safety testing schedule associated with the registration of crop and plant protection products (pesticides): present status. Arch Toxicol. 79(11):615-26.
8. Christopher C Wendler. Identification of the heart as the critical site of adenosine mediated embryo protection. 1997. J Clin Invest 100:169-79
9. Chanda S et al. (2007) 26-Week dermal oncogenicity study evaluating pure trans-capsaicin in Tg.AC hemizygous mice (FBV/N). Int J Toxicol. 26(2):123-33.
10. Cohen SM et al. (2001) Alternative models for carcinogenicity testing. Toxicol Sci. 64(1):14-9.
11. Cohen SM et al. (2001) Alternative models for carcinogenicity testing: weight of evidence evaluations across models. Toxicol Pathol. 29 Suppl:183-90.
12. Eastin WC et al. (2001) Tg.AC genetically altered mouse: assay working group overview of available data. 2001. Toxicol Pathol. 29 Suppl : 60-80.
13. Fuhrman Jet al. (2005) Mechanisms of SEPA 0009-inducedtumorigenesisinv-ras Ha transgenic Tg.AC mice. Toxicol Pathol. 33(6):623-30.
14. Gaylor DW et al. (2005) Are tumor incidence rates from chronic bioassays telling us what we need to know about carcinogens? Regul Toxicol Pharmacol. 41(2):128-33.
15. Goodman JI. A perspective on current and future uses of alternative models for carcinogenicity testing. 2001. Toxicol Pathol. 29 Suppl:173-6.
16. Holden HE, Stoll RE, Spalding JW and Tennant RW. Hemizygous Tg.AC transgenic mouse as a potential alternative to the two-year mouse carcinogenicity bioassay: evaluation of husbandry and housing factors. 1998. J Appl Toxicol. 18(1):19-24.
17. Jacobson-Kram D, Sistare FD and Jacobs AC. Use of transgenic mice in carcinogenicity hazard assessment. 2004. Toxicol Pathol. 32 Suppl 1:49-52.Review.
18. Johannsen FR and Levinskas GJ. Comparative chronic toxicity and carcinogenicity of acrylonitrile by drinking water and oral intubation to Spartan Sprague-Dawley rats. 2002. Toxicol Lett. 132(3):197-219.

19. JM Choi & S Devkota. EI24 regulates epithelial-to- mesenchymal transition & tumor progression by suppressing TRAF2-mediated NF-κB activity. 2014. Oncotarget 4(12):2383-96
20. J Roh. Perturbation of NCOA6 Leads to Dilated Cardiomyopathy. 2014. Cell Reports 8:991-998
21. JY Ahn. Proteomic analysis of domestic pig pancreas during development using two-dimensional electrophoresis and matrix-assisted laser desorption/ionization-time of flight mass spectrometry. 2014. Lab Anim Res 30(2):45-53
22. Kirkland D, Pfuhler S, Tweats D, Aardema M, Corvi R, Darroudi F, Elhajouji A, Glatt H, Hastwell P, Hayashi M, Kasper P, Kirchner S, Lynch A, Marzin D, Maurici D, Meunier JR, Müller L, Nohynek G, Parry J, Parry E, Thybaud V, Tice R, van Benthem J, Vanparys P and White P. How to reduce false positive results when undertaking in vitro genotoxicity testing and thus avoid unnecessary follow-up animal tests: Report of an ECVAM Workshop. 2007. Mutat Res. 628(1):31-55.
23. Koujitani T, Yasuhara K, Tamura T, Onodera H, Takagi H, Takizawa T, Hirose M, Hayashi Y and Mitsumori K. Lack of modifying effects of eugenol on development of lung proliferative lesions induced by urethane in transgenic mice carrying the human prototype c-Ha-ras gene. 2001. J Toxicol Sci. 26(3):129-39.
24. Lina BA, Woutersen RA, Bruijntjes JP, van Benthem J, van den Berg JA, Monbaliu J, Thoolen BJ, Beems RB and van Kreijl CF. Evaluation of the Xpa-deficient transgenic mouse model for short-term carcinogenicity testing: 9-month studies with haloperidol, reserpine, phenacetin, and D-mannitol. 2004. Toxicol Pathol. 32(2):192-201.
25. MacDonald J, French JE, Gerson RJ, Goodman J, Inoue T, Jacobs A, Kasper P, Keller D, Lavin A, Long G, McCullough B, Sistare FD, Storer R and van der Laan JW. The utility of genetically modified mouse assays for identifying human carcinogens: a basic understanding and path forward. The Alternatives to Carcinogenicity Testing Committee ILSI HESI. 2004. Toxicol Sci. 77(2):188-94.
26. Mauthe RJ, Gibson DP, Bunch RT and Custer L. The syrian hamster embryo (SHE) cell transformation assay: review of the methods and results. 2001. Toxicol Pathol. 29 Suppl:138-46.
27. McClain RM, Keller D, Casciano D, Fu P, MacDonald J, Popp J and Sagartz J. Neonatal mouse model: review of methods and results. 2001. Toxicol Pathol. 29 Suppl:128-37.
28. Mitsumori K, Koizumi H, Nomura T and Yamamoto S. Pathological features of spontaneous and induced tumors in transgenic mice carrying a human prototype c-Ha-ras gene used for six-month carcinogenicity studies. 1998. Toxicol Pathol. 26(4):520-31.
29. National Toxicology Program, Public Health Service, National Institutes of Health, US Departmentof Health and Human Services. NTP toxicology and carcinogenesis studies of triethanolamine (CasNo.102-71-6) in B6C3F1 mice (dermalstudies). 2004. Natl Toxicol Program Tech Rep Ser. 518:5-163.
30. National Toxicology Program, Public Health Services, National Institutes of Health, US Department of Health and Human Services. NTP technical report on the toxicology and carcinogenesis studies of Elmiron (CasNo.37319-17-8) in F344/N rats and B6C3F1 mice (GavageStudies). 2004. Natl Toxicol Program Tech Rep Ser. (512):7-289.
31. National Toxicology Program. Toxicology and carcinogenesis studies of indium phosphide (CAS No. 22398-90-7) in F344/N rats and B6C3F1 mice (inhalation studies). 2001. Natl Toxicol Program Tech Rep Ser. (499):7-340.

32. National Toxicology Program. Toxicology and carcinogenesis studies of p-nitrotoluene (CAS no. 99-99-0) in F344/N rats and B6C3F(1) mice (feed studies). 2002. Natl Toxicol Program Tech Rep Ser. (498):1-277.
33. Okamura M, Moto M, Muguruma M, Ito T, Jin M, Kashida Y and Mitsumori K. A 26-week carcinogenicity study of 2-amino-3-methylimidazo[4,5-f]quinoline in rasH2 mice. 2006. Toxicol Pathol. 34(2):199-205.
34. Omenn GS. Assessment of human cancer risk: challenges for alternative approaches. 2001. Toxicol Pathol. 29 Suppl:5-12.
35. Pettit SD. Panel discussion on the application of alternative models to cancer risk assessment. 2001. Toxicol Pathol. 29 Suppl:191-5.
36. Robinson DE and MacDonald JS. Background and framework for ILSI's collaborative evaluation program on alternative models for carcinogenicity assessment. 2001. Toxicol Pathol. 29 Suppl:13-9.
37. Sehata S, Maejima T, Watanabe M, Ogata S, Makino T, Tanaka K, Manab S and Takaoka M. Twenty-six-Week carcinogenicity study of chloroform in CB6F1 rasH2-transgenicmice. 2002. Toxicol Pathol. 30(3):328-38.
38. Spalding JW, Momma J, Elwell MR and Tennant RW. Chemically induced skin carcinogenesis in a transgenic mouse line (TG.AC) carrying a v-Ha-ras gene. 1993. Carcinogenesis. 14(7):1335-41.
39. Storer RD, French JE, Haseman J, Hajian G, LeGrand EK, Long GG, Mixson LA, Ochoa R, Sagartz JE and Soper KA. P53+/- hemizygous knockout mouse: overview of available data. 2001. Toxicol Pathol. 29 Suppl:30-50.
40. SS Yi. Proteomic analysis of liver in miniature pigs according to developmental stages using two-dimensional electrophoresis and matrix-assisted laser desorption/ionization-time of flight mass spectrometry. 2013. Lab Anim Res 29(3):162-7
41. SS Yi. Proteomic analysis of pancreas in miniature pigs according to developmental stages using two-dimensional electrophoresis and matrix-assisted laser desorption/ionization-time of flight mass spectrometry. 2014. Lab Anim Res 30(1):1-7
42. Tamaoki N. The rasH2 transgenic mouse: nature of the model and mechanistic studies on tumorigenesis. 2001. Toxicol Pathol. 29 Suppl:81-9.
43. Toyosawa K, Okimoto K, Kobayashi I, Kijima K, Kikawa E, Kohchi M, Koujitani T, Tanaka K and Matsuoka N. Di(2-ethylhexyl)phthalate induces hepatocellular adenoma in transgenic mice carrying a human prototype c-Ha-ras gene in a 26-week carcinogenicity study. 2001. Toxicol Pathol. 29(4):458-66.
44. Usui T, Mutai M, Hisada S, Takoaka M, Soper KA, McCullough B and Alden C. CB6F1-rasH2 mouse: overview of available data. 2001. Toxicol Pathol. 29 Suppl:90-108.
45. van der Laan JW and Spindler P. The in vivo rodent test systems for assessment of carcinogenic potential. 2002. Regul Toxicol Pharmacol. 35(1):122-5.
46. Van Kreijl CF, McAnulty PA, Beems RB, Vynckier A, van Steeg H, Fransson-Steen R, Alden CL, Forster R, van der Laan JW and Vandenberghe J. Xpa and Xpa/p53+/- knockout mice: overview of available data. 2001. Toxicol Pathol. 29 Suppl:117-27.
47. Van Steeg H, de Vries A, van Oostrom CTh, van Benthem J, Beems RB and van Kreijl CF. DNA repair-deficient Xpa and Xpa/p53+/- knock-out mice: nature of the models. 2001. Toxicol

Pathol. 29 Suppl:109-16.
48. Weaver JL, Contrera JF, Rosenzweig BA, Thompson KL, Faustino PJ, Strong JM, Ellison CD, Anderson LW, Prasanna HR, Long-Bradley PE, Lin KK, Zhang J and Sistare FD. An evaluation of the hemizygous transgenic Tg.AC mouse for carcinogenicity testing of pharmaceuticals. I. Evidence for a confounding nonresponder phenotype. 1998. Toxicol Pathol. 26(4):532-40.
49. Wyde ME, Braen AP, Hejtmancik M, Johnson JD, Toft JD, Blake JC, Cooper SD, Mahler J, Vallant M, Bucher JR and Walker NJ. Oral and dermal exposure to 2,3,7,8-tetrachlorodibenzo-p-dioxin (TCDD) induces cutaneous papillomas and squamous cell carcinomas in female hemizygous Tg.AC transgenic mice. 2004. Toxicol Sci. 82(1):34-45.
50. Y Kim & JS Goo. Identification of the responsible proteins for increasedselenium bioavailability in the brain of transgenic rats overexpressing selenoprotein M. 2014. Int J Mol Med 34:1688-1698
51. Yamamoto S, Mitsumori K, Kodama Y, Matsunuma N, Manabe S, Okamiya H, Suzuki H, Fukuda T, Sakamaki Y, Sunaga M, Nomura G, Hioki K, Wakana S, Nomura T and Hayashi Y. Rapid induction of more malignant tumors by various genotoxic carcinogens in transgenic mice harboring a human prototype c-Ha-ras gene than in control non-transgenic mice. 1996. Carcinogenesis. 17(11):2455-61.
52. Zhu H, Wang Y, Chen J, Cheng G, Xue J. Transgenic mice expressing hepatitis B virus X protein are more susceptible to carcinogen induced hepatocarcinogenesis. Exp Mol Pathol, 2004 Feb;76(1):44-50.
53. Zhu. Coactivator PRIP, the Peroxisome Proliferator-activated Receptor-interacting Protein, Is a Modulator of Placental, Cardiac, Hepatic, and Embryonic Development. 2003. JBC 278:1986-1990
54. 국가마우스표현형 분석사업 (KMPC), 과제 계획서(2013), 미래창조과학부
55. 맞춤형 미래선도 모델동물자원 활용 구축 연구, 1차 연차실적계획서(2014), 식품의약품안전처
56. 이화여대, GEM 기반구축사업의 필요성 검토 및 사전기획연구 (2009)
57. KGEMC, 유전자변형마우스(GEM) 기반구축사업 연구개발계획서 (2010)
58. IKMC 홈페이지, http://www.knockoutmouse.org
59. IMPC 홈페이지, http://www.mousephenotype.org
60. 60.Adams, JM, Cory S, 1998. The Bcl-2 proteinfamily: arbiters of cell survival. Science (NewYork, NY)281, 1322 - 1326.
61. Albreht, A., Vovk, I., Simonovska, B., Srbinoska, M., 2009. Identification of shikonin and its ester derivatives from the roots of *Echium italicum* L. Journal of Chromatography A 1216, 3156 - 3162.
62. Antonsson, B., 2001. Bax and other pro-apoptotic Bcl-2 family "killer-proteins" and their victim the mitochondrion. Cell and Tissue Research 306, 347 - 361.
63. Baxter PS, Martel MA, McMahon A, Kind PC, Hardingham GE. 2011. Pituitary adenylate cyclase-activating peptide induces long-lasting neuroprotection through the in-duction of activity-dependent signaling via the cyclic AMP response element-binding protein-regulated transcription co-activator 1. J Neurochem 118, 365 - 378.
64. Blum D, Torch S, Lambeng N, Nissou M, Benabid AL, Sadoul R, et al. 2001. Molecular pathways involved in the neurotoxicity of 6-OHDA, dopamine and MPTP: contribution to the apoptotic theory in Parkinson's disease. Prog Neurobiol 65, 135 - 72.
65. Bove J, Perier C. 2012. Neurotoxin-based models of Parkinson's disease. Neuroscience 211,

51 - 76.
66. Brandenburg LO, Kipp M, Lucius R, Pufe T, Wruck CJ. 2010. Sulforaphane suppresses LPS-induced inflammation in primary rat microglia Inflammation research : official journal of the European Histamine Research Society ...[et al.]. 59, 443-450.
67. Chen PC, Vargas MR, Pani AK, Smeyne RJ, Johnson DA, Kan YW, et al. 2009. Nrf2-mediated neuroprotection in the MPTP mouse model of Parkinson's disease: critical role for the astrocyte. Proc Natl Acad Sci U S A 106, 2933 - 8.
68. Chen DF, Zhang SX, Xie L, Xie JX, Chen K, Kashiwada Y, Zhou BN, Wang P, Cosentino LM, Lee KH. 1997. Anti-AIDS agents-XXVI. Structure-activity correlations of gomisin-G-related anti-HIV lignans from *Kadsura interior* and of related synthetic analogues Bioorganic & medicinal chemistry. 5, 1715-1723.
69. Chen X, Yang L, Zhang N, Turpin JA, Buckheit RW, Osterling C, Oppenheim JJ, Howard O M. 2003. Shikonin, a component of Chinese herbal medicine, inhibits chemokine receptor function and suppresses human immuno deficiency virus type 1. Antimicrobial Agents and Chemotherapy 47, 2810 - 2816.
70. Cheng JC, Esparza S, Sandoval S, Shankar D, Fu C, Sakamoto KM. 2007. Potential role of CREB as a prognostic marker in acute myeloid leukemia. Future Oncol 3, 475 - 80.
71. Choi YW, Takamatsu S, Khan SI, Srinivas PV, Ferreira D, Zhao J, et al. 2006. Schisandrene, a dibenzocyclooctadiene lignan from *Schisandra chinensis*: structure-antioxidant activity relationships of dibenzocyclooctadiene lignans. J Nat Prod 69, 356 - 359.
72. Chung HS, Kang M, Cho C, Park S, Kim H, Yoon YS, Kang J, Shin MK, Hong MC, Bae H. 2005. Inhibition of lipopolysaccharide and interferon-gamma-induced expression of inducible nitric oxide synthase and tumor necrosis factor-alpha by Lithospermi radix in mouse peritoneal macrophages. Journal of Ethnopharmacology 102, 412 - 417.
73. Cohen GM. 1997. Caspase:the executioners of apoptosis. The Biochemical Journal 326, 1 - 16.
74. Dai JN, Zong Y, Zhong LM, Li YM, Zhang W, Bian LG, Ai QL, Liu YD, Sun J, Lu D. 2011. Gastrodin inhibits expression of inducible NO synthase, cyclooxygenase-2 and proinflammatory cytokines in cultured LPS-stimulated microglia via MAPK pathways PloS one. 6, e21891.
75. D'Aversa TG, Eugenin EA, Berman JW, 2008. CD40-CD40 ligand interactions in human microglia induce CXCL8 (interleukin-8) secretion by a mechanism dependent on activation of ERK1/2 and nuclear translocation of nuclear factor-kappa B (NFkappaB) and activator protein-1 (AP-1) Journal of neuroscience research. 86, 630-639.
76. Dehmer T, Heneka MT, Sastre M, Dichgans J, Schulz JB. 2004. Protection by pioglitazone in the MPTP model of Parkinson's disease correlates with I kappa B alpha induction and block of NF kappa B and iNOS activation Journal of neurochemistry. 88, 494-501.
77. Drukala J, Rajwa B, Pietrzkowski Z, Korohoda W. 2003. Comparison of daunomycin influence upon human keratinocytes and melanoma HTB140 cells. Image cytometry study. Anticancer Research 23, 419 - 423.
78. Eikelenboom P, Veerhuis R, Familian A, Hoozemans JJ, van Gool WA, Rozemuller AJ, 2008. Neuroinflammation in plaque and vascular beta-amyloid disorders: clinical and therapeutic implications Neuro-degenerative diseases. 5, 190-193.
79. Floden AM, Combs CK. 2011. Microglia demonstrate age-dependent interaction with amyloid-beta fibrils Journal of Alzheimer's disease : JAD. 25, 279-293.

80. Gao D, Hiromura M, Yasui H, Sakurai H. 2002. Direct reaction between shikonin and thiols induces apoptosis in HL60 cells. Biological and Pharmaceutical Bulletin 25, 827 – 832.
81. Giulian D, Baker TJ. 1986. Characterization of ameboid microglia isolated from developing mammalian brain The Journal of neuroscience : the official journal of the Society for Neuroscience. 6, 2163-2178.
82. Glinka Y, Gassen M, Youdim MB. 1997. Mechanism of 6-hydroxydopamine neurotoxicity. J Neural Transm Suppl 50, 55 – 66.
83. Glinka Y, Tipton KF, Youdim MB. 1996. Nature of inhibition of mitochondrial respiratory complex I by 6-hydroxydopamine. J Neurochem 66, 2004 – 10.
84. Gomez-Lazaro M, Galindo MF, Concannon CG, Segura MF, Fernandez-Gomez FJ, Llecha N, et al. 2008. 6-Hydroxydopamine activates the mitochondrial apoptosis pathway through p38 MAPK-mediated, p53-independent activation of Bax and PUMA. J Neurochem 104, 1599 – 612.
85. Gorman AM, Orrenius S, Ceccatelli S. 1998. Apoptosis in neuronal cells: role of caspases. Neuroreport 9, R49 – 55.
86. Gross A, McDonnell JM, Korsmeyer SJ, 1999. Bcl-2 family members and the mitochondria in apoptosis. Genes and Development 13, 1899 – 1911.
87. Guo LY, Hung TM, Bae KH, Shin EM, Zhou HY, Hong YN, et al. 2008. Anti-inflammatory effects of schisandrin isolated from the fruit of *Schisandra chinensis* Baill. Eur J Pharmacol 591, 293 – 9.
88. Hashimoto S, Xu M, Masuda Y, Aiuchi T, Nakajo S, Cao J, Miyakoshi M, Ida Y, Nakaya K. 1999. β-Hydroxyisovalerylshikonin inhibits the cell growth of various cancer cell lines and induces apoptosis in leukemia HL-60 cells through a mechanism different from those of Fas and etoposide. Journal of Biochemistry 125, 17 – 23.
89. Hoang MT, Eichenfield LF. 2000.The rising incidence of melanoma in children and adolescents. Dermatology Nursing 121, 192 – 193.
90. Hong SJ, Dawson TM, Dawson VL. 2004. Nuclear and mitochondrial conversations in cell death: PARP-1 and AIF signaling. Trends Pharmacol Sci 25, 259 – 64.
91. Hsu PC, Huang YT, Tsai ML, Wang YJ, Lin JK, Pan M.H. 2004. Induction of apoptosis by shikonin through coordinative modulation of the Bcl-2 family, p27, and p53, release of cytochrome C, and sequential activation of caspases in human colorectal carcinoma cells. Journal of Agricultural and Food Chemistry 52, 6330 – 6337.
92. Im JY, Kim D, Lee KW, Kim JB, Lee JK, Kim DS, Lee YI, Ha KS, Joe CO, Han PL. 2004. COX-2 Regulates the insulin-like growth factor I-induced potentiation of Zn(2+)-toxicity in primary cortical culture Molecular pharmacology. 66, 368-376.
93. Innamorato NG, Rojo AI, Garcia-Yague AJ, Yamamoto M, de Ceballos ML, Cuadrado A. 2008. The transcription factor Nrf2 is a therapeutic target against brain inflammation. J Immunol 181, 680 – 9.
94. Ito Y, Onobori K, Yamazaki T, Kawamura Y. 2011. Tigloylshikonin, a new minor shikonin derivative, from the roots and the commercial root extract of *Lithospermum erythrorhizon*. Chemical and Pharmaceutical Bulletin 59, 117 – 119.
95. Jang S, Kelley KW, Johnson R.W. 2008. Luteolin reduces IL-6 production in microglia by inhibiting JNK phosphorylation and activation of AP-1 Proceedings of the National Academy of Sciences of the United States of America. 105, 7534-7539.

96. Jin R, Kurashige S. 1996. Effects of Chinese herbs on macrophage functions in N-butyl-N-butanolnitrosoamine treated mice. Immunopharmacology and Immunotoxicology 18, 105 - 114.
97. Jin R, Wan LL, Mitsuishi T, Kodama K, Kurashige S. 1994. Immunomodulative effects of Chinese herbs in mice treated with anti-tumor agent cyclophosphamide. Yakugakuzasshi: Journal of the Pharmaceutical Society of Japan 114, 533 - 538.
98. Jonstone R.W. 2002. Apoptosis: a link between cancer genetics and chemotherapy. Cell 108, 153 - 164.
99. Katoh Y, Itoh K, Yoshida E, Miyagishi M, Fukamizu A, Yamamoto M. 2001. Two domains of Nrf2 cooperatively bind CBP, a CREB binding protein, and synergistically activate transcription. Genes Cells 6, 857 - 68.
100. Kawai Y, Garduno L, Theodore M, Yang J, Arinze IJ. 2011. Acetylation-deacetylation of the transcription factor Nrf2 (nuclear factor erythroid 2-related factor 2) regulates its transcriptional activity and nucleocytoplasmic localization. J Biol Chem 286, 7629 - 40.
101. Kim SJ, Min HY, Lee EJ, Kim YS, Bae K, Kang SS, et al. 2010. Growth inhibition and cell cycle arrest in the G0/G1 by schizandrin, a dibenzocyclooctadiene lignan isolated from *Schisandra chinensis*, on T47D human breast cancer cells. Phytother Res 24, 193 - 7.
102. Kim JE, Kim SG, Goo JS, Park DJ, Lee YJ, Hwang IS, Lee, HR, Choi SI, Lee YJ, Oh CH, Choi YW, Hwang DY. 2012. The alpha-iso-cubebenol compound isolated from *Schisandra chinensis* induces p53-independent pathway-mediated apoptosis in hepatocellular carcinoma cells Oncology reports. 28, 1103-1109.
103. Kim MJ, Seong AR, Yoo JY, Jin CH, Lee YH, Kim YJ, Lee J, Jun WJ, Yoon HG. 2011. Gallic acid, a histone acetyltransferase inhibitor, suppresses beta-amyloid neurotoxicity by inhibiting microglial-mediated neuroinflammation Molecular nutrition & food research. 55, 1798-1808.
104. Klintworth H, Newhouse K, Li T, Choi WS, Faigle R, Xia Z. 2007. Activation of c-Jun N-terminal protein kinase is a common mechanism underlying paraquat- and rotenone-induced dopaminergic cell apoptosis. Toxicol Sci 97, 149 - 62.
105. Lee J, Kim CH, Simon DK, Aminova LR, Andreyev AY, Kushnareva YE, et al. 2005. Mitochondrial cyclic AMP response element-binding protein (CREB) mediates mitochondrial gene expression and neuronal survival. J Biol Chem 280, 40398 - 401.
106. Lee SK, Kim SD, Lee HY, Baek SH, Ko MJ, Son BG, et al. 2010. Alpha-iso-cubebene, a natural compound isolated from *Schisandra chinensis* fruit, has therapeutic benefit against polymicrobial sepsis. Biochem Biophys Res Commun 426, 226 - 31.
107. Lee YJ, Park SY, Kim SG, Park da J, Kang JS, Lee SJ, et al. 2010. Identification of a novel compound that inhibits iNOS and COX-2 expression in LPS-stimulated macrophages from *Schisandra chinensis*. Biochem Biophys Res Commun 391, 1687 - 92.
108. Lee YJ, Park SY, Kim SG, Park DJ, Kang JS, Lee SJ, Yoon S, Kim YH, Bae YS, Choi YW. 2010a. Identification of a novel compound that inhibits iNOS and COX-2 expression in LPS-stimulated macrophages from *Schisandra chinensis* Biochemical and biophysical research communications. 391, 1687-1692.
109. Lee YJ, Shim JW, Lee YJ, Park YH, Lee HY, Kim SD, Choi YW, Bae YS. 2009. Identification of a novel compound that stimulates intracellular calcium increase and CXCL8 production in human neutrophils from *Schisandra chinensis* Biochemical and biophysical research

communications. 379, 928-932.
110. Li HY, Wu SY, Shi N. 2007. Transcription factor Nrf2 activation by deltamethrin in PC12 cells: involvement of ROS. Toxicol Lett 171, 87 - 98.
111. Lin YC, Uang HW, Lin RJ, Chen IJ, Lo YC, 2007. Neuroprotective effects of glyceryl nonivamide against microglia-like cells and 6-hydroxydopamine-induced neurotoxicity in SH-SY5Y human dopaminergic neuroblastoma cells The Journal of pharmacology and experimental therapeutics. 323, 877-887.
112. Lindequist, U., Niedermeyer, T.H.J., Julich, W.D., 2005. The pharmacological potential of mushrooms. Evidence Based Complementary and Alternative Medicine 2, 285 - 299.
113. Lirussi D, Li J, Prieto JM, Gennari M, Buschiazzo H, Rios JL, ZaidenbergA. 2004. Inhibition of *Trypanosoma cruzi* by plant extracts used in Chinese medicine. Fitoterapia 75, 718 - 723.
114. Liu DZ, Liang HJ, Chen CH, Su CH, Lee TH, Huang CT, Hou WC, Lin SY, Zhong WB, Lin PJ, Hung LF, Liang YC. 2007. Comparative anti-inflammatory characterization of wild fruiting body, liquid-state fermentation, and solid-state culture of *Taiwanofungus camphoratus* in microglia and the mechanism of its action Journal of Ethnopharmacology. 113, 45-53.
115. Mao X, Yu CR, Li WH, Li WX. 2008. Induction of apoptosis by shikonin through a ROS/JNK-mediated process in Bcr/Abl-positive chronic myelogenous leukemia (CML)cells. Cell Research 18, 879 - 888.
116. Martin I, Dawson VL, Dawson TM. 2011. Recent advances in the genetics of Parkinson's disease. Annu Rev Genomics Hum Genet 12, 301 - 25.
117. Martinez TN, Greenamyre JT. 2012. Toxin models of mitochondrial dysfunction in Parkinson's disease. Antioxid Redox Signal 16, 920 - 34.
118. Nakaso K, Ito S, Nakashima K. 2008. Caffeine activates the PI3K/Akt pathway and prevents apoptotic cell death in a Parkinson's disease model of SH-SY5Y cells. Neurosci Lett 432, 146 - 50.
119. Nunez G, Benedic, MA, Hu Y, Inohara N. 1998. Caspases: the proteases of the apoptotic pathway. Oncogene 17, 3237 - 3245.
120. Oh YT, Lee JY, Lee J, Lee JH, Kim JE, Ha J, Kang, I. 2010. Oleamide suppresses lipopolysaccharide-induced expression of iNOS and COX-2 through inhibition of NF-kappa B activation in BV2 murine microglial cells Neuroscience letters. 474, 148-153.
121. Olson JK, Miller SD. 2004. Microglia initiate central nervous system innate and adaptive immune responses through multiple TLRs Journal of immunology (Baltimore, Md.: 1950). 173, 3916-3924.
122. Ozaki Y, Ohno A, Saito Y, Satake M. 1994. Accelerative effect of shikonin, alkannin and acetylshikonin on the proliferation of granulation tissue in rats. Biological and Pharmaceutical Bulletin 17, 1075 - 1077.
123. Pan XD, Zhu YG, Lin N, Zhang J, Ye QY, Huang HP, Chen X.C. 2011. Microglial phagocytosis induced by fibrillar beta-amyloid is attenuated by oligomeric betaamyloid: implications for Alzheimer's disease Molecular neurodegeneration. 6, 45-1326-6-45.
124. Papageorgiou VP. 1979. ^{1}H NMR spectra of naturally occurring isohexenyl-naphthazar in pigments. Planta Medica 37, 185 - 187.
125. Papageorgiou VP, Assimopoulou AN, Couladouros EA, Hepworth D, Nicolaou KC. 1999. The chemistry and biology of alkannin, shikonin, and related naphthazarin S. natural products.

Angew and te Chemie International Edition in English 38, 270 – 300.
126. Park SY, Kim JH, Lee SJ, Kim Y. 2013. Involvement of PKA and HO-1 signaling in anti-inflammatory effects of surfactin in BV-2 microglial cells. Toxicol Appl Pharmacol 268, 68 – 78.
127. Park SY, Park TG, Lee SJ, Bae YS, Ko MJ, Choi YW. 2014. Alpha-iso-cubebenol inhibits inflammation-mediated neurotoxicity and amyloid beta 1-42 fibril-induced microglial activation. J Pharm Pharmacol 66, 93 – 105.
128. Park SY, Park DJ, Kim YH, Kim Y, Choi YW, Lee SJ. 2011. *Schisandra chinensis* alpha-iso-cubebenol induces heme oxygenase-1 expression through PI3K/Akt and Nrf2 signaling and has anti-inflammatory activity in *Porphyromonas gingivalis* lipopolysaccharide-stimulated macrophages International immunopharmacology. 11, 1907-1915.
129. Parvathy S, Rajadas J, Ryan H, Vaziri S, Anderson L, Murphy GMJr. 2009. Abeta peptide conformation determines uptake and interleukin-1alpha expression by primary microglial cells Neurobiology of aging. 30, 1792-1804.
130. Poulose SM, Fisher DR, Larson J, Bielinski DF, Rimando AM, Carey AN, Schauss AG, Shukitt-Hale B. 2012. Anthocyanin-rich acai (*Euterpe oleracea* Mart.) fruit pulp fractions attenuate inflammatory stress signaling in mouse brain BV-2 microglial cells Journal of Agricultural and Food Chemistry. 60, 1084-1093.
131. Presgraves SP, Ahmed T, Borwege S, Joyce JN. 2004. Terminally differentiated SH-SY5Y cells provide a model system for studying neuroprotective effects of dopamine agonists. Neurotox Res 5, 579 – 98.
132. Qiang FX, Guo YJ. 2001. Apoptosis in oncology. Cell Research 11, 1 – 7.
133. Rodriguez-Pallares J, Rey P, Parga JA, Munoz A, Guerra MJ, Labandeira-Garcia JL. 2008. Brain angiotensin enhances dopaminergic cell death via microglial activation and NADPH-derived ROS Neurobiology of disease. 31, 58-73.
134. Savitt JM, Dawson VL, Dawson TM. 2006. Diagnosis and treatment of Parkinson disease: molecules to medicine. J Clin Invest 116, 1744 – 54.
135. Scapagnini G, Vasto S, Abraham NG, Caruso C, Zella D, Fabio G. 2011. Modulation of Nrf2/ARE pathway by food polyphenols: a nutritional neuroprotective strategy for cognitive and neurodegenerative disorders. Mol Neurobiol 44, 192 – 201.
136. Schapira AH, Gegg M. 2011. Mitochondrial contribution to Parkinson's disease pathogenesis. Parkinsons Dis 2011, 159 – 60.
137. Schneider L, Giordano S, Zelickson BR, Johnson M, Benavides G, Ouyang X, et al. 2011. Differentiation of SH-SY5Y cells to a neuronal phenotype changes cellular bioener- getics and the response to oxidative stress Free Radic Biol Med 51, 2007 – 17.
138. Shen CC, Syu WJ, Li SY, Lin CH, Lee GH, Sun CM. 2002. Antimicrobial activities of naphthazarins from *Arnebia euchroma*. Journal of Natural Products 65, 1857 – 1862.
139. Singh B, Sharma MK, Meghwal PR, Sahu PM, Singh S. 2003.Anti-inflammatory activity of shikonin derivatives from *Arnebia hispidissima*. Phytomedicine: International Journal of Phytotherapy and Phytopharmacology 10, 375 – 380.
140. Tobon-Velasco JC, Limon-Pacheco JH, Orozco-Ibarra M, Macias-Silva M, Vazquez- Victorio G, Cuevas E, et al. 2013. 6-OHDA-induced apoptosis and mitochondrial dys-function are mediated by early modulation of intracellular signals and interaction of Nrf2 and NF-kappaB

factors. Toxicology 304, 109 - 19.
141. Tseng CJ, Wang YJ, Liang YC, Jeng JH, Lee WS, Lin JK, Chen CH, Liu IC, Ho YS. 2002. Microtubule damaging agents induce apoptosis in HL60 cells and G2/M cell cycle arrest in HT29 cells. Toxicology 175, 123 - 142.
142. Tukel C, Wilson RP, Nishimori JH, Pezeshki M, Chromy BA, Baumler AJ. 2009. Responses to amyloids of microbial and host origin are mediated through toll-like receptor 2 Cell host & microbe. 6, 45-53.
143. Williams GT, Smith CA. 1993. Molecular regulation of apoptosis: genetic controls on cell death. Cell 74, 777 - 779.
144. Wu Y, Zhai H, Wang Y, Li L, Wu J, Wang F, Sun S, Yao S, Shang Y. 2012. Aspirin-triggered lipoxin A(4) attenuates lipopolysaccharide-induced intracellular ROS in BV2 microglia cells by inhibiting the function of NADPH oxidase Neurochemical research. 37, 1690-1696.
145. Wu Z, Wu L, Li L, Tashiro SI, Onodera S, Ikejima T. 2004a. p53 Mediated cell cycle arrest and apoptosis induced by shikonin via caspase-9 dependent mechanism in human malignant melanoma A375-S2 cells. Journal of Pharmacological Sciences 94, 166 - 176.
146. Wu Z, Wu LJ, Li .H, Tashiro S, Onodera S, Ikejima T. 2004b. Shikonin regulates HeLa cell death via caspase-3 activation and blockage of DNA synthesis. Journal of Asian Natural Products Research 6, 155 - 166.
147. Yeh CC, Kuo HM, Li TM, Lin JP, Yu FS, Lu HF, Chung JG, Yang JS. 2007. Shikonin-induced apoptosis involves caspase-3 activity in a human bladder cancer cellline (T24). In Vivo (Athens, Greece) 21, 1011 - 1019.
148. Zeng Y, Liu G, Zhou LM. 2009. Inhibitory effect of acetylshikonin on human gastric carcinoma cell line SGC-7901 in vitro and in vivo. World Journal of Gastroenterology 15, 1816 - 1820.
149. Zhang H, Wang ZQ, Zhao DY, Zheng DM, Feng J, Song LC, et al. 2011. AIF-mediated mitochondrial pathway is critical for the protective effect of diazoxide against SH-SY5Y cell apoptosis. Brain Res 1370, 89 - 98.
150. Zhang L, Wu C, Zhao S, Yuan D, Lian G, Wang X, Wang L, Yang J. 2010. Demethoxycurcumin, a natural derivative of curcumin attenuates LPS-induced proinflammatory responses through down-regulation of intracellular ROS-related MAPK/NF kappa B signaling pathways in N9 microglia induced by lipopolysaccharide International Immunopharmacology. 10, 331-338.
151. Zhu C, Wang X, Huang Z, Qiu L, Xu F, Vahsen N, et al. 2007. Apoptosis-inducing factor is a major contributor to neuronal loss induced by neonatal cerebral hypoxia-ischemia. Cell Death Differ 14, :775 - 84.
152. Zornig M, Hueber A, Baum W, Evan G. 2001. Apoptosis regulators and their role in tumorigenesis. Biochimicaet Biophysica Acta 1551, 1 - 37.

부 록

1. CRO 관련 SOP

2. 사업성검토 보고서

(자초추출물, α-iso-Cubebenol, EC-18, Gomisin J)

3. 논문게재실적

4. 각종 비임상시험 데이터 Summary

1. CRO 운용 관련 SOP

<제정 표준작업수순서 (SOP) 예시>

SOP번호	조직 및 업무분장	제정일자	2012-11-30
SOP/AGR/001	**Organization and Job Descriptions**	개정일자(차수)	(0)

1. 목적

㈜바이오톡스텍 내부 조직으로서 가칭 '농업전문CRO'에서 기획, 실시되는 시험의 신뢰성을 확보하기 위하여 조직의 책임과 권한을 명확히 함.

2. 적용범위

㈜바이오톡스텍 내부 조직으로서 가칭 '농업전문CRO'에서 시험 등을 실행, 유지하는 구성원에 적용한다.

3. 조직의 구성 및 운영

3.1 조직 구성은 추후 확정한다.

3.2 주요 업무에 대한 의결은 "운영위원회"를 통하여 결정하고 운영자의 승인을 받는다.

3.3 각 구성원의 역할, 책임 및 권한은 "업무분장표"에 따르며, "업무분장표"는 운영자의 승인을 받는다.

4. 책임과 권한

4.1 운영자

4.1.1 소속된 개개인이 규정에 명시된 책무를 수행하였음을 확인 한다.

4.1.2 담당자의 자격, 훈련, 경험, 책무분담에 대한 기록의 관리유지를 확인한다.

4.1.3 담당자 별로 그들이 실시해야 하는 책무를 명확히 이해하고 관련된 교육이 실시되고 있는지 확인한다.

4.1.4 기술적으로 타당한 표준작업수순서(SOP, Standard Operating Procedure)가 작성되고 준수되는지를 확인하고, 모든 표준작업수순서의 제정, 개정 및 폐기를 승인한다.

4.1.5 모든 관련 표준작업수순서 파일을 유지토록 한다.

4.2 팀장

4.2.1 팀원의 역할, 책임 및 권한에 대하여 업무 분장표를 작성한다.

4.2.2 팀원의 자격을 평가하고 업무 수행에 대하여 관리 감독한다.

4.2.3 년간 교육 훈련 계획서를 작성하고, 팀원의 자질 향상을 위해 교육을 실시한다.

4.2.4 팀별 업무 목표 및 추진 계획을 설정, 실행한다.

4.2.5 해당 SOP의 제정, 개정 내용을 검토하고, 유지, 관리한다.

4.2.6 시정 및 예방조치 사안에 대하여 계획을 수립하고 실시한다.

4.3 담당자

4.3.1 담당자는 관련된 해당 규정의 조항을 숙지하고 있어야 한다.

4.3.2 담당자는 적절한 표준작업수순서에 따라 업무를 수행하고, 문제 발생시 운영자에게 보고한다.

5. 기록 및 보관

모든 기록의 관리는 ㈜바이오톡스텍 "자료관리(SOP/GER/006)"에 따른다.

2. 사업화 보고서 표지(비임상 물질에 대한 보안사항으로 표지, 목차만 공개)

일 반 보 고 서

Acetylshikonin(자초추출물) 사업성 검토

비임상전문CRO Biotoxtech

연 구 책 임 자 강 종 구 2014. 3. 12

목 차

일 반 보 고 서

α-Iso-cubebenol 사업성 검토

비임상전문CRO
Biotoxtech

연 구 책 임 자 강 종 구 2014. 11. 21

㈜바이오톡스텍

목 차

일 반 보 고 서

EC-18 (1-palmitoyl-2-linoleoyl-3-acetylglycerol, PLAG) 사업성 검토

비임상전문CRO
Biotoxtech

연 구 책 임 자 강 종 구 2014. 5. 18

목 차

일 반 보 고 서

Gomisin J 사업성 검토

비임상전문CRO
Biotoxtech

연 구 책 임 자 강 종 구 2013. 12. 2

㈜ 바이오톡스텍

목 차

3. 논문게재 실적

Vascular Pharmacology 57 (2012) 124–130

Contents lists available at SciVerse ScienceDirect

Vascular Pharmacology

journal homepage: www.elsevier.com/locate/vph

Gomisin J from *Schisandra chinensis* induces vascular relaxation via activation of endothelial nitric oxide synthase

Ji Young Park [a], Young Whan Choi [b], Jung Wook Yun [a], Jin Ung Bae [a], Kyo Won Seo [a], Seung Jin Lee [a], So Youn Park [a], Chi Dae Kim [a,*]

[a] Department of Pharmacology, College of Medicine, and MRC for Ischemic Tissue Regeneration, Pusan National University, Yangsan, Gyeongnam 626-870, Republic of Korea
[b] College of Natural Resources & Life Sciences, Pusan National University, Gyeongnam 627-706, Republic of Korea

ARTICLE INFO

Article history:
Received 12 December 2011
Received in revised form 14 May 2012
Accepted 13 June 2012

Keywords:
Gomisin J
Vasorelaxation
Endothelium
Nitric oxide
eNOS

ABSTRACT

Gomisin J (GJ) is a lignan contained in *Schisandra chinensis* (SC) which is a well-known medicinal herb for improvement of cardiovascular symptoms in Korean. Thus, the present study examined the vascular effects of GJ, and also determined the mechanisms involved. Exposure of rat thoracic aorta to GJ (1–30 μg/ml) resulted in a concentration-dependent vasorelaxation, which was more prominent in the endothelium (ED)-intact aorta. ED-dependent relaxation induced by GJ was markedly attenuated by pretreatment with L-NAME, a nitric oxide synthase (NOS) inhibitor. In the intact endothelial cells of rat thoracic aorta, GJ also enhanced nitric oxide (NO) production. In studies using human coronary artery endothelial cells, GJ enhanced phosphorylation of endothelial NOS (eNOS) at Ser^{1177} with increased cytosolic translocation of eNOS, and subsequently increased NO production. These effects of GJ were attenuated not only by calcium chelators including EGTA and BAPTA-AM, but also by LY294002, a PI3K/Akt inhibitor, indicating calcium- and PI3K/Akt-dependent activation of eNOS by GJ. Moreover, the levels of intracellular calcium were increased immediately after GJ administration, but Akt phosphorylation was started to increase at 20 min of GJ treatment. Based on these results with the facts that ED-dependent relaxation occurred rapidly after GJ treatment, it was suggested that the ED-dependent vasorelaxant effects of GJ were mediated mainly by calcium-dependent activation of eNOS with subsequent production of endothelial NO.

1. Introduction

Schisandra chinensis (SC) has long been used as a tonic, a sedative, an anti-aging and an astringent agent, and also for treatment of cardiovascular symptoms in Korea, China and Japan (Chen and Li, 1993; Huang et al., 2005). The major bioactive components of SC fruits are lignans such as schizandrins and gomisins including gomisin J (GJ), gomisin N and gomisin A (Choi et al., 2006; Lu and Chen, 2009). In our previous study, hexane extracts of SC were found to cause vasorelaxation in endothelium (ED)-intact vasculature as well as in ED-denuded rat thoracic aortas (Park et al., 2009a). The relaxant effect of SC extracts on ED-intact vasculature was more prominent than that on ED-denuded aorta (Park et al., 2009a). Thus, Park et al. (2009a) suggested that vascular relaxation evoked by SC extracts was mediated mainly by the ED-dependent nitric oxide (NO) pathway.

Compounds that can enhance endothelial function through the NO pathway may have potential for use in prevention and treatment of cardiovascular diseases, such as hypertension and atherosclerosis (Landmesser and Drexler, 2005). The anti-atherosclerotic properties of endothelial NO synthase (eNOS), including inhibition of platelet aggregation, leukocyte adhesion, smooth muscle cell proliferation, and expression of atherosclerosis related genes, have been demonstrated (Herman and Moncada, 2005). The activity of eNOS is reportedly increased not only by translocation of eNOS from cellular membrane to cytosol, but also by Akt-dependent phosphorylation of eNOS at Ser^{1179} (Dimmeler et al., 1999; Fleming et al., 2001). Whereas cytosolic translocation of eNOS is dependent on binding of calmodulin, thereby requiring elevation of intracellular calcium concentration, phosphorylation of eNOS at Ser^{1177} has been demonstrated to occur even in calcium-free conditions (Dimmeler et al., 1999). Previous studies have demonstrated that gomisin A induced vasodilation via increased NO production in endothelial cells (Park et al., 2009b; Seok et al., 2011). However, the vascular effects of other lignans including GJ were not fully clarified.

GJ is a small molecular weight lignan contained in SC. Previous studies have shown that GJ protected hydrogen peroxide-induced cell death (Yoshikawa et al., 2006) and LPS-induced inflammatory reaction (Oh et al., 2010). GJ has also been shown to inhibit lipid peroxidation in rat liver mitochondria and to protect cultured myocardial

Abbreviations: SC, *Schisandra chinensis*; GJ, gomisin J; NO, nitric oxide; eNOS, endothelial nitric oxide synthase; ED, endothelium; HCAEC, human coronary artery endothelial cell.

* Corresponding author at: Department of Pharmacology, School of Medicine, Pusan National University, Yangsan, Gyeongnam 626-870, Republic of Korea. Tel: +82 51 510 8063; fax: +82 51 510 8068.
E-mail address: chidkim@pusan.ac.kr (C.D. Kim).

1537-1891/$ – see front matter © 2012 Elsevier Inc. All rights reserved.
doi:10.1016/j.vph.2012.06.002

cells from injury by calcium paradox (Peng et al., 1996). To date, however, knowledge of the pharmacological mechanism of GJ on the cardiovascular system is very limited. Thus, in the present study, we examined the effects of GJ on vasodilatation as well as NO synthesis in rat thoracic aorta. In addition, in order to determine possible mechanisms involved in vascular relaxation induced by GJ, the role of GJ on the regulation of eNOS activity with subsequent production of NO was also determined using human vascular endothelial cells.

2. Materials and methods

2.1. Plant material

Schisandra chinensis (SC) fruits were collected on September 2005 from Mungyeong, Korea. A voucher specimen (accession number SC-PDRL-1) has been deposited in the Herbarium of Pusan National University. SC was identified by one of the authors (Young Whan Choi).

2.2. Isolation of gomisin J

The dried fruits of SC were ground to a fine powder and extracted with n-hexane. The suspension was filtered, evaporated, lyophilized, and then the hexane extract was obtained. The hexane extract was chromatographed on a silica gel column (40 m, J.T. Baker, NJ, USA) with a step gradient of ethyl acetate in hexane. Fraction 26 was separated on a silica gel column with 1% acetone in CH_2Cl_2 to get 26IA-26IT. Fraction 26IJ was re-separated on a silica gel column with 1% acetone in CH_2Cl_2 to give gomisin J.

Positive GC-MS indicated a molecular ion at *m/z* 389 corresponding to $[M+H]^+$, indicating a molecular formula of $C_{22}H_{28}O_6$. The IR spectrum indicated that GJ is a cyclooctadiene lignan having a hydroxyl group. ^{13}C NMR and DEPT spectra showed 22 signals, including 12 carbons for two aromatic rings, and four *O*-methyls at δ_C 60.9 (×2), 60.0 (×2). It also showed the presence of two benzylic methylenes at 38.7 and 35.1, and two tertiary carbons at δ_C 21.7 and 12.4. The proton NMR spectrum of GJ showed the presence of two secondary methyls (δ 0.97 and 0.73, each d, J = 7 Hz), two benzylic methylene (δ_H 0.02–2.25, 4H, m), four methoxyls (δ_H 3.54 and 3.94, each 6H, s), two hydroxyls (δ_H 5.91, 2H, br s, D_2O exchangeable) and two aromatic protons (δ_H 6.64, 2H, s). The appearance of two distinct methyl signals and two distinct methoxyl signals suggested that one methyl (δ 0.73) and two methoxyls (δ 3.54) are shielded by the aromatic rings, and therefore that GJ has a *cis*-dimethyl moiety on the cyclooctadiene rings and two methoxyls at C-1 and C-15 on the aromatic rings (Ikeya et al., 1979) (Fig. 1).

2.3. Chemicals

Phenylephrine hydrochloride (PE), acetylcholine chloride, N^G-nitro-L-arginine methyl ester (L-NAME), indomethacin, tetraethylammonium, and EGTA were purchased from Sigma-Aldrich (St. Louis, MO). 1,2-Bis-(*o*-aminophenoxy) ethane-*N,N,N′,N′*-tetraacetic acid tetraacetoxy methyl ester (BAPTA-AM) was purchased from Calbiochem (Gibbstown, NJ). DAF-FM DA was purchased from Molecular Probes (Karlsruhe, Germany), and all other chemicals were reagent grade. The solid form of GJ was dissolved in 100% DMSO at a concentration of 100 mg/l as stock solutions, and subsequently diluted in media in all experiments.

2.4. Preparation of aortic rings and tension measurement

All animal procedures were conducted in accordance with the Animal Care Guidelines of Pusan National University Institutional Animal Care and Use Committee. Sprague–Dawley rats (250–300 g) were anesthetized with sodium pentobarbital (50 mg/kg, i.p.), and then thoracic aorta was rapidly removed. The aortic rings (2–3 mm in width) were suspended in a 10-ml organ chambers filled with Krebs' solution (37 °C) at a resting tension of 2 g. After aortic rings were allowed to equilibrate for 90 min, sustained and stable contraction was induced by PE (10^{-5} M). Changes in isometric tension were recorded using a force-displacement transducer (Grass FT 0.3, Quincy, MA, USA) connected to a Power Lab system 400 (ML 118, PowerLab, AD Instruments, Medford, MA).

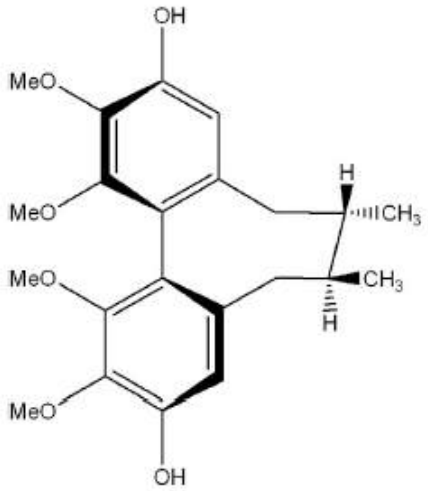

Fig. 1. Structure of gomisin J.

Vasodilatory potency of GJ was studied by cumulative addition of GJ at concentrations of 1–30 μg/ml. Involvement of endothelium (ED) in GJ-induced relaxation was also examined by comparing the magnitude of relaxation between endothelium-denuded and endothelium-intact specimens. Endothelium was removed by gently rubbing the intimal surface with a cotton swab. For pharmacological characterization of GJ-induced vasodilatation, aortic specimens were pretreated with various inhibitors including L-NAME (a nitric oxide synthase inhibitor), tetraethylammonium (a nonselective K^+ channel blocker), and indomethacin (a cyclooxygenase inhibitor) for 20 min before the PE-induced contraction. Relaxations are expressed as the percentage of relaxation of PE-induced tone.

2.5. Measurement of NO in aortic tissues

4-Amino-5-methylamino-2′,7′-difluorofluorescein diacetate (DAF-FM DA) is converted via a NO-specific mechanism to an intensely fluorescent triazole derivative (Kojima et al., 1998). Thus, DAF-FM DA, a membrane permeable fluorescent indicator for NO, was used to detection of NO produced by GJ. For the fluorometric measurement of NO, aortic rings were incubated for 2 h in the darkness in Krebs' solution containing DAF-FM DA (10 μM), and GJ was then administered in the presence or absence of L-NAME (100 μM). After then, the aortic rings were removed and frozen at −20 °C, and cut into 10 μm-thick sections in a microtome (MICROM, Germany). Fluorescence was detected using an Axivert 200 fluorescence microscope (Carl Zeiss, Oberkochem, Germany) and quantified by Metamorph software (Molecular Devices, Sunnyvale, CA).

2.6. Measurement of NO in endothelial cells

Human coronary artery endothelial cells (HCAEC) were obtained from Lonza (Walkersville, MD) and cultured in endothelial growth

medium-2 (EGM-2 MV, Lonza). After reaching subconfluency, the cells were incubated in red phenol-free EBM containing GJ, and DAF-FM DA was then loaded into the cells. After incubation in 37 °C for 5 min, the cells were washed mildly three times by PBS to eliminate any interference. Fluorescence was detected using an Axivert 200 fluorescence microscope (Carl Zeiss) and quantified by Metamorph software (Molecular Devices).

2.7. Measurement of eNOS activity

The change in eNOS activity in response to GJ was quantified by use of a NOS colorimetric assay kit (Calbiochem, Ra Jolla, CA). This assay measures eNOS activity based on the enzymatic conversion of nitrate to nitrite by nitrate reductase. The reaction is followed by colorimetric detection of nitrite as an azo dye product (540 nm) of the Griess reaction. eNOS activity was measured in cell culture supernatants after incubation of GJ. ELISA assay was quantified using the Power Wave ×340 (Bio-Tek Instrument Inc, Winooski, VT).

2.8. Western blotting for eNOS and Akt

Cells were washed in PBS after stimulation with GJ, and then scraped using an ice-cold lysis buffer (20 mM Tris–HCl, pH 7.4, 1 mM EGTA, 1 mM EDTA, 150 mM NaCl, 1% Triton-X, 1 mM Na_3Vo_4, 10% glycerol). For eNOS translocation, the cell lysate was ultracentrifuged at 100,000×*g* for 90 min at 4 °C to obtain the membrane (pellet) and cytosolic (supernatant) fractions. Equal amounts of protein per sample were separated on 8% SDS-PAGE gels, and subsequently transferred to a polyvinylidene fluoride membrane. The membranes were incubated with purified mouse anti-eNOS (1:1000, BD Biosciences), and washed and further incubated with the secondary antibody. For measurement of eNOS phosphorylation, total cellular lysate was subjected to 8% SDS-PAGE, and subsequently transferred to a polyvinylidene fluoride membrane. After blocking with 5% skim milk, the membranes were incubated with purified mouse anti-eNOS (1:1000, BD Biosciences) and purified mouse anti-phospho Ser^{1177} eNOS (1:1000, BD Biosciences). For measurement of Akt phosphorylation, the membranes were incubated with anti-Akt (1:1000, Cell Signaling Technology) and anti-phospho Akt (1:1000, Cell signaling Technology), and further incubated with the secondary antibody. The bands were visualized by addition of enhanced chemiluminescence detection reagents.

2.9. Measurement of intracellular calcium levels

Intracellular calcium concentration was measured using Fura-2/AM, a calcium-sensitive fluorescent dye. In brief, cells were incubated with 3 μM Fura-2/AM at 37 °C in fresh serum-free EBM medium for 60 min. Cells were resuspended in Locke's solution (154 mM NaCl, 5.6 mM KCl, 1.2 mM $MgCl_2$, 5 mM HEPES, pH 7.3, 10 mM glucose, 2.2 mM $CaCl_2$, and 0.2 mM EGTA). Fluorescence was measured in fluorescence spectrophotometer (RF-5301-PC; Shimadzu, Kyoto, Japan) with emission wavelength at 500 nm using an excitation wavelength of 340 nm and 380 nm.

2.10. Statistical analysis

Results are expressed as the mean ± SEM. The significance of the results was analyzed by one-way analysis of variance (ANOVA) followed by Tukey's Multiple Comparison Test. *P* values less than 0.05 were considered significant.

3. Results

3.1. Gomisin J induces vascular relaxation

After stabilization of the resting tension of each vascular specimen, sustained and stable contraction of 1.5 ± 0.4 g was maintained by addition of PE (10^{-5} M). When the contraction by PE was stabilized, GJ was added from 1 to 30 μg/ml. In the ED-denuded aortic rings, vascular tension was reduced by GJ in a concentration-dependent manner, indicating occurrence of endothelium-independent relaxation. In the ED-intact aortic ring preparations, vascular tension induced by PE was markedly reduced by GJ in a concentration-dependent manner with the maximum value of 58.6 ± 3.7% at a concentration of 30 μg/ml. The vasorelaxant effects of GJ in ED-intact vasculature were more prominent than those in ED-denuded vasculature (Fig. 2).

3.2. Role of NO in gomisin J-induced vasorelaxation

In ED-intact vasculature, GJ-induced vasorelaxation was significantly attenuated by L-NAME (10^{-4} M), but not by indomethacin (10^{-5} M) as a cyclooxygenase inhibitor and tetraethylammonium (10^{-3} M) as a non-selective blocker of potassium channels (Fig. 3). This result suggested that the NO-mediated pathway was involved in GJ-induced relaxation in endothelium-intact aorta. To determine the effect of GJ on ED-dependent production of NO, NO production in aortic tissues was measured by DAF-FM DA, a fluorescent NO-sensitive dye, using a fluorescence microscope. As shown in Fig. 4A, GJ enhanced NO production in the endothelial layer of rat thoracic aorta in a concentration-dependent manner. In addition, GJ-induced NO production in aortic tissues was also significantly attenuated by L-NAME (10^{-4} M) (Fig. 4B and C).

3.3. Gomisin J-induced NO production in HCAEC

To determine the role of GJ in endothelial production of NO, we measured GJ-induced NO production in HCAEC by DAF-FM DA in the absence or presence of L-NAME. As shown in Fig. 5A, GJ induced an increase in DAF-FM DA fluorescence in a concentration-dependent

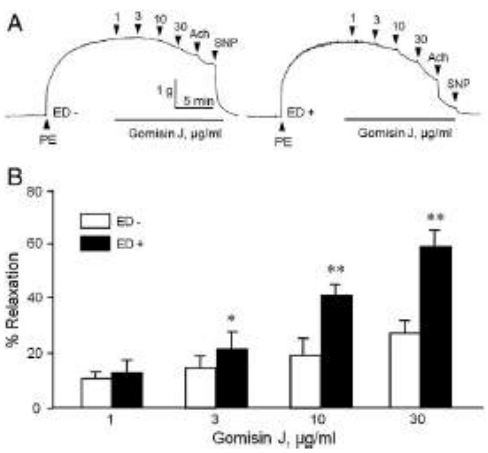

Fig. 2. Gomisin J-induced relaxation in aortic rings without endothelium (ED−) or with endothelium (ED+). (A) Representative tracings show the vasorelaxant effects of GJ (1–30 μg/ml) in phenylephrine (PE, 10^{-5} M)-precontracted aortic rings. Ach, 10^{-6} M acetylcholine; SNP, 10^{-7} M sodium nitroprusside. (B) Quantitative data of GJ-induced vasorelaxation in ED− (n = 5) or ED+ group (n = 6). Data were expressed as means ± SEM. *P<0.05, **P<0.01 vs. corresponding value in ED− group.

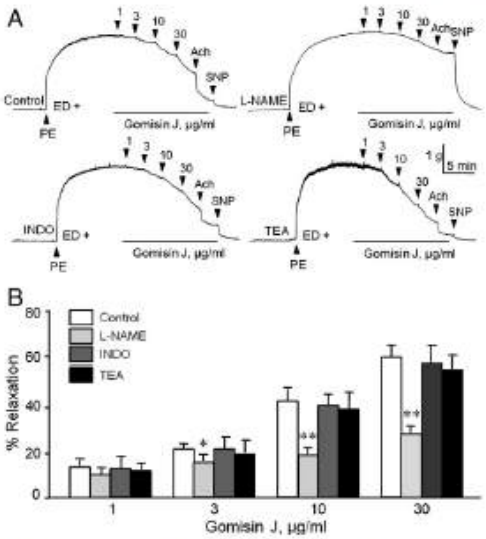

Fig. 3. Pharmacological characterization of gomisin J-induced vasorelaxation. GJ-induced relaxation was significantly attenuated when the endothelium (ED)-intact specimens were exposed to N^G-nitro-L-arginine methyl ester (L-NAME, 10^{-4} M), but remained unaffected by indomethacin (INDO, 10^{-5} M) and tetraethylammonium (TEA, 10^{-3} M). (A) Representative tracings. (B) Quantitative data were expressed as means ± SEM from 5 experiments. *$P<0.05$, **$P<0.01$ vs. corresponding control value.

manner. NO production was rapid, and was observed within 5 min of GJ addition, and reached a maximum at 20 min (data not shown). GJ-induced NO production in endothelial cells was also significantly attenuated by L-NAME (10^{-4} M), suggesting a potential role for GJ in regulation of eNOS activity in endothelial cells (Fig. 5B and C).

3.4. Signaling pathways involved in gomisin J-induced NO production

To determine involvement of various signaling pathways including calcium and PI3K/Akt pathways in GJ-induced NO production, this study evaluated the effects of various pharmacological inhibitors, including BAPTA-AM and EGTA as intracellular and extracellular calcium chelators, respectively, and LY294002 as a PI3K/Akt inhibitor. As shown in Fig. 6, GJ-induced NO production in HCAEC was significantly attenuated not only by calcium chelators, but also by a PI3K/Akt inhibitor. The inhibitory effect by calcium chelators was more prominent than that by a PI3K/Akt inhibitor. In addition, the increase in eNOS activity as measured by L-NAME-inhibitable nitrite production was also markedly inhibited by a PI3K/Akt inhibitor as well by calcium chelators. This observation suggests that acute NO production by GJ was mediated through calcium signaling as well as PI3K/Akt pathways.

3.5. Role of gomisin J on the regulation of eNOS activity

In order to evaluate the potential role of eNOS in GJ-induced NO production, the effect of GJ on both cytosolic translocation and phosphorylation of eNOS at Ser^{1177} was determined. As shown in Fig. 7A and B, treatment of HCAEC with 1 μg/ml GJ resulted in time-dependent translocation of eNOS from the plasma membrane to the cytosol, which was rapid, and observed within 5 min of GJ addition.

GJ also showed an effect on phosphorylation of eNOS at Ser^{1177} in a time-dependent manner (Fig. 7C and D). Phosphorylation of eNOS was also rapid, and reached a maximum at 10 min after GJ treatment. The GJ-induced phosphorylation of eNOS was significantly attenuated not only by calcium chelators, but also by a PI3K/Akt inhibitor (Fig. 7E and F).

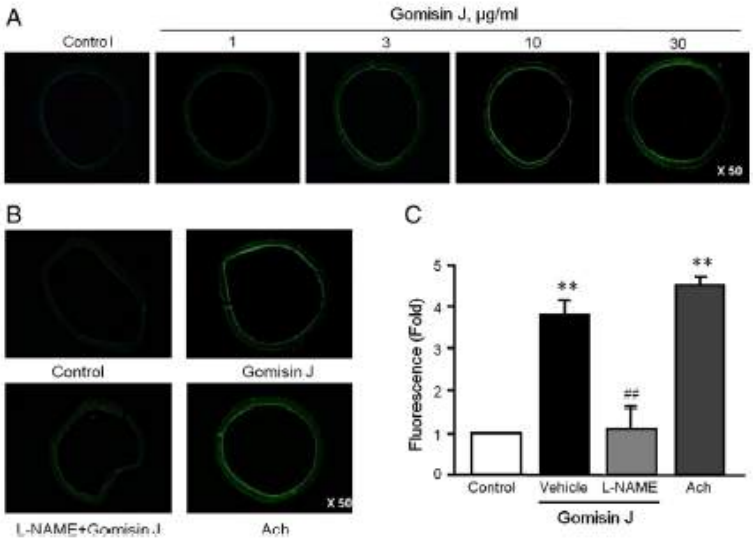

Fig. 4. Gomisin J-induced NO production in aortic tissues. Aortic tissues were treated with GJ (1–30 μg/ml) for 30 min, and then NO production was measured by DAF-FM using a fluorescent microscope. (A) Representative photographs from 4 independent experiments. (B) Representative photographs for GJ-induced NO production in aortic tissues in the presence of L-NAME (10^{-4} M). Acetylcholine (Ach, 10^{-6} M) was used as a positive control. (C) Quantitative data was expressed as ratio of control value, and data were represented as means ± SEM from 4 experiments. **$P<0.01$ vs. control; ##$P<0.01$ vs. vehicle.

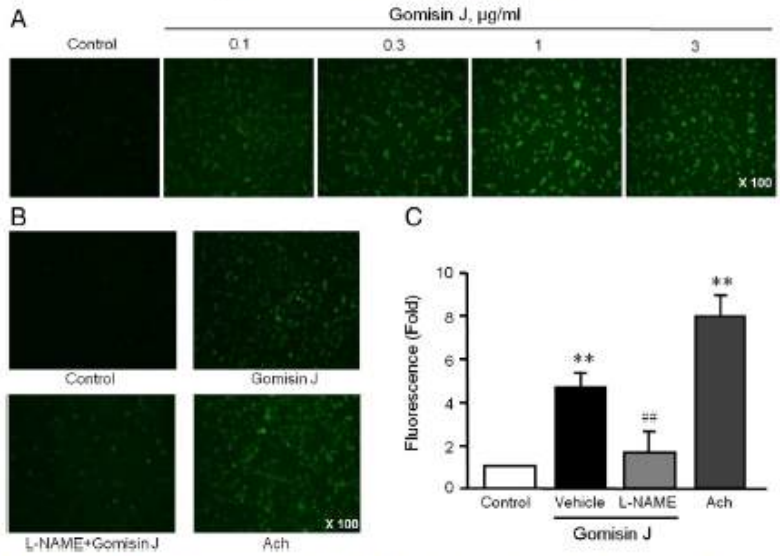

Fig. 5. Gomisin J-induced NO production in HCAEC. Cells were treated with GJ (0.1–3 μg/ml) for 30 min, and then NO production was measured by DAF-FM. (A) Representative photographs from 4 independent experiments. (B) Representative photographs for GJ-induced NO production in HCAEC in the presence of L-NAME (10^{-4} M). Acetylcholine (Ach, 10^{-6} M) was used as a positive control. (C) Quantitative data were expressed as ratio to the control, and data were represented as means ± SEM from 4 experiments. **P<0.01 vs. control; ##P<0.01 vs. vehicle.

3.6. Direct effects of gomisin J on intracellular calcium levels and Akt phosphorylation

In order to evaluate the direct role of GJ on the regulation of intracellular calcium levels in endothelial cells, we determined the levels of intracellular calcium using Fura-2/AM. The levels of intracellular calcium were rapidly and dose-dependently increased in HCAEC treated with GJ, suggesting a potential role of intracellular calcium in GJ-induced activation of eNOS (Fig. 8A).

We next explored the direct pieces of evidence that GJ activated Akt in endothelial cells. Treatment of HCAEC with 1 μg/ml GJ resulted in time-dependent phosphorylation of Akt. Phosphorylation of Akt was observed at 20 min of GJ addition, and reached a maximum at 30 min (Fig. 8B). Thus, it was suggested that nitric oxide derived

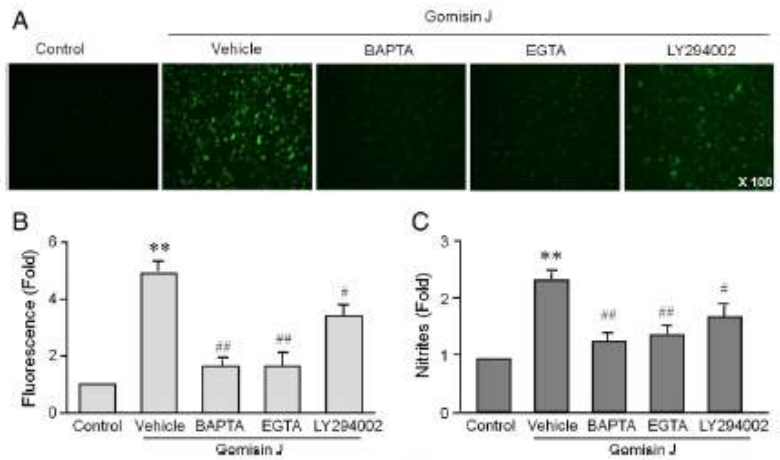

Fig. 6. Effects of calcium chelators and an Akt inhibitor on both NO production and eNOS activity in HCAEC. (A) Representative photographs for GJ (1 μg/ml) induced NO production in HCAEC, and its inhibition by various inhibitors including BAPTA-AM (2×10^{-5} M), EGTA (10^{-3} M), and LY294002 (10^{-5} M). (B) Quantitative data of NO production were expressed as ratio to the control value, and represented as means ± SEM from 5 experiments. **P<0.01 vs. control; #P<0.05, ##P<0.01 vs. vehicle. (C) The activity of eNOS as measured by L-NAME-inhibitable nitrite production was expressed as ratios to the control value, and was represented as means ± SEM from 5 experiments. **P<0.01 vs. control; #P<0.05, ##P<0.01 vs. vehicle.

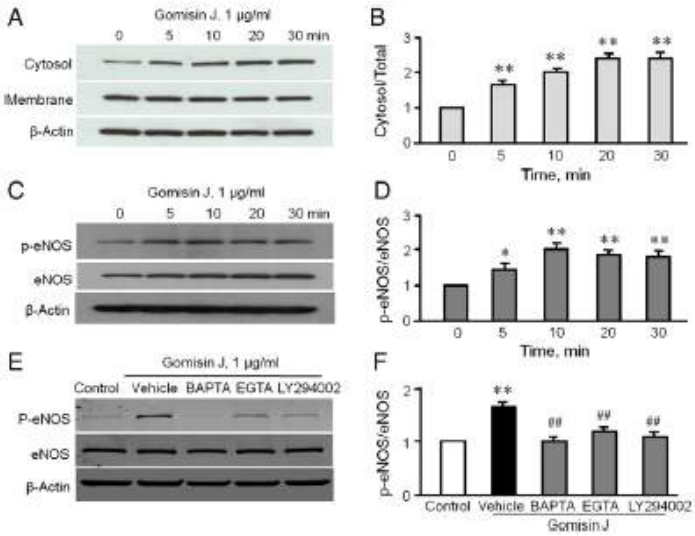

Fig. 7. Effects of gomisin J on cytosolic translocation and phosphorylation of eNOS in HCAEC. (A), (C) and (E) show representative blots for the time-course effects of GJ (1 μg/ml) on eNOS translocation, phosphorylation at Ser^{1177}, and its inhibition by calcium chelators (BAPTA-AM, 2×10^{-5} M; EGTA, 10^{-3} M) and a PI3K/Akt inhibitor (LY294002, 10^{-5} M), respectively. (B), (D), and (F) show respective quantification data. Data were expressed as ratio of cytosolic eNOS/total eNOS (cytosolic eNOS + membrane eNOS) and phosphorylated eNOS/eNOS, and represented as means ±SEM of 4–6 experiments. *$P<0.05$, **$P<0.01$ vs. corresponding control. ##$P<0.01$ vs. vehicle.

from calcium-mediated activation of eNOS might be mostly involved in GJ-induced vasorelaxation because GJ rapidly induced vasorelaxation in PE-contracted vasculature.

4. Discussion

Acute exposure of rat thoracic aorta to GJ, a major ingredient of *Schisandra chinensis* (SC), caused vasorelaxation in both endothelium (ED)-intact and ED-denuded vasculature. The vasorelaxant effects of GJ in ED-intact aorta were found to be more prominent than those in ED-denuded vasculature, and were markedly attenuated by pretreatment with L-NAME. In addition, GJ induced an increase in nitric oxide (NO) production in endothelial layer of rat thoracic aorta as well as in human coronary artery endothelial cells. These results suggested that the vasorelaxation induced by GJ was mainly mediated by an NO-dependent pathway.

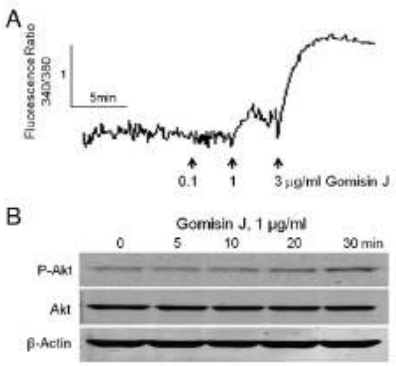

Fig. 8. Effects of gomisin J on intracellular calcium levels and Akt phosphorylation. (A) Representative tracing for the dose-response effects of GJ on intracellular calcium (n =5). HCAEC were incubated with the calcium indicator dye Fura 2-AM and then treated with GJ (0.1, 1 and 3 μg/ml). Cellular fluorescence was measured in fluorescence spectrophotometer. (B) Time-course effects of GJ (1 μg/ml) on the levels of p-Akt and total Akt in HCAEC treated with GJ for the indicated time. Representative photographs from 5 independent experiments.

In our previous study, hexane extracts of SC and gomisin A caused a vasorelaxation in both ED-intact and ED-denuded rat aortas (Park et al., 2007; 2009a). Endothelium-independent relaxation by SC extract and gomisin A has been ascribed to inhibition of MLC phosphorylation (Park et al., 2009a) and the Rho A/Rho-kinase pathway (Seok et al., 2011), respectively. However, the relaxant effect by SC extract and gomisin A on ED-intact aorta was more prominent than that on ED-denuded aorta (Park et al., 2007; 2009a). The previous study also demonstrated that gomisin A induced vasorelaxation via increased NO production in endothelial cells (Park et al., 2009b), suggesting a pivotal role of ED in vasorelaxation induced by SC extracts. In line with these results, the vasorelaxant effects of GJ were also more prominent in ED-intact vasculature. Thus, it was also suggested that vascular relaxation evoked by GJ was mediated mainly by an ED-dependent NO pathway.

NO, which is produced by eNOS, is a potent vasodilator by stimulation of soluble guanylate cyclase. This enzyme catalyzes the conversion of GTP to cGMP (Rapoport and Murad, 1983; Haug et al., 1999; Schlossmann et al., 2000; Ammendola et al., 2001). The rise of cGMP initiates reactions that result in relaxation of vascular smooth muscle (Marin and Rodriguez-Martinez, 1997; Fujita et al., 1998). In the present study, using pharmacological inhibitors, vasorelaxation induced by GJ was markedly attenuated by pretreatment with L-NAME (a nitric oxide synthase inhibitor), but not by tetraethylammonium (a nonselective blocker of K^+ channels) and indomethacin (a cyclooxygenase inhibitor). These results suggested that the vascular effect of GJ was mediated by NO, not by endothelium-derived prostacyclin or activation of K^+ channels. In addition, direct determination of an increase in NO production in the endothelial layer of rat thoracic aorta after treatment with GJ confirmed our pharmacological data, which indicated possible involvement of NO in GJ-induced vasorelaxation.

Endothelial NOS is tightly regulated not only at the transcriptional level but also by several post-transcriptional mechanisms (Fleming et al., 1997; Fleming and Busse, 2003). In the present study, GJ rapidly stimulated NO production in the endothelial layer as well as in HCAEC. In addition, acute exposure of endothelial cells to GJ did not have an effect on the level of eNOS proteins. Thus, it was suggested that GJ induced an increase in eNOS activity at the posttranscriptional level in human vascular endothelial cells.

The fact that eNOS activation can be both calcium-dependent and -independent has been well established (Omura et al., 2001). In endothelial cells, agonist-induced eNOS activation follows its dissociation from caveolin-1 and subsequent translocation into the cytosol, which requires increases in intracellular calcium and binding to CaMI (Fleming, 2010). In addition, activation of eNOS can take place independently of CaM binding and enzyme translocation while requiring small increases in intracellular calcium. In endothelial cells, eNOS can also be activated by Akt-dependent phosphorylation of eNOS at Ser^{1179} (Dimmeler et al., 1999; Fleming et al., 2001). Whereas cytosolic translocation of eNOS is dependent on intracellular calcium concentration, the phosphorylation of eNOS at Ser^{1177} has been demonstrated to occur even in calcium-free conditions (Dimmeler et al., 1999).

Most ligands, including bradykinin and acetylcholine, stimulate eNOS by raising the intracellular calcium concentration, which in turn forms a calcium/calmodulin complex that binds to eNOS (Michel and Feron, 1997). As in this study, our previous study showed that gomisin A increased endothelial eNOS activity via intracellular calcium-mediated cytosolic translocation of eNOS (Park et al., 2009b). In line with our previous study, the present study also demonstrated that GJ induced cytosolic translocation of eNOS within 5 min after GJ application. However, in contrast to gomisin A, which did not increase eNOS phosphorylation (Park et al., 2009b), GJ induced a rapid increase in phosphorylation of eNOS at Ser^{1179}, suggesting a potential role for the PI3K/Akt pathway in GJ-induced eNOS activation. In addition, GJ-induced NO production was attenuated not only by the acute removal of external calcium by EGTA or the buffering of cytosolic free calcium by BAPTA, but also by LY294002, a PI3K/Akt inhibitor. In parallel, eNOS phosphorylation by GJ was also attenuated by calcium chelators as well as by a PI3K/Akt inhibitor, indicating calcium- and PI3K/Akt-dependent activation of eNOS. In the present study, the levels of intracellular calcium were increased immediately after GJ treatment, but Akt phosphorylation was started to increase at 20 min of GJ addition. Considering these results with the facts that ED-dependent relaxation occurs rapidly after GJ administration, our present study suggests that the ED-dependent vasorelaxant effects of GJ are mediated mainly by calcium-dependent activation of eNOS with subsequent enhancement of endothelial NO production.

In summary, GJ activates eNOS via calcium-dependent and Akt-dependent pathways in HCAEC, and subsequently increases NO production and causes ED-dependent vasorelaxation. Furthermore, it is of note that the exact mechanism linking phosphorylation and translocation of eNOS and subsequent activation of eNOS after GJ stimulation still remain elusive. These observations may be important in understanding the mechanism of the action of GJ in vasculature and also in the therapeutic use of GJ for treatment of cardiovascular diseases such as hypertension and atherosclerosis.

Acknowledgments

This study was supported by the MRC Program of the MEST/KOSEF (2005-0049477), and Bio-industry Technology Development Program, Ministry for Food, Agriculture, Forestry and Fisheries, Republic of Korea (311054-03-1-HD120).

References

Ammendola, A., Geiselhoringer, A., Hofmann, F., Schlossmann, J., 2001. Molecular determinants of the interaction between the inositol 1,4,5-triphosphate receptor-associated cGMP kinase substrate (IRAG) and cGMP kinase I_β. J. Biol. Chem. 276, 24153–24159.
Chen, S.Y., Li, F., 1993. Tonics and astringents. In: Diebschlag, F. (Ed.), Clinical Guide to Chinese Herbs and Formulae. Churchill Livingstone, London, p. 75.
Choi, Y.W., Takamatsu, S., Khan, S.I., Srinivas, P.V., Ferreira, D., Zhao, J., Khan, I.A., 2006. Schisandrene, a dibenzocyclooctadiene lignan from *Schisandra chinensis*: structure–antioxidant activity relationships of dibenzocyclooctadiene lignans. J. Nat. Prod. 69, 356–359.
Dimmeler, S., Fleming, I., Fisslthaler, B., Hermann, C., Busse, R., Zeiher, A.M., 1999. Activation of nitric oxide synthase in endothelial cells by Akt-dependent phosphorylation. Nature 399, 601–605.
Fleming, I., 2010. Molecular mechanisms underlying the activation of eNOS. Pflugers Arch. 459, 793–806.
Fleming, I., Busse, R., 2003. Molecular mechanisms involved in the regulation of the endothelial nitric oxide synthase. Am. J. Physiol. Regul. Integr. Comp. Physiol. 284, R1–R12.
Fleming, I., Bauersachs, J., Busse, R., 1997. Calcium-dependent and calcium-independent activation of the endothelial NO synthase. J. Vasc. Res. 34, 165–174.
Fleming, I., Fisslthaler, B., Dimmeler, S., Kemp, B.E., Busse, R., 2001. Phosphorylation of Thr(495) regulates Ca(2+)/calmodulin-dependent endothelial nitric oxide synthase activity. Circ. Res. 88, E68–E75.
Fujita, S., Roerig, D.L., Bosnjak, Z.J., Stowe, D.F., 1998. Effects of vasodilators and perfusion pressure on coronary flow and simultaneous release of nitric oxide from guinea pig isolated hearts. Cardiovasc. Res. 38, 655–667.
Haug, L.S., Jensen, V., Hvalby, O., Walaas, S.I., Ostvold, A.C., 1999. Phosphorylation of the inositol 1,4,5-trisphosphate receptor by cyclic nucleotide-dependent kinases in vitro and in rat cerebellar slices in situ. J. Biol. Chem. 274, 7467–7473.
Herman, A.G., Moncada, S., 2005. Therapeutic potential of nitric oxide donors in the prevention and treatment of atherosclerosis. Eur. Heart J. 26, 1945–1955.
Huang, T., Shen, P., Shen, Y., 2005. Preparative separation and purification of deoxyschisandrin and γ-schisandrin from *Schisandra chinensis* (Turcz.) Baill by high-speed counter-current chromatography. J. Chromatogr. A 1066, 239–242.
Ikeya, Y., Taguchi, H., Yosioka, I., Kobayashi, H., 1979. The constituents of *Schisandra chinensis* Baill. I. Isolation and structure determination of five new lignans, gomisin A, B, C, F and G, and the absolute structure of schizandrin. Chem. Pharm. Bull. 27, 1383–1394.
Kojima, H., Sakurai, K., Kikuchi, K., Kawahara, S., Kirino, Y., Nagoshi, H., Hirata, Y., Nagano, T., 1998. Development of a fluorescent indicator for nitric oxide based on the fluorescein chromophore. Chem. Pharm. Bull. 46, 373–375.
Landmesser, U., Drexler, H., 2005. The clinical significance of endothelial dysfunction. Curr. Opin. Cardiol. 20, 547–551.
Lu, Y., Chen, D.F., 2009. Analysis of *Schisandra chinensis* and *Schisandra sphenanthera*. J. Chromatogr. A 1216, 1980–1990.
Marin, J., Rodriguez-Martinez, M.A., 1997. Role of vascular nitric oxide in physiological and pathological conditions. Pharmacol. Ther. 75, 111–134.
Michel, T., Feron, O., 1997. Nitric oxide synthases: which, where, how, and why? J. Clin. Invest. 100, 2146–2152.
Oh, S.Y., Kim, Y.H., Bae, D.S., Um, B.H., Pan, C.H., Kim, C.Y., Lee, H.J., Lee, J.K., 2010. Anti-inflammatory effects of gomisin N, gomisin J, and schisandrin C isolated from the fruit of *Schisandra chinensis*. Biosci. Biotechnol. Biochem. 74, 285–291.
Omura, M., Kobayashi, S., Mizukami, Y., Mogami, K., Todoroki-Ikeda, N., Miyake, T., Matsuzaki, M., 2001. Eicosapentaenoic acid (EPA) induces Ca(2+)-independent activation and translocation of endothelial nitric oxide synthase and endothelium-dependent vasorelaxation. FEBS lett. 487, 361–366.
Park, J.Y., Lee, S.J., Yun, M.R., Seo, K.W., Bae, S.S., Park, J.W., Lee, Y.J., Shin, W.J., Choi, Y.W., Kim, C.D., 2007. Gomisin A from *Schisandra chinensis* induces endothelium-dependent and direct relaxation in rat thoracic aorta. Planta Med. 73, 1537–1542.
Park, J.Y., Shin, H.K., Lee, Y.J., Choi, Y.W., Bae, S.S., Kim, C.D., 2009a. The mechanism of vasorelaxation induced by *Schisandra chinensis* extract in rat thoracic aorta. J. Ethnopharmacol. 121, 69–73.
Park, J.Y., Shin, H.K., Choi, Y.W., Lee, Y.J., Bae, B.R., Han, J., Kim, C.D., 2009b. Gomisin A induces Ca2+-dependent activation of eNOS in human coronary artery endothelial cells. J. Ethnopharmacol. 125, 291–296.
Peng, H.L., Chen, D.F., Lan, H.X., Zhang, X.M., Gu, Z., Jiang, M.H., 1996. Anti-lipid peroxidation of gomisin J on liver mitochondria and cultured myocardial cells. Zhongguo Yao Li Xue Bao 17, 538–541.
Rapoport, R.M., Murad, F., 1983. Agonist-induced endothelium-dependent relaxation in rat thoracic aorta may be mediated through cGMP. Circ. Res. 52, 352–357.
Schlossmann, J., Ammendola, A., Ashman, K., Zong, X., Huber, A., Neubauer, G., Wang, G.X., Allescher, H.D., Korth, M., Wilm, M., Hofmann, F., Ruth, P., 2000. Regulation of intracellular calcium by a signaling complex of IRAG, IP3 receptor and cGMP kinase I_β. Nature 404, 197–201.
Seok, Y.M., Choi, Y.W., Kim, G.D., Kim, H.Y., Takuwa, Y., Kim, I.K., 2011. Effects of gomisin A on vascular contraction in rat aortic rings. Naunyn Schmiedebergs Arch. Pharmacol. 383, 45–56.
Yoshikawa, A., Saito, Y., Maruyama, K., 2006. Lignan compounds and 4,4′-dihydroxybiphenyl protect C2C12 cells against damage from oxidative stress. Biochem. Biophys. Res. Commun. 344, 394–399.

Hypertension Research (2012) 35, 928–934

www.nature.com/hr

Open

ORIGINAL ARTICLE

Antihypertensive effect of gomisin A from *Schisandra chinensis* on angiotensin II-induced hypertension via preservation of nitric oxide bioavailability

Ji Young Park[1,3], Jung Wook Yun[1,3], Young Whan Choi[2], Jin Ung Bae[1], Kyo Won Seo[1], Seung Jin Lee[1], So Youn Park[1], Ki Whan Hong[1] and Chi Dae Kim[1]

Gomisin A (GA) is a small molecular weight lignan present in *Schisandra chinensis*, and has been demonstrated to have vasodilatory activity. In the present study, we investigated the effect of GA on blood pressure (BP) in angiotensin II (Ang II)-induced hypertensive mice. C57/BL6 mice infused subcutaneously with Ang II (1 and 2 μg kg^{-1} per min for 2 weeks) showed an increase in BP with a decrease in nitric oxide (NO) metabolites in plasma, and a negative correlation between these two parameters was demonstrated. In the thoracic aorta from Ang II-induced hypertensive mice, a decrease in vascular NO that was accompanied by a diminution of phosphorylated endothelial nitric oxide synthase (eNOS), as well as by increased reactive oxygen species (ROS) production, was demonstrated. These alterations in BP, eNOS phosphorylation and ROS production in the vasculature of Ang II-treated mice were markedly and dose-dependently reversed by simultaneous administration of GA (2 and 10 μg kg^{-1} per min). In addition, Ang II-induced ROS production in cultured vascular cells such as endothelial cells and vascular smooth muscle cells was markedly attenuated by GA. These results suggested that GA attenuated the increase in BP via preservation of vascular NO bioavailability not only by inhibiting ROS production but also by preventing the impairment of eNOS function in the vasculature of Ang II-induced hypertensive mice.
Hypertension Research (2012) **35,** 928–934; doi:10.1038/hr.2012.50; published online 26 April 2012

Keywords: angiotensin II; gomisin A; nitric oxide; ROS

INTRODUCTION

An increase in arterial blood pressure (BP) is generally regarded as a major risk factor for heart attack and stroke.[1] Dysfunctional endothelium, characterized by a reduced nitric oxide (NO) production, is recognized as an independent factor for an increase in arterial BP.[2] It is well known that impairment in endothelial nitric oxide synthase (eNOS) activity has an important role in the pathogenesis of endothelial cell dysfunction. Previous studies indicate that eNOS is upregulated by post-translational modifications, such as Akt-induced phosphorylation.[3–4] Thus, a decline in NO bioavailability may be caused by alterations in cellular signaling involved in eNOS phosphorylation as well as by an accelerated NO degradation by reactive oxygen species (ROS).[5]

An increasing body of evidence suggests novel roles for angiotensin II (Ang II) in regulating the balance between NO and ROS in the vasculature.[6–7] Ang II activates NAD(P)H oxidase and induces ROS generation in vascular smooth muscle cells, endothelial cells and intact arteries.[8] An important source of ROS in endothelial and vascular smooth muscle cells is NADPH oxidase.[9–10] Moreover, the strict cross talk between Ang II and NADPH oxidase was also confirmed by *in vivo* studies.[8] Indeed, many of the consequences of Ang II exposure, including hypertension and vascular remodeling, are reportedly related to the formation of ROS.[11–12]

In traditional Korean herbal medicine, *Schisandra chinensis* (SC) has long been used for its antioxidant, tonic and sedative effects. It is also known to have potent antioxidative and anti-inflammatory effects.[13–15] Recently, we demonstrated that gomisin A (GA) isolated from SC induced vasorelaxation in isolated rat thoracic aorta in endothelium-dependent and -independent manners,[16–17] suggesting that GA might prevent the increase in arterial BP, however, the effect of GA on BP in an animal model of hypertension has not been clarified.

In the present study, we evaluated the effect of continuous infusion of GA on the increase in arterial BP in Ang II-induced hypertensive mice. In addition, as GA prevented the loss of NO in isolated blood vessels from Ang II-induced hypertensive mice, we also investigated

[1]Department of Pharmacology, School of Medicine, and MRC for Ischemic Tissue Regeneration, Pusan National University, Gyeongnam, Republic of Korea and [2]College of Natural Resources & Life Sciences, Pusan National University, Gyeongnam, Republic of Korea
[3]These authors contributed equally to this work.
Correspondence: Professor CD Kim, Department of Pharmacology, School of Medicine, and MRC for Ischemic Tissue Regeneration, Pusan National University, Yangsan, Gyeongnam 626-870, Republic of Korea.
E-mail: chidkim@pusan.ac.kr
Received 2 November 2011; revised 14 February 2012; accepted 8 March 2012; published online 26 April 2012

the possible mechanisms involved in GA-mediated preservation of NO bioavailability in the vasculature of Ang II-treated mice.

METHODS

Plant collection and extraction of GA

The fruits of SC were collected in September 2005 from Mungyeong, Korea. A voucher specimen (accession number SC-PDRL-1) was deposited in the Herbarium of Pusan National University. Pure GA was extracted from the dried fruits of SC, and identified by HPLC on a Phenomenex Luna C18 column (Phenomenex, Torrance, CA, USA, 150 × 4.6 mm I.D.; 5 μm particle size). The chemical structure of GA was verified by liquid chromatography-mass spectrometry (LC-MS, Bruker BioApex FT mass spectrometer, Bruker, Billerica, MA, USA) and NMR analysis (Bruker DRX 400 spectrometer, Bruker, Pullman, WA, USA). The solid form of GA (MW = 416.46) was dissolved in DMSO, and subsequently diluted in media in all experiments.

Cell culture

The mouse aorta was dissected, cut into 1–2 mm^2 segments, and then placed as explants in cell culture dishes containing DMEM (Gibco BRL, Grand Island, NY, USA) with 10% fetal bovine serum. VSMC purity was determined by staining with smooth muscle-specific actin monoclonal antibodies (Sigma-Aldrich Co., St Louis, MO, USA).

Human coronary artery endothelial cells and human umbilical vein endothelial cells were obtained from Lonza (Walkersville, MD, USA). Cells were cultured in endothelial growth medium-2 (EGM-2 MV, Lonza). Cells between passages 4 and 6 were used in the present study.

Animals and experimental design

All animal procedures were conducted in accordance with the Animal Care Guidelines of Pusan National University Institutional Animal Care and Use Committee. Male C57BL/6 mice (20–25 g) were implanted with a subcutaneous osmotic minipump (Alzet model 1002, Alza Corp., Vacaville, CA, USA) filled with either Ang II (Sigma Chemical Co., St Louis, MO, USA) or NaCl (sham-treated mice) for 14 days. The average Ang II infusion rate was 1 and 2 $\mu g\,kg^{-1}$ per min. To determine the effects of GA on Ang II-induced hypertension, some animals were treated concomitantly with a subcutaneously implanted osmotic minipump containing GA (2 or 10 $\mu g\,kg^{-1}$ per min) for 14 days. The systolic BP was measured by tail cuff plethysmography with the aid of a computerized system (BP2000 Blood Pressure Analysis System, Visitech Systems, Apex, NC, USA).

Measurement of NO metabolites in plasma

Accumulation of nitrate and nitrite, the end products of NO metabolism used as indices of NOS activity, was measured in plasma as previously described.[18] In brief, plasma samples were deproteinized by ultrafiltration using centrifugal concentrators (Nanosep, Pall Filtron, Northborough, MA, USA). The supernatant was reacted with Griess solution (Promega, Madison, WI, USA) for 15 min. The absorbance of samples was measured at 540 nm on Emax ELISA microplate reader using SoftMax Pro Software (Bio-Tek Instruments Inc., Winooski, VT, USA).

Measurement of vascular concentration of NO

At the end of the study period, the mice were anesthetized with chloral hydrate (450 mg kg^{-1}, i.p.). The thoracic aorta was rapidly excised, and dissected from adhering connective and adipose tissue. For the fluorometric experiments, the aortic rings (3 mm in width) were incubated for 2 h in the dark in Krebs' buffer containing 10 μM DAF-FM DA (Molecular Probes, Karlsruhe, Germany), a fluorescent NO-sensitive dye. The aortic rings were rapidly removed and frozen at −20 °C. Aortic rings were cut into 10 μm-thick sections in a microtome (HM550, MICROM GmbH, Walldorf, Germany) and placed onto microscope slides without any mounting medium or coverslip. Fluorescence was detected using an Axiovert 200 fluorescence microscope (Carl Zeiss, Oberkochem, Germany).

Measurement of ROS

Vascular superoxide anion production was measured using lucigenin-enhanced chemiluminescence method. The aortic ring segments were cryocut into 3 μm thick sections and mounted on gelatin chromalumin-coated slides. The sections were incubated for 30 min with 5 μM DHE. After the sections were washed two times with PBS, fluorescence of DHE was detected using an Axiovert 200 fluorescence microscope (Carl Zeiss).

Intracellular ROS was measured using DCFH-DA (Molecular Probes), which can then react with ROS to form highly fluorescent DCF.[19] The vascular smooth muscle cells and endothelial cells grown in 12-well plates were incubated with 10 μM DCFH-DA for 30 min. After incubation, the cells were washed with PBS, and then the fluorescence of DCFH-DA was detected using an Axiovert 200 fluorescence microscope (Carl Zeiss).

Western blot analysis for eNOS and phosphorylated-eNOS

Mouse aortic tissue was homogenized and equal amounts (20 μg) of protein per sample were separated on 8% SDS-PAGE gels and subsequently transferred to polyvinylidene fluoride membrane. After blocking with 5% skim milk, the membranes were incubated with purified mouse anti-eNOS (1:1000, BD Biosciences) and purified mouse anti-phospho Ser1177 eNOS (1:1000, BD Biosciences) at 4 °C overnight. The membranes were then washed and further incubated with secondary antibody, and the bands were visualized by the addition of enhanced chemiluminescence detection reagents.

Statistics

The results were expressed as mean ± s.e.m. Statistical significance of difference between groups was analyzed by one-way analysis of variance (ANOVA) followed by Tukey's multiple comparison test using statistical software (Prism, version 3.03; GraphPad Software Inc., San Diego, CA, USA). $P<0.05$ was regarded as significant.

RESULTS

Characterization of Ang II-induced hypertension

At the beginning of the experiment, BP of control and Ang II (1 and 2 μg kg per min)-treated mice were 93.5 ± 4.1, 98.1 ± 3.0 and 91.6 ± 4.1 mm Hg, respectively. While the BP of control mice remained constant throughout the period of investigation, the BP of Ang II (1 and 2 $\mu g\,kg^{-1}$ per min)-treated mice started to increase at day 4 and peaked at day 6 of the experimental period (139.9 ± 5.7 mm Hg), and then the elevated BP was sustained at a high level for 14 days. The effects of Ang II at 2 $\mu g\,kg^{-1}$ per min on BP were more prominent and stable than those at 1 $\mu g\,kg^{-1}$ per min (Figure 1). However, there were no significant differences between groups with regard to heart rates (517 ± 20 beats per min in control group, 544 ± 59 and 546 ± 29 beats per min in Ang II 1 and 2 $\mu g\,kg^{-1}$ per min-treated groups, respectively).

Role of Ang II on vascular NO production

In good agreement with previous reports in which Ang II inhibited eNOS activity,[20–21] NO concentration was diminished in aortic tissues from Ang II-treated mice compared with those from control mice (Figure 2a). Likewise, the concentration of nitrate/nitrite, metabolites of NO, was also diminished in the plasma of Ang II-treated mice in a dose-dependent manner (Figure 2b). When the relationship between systolic BP and plasma concentration of nitrites was examined in each mouse, systolic BP was found to be negatively correlated with plasma concentration of NO metabolites (Figure 2c). This suggests that the elevation in BP in Ang II-treated mice may be a consequence of reduction in the bioavailability of NO.

Antihypertensive effect of GA on Ang II-induced hypertension

As the effects of Ang II at 2 $\mu g\,kg^{-1}$ per min on BP were more prominent and stable than those at 1 $\mu g\,kg^{-1}$ per min, the following

experiments were performed in mice treated with Ang II at 2 μg kg^{-1} per min. As shown in Figure 3, concomitant treatment with GA (2 and 10 μg kg^{-1} per min) in Ang II-treated mice significantly attenuated the increase in BP in a dose-dependent manner. However, there were no significant differences between groups with regard to heart rates (546 ± 29 beats per min in control group; 532 ± 47 and 542 ± 67 beats per min in GA 2 and 10 μg kg^{-1} per min-treated groups, respectively).

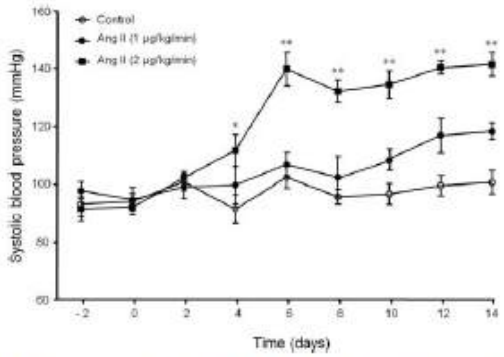

Figure 1 Effect of Ang II infusion on systolic blood pressure. Time course of systolic blood pressure in C57BL/6 mice treated with a subcutaneous osmotic minipump filled with Ang II (1 and 2 μg kg^{-1} per min) for 14 days. Data were expressed as mean ± s.e.m. from 5–7 independent experiments. $^{*}P<0.05$, $^{**}P<0.01$ vs. corresponding value in control.

Effect of GA on impaired NO production in Ang II-treated mice

Vascular NO production as assayed with DAF-FM DA was markedly reduced in Ang II-infused animals compared with controls. With simultaneous chronic administration of GA (2 and 10 μg kg^{-1} per min) in Ang II-induced hypertensive mice, the diminished NO concentration in isolated aorta from Ang II-treated mice was restored in a dose-dependent manner (Figure 4a). In line with vascular production of NO, the decreased plasma concentration of NO

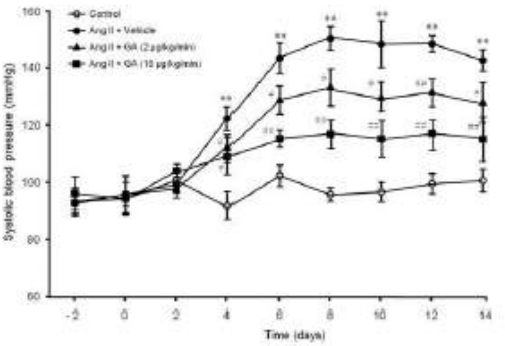

Figure 3 Preventive effect of GA on Ang II-induced hypertension. Time course of systolic blood pressure in Ang II-induced hypertensive mice treated with various concentrations of GA. Data are expressed as mean ± s.e.m. from 7–13 independent experiments. $^{**}P<0.01$ vs. corresponding value in control. $^{\#}P<0.05$; $^{\#\#}P<0.01$ vs. corresponding value in vehicle group.

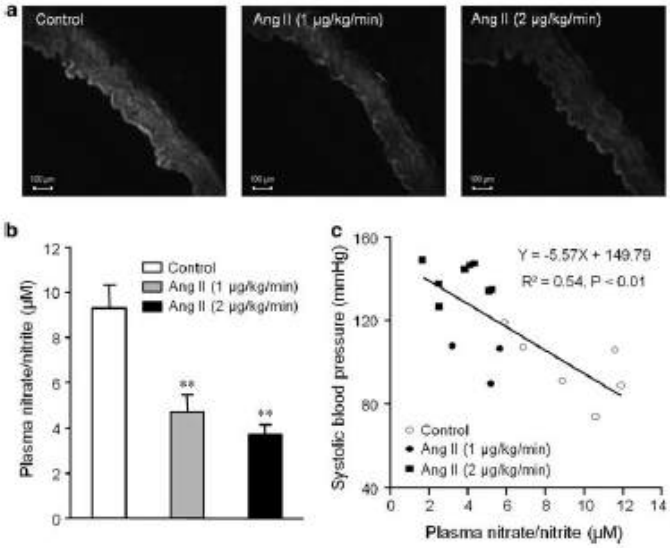

Figure 2 Effect of Ang II infusion on NO production. (**a**) Vascular NO production in aortic segments from control and Ang II-treated mice were measured by DAF2-FM staining. Photographs are representative of five independent experiments. (**b**) Plasma concentration of NO metabolites as an index for plasma NO concentration from control and Ang II-treated mice was measured by Griess reagent. Data are expressed as mean ± s.e.m. from 4–7 independent experiments. $^{**}P<0.01$ vs. control. (**c**) Interaction between blood pressure and plasma nitrate/nitrite concentration in each mouse shows a negative correlation. A full color version of this figure is available at the *Hypertension Research* journal online.

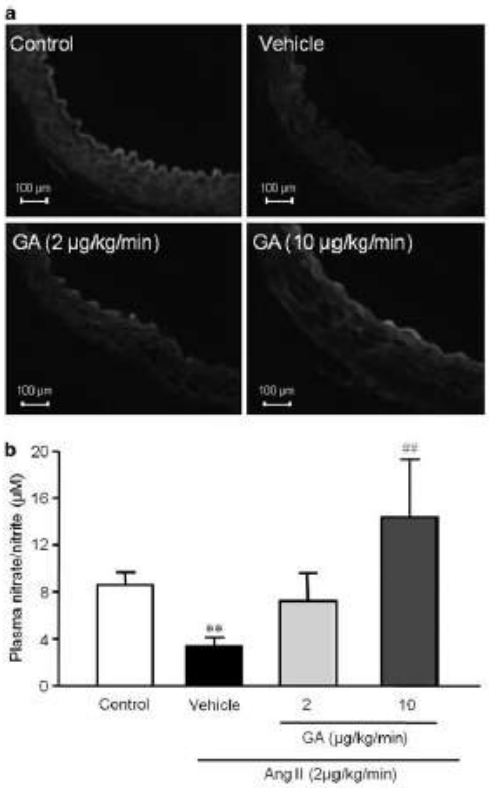

Figure 4 Effect of GA on impaired NO production in Ang II-treated mice. (**a**) Representative photographs of the preservation of NO production by GA in aortic tissues from Ang II-treated mice ($n=4$). (**b**) The decreased plasma concentration of NO metabolites in Ang II-treated mice was significantly preserved by simultaneous chronic administration of GA (2 and 10 μg kg^{-1} per min). Data were expressed as mean±s.e.m. from 4–7 independent experiments. $^{**}P<0.01$ vs. control. $^{\#\#}P<0.01$ vs. vehicle. A full color version of this figure is available at the *Hypertension Research* journal online.

metabolites in Ang II-treated mice was also significantly preserved by GA treatment (2 and 10 μg kg^{-1} per min) (Figure 4b).

Effect of GA on impaired eNOS activity in Ang II-treated mice

Phosphorylation of eNOS at Ser1177 enhances eNOS activity.[22] Thus, to assess the involvement of Ang II in the regulation of eNOS activity, we studied the effects of Ang II on the level of eNOS and phosphorylated-eNOS protein expression in aortic tissues from control and Ang II-treated mice. As shown in Figures 5a and b, the expression level of phosphorylated-eNOS at Ser1177, but not eNOS expression, was markedly diminished in aortic tissue from Ang II-treated mice as compared with those from control mice. This attenuation in eNOS phosphorylation was inhibited by simultaneous treatment with GA in a dose-dependent manner.

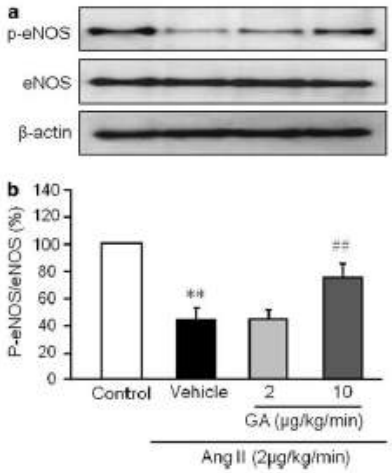

Figure 5 Effect of GA on impaired eNOS phosphorylation at Ser1177 in Ang II-treated mice. (**a**) Levels of phosphorylated eNOS (p-eNOS) at Ser1177, eNOS and β-actin protein were determined by western blot analysis. One representative blot out of six independent experiments is shown. (**b**) Each bar represents mean±s.e.m. from 4–6 independent experiments. $^{**}P<0.01$ vs. control. $^{\#\#}P<0.01$ vs. vehicle.

Effects of GA on Ang II-enhanced ROS production

Ang II is known as a regulatory factor in vascular oxidation–reduction signaling to enhance superoxide production.[9] Likewise, ROS production as measured by DHE was significantly increased in isolated aorta from Ang II-treated mice. The increased ROS production by Ang II was markedly attenuated in the aortic tissues from Ang II-treated mice with simultaneous treatment of GA (Figure 6a). Likewise, when vascular cells such as vascular smooth muscle cell and endothelial cells were exposed to Ang II (1–10 μM) for 24 h, ROS production in cells was gradually increased in a concentration-dependent manner (data not shown). The Ang II (10 μM)-induced increase in ROS production in cultured vascular cells was also markedly attenuated by pretreatment with GA (1–10 μM) in a dose-dependent manner (Figure 6b).

DISCUSSION

The present study provides evidence that increased arterial BP in mice infused subcutaneously with Ang II was markedly attenuated by chronic administration of GA. The beneficial effects of GA on Ang II-induced hypertension were associated with preservation of NO bioavailability in the vasculature. Moreover, GA treatment in this study was started at the prehypertensive stage, suggesting that GA had a prophylactic effect against the development of hypertension induced by Ang II.

Disruption of the NO pathway by L-NAME was demonstrated by reduced plasma nitrate/nitrite levels.[23] Similarly, long-term treatment with Ang II also resulted in a significant reduction in the acetylcholine-induced increase in plasma NO concentration in rabbits.[24] In the Ang II-infused rat model by Mollnau *et al.*[25] showed that NO in the aortic segments was markedly reduced. In line with these previous studies, in mice infused subcutaneously with Ang II, we also found an increase in arterial BP with a decrease in NO

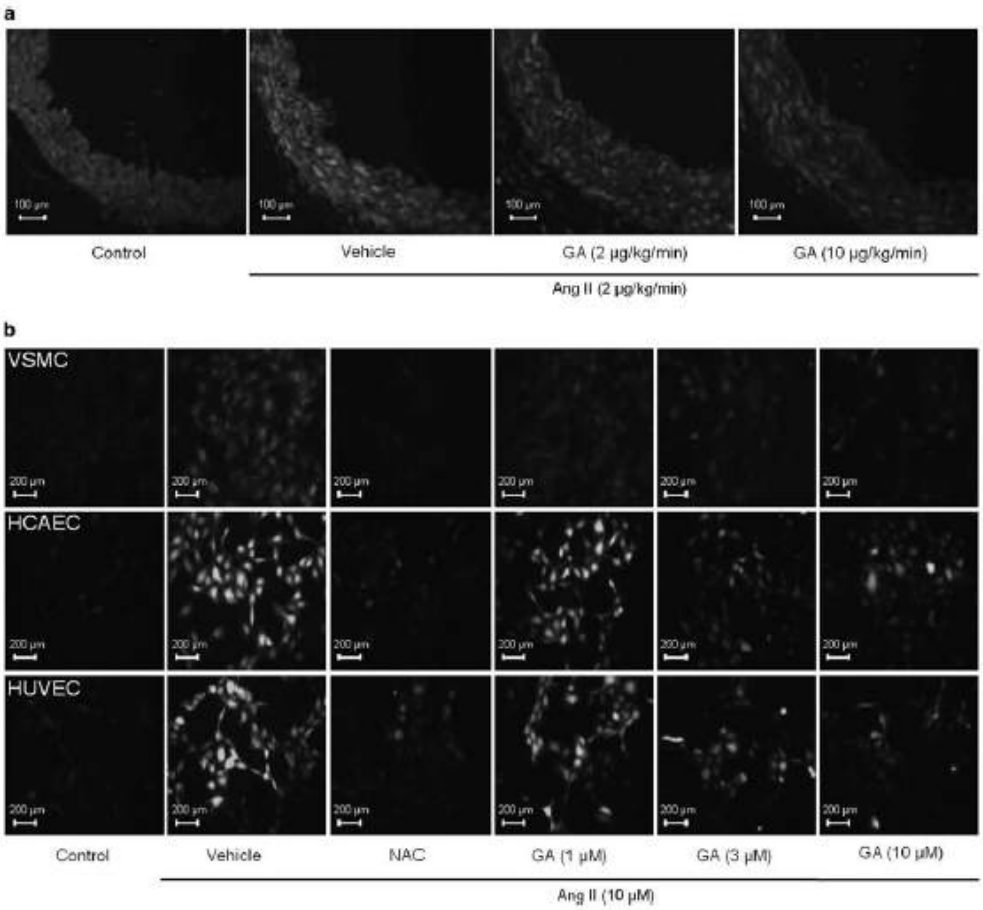

Figure 6 Effects of GA on Ang II-enhanced ROS production. (**a**) Representative photographs of ROS production as measured by DHE in aortic tissues from control, Ang II-treated mice without or with simultaneous treatment of GA ($n=5$). (**b**) Vascular smooth muscle cells (VSMC), human coronary artery endothelial cell (HCAEC) and umbilical vein endothelial cell (HUVEC) were exposed to Ang II (10 μM) for 24 h, and then ROS production in cells was determined using DCF fluorescence. Photographs are representative of 5–6 experiments. A full color version of this figure is available at the *Hypertension Research* journal online.

metabolites in plasma, and a negative correlation between these two parameters. Thus, the dysfunctional endothelium, characterized by less production of NO as well as a decrease in NO bioavailability, appeared to lead to an increase in arterial BP in Ang II-infused mice.

A decline in NO bioavailability may be caused by alterations in cellular signaling involved in eNOS activation or by accelerated NO degradation by ROS.[26] Our study showed that the decreased plasma concentration of NO metabolites in Ang II-treated mice was accompanied by diminished NO concentration in the aortic segments, suggesting a potential relationship between these two parameters. Moreover, the decreased level of NO in the vasculature might result from a decrease in NO synthesis by inhibition of eNOS activity or an increase in NO inactivation by enhanced vascular production of ROS.

To determine the involvement of Ang II in the regulation of eNOS activity, we studied the effects of Ang II on the level of eNOS and phosphorylated-eNOS protein expression in aortic tissues from control and Ang II-treated mice. In the segments of aorta isolated from mice treated with Ang II, a clear impairment in endothelial function was observed; however, eNOS expression was unaltered by Ang II treatment.[27] In line with this report, our present results showed that expression level of phosphorylated-eNOS at Ser1177, but not eNOS expression, was markedly diminished in the aortic tissue from Ang II-treated mice compared with those from control mice. Thus, it was suggested that the impaired vascular production of NO might be partially involved in the decrease in NO bioavailability in Ang II-treated mice, subsequently leading to an increase in arterial BP.

Many of the consequences of Ang II exposure, including hypertension and vascular remodeling, are reportedly related to ROS formation as a consequence of the activation of NADPH oxidases.[11,28] Sachse and Wolf[29] also provide evidence that Ang II stimulates intracellular formation of superoxide by upregulating subunits of the membrane-bound NAD(P)H oxidase and by facilitating assembly of subunits. In endothelial cells, Ang II activates mainly the Nox2 (gp91phox) and Nox4 subunits, and genetic disruption of Nox2 prevents the endothelial dysfunction observed in a high-renin model of hypertension.[30] We therefore assessed ROS production in the vasculature isolated from Ang II-infused mice. Our present study clearly showed that ROS production in the aortic tissue from Ang II-treated mice was markedly increased. Moreover, in an *in vitro* study using VSMC and endothelial cells to determine the cellular source for Ang II-induced ROS generation, Ang II enhanced ROS generation in endothelial cells as well as in VSMC. Thus, it was suggested that hypertension caused by Ang II was mediated in part via a decrease in NO bioavailability by an increased production of ROS in the vasculature.

Traditionally, SC has been used as a Korean herbal medicine for its antioxidant, antitussive, tonic and sedative effects. SC fruits contain a variety of pharmacologically active lignans. GA and the major bioactive compounds are lignans with a dibenzocyclooctadiene skeleton.[15,31–32] We recently showed that GA induced vasorelaxation in isolated rat thoracic aorta in an endothelium-dependent and -independent manner.[16] Moreover, GA enhanced NO production by activation of eNOS in human coronary endothelial cells.[17] Our previous reports describing a pivotal role of GA in vascular relaxation[16-17] suggest that GA might have a potential role in the prevention of hypertension induced by various causes.

In the present study, chronic administration of Ang II into mice caused an increase in arterial BP with a diminished plasma concentration of NO metabolites, which was prevented by continuous infusion of GA. The effect of GA on NO bioavailability in Ang II-infused mice might result from its preventive roles on impaired NO synthesis or increased NO inactivation by ROS. To determine the role of GA in NO synthesis, the effect of GA on the regulation of eNOS activity was investigated. The present study showed that GA attenuated the decrease in phosphorylated-eNOS (Ser1177) expression, leading to restoration of diminished plasma nitrate/nitrite levels. In our previous study, GA rapidly stimulated NO production and eNOS activation via enhanced eNOS translocation with little effect on the expression of both total eNOS and phosphorylated-eNOS protein.[17] Likewise, the level of eNOS expression in the endothelial layer of the thoracic aorta from Ang II-treated mice was neither decreased compared with that in control nor affected by GA treatment. Interestingly, although GA did not enhance eNOS phosphorylation in endothelial cells in our previous study,[17] our present study showed that the diminished level of phosphorylated-eNOS in Ang II-treated mice was instead markedly preserved in mice treated with GA. This indicates that GA might have a preventive role in Ang II-induced impairment of eNOS phosphorylation without affecting eNOS phosphorylation in the resting state. However, further experiments are necessary to determine the effect of GA on the cross-talk between Ang II and eNOS function.

Moreover, the increased ROS production in isolated aorta from Ang II-treated mice was markedly attenuated in the aortic tissues from Ang II-treated mice co-treated with GA. In addition, in agreement with previous studies in which Ang II enhanced ROS production in endothelial cells and vascular smooth muscle cells,[33–34] this study also showed that Ang II increased ROS in vascular cells. In line with the results from the *in vivo* study, Ang II-induced ROS production in cultured vascular cells was also markedly attenuated by pretreatment with GA. Recently, it was reported that treatment with antioxidants blunted the increase in BP caused by Ang II.[23,35] Likewise, the results of our present study suggested that the antioxidative property-related protection against ROS-mediated degradation of NO in the vasculature may contribute at least partly to the antihypertensive effect of GA.

In conclusion, chronic administration of GA had an antihypertensive effect in Ang II-induced hypertensive mice. Its beneficial effects on NO bioavailability, which are mediated by preservation of vascular NO, seem to be related to the antihypertensive activity. Based on these results, it was suggested that GA attenuated the increase in arterial BP *via* preservation of vascular NO bioavailability not only by inhibiting ROS production but also by preventing the impairment of eNOS function in the vasculature of Ang II-induced hypertensive mice.

CONFLICT OF INTEREST

The authors declare no conflict of interest.

ACKNOWLEDGEMENTS

This study was supported by the MRC Program of the MEST/KOSEF (2005-0049477), Bio-industry Technology Development Program and Ministry for Food, Agriculture, Forestry and Fisheries, Republic of Korea (311054-03-1-HD120).

1 Ngueleack TB, Dongmo AB, Dimo T, Kamanyi A. Phytopharmacology of some medicinal plants used in Cameroonian traditional medicine to handle cardiovascular diseases. In Anna Capasso (ed) *Recent Developments in Medicinal Plant Research*, 2007, pp 147–167. ISBN 978-81-308-0160-5.
2 Davignon J, Ganz P. Role of endothelial dysfunction in atherosclerosis. *Circulation* 2004; **109**: III27–III32.
3 Fulton D, Gratton JP, Sessa WC. Post-translational control of endothelial nitric oxide synthase: why isn't calcium/calmodulin enough? *J Pharmacol Exp Ther* 2001; **299**: 818–824.
4 Venema RC. Post-translational mechanisms of endothelial nitric oxide synthase regulation by bradykinin. *Int Immunopharmacol* 2002; **2**: 1755–1762.
5 Schulz E, Jansen T, Wenzel P, Daiber A, Münzel T. Nitric oxide, tetrahydrobiopterin, oxidative stress, and endothelial dysfunction in hypertension. *Antioxid Redox Signal* 2008; **10**: 1115–1126.
6 Watanabe T, Barker TA, Berk BC. Angiotensin II and the endothelium: diverse signals and effects. *Hypertension* 2005; **45**: 163–169.
7 Nakashima H, Suzuki H, Ohtsu H, Chao JY, Utsunomiya H, Frank GD, Eguchi S. Angiotensin II regulates vascular and endothelial dysfunction: recent topics of angiotensin II type-1 receptor signaling in the vasculature. *Curr Vasc Pharmacol* 2006; **4**: 67–78.
8 Virdis A, Duranti E, Taddei S. Oxidative stress and vascular damage in hypertension: role of angiotensin II. *Int J Hypertens* 2011; **2011**: 916310.
9 Griendling KK, Minieri CA, Ollerenshaw JD, Alexander RW. Angiotensin II stimulates NADH and NADPH oxidase activity in cultured vascular smooth muscle cells. *Circ Res* 1994; **74**: 1141–1148.
10 Somers MJ, Mavromatis K, Galis ZS, Harrison DG. Vascular superoxide production and vasomotor function in hypertension induced by deoxycorticosterone acetate-salt. *Circulation* 2000; **101**: 1722–1728.
11 Garrido AM, Griendling KK. NADPH oxidases and angiotensin II receptor signaling. *Mol Cell Endocrinol* 2009; **302**: 148–158.
12 Murdoch CE, Alom-Ruiz SP, Wang M, Zhang M, Walker S, Yu B, Brewer A, Shah AM. Role of endothelial Nox2 NADPH oxidase in angiotensin II-induced hypertension and vasomotor dysfunction. *Basic Res Cardiol* 2011; **106**: 527–538.
13 Chen DF, Zhang SX, Xie L, Xie JX, Chen K, Kashiwada Y, Zhou BN, Wang P, Cosentino LM, Lee KH. Anti-AIDS agents-XXVI. Structure-activity correlations of gomisin-G-related anti-HIV lignans from Kadsura interior and of related synthetic analogues. *Bioorg Med Chem* 1997; **5**: 1715–1723.
14 Chiu PY, Mak DH, Poon MK, Ko KM. *In vivo* antioxidant action of a lignan-enriched extract of schisandra fruit and an anthraquinone-containing extract of polygonum root in comparison with schisandrin B and emodin. *Planta Med* 2002; **68**: 951–956.
15 Choi YW, Takamatsu S, Khan SI, Srinivas PV, Ferreira D, Zhao J, Khan IA. Schisandrene, a dibenzocyclooctadiene lignan from Schisandra chinensis: structure-antioxidant activity relationships of dibenzocyclooctadiene lignans. *J Nat Prod* 2006; **69**: 356–359.

16 Park JY, Lee SJ, Yun MR, Seo KW, Bae SS, Park JW, Lee YJ, Shin W, Choi YW, Kim CD. Gomisin A from Schisandra chinensis induces endothelium-dependent and direct relaxation in rat thoracic aorta. *Planta Med* 2007; **73**: 1537–1542.
17 Park JY, Shin HK, Choi YW, Lee YJ, Bae SS, Han J, Kim CD. Gomisin A induces Ca^{2+}-dependent activation of eNOS in human coronary artery endothelial cells. *J Ethnopharmacol* 2009; **125**: 291–296.
18 Kukongviriyapan V, Sompam N, Senggunprai L, Prawan A, Kukongviriyapan U, Jetsrisuparb A. Endothelial dysfunction and oxidant status in pediatric patients with hemoglobin E-beta thalassemia. *Pediatr Cardiol* 2008; **29**: 130–135.
19 Amer J, Goldfarb A, Fibach E. Flow cytometric measurement of reactive oxygen species production by normal and thalassaemic red blood cells. *Eur J Haematol* 2003; **70**: 84–90.
20 Lin LY, Lin CY, Su TC, Liau CS. Angiotensin II-induced apoptosis in human endothelial cells is inhibited by adiponectin through restoration of the association between endothelial nitric oxide synthase and heat shock protein 90. *FEBS Lett* 2004; **574**: 106–110.
21 Marrero MB, Venema VJ, Ju H, He H, Liang H, Caldwell RB, Venema RC. Endothelial nitric oxide synthase interactions with G-protein-coupled receptors. *Biochem J* 1999; **343**: 335–340.
22 Sessa WC. eNOS at a glance. *J Cell Sci* 2004; **117**: 2427–2429.
23 Nakmareong S, Kukongviriyapan U, Pakdeechote P, Donpunha W, Kukongviriyapan V, Kongyingyoes B, Sompamit K, Phisalaphong C. Antioxidant and vascular protective effects of curcumin and tetrahydrocurcumin in rats with L-NAME-induced hypertension. *Naunyn Schmiedebergs Arch Pharmacol* 2011; **383**: 519–529.
24 Imanishi T, Kobayashi K, Kuroi A, Mochizuki S, Goto M, Yoshida K, Akasaka T. Effects of angiotensin II on NO bioavailability evaluated using a catheter-type NO sensor. *Hypertension* 2006; **48**: 1058–1065.
25 Mollnau H, Wendt M, Szocs K, Lassegue B, Schulz E, Oelze M, Li H, Bodenschatz M, August M, Kleschyov AL, Tsilimingas N, Walter U, Forstermann U, Meinertz T, Griendling K, Munzel T. Effects of angiotensin II on the expression and function of NAD(P)H oxidase and components of nitric oxide/cGMP signaling. *Circ Res* 2002; **90**: e58–e65.
26 Cai H, Harrison DG. Endothelial dysfunction in cardiovascular diseases the role of oxidant stress. *Circ Res* 2000; **87**: 840–844.
27 Loot AE, Schreiber JG, Fisslthaler B. Angiotensin II impairs endothelial function via tyrosine phosphorylation of the endothelial nitric oxide synthase. *J Exp Med* 2009; **206**: 2889–2896.
28 Ikeda Y, Aihar K, Yoshida S, Sato T, Yagi S, Iwase T, Sumitomo Y, Ise T, Ishikawa K, Azuma H, Akaike M, Kato S, Matsumoto T. Androgen-androgen receptor system protects against angiotensin II-induced vascular remodeling. *Endocrinology* 2009; **150**: 2857–2864.
29 Sachse A, Wolf G. Angiotensin II-induced reactive oxygen species and the kidney. *J Am Soc Nephrol* 2007; **18**: 2439–2446.
30 Jung O, Schreiber JG, Geiger H, Pedrazzini T, Busse R, Brandes RP. gp91 phox-containing NADPH oxidase mediates endothelial dysfunction in renovascular hypertension. *Circulation* 2004; **109**: 1795–1801.
31 Kuo YH, Kuo LM, Chen CF. Four new C19 homolignans, schiarisanrins A, B, and D and cytotoxic schiarisanrin C, from Schizandra arisanensis. *J Org Chem* 1997; **62**: 3242–3245.
32 Chen YG, Qin GW, Xie YY, Cheng KF, Lin ZW, Sun HD, Kang YH, Han BH. Lignans from Kadsura angustifolia. *J Asian Nat Prod Res* 1998; **1**: 125–131.
33 Zhang H, Schmeisser A, Garlichs CD, Plötze K, Damme U, Mügge A, Daniel WG. Angiotensin II-induced superoxide anion generation in human vascular endothelial cells: role of membrane-bound NADH-/NADPH-oxidases. *Cardiovasc Res* 1999; **44**: 215–222.
34 Lavigne MC, Malech HL, Holland SM, Leto TL. Genetic demonstration of p47phox-dependent superoxide anion production in murine vascular smooth muscle cells. *Circulation* 2001; **104**: 79–84.
35 Virdis A, Neves MF, Amiri F, Touyz RM, Schiffrin EL. Role of NAD(P)H oxidase on vascular alterations in angiotensin II-infused mice. *J Hypertens* 2004; **22**: 535–542.

Biochemical and Biophysical Research Communications 427 (2012) 547–552

Contents lists available at SciVerse ScienceDirect

Biochemical and Biophysical Research Communications

journal homepage: www.elsevier.com/locate/ybbrc

Therapeutic effects of α-iso-cubebenol, a natural compound isolated from the *Schisandra chinensis* fruit, against sepsis

Sung Kyun Lee [a,b], Sang Doo Kim [a], Minsoo Kook [a], Ha Young Lee [a,b], Joon Seong Park [c], Young Hoon Park [d], Jum Soon Kang [d], Won Jung Jung [d], Young Whan Choi [d,*], Yoe-Sik Bae [a,b,e,*]

[a] Department of Biological Sciences, Sungkyunkwan University, Suwon 440-746, South Korea
[b] Mitochondria Hub Regulation Center, Dong-A University, Busan 602-714, South Korea
[c] Department of Hematology–Oncology, Ajou University School of Medicine, Suwon 443-721, South Korea
[d] Department of Horticultural Bioscience, College of Natural Resources and Life Science, Pusan National University, Miryang 627-706, South Korea
[e] Samsung Advanced Institute for Health Sciences and Technology, Sungkyunkwan University, Seoul 135-710, South Korea

ARTICLE INFO

Article history:
Received 13 September 2012
Available online 26 September 2012

Keywords:
Sepsis
α-Iso-cubebenol
Inflammation
Organ failure

ABSTRACT

α-Iso-cubebenol, a natural compound isolated from the *Schisandra chinensis* fruit, strongly enhances survival rate in cecal ligation and puncture (CLP) challenge-induced sepsis. Mechanistically, α-iso-cubebenol markedly reduces viable bacteria in the peritoneal fluid and peripheral blood, by increasing production of superoxide anion. α-Iso-cubebenol also significantly attenuates widespread immune cell apoptosis in a mouse CLP sepsis model, and inhibits the production of proinflammatory cytokines including interleukin-1β (IL-1β) and IL-6 in CLP mice and lipopolysaccharide-stimulated splenocytes. Taken together, the results indicate that α-iso-cubebenol can reverse the progression of septic shock by triggering multiple protective downstream signaling pathways to enhance microbial killing and maintain organ function and leukocyte survival.

1. Introduction

Sepsis, a systemic inflammatory response, is caused by viable bacteria or bacterial products such as lipopolysaccharide (LPS) [1]. More than 750,000 patients develop sepsis annually in the United States, and the incidence rate is gradually increasing [2]. The number of hospitalizations with sepsis in the US increased from 300,000 to around 800,000 from 2000 to 2007 [3]. Although the mortality rate of sepsis decreased somewhat from 2000 to 2007, sepsis remains the major cause of death in intensive care units, and the overall mortality associated with sepsis ranges from 30% to 70% [2]. Only 2% of hospitalizations are for sepsis, yet it makes up 17% of in-hospital deaths in the US [4]. Sepsis-induced lethality is accompanied by the failure of an appropriate immune response against invading pathogens [5,6]. The inability of the innate immune system to respond during early sepsis (i.e., the first 6 h) results in increased mortality. Excessive lymphocyte apoptosis can occur during sepsis, which results in the clinical signs of multi-organ failure [7,8]. Since sepsis is caused by viable bacteria or bacterial products, the levels of proinflammatory cytokines such as tumor necrosis factor (TNF) and interleukin (IL)-1β are substantially increased during sepsis [9–11]. Thus, an effective treatment for sepsis should control bacteria, prevent production of inflammatory cytokines, and block widespread leukocyte apoptosis.

We previously isolated a novel natural compound, α-iso-cubebenol, from the *Schisandra chinensis* fruit and demonstrated that the compound inhibits inducible nitric oxide synthase and cyclooxygenase-2 expression in lipopolysaccharide (LPS)-stimulated macrophages [12]. Subsequently, α-iso-cubebenol has been reported to induce heme oxygenase-1 expression and have anti-inflammatory activity in *Porphyromonas gingivalis* LPS-stimulated macrophages [13]. In this study we investigated the *in vivo* efficacy of α-iso-cubebenol in a preclinical mouse model of sepsis. We also examined the mechanisms of septic protection by this novel natural compound.

2. Materials and methods

2.1. Purification of α-iso-cubebenol

α-Iso-cubebenol (CAS registry number: 1219105-52-8) was purified from the dried fruit of *S. chinensis* as described previously [12]. The fruit of *S. chinensis* (Turcz.) Baill was collected in September 2005 from Moonkyong, Korea. A voucher specimen (Accession

* Corresponding authors. Addresses: Department of Horticultural Bioscience, College of Natural Resources and Life Science, Pusan National University, Miryang 627-706, South Korea. Fax: +82 55 350 5529 (Y.W. Choi), Department of Biological Sciences, Sungkyunkwan University, Suwon 440-746, South Korea. Fax: +82 31 290 7015 (Y.-S. Bae).
E-mail addresses: ywchoi@pusan.ac.kr (Y.W. Choi), yoesik@skku.edu (Y.-S. Bae).

0006-291X/$ - see front matter © 2012 Elsevier Inc. All rights reserved.
http://dx.doi.org/10.1016/j.bbrc.2012.09.094

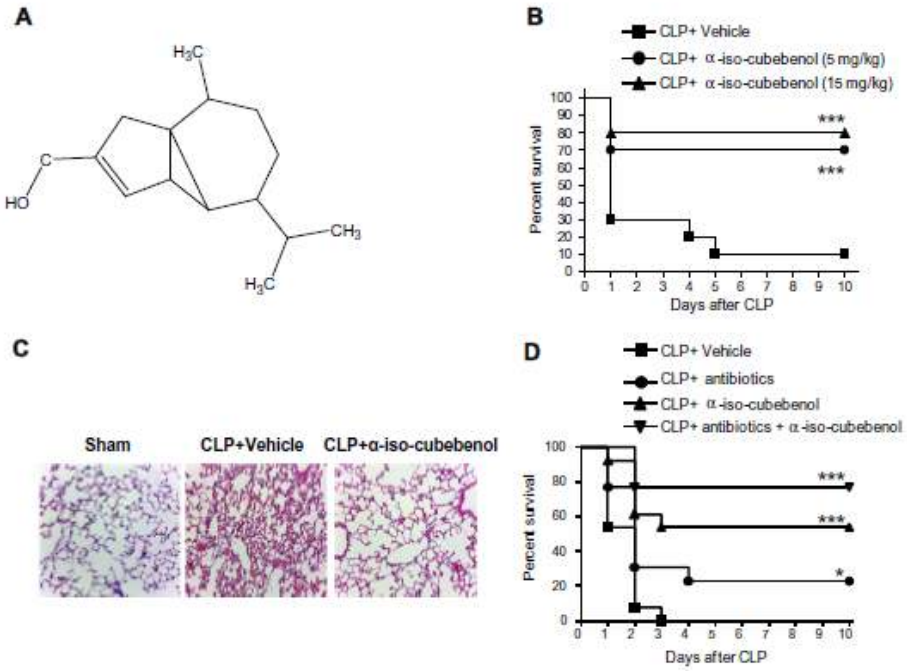

Fig. 1. α-iso-cubebenol protects against CLP-induced mortality. (A) The chemical structure of α-iso-cubebenol. (B) Several doses (0, 5, 15 mg/kg) of α-iso-cubebenol were injected subcutaneously four times into CLP mice at 2, 14, 26, and 38 h post-CLP. (C) Vehicle (0.8% DMSO in PBS) or α-iso-cubebenol (15 mg/kg) was administered 2 and 14 h after CLP. The mice were sacrificed 24 h after surgery and the lungs stained with hematoxylin and eosin (magnification, 100×). (D) Vehicle (0.8% DMSO in PBS), α-iso-cubebenol (15 mg/kg) or antibiotics (10 mg/kg gentamycin plus 10 mg/kg cephalosporin), or α-iso-cubebenol plus antibiotics were injected subcutaneously four times into CLP mice at 2, 14, 26, and 38 h post-CLP. $^{*}P < 0.05$, $^{***}P < 0.001$ compared to vehicle control by ANOVA (B and D). Sample size: $n = 10$ mice/group (B) or 13 mice/group (D). The data are representative of 8 mice/group (C).

No. SC-PDRL-1) has been deposited in the Herbarium of Pusan National University. The plant was identified by one of the authors (Y. Choi). The dried fruit of *S. chinensis* (2.5 kg) ground to a fine powder and then successively extracted at room temperature with *n*-hexane, $CHCl_3$, and MeOH. The hexane extract (308 g) was evaporated *in vacuo* and chromatographed on a silica gel (40 μm; Baker, Phillipsburg, NJ, USA) column (100 × 10 cm) with a step gradient of EtOAc in hexane (0%, 5%, and 20%) and 5% MeOH in $CHCl_3$ to obtain 38 fractions as described [14]. Fraction 9 (KH9, 4866 mg) was separated on a silica gel column (100 × 3.0 cm) with a step gradient (1%, 10%, and 15%) of acetone in $CHCl_3$ to obtain 21 fractions. Of these 21 fractions, fraction 2 (KH9IG, 529.9 mg) was separated on a silica gel column (100 × 3.0 cm) with 5% acetone in $CHCl_3$ to yield α-iso-cubebenol (162.9 mg). Pure α-iso-cubebenol was identified by HPLC on a Phenomenex Luna C18 column (150 × 4.6 mm internal diameter, 5 μm particle size; Phenomenex, Los Angeles, CA, USA) with a methanol–acetonitrile gradient, at a flow rate of 1.0 ml/min. The purity of α-iso-cubebenol was over 96%.

2.2. Animals and sepsis model

Six week old male wild type ICR mice were used as an experimental sepsis model as described [15]. For cecal ligation and puncture (CLP), mice were anesthetized with intraperitoneal injections of Zoletil (50 mg/kg) and Rompun (10 mg/kg), after which a small abdominal midline incision was made to expose the cecum. The cecum was then ligated below the ileocecal valve, punctured twice through both surfaces (or once for measurement of cytokine production) using a 22-gauge needle, and the abdomen was closed. Sham CLP mice were subjected to the same procedure but without ligation and puncture of the cecum. Survival was monitored once daily for 10 days.

2.3. Measurement of bactericidal activity in vivo

Twenty-four hours after CLP, peritoneal lavage fluid and peripheral blood were collected and cultured overnight on blood-agar base plates (Trypticase Soy Agar Deeps; Becton Dickinson, Franklin Lakes, NJ, USA) at 37 °C. Colony forming units (CFUs) were determined as described previously [15].

2.4. Measurement of phagocytic activity

Raw 264.7 cells (2×10^5) were resuspended in 100 μl phosphate-buffered saline (PBS) containing 1% human AB serum and 0.02% sodiumazide, preincubated with or without α-iso-cubebenol for 30 min. The cells were further incubated with FITC-dextran (1 mg/ml) at 37 °C for 30 min. The incubations were stopped by adding 2 ml ice-cold PBS containing 1% human serum. After fixing the cells with 3.7% formaladehyde, phagocytic uptake was analyzed on a flow cytometer (FACS Canto II).

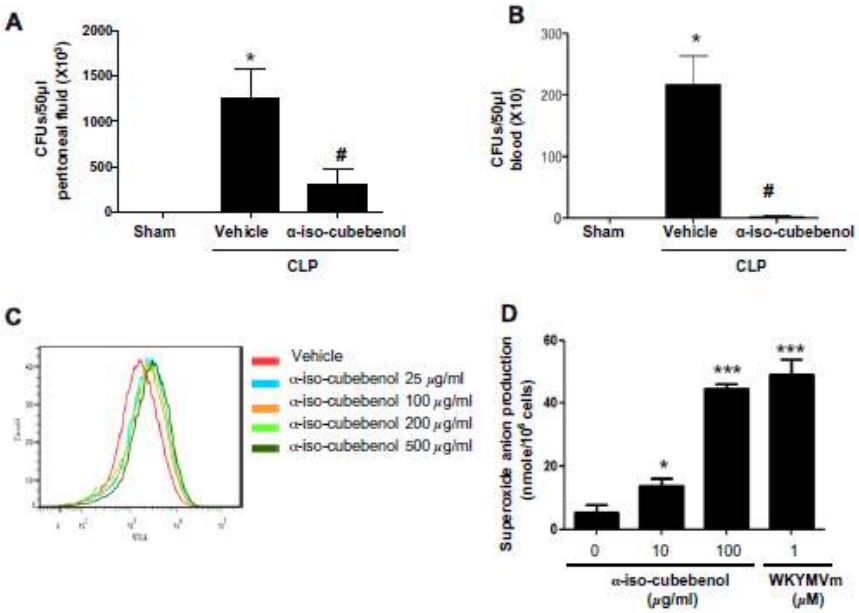

Fig. 2. α-Iso-cubebenol stimulates bactericidal activity. (A and B) Vehicle (0.8% DMSO in PBS) or α-iso-cubebenol (15 mg/kg) was injected two times into CLP mice 2 and 14 h post-CLP. Peritoneal lavage fluid (A), or peripheral blood (B) collected 24 h after sham operation, CLP, or CLP plus α-iso-cubebenol administration was cultured overnight on blood-agar base plates at 37 °C, and CFUs were determined. (C) Raw 264.7 cells (2×10^5) were resuspended in 100 μl PBS and preincubated with or without α-iso-cubebenol for 30 min. Then the cells were further incubated with FITC-dextran (1 mg/ml) at 37 °C for 30 min. After fixing the cells, phagocytic uptake was analyzed on a flow cytometer. The result is representative of three independent experiments. (D) Freshly isolated human neutrophils were stimulated with vehicle (0.1% DMSO in PBS) or α-iso-cubebenol (10 or 100 μg/ml) for 5 min. The amount of superoxide anions produced from neutrophils was measured using a cytochrome c reduction assay. Data are expressed as the mean ± SEM; n = 8. *, $P < 0.05$, compared with the value obtained from the sham control (A, B); #, $P < 0.05$, significantly different from the CLP alone control (A, B). *$P < 0.05$; ***$P < 0.001$ compared to the vehicle control (D).

2.5. Measurement of superoxide anion production

Superoxide anion generation was determined by measuring cytochrome c reduction using a microtiter 96-well plate ELISA reader (Bio-Tek instruments, EL312e, Winooski, VT, USA), as previously described [16]. Human neutrophils were isolated according to the standard procedures of dextran sedimentation, hypotonic lysis of erythrocytes, and use of a lymphocyte separation medium gradient as described previously [15]. The isolated human neutrophils were used promptly. Human neutrophils (2×10^6 cells in RPMI 1640 medium) were preincubated with 50 μM of cytochrome c at 37 °C for 5 min and subsequently incubated with each stimulant. Superoxide generation was determined by measuring light absorption changes at 550 nm over 5 min, at 1 min intervals.

2.6. Terminal deoxynucleotidyl transferase dUTP nick end labeling (TUNEL) assay

Mice were subjected to CLP surgery and given vehicle (0.8% DMSO in PBS) or α-iso-cubebenol at a dose of 15 mg/kg 2 and 14 h post-surgery. The mice were euthanized 24 h after surgery, after which their spleens and thymuses were isolated. The TUNEL assay was performed in frozen tissue sections using a standard histological protocol. The sections were permeabilized with Triton X-100 at 4 °C for 2 min and flooded with terminal deoxynucleotidyl transferase and digoxigenin-dUTP reaction buffer (TUNEL) reagent for 60 min at 37 °C. The percentage of apoptotic (TUNEL-positive) cells was determined by counting 500 splenocytes under a light microscope [17].

2.7. Immunohistochemistry

Immunohistochemistry was conducted using frozen tissue sections using a standard histological protocol. After incubation with primary antibodies against cleaved caspase-3 (Cell Signaling Technology, Danvers, MA, USA), all sections were stained with horseradish peroxidase-conjugated secondary antibody.

2.8. Cytokine measurement

To measure CLP-induced cytokine production in peritoneal lavage fluid, mice were given α-iso-cubebenol at 2 and 14 h after CLP. Peritoneal lavage fluid was collected at 24 h post-CLP, and the cytokines present in the peritoneal fluid were measured by enzyme-linked immunosorbant assay (ELISA; BD Biosciences Pharmingen, San Jose, CA, USA).

2.9. Cytokine release from splenocytes in vitro

Mouse splenocytes (3×10^6 cells/0.3 ml) were placed in RPMI 1640 medium containing 5% fetal bovine serum (FBS) in 24-well plates and kept in a 5% CO_2 incubator at 37 °C. Mouse splenocytes were stimulated with PBS or LPS (100 ng/ml). After 15 min, cells were subsequently stimulated with vehicle (0.1% DMSO in PBS)

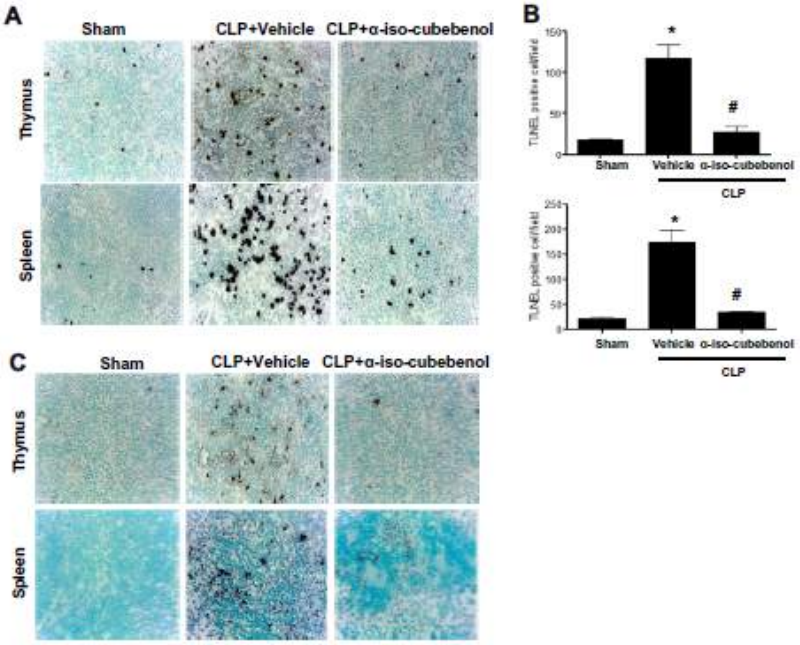

Fig. 3. α-Iso-cubebenol protects against widespread CLP-induced leukocyte apoptosis. (A) Vehicle (0.8% DMSO in PBS) or α-iso-cubebenol (15 mg/kg) was injected two times into CLP mice 2 and 14 h post-CLP. The spleens and the thymuses were collected 24 h after sham, CLP plus vehicle, or CLP plus α-iso-cubebenol administration, and used for a TUNEL assay. (B) TUNEL-positive cells from the spleens and thymuses of mice described in (A) were quantified. Data are expressed as the mean ± SEM ($n = 8$). *$P < 0.05$, compared with the value obtained from the sham control; #$P < 0.05$, significantly different from the CLP alone control. (C) The spleens and thymuses from the mice described in (A) were subjected to immunohistochemistry with cleaved-caspase-3 antibody (magnification, 100×). Data are representative of eight mice per group (A and C).

or α-iso-cubebenol (100 or 250 μg/ml) for 4 h. Cell-free supernatants were collected, centrifuged, and measured for IL-1β, IL-6, and IFN-γ production by ELISA (BD Biosciences Pharmingen).

2.10. Statistical analyses

Survival data were analyzed using the log-rank test. All other data were evaluated using ANOVA or *t*-test. The Bonferroni test was used for post hoc comparisons, and statistical significance was set *a priori* at $P < 0.05$.

3. Results

3.1. α-Iso-cubebenol administration protects against sepsis-induced mortality

We first investigated whether α-iso-cubebenol, its chemical structure was shown in Fig. 1A, has anti-septic activity against polymicrobial sepsis using a CLP sepsis model. α-Iso-cubebenol administration strongly protected against mortality induced by CLP in a dose-dependent manner (Fig. 1B). Survival was strongly enhanced, reaching 80% when 15 mg/kg of α-iso-cubebenol was injected 2 h post-CLP and additionally three times at 12 h intervals (Fig. 1B). Inflammation of vital organs such as lung is associated with sepsis-induced mortality [1]. In this study, we also observed that CLP caused severe alveolar congestion and extensive thrombotic lesions in the lungs. Administration of α-iso-cubebenol markedly improved the pulmonary histopathology (Fig. 1C).

In the clinical setting, septic patients always receive antibiotics. The effect of α-iso-cubebenol treatment on survival in mice subjected to CLP in the presence of concomitant treatment with appropriate antibiotic regimen was tested. As shown in Fig. 1D, the administration of 10 mg/kg of both antibiotics (gentamycin plus cephalosporin) slightly increased the survival rate in the severe sepsis model. The administration of α-iso-cubebenol also slightly enhanced therapeutic effect against severe sepsis. Combination of α-iso-cubebenol with the antibiotics additionally increased survival rate (Fig. 1D).

3.2. α-Iso-cubebenol administration strongly enhances bacterial clearance

Since CLP surgery causes the release of intestinal contents including viable bacteria, CLP-induced lethality has been reported to be positively correlated with bacterial colony counts in the peripheral blood and peritoneal fluid [1]. Because α-iso-cubebenol administration markedly increased survival rate (Fig. 1), we examined the effects of α-iso-cubebenol on bacterial colony number in the CLP model. α-Iso-cubebenol administration strongly decreased bacterial numbers in the peritoneal fluid as well as peripheral blood (Fig. 2A and B). α-Iso-cubebenol administration significantly reduced the number of intraperitoneal bacteria by 80% (Fig. 2A), and almost completely eliminated intravascular bacteria (Fig. 2B). Since bactericidal activity is mediated by phagocytes which engulf bacteria [18], we also checked whether α-iso-cubebenol could affect phagocytic activity of mouse macrophages using fluorescein isothiocynate (FITC)-labeled dextran. Stimulation of Raw 264.7

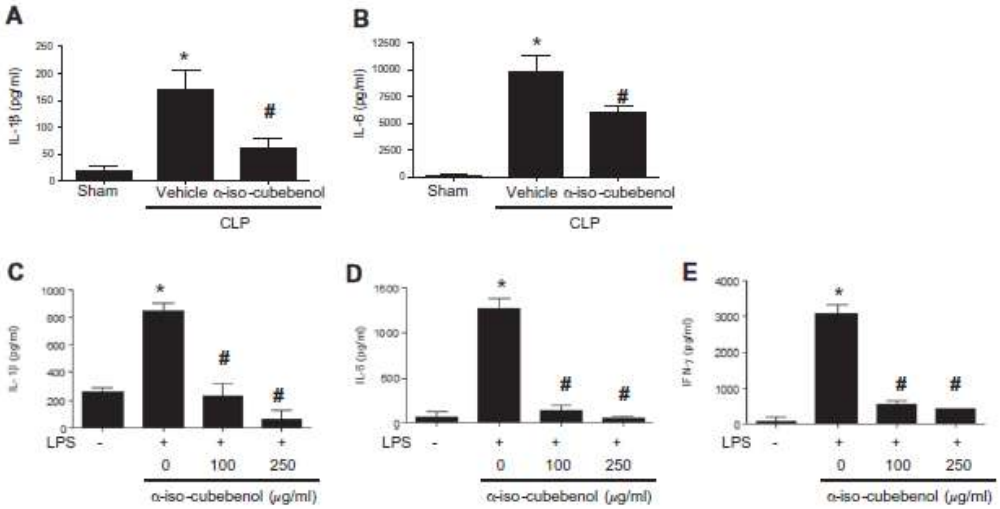

Fig. 4. Effects of α-iso-cubebenol on CLP- or LPS-induced cytokine production. (A–C) Vehicle (0.8% DMSO in PBS) or α-iso-cubebenol (15 mg/kg) was injected two times into CLP mice at 2 and 14 h post-CLP. Separate groups of animals were subjected to sham, CLP plus vehicle, or CLP plus α-iso-cubebenol treatment. Peritoneal fluids were collected at 24 h after CLP. Cytokine levels in the peritoneal fluid were determined by ELISA analysis. Panels A and B display results for IL-1β and IL-6, respectively. (C–E) Mouse splenocytes were stimulated with PBS or LPS (100 ng/ml). After 15 min, cells were subsequently stimulated with vehicle (0.1% DMSO in PBS) or α-iso-cubebenol (100 or 250 μg/ml) for 4 h. IL-1β (C), IL-6 (D), and IFN-γ (E) levels were measured by ELISA. Data are expressed as the mean ± SEM ($n = 8$). *$P < 0.05$, compared with the value obtained from the sham (A and B) or not treated (C–E) control; #$P < 0.05$, significantly different from the CLP alone (A and B) or LPS alone (C–E) control.

cells with α-iso-cubebenol increased phagocytic activity (Fig. 2C). FITC-positive cells were increased from 45% to 72% by stimulation of the cells with α-iso-cubebenol (Fig. 2C). Bactericidal activity also has been demonstrated to be mediated by the phagocytic activity and reactive oxygen species generation of phagocytic cells such as neutrophils and macrophages [19]. α-Iso-cubebenol also strongly increased the production of superoxide anions in human neutrophils (Fig. 2D). These results suggest that α-iso-cubebenol stimulates bactericidal activity by enhancing phagocytic activity and superoxide anion production of phagocytes.

3.3. α-Iso-cubebenol administration inhibits CLP-induced lymphocyte apoptosis

Apoptosis of splenocytes and thymocytes is dramatically increased during the progression of sepsis. CLP treatment also increased the apoptosis of splenocytes and thymocytes, as detected by DNA fragmentation analysis (TUNEL assay) (Fig. 3A). α-Iso-cubebenol administration dramatically inhibited CLP-induced apoptosis of splenocytes and thymocytes (Fig. 3A). The numbers of apoptotic cells were quantified by counting TUNEL-positive cells (Fig. 3B). Apoptotic splenocytes and thymocytes in the α-iso-cubebenol administrated groups decreased to almost the level of sham control groups (Fig. 3B). Caspase-3 mediates the apoptosis of splenocytes and thymocytes in CLP sepsis [20]. Consistently, α-iso-cubebenol administration almost completely inhibited CLP-induced caspase-3 activity in splenocytes and thymocytes (Fig. 3C).

3.4. α-Iso-cubebenol inhibits proinflammatory cytokine production in vivo and in vitro

Pathogenesis of sepsis is associated with high levels of proinflammatory cytokines such as IL-1β and IL-6 [1]. To test the effects of α-iso-cubebenol on CLP-induced cytokine production, we measured the levels of IL-1β and IL-6 in peritoneal fluid with or without α-iso-cubebenol administration 24 h after CLP. As shown in Fig. 4A and B, CLP induced a dramatic increase in the production of the proinflammatory cytokines IL-1β and IL-6 within 24 h. α-Iso-cubebenol administration significantly decreased IL-1β and IL-6 levels at 24 h after CLP (Fig. 4A and B).

Next, we also examined whether α-iso-cubebenol could act directly on leukocytes to inhibit LPS-stimulated proinflammatory cytokine production. As reported, stimulation of freshly isolated splenocytes with 100 ng/ml LPS (as a prototypical microbial signal) strongly increased the levels of proinflammatory cytokines such as IL-1β, IL-6, and IFN-γ (Fig. 4C–E). α-Iso-cubebenol (100 μg/ml or 250 μg/ml) significantly decreased LPS-stimulated cytokine levels in splenocytes (Fig. 4C–E).

4. Discussion

With improvements in hospital care and increased awareness of deadly diseases, mortality rates from sepsis have decreased in recent years [3,4]. However, 1 in 1200 Americans die of severe sepsis annually [3,4]. Even though 17% of in-hospital deaths in the US are caused by sepsis, drugs that combat sepsis without antibiotics are not clinically available. Xigris, which had been approved by the US FDA as a therapeutic agent against sepsis, was withdrawn from the market. Thus, researchers are searching for new targets and therapeutic molecules to treat sepsis. In this study, we demonstrate that the therapeutic administration of α-iso-cubebenol after induction of sepsis by CLP can effectively inhibit CLP-induced lethality in mice. α-Iso-cubebenol appears to exert its therapeutic activity against sepsis through multiple mechanisms: (1) increase in bactericidal activity, (2) inhibition of leukocyte apoptosis, and (3) inhibition of proinflammatory cytokine secretion.

Sepsis-induced mortality is closely associated with organ failure, which can be caused by lymphocyte apoptosis [1]. Here

we observed the anti-apoptotic effects of α-iso-cubebenol in CLP sepsis mice (Fig. 3A and B). Among many mediators involved in lymphocyte apoptosis, caspase-3 is regarded to be a key player [20]. α-Iso-cubebenol administration dramatically inhibited CLP-induced caspase-3 activation (Fig. 3C). Therefore, α-iso-cubebenol may contribute to increase the survival rate of CLP mice by blocking lymphocyte apoptosis via inhibition of caspase-3.

α-Iso-cubebenol administration affects the cytokine profile in CLP sepsis mice. The production of proinflammatory cytokines including IL-1β and IL-6 is inhibited by α-iso-cubebenol (Fig. 4A and B), and LPS-induced production of IL-1β, IL-6, and IFN-γ in splenocytes is also inhibited (Fig. 4C–E). Since TLR4 mediates LPS-stimulated cellular signaling which leads to the induction of many proinflammatory molecules [21], α-iso-cubebenol may act by blocking LPS-induced TLR4-mediated signaling. Previously, we demonstrated that α-iso-cubebenol inhibits the expression of LPS-induced nitric oxide synthase and cydooxygenase-2 in the Raw 264.7 mouse macrophage cell line [12]. Mechanistically, α-iso-cubebenol strongly inhibited nuclear translocation of the NF-κB p65 subunit in response to LPS in macrophages [12]. Therefore, α-iso-cubebenol may inhibit the production of LPS-induced proinflammatory cytokines by inhibiting NF-κB activity downstream of TLR4.

In conclusion, a novel natural product isolated from the *S. chinensis* fruit, α-iso-cubebenol, shows therapeutic effects against sepsis by enhancing bactericidal activity, inhibiting lymphocyte apoptosis, and modulating cytokine profile. α-Iso-cubebenol and its unidentified target(s) may prove useful in the development of efficient therapeutic agents against polymicrobial sepsis.

Acknowledgments

This research was supported by Ministry for Food, Agriculture, Forestry and Fisheries, Republic of Korea (311054031HD120) and by National Research Foundation of Korea (NRF) Grants funded by the Korean government (MEST) (Nos. 2009 0093198, 35B-2011-1-E00012).

We thank Dr. Brian A. Zabel of Palo Alto Institute for Research and Education for helpful discussion.

SL, YC, and YB have pending patent applications. The other authors have no financial conflicts of interest.

References

[1] J. Cohen, The immunopathogenesis of sepsis, Nature 420 (2002) 885–891.
[2] D.C. Angus, W.T. Linde-Zwirble, J. Lidicker, G. Clermont, J. Carcillo, M.R. Pinsky, Epidemiology of severe sepsis in the United States: analysis of incidence, outcome, and associated costs of care, Crit. Care Med. 29 (2001) 1303–1310.
[3] G. Kumar, N. Kumar, A. Taneja, T. Kaleekal, S. Tarima, E. McGinley, E. Jimenez, A. Mohan, R.A. Khan, J. Whittle, E. Jacobs, R. Nanchal, Milwaukee Initiative in Critical Care Outcomes Research Group of Investigators, Nationwide trends of severe sepsis in the 21st century (2000–2007), Chest 140 (2011) 1223–1231.
[4] M.J. Hall, S.N. Williams, C.J. Defrances, A. Golosinskiy, Inpatient care for septicemia or sepsis: a challenge for patients and hospitals, NCHS Data Brief (2011) 1–8.
[5] W.D. Döcke, F. Randow, U. Syrbe, D. Krausch, K. Asadullah, P. Reinke, et al., Monocyte deactivation in septic patients: restoration by IFN-gamma treatment, Nat. Med. 3 (1997) 678–681.
[6] B.J. Czermak, V. Sarma, C.L. Pierson, R.L. Warner, M. Huber-Lang, N.M. Bless, et al., Protective effects of C5a blockade in sepsis, Nat. Med. 5 (1999) 788–792.
[7] R.S. Hotchkiss, K.W. Tinsley, P.E. Swanson, R.E. Schmieg Jr., J.J. Hui, K.C. Chang, et al., Sepsis-induced apoptosis causes progressive profound depletion of B and CD4+ T lymphocytes in humans, J. Immunol. 166 (2001) 6952–6963.
[8] S.D. Wang, K.J. Huang, Y.S. Lin, H.Y. Lei, Sepsis-induced apoptosis of the thymocytes in mice, J. Immunol. 152 (1994) 5014–5021.
[9] C.A. Gogos, E. Drosou, H.P. Bassaris, A. Skoutelis, Pro- versus anti-inflammatory cytokine profile in patients with severe sepsis: a marker for prognosis and future therapeutic options, J. Infect. Dis. 181 (2000) 176–180.
[10] K. Reinhart, W. Karzai, Anti-tumor necrosis factor therapy in sepsis: update on clinical trials and lessons learned, Crit. Care Med. 29 (2001) S121–S125.
[11] L. Ulloa, K.J. Tracey, The "cytokine profile": a code for sepsis, Trends Mol. Med. 11 (2005) 56–63.
[12] Y.J. Lee, S.Y. Park, S.G. Kim, D.J. Park, J.S. Kang, S.J. Lee, S. Yoon, Y.H. Kim, Y.S. Bae, Y.W. Choi, Identification of a novel compound that inhibits iNOS and COX-2 expression in LPS-stimulated macrophages from *Schisandra chinensis*, Biochem. Biophys. Res. Commun. 391 (2010) 1687–1692.
[13] S.Y. Park, D.J. Park, Y.H. Kim, Y. Kim, Y.W. Choi, S.J. Lee, *Schisandra chinensis* α-iso-cubebenol induces heme oxygenase-1 expression through PI3K/Akt and Nrf2 signaling and has anti-inflammatory activity in *Porphyromonas gingivalis* lipopolysaccharide-stimulated macrophages, Int. Immunopharmacol. 11 (2011) 1907–1915.
[14] Y.W. Choi, H.J. Kim, S.S. Park, J.H. Chung, H.W. Lee, S.O. Oh, B.S. Kim, J.B. Kim, H.Y. Chung, B.P. Yu, C.D. Kim, S. Yoon, Inhibition of endothelial cell adhesion by the new anti-inflammatory agent alpha-iso-cubebene, Vascul. Pharmacol. 51 (2009) 215–224.
[15] S.D. Kim, H.Y. Lee, J.W. Shim, H.J. Kim, Y.H. Yoo, J.S. Park, et al., Activation of CXCR2 by extracellular matrix degradation product acetylated Pro-Gly-Pro has therapeutic effects against sepsis, Am. J. Respir. Crit. Care Med. 184 (2011) 243–251.
[16] H.Y. Lee, S.H. Jo, C. Lee, S.H. Baek, Y.S. Bae, Differential production of leukotriene B4 or prostaglandin E2 by WKYMVm or serum amyloid A via formyl peptide receptor-like 1, Biochem. Pharmacol. 72 (2006) 860–868.
[17] J. Wang, J.P. Silva, C.M. Gustafsson, P. Rustin, N.G. Larsson, Increased *in vivo* apoptosis in cells lacking mitochondrial DNA gene expression, Proc. Natl. Acad. Sci. USA 98 (2001) 4038–4043.
[18] J.C. Simard, M.M. Simon, P.A. Tessier, D. Girard, Damage-associated molecular pattern S100A9 increases bactericidal activity of human neutrophils by enhancing phagocytosis, J. Immunol. 186 (2011) 3622–3631.
[19] C. Erridge, Endogenous ligands of TLR2 and TLR4: agonists or assistants?, J. Leukoc. Biol. 87 (2010) 989–999.
[20] R.F. Guo, M. Huber-Lang, X. Wang, V. Sarma, V.A. Padgaonkar, R.A. Craig, N.C. Riedemann, S.D. McClintock, T. Hlaing, M.M. Shi, P.A. Ward, Protective effects of anti-C5a in sepsis-induced thymocyte apoptosis, J. Clin. Invest. 106 (2000) 1271–1280.
[21] R. Salomao, M.K. Brunialti, M.M. Rapozo, G.L. Baggio-Zappia, C. Galanos, M. Freudenberg, Bacterial sensing, cell signaling, and modulation of the immune response during sepsis, Shock 38 (2012) 227–242.

Biochemical and Biophysical Research Communications 431 (2013) 433–436

Contents lists available at SciVerse ScienceDirect

Biochemical and Biophysical Research Communications

journal homepage: www.elsevier.com/locate/ybbrc

Role of CXCR2 on the immune modulating activity of α-iso-cubebenol a natural compound isolated from the *Schisandra chinensis* fruit

Young Su Jung [a,c,1], Sung Kyun Lee [a,c,1], Chang Youp Ok [a], Eun Jung Cho [b,c], Joon Seong Park [d], Young Whan Choi [e,*], Yoe-Sik Bae [a,c,f,*]

[a] Department of Biological Science, Sungkyunkwan University, Suwon 440-746, South Korea
[b] Institute of Basic Science, Sungkyunkwan University, Suwon 440-746, South Korea
[c] Mitochondria Hub Regulation Center, Dong-A University, Busan 602-714, South Korea
[d] Department of Hematology–Oncology, Ajou University School of Medicine, Suwon 443-721, South Korea
[e] Department of Horticultural Bioscience, College of Natural Resources and Life Science, Pusan National University, Miryang 627-706, South Korea
[f] Samsung Advanced Institute for Health Sciences and Technology, Sungkyunkwan University, Seoul 135-710, South Korea

ARTICLE INFO

Article history:
Received 18 December 2012
Available online 16 January 2013

Keywords:
α-Iso-cubebenol
CXCR2
Inflammation
Sepsis

ABSTRACT

Previously, we demonstrated that α-iso-cubebenol, a natural compound isolated from the fruits of *Schisandra chinensis*, strongly enhances therapeutic efficacy against cecal ligation and puncture challenge-induced sepsis. In this study, we found that α-iso-cubebenol stimulated calcium increase and degranulation in human neutrophils. α-Iso-cubebenol also strongly induced neutrophil chemotaxis, which was completely blocked by a CXCR2 antagonist, SB225002. The increased survival rate by α-iso-cubebenol was also significantly attenuated by SB225002. Taken together, the results indicate that α-iso-cubebenol-induced anti-septic activity was mediated by CXCR2, suggesting CXCR2 as an important target for the regulation of sepsis and inflammation.

1. Introduction

It has been known that sepsis, a systemic inflammatory response, is caused by viable bacteria or bacterial products such as lipopolysaccharide (LPS) [1]. The number of hospitalizations with sepsis in the US has annually increased, reaching around 800,000 in 2007 [2]. Moreover, the overall mortality associated with sepsis ranges from 30% to 70%, and sepsis remains the major cause of death in intensive care units in the US. Currently, no therapeutic agents approved from the US FDA are available, and various studies have been on going to identify efficient target molecules for the development of therapeutic agents against sepsis.

CXCR2 is a well-known chemokine receptor, which is expressed on several leukocytes such as neutrophils, monocytes, and macrophages [3]. CXCL8, an endogenous ligand for CXCR2, binds to CXCR2 in humans [4,5], and mouse chemokines, including CXCL1 (KC, keratinocyte-derived chemokine), bind to mouse CXCR2. Physiologically, the activation of CXCR2 by CXCL8 or CXCL1 induces leukocyte chemotactic migration in neutrophils and monocytes [6,7]. In addition to CXCL8 and CXCL1, N-terminal acetylated tripeptide, Ac-PGP, has been reported to act on CXCR2 [8,9]. Although some reports revealed that neutralizing antibodies against CXCR2 or inhibitory molecules for CXCR2 show therapeutic activity against sepsis, we strongly demonstrated that the activation of CXCR2 by Ac-PGP shows therapeutic efficacy against sepsis [9].

Previously, we isolated a novel natural compound, α-iso-cubebenol, from the fruits of *Schisandra chinensis* and demonstrated that the compound shows therapeutic activity against cecal ligation and puncture (CLP) sepsis model [10,11]. Furthermore, α-iso-cubebenol strongly increased the survival rate in the CLP model by increasing the bactericidal activity of phagocytes, and by attenuating inflammatory cytokine production and blocking leukotycte apoptosis [11]. In this study, we investigated the in vitro activity of α-iso-cubebenol on neutrophil activity. We also examined the role of an important chemokine receptor, CXCR2, on the *in vivo* efficacy of α-iso-cubebenol in a preclinical mouse model of sepsis.

2. Materials and methods

2.1. Materials

α-Iso-cubebenol was purified from the dried fruits of *S. chinensis* as described previously [10]. Peripheral blood mononuclear cell separation medium (Histopaque-1077) was from Sigma (St. Louis,

* Corresponding authors. Address: Department of Horticultural Bioscience, College of Natural Resources and Life Science, Pusan National University, Miryang, Miryang 627-706, South Korea. Fax: +82 55 350 5529 (Y.W. Choi), Department of Biological Science, Institute of Basic Science, Sungkyunkwan University, Suwon 440-746, South Korea. Fax: +82 31 290 7015 (Y.-S. Bae).
E-mail addresses: ywchoi@pusan.ac.kr (Y.W. Choi), yoesik@skku.edu (Y.-S. Bae).
[1] These authors contributed equally to this work.

0006-291X/$ - see front matter © 2013 Elsevier Inc. All rights reserved.
http://dx.doi.org/10.1016/j.bbrc.2012.12.152

MO). Fura-2 pentaacetoxymethylester (fura-2/AM) was purchased from Molecular Probes (Eugene, OR).

2.2. Isolation of human neutrophils

Peripheral blood leukocytes were isolated from healthy donors. Human neutrophils were isolated according to the standard procedures for dextran sedimentation, hypotonic lysis of erythrocytes, and lymphocyte separation medium gradient as described previously [12]. Isolated human neutrophils were used promptly.

2.3. Measurement of intracellular Ca^{2+} increase

The level of $[Ca^{2+}]_i$ was measured using Grynkiewicz's method with fura-2/AM [13,14]. Briefly, prepared cells were incubated with 3 μM fura-2/AM at 37 °C for 50 min in fresh serum-free RPMI 1640 medium under continuous stirring. Following this, 2×10^6 cells were aliquoted for each assay in Ca^{2+}-free Locke's solution (154 mM NaCl, 5.6 mM KCl, 1.2 mM $MgCl_2$, 5 mM HEPES, pH 7.3, 10 mM glucose, and 0.2 mM EGTA) and incubated with the indicated concentrations of α-iso-cubebenol. Fluorescence changes at dual excitation wavelengths of 340 nm and 380 nm and at an emission wavelength of 500 nm were measured, and the calibrated fluorescence ratio was translated into $[Ca^{2+}]_i$.

2.4. β-Hexosaminidase secretion assay

The amount of released β-hexosaminidase was measured as described previously [15]. Briefly, neutrophils (2×10^5/well) were cultured overnight in 24-well tissue culture plates. The cells were then washed twice with Tyrode's buffer (137 mM NaCl, 12 mM $NaHCO_3$, 5.6 mM glucose, 2.7 mM KCl, 1 mM $CaCl_2$, 0.5 mM $MgCl_2$, 0.4 mM NaH_2PO_4, 0.1 g/100 ml BSA, and 25 mM HEPES, pH 7.4) and stimulated with α-iso-cubebenol. The reaction was terminated 20 min after stimulation by placing the plate on ice. The amount of β-hexosaminidase secreted into the medium was determined by incubating 50 μl of supernatant or cell lysate with 25 μl of 5 mM *p*-nitrophenyl-*N*-acetyl-β-D-glucosamide in 0.1 M sodium citrate buffer (pH 3.8) at 37 °C for 2 h. At the end of incubation, 50 μl of 0.4 M Na_2CO_3 was added. Absorbance was monitored at 405 nm. Values are expressed as a percentage of the total β-hexosaminidase present in the cells.

2.5. Chemotaxis assay

Chemotaxis assays were performed using multiwell chambers (Neuroprobe Inc., Gaithersburg, MD) [16]. Briefly, prepared human neutrophils were suspended in RPMI 1640 medium at a concentration of 1×10^6 cells/ml, and 25 μl was placed onto the upper well of the chamber that was separated by a 3 μm polyhydrocarbon filter from an α-iso-cubebenol-containing lower well. After incubation for 90 min at 37 °C, nonmigrated cells were removed by scraping, and cells that migrated across the filter were dehydrated, fixed, and stained with hematoxylin (Sigma, St. Louis, MO). Stained cells were counted per well under light microscope [16].

2.6. Animals and sepsis model

Six week aged male wild type albino institute of cancer research center (ICR) mice were used as an experimental sepsis model as described [17]. For cecal ligation and puncture (CLP), mice were anesthetized with intraperitoneal injections of Zoletil (50 mg/kg) and Rompun (10 mg/kg), after which a small abdominal midline incision was made to expose the cecum. The cecum was then ligated below the ileocecal valve, punctured twice through both surfaces (or once for measurement of cytokine production) using a 22-gauge needle, and then the abdomen was closed. Sham CLP mice were subjected to the same procedure but without ligation and puncture of the cecum. Survival was monitored once daily for 10 days.

2.7. Statistical analyses

Survival data were analyzed using the log-rank test. All other data were evaluated using the ANOVA or *t*-test. The Bonferroni test was used for post hoc comparisons, and statistical significance was set *a priori* at $P < 0.05$.

3. Results

3.1. α-Iso-cubebenol stimulates calcium increase in human neutrophil

Previously, we reported that isolated α-iso-cubebenol strongly protected against mortality induced by CLP [11]. α-Iso-cubebenol also markedly increased superoxide anion production from human neutrophils [11]. We also demonstrated that the production of superoxide anion is mediated by intracellular calcium increase in human neutrophils [18]. To test the possibility that α-iso-cubebenol also stimulates calcium increase in human neutrophils, we treated fura-2/AM-loaded human neutrophils with various concentrations of α-iso-cubebenol. Stimulation of human neutrophils with α-iso-cubebenol induced an increase of intracellular calcium concentration in a concentration-dependent manner, showing maximal activity at 100 μg/ml (Fig. 1A). Intracellular calcium increase can be induced by activation of phospholipase C (PLC) activity or activation of membrane-bound calcium channel [19]. The α-iso-cubebenol-induced calcium increase was almost markedly inhibited by the PLC-selective inhibitor, U-73122, but not by its inactive analogue, U-73343 (Fig. 1B). However, several inhibitors for membrane-bound calcium channels such as SK&F, diltiazem, or nifedifine did not inhibit the α-iso-cubebenol-induced calcium increase (Fig. 1B).

3.2. α-Iso-cubebenol stimulates degranulation in human neutrophils

Activated neutrophil secretes granule contents, which mediate defensive activity in the innate immune response [20]. In this

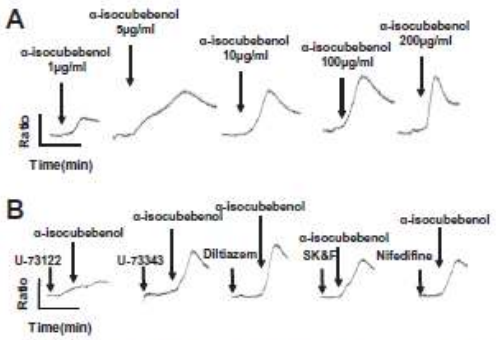

Fig. 1. α-Iso-cubebenol stimulates $[Ca^{2+}]_i$ release in human neutrophils. Human neutrophils were stimulated with various concentrations (1, 5, 10, 50, 100, or 200 μg/ml) of α-iso-cubebenol (A). Human neutrophils were preincubated with U-73122 (5 μM), U-73343 (5 μM), diltiazem (10 μM), SK&F (10 μM), or nifedifine (1 μM), and then stimulated with α-iso-cubebenol (10 μg/ml) (B). The relative $[Ca^{2+}]_i$ are expressed as fluorescence ratios. The data represents three independent experiments (A and B).

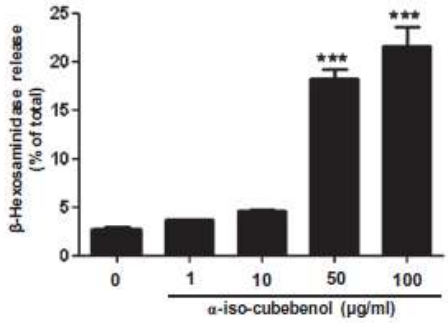

Fig. 2. α-Iso-cubebenol stimulates degranulation activity in human neutrophils. Various concentrations (0, 1, 10, 50, or 100 μg/ml) of α-iso-cubebenol were administered to human neutrophils. The α-iso-cubebenol-induced secretion of β-hexosaminidase was determined. Data are expressed as mean ± SE; $n = 8$. ***$P < 0.001$, compared with the value obtained from the untreated control.

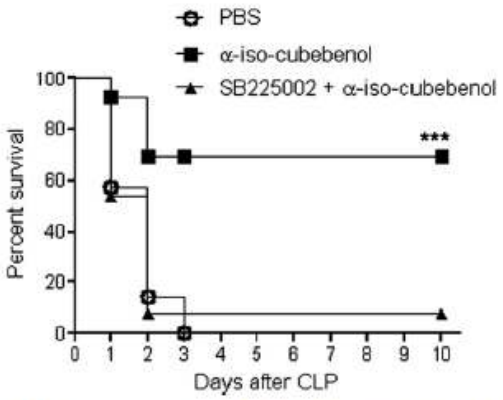

Fig. 4. Role of CXCR2 on α-iso-cubebenol-induced protection against CLP-induced mortality. Vehicle (0.8% DMSO in PBS), α-iso-cubebenol (15 mg/kg), or SB225002 (15 mg/kg) plus α-iso-cubebenol (15 mg/kg) were injected subcutaneously four times into CLP mice at 2, 14, 26, and 38 h post-CLP. Sample size: $n = 9$–10 mice/group. ***$P < 0.001$ compared to the vehicle control by ANOVA.

study, we investigated the effect of α-iso-cubebenol on degranulation-stimulating activity in human neutrophils. As shown in Fig. 2, stimulation of human neutrophils with various concentrations of α-iso-cubebenol induced degranulation. To test the effect of calcium signaling on α-iso-cubebenol-stimulated degranulation in human neutrophils, we incubated human neutrophils with the calcium chelator, BAPTA/AM, prior to α-iso-cubebenol addition. The α-iso-cubebenol-stimulated degranulation activity was completely inhibited by BAPTA/AM, indicating the involvement of calcium increase in α-iso-cubebenol-stimulated degranulation (data not shown).

3.3. α-Iso-cubebenol stimulates human neutrophil chemotaxis via CXCR2

Neutrophil chemotactic migration is a very essential process in the modulation of innate immunity and inflammatory response [21]. Many chemoattractants regulate neutrophil chemotaxis; pertussis toxin-sensitive G-protein-coupled receptors such as chemokine receptors are activated by these chemoattractants [22,23]. Here we examined whether α-iso-cubebenol would regulate neutrophil chemotaxis. As shown in Fig. 3A, stimulation of human neutrophils strongly induced neutrophil chemotaxis.

Neutrophils express several chemokine receptors [21]. Among these chemokine receptors, CXCR2, a receptor for CXCL8, has been known to mediate neutrophil chemotaxis and calcium increase [4,6]. Here we tested the possibility of CXCR2 involvement in α-iso-cubebenol-induced neutrophil chemotaxis using a CXCR2-selective antagonist, SB225002. Interestingly, α-iso-cubebenol-induced neutrophil chemotaxis was inhibited by SB225002 (Fig. 3B).

3.4. α-Iso-cubebenol shows anti-septic activity via CXCR2

Since we demonstrated that α-iso-cubebenol has therapeutic effects against sepsis in our previous report [11], and that α-iso-cubebenol-induced neutrophil chemotaxis is blocked by the CXCR2 antagonist (Fig. 3B), we tested the role of CXCR2 on α-iso-cubebenol-induced anti-septic activity. α-Iso-cubebenol-induced increase of survival rate in the CLP sepsis model was completely inhibited by administration of the CXCR2 antagonist (Fig. 4). α-Iso-cubebenol administration-induced attenuation of lung inflammation

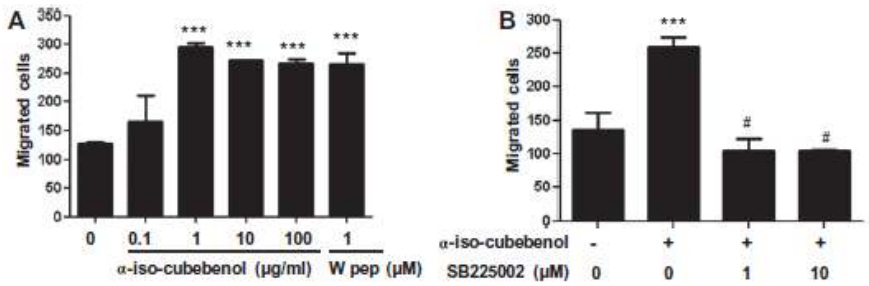

Fig. 3. α-Iso-cubebenol stimulates neutrophil chemotaxis via CXCR2. Human neutrophils (1×10^6 cells/ml of serum-free RPMI) were added to the upper wells of a 96-well chemotaxis chamber, and migration across a 3-μm pore size polycarbonate membrane was assessed after 1.5-h of incubation at 37 °C. Various concentrations (0, 0.1, 1, 10, or 100 μg/ml) of α-iso-cubebenol or 1 μM WKYMVm were used for chemotaxis assay (A). Vehicle or two different concentrations (1 or 10 μM) of SB225002 pretreated cells were subjected to chemotaxis assay with 10 μg/ml of α-iso-cubebenol (B). The number of migrated cells was determined by counting in a high-power field (400×). Data are presented as mean ± SE of three independent experiments performed in duplicate. ***$P < 0.001$, compared with the value obtained from the untreated control. #$P < 0.05$, significantly different from the α-iso-cubebenol alone control (B).

against CLP sepsis was also markedly reversed by administration of the CXCR2 antagonist (data not shown).

4. Discussion

Although mortality rates from sepsis have decreased in recent years, the figure is still around 30% [1,2]. Moreover 1 in 1200 Americans die of severe sepsis annually [1,2]. After Xigris, a therapeutic agent against sepsis approved by the US FDA, has been withdrawn from the market, researchers have been avidly researching for new targets and therapeutic molecules to treat sepsis. In our previous report, we demonstrated that α-iso-cubebenol, a natural compound isolated from the fruits of *S. chinensis*, has strong therapeutic effects against polymicrobial sepsis [11]. In the present study, we demonstrated that the therapeutic effect of α-iso-cubebenol after induction of sepsis by CLP is mediated by an important chemokine receptor, CXCR2. We clearly revealed that the therapeutic effect of α-iso-cubebenol requires compound engagement with CXCR2, since pretreatment of mice with the CXCR2-specific antagonist (SB225002) abolished the efficacy of α-iso-cubebenol in CLP-induced sepsis, thus indicating that α-iso-cubebenol acts via CXCR2 to prevent septic mortality.

Previous studies have indicated that stimulation of CXCR2 by its endogenous ligands such as CXCL8 and CXCL1 induces leukocyte chemotactic migration in neutrophils and monocytes [24,25]. Moreover, clinical data showed that CXCR2 but not CXCR1 is down-regulated by 50% in the neutrophils of sepsis patients compared to normal controls [26]. Since CXCR2 is important for the recruitment of inflammatory cells including neutrophils and monocytes, it has been regarded that blocking of CXCR2 using antibodies or antagonists would show increased survival rate in experimental sepsis models [27]. Novel lipid-conjugated peptide molecules derived from the CXCR2 intracellular region (x1/2pal-3: pal-RTLFKAHMGQKHR), which blocks CXCR2-mediated signaling by CXCL8 or CXCL1, also showed a marked therapeutic effect against cecal ligation and puncture (CLP)-septic mice [28]. Collectively, CXCR2 and its cognate ligands have been considered as important proinflammatory response-inducing targets. However, in our previous report we demonstrated that administration of Ac-PGP, a novel agonist which binds to CXCR2, elicit strong therapeutic efficacy in a CLP sepsis model by increasing bactericidal activity, decreasing inflammatory cytokines, and blocking leukocyte apoptosis [9]. Our previous report and other group's reports collectively suggest that CXCR2 can be differentially regulated in a ligand-selective manner to cause promotion or inhibition of sepsis pathogenesis. In this study, we also exhibited that α-iso-cubebenol shows anti-septic activity via CXCR2. This finding strongly supports our notion that activation of CXCR2 can be a good approach to develop efficient therapeutic agents against sepsis.

In conclusion, α-iso-cubebenol, a novel natural product isolated from the fruits of *S. chinensis*, stimulated neutrophils, resulting in calcium increase, degranulation, and chemotactic migration via CXCR2. Since the α-iso-cubebenol-induced therapeutic effect against sepsis was also blocked by the CXCR2 antagonist, α-iso-cubebenol, and its target, CXCR2, may prove useful in the treatment of polymicrobial sepsis.

5. Acknowledgements

This research was supported by Ministry for Food, Agriculture, Forestry and Fisheries, Republic of Korea (311054031HD120) and by National Research Foundation of Korea(NRF) grants funded by the Korean government (MEST) (Nos. 2009 0093198, 2012R1A2A2A01007751).

References

[1] J. Cohen, The immunopathogenesis of sepsis, Nature 420 (2002) 885–891.
[2] G. Kumar, N. Kumar, A. Taneja, T. Kaleekal, S. Tarima, E. McGinley, E. Jimenez, A. Mohan, R.A. Khan, J. Whittle, E. Jacobs, R. Nanchal, Milwaukee initiative in critical care outcomes research group of investigators. Nationwide trends of severe sepsis in the 21st century (2000–2007), Chest 140 (2011) 1223–1231.
[3] R.W. Chapman, J.E. Phillips, R.W. Hipkin, A.K. Curran, D. Lundell, J.S. Fine, CXCR2 antagonists for the treatment of pulmonary disease, Pharmacol. Ther. 121 (2009) 55–68.
[4] L. Wu, N. Ruffing, X. Shi, W. Newman, D. Soler, C.R. Mackay, S. Qin, Discrete steps in binding and signaling of interleukin-8 with its receptor, J. Biol. Chem. 271 (1996) 31202–31209.
[5] W.A. Boisvert, L.K. Curtiss, R.A. Terkeltaub, Interleukin-8 and its receptor CXCR2 in atherosclerosis, Immunol. Res. 21 (2000) 129–137.
[6] M. Baggiolini, A. Walz, S.L. Kunkel, Neutrophil-activating peptide-1/interleukin 8, a novel cytokine that activates neutrophils, J. Clin. Invest. 84 (1989) 1045–1049.
[7] B. Mehrad, R.M. Strieter, T.A. Moore, W.C. Tsai, S.A. Lira, T.J. Standiford, CXC chemokine receptor-2 ligands are necessary components of neutrophil-mediated host defense in invasive pulmonary aspergillosis, J. Immunol. 163 (1999) 6086–6094.
[8] N.M. Weathington, A.H. van Houwelingen, B.D. Noerager, P.L. Jackson, A.D. Kraneveld, F.S. Galin, G. Folkerts, F.P. Nijkamp, J.E. Blalock, A novel peptide CXCR ligand derived from extracellular matrix degradation during airway inflammation, Nat. Med. 12 (2006) 317–323.
[9] S.D. Kim, H.Y. Lee, J.W. Shim, H.J. Kim, Y.H. Yoo, J.S. Park, S.H. Baek, B.A. Zabel, Y.S. Bae, Activation of CXCR2 by extracellular matrix degradation product acetylated Pro-Gly-Pro has therapeutic effects against sepsis, Am. J. Respir. Crit. Care Med. 184 (2011) 243–251.
[10] Y.J. Lee, S.Y. Park, S.G. Kim, D.J. Park, J.S. Kang, S.J. Lee, S. Yoon, Y.H. Kim, Y.S. Bae, Y.W. Choi, Identification of a novel compound that inhibits iNOS and COX-2 expression in LPS-stimulated macrophages from Schisandra chinensis, Biochem. Biophys. Res. Commun. 391 (2010) 1687–1692.
[11] S.K. Lee, S.D. Kim, M. Kook, H.Y. Lee, J.S. Park, Y.H. Park, J.S. Kang, W.J. Jung, Y.W. Choi, Y.S. Bae, Therapeutic effects of α-iso-cubebenol, a natural compound isolated from the Schisandra chinensis fruit, against sepsis, Biochem. Biophys. Res. Commun. 427 (2012) 547–552.
[12] Y.S. Bae, H. Bae, Y. Kim, T.G. Lee, P.G. Suh, S.H. Ryu, Identification of novel chemoattractant peptides for human leukocytes, Blood 97 (2001) 2854–2862.
[13] G. Grynkiewicz, M. Poenie, R.Y. Tsien, A new generation of Ca^{2+} indicators with greatly improved fluorescence properties, J. Biol. Chem. 260 (1985) 3440–3450.
[14] Y.S. Bae, H.Y. Lee, E.J. Jo, J.I. Kim, H.K. Kang, R.D. Ye, J.Y. Kwak, S.H. Ryu, Differential activation of formyl peptide receptor-like 1 by peptide ligands, J. Immunol. 171 (2003) 6807–6813.
[15] Y.S. Bae, J.Y. Song, Y. Kim, R. He, R.D. Ye, J.Y. Kwak, P.G. Suh, S.H. Ryu, Differential activation of formyl peptide receptor signaling by peptide ligands, Mol. Pharmacol. 64 (2003) 841–847.
[16] Y.S. Bae, H.Y. Lee, E.J. Jo, J.I. Kim, H.K. Kang, R.D. Ye, J.Y. Kwak, S.H. Ryu, Identification of peptides that antagonize formyl peptide receptor-like 1-mediated signaling, J. Immunol. 173 (2004) 607–614.
[17] S.D. Kim, Y.K. Kim, H.Y. Lee, Y.S. Kim, S.G. Jeon, S.H. Baek, D.K. Song, S.H. Ryu, Y.S. Bae, The agonists of formyl peptide receptors prevent development of severe sepsis after microbial infection, J. Immunol. 185 (2010) 4302–4310.
[18] Y.S. Bae, S.A. Ju, J.Y. Kim, J.K. Seo, S.H. Baek, J.Y. Kwak, B.S. Kim, P.G. Suh, S.H. Ryu, Trp-Lys-Tyr-Met-Val-D-Met stimulates superoxide generation and killing of Staphylococcus aureus via phospholipase D activation in human monocytes, J. Leukoc. Biol. 65 (1999) 241–248.
[19] M.J. Berridge, Inositol trisphosphate and calcium signaling, Nature 361 (1993) 315–325.
[20] M.R. Logan, S.O. Odemuyiwa, R. Moqbel, Understanding exocytosis in immune and inflammatory cells: the molecular basis of mediator secretion, J. Allergy Clin. Immunol. 111 (2003) 923–932.
[21] N. Borregaard, Neutrophils, from marrow to microbes, Immunity 33 (2010) 657–670.
[22] Y. Kobayashi, The role of chemokines in neutrophil biology, Front. Biosci. 13 (2008) 2400–2407.
[23] A. Walther, K. Riehemann, V. Gerke, A novel ligand of the formyl peptide receptor: annexin I regulates neutrophil extravasation by interacting with the FPR, Mol. Cell 5 (2000) 831–840.
[24] M. Baggiolini, Reflections on chemokines, Immunol. Rev. 177 (2000) 5–7.
[25] M. Baggiolini, B. Dewald, B. Moser, Human chemokines: an update, Annu. Rev. Immunol. 15 (1997) 675–705.
[26] C.J. Cummings, T.R. Martin, C.W. Frevert, J.M. Quan, V.A. Wong, S.M. Mongovin, T.R. Hagen, K.P. Steinberg, R.B. Goodman, Expression and function of the chemokine receptors CXCR1 and CXCR2 in sepsis, J. Immunol. 162 (1999) 2341–2346.
[27] T.L. Ness, C.M. Hogaboam, R.M. Strieter, S.L. Kunkel, Immunomodulatory role of CXCR2 during experimental septic peritonitis, J. Immunol. 171 (2003) 3775–3784.
[28] N.C. Kaneider, A. Agarwal, A.J. Leger, A. Kuliopulos, Reversing systemic inflammatory response syndrome with chemokine receptor pepducins, Nat. Med. 11 (2005) 661–665.

EI24 regulates epithelial-to-mesenchymal transition and tumor progression by suppressing TRAF2-mediated NF-κB activity

Jung-Min Choi[1,*], Sushil Devkota[1,*], Young Hoon Sung[1], and Han-Woong Lee[1,2]

[1] Department of Biochemistry, College of Life Science and Biotechnology, Yonsei University, Seoul 120-749, Korea,

[2] Laboratory Animal Research Center, Yonsei University, Seoul 120-749, Korea

[*] denotes equal contribution

***Correspondence to**: Han-Woong Lee, **email**: hwl@yonsei.ac.kr*

***Keywords**: EI24, EMT, Tumor progression, NF-κB*

***Received**: September 26, 2013 **Accepted**: November 16, 2013 **Published**: November 17, 2013*

ABSTRACT:

Tumor metastasis is a multistep process that requires the concerted activity of discrete biological functions. The epithelial-to-mesenchymal transition (EMT) is the most critical mechanism implicated in tumor progression that is controlled by the inflammatory microenvironment. Understanding how an inflammatory microenvironment is maintained and contributes to tumor progression will be crucial for the development of new effective therapies. Here, we report that *etoposide induced 2.4 (EI24)* has a multifaceted role against tumor progression that is regulated by both EMT and inflammation. Decreased expression levels of EI24 in epithelial tumor cells induced EMT in association with increased cell motility and invasiveness and resistance to anoikis. Overexpression of EI24 resulted in the opposite cell biological characteristics and suppressed in vivo metastatic behavior. EI24 attenuated NF-κB activity by binding to the Complex I component TRAF2 and inducing its lysosome-dependent degradation, leading to transcriptional alterations of EMT- and inflammation-related genes. Analysis of clinical samples demonstrated that reduced EI24 expression and copy number was positively correlated with tumor malignancy and poor prognosis. Collectively, these findings establish EI24 as a critical suppressor of tumor progression and implicate EI24 expression level in malignant tumors as a useful therapeutic and diagnostic marker.

INTRODUCTION

Tumor metastasis, the spread of cancer cells from the primary neoplasm to distant organs, is a sequential and multistep process that is the most common cause of death in cancer patients [1]. Malignant tumor cells acquire several traits including increased cell motility, loss of cell-to-cell adhesion, invasion into lymphatic and/or blood circulation, and resistance to anoikis [2]. To acquire malignancy, cancer cells must undergo a loss of epithelial phenotypes and acquire characteristics of a mesenchymal state. This process, called the epithelial-to-mesenchymal transition (EMT), changes many of the cellular properties described above [3].

NF-κB mediates molecular crosstalk between inflammation and many other physiological processes through the transcriptional regulation of pro-inflammatory genes [4]. The transcriptional activity of NF-κB is controlled by Complex I of the tumor necrosis factor receptor type 1 (TNFR1) signaling pathway, which contains TNFR1-associated DEATH domain protein (TRADD) and TNFR-associated factors 2/5 (TRAF2/5). In the canonical pathway, IκBα is phosphorylated in an IKKβ- and NEMO-dependent manner, resulting in the nuclear translocation of heterodimers containing NF-κB p65 [5]. Thus, inhibition of IKKβ/NF-κB signaling could be an effective tool for the inhibition of tumor progression through reduced expression of a number of pro-malignant genes [6, 7].

The pro-apoptotic gene *EI24* plays an important role in the negative regulation of cell growth through its tumor suppressor activities [8]. The genomic locus of *EI24* at chromosome 11q23-q24 is a hot spot region for mutations in human tumors and is often correlated with

poor prognosis [9]. Additionally, loss of EI24 expression is associated with the development of invasive ductal [10] and cervical [11] carcinomas. However, the involvement of EI24 in tumor malignancy and the underlying molecular mechanisms are not well characterized.

In this study, we examined the functional significance of EI24 in the regulation of EMT and tumor progression by investigating the properties of cancer cells in which EI24 was either overexpressed or downregulated and the physiological activity of these cells in a mouse model of cancer. We found that, mechanistically, EI24 attenuated NF-κB activity by binding to the Complex I component TRAF2 and causing its lysosome-dependent degradation, thereby suppressing the transcription of pro-inflammatory genes that contribute to tumor progression. Furthermore, our data showed that decreased EI24 expression correlated with high tumorigenic potential of various cancer cells and with poor prognosis in human cancer patients.

RESULTS

EI24 inhibits cell motility and enhances cell-cell adhesion

Because increased cell motility is a key step in tumor progression [12], we first investigated the effect of EI24 on the motility phenotypes of several cancer cell lines. Overexpression of EI24 in metastatic B16F10 cells (F10-Ei24 cells) significantly reduced migration compared with that of the control cells (Figure 1A, 1B). Conversely, stable EI24 knockdown (ZR-shEI24 cells) increased cell migration (Figure 1C, 1D). Consistent with these data, F10-Ei24 cells exhibited a retarded wound-healing capacity (Supplemental Figure 1A), whereas EI24 knockdown in B16F10 cells (F10-shEi24) increased wound-healing capacity (Supplemental Figure 1B). As rearrangement of the actin cytoskeleton is an important factor in cell migration [13], we monitored F-actin arrangements and focal adhesion distribution in the context of overexpression or knockdown of EI24. The formation of stress fibers and focal adhesions was diminished in F10-Ei24 cells, whereas ZR-shEI24 cells displayed well-organized stress fibers linked with focal adhesions (Figure 1E, 1F). These data indicate that EI24 decreases cell migration by suppressing the formation of stress fibers and focal adhesions.

The adhesive strength of cells also has a critical influence on cell motility [14], therefore we measured the effect of EI24 overexpression on cell-cell adhesion. F10-Ei24 cells exhibited increased cell aggregation in hanging drop cultures (Figure 1G). A similar effect of EI24 overexpression was observed in breast cancer 4T1 cells (Supplemental Figure 1C). In contrast, EI24 knockdown significantly decreased cell-cell adhesion of

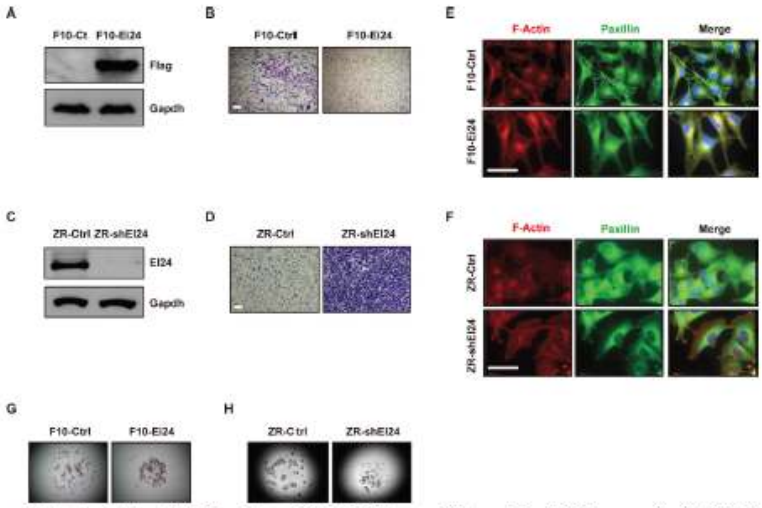

Figure 1: EI24 regulates the cell motile phenotype. (A) and (C) Immunoblot analysis of EI24 expression in B16F10 cells expressing either control vector (F10-EV) or EI24 (F10-Ei24, A), and in ZR-75-1 cells stably expressing control (ZR-Ctrl) or EI24-specific shRNA (ZR-shEI24, C). (B) and (D) Cell migration assays with F10-Ei24 (B) and ZR-shEI24 cells (D). The cells were visualized by staining with crystal violet. Data are representative of at least two independent experiments. Scale bars represent 200 μm. (E) and (F) Actin cytoskeletal structures in B16F10 (E) and ZR-75-1 (F) variant cells were visualized by immunofluorescence (IF) staining using anti-Phalloidin and anti-Paxillin antibodies. Scale bars represent 50 μm. (G) and (H) Cell-cell adhesion in F10-Ei24 (G) and ZR-shEI24 (H) cells was evaluated using the hanging drop assay. Data are representative of five independent drops.

ZR-75-1 and NMuMG cells (Figure 1H, Supplemental Figure 1D). These findings indicate that EI24 is necessary for maintenance of cell-cell interactions.

Decreased EI24 expression induces EMT

Because the increased cell motility, cytoskeleton rearrangements, and decreased cell-cell adhesion induced by reduced levels of EI24 are reminiscent of EMT, we examined whether EI24 ablation affected the epithelial characteristics of cancer cells. Gene set enrichment analysis (GSEA) showed a strong correlation between EI24 knockdown in ZR-75-1 cells and gene signatures that are invoked during the EMT process [15-17] (Supplemental Figure 2A-C). Additionally, gene sets characteristic of phenotypic changes and molecular signaling alterations that are prerequisites for EMT were enriched in ZR-shEI24 cells (Supplemental Table 1, 2). In this context, we investigated whether reduced expression of EI24 induces EMT. Consistent with the molecular transition, EI24 knockdown induced a morphological change of ZR-75-1 cells to the fibroblast-like scattered morphology of mesenchymal cells (Figure 2A). A significant reduction in the expression of epithelial markers such as E-cadherin, β-catenin, and γ-catenin and emergence of the mesenchymal marker vimentin further supported the induction of EMT by EI24 knockdown (Figure 2B). Moreover, expression of the epithelial marker E-Cadherin in the cell-to-cell contacts was significantly decreased, coincident with increased expression of the mesenchymal marker vimentin (Figure 2C). We consistently found that the level of *CDH1* mRNA was significantly lowered whereas the mRNA levels of *VIM* and *FN1* were considerably increased in EI24 knockdown cells (Figure 2D). Notably, mRNA levels of

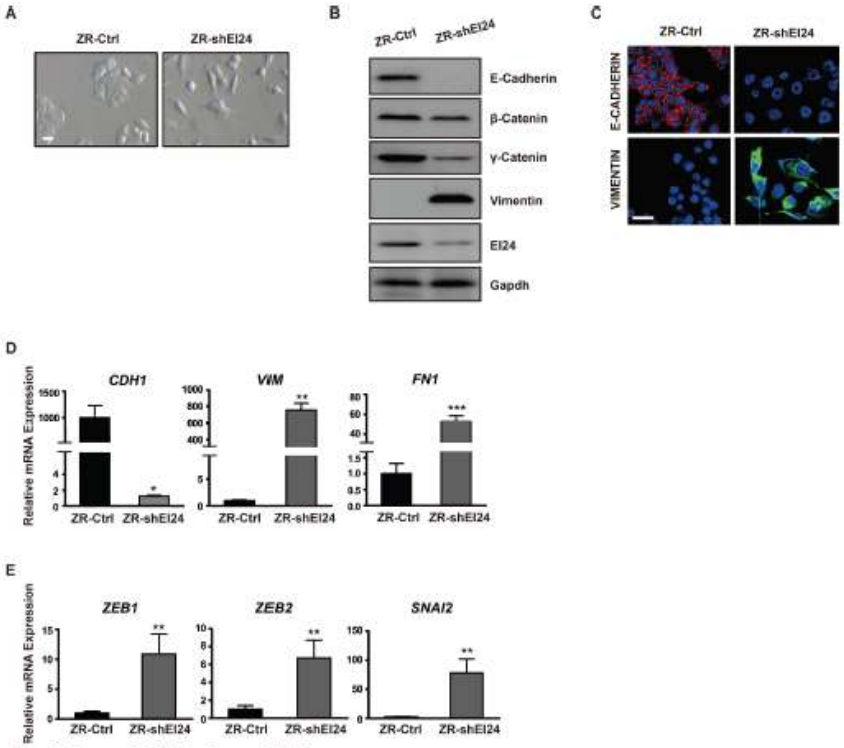

Figure 2: Knockdown of EI24 induces EMT. (A) Phase contrast microscopy of ZR-75-1 cells stably expressing control or EI24-specific shRNA. Scale bar represents 100 μm. (B) Immunoblot analysis of changes in the expression of epithelial and mesenchymal markers in control and ZR-shEI24 cells. (C) Confocal microscopic analysis of E-cadherin and Vimentin expression in ZR-Ctrl and ZR-shEI24 cells. Scale bar represents 50 μm. (D) and (E) Real-time quantitative PCR (qPCR) analysis of transcriptional regulation of the expression of epithelial and mesenchymal markers (D) and EMT-related transcription factors (E) in control and ZR-shEI24 cells. Data are means of measurements from two independent experiments performed in triplicate; P values were calculated by unpaired t-test using GraphPad Prism software. *p <0.05, **p <0.01, ***p <0.0001.

EMT-related transcription factors including *ZEB1*, *SIP1*, and *SLUG* were also significantly increased in ZR-shEI24 cells (Figure 2E). Collectively, these data indicate that EI24 plays an important role in maintaining epithelial characteristics; thus, reduced expression of EI24 promotes the initiation of EMT.

Reduced EI24 expression potentiates malignant properties of tumor cells

Since EMT is a characteristic feature of malignant tumors, we investigated cellular properties that are accompanied by EMT in the context of EI24 dysregulation. Matrigel invasion assays revealed that EI24 overexpression inhibited the invasive capacity of malignant B16F10 cells (Figure 3A, top panel). In contrast, ZR-shEI24 cells showed increased invasiveness (Figure 3A, bottom panel). ZR-shEI24 cells in 3D-culture consistently displayed invasive characteristics compared with the rounded morphology of the control cells (Figure 3B). We next examined the effect of EI24 on anchorage independent survival by measuring the cell viability after inducing the anoikis. After 72 hours, the EI24 knockdown cells survived approximately 15% more than the control cells (Figure 3C). This result indicates that loss of EI24

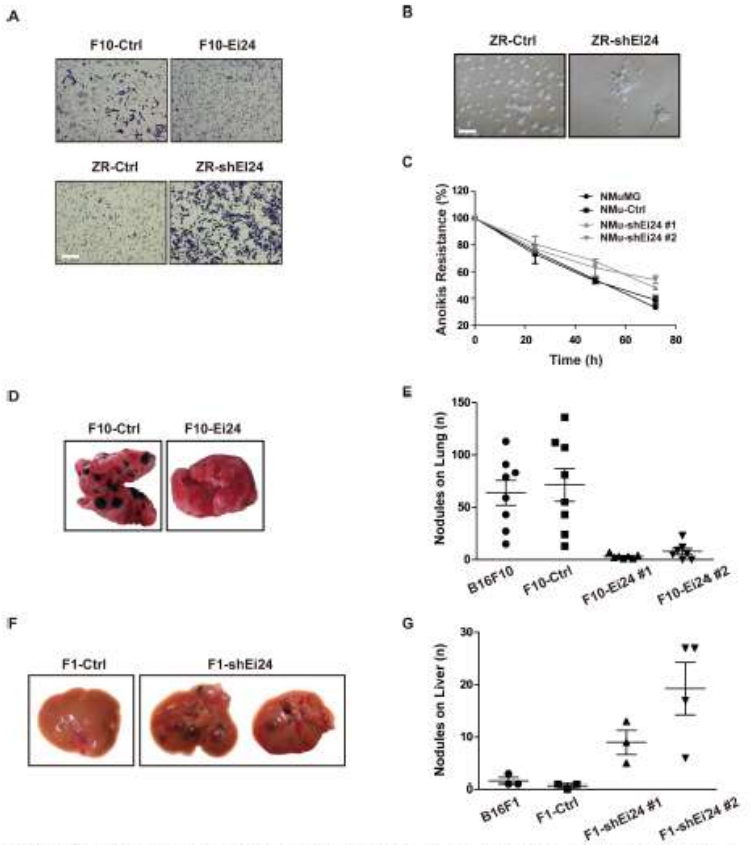

Figure 3: Knockdown of EI24 promotes malignant characteristics that accompany EMT. (A) The indicated cell lines were added to Matrigel-coated transwell inserts, and invading cells were visualized after 16 hours by crystal violet staining. Scale bar represents 200 μm. (B) Formation of invasive acini was evaluated using the 3D matrigel assay. The data are representative of at least two independent experiments. Scale bar represents 100 μm. (C) NMuMG-Ctrl and NMuMG-shEi24 cells were maintained in suspension using ultra-low-attachment plates and cell viability was analyzed at the indicated time points. (D) and (E) F10-Ctrl or F10-EI24 cells were intravenously injected into C57BL/6NTac mice and specific metastatic ability was analyzed by counting nodules in the lungs; $n \geq 7$; one-way analysis of variance, $p < 0.0001$. (F) and (G) F1-Ctrl or F1-EI24 cells were intravenously injected into C57BL/6NTac mice and their specific metastatic ability was analyzed by counting nodules in the liver; $n \geq 3$; one-way analysis of variance, $p < 0.01$.

protects cells from anoikis. Taken together, acquisition of invasive characteristics and resistance to anoikis upon reduced levels of EI24 facilitates the enhanced malignancy of tumor cells.

To validate our in vitro findings using in vivo analyses, we adopted a well-established mouse model of experimental metastasis by injecting B16 variant cells intravenously into congenic C57BL/6NTac mice [18]. Control B16F10 cells formed large numbers of visible metastasized nodules, whereas the formation of lung nodules was significantly attenuated in mice injected with F10-Ei24 cells (Figure 3D, 3E). When liver-colonizing B16F1 variant cells were injected into C57BL/6NTac mice [19], Ei24 knockdown increased the formation of metastatic nodules in the mouse liver, compared to the number of nodules formed by control cells (Figure 3F, 3G). Collectively, these data support the notion that reduced expression of EI24 promotes tumor malignancy in vitro and in vivo.

EI24 inhibits NF-κB transcriptional activity and the expression of inflammation-associated target genes

To elucidate the molecular mechanism governing EI24-mediated regulation of EMT, we treated ZR-shEI24 cells with specific inhibitors of several pathways. Although most of the inhibitors had no effect, the NF-κB inhibitor BAY 11-7082 restored the epithelial morphology (Supplemental Figure 3A). From these data, we surmised that EI24 suppresses EMT by negatively regulating NF-κB signaling. Consistent with this, overexpression of EI24 suppressed NF-κB reporter activity in MDA-MB-231 cells (Figure 4A). These observations were also confirmed using EI24 overexpression and knockdown

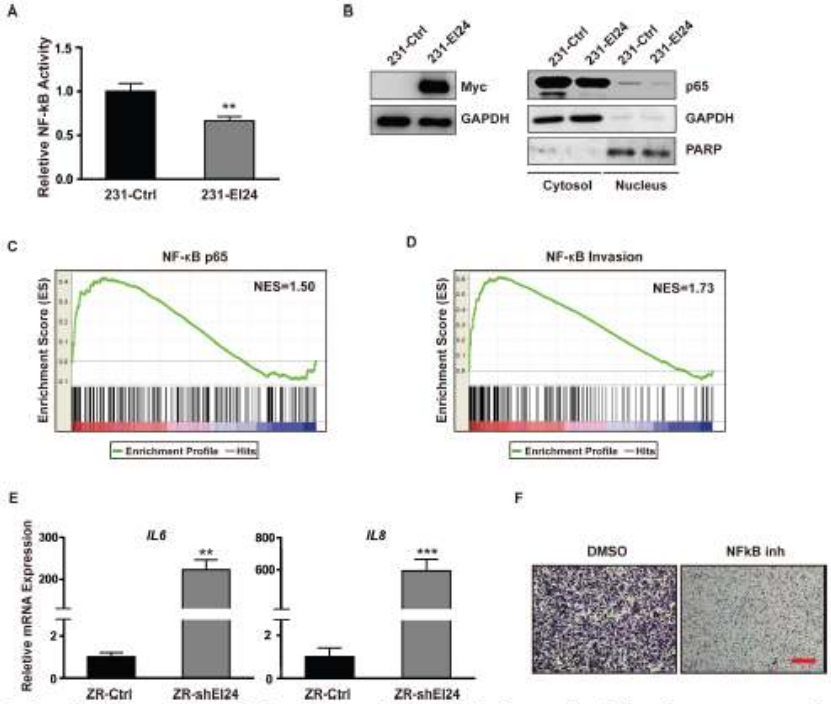

Figure 4: NF-κB activation and upregulation of genes involved in inflammation-induced tumor progression by EI24 knockdown. (A) The transcriptional activity of NF-κB in control and EI24-overexpressing MDA-MB-231 cells was evaluated using a NF-κB luciferase reporter assay. Data shown are mean ± S.D. n = 6, **p <0.0001. (B) Immunoblot analysis of p65 expression levels in nuclear extracts from control and EI24-overexpressing MDA-MB-231 cells. (C) and (D) GSEA for gene signatures in EI24 knockdown cells indicating genes that contain p65-binding sites in their promoter regions (p <0.001; C) and genes that are targets of NF-κB and are associated with tumor invasiveness (p <0.001; D). NES, normalized enrichment score. (E) Relative mRNA expression levels of the indicated genes in control and ZR-shEI24 cells analyzed by real-time qPCR. Data shown are the mean ± S.D. of two independent experiments with each sample assayed in triplicate; P values were calculated by unpaired t-test using GraphPad Prism software. *p <0.005, **p <0.0001, ***p <0.0005. (F) Cell migratory potential was measured after treatment of ZR-shEI24 cells with an NF-κB inhibitor. The red scale bar represents 200 μm.

systems in HeLa cells (Supplemental Figure 3B, 3C). EI24 overexpression in MDA-MD-231 cells significantly decreased nuclear localization of the p65 subunit of NF-κB (Figure 4B), whereas F10-shEI24 cells exhibited an increase in p65 in the nucleus (Supplemental Figure 3D). Furthermore, when GSEA was performed using a gene set from the Molecular Signatures Database (MSigDB) that contained the GGGRATTTCC motif, the consensus binding sequence for p65 transcription factors, in their promoter regions [20] this gene signature was enriched in ZR-shEI24 cells (Figure 4C). Notably, the expression levels of NF-κB target genes that are associated with tumor invasiveness [21] were also significantly enhanced in ZR-shEI24 cells (Figure 4D). For example, ZR-shEI24 cells exhibited upregulation of *IL6* and *IL8*, NF-κB target genes that are involved in inflammation-induced tumor metastasis (Figure 4E). Consistent with these data, *IL6* and *IL8* were downregulated in MDA-MB-231 cells upon overexpression of EI24 (Supplemental Figure 3E). Moreover, treatment of ZR-shEI24 cells with the NF-

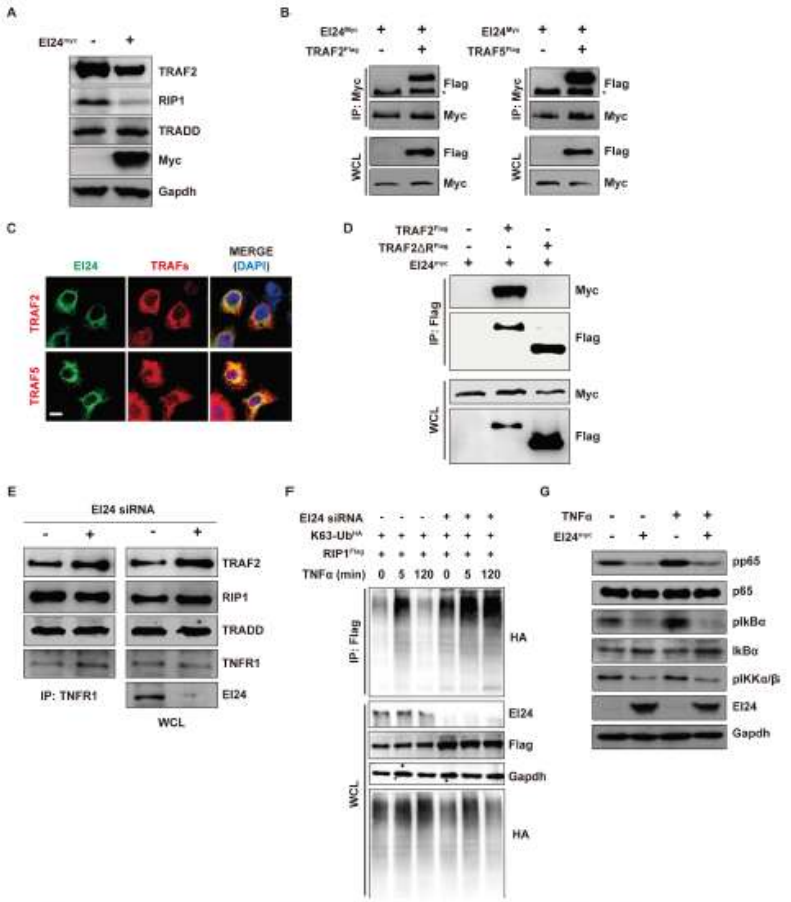

Figure 5: EI24 binds to and promotes degradation of Complex I components, thus inhibiting downstream signaling. (A) Immunoblot analysis of degradation of TRAF2, RIP1, and TRADD induced by EI24. (B) Interaction between EI24 and TRAF2/5 in 293T cells assessed using immunoprecipitation. (C) Colocalization of EI24 with TRAF2/5 in HeLa cells. Scale bar represents 10 μm. (D) Immunoprecipitation experiments showing that the RING domain of TRAF2 is required for its interaction with EI24. (E) siRNA-mediated knockdown of EI24 increases the binding of TRAF2 to TNFR1. Binding of TNFR1 with TRAF2, TRADD, and RIP1 was examined in control and EI24 knockdown 293T cells. WCL, whole cell lysate. (F) EI24 knockdown results in accumulation of K63-linked RIP1. RIP1-K63 ubiquitination was examined in the presence of TNFα at the indicated time points. (G) Downstream molecules of Complex I-mediated signaling were evaluated upon EI24 overexpression. Levels of phospho (p)-IKKα/β, p-IκBα, IκBα, p-p65, and p65 in MDA-MB-231 cells were determined by immunoblotting.

κB inhibitor BAY 11-7082 significantly decreased cell migration compared with the control treatment (Figure 4F). Taken together, these data demonstrate that EI24 attenuates NF-κB-mediated tumor malignancy.

EI24 knockdown promotes sustained TNFR1 Complex I signaling

Next, we focused on identifying upstream components of the molecular mechanism by which loss of EI24 increases NF-κB transcriptional activity. Among several pathways that converge on NF-κB, the most prominent is the Complex I (TRADD, RIP1, and TRAF2) signaling cascade induced by the binding of TNFα to its receptor [5]. We confirmed involvement of EI24 in this process by GSEA using gene signatures of the TNFα pathway acting through NF-κB [22] in EI24 knockdown cells (Supplemental Figure 4A). Because TRAF2 is known to be a mediator of inflammatory cytokine-induced NF-κB activation [23] and reduced levels of EI24 resulted in the promotion of tumor invasiveness through NF-κB (Figure 4), we examined whether the increase in NF-κB transcriptional activity upon EI24 knockdown is mediated through activation of Complex I signaling. First, we assessed changes in protein levels of Complex I

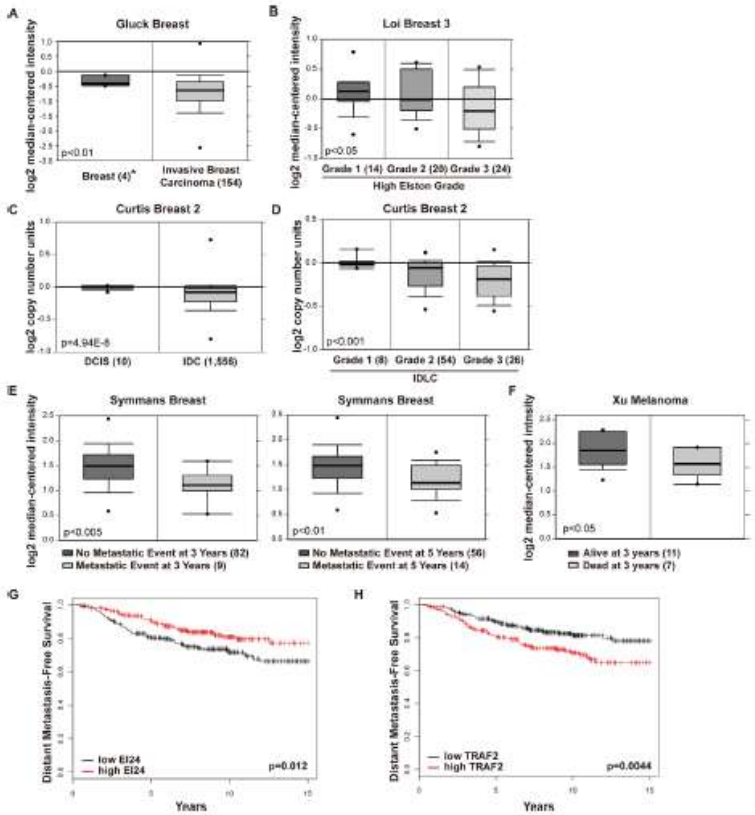

Figure 6: Decreased expression of EI24 correlates with increased tumor invasiveness and poor prognosis in human patients. (A) Box plots showing EI24 gene expression in normal breast tissue and invasive breast carcinoma of breast cancer patients. (B) Box plots showing EI24 gene expression in high Elston-Ellis grade breast carcinomas. (C) and (D) Box plots showing EI24 gene copy numbers in DCIS and IDC (C), and in IDLC of various tumor grades (D). (E) EI24 gene expression in patients with breast cancer and its association with clinical outcomes at 3 and 5 years in patients with one or more metastatic events. (F) EI24 gene expression in melanoma patients and clinical outcomes at 3 years. (G) and (H) Kaplan-Meier plots of distant metastasis-free survival of human breast cancer patients. ER-positive patients (n = 417) were evaluated from 2011 version of database and categorized by median expression of EI24 (probe set 208289_s_t, G) or TRAF2 (probe set 204413_at, H). The p-values were calculated using the log-rank test. *Numbers in parentheses indicate number of samples included in the study.

components. RIP1, TRAF2, and TRAF5 were significantly downregulated by EI24 overexpression and upregulated by EI24 knockdown (Figure 5A, Supplemental Figure 4B, 4C). Based on previous reports showing that EI24 acts as an inducer of autophagy [24, 25], we examined whether inhibition of lysosome function rescues the degradation of TRAF2 and TRAF5 that is mediated by overexpression of EI24 and found that treatment with the lysosome inhibitor bafilomycin A1 impeded EI24-mediated degradation of TRAF2 and TRAF5 (Supplemental Figure 4D). This result suggests that the regulation of NF-κB activity by EI24 is mediated through lysosomal degradation of Complex I components.

Since TNFα-induced NF-κB signaling in mice is impaired only when *Traf2* and *Traf5* are deficient [26], it is plausible that the simultaneous downregulation of TRAF2 and TRAF5 by EI24 results in activation of the NF-κB pathway. To examine whether the degradation of TRAF2 and TRAF5 by EI24 is mediated through a physical interaction between these proteins we performed immunoprecipitation and immunofluorescence assays in 293T and HeLa cells and showed that EI24 bound to and colocalized with both TRAF2 and TRAF5 (Figure 5B, 5C, Supplemental Figure 4E). Domain mapping assays revealed that the Really Interesting New Gene (RING)-domain of TRAF2 facilitates the binding of TRAF2 with EI24 and the degradation of TRAF2 (Figure 5D, Supplemental Figure 4F). Furthermore, knockdown of EI24 resulted in increased binding of TRAF2 to TNFR1 without affecting the interaction between RIP1 and TRADD in Complex I (Figure 5E). These data indicate a role of EI24 recruitment and degradation of the components of Complex I in the alleviation of TNFR1 signaling.

TRAF2 is a key component of NF-κB signaling through its role as an RING-domain-containing E3 ubiquitin ligase that mediates the K63-linked polyubiquitination of RIP1 [27]. In turn, K63-linked polyubiquitinated RIP1 functions as a scaffold for the assembly of factors that activate IKK in NF-κB activation-dependent inflammatory signaling pathways [28]. Because knockdown of EI24 resulted in the accumulation of TRAF2, we examined the K63-ubiquitination status of RIP1. After treatment with TNFα, K63-linked ubiquitination of RIP1 was sustained for 2 hours in EI24 knockdown cells but was almost completely absent in control cells at the same time point (Figure 5F). These data imply that in the course of signal transduction a

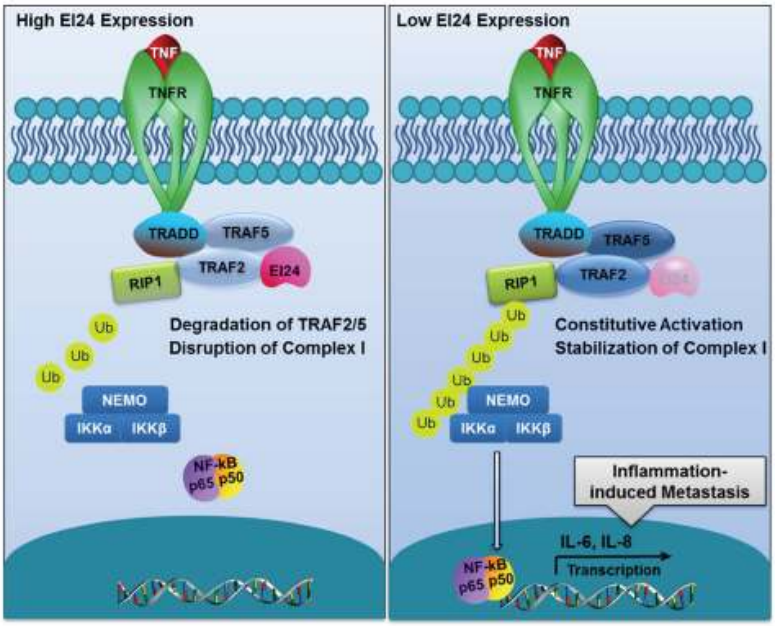

Figure 7: Proposed model of EI24-mediated suppression of tumor progression through the alleviation of NF-κB signaling. In the presence of EI24, TRAF2/5 in Complex I are bound with EI24 and subsequently degraded, functioning as a negative regulatory mechanism for the attenuation of downstream NF-κB signaling. When the EI24 level is low, TRAF2 accumulates and promotes Complex I assembly, activation, and the nuclear translocation of NF-κB, resulting in the induction of inflammation-related cytokine expression.

reduction in the EI24 level plays an important function in sustaining activation of downstream NF-κB signaling by maintaining K63-ubiquitination of RIP1. Consequently, the downstream molecules of Complex I accumulated upon EI24 knockdown, resulting in activation of IKKβ, IκBα, and p65 (Supplemental Figure 4G). We also verified that the TNFα-mediated activation of NF-κB was significantly suppressed by ectopic EI24 expression in MDA-MB-231 cells (Figure 5G). Conversely, knockdown of EI24 augmented TNFα-mediated NF-κB activation (Supplemental Figure 4H). Taken together, these data demonstrate that EI24 acts as a negative regulator of TRAF2 signaling by degrading Complex I components, leading to decreased NF-κB transcriptional activity.

EI24 expression is inversely correlated with tumor invasiveness and poor prognosis in human patients

To validate our findings from cell lines and mouse models in human patients, we searched publicly accessible microarray datasets for correlations between EI24 expression and clinically relevant parameters [29]. The Gluck breast dataset [30] showed markedly reduced *EI24* mRNA expression in invasive breast carcinomas compared with that in normal breast tissues (Figure 6A). In a dataset from The Cancer Genome Atlas (TCGA), EI24 expression was downregulated in invasive ductal breast carcinomas (IDCs) and invasive lobular breast carcinomas (ILCs) compared with normal breast samples (Supplemental Figure 5A). Furthermore, EI24 expression correlated negatively with the progression stage of breast cancer (Figure 6B) measured using the Elston-Ellis grading system [31]. Consistent with the EI24 expression pattern, the copy number of the *EI24* gene was decreased in IDC [32] compared with ductal carcinoma in situ (DCIS, Figure 6C). Furthermore, *EI24* copy number loss correlated with high tumor grade in IDC and ILC (Figure 6D). We also detected loss of *EI24* copy number in the most common types of invasive breast cancer, such as IDC, ILC, and mixed ductal/lobular carcinoma (IDLC), in the TCGA database (Supplemental Figure 5B). Similar *EI24* gene expression patterns were observed in metastatic tumors from various types of cancers (Supplemental Figure 5C). These findings demonstrate that the expression level and copy number of the *EI24* gene might be good prognostic markers in breast cancer patients.

Based on these data, we analyzed the correlation between EI24 expression level and clinical outcomes in patients with breast tumors. In the Symmans 2 and Loi breast cancer datasets [33, 34], estrogen receptor (ER)-positive breast cancer patients with metastatic events at both 3 and 5 years expressed lower levels of EI24 compared with their non-metastatic counterparts (Figure 6E, Supplemental Figure 6A). Furthermore, *EI24* gene copy numbers were lower in the group of patients with a metastatic event at 5 years than in patients without a metastatic event (Supplemental Figure 6B). Patients with melanoma who died with metastases at 3 years [35] had lower tumor EI24 expression than patients who were alive at 3 years (Figure 6F). To determine the prognostic importance of EI24 expression, the survival rate of metastatic tumor patients was evaluated using the method described in a previous study [36]. Although there was not a statistically significant correlation between the survival rate of ER-negative breast cancer patients and the expression levels of EI24 and TRAF2 in patients without distant metastasis (Supplemental Figure 6C, 6D), there was a significant correlation between poor survival rate and low EI24 and high TRAF2 expression in ER-positive breast cancer patients (Figure 6G, 6H). Collectively, data from clinical tumor samples reinforce the important role of EI24 in suppressing tumor malignancy.

Taken together, these results support a model in which EI24 coordinates EMT and tumor progression through the regulation of TRAF2-mediated NF-κB activity. The pathway identified in this study is illustrated in Figure 7.

DISCUSSION

In this study, we demonstrated that the reduced expression of a single gene, *EI24*, results in the acquisition of systemic traits that strongly favor tumor progression. Reduction of EI24 expression in tumor cells resulted in the acquisition of various mesenchymal characteristics through the induction of EMT and upregulation of inflammation-related gene expression. We further showed that EI24 promotes tumor progression in a NF-κB-dependent manner by sustaining TNFR1-Complex I activity. In contrast, ectopic expression of EI24 in tumor cells suppressed malignant progression. The multifaceted functions of EI24 in processes required for tumor malignancy make this gene an attractive candidate for therapeutic intervention. Previous studies have shown that the transcriptional activity of NF-κB is required for maintenance of an invasive phenotype in cancers through the upregulation of inflammatory cytokines [37]. Furthermore, NF-κB directly or indirectly regulates mesenchymal markers and EMT-related transcription factors [38]. We found that the induction of EMT upon EI24 ablation was mechanistically similar to the process driven by activation of NF-κB signaling during tumor progression. Based on these observations, we conclude that EI24 inhibits transcriptional activities required for execution of the EMT program in malignant tumor cells.

Since NF-κB is essential for the induction and maintenance of EMT and tumor progression [7], identification of regulators that might be manipulated to decrease NF-κB activity could lead to an ideal therapeutic strategy. Here, we show that the induction of tumor

progression by EI24 knockdown involves the activation of NF-κB signaling. A reduction in the level of EI24 induces the expression of the inflammatory cytokines IL-6 and IL-8 that are implicated in tumor malignancy in ZR-75-1 cells, which do not intrinsically express these cytokines. Thus, attenuation of NF-κB signaling by endogenous EI24 is crucial for the suppression of inflammation-induced tumor progression. Since NF-κB is specifically involved in EI24-mediated suppression of EMT without the involvement of other signaling pathways such as PI3K, TGFβ, and p38 MAPK, the therapeutic approach proposed in this study could be a good way to treat tumor progression without severe side effects.

Deubiquitinases such as CYLD or A20 have been proposed as therapeutic targets in inflammatory disorders that involve dysregulation of NF-κB through the regulation of Complex I activity [39]. Moreover, a recent study suggested that degradation of TRAF2 by CHIP results in reduced tumor invasiveness by inactivating NF-κB activity [40]. Here, we demonstrate that lysosome-dependent degradation of the Complex I components TRAF2/5 by EI24 is a novel mechanism for attenuating NF-κB signaling. Thus, as an alternative to CYLD or A20, induction of EI24, which plays a pleiotropic anti-metastatic role, provides a novel molecular target for attenuating NF-κB activation. Consistent with this proposal, a recent study described a therapeutic intervention that targets TRAF protein for the treatment of a cytokine-driven inflammatory disease [41].

Loss of p53 creates an inflammatory microenvironment in an NF-κB-dependent manner to facilitate EMT during tumor progression [42]. Since EI24 contributes to generation of the NF-κB-dependent inflammatory microenvironment and is a transcriptional target of p53, the induction of EMT upon p53 loss may be equivalent to that induced by depletion of EI24 expression. Thus, EI24 may be the effector molecule for p53-mediated suppression of EMT and tumor progression, although further studies are needed to delineate the role of the p53-EI24 axis in these processes.

We used clinical samples from cancer patient-based datasets to investigate the role of EI24 in EMT and tumor progression. Using widely accepted parameters such as changes in mRNA expression and gene copy number variation, our study confirmed that a low level of EI24 correlates with tumor malignancy in humans. Although the current study primarily included melanoma and breast cancers, we also observed decreased EI24 expression in clinical datasets of metastatic ovarian, prostate, and colorectal cancers. Further extensive investigations are needed to elucidate the precise role of EI24 in these cancers.

Collectively, these studies indicate that the expression level of EI24 in malignant tumors could be a useful diagnostic marker. Furthermore, induction of the *EI24* gene may be an effective therapeutic intervention for patients whose tumors carry an intact genomic profile of *EI24*.

MATERIALS AND METHODS

Cell culture and generation of stable cell lines

The melanoma B16F1 cells were obtained from the Korean Cell Line Bank (cellbank.snu.ac.kr), and breast cancer NMuMG and MDA-MB-231 cells from the American Type Culture Collection (ATCC; www.atcc.org). 4T1 and ZR-75-1 were kindly provided by Drs. Goo Taeg Oh (Ewha University), Sung Hee Baek (Seoul National University), and Jaewhan Song (Yonsei University), respectively. B16F1, B16F10, and MDA-MB-231 cells were cultured in Dulbecco's modified Eagle medium (DMEM, HyClone) supplemented with 10% FBS (HyClone). ZR-75-1 and 4T1 cells were maintained in Roswell Park Memorial Institute Medium (RPMI1640, HyClone) supplemented with 10% FBS. NMuMG cells were grown according to ATCC guidelines.

Human and mouse stable EI24-overexpressing and control (empty vector-harboring) cell lines were generated by transfection with a plasmid containing flag-tagged EI24 or the corresponding empty vector (pcDNA3.1). Clones were selected using G418-containing medium and examined for EI24 expression by immunoblotting. Human and mouse EI24-knockdown stable cell lines were generated as described previously [43].

Plasmids and reagents

The mouse EI24 constructs were generated as described previously [10]. The human *EI24* ORF was purchased from OriGene and subcloned into the pCS5-3xMyc vector for tagging with myc. TRAF2, TRAF5, RIP1, K63-3x-HA-Ub, and TRADD constructs were generously provided by Dr. Jaewhan Song (Yonsei University). shRNAs against human and mouse EI24 were purchased from Sigma-Aldrich. siRNA sequence against human EI24 is described previously [25]. BAY 11-7082, SB203580, SB435142, and Wortmannin were purchased from Tocris.

Immunoblotting, immunoprecipitation, and antibodies

Protein extraction and immunoprecipitation were performed as described previously [44]. Exposures were acquired using a LAS-3000 Imager (Fujifilm). The following antibodies were used: anti-EI24 [44], anti-E-cadherin (Cell Signaling Technology, #4065), anti-β-catenin (BD Transduction, #610153), anti-γ-catenin (Cell

Signaling Technology, #2309), anti-vimentin (Abcam, #ab8978), anti-TRAF2 (Cell Signaling Technology, #4724), anti-RIP1 (BD Transduction, #610459), anti-TRADD (Santa Cruz Biotechnology, #sc-7868), anti-TNFR1 (R&D systems #AF225 for IP; Santa Cruz Biotechnology #sc-8436 for IB), anti-poly (ADP-ribose) polymerase (PARP; Cell Signaling Technology, #9542), anti-p65 (Cell Signaling Technology, #8242), anti-phospho (p)-p65 (Cell signaling Technology #3033), anti-IKKβ (Cell Signaling Technology, #2370), anti-p-IKKα/β (Cell Signaling Technology, #2697), anti-IκBα (Cell Signaling Technology, #4814), anti-p-IκBα (Cell Signaling Technology, #2859), anti-MYC (Cell Signaling Technology, #2276 and #2278), anti-HA (Santa Cruz Biotechnology, #sc-7392), and anti-FLAG (Sigma, #F3165).

Ubiquitination assay

Cells were harvested in PBS containing 2 mM N-ethylmaleimide (NEM) and lysed in Tris-buffered saline (TBS) containing 1% SDS and 20 mM NEM. The lysate was boiled, sonicated, and centrifuged at 14,000 g for 15 min. The supernatant was diluted in NP-40 buffer containing 2 mM NEM, and immunoprecipitation was carried out using standard methods.

RNA isolation and real-time qPCR

Total RNA was prepared with Trizol reagent (Invitrogen). One microgram of total RNA was reverse-transcribed to cDNA using the Superscript III First-Strand Synthesis System with oligo-dT primers (Invitrogen). Real-time qPCR was performed using IQ SYBR Green SuperMix on an iQ5 Real-Time PCR System (Bio-Rad), with each sample measured in triplicate. Relative gene expression values were calculated using the iQ5 optical system software (Bio-Rad) after normalization to the expression levels of *GAPDH*. The sequences of primers were designed using IDT SciTools (www.idtdna.com) and are as follows: human *EI24* forward, 5′- AATGCACCAGCGGTTGTCTAA-3′; human *EI24* reverse, 5′-GATAGAGAAAAGGCAGCCACTGA-3′, human *CDH1* forward, 5′-CTACGGAGGAGAACGGTGGT-3′; human *CDH1* reverse. Primer sequences for assessment of human *IL6* and *IL8* [45] and other EMT-related genes [46] were described previously.

Migration and invasion assay

Migration assays were performed using the Transwell Permeable Support System (Corning Costar) with a fibronectin pre-coated polycarbonate membrane (8 μm pore size). The invasion assay was performed with the BD BioCoat Matrigel Invasion Chamber (BD Bioscience). For both assays, cancer cell lines cultured in serum-free medium were seeded on the top of the upper chamber, while the bottom chambers were filled with regular culture media. Cells that had moved and were attached to the lower side of the membrane were fixed and cells remaining in the upper chamber were removed using a cotton swab. Cells that had migrated to the lower side of the membrane were stained with crystal violet and assessed the migration and invasion abilities of the cells.

Hanging drop assays

Approximately 25,000 single cells were dropped onto the lid of a 60-mm culture dish (Nunc). The corresponding bottom surfaces of each dish contained the appropriate culture media to maintain humidity. The images of drops were captured with an inverted microscope (×4 magnification; Nikon). At least five independent drops were analyzed for each experiment. The area of cell clusters was determined using the NIS-Element Analysis Tool for the Nikon microscope (Nikon).

Anoikis assay

Equal volumes and numbers of cells were maintained in ultra-low-attachment plates (Corning Costar) to induce anoikis. Live/dead cells were scored by manual counting following Trypan Blue staining (Sigma-Aldrich) at the indicated time points according to the manufacturer's instructions.

3D Matrigel culture

ZR-Ctrl and ZR-shEI24 cells in growth medium containing 2% Matrigel were seeded on 8-well chamber slides (BD Biosciences) pre-coated with Matrigel. Cell morphology was assessed and the cells were photographed under a microscope (Nikon) over time until invasive acini appeared.

Immunocytochemistry

Cells were seeded on 4- or 8-well chamber slides (BD Bioscience) at a density of 3×10^4 cells per slide. The cells were fixed with 4% paraformaldehyde, permeabilized with 0.1% Triton X-100 (Amersham), and then blocked with 2.5% bovine serum albumin (Sigma-Aldrich) for 30 min and incubated with primary antibodies overnight. After staining with Alexa Flour 488- or Alexa Flour 568-conjugated secondary antibodies (Invitrogen) and extensive washing, the slides were mounted with ProLong Gold antifade reagent in the presence of DAPI

for visualization of the nuclei (Invitrogen). Images were captured using a fluorescence microscope (Nikon) or a confocal microscope (Zeiss). The following antibodies were used for immunocytochemistry: anti-Paxillin (BD Transduction, #610569), anti-E-cadherin (Cell Signaling Technology, #4065), anti-Vimentin (Abcam, #ab8978), anti- Rhodamine phalloidin (Invitrogen, R415), anti-MYC (Cell Signaling Technology, #2276 and #2278), and anti-FLAG (Sigma, #F3165).

Luciferase reporter assay

Luciferase reporter assays were performed with the Dual-Luciferase Reporter Assay System (Promega) according to the manufacturer's instructions. Cells were transfected with 4x-κB-luc and pRL-tk, the internal control encoding Renilla luciferase, using lipofectamine 2000 (Invitrogen). After 24 hours, the luciferase activity was measured using a luminometer (Turner Biosystems, Promega) and the relative luciferase reporter activity was calculated after normalization of the firefly luciferase reporter activity to the Renilla luciferase activity.

Animals and in vivo metastasis assay

Wild-type C57BL/6NTac mice were purchased from Taconic (USA). Mice were housed in a specific pathogen-free facility at Yonsei University Laboratory Animal Research Center with a 12-hour dark-light cycle and handled according to the Institutional Animal Care and Use Committee standards. For analysis of in vivo metastasis of melanoma cells, wild-type C57BL/6NTac mice (6-8 weeks old) were injected with 3×10^4 cells resuspended in PBS via the tail veins and sacrificed after 2-3 weeks. Metastatic nodules in the lung and liver were counted under a microscope (Nikon).

Microarray and Oncomine analyses

Gene expression profiling studies of ZR-shEI24 and control cells were performed using the GeneChip human exon 1.0 st array (Affymetrix). RNA samples were prepared using the RNeasy Mini Kit (QIAGEN), and microarray studies were carried out following standard protocols of DNALink, Inc. (http://www.dnalink.com). The expression microarray data will be deposited in the GEO database.

To examine *EI24* gene expression and copy number variation in human patients, we used several datasets from the Oncomine Premium Edition Database (Compendia Biosciences, USA; www.oncomine.org). Statistical analysis of differences in expression was performed using ONCOMINE algorithms as described previously [29].

Gene Set Enrichment Analysis (GSEA)

Version 2.0.10 of the GSEA desktop application was provided by the Broad Institute of MIT and Harvard University (www.broad.mit.edu/gsea) and used as described previously [47]. Gene signatures were obtained from MSigDB v3.1 or from published gene lists as described in the main text. The parameters and presentations of GSEA were processed as described previously [42].

Statistical analysis

Data are presented as mean ± S.D. For statistical analysis we used the GraphPad Prism software. The statistical analyses were conducted using the unpaired t-test unless otherwise stated. Values of $p < 0.05$ were considered statistically significant.

ACKNOWLEDGEMENTS

This research was supported by grants from the National Research Foundation of Korea (NRF) funded by the MEST (2009-0081177 and 2010-0020878), National R&D Program for Cancer Control, MoHWFA (1020220), and Bio-industry Technology Development Program, MAFRA (311054-03-2-HD110), Republic of Korea.

Conflict of Interest

Authors have no potential conflict of interests.

REFERENCES

1. Fidler IJ. The pathogenesis of cancer metastasis: the 'seed and soil' hypothesis revisited. Nature reviews Cancer. 2003; 3(6):453-458.
2. Gupta GP and Massague J. Cancer metastasis: building a framework. Cell. 2006; 127(4):679-695.
3. Thiery JP and Sleeman JP. Complex networks orchestrate epithelial-mesenchymal transitions. Nature reviews Molecular cell biology. 2006; 7(2):131-142.
4. Mantovani A. Molecular pathways linking inflammation and cancer. Current molecular medicine. 2010; 10(4):369-373.
5. Oeckinghaus A, Hayden MS and Ghosh S. Crosstalk in NF-kappaB signaling pathways. Nature immunology. 2011; 12(8):695-708.
6. Grivennikov SI, Greten FR and Karin M. Immunity, inflammation, and cancer. Cell. 2010; 140(6):883-899.
7. Huber MA, Azoitei N, Baumann B, Grunert S, Sommer A, Pehamberger H, Kraut N, Beug H and Wirth T. NF-kappaB is essential for epithelial-mesenchymal transition

Lab Anim Res 2013: 29(3), 162-167
http://dx.doi.org/10.5625/lar.2013.29.3.162

Laboratory Animal Research
http://submissions.kalas.or.kr

Proteomic analysis of liver in miniature pigs according to developmental stages using two-dimensional electrophoresis and matrix-assisted laser desorption/ionization-time of flight mass spectrometry

Sun-Shin Yi[1], Sae-Jin Oh[2], Il-Yong Kim[3], Hye-Jung Yeom[4], Su-Cheong Yeom[5], Seung-Yong Hwang[6], Je-Kyung Seong[3,7]*

[1]*Department of Biomedical Laboratory Science, College of Biomedical Sciences, Soonchunhyang University, Asan, Korea*
[2]*Department of Pathology and Laboratory of Immune Regulation, College of Medicine, Seoul National University, Seoul, Korea*
[3]*Laboratory of Developmental Biology and Genetics, College of Veterinary Medicine, Seoul National University, Seoul, Korea*
[4]*Transitional Research Institute, College of Medicine, Seoul National University, Seoul, Korea*
[5]*Biomedical Center for Animal Resource and Development, Bio-Max Institute, Seoul National University, Seoul, Korea*
[6]*Department of Biochemistry, Hanyang University, Ansan, Korea*
[7]*Interdisciplinary Program for Bioinformatics, Program for Cancer Biology and Bio-Max Institute, Seoul National University, Seoul, Korea*

Due to the shortage of human organ donors for transplant, various studies of xenotransplantation, or the use of animal organs instead of human organs, have been carried out. The organs of porcine are thought to be safer and of a more suitable size for xenotransplantationthan those of nonhuman primates. Understanding the levels of expression of proteins, and their post-translational regulation, would be very practical between different species and among developing stages, though the molecular profiling for xenotransplantation has been rarely studied for porcine, while that of human and rodent is well known. Here, in this present study, we report protein regulation of the developing stages of liver (4-day old neonate, 19-day old piglet and 14-month old adult miniature pigs) using 2-DE and MALDI-TOF. From images of the three different stages, a total of 8 spotswhich were differently regulated were identified, and 5 spots were identified with MALDI-TOF MS. The data presented within this study provides critical direction relating to the development of livers of miniature pigs, which will assist future proteome analysis of the liver, and advance our understanding of the hurdles facing xenotransplantaion.

Key words: Liver, MALDI-TOF, miniature pig, proteome, 2-DE, xenotransplantation

Received 24 May 2013; Revised version received 18 July 2013; Accepted 23 July 2013

A comprehensive understanding of the regulation and range of gene expression is very important to elucidate the biological role of the encoded protein. Changes of gene expression configuration can also provide evidence concerning regulatory mechanisms, cellular functions and biochemical pathways [1]. Accordingly, research interest has focused on the identification and characterization of the functional protein products encoded by cell genome, whether independent or organized as a tissue [2].

Protein-based methods are very important because they characterize translational and post-translational modifications. Of the methods, two-dimensional electrophoresis (2DE) and matrix-assisted laser desorption/ionization-time of flight mass spectrometry (MALDI-TOF MS) monitoring of proteome levels are considered

*Corresponding author: Je-Kyung Seong, Laboratory of Developmental Biology and Genetics, College of Veterinary Medicine, Seoul National University, Seoul 151-742, Korea
Tel: +82-2-883-8395; Fax: +82-2-875-8395; E-mail: snumouse@snu.ac.kr

to very promising tools.

The increasing shortage of human donor organ has spurred interest in the possible use of animal organs, particularly nonhuman primates, for human transplantation [3,4]. Presently, the use of nonhuman primate organs as replacements is dangerous, and their organs are too small to permit proper function in human adults [4]. Therefore, at present, most research focuses on the use of pigs instead of nonhuman primates for organ transplantation [5].

Especially, inbred miniature pigs have been introduced by a selective breeding program over the past 25 years, with the goal of successful organ xenotransplantation [4]. However, as with any xenotransplantation effort, the species barrier is an imposing and potentially dangerous obstacle [4]. The barriers to xenotransplantation involving miniature pigs include: 1) rejection due to the immunologic barrier between human and pig, 2) possibility of pathogen infection of human from pigs, 3) problems of physiologic and anatomic incompatibility among species, and 4) social agreements for response of patients.

Overcoming these issues is crucial if xenotransplantation is to be realized. To transplant pigs' organs into humans, we have to know the characteristics of proteins expressed in each organ. Protein expression in organs under the normal condition is unknown, although organs of miniature pigs are similar physiologically and anatomically with those of humans. Little is known regarding characteristics of expressed proteins according to postnatal developmental stages.

The proteome of the pig liver remains largely unexplored. Presently, we focused on the liver, with the hope of acquiring a similar level of information as has been achieved in rodents and humans. A four-day-old miniature pig (neonate),19-day-old miniature pig (piglet), and 14-month-old miniature pig (adult) were used as representative of developmental stages. The liver of each animal was analyzed by 2DE. Various protein expression spots among the three stages were chosen and the proteins were identified by MALDI-TOF MS. Unfortunately, since databases of various proteins in pigs are not as well-established asthose of humans and rodents, it was hard to identify these proteins. Still, the present findings are the first description of differentially expressed protein profiles of liver in miniature pigs according to postnatal development stage.

Materials and Methods

Laboratory animals

The miniature pigs were housed in the air barrier facility of the Center for Animal Resource Development at Seoul National University. Three pigs of different ages and developmental stages described above were used. Intramuscular anesthesia was achieved using a mixture of 2 mL ketamine · HCl (50 mg/mL/kg), 1 mL xylazin (2.3 mg/mL/kg) and 1 mL Atropine sulfate (0.5 mg/mL/10 kg) during every painful/stressful procedure. The abdomen of each pig was shaved and disinfected with polyvinylpyrrolidone-iodine. The animals were immobilized on a surgical plane-table by adhesive ties. A median laparotomy was performed. The livers from the animals were nipped off aseptically and stored in liquid nitrate tank while being transported to the laboratory. These procedures were reviewed by the Institutional Animal and Care and Use Committee, Seoul National University, according to the university regulations.

Sample preparation for 2DE

The livers were removed immediately after sacrifice and stored at −70°C until used. Frozen tissues (1 g) were pulverized under liquid nitrogen into a fine powder using a mortar and pestle. Protein samples were collected and homogenized in 900 μL lysis buffer (7 M urea, 2 M thiourea, 2% w/v CHAPS, 2% Pharmalyte pH 3-10, 100 mMDTE). Samples were centrifuged at 50,000 rpm at 4°C for 1 h. The supernatant was carefully removed and immediately frozen at −70°C.

2DE

2D-polyacrylamide gel electrophoresis (PAGE) was performed as previously described [6]. Aliquots containing 1 mg total protein were diluted in lysis buffer to a total volume of 450 μL. The samples were applied to a 240 mm, immobilized, nonlinear pH 3-10 IPG Drystrip (Amersham Pharmacia Biotech, Piscataway, NJ), which was rehydrated for at least 12 h. After rehydration, the strips were focused at 30 V for 3 h, 100 V for 1 h, 200 V for 1 h, 500 V for 1 h, 1,000 V for 1 h and finally at 8,000 V for 11 h to obtain approximately 90,000 Vh (Ettan™IPGphor™ II IEF systems; Amersham Pharmacia Biotech). Once isoelectric focusing was completed, the strips were equilibrated in 6 M urea containing 20% v/v glycerol, 2% w/v sodium dodecyl sulfate (SDS) and

0.01% w/v full term for BPB with 10 mM Tributyl phosphine (Flukachemie, Buchs, Switzerland). SDS-PAGE was performed using and 8-18% separating gel without a stacking gel using the EttanDalt system (Amersham Pharmacia, Piscataway, NJ). The second dimension electrophoresis was carried out overnight at 3 W/gel at 20℃. The gels were stained with Coomassie G-250 (Bio-Rad Laboratories, Hercules, CA,USA).

Protein visualization and image analysis

The gels were stained with Coomassie G-250 (Bio-Rad) as previously described [7]. The stained gels were scanned using a GS 800 photometer (Bio-Rad) and analyzed with the ImageMaster™ 2D Platinum Software version 5.0 (GeneBio, Geneva, Switzerland). The digitalized 2DE gel images were compared by a matching method. Differentially expressed spots among groups (>3-fold and <1/3-fold) were analyzed and annotated.

In-gel digestion

The spots were cut into smaller pieces and digested using 12.5 ng/μL typsin (Promega, Madison, WI, USA) in 50 mM ammonium bicarbonate, pH 8.0, as previously described (Gorg *et al.*, 2000). For MALDI-TOF MS analysis, the tryptic peptides were concentrated on a POROS 50 R2 column (Applied BioSystems, Foster City, CA, USA). After subsequent washing steps of column with 70% acetonitrile (can) in 5% FA, 100% can and 5% FA, the samples were loaded into a POROS 50 R2 column and washed with 5% FA. The sample was eluted with 2 μL of matrix solution consisting of 10 mg/mL α-cyano-4-hydroxy-cinnamic acid (Sigma-Aldrich, St. Louis, MO, USA) and then dropped onto MALDI sample plate [8].

Protein identification by MALDI-TOF

MALDI-TOF MS was performed using the Voyager DE-PRO spectrometer (Applied Biosystems), equipped with a 337 nm nitrogen laser. The instrument was operated at an accelerating voltage of 20 kV, positive ion reflection mode, voltage grid 74.5%, guide wire voltage 0% and delay-time of 120 ns. The spectra were internally calibrated using the trypsin autolysis products (842.51 [M+H] and 2211.11 [M+H]), and searching in Swiss-Prot identified the proteins and NCBI database using Mascot (Matrix Science, London, UK). Monoisotopic peaks [MH+] were selected and all the searches were analyzed with a 50 ppm mass tolerance.

Results

Protein identification

Profiles of differentially expressed liver proteins were identified with age. The liver proteins were extracted and analyzed by 2D-PAGE. After 2D gels were visualized by Coomassie blue staining, 2DE was repeated for the three pairs of matched samples, three times independently (Figure 1). For each sample, the three gels with the best

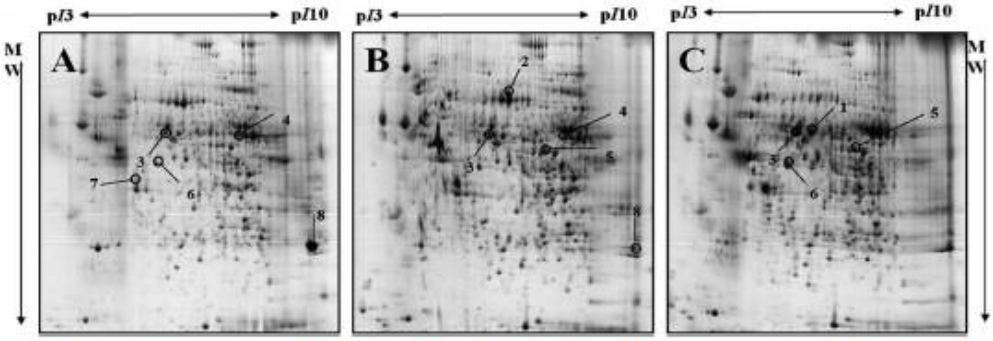

Figure 1. Representative 2-DE gels of livers 4-day, 19-day and 14-month old miniature pigs by developmental stages, which is visualized by Commassie blue staining. Samples of 1 mg protein were separated on pH3-10 non-linear IPG strip (24 cm) following by 8-18% gradient SDS-PAGE gels as the second dimension. Proteins were detected by Coomassie brilliant blue G-250 and compared using ImageMaster™ 2D Platinum Software version 5.0; A: 2-DE gel of 4-day old miniature pig (neonate), B: 2-DE gel of 19-day old miniature pig, C: 2-DE gel of 14-month old miniature pig. The closed circles indicate 13 differentially expressed protein spots among 4-day old miniature neonate pig, 19-day old miniature piglet, 14-month old miniature adult pig.

Table 1. Identified proteins in the liver of miniature pigs by 2DE and MALDI-TOF MS

Spot No.	Name	Accession No.	Sequence Coverage (%)	MW(Da)/pI	Score	Expect	Species	Database
1	Aldehyde dehydrogenase mitochondrial precursor	P20000	14%	56673/7.55	65	3.40e-02	Bovine	Swissprot
2	Serum Albumin precursor	P08835	20%	69647/6.08	107	2.00e-06	Pig	Swissprot
3	Keratin, Type II cytoskeletal-8	P05786	11%	53463/5.60	31	7.50e+01	Bovine	Swissprot
4	Unknown	-	-	-	-	-	-	-
5	Unknown	-	-	-	-	-	-	-
6	Proliferation-associated protein 2G4	Q9UQ80	17%	43628/6.13	34	4.50e+01	Human	Swissprot
7	Lamda-cristallin homolog	Q8SPX7	14%	34918/6.17	26	2.60e+02	Bovine	Swissprot
8	Unknown	-	-	-	-	-	-	-

resolution were selected for analysis. Analysis of spot intensities was calculated and the resulting dataset was found by Image master™ software (Geneva Bioinformatics, S.A, Geneva, Switzerland). Among the 399 protein spots detected, eight different spots were identified. The protein spots that were up-regulated>3-fold or down-regulated<1/3-fold were selected. The selected spots were cut out from the gels and subjected to in-gel digestion with trypsin and peptide fingerprinting by MALDI-TOF MS. The peptide mass data were identified by Mascot. In this way, eight spots displayed a difference between the pigs were evident. Five spots were able to be identified by a protein function search at http://www.ebi.ac.uk/ego (Table 1).

Classification of the identified proteins

The increase and decrease of the selected spot intensities were inspected among the three gels from neonate miniature pig to miniature adult pig (Figure 2). The expression levels of aldehyde dehydrogenase mitochondrial precursor (spot no. 1), was unchanged to up-regulated. The expression levels of serum albumin (spot no. 2) and lamda-crystallin homolog (spot no. 7) were down-regulated. Although spot no. 5 displayed a similar spot intensity patterns, correct identification could not be performed. The expression levels of keratin, a type II cytoskeletal-3 protein, were up-regulated. Proliferation-associated protein 2G4 expression was up-regulated. Although spots no. 4 and no. 8 displayed similar intensity patterns, correct identification could not be performed.

Discussion

This study is, to our knowledge, the first report of protein expression of liver in miniature pig using proteome analysis according to the developmental stage. Few studies have explored the proteome of the whole liver of pigs. A comprehensive understanding of proteins expressed in the liver can provide biological information. About 400 proteins with an isoelectric point of pH 3-10 and Mr of 10-100 kDa were detected. Of 399 spots, eightprotein spots were significantly changed among groups and five spots were identified. Aldehyde dehydrogenase mitochondrial precursor belongs to the aldehyde dehydrogenase family and is associated with ethanol utilization [9]. Serum albumin is the main protein of plasma and has a good binding capacity for water Ca^{2+}, Na^{+}, K^{+}, fatty acids,hormones, bilirubin and drugs. Its main function is the regulation of the colloidal osmotic pressure of blood [10]. Keratin, a type II cytoskeletal-8 protein, helps to link the contractile-apparatus to dystrophin at the costameres of striated muscle and is expressed in bladder, liver, exocervix and esophagus [11]. Proliferation-associated protein 2G4 may play a role in an ERBB3-regulated signal transduction pathway andseems to be involved in growth regulation. Itacts a co-repressorof the androgen receptor and is regulated by the ERBB3 ligandneuregulin-1/heregulin (HRG). It inhibits transcription of someE2F1-regulated promoters, probably by recruiting histone acetylase (HAT) activity. It binds RNA and associates with 28S, 18S and 5.8S maturerRNAs, several rRNA precursors and probably U3 small nucleolar RNA [12]. It may be involved in regulation of the intermediate and late steps ofrRNA processing. It may also be involved in ribosome assembly andmediatescap-independent translation of specific viral IRESs. Lamda-crystallin belongs to the 3-hydroxyacyl-CoA dehydrogenase family and is a lens component. However, it is report to be highly expressed

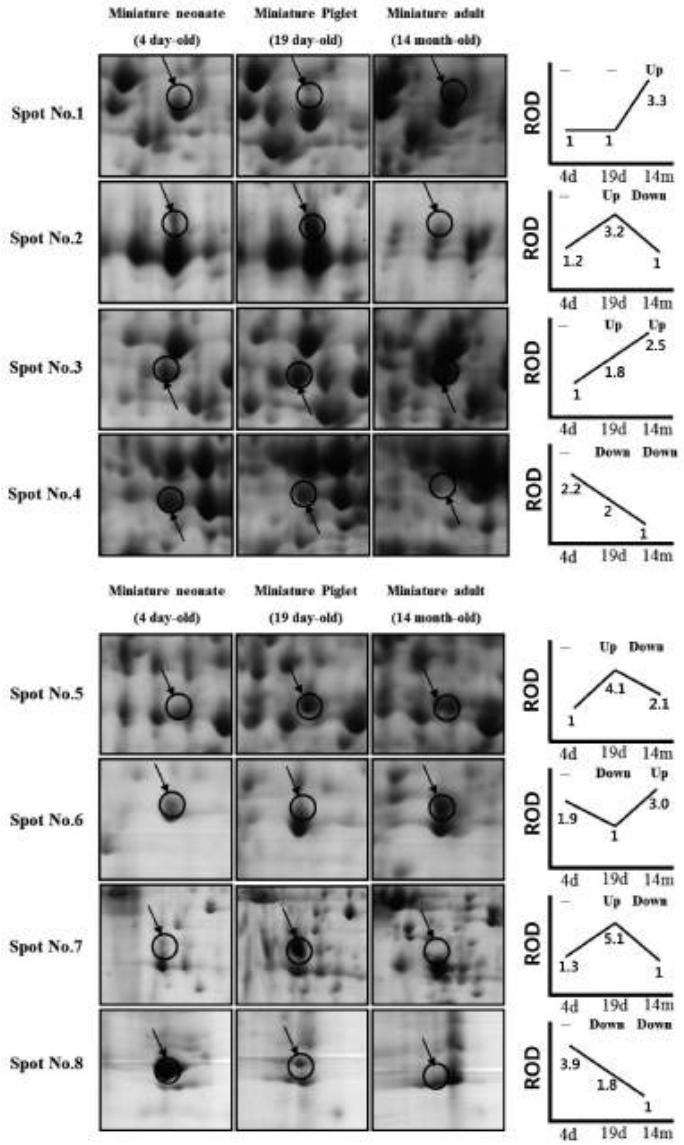

Figure 2. Two-DE images of alterative spots of pancreas according to developmental stage. The circles indicate differentially expressed protein spots and the expression patterns of the different three stages were described as simple line graphs.

in liver and kidney, and might be related to carcinogenesis of liver cancer [13].

Of the fiveidentified spot proteins, except for proliferation-associated protein 2G4, the proteins areexpressed in the liver. However, the identification was done with using other species' homology except serum albumin precursor. Chen et al. and Moller et al. also used human, cattle, mouse, rat homology due to

shortage of database information of the pig [14,15].

Proteome analysis for xenotransplantation has been used for the investigation of target proteins for drugs and to explore the trend of protein expression after transplantation of tumor tissues into animals [16,17]. Anti-cancer drugs have been applied after transplantation of human tumor tissues into animals and the alterations of protein expression between the tumor transplanted tissue group and non-treated tissue group have been compared, with the aim of clarifying the effects of anti-cancer drugs at the protein expression level. To date, the characteristics of protein expression according to developmental stage for xenotransplantation has been essentially not studied. For xenotransplantation pigs are thought to have more potential value than non-human primates.However, one hindrance to this potential has been the paucity of mapping of the protein complement of various organs due to the scant database comparing humans and mice. At present, there are >50,000 and 25,000 database entries for humans and mice, respectively, whereas only 1072 entries for pigs were available in the MSDB database [1]. In addition, we could not confirm the proteomes (spots) identified by the 2DE and MALDI-TOF due to the lack of commercial antibodies. Knowledge of the alteration of the protein complement would provide valuable information to overcome the problems posed by the immunologic barrier, microbiologic differences and xenospecies, which present hinder xenotransplantation [3,18]. Although there is limited data for the livers of miniature pigs due to the lack of a database, the data presented in this study provides for a first reference point for the developmental livers of miniature pigs, providing critical direction for further proteome analysis of livers in future studies.

Acknowledgments

This research was supported by Bio-Industry Technology Development Program Ministry of Agriculture, Food and Rural Affairs to Prof. Je-Kyung Seong (311054-03-2-HD110) and supported by the Soonchunhyang University Fund to Prof. Sun-Shin Yi.

References

1. Junghans P, Kaehne T, Beyer M, Metges CC, Schwerin M. Dietary protein-related changes in hepatic transcription correspond to modifications in hepatic protein expression in growing pigs. J Nutr 2004; 134(1), 43-47.
2. Pan TL, Goto S, Lord R, Huang YC, Huang CM, Wang PW, Lin YC, Kawamoto S, Ono K, Liao PC, Lin CL, Lai CY, Chang HL, Lan CH, Lee TH, Wang YC, Wu ML, Jawan B, Cheng YF, Chen ST, Chen CL. Proteome analysis in liver transplantation. Transplant Proc 2001; 33(1-2): 156.
3. Platt JL. Physiologic barriers to xenotransplantation. Transplant Proc 2000; 32(7): 1547-1548.
4. Cooper DK, Gollackner B, Sachs DH. Will the pig solve the transplantation backlog? Annu Rev Med 2002; 53: 133-147.
5. Tucker A, Belcher C, Moloo B, Bell J, Mazzulli T, Humar A, Hughes A, McArdle P, Talbot A. The production of transgenic pigs for potential use in clinical xenotransplantation: baseline clinical pathology and organ size studies. Xenotransplantation 2002; 9(3): 203-208.
6. Steiner S, Anderson NL. Pharmaceutical proteomics. Ann N Y Acad Sci 2000; 919: 48-51.
7. Görg A, Obermaier C, Boguth G, Harder A, Scheibe B, Wildgruber R, Weiss W. The current state of two-dimensional electrophoresis with immobilized pH gradients. Electrophoresis 2000; 21(6): 1037-1053.
8. Shevchenko A, Wilm M, Vorm O, Mann M. Mass spectrometric sequencing of proteins silver-stained polyacrylamide gels. Anal Chem 1996; 68(5): 850-858.
9. Alnouti Y, Klaassen CD. Tissue distribution, ontogeny, and regulation of aldehyde dehydrogenase (Aldh) enzymes mRNA by prototypical microsomal enzyme inducers in mice. Toxicol Sci 2008; 101(1): 51-64.
10. Akram M, Ali Shah SM, Asif HM, Shaheen G, Shamim T, Khan MI, Ullah A, Ahmed K. Comparative study of similarity and identity of human albumin with some selected organism albumin. J Med Plants Res2011; 5(19): 4974-4976.
11. Magin TM, Jorcano JL, Franke WW. Cytokeratin expression in simple epithelia. II. cDNA cloning and sequence characteristics of bovine cytokeratin A (no. 8). Differentiation 1986; 30(3): 254-264.
12. Parker KA, Bruzik JP, Steitz JA. An in vitro interaction between the human U3 snRNP and 28S rRNA sequences near the alpha-sarcin site. Nucleic Acids Res 1988; 16(22): 10493-10509.
13. Chen J, Yu L, Li D, Gao Q, Wang J, Huang X, Bi G, Wu H, Zhao S. Human CRYL1, a novel enzyme-crystallin overexpressed in liver and kidney and downregulated in 58% of liver cancer tissues from 60 Chinese patients, and four new homologs from other mammalians. Gene 2003; 302(1-2): 103-113.
14. Chen FC, Chuang TJ. ESTviewer: a web interface for visualizing mouse, rat, cattle, pig and chicken conserved ESTs in human genes and human alternatively spliced variants. Bioinformatics 2005; 21(10): 2510-2513.
15. Moller M, Berg F, Riquet J, Pomp D, Archibald A, Anderson S, Feve K, Zhang Y, Rothschild M, Milan D, Andersson L, Tuggle CK. High-resolution comparative mapping of pig Chromosome 4, emphasizing the FAT1 region. Mamm Genome 2004; 15(9): 717-731.
16. Kahlem P, Dörken B, Schmitt CA. Cellular senescence in cancer treatment: friend or foe? J Clin Invest 2004; 113(2): 169-174.
17. Besada V, Diaz M, Becker M, Ramos Y, Castellanos-Serra L, Fichtner I. Proteomics of xenografted human breast cancer indicates novel targets related to tamoxifen resistance. Proteomics 2006; 6(3): 1038-1048.
18. Coggin JH Jr, Barsoum AL, Rohrer JW, Thumher M, Zeis M. Contemporary definitions of tumor specific antigens, immunogens and markers as related to the adaptive responses of the cancer-bearing host. Anticancer Res 2005; 25(3c): 2345-2355.

JPP JOURNAL OF Pharmacy and Pharmacology
ROYAL PHARMACEUTICAL SOCIETY
JPP
Journal of Pharmacy
And Pharmacology
Research Paper

α-Iso-cubebenol inhibits inflammation-mediated neurotoxicity and amyloid beta 1–42 fibril-induced microglial activation

Sun Young Park[a], Tae Gyeong Park[b], Sang-Joon Lee[c], Yoe-Sik Bae[d], Min J. Ko[b] and Young-Whan Choi[b]

[a]Bio-IT Fusion Technology Research Institute, [b]Department of Horticultural Bioscience, [c]Department of Microbiology, Pusan National University, Busan, Korea and [d]Department of Biological Sciences, Sungkyunkwan University, Suwon, South Korea

Keywords
amyloid β; α-iso-cubebenol; microglia; neuroinflammation; nuclear factor-κB; reactive oxygen species

Correspondence
Young-Whan Choi, Department of Horticultural Bioscience, Pusan National University, Miryang 627-706, South Korea.
E-mail: ywchoi@pusan.ac.kr

Received June 3, 2013
Accepted September 16, 2013

doi: 10.1111/jphp.12160

Abstract

Objectives To examine the antineuroinflammatory and neuroprotective activity of α-iso-cubebenol and its molecular mechanism of action in amyloid β (Aβ) 1–42 fibril-stimulated microglia.

Methods Aβ 1–42 fibrils were used to induce a neuroinflammatory response in murine primary microglia and BV-2 murine microglia cell lines. Cell viability was monitored by 3-(4,5-dimethylthiazol-2-yl)-2,5-diphenyltetrazolium bromide assay, protein expression and phosphorylation were determined by Western blot analysis, and matrix metalloproteinase-9 (MMP-9) activity was determined by gelatin zymography assay. In addition, prostaglandin E2 (PGE2), pro-inflammatory cytokines and chemokines were measured by ELISA, and the transactivity of nuclear factor (NF)-κB was determined by a reporter assay.

Key findings α-Iso-cubebenol significantly inhibited Aβ 1–42 fibril-induced MMP-9, inducible nitric oxide synthase and cyclooxygenase-2 expressions and activity, without affecting cell viability. α-Iso-cubebenol also suppressed the production of tumour necrosis factor-α, IL-1β, IL-6, monocyte chemoattractant protein-1 and reactive oxygen species in a dose-dependent manner, while decreasing the nuclear translocation and transactivity of NF-κB by inhibiting the phosphorylation and degradation of the inhibitor of κB (IκB)α. α-Iso-cubebenol suppressed the phosphorylation of mitogen-activated protein kinase (MAPK) in Aβ 1–42 fibril-stimulated microglia. Primary cortical neurons were protected by the inhibitory effect of α-iso-cubebenol on Aβ 1–42 fibril-induced neuroinflammatory response.

Conclusions α-Iso-cubebenol suppresses Aβ 1–42 fibril-induced neuro-inflammatory molecules in primary microglia via the suppression of NF-κB/inhibitor of κBα and MAPK. Importantly, the antineuroinflammatory potential of α-iso-cubebenol is critical for neuroprotection.

Introduction

Schisandra chinensis is a woody vine that is widely distributed throughout Korea, Russia, Japan and China. *S. chinensis* is used in food, wine, tea and traditional medicine. Dibenzocyclooctadiene lignans, which are the main active ingredient of *S. chinensis*, have a variety of biological effects, including anti-oxidative, hepatoprotective, anti-inflammatory, detoxifying and neuroprotective effects.[1–3] Several investigators have demonstrated that dibenzocyclooctadiene lignans can inhibit the production of amyloid β (Aβ) and protect neuronal cells against Aβ-induced neurotoxicity. According to our previous study, α-iso-cubebenol suppresses *Porphyromonas gingivalis*-induced inflammatory responses through the inhibition of the pro-inflammatory response via nuclear factor (NF)-regulated factor 2 and heme oxygenase-1 signalling in phorbol myristate acetate-differentiated human monocytic

leukemia cell line cells.[4] However, the effects of the novel α-iso-cubebenol isolated from *S. chinensis* on Aβ-inducedneuroinflammatory response-mediated neurotoxicity have not been investigated.

Neuroinflammatory responses play an important role in the pathogenesis of various neurodegenerative diseases, such as Alzheimer's disease, Parkinson's disease and multiple sclerosis.[5] Microglia are resident immune cells in the central nervous system (CNS) that can be activated in response to environmental toxins, neuronal death and neuronal damage. Microglia can also defend the host against invasive pathogens and clear toxic cellular debris. However, overactivation under abnormal physical situations causes these cells to induce too many neuroinflammatory responses, leading to neuroinflammation-mediated neuronal cell death and brain injury.[6,7] Therefore, the regulation of microglial activation is a crucial therapeutic target against neurodegenerative disease. In addition, epidemiological studies have shown that treatment with non-steroidal anti-inflammatory drugs can decrease the risk of developing neurodegenerative diseases.[8]

Alzheimer's disease is characterized by extracellular deposition of the Aβ peptide in plaques that colocalize with various neuroinflammatory molecules and activated microglia.[9] Aβ peptides consist of 39–42 amino acid residues that are formed as a result of sequential cleavage of the neuronal membrane protein amyloid precursor protein by β- and γ-secretase in the amyloidogenic pathway. Aβ peptides can form the following toxic species: Aβ peptide dimers, oligomers and fibrils. For example, Aβ 1–42 fibrils, which are composed of 42 amino acid residues, have yielded potent induction of neuronal cell death via the induction of the production of reactive oxygen species (ROS), nitric oxide (NO), neuroinflammatory cytokines, chemokines and several reports have identified the underlying signalling mechanisms.[10,11]

The expression of neuroinflammatory molecules is primarily controlled at the transcriptional level. The transcriptional induction of neuroinflammatory molecules, such as cytokines or inducible NO synthase (iNOS), is dependent on the activity of transcription factors, such as the NF-κB, the activator protein-1, the interferon regulatory factor-1 and Oct. Among these transcription factors, NF-κB has been shown to play a major role in the transcription of neuroinflammatory molecules in response to Aβ 1–42 fibrils.[9] NF-κB is a heterodimeric transcription factor composed of p50 and p65. In unstimulated cells, NF-κB is present in the cytosol bound to the inhibitor of κBα (IκBα). After stimulation by factors such as Aβ 1–42 fibrils, IκB undergoes phosphorylation and degradation. In this process, free NF-κB dimers translocate to the nucleus, bind to the promoter regions of neuroinflammatory molecules and induce their transcription. The mitogen-activated protein kinase (MAPK) signalling pathway is also involved in Aβ 1–42 fibril-induced microglial activation. MAPK are classified into three components: the extracellular signal-regulated kinase (ERK), c-Jun NH(2)-terminal kinase (JNK) and p38 MAPK, which are involved in the expression and activation of neuroinflammatory molecules, such as iNOS, cyclooxygenase-2 (COX-2) and matrix metalloproteinase-9 (MMP-9).[12,13]

In this study, we present the first evidence that α-iso-cubebenol isolated from the *S. chinensis* fruit exhibits significant antineuroinflammatory and neuroprotective properties against Aβ 1–42 fibril-induced neuroinflammatory responses in microglia. This study highlights the important role of neuroprotection in mediating Aβ 1–42 fibril-induced neuroinflammatory responses in neurons and microglia, and provides insight into the development of antineuroinflammatory treatments for neurodegenerative diseases.

Material and Methods

Materials

Aβ 1–42 fibrils were obtained from Bachem Bioscience (King of Prussia, PA, USA). The cell culture media Dulbecco's Modified Eagle Medium (DMEM), DMEM/F12 and fetal bovine serum (FBS) were purchased from Gibco BRL (now Invitrogen Corporation, Carlsbad, CA, USA). Other reagents were purchased from Sigma (St. Louis, MO, USA). Protoporphyrin IX (SnPP) and antibodies against iNOS, COX-2, NF-κB, IκBα, TATA-binding protein and α-tubulin were purchased from Santa Cruz Biotechnology (Santa Cruz, CA, USA). Antibodies against phosphorylated p38 (p-p38) (Thr180/Tyr182), p-JNK (Thr183/Tyr185), p-ERK (Thr202/Tyr204), p-p65 (Ser536), p-IκB α (Ser32), and MMP-9 were purchased from Cell Signaling Technology (Beverly, MA, USA). The FuGENE 6 transfection reagent was purchased from Roche (Indianapolis, IN, USA). Mouse monoclonal antibodies against CD11b were purchased from BD Pharmingen (San Diego, CA, USA).

Plant material

The fruits of *S. chinensis* (Turcz.) Baill were collected in September 2005 from Moonkyong, Korea. A voucher specimen (accession number SC-PDRL-1) was deposited in the herbarium of Pusan National University (Miryang, Korea). The plant was identified by one of the authors (YW Choi).

Extraction of the new compound α-iso-cubebenol

The dried fruits of *S. chinensis* (2.5 kg) were ground to a fine powder and then extracted successively at room

temperature with *n*-hexane, $CHCl_3$ and MeOH. The hexane extract (308 g) was evaporated *in vacuo* and chromatographed on a silica gel column (100 × 10 cm) (40 μm; Baker, Phillipsburg, NJ, USA) with a step gradient (0%, 5% and 20%) of EtOAc in hexane and 5% MeOH in $CHCl_3$ to obtain 38 fractions, as described previously.[14] Fraction 9 (KH9, 4866 mg) was separated on a silica gel column (100 × 3.0 cm) with a step gradient (1%, 10% and 15%) of acetone in $CHCl_3$, to obtain 21 fractions. Next, fraction 2 (KH9IG, 529.9 mg) was separated on a silica gel column (100 × 3.0 cm) with 5% acetone in $CHCl_3$ to yield α-iso-cubebenol (162.9 mg), as described previously.[3] Pure α-iso-cubebenol was identified by HPLC on a Luna C18 column (150 × 4.6 mm internal diameter (ID); 5-μm particle size; Phenomenex, Los Angeles, CA, USA) with a methanol–acetonitrile gradient at a flow rate of 1.0 ml/min. The structure of α-iso-cubebenol isolated from *S. chinensis* fruits was identified by its ^1H and ^{13}C nuclear magnetic resonance spectra (including Dept, heteronuclear single-quantum correlation and heteronuclear multiple-bond correlation spectroscopy) in $CDCl_3$, as described previously.[14]

Ethics statement

All of the animal procedures were in accordance with the National Institute of Health of Korea Guidelines for the Care and Use of Laboratory Animals, and all the experiments were approved by the Pusan National University Institutional Animal Care and Use Committee (PNU-IACUC; Approval Number PNU-2010-0102)

Isolation and culture of mouse primary microglia and cortical neurons

Imprinting Control Region (ICR) mice were purchased from the Dae Han Laboratory Animal Center (Tae-Jon, Korea). They were kept in a room with controlled temperature (20 ± 2°C) under a 12 h light/12 h dark cycle. Isolated primary microglia cultures were prepared as described previously.[15] Briefly, primary-mixed glial cell cultures from whole brains of ICR mice at postnatal days 2–5 were prepared in culture flasks and maintained in DMEM/F12 containing 10% FBS, 0.1 mM non-essential amino acids, 1 mM sodium pyruvate, 2 mM L-glutamine and 50 mg/ml penicillin/streptomycin at 37°C under 5% CO_2. After 2 weeks, the culture flasks were shaken on an orbital shaker at 180 rpm at 37°C for 5 h, and the medium was harvested. The attached cells were removed by trypsinization and seeded onto new plates for further study. To monitor purity, cells were immunostained with an anti-CD11b antibody: more than 90% of cells were stained positively. Primary-culture cortical neurons were prepared as described previously.[16] Dissociated cortical cells were plated in minimal essential medium supplemented with 20 mM glucose, 5% FBS, 5% horse serum and 2 mM glutamine at a density of five hemispheres/plate (approximately 4×10^5 cells per well) in poly-D-lysine- (100 μg/ml) and laminin (4 μg/ml)-coated 24-well plates, and maintained at 37°C in a humidified 5% CO_2 incubator. The cortical cultures were used at day 14 for 3-(4,5-dimethylthiazol-2-yl)-2,5-diphenyltetrazolium bromide (MTT) and TdT-mediated dUTP-biotin nick end-labelling (TUNEL) assays. Mouse BV-2 murine microglia cell lines (BV-2) were kindly provided by Professor Youn-Chul Kim from Wonkwang University (Iksan, Korea) and cultured in DMEM supplemented with 5% heat-inactivated FBS and 0.1% penicillin–streptomycin at 37°C in a humidified atmosphere of 5% CO_2 and 95% air.

Gelatin zymography assay

The activity of MMP-9 in the conditioned medium was determined by gelatin zymography protease assays. Briefly, 2×10^5 primary microglia were seeded in six-well plates and allowed to grow to 80% confluency. The primary microglia were incubated with various concentrations of α-iso-cubebenol for 1 h, followed by incubation with Aβ 1–42 fibrils for 24 h. Conditioned media were collected, cleared by centrifugation, mixed with 2× sodium dodecyl sulfate (SDS) sample buffer (Invitrogen Corporation) and electrophoresed in a 10% polyacrylamide gel containing 0.1% (w/v) gelatin. After electrophoresis, the gels were incubated in renaturing buffer (2.5% Triton X-100) with gentle agitation to remove SDS and incubated in a developing buffer (50 mM Tris-HCl buffer, pH 7.4 and 10 mM $CaCl_2$) overnight at 37°C, to digest the gelatin. Gels were then stained with SimplyBlue SafeStain (Invitrogen Corporation) until clear bands appeared, indicating gelatin digestion. Relative MMP-9 activity was expressed as the relative intensity of bands (fold of control), as estimated using the Image Quant TL software (GE Healthcare, Little Chalfont, UK).

Measurement of the concentration of tumour necrosis factor-α, interleukin-1β, interleukin-6, monocyte chemo attractant protein-1 and prostaglandin E2

Primary microglia were first incubated with various concentrations of an ethyl acetate extract of α-iso-cubebenol for 1 h and then with Aβ 1–42 fibrils for 24 h. Subsequently, tumour necrosis factor-α (TNF-α), IL-1β, IL-6, monocyte chemoattractant protein-1 (MCP-1) and prostaglandin E2 (PGE2) levels were quantified in the culture media using an ELISA kit (R&D Systems, Minneapolis, MN, USA), according to the manufacturer's instructions.

Measurement of reactive oxygen species

To evaluate the levels of intracellular ROS, primary microglia were treated with the indicated concentration of α-iso-cubebenol or *N*-acetylcysteine (10 mM) for 1 h, and then incubated with Aβ 1–42 fibrils (5 μM) for 24 h. Primary microglia were treated with 5-(and-6)-chloromethyl-2′,7′-dichlorodihydrofluorescein diacetate, acetyl este (CM-H_2DCFDA), which is an indicator of general oxidative stress, for 1 h at 37°C under 5% CO_2. The primary microglia were then harvested and washed three times with phosphate-buffered saline (PBS), after which the fluorescence intensity was measured by flow cytometry using an excitation wavelength of 488 nm and an emission wavelength of 525 nm. Data analyses were performed using the CXP software 2.0 (Beckman Coulter, Brea, CA, USA).

Transient transfection and dual-luciferase assay

The BV-2 were transfected with the κB-luc reporter plasmid consisting of 3 kB concatemers from the Igγ chain and the firefly luciferase gene using the FuGENE-HD reagent (Roche), according to the manufacturer's instructions. Twenty-four hours later, BV-2 were incubated with the indicated concentrations of α-iso-cubebenol for 1 h, followed by stimulation with Aβ 1–42 fibrils (5 μM) for 24 h. A *Renilla* luciferase control plasmid, Renilla luciferase reporter plasmid (Promega, Madison, WI, USA), was cotransfected as an internal control of transfection efficiency. Luciferase activity was assayed using the dual-luciferase assay kit (Promega), according to the manufacturer's instructions. Luminescence was measured using a microplate luminometer (Wallac 1420, Perkin Elmer, Monza, Italy).

Preparation of cytosolic and nuclear extracts

BV-2 were washed three times with cold PBS, and the cell pellets were suspended in buffer A (10 mM 4-(2-hydroxyethyl)piperazine-1-ethanesulfonic acid potassium salt-potassium hydroxide (HEPES-KOH) (pH 7.9), 1.5 mM $MgCl_2$, 10 mM KCl, 0.5 mM dithiothreitol (DTT) and 0.2 mM protease inhibitor (PI)) and incubated for 5 min on ice. Detergent was added to the cell extract (Active Motif, Carlsbad, CA, USA); the cell extract was incubated on ice for 5 min, then centrifuged at 13 000 rpm for 1 min at 4°C, and supernatants (cytosolic extract) were collected and stored at –70°C. Nuclear proteins were extracted by adding complete lysis buffer B (10 mM HEPES-KOH (pH 7.9), 1.5-mM $MgCl_2$, 10-mM KCL, 0.5-mM DTT, 0.2 mM PI, 25% (w/v) glycerin, 420-mM NaCl and 0.2-mM EDTA) for 30 min at 4°C with occasional vortexing. After centrifugation at 13 000 rpm for 5 min at 4°C, supernatants were collected and stored at –70°C.

Western blot analysis

The primary microglia and BV-2 were harvested in ice-cold lysis buffer consisting of 1% Triton X-100, 1% deoxycholate and 0.1% SDS. The protein content of the cell lysates was determined using the Bradford reagent (Bio-Rad, Hercules, CA, USA). Total proteins in each sample (50 μg) were resolved by 7.5% SDS–polyacrylamide gel electrophoresis, transferred to a polyvinylidene difluoride membrane and incubated with the appropriate antibodies. The proteins were visualized using an enhanced chemiluminescence detection system (Amersham Biosciences, Piscataway, NJ, USA) with horseradish peroxidase-conjugated antirabbit or antimouse secondary antibodies. Images were acquired using an Image Quant 350 analyser (Amersham Biosciences).

Neurotoxicity of microglial-conditioned medium

Primary microglia were treated with Aβ 1–42 fibrils or α-iso-cubebenol for 24 h and then centrifuged to obtain a cell-free supernatant. Primary cortical neurons were subsequently treated with microglia-conditioned medium, after which their viability was assessed by MTT assay and TUNEL assay after a 24-h incubation.

TdT-mediated dUTP-biotin nick end-labelling assay

Primary cortical neurons were evaluated by a TUNEL assay using the APO-BrdU™ TUNEL Assay Kit (Invitrogen, San Diego, CA, USA), according to the manufacturer's instructions. The results were analysed by flow cytometry (fluorescent isothiocyanate, excitation at 488 nm and emission at 520 nm). Data analyses were performed using the CXP software 2.0 (Beckman Coulter).

Statistical analyses

Data are expressed as the mean ± standard error. Statistical analyses were performed using the Statistical Package for the Social Sciences (SPSS) software (version 18.0; SPSS Inc., Chicago, IL, USA), to identify significant differences based on either one-way or two-way analysis of variance, followed by Dunn's post-hoc tests. *P*-values <0.05 were considered statistically significant. Each experiment was repeated at least three times.

Results

α-Iso-cubebenol inhibits amyloid β 1–42 fibril-induced matrix metalloproteinase-9, inducible nitric oxide synthase and cyclooxygenase-2 expression and activation in primary microglia

Primary microglia were treated with α-iso-cubebenol in the absence or presence of Aβ 1–42 fibrils, and an MTT-based cell viability assay was performed. Treatment with α-iso-cubebenol alone or with Aβ 1–42 fibrils for 24 h did not cause any change in cell viability. Moreover, α-iso-cubebenol did not exhibit cytotoxicity, rather an MTT assay indicated that it tended to ameliorate the cytotoxicity caused by Aβ 1–42 fibrils (Figure 1a). To evaluate the effects of α-iso-cubebenol on Aβ 1–42 fibril-induced MMP-9, iNOS and COX-2 expression and activation, primary microglia were pretreated for 1 h with different concentrations of α-iso-cubebenol, followed by incubation with Aβ 1–42 fibrils for 24 h, after which the levels of MMP-9, NO and PGE2 activity in culture media were determined by gelatinolytic, Griess and ELISA assays. As shown in Figure 1, the stimulation of primary microglia with Aβ 1–42 fibrils led to a marked increase in the relative activity of MMP-9 and production of NO and PGE2 (Figure 1b and 1d). Treatment of primary microglia with α-iso-cubebenol significantly reduced Aβ 1–42 fibril-induced MMP-9 activity, and NO and PGE2 production. α-Iso-cubebenol alone had no effect on MMP-9 activity, and NO and PGE2 production. Furthermore, we investigated whether α-iso-cubebenol had similar inhibitory effects on Aβ 1–42 fibril-induced MMP-9, iNOS and COX-2 expression. As shown in Figure 1b, treatment with Aβ 1–42 fibrils alone led to a marked increase in MMP-9, iNOS and COX-2 expression compared with the control. However, pretreatment with α-iso-cubebenol significantly suppressed the increase in MMP-9, iNOS and COX-2 expression in a concentration-dependent manner (Figure 1b). α-Iso-cubebenol alone had no effect on MMP-9, iNOS and COX-2 expression. Our results indicate that α-iso-cubebenol has a potent inhibitory effect against increased MMP-9, iNOS and COX-2 expression and activation in Aβ 1–42 fibril-stimulated primary microglia.

α-Iso-cubebenol attenuates amyloid β 1–42 fibril-stimulated tumour necrosis factor-α, interleukin-1β, interleukin-6 and monocyte chemoattractant protein-1 production in primary microglia

Proneuroinflammatory cytokines and chemokines, such as TNF-α, IL-1β, IL-6 and MCP-1, play central roles in microglia-mediated neuroinflammatory responses.[17] To examine whether α-iso-cubebenol affects the Aβ 1–42 fibril-induced TNF-α, IL-1β, IL-6 and MCP-1 production, the levels of these compounds were measured after Aβ 1–42 fibril stimulation in the presence or absence of α-iso-cubebenol. The production of TNF-α, IL-1β, IL-6 and MCP-1 induced by Aβ 1–42 fibrils was significantly inhibited by α-iso-cubebenol in a dose-dependent manner in primary microglia, whereas α-iso-cubebenol alone had no effect on the production of TNF-α, IL-1β, IL-6 and MCP-1 in primary microglia (Figure 2).

Attenuation of reactive oxygen species production by α-iso-cubebenol in amyloid β 1–42 fibril-stimulated primary microglia

During overneuroinflammation, activated microglia show markedly increased oxygen uptake, resulting in an enormous release of ROS. Recent studies have demonstrated that Aβ 1–42 fibril-induced microglia-derived ROS are involved in oxidative neuronal damage.[18] In this study, we investigated ROS production using CM-H_2DCFDA, which is an indicator that measures intracellular ROS. As shown in Figure 3, a right shift in ROS production was observed relative to the control, whereas primary microglia treated with α-iso-cubebenol for 1 h, followed by incubation with Aβ 1–42 fibrils, showed a left shift. These flow cytometry data suggest that α-iso-cubebenol significantly attenuates ROS production in Aβ 1–42 fibril-stimulated primary microglia. These results indicate that α-iso-cubebenol inhibits the Aβ 1–42 fibril-induced neuroinflammatory response via the inhibition of ROS generation.

α-Iso-cubebenol inhibits amyloid β 1–42 fibril-induced nuclear factor-κB activation and inhibitor of κBα phosphorylation and degradation in BV-2

NF-κB is a major transcription factor that has been shown to be essential for the expression of neuroinflammatory molecules, such as cytokines, iNOS and MMP-9.[19] Overneuroinflammatory responses, including Aβ 1–42 fibrils, rapidly activate the NF-κB signalling pathway. Therefore, we investigated whether the inhibitory effect of α-iso-cubebenol on the expression of neuroinflammatory molecules is mediated by NF-κB signalling pathways. As shown in Figure 4a and 4b, treatment with Aβ 1–42 fibrils for 1 h led to the phosphorylation and nuclear translocation of the NF-κB subunit p65 in BV-2. Moreover, after treatment with α-iso-cubebenol, the phosphorylation and nuclear translocation of p65 were effectively reduced in a dose-dependent manner. During NF-κB activation, the phosphorylation and degradation of IκBα are necessary to release NF-κB and allow subsequent translocation to the nucleus. We evaluated the effects of α-iso-cubebenol on the

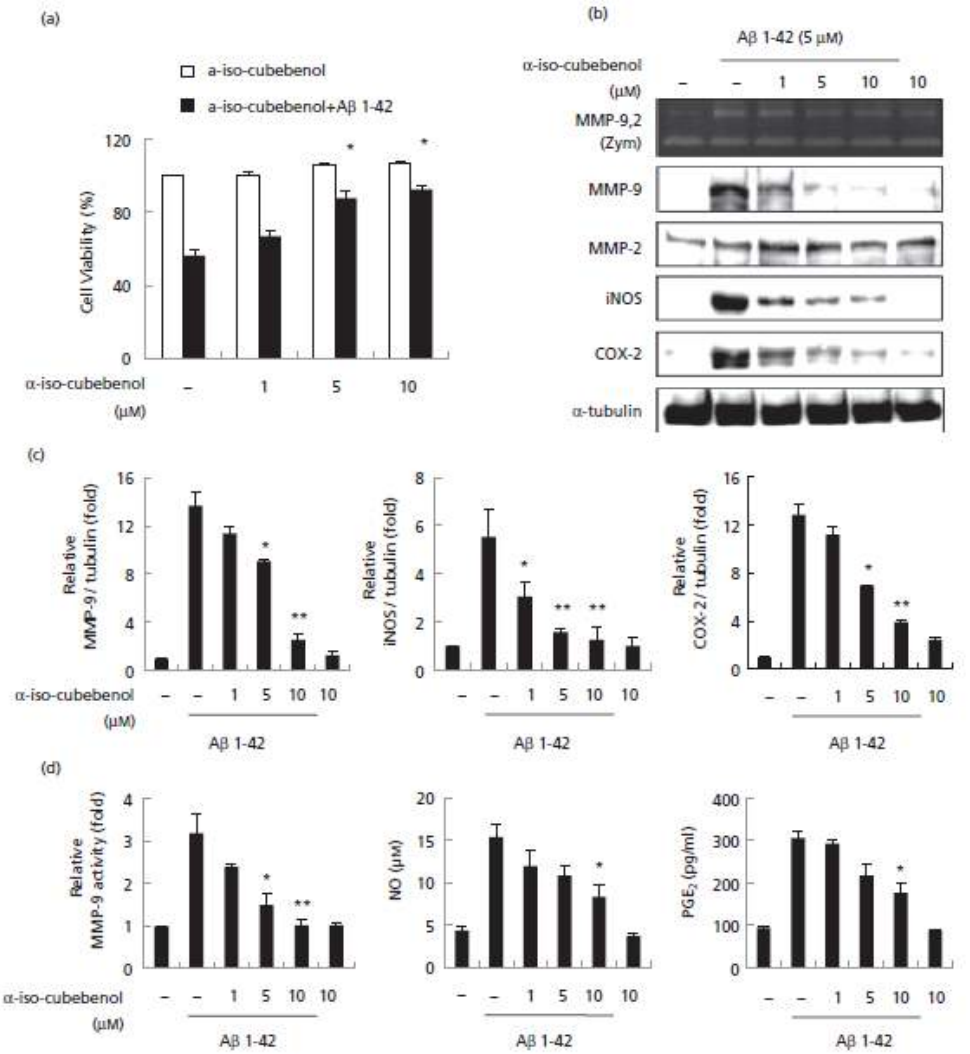

Figure 1 Effect of α-iso-cubebenol on the production of various neuroinflammatory molecules mediated by amyloid β 1–42 fibrils in microglia. (a) Mouse primary microglia were treated with the indicated concentration of α-iso-cubebenol for 1 h, followed by incubation with amyloid β 1–42 fibrils (5 μM) for 24 h. Cell viability was assessed by 3-(4,5-dimethylthiazol-2-yl)-2,5-diphenyltetrazolium bromide (MTT) assay, and the results are presented as the percentage of surviving cells relative to control cells. (b) Mouse primary microglia were treated with the indicated concentration of α-iso-cubebenol for 1 h, followed by incubation with amyloid β 1–42 fibrils (5 μM). After 24 h of stimulation, matrix metalloproteinase-9 enzymatic activity was analysed by gelatin zymography. The expression levels of matrix metalloproteinase-9, inducible nitric oxide synthase, cyclooxygenase-2 and tubulin were detected by Western blotting using specific antibodies. (c) The expression level of matrix metalloproteinase-9, inducible nitric oxide synthase and cyclooxygenase-2 was quantified using the image Quant TL software. (d) The enzymatic activity of matrix metalloproteinase-9 was quantified using the image Quant TL software. Nitrite content was measured using the Griess reaction. The concentration of prostaglandin E2 (PGE2) in the culture media was measured using a commercial enzyme-linked immunosorbent assay kit. Each bar represents the mean ± standard error. from three independent experiments per group. $^{*}P < 0.05$ or $^{**}P < 0.01$ versus the amyloid β 1–42 fibril-treated group.

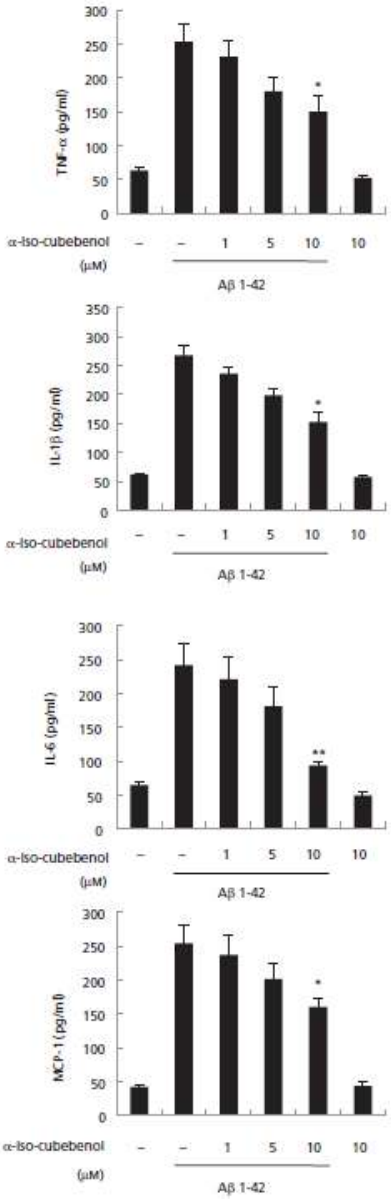

Figure 2 Effect of α-iso-cubebenol on amyloid β 1–42 fibril-induced tumour necrosis factor-α, interleukin-β, interleukin-6 and monocyte chemoattractant protein-1 production in primary microglia. Mouse primary microglia were treated with the indicated concentrations of α-iso-cubebenol for 1 h, followed by incubation with amyloid β 1–42 fibrils (5 μM) for 24 h. The concentrations of tumour necrosis factor-α, interleukin-β, interleukin-6 and monocyte chemoattractant protein-1 in the culture media were measured using a commercial enzyme-linked immunosorbent assay kit. Each bar represents the mean ± standard error from three independent experiments per group. $^{*}P < 0.05$ or $^{**}P < 0.01$ vs. the amyloid β 1–42 fibril-treated group.

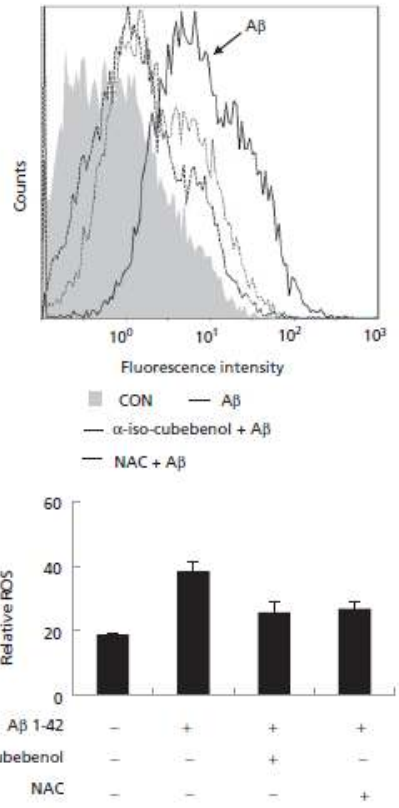

Figure 3 Effect of α-iso-cubebenol on amyloid β 1–42 fibril-induced reactive oxygen species production in primary microglia. Primary microglia were treated with α-iso-cubebenol for 1 h, followed by incubation with amyloid β 1–42 fibrils (5 μM). After 24 h of stimulation, primary microglia were incubated with CM-H_2DCFDA for an additional hour. Subsequently, the intracellular levels of reactive oxygen species were determined by flow cytometry.

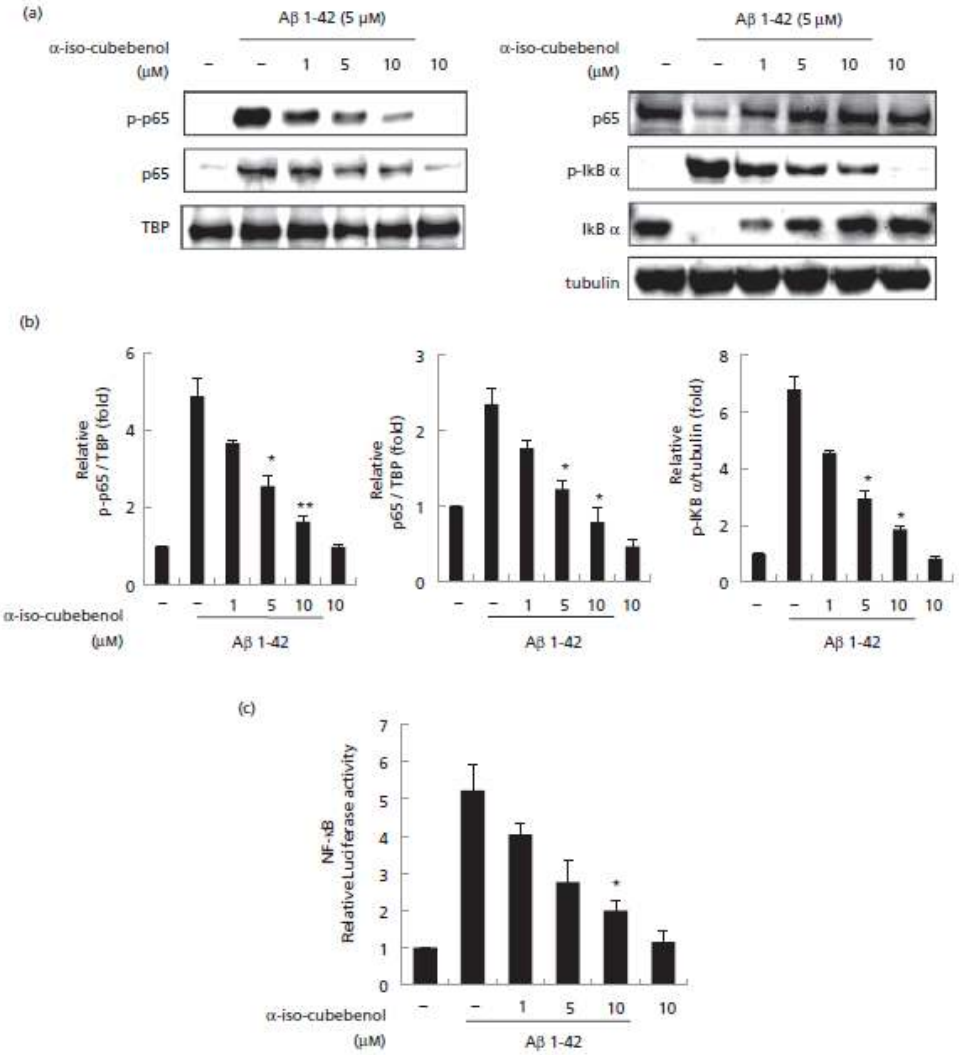

Figure 4 Effect of α-iso-cubebenol on the amyloid β 1–42 fibril-induced activation of nuclear factor-κB. (a) BV-2 murine microglia cell lines (BV-2) were treated with α-iso-cubebenol for 1 h, followed by incubation with amyloid β 1–42 fibrils (5 μM) for 0.5 h. The nuclear extracts were analysed by Western blotting with anti-nuclear factor-κB p65 and antiphosphonuclear factor-κB p65 antibodies. Cytosolic extracts were analysed by Western blotting with antinuclear factor-κB p65, anti-inhibitor of κBα, and anti-p-inhibitor of κBα antibodies. (b) The expression levels of phosphonuclear factor-κB p65, nuclear factor-κB p65 and phospho-inhibitor of κBα were quantified using the image Quant TL software. (c) BV-2 were cotransfected with the κB-luc reporter and the control *Renilla* luciferase plasmid, Renilla luciferase reporter plasmid (pRL-CMV). After 24 h, BV-2 were incubated with the indicated concentrations of α-iso-cubebenol for 1 h, followed by stimulation with amyloid β 1–42 fibrils (5 μM) for 24 h. Each bar represents the mean ± S.E. from three independent experiments per group. $^{*}P < 0.05$ or $^{**}P < 0.01$ vs. the amyloid β 1–42 fibril-treated group.

Aβ 1–42 fibril-induced phosphorylation and degradation of IκBα in BV-2. We found that α-iso-cubebenol suppressed the Aβ 1–42 fibril-induced phosphorylation and degradation of IκBα in a concentration-dependent manner. To confirm the effects of α-iso-cubebenol on the transactivity of NF-κB, we measured the activity of a luciferase reporter gene containing the NF-κB binding regions. As shown in Figure 4c, treatment with Aβ 1–42 fibrils increased the promoter activity of NF-κB in BV-2 by 5.3-fold, whereas treatment with 10 μM α-iso-cubebenol decreased the Aβ 1–42 fibril-stimulated promoter activity of NF-κB by 2.1-fold. These findings suggest that α-iso-cubebenol is capable of disrupting the activation of NF-κB by Aβ 1–42 fibrils in BV-2, resulting in the prevention of the expression of overneuroinflammatory molecules.

α-Iso-cubebenol inhibits the amyloid β 1–42 fibril-induced phosphorylation of mitogen-activated protein kinase in primary BV-2

MAPK signalling pathways are among the important signalling pathways that control neuroinflammatory molecules, such as cytokines, iNOS and MMP-9 in activated microglia during Aβ 1–42 fibril-induced neuroinflammatory responses.[20] We evaluated the effects of α-iso-cubebenol on the Aβ 1–42 fibril-induced phosphorylation of three MAPK molecules – ERK, JNK and p38 – in BV-2. Stimulation with Aβ 1–42 fibrils induced the phosphorylation of the three MAPK molecules within 1 h, and α-iso-cubebenol suppressed the phosphorylation of the three MAPK molecules in Aβ 1–42 fibril-stimulated BV-2 in a concentration-dependent manner (Figure 5). These results showed that α-iso-cubebenol suppresses the expression of neuroinflammatory molecules via MAPK signal transduction pathways.

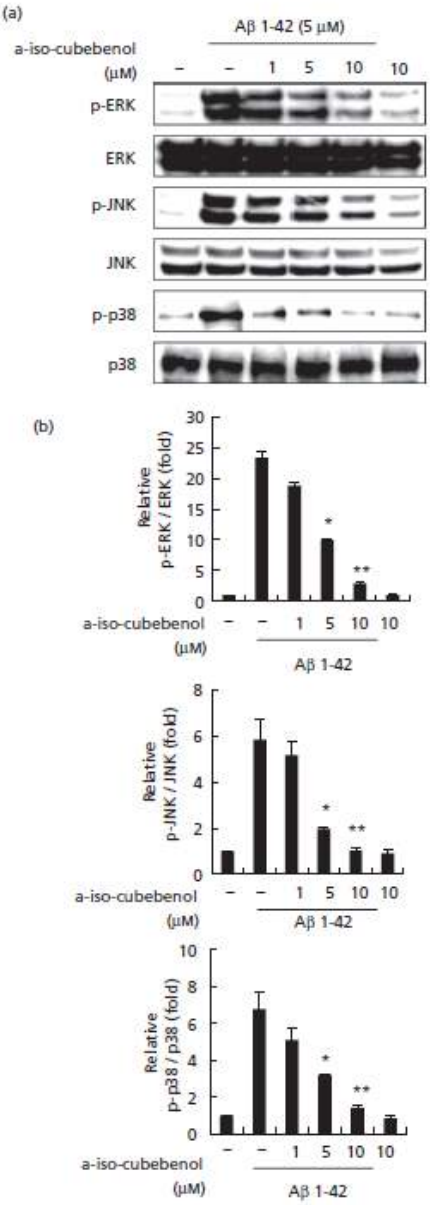

Figure 5 Effect of α-iso-cubebenol on amyloid β 1–42 fibril-induced activation of mitogen-activated protein kinase. (a) BV-2 murine microglia cell lines (BV-2) were treated with α-iso-cubebenol for 1 h, followed by incubation with amyloid β 1–42 fibrils (5 μM) for 0.5 h. An equal amount of cell extracts were then analysed by Western blotting with an anti-p-extracellular signal-regulated kinase 1/2, anti-p-c-Jun NH(2)-terminal kinase, or anti-p-p38 antibody. Extracellular signal-regulated kinase1/2, c-Jun NH(2)-terminal kinase or p38 bands indicated that the induction of total extracellular signal-regulated kinase 1/2, c-Jun NH(2)-terminal kinase or p38 protein expression did not change. (b) The expression level of p-extracellular signal-regulated kinase, p-c-Jun NH(2)-terminal kinase and p-p38 was quantified using the image Quant TL software. Each bar represents the mean ± standard error from three independent experiments per group. $^{*}P < 0.05$ or $^{**}P < 0.01$ versus the amyloid β 1–42 fibril-treated group.

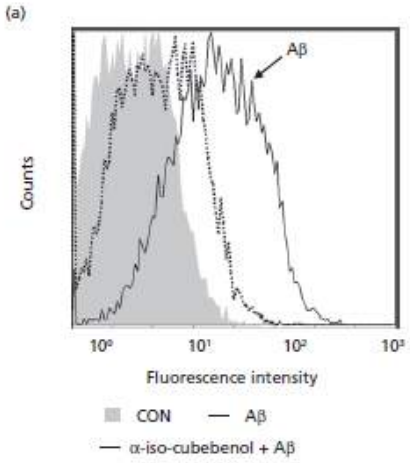

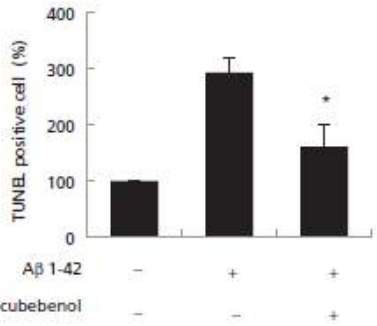

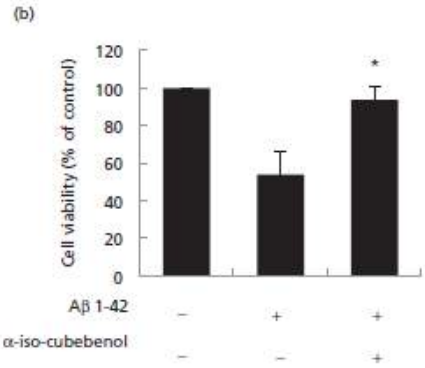

Figure 6 Neuroprotective effect of α-iso-cubebenol via the inhibition of amyloid β 1–42 fibril-activated microglia. Primary microglia were stimulated with amyloid β 1–42 fibrils or α-iso-cubebenol for 24 h, after which media were transferred to primary cortical neurons. Primary cortical neurons were then assessed by TdT-mediated dUTP-biotin nick end-labelling assay (a) and 3-(4,5-dimethylthiazol-2-yl)-2,5-diphenyltetrazolium bromide (MTT) assay (b) after a 24-h incubation period. Each bar represents the mean ± standard error from three independent experiments per group. *$P < 0.05$versus the amyloid β 1–42 fibril-treated group.

α-Iso-cubebenol protects cortical neurons from amyloid β 1–42 fibril-induced neuroinflammatory responses

Microglia have previously been shown to mediate neuroinflammatory responses, causing toxicity to neighbouring neuronal cells. Microglia-mediated neuroinflammatory toxicity is a major contributor to neuronal cell death in neurodegenerative diseases, including Alzheimer's disease and Parkinson's disease.[21,22] To determine the role of α-iso-cubebenol in the death of microglia-mediated neuroinflammatory toxicity-induced cortical neurons, we simultaneously treated primary cortical neurons with Aβ 1–42 fibril-stimulated microglia-conditioned medium or Aβ 1–42 fibrils and α-iso-cubebenol-stimulated microglia-conditioned medium. Treatment with Aβ 1–42 fibril-stimulated microglia-conditioned medium led to the death of primary cortical neurons at 24 h after exposure, resulting in about 297% TUNEL-positive cells. However, treatment with Aβ 1–42 fibril-stimulated microglia-conditioned medium induced cell death, which could be prevented by α-iso-cubebenol. Moreover, an MTT-based cell-viability assay revealed that α-iso-cubebenol exerted a protective effect (Figure 6). Collectively, these results indicate that α-iso-cubebenol protects primary cortical neurons against Aβ 1–42 fibril-stimulated microglia-mediated neurotoxicity.

Discussion

Natural products have long been used for the treatment of various neurodegenerative diseases in Asian countries. Therefore, we examined the ability of several natural products to protect against the deleterious effects of Aβ 1–42 fibrils, such as their antineuroinflammatory and neuroprotective properties.[10] Previous photochemical studies showed that *S. chinensis* contains bioactive compounds that are generally considered the source of its biological activity and therapeutic uses. Several published studies have demonstrated its anticancer, anti-inflammatory, anti-oxidant, pro-apoptotic and

hepatoprotective activity.[23–25] In this study, we explored the possible effects of α-iso-cubebenol against Aβ 1–42 fibril-stimulated microglia-mediated neurotoxicity.

Several studies have reported that the anti-oxidant defence mechanisms of natural products in Aβ 1–42 fibril-stimulated microglia maintain low levels of intracellular ROS.[26][27] We also demonstrated that attenuation of ROS production by α-iso-cubebenol might have therapeutic potential for neurodegenerative disorders. Accumulating evidence has suggested that iNOS, COX-2 and MMP-9 expression and activation are highly correlated with Aβ 1–42 fibril-induced neuroinflammatory responses.[11] Agents that downregulate iNOS, COX-2 and MMP-9 have also been shown to inhibit overneuroinflammatory responses.[10] In fact, here, we demonstrated that α-iso-cubebenol yielded a strong suppressive effect on Aβ 1–42 fibril-induced iNOS, COX-2 and MMP-9 expression and activation in primary microglia. Overproduction of neuroinflammatory cytokines, such as TNF-α, IL-1β and IL-6, in response to Aβ 1–42 fibrils contributes to the development of many neurodegenerative diseases, and can be considered a histopathological hallmark of various neurological diseases of the CNS. The neuroinflammatory chemokine MCP-1 is a potent chemoattractant that is capable of promoting microglia recruitment into neurodegenerative sites, thus potentiating the neuroinflammatory response. The results of this study suggest that α-iso-cubebenol inhibits the production of TNF-α, IL-1β, IL-6 and MCP-1 in Aβ 1–42 fibril-stimulated primary microglia.

Aβ 1–42 fibrils increase the neuroinflammatory response of microglia by inducing neuroinflammatory cytokines, chemokines and mediators via the NF-κB and MAPK signalling pathways. NF-κB regulates the transcription of neuroinflammation-mediated genes and is localized in the cytoplasm, where it binds to IκBα. Upon stimulation, IκBα is rapidly phosphorylated by IκB kinase (IKK) α/β and degraded via the ubiquitin–proteasome pathway. Degradation of IκBα exposes the nuclear-localization signals on NF-κB, which then translocates to the nucleus for the transcriptional regulation of neuroinflammation-mediated genes. Remarkably, phosphorylation of NF-κB p65 (Ser536) by IKK α/β is an important process in NF-κB activation.[11,28] We investigated the nuclear translocation and phosphorylation level of NF-κB p65 and found increased levels of p65 nuclear translocation and phosphorylation at Ser536 in Aβ 1–42 fibril-stimulated BV-2. Optimal activation of NF-κB p65 requires its phosphorylation at Ser536, which has been shown to enhance its transactivation potential. However, α-iso-cubebenol significantly inhibited the Aβ 1–42 fibril-induced nuclear translocation and phosphorylation of NF-κB p65. Further investigation of the effects of α-iso-cubebenol on IκBα signalling revealed that treatment with α-iso-cubebenol significantly inhibited the Aβ 1–42 fibril-induced phosphorylation and degradation of IκBα. We also found that α-iso-cubebenol inhibited Aβ 1–42 fibril-induced transcriptional activity of NF-κB p65, confirming the essential role of NF-κB in Aβ 1–42 fibril-induced neuroinflammatory responses of BV-2. Activation of MAPK may act upstream of NF-κB signalling. MAPK are involved in the regulation of neuroinflammatory responses, and their phosphorylation will ultimately signal the activation of neuroinflammatory responses.[9] However, overphosphorylation of MAPK will result in excessive production of neuroinflammatory molecules, which will lead to neurodegenerative disorders.[12,13] The results of this study indicated that α-iso-cubebenol treatment reduced the Aβ 1–42 fibril-induced phosphorylation of ERK (Thr185/Tyr187), JNK (Thr183/Tyr185) and p38 MAPK (Thr180/Tyr182). Overall, these results demonstrated that treatment with α-iso-cubebenol reduces Aβ 1–42 fibril-induced neuroinflammatory responses in BV-2 by inhibiting NF-κB and MAPK activation. It was indicated that activated microglia-derived pro-inflammatory cytokines, including TNF-α, IL-β, IL-6 and NO, and ROS induce neuronal damage in cocultured conditions. This phenomenon has also been observed in neurodegenerative diseases, in neuroinflammation and in infection *in vivo*.[22,29] In this study, α-iso-cubebenol had an inhibitory effect on neuroinflammatory responses by affecting various intracellular signalling pathways, including MAPK and NF-κB, in microglia.

Conclusions

Overall, our study provided evidence that α-iso-cubebenol at non-toxic concentrations inhibited Aβ 1–42 fibril-induced neuroinflammatory responses via the down-regulation of ROS, cytokines and chemokines, and the activation of mediators. Moreover, we showed that the molecular mechanism via which α-iso-cubebenol inhibited the expression of Aβ 1–42 fibril-induced neuroinflammatory molecules was mediated by its suppressive effect on NF-κB and MAPK activation. Thus, it could be inferred that α-iso-cubebenol has a protective effect on the death of cortical neurons caused by neuroinflammatory molecules from activated microglia. Given that neurodegenerative disease is often associated with poor prognosis, there is a need to discover and develop new therapeutic strategies. The finding that α-iso-cubebenol inhibits microglia-mediated neurotoxicity indicates that it is a promising agent for the treatment of neurodegenerative diseases such as Alzheimer's disease.

Declarations

Conflict of interest

The Author(s) declare(s) that they have no conflicts of interest to disclose.

Acknowledgements

This research was supported by the Basic Science Research Program through the National Research Foundation of Korea (NRF) and funded by the Ministry of Education, Science and Technology (2012R1A1A3010601). This study was supported by a grant (code #7–19-42) from the Rural Development Administration, Republic of Korea.

References

1. Chen DF *et al.* Anti-AIDS agents–XXVI. Structure-activity correlations of gomisin-G-related anti-HIV lignans from Kadsura interior and of related synthetic analogues. *Bioorg Med Chem* 1997; 5: 1715–1723.
2. Kim JE *et al.* The alpha-iso-cubebenol compound isolated from *Schisandra chinensis* induces p53-independent pathway-mediated apoptosis in hepatocellular carcinoma cells. *Oncol Rep* 2012; 28: 1103–1109.
3. Lee YJ *et al.* Identification of a novel compound that inhibits iNOS and COX-2 expression in LPS-stimulated macrophages from *Schisandra chinensis*. *Biochem Biophys Res Commun* 2010; 391: 1687–1692.
4. Park SY *et al.* *Schisandra chinensis* alpha-iso-cubebenol induces heme oxygenase-1 expression through PI3K/Akt and Nrf2 signaling and has anti-inflammatory activity in *Porphyromonas gingivalis* lipopolysaccharide-stimulated macrophages. *Int Immunopharmacol* 2011; 11: 1907–1915.
5. Dehmer T *et al.* Protection by pioglitazone in the MPTP model of Parkinson's disease correlates with I kappa B alpha induction and block of NF kappa B and iNOS activation. *J Neurochem* 2004; 88: 494–501.
6. Brandenburg LO *et al.* Sulforaphane suppresses LPS-induced inflammation in primary rat microglia. *Inflamm Res* 2010; 59: 443–450.
7. Liu DZ *et al.* Comparative anti-inflammatory characterization of wild fruiting body, liquid-state fermentation, and solid-state culture of *Taiwanofungus camphoratus* in microglia and the mechanism of its action. *J Ethnopharmacol* 2007; 113: 45–53.
8. Poulose SM *et al.* Anthocyanin-rich acai (Euterpe oleracea Mart.) fruit pulp fractions attenuate inflammatory stress signaling in mouse brain BV-2 microglial cells. *J Agric Food Chem* 2012; 60: 1084–1093.
9. Parvathy S *et al.* Abeta peptide conformation determines uptake and interleukin-1alpha expression by primary microglial cells. *Neurobiol Aging* 2009; 30: 1792–1804.
10. Eikelenboom P *et al.* Neuroinflammation in plaque and vascular beta-amyloid disorders: clinical and therapeutic implications. *Neurodegener Dis* 2008; 5: 190–193.
11. Floden AM, Combs CK. Microglia demonstrate age-dependent interaction with amyloid-beta fibrils. *J Alzheimers Dis* 2011; 25: 279–293.
12. Olson JK, Miller SD. Microglia initiate central nervous system innate and adaptive immune responses through multiple TLRs. *J Immunol* 2004; 173: 3916–3924.
13. D'Aversa TG *et al.* CD40-CD40 ligand interactions in human microglia induce CXCL8 (interleukin-8) secretion by a mechanism dependent on activation of ERK1/2 and nuclear translocation of nuclear factor-kappaB (NFkappaB) and activator protein-1 (AP-1). *J Neurosci Res* 2008; 86: 630–639.
14. Lee YJ *et al.* Identification of a novel compound that stimulates intracellular calcium increase and CXCL8 production in human neutrophils from *Schisandra chinensis*. *Biochem Biophys Res Commun* 2009; 379: 928–932.
15. Giulian D, Baker TJ. Characterization of ameboid microglia isolated from developing mammalian brain. *J Neurosci* 1986; 6: 2163–2178.
16. Im JY *et al.* COX-2 Regulates the insulin-like growth factor I-induced potentiation of Zn(2+)-toxicity in primary cortical culture. *Mol Pharmacol* 2004; 66: 368–376.
17. Jang S *et al.* Luteolin reduces IL-6 production in microglia by inhibiting JNK phosphorylation and activation of AP-1. *Proc Natl Acad Sci U S A* 2008; 105: 7534–7539.
18. Pan XD *et al.* Microglial phagocytosis induced by fibrillar beta-amyloid is attenuated by oligomeric beta-amyloid: implications for Alzheimer's disease. *Mol Neurodegener* 2011; 6: 45.
19. Oh YT *et al.* Oleamide suppresses lipopolysaccharide-induced expression of iNOS and COX-2 through inhibition of NF-kappaB activation in BV2 murine microglial cells. *Neurosci Lett* 2010; 474: 148–153.
20. Dai JN *et al.* Gastrodin inhibits expression of inducible NO synthase, cyclooxygenase-2 and proinflammatory cytokines in cultured LPS-stimulated microglia via MAPK pathways. *PLoS ONE* 2011; 6: e21891.
21. Kim MJ *et al.* Gallic acid, a histone acetyltransferase inhibitor, suppresses beta-amyloid neurotoxicity by inhibiting microglial-mediated neuroinflammation. *Mol Nutr Food Res* 2011; 55: 1798–1808.

NeuroToxicology 44 (2014) 160–168

Contents lists available at ScienceDirect

NeuroToxicology

Involvement of activation of the Nrf2/ARE pathway in protection against 6-OHDA-induced SH-SY5Y cell death by α-iso-cubebenol

Sun Young Park [a], Do Yeon Kim [b], Jong-koo Kang [c], Geuntae Park [a,d], Young-Whan Choi [c,e,*]

[a] Bio-IT Fusion Technology Research Institute, Pusan National University, Busan 609-735, Republic of Korea
[b] Department of Horticultural Bioscience, Pusan National University, Miryang 627-706, Republic of Korea
[c] College of Veterinary Medicine, Chungbuk National University, Cheongju 361-763, Republic of Korea
[d] Institute for Research &Industry Cooperation, Pusan National University, Busan 609-735, Republic of Korea
[e] life and Industry Convergence Research Institute, Pusan National University, Miryang 627-706, Republic of Korea

ARTICLE INFO

Article history:
Received 12 March 2014
Accepted 24 June 2014
Available online 2 July 2014

Keywords:
α-iso-cubebenol
6-OHDA
Oxidative stress
Apoptosis
CREB

ABSTRACT

Free radical-mediated neurodegeneration is one of the many causes of Parkinson's disease (PD). As part of our ongoing studies on the identification of biologically active *Schisandra chinensis* components, we have isolated and structurally elucidated α-iso-cubebenol. This study was carried out in an attempt to clarify the neuroprotective effect of α-iso-cubebenol on toxin-insulted dopaminergic neuronal death using 6-hydroxy-dopamine (6-OHDA)-induced dopaminergic SH-SY5Y cells. α-iso-cubebenol significantly attenuated the loss of mitochondrial function (MTT assay) and membrane integrity (lactate dehydrogenase assay) associated with 6-OHDA-induced neurotoxicity. Pretreatment of the cells with α-iso-cubebenol diminished the intracellular accumulation of reactive oxygen species (ROS) and calcium in response to 6-OHDA. Moreover, α-iso-cubebenol protected against 6-OHDA-induced neurotoxicity through inhibition of SH-SY5Y cell apoptosis. In addition, JC-1 staining, which is a well-established measure of mitochondrial damage, was decreased after treatment with α-iso-cubebenol. Notably, α-iso-cubebenol inhibited the release of mitochondrial flavoprotein apoptosis inducing factor (AIF) from the mitochondria to the cytosol and nucleus following 6-OHDA treatment. In addition, α-iso-cubebenol reduced the 6-OHDA-induced phosphorylation of ERK and induced the phosphorylation of PKA, PKB, and CREB in a dose-dependent manner. Moreover, α-iso-cubebenol stimulated the activation of Nrf2, a downstream target of CREB. Furthermore, α-iso-cubebenol stimulated the expression of multiple antioxidant response genes (NQO-1 and HO-1). Finally, CREB and Nrf2 siRNA transfection diminished α-iso-cubebenol-mediated neuroprotection.

1. Introduction

Parkinson's disease (PD) is a progressive neurodegenerative disorder characterized by the selective loss of dopaminergic neurons in substantia nigra pars compacta (SNc). Substantial evidence suggests that oxidative stress, mitochondrial dysfunction, environmental toxins, apoptosis, and inflammatory response are implicated in the pathogenesis of PD (Martin et al., 2011; Savitt et al., 2006). 6-OHDA, a hydroxylated analog of dopamine, has been used in vivo and in vitro to model PD. 6-OHDA treatment is associated with enhanced oxidative stress and/or mitochondrial damage, which lead to dopaminergic neuron damage (Tobon-Velasco et al., 2013). Subsequently, 6-OHDA-induced neurotoxicity results in an induction of BAX, which promotes cell death by inducing mitochondrial damage and a decrease in BCL-2, which is known to reduce cell death by preventing mitochondrial damage (Glinka et al., 1997). AIF is released from the mitochondrial intermembrane spaces and is translocated to the nucleus, which leads to DNA fragmentation and subsequent cell death (Hong et al., 2004). In addition, oxidative stress induced by 6-OHDA activates MAPK family members including ERK, JNK, and p38 MAPK kinases, which also regulate the transcription of neuronal cell death-related genes. MAPK pathways are activated by ultraviolet light, cytokines, and neurotoxins. Activation of MAPK pathways leads to neuronal cell death and differentiation (Klintworth et al., 2007; Gomez-Lazaro et al., 2008). Thus, studying naturally occurring drugs that can counteract 6-OHDA-induced neurotoxicity may lead to the development of helpful strategies for the treatment and prevention of PD.

* Corresponding author at: Department of Horticultural Bioscience, Pusan National University, Miryang 627-706, Republic of Korea. Tel.: +82 55 350 5522; fax: +82 55 350 5529.
E-mail addresses: ywchoi@pusan.ac.kr, sundeng99@pusan.ac.kr (Y.-W. Choi).

http://dx.doi.org/10.1016/j.neuro.2014.06.011
0161-813X/

Neuronal cells have developed several neuroprotective mechanisms to prevent oxidative stress. These neuroprotective mechanisms entail antioxidant-related molecules. Nrf2 is an important transcription factor. Its activation leads to the expression of antioxidant-related genes. Under normal conditions, Nrf2 is sequestered in Kelch-like ECH-associated protein 1 (Keap1) and degraded by the ubiquitin-dependent 26S proteasome system. Upon activation, Nrf2 is released from Keap1 and translocates to the nucleus, heterodimerizes with Maf, and binds antioxidant response elements (AREs) located in the promoter regions of antioxidant-related genes, including HO-1 and NQO1 (Chen et al., 2009; Innamorato et al., 2008; Li et al., 2007; Scapagnini et al., 2011). CREB has been shown to be a key transcription factor involved in neuroprotective mechanisms and cell survival. CREB specifically binds to the cAMP response element (CRE) sites of promoters to modulate transcription activity and enhance neuroprotective mechanisms (Cheng et al., 2007; Katoh et al., 2001; Lee et al., 2005). The CREB/Nrf2 pathway is activated by PKA, PKB, and MAPKs. However, these signaling pathways, which lead to CREB/Nrf2 activation, vary depending on cell types and stimuli (Park et al., 2013; Baxter et al., 2011; Nakaso et al., 2008).

In recent years, considerable attention has been focused on identifying naturally existing neuroprotective agents with antioxidant activity or mitochondria or proteasome function stabilizing ability (Schapira and Gegg, 2011). Naturally occurring drugs are an appealing source for novel compounds with powerful biological and pharmacological activities. *Schisandra chinensis* is a woody vine that is widely distributed throughout Korea, China, Russia, and Japan. *Schisandra chinensis* has been extensively used in traditional medicine as a health food against enuresis, asthma, sexual weakness, impotence, gonorrhea, dysentery, protracted diarrhea, thirst, and diabetes. Several investigators have shown that the major constituents of its fruit have biological and medicinal properties (Choi et al., 2006; Guo et al., 2008; Kim et al., 2010). Furthermore, we have recently isolated α-iso-cubebenol from *Schisandra chinensis*, which has been intensively studied from both a pharmacological and a phytochemical point of view (Lee et al., 2010, 2012; Park et al., 2014).

This study was conducted to evaluate the role and possible mechanisms of α-iso-cubebenol on cell death in 6-OHDA-induced human neuroblastoma SH-SY5Y cells. We investigated and elucidated the molecular mechanisms underlying the activation of the CREB/Nrf2 pathway by α-iso-cubebenol. We show that α-iso-cubebenol induces gene expression in a CREB/Nrf2-dependent manner. Ultimately, the present study indicates that α-iso-cubebenol protects against 6-OHDA-induced neuronal cell death in part through the CREB/Nrf2 pathway.

2. Materials and methods

2.1. Reagents

Dulbecco's modified Eagle medium (DMEM) and fetal bovine serum (FBS) were purchased from Gibco/BRL (Grand Island, NY). 3-[4,5-Dimethylthiazol-2-yl]-2,5-diphenyltetrazoliumbromide (MTT) and other reagents were purchased from Sigma–Aldrich (St. Louis, MO). Silencing RNAs against CREB and Nrf2 as well as antibodies for α-tubulin, TBP, ERK, JNK, p38, Nrf2, HO-1, and NQO1 were purchased from Santa Cruz Biotechnology (Santa Cruz, CA). Antibodies against AIF, COXIV, p-ERK, p-JNK, p-p38, p-PKA, PKA, p-CREB, and CREB were purchased form Cell Signaling Technology (Beverly, MA). FuGENE HD transfection reagent and X-tremeGENE siRNA Transfection Reagent were obtained from Roche (Indianapolis, IN). The cytotoxicity detection kit (LDH assay) was purchased from Roche Applied Science (Rotkreuz, Switzerland) and APO-BrdU™ TUNEL Assay Kit was purchased from Invitrogen (San Diego, CA). A nuclear extraction kit was purchased from Active Motif (San Diego, CA). Mitochondria Isolation kit was purchased from Thermo Scientific (Rockford, IL).

2.2. Cell culture

The human neuroblastoma SH-SY5Y cell line was obtained from the American Type Culture Collection (ATCC; Manassas, VA) and grown as monolayers in DMEM supplemented with 10% heat-inactivated FBS. SH-SY5Y cells were incubated at 37 °C in a humidified atmosphere containing 5% CO_2. To avoid changes in cell characteristics caused by extended periods of cell culture, all experiments were conducted with cells between passages 15 and 25. Each cell suspension was subcultured by trypsin/EDTA treatment every 3 days in order to maintain exponential growth.

2.3. Cell viability assay

Cells were seeded in wells of a 24-well plate at a density of 4×10^4 cells/well. Cells were incubated with the α-iso-cubebenol (5, 10 and 20 μM) for 12 h, followed by 6-OHDA (200 μM) treatment for 24 h. MTT solution (50 μg/mL) was added to each well. The plates were then incubated for an additional 4 h at 37 °C in a 5% CO_2 atmosphere, after which the supernatant was removed. Formazan crystals that had formed in viable cells were solubilized using dimethylsulfoxide. The absorbance in each well was measured at 570 nm using a microplate reader (Wallac 1420; Boston, MA).

2.4. Lactate dehydrogenase (LDH) release assay

Cells were seeded in wells of a 24-well plate at a density of 4×10^4 cells/well. Cells were incubated with the α-iso-cubebenol (5, 10 and 20 μM) for 12 h, followed by 6-OHDA (200 μM) treatment for 24 h. Extracellular LDH activity was measured using a cytotoxicity detection kit according to the manufacturer's protocol. Briefly, cells were seeded in 96-well plates and then subjected to the indicated treatments. For analysis, the supernatant was extracted from each well, and catalyst solutions were added to each well and incubated for 30 min at room temperature. The absorbance in each well was measured at 490 nm using a microplate reader (Wallac 1420; Boston, MA).

2.5. Measurement of intracellular reactive oxygen species (ROS) and calcium

Cells were seeded in wells of a 6-well plate at a density of 2×10^5 cells/well. Cells were incubated with the α-iso-cubebenol (5, 10 and 20 μM) for 12 h, followed by 6-OHDA (200 μM) treatment for 24 h. To evaluate the levels of intracellular ROS and calcium, cells were treated with CM-H_2DCFDA or Fluo 4-AM, respectively, for 1 h at 37 °C under 5% CO_2. The cells were then harvested and washed three times with phosphate-buffered saline (PBS). The fluorescence intensity was then measured by flow cytometry at an excitation wavelength of 488 nm and an emission wavelength of 525 nm. Data analyses were performed using CXP software 2.0 (Beckman Coulter; Pasadena, CA).

2.6. Sub-G1 measurement

Cells were seeded in wells of a 6-well plate at a density of 2×10^5 cells/well. Cells were incubated with the α-iso-cubebenol (5, 10 and 20 μM) for 12 h, followed by 6-OHDA (200 μM) treatment for 24 h. Cells were collected by centrifuging at 800 rpm for 3 min after treatment, washed twice in PBS, and fixed with 75% ethanol overnight. Prior to flow cytometry analysis, the fixed cells

were washed with PBS and incubated with a final concentration of 50 μg/mL propidium iodide for 10 min in the dark. The percent of apoptosis was calculated as the percentage of the sub-G1 peak as determined by CXP software 2.0 (Beckman Coulter).

2.7. Terminal deoxynucleotidyl transferase dUTP nick end labeling (TUNEL) assay

Cells were seeded in wells of a 6-well plate at a density of 2×10^5 cells/well. Cells were incubated with the α-iso-cubebenol (5, 10 and 20 μM) for 12 h, followed by 6-OHDA (200 μM) treatment for 24 h. Cells were evaluated using a TUNEL assay with the APO-BrdU™ TUNEL Assay Kit (Invitrogen) according to the manufacturer's instructions. The results were analyzed by flow cytometry (fluorescein isothiocyanate, excitation at 488 nm and emission at 520 nm). Data analyses were performed using CXP 2.0 (Beckman Coulter).

2.8. Mitochondrial membrane potential (MMP, $\Delta\psi_m$) assay

Cells were seeded in wells of a 6-well plate at a density of 2×10^5 cells/well. Cells were incubated with the α-iso-cubebenol (5, 10 and 20 μM) for 12 h, followed by 6-OHDA (200 μM) treatment for 24 h. Mitochondrial membrane potential ($\Delta\psi_m$) was determined by flow cytometry using J-aggregate-forming lipophilic cationic probe 5,5′,6,6′-tetrachloro-1,1′,3,3′-tetraethyl benzimidazol

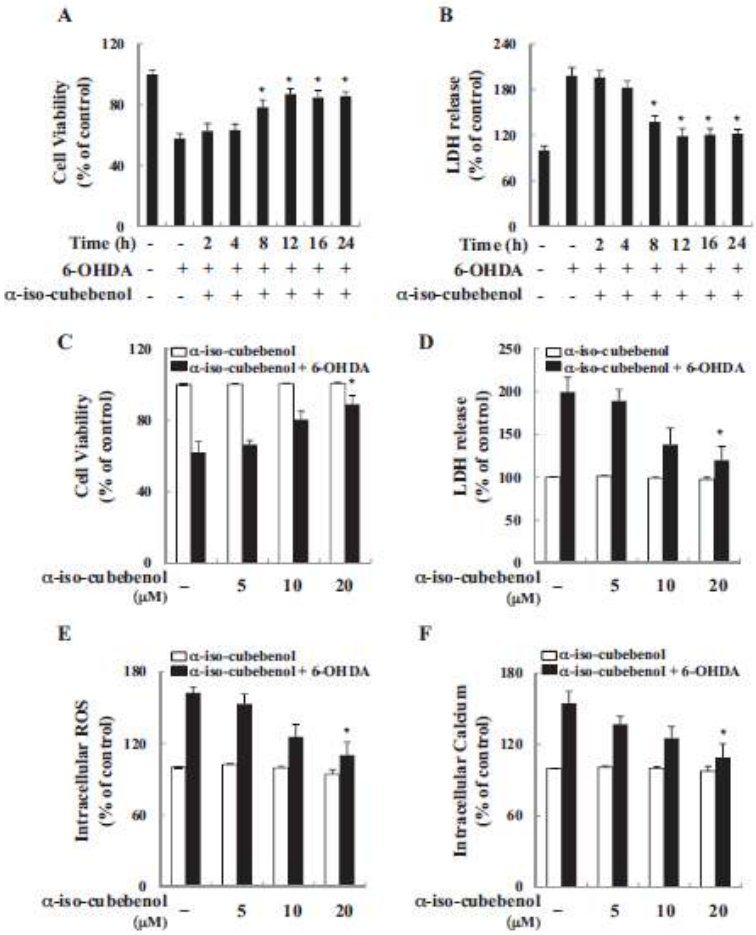

Fig. 1. Effects of α-iso-cubebenol on the 6-OHDA-induced cell death and intracellular ROS and calcium accumulation. Human neuroblastoma SH-SY5Y cells were treated with 20 μM of α-iso-cubebenol for the indicated times and 6-OHDA (200 μM) for 24 h. Cell viability was determined by an MTT assay (A) and a LDH release assay (B). Cells were treated with α-iso-cubebenol (5, 10 and 20 μM) for 12 h, followed by 6-OHDA (200 μM) treatment for 24 h. Cell viability was determined using the MTT assay (C) and an LDH release assay (D). (E) Intracellular ROS levels were detected using H_2DCFDA by flow cytometry. (F) Intracellular calcium was assessed using Fluo-4 AM by flow cytometry. Each bar represents the mean ± SE from three independent experiments per group. *$P < 0.05$ vs. the 6-OHDA-treated group.

carbocyanine iodide (JC-1). Cells were stained with JC-1 and analyzed by subsequent flow cytometry with the CXP software 2.0 (Beckman Coulter). JC-1 red fluorescence, indicating intact $\triangle\psi_m$, was excited at 488 nm, and emission was detected using a 613 ± 20-nm band pass filter. For each sample, 10,000 cells were acquired and analyzed by flow cytometry. Data were analyzed using the fluorescence intensity of the analyzed cell population.

2.9. Protein extracts and western blot analysis

Cells were seeded in wells of a 6-well plate at a density of 2×10^5 cells/well. Cells were incubated with the α-iso-cubebenol (5, 10 and 20 μM) for 12 h, followed by 6-OHDA (200 μM) treatment for 24 h. The cytosol, nuclear, and mitochondria extracts were isolated using a nuclear extraction kit according to the manufacturer's instructions. The protein content of the cell lysates was then determined using the Bradford reagent (Bio-Rad). The proteins in each sample were resolved by sodium dodecyl sulfate-polyacrylamide gel electrophoresis, transferred to a polyvinylidenedifluoride membrane, and exposed to the appropriate antibody. The proteins were visualized by an enhanced chemiluminescence detection system (Amersham Biosciences; Piscataway, NJ) using a horseradish peroxidase-conjugated anti-rabbit or anti-mouse secondary antibody. Images were acquired using an ImageQuant 350 analyzer (Amersham Biosciences).

2.10. Transient transfection with siRNA

Transfection of the cells with small interfering RNA (siRNA) was performed using the X-tremeGENE siRNA Transfection Reagent (Roche Applied Science) according to the manufacturer's instructions. Commercially available mouse CREB- and Nrf2-specific siRNAs (Santa Cruz Biotechnology) and negative control siRNAs (Santa Cruz Biotechnology) were used for transfection. Briefly, X-tremeGENE siRNA Transfection Reagent (10 μL) was added to 100 μL of serum-free medium containing 2 μg of each siRNA and incubated for 20 min at room temperature. Gene silencing was measured after 48 h by western blotting. Cells were transfected with si-control and si-CREB or si-Nrf2. At 48 h after transfection, the cells were treated with α-iso-cubebenol (20 μM) for 1 h and then stimulated with 6-OHDA (200 μM) for 24 h.

2.11. Transient transfection and dual luciferase assay

Cells were transfected with the CRE and ARE reporter plasmids or an HO-1 promoter reporter plasmid using FuGENE-HD reagent according to the manufacturer's instructions. A *Renilla* luciferase control plasmid, pRL-CMV, was co-transfected as an internal control for transfection efficiency. Luciferase activity was assayed using a dual-luciferase assay kit according to the manufacturer's instructions. Luminescence was measured using a microplate luminometer (Wallac 1420; Boston, MA). Cells were transfected with CRE and ARE reporter plasmids or an HO-1 promoter reporter plasmid. At 24 h after transfection, the cells were treated with α-iso-cubebenol (20 μM) for 1 h and then stimulated with 6-OHDA (200 μM) for 24 h.

2.12. Statistical analysis

Data are expressed as the mean ± S.E. Statistical analysis was performed using the Statistical package for the Social Sciences (SPSS) software (version 18.0) to identify significant differences based on either one- or two-way analysis of variance (ANOVA) followed by Dunn's post hoc tests. *P* values <0.05 were considered statistically significant. Each experiment was repeated at least thrice.

3. Results

3.1. α-iso-cubebenol protects human neuroblastoma SH-SY5Y cells against 6-OHDA-induced cell death as well as ROS and calcium accumulation

In preliminary studies, it is important to screen for possible pretreatment vs. simultaneous effects of α-iso-cubebenol in SH-SY5Y cells. Therefore, we measured cell viability using the MTT and LDH release assays. Cells were pre-treated with α-iso-cubebenol for 2–24 h, and then exposed to 6-OHDA for 24 h. As resulted, only 57.8% of the cells stimulated with 6-OHDA remained viable compared to those not stimulated with 6-OHDA. However, pre-treatment with α-iso-cubebenol improved the viability of 6-OHDA-stimulated cells (Fig. 1A and B). Based on these results, pre-treated with α-iso-cubebenol for 12 h was used for the subsequent studies. Next, Cells were pre-incubated with various concentration of α-iso-cubebenol and treated with 6-OHDA. It was found that α-iso-cubebenol blocked 6-OHDA-induced cell death in a dose-dependent manner (Fig. 1C and D). Next, we detected ROS and calcium accumulation after treatment with α-iso-cubebenol or 6-OHDA by flow cytometry. ROS and calcium accumulation was assessed using the ROS-sensitive fluorescence indicator CM-H_2DCFDA and the calcium-sensitive fluorescence indicator Fluo 4-AM. After 24 h of 6-OHDA treatment, accumulation of ROS and calcium was observed. The presence of α-iso-cubebenol inhibited the 6-OHDA-induced accumulation of ROS and calcium. As a control, α-iso-cubebenol alone had no obvious effect on ROS and calcium accumulation in SH-SY5Y cells compared to the untreated control group (Fig. 1E and F). Based on these data, we concluded that pretreatment with α-iso-cubebenol exerted a potent neuroprotective effect against 6-OHDA-induced oxidative stress through inhibition of ROS and calcium accumulation.

3.2. α-iso-cubebenol-mediated protection of SH-SY5Y cells occurs through inhibition of apoptotic death induced by 6-OHDA

To examine whether 6-OHDA-induced SH-SY5Y cell death occurred by an apoptotic-like mechanism, we utilized flow cytometry to measure the relative amounts of TUNEL-stained cells. TUNEL-stained cells showed nuclear DNA fragmentation that results from apoptotic signaling cascades. Flow cytometric analysis

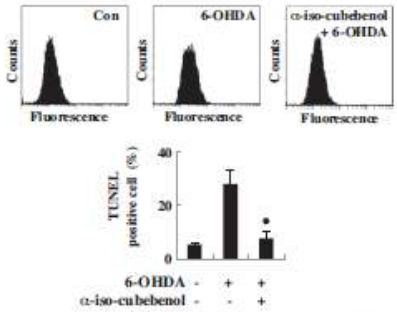

Fig. 2. Effects of α-iso-cubebenol on the 6-OHDA-induced apoptotic cell death. Cells were pretreated with α-iso-cubebenol (5, 10 and 20 μM) for 12 h, followed by 6-OHDA (200 μM) treatment for 24 h. Cell apoptosis was measured by labeling cells using the TUNEL assay. TUNEL-stained cells were quantified by flow cytometry. The number in each panel is the percentage of TUNEL-positive cells. The results are expressed as the ratio of TUNEL-positive cells observed in the same field. Each bar represents the mean ± SE from three independent experiments per group. *$P < 0.05$ vs. the 6-OHDA-treated group.

of the TUNEL assay revealed that 6-OHDA treatment increased the number of TUNEL-stained cells. After 24 h of incubation with 6-OHDA in the absence of pre-incubation with α-iso-cubebenol, the number of TUNEL-stained cells increased from 5.5% to 28.1%. However, α-iso-cubebenol pretreatment completely attenuated the effect of 6-OHDA, suggesting that α-iso-cubebenol could protect SH-SY5Y neuronal cells against 6-OHDA-induced apoptotic death (Fig. 2).

3.3. α-iso-cubebenol protection of SH-SY5Y cells occurs through inhibition of apoptotic death induced by 6-OHDA

There have been numerous reports with regard to the association between mitochondrial dysfunction and neurodegenerative diseases such as PD (Martinez and Greenamyre, 2012). In neuronal cells, 6-OHDA treatment impairs intracellular calcium homeostasis, and leads to mitochondria dysfunction and apoptotic death (Tobon-Velasco et al., 2013; Glinka et al., 1996). To monitor mitochondrial damages, we examined mitochondrial membrane potential using the molecular probe JC-1 in SH-SY5Y cells that were pretreated with 20 μM of α-iso-cubebenol and then treated with 200 mM 6-OHDA for 24 h. As shown in Fig. 3A, treatment with 6-OHDA induced a loss or collapse of mitochondrial membrane potential in SH-SY5Y cells when compared with the control cells. However, pretreatment with α-iso-cubebenol inhibited the 6-OHDA induced loss or collapse of mitochondrial membrane potential. Mitochondria related cell death signals drive neuronal cells to apoptosis through translocation of death factors such as AIF into the cytosol, and then to the nucleus. AIF

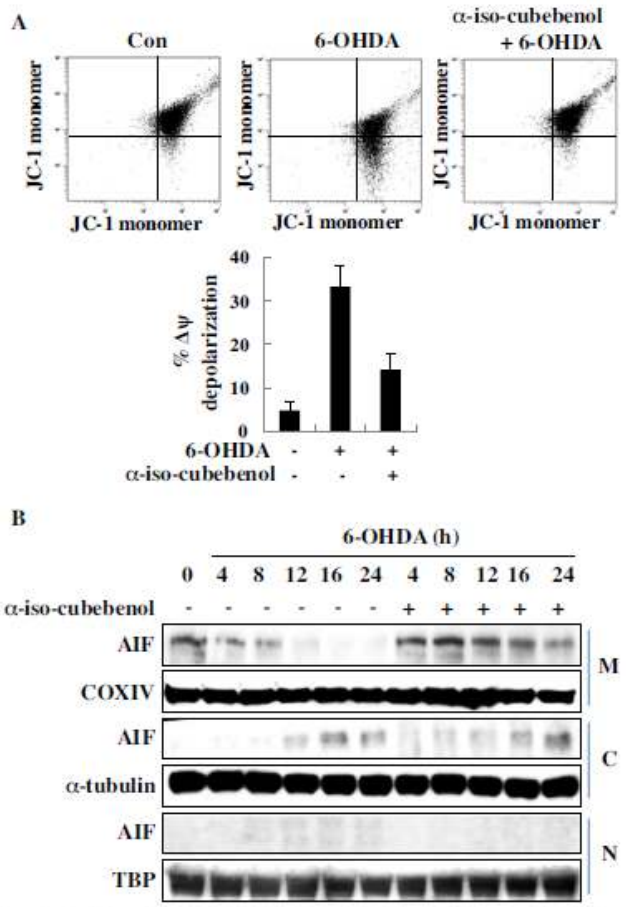

Fig. 3. Effects of α-iso-cubebenol on mitochondrial membrane potential (MMP, $\Delta\psi_m$) and AIF translocation. Cells were treated with α-iso-cubebenol (20 μM) for 12 h and then incubated with 6-OHDA (200 μM) for 24 h. (A) Cells were stained with JC-1 dye probe and analyzed by flow cytometry. Higher numbers of cells in the lower right quadrant indicated a higher percentage of cells that emitted only green fluorescence, which is attributed to depolarized mitochondrial membrane. (B) Relative intensity of Flow cytometry data was transformed into histogram. (C) Cells were incubated with α-iso-cubebenol (20 μM) for 12 h, then stimulated with 6-OHDA (200 μM) for the indicated time; subcellular proteins were isolated from mitochondrial (M), cytosol (C) and nucleus (N), and then AIF protein levels were analyzed by western blot.

participates in chromatin condensation and large-scale DNA fragmentation (Zhang et al., 2011; Zhu et al., 2007). In addition, we investigated the inhibitory effect of α-iso-cubebenol on the 6-OHDA-induced release of AIF from mitochondria. As shown in western blot analysis, α-iso-cubebenol attenuated the 6-OHDA-induced release of AIF from mitochondria, and sustained AIF expression in the mitochondria (Fig. 3B). These data clearly suggest that α-iso-cubebenol protects SH-SY5Y cells by preventing 6-OHDA-induced mitochondrial dysfunction via inhibiting release of AIF from the mitochondria.

3.4. Effect of α-iso-cubebenol on 6-OHDA-induced phosphorylation of the MAPKs ERK, JNK, and p38

MAPKs such as ERK, JNK, and p38 are activated and involved in 6-OHDA-induced neuronal cell death (Klintworth et al., 2007; Gomez-Lazaro et al., 2008). To analyze the molecular mechanism underlying the neuroprotective effect of α-iso-cubebenol, we further examined its inhibitory effect on phosphorylation of MAPKs, which are upstream signaling molecules in the neuronal cell death response. α-iso-cubebenol-treated cells were evaluated by western blot analysis to determine whether α-iso-cubebenol treatment affected the phosphorylation of MAPKs. SH-SY5Y cells were preincubated with 20 μM α-iso-cubebenol for 12 h and then treated with 200 μM 6-OHDA for 4–24 h. Western blot analysis revealed that 6-OHDA markedly increased the phosphorylation of ERK, JNK, and p38 MAPK at 12–24 h, while α-iso-cubebenol reduced 6-OHDA-induced phosphorylation of ERK (Fig. 4). These data indicated that ERK inhibition is involved in the inhibitory effect of α-iso-cubebenol on 6-OHDA-induced neuronal cell death.

3.5. α-iso-cubebenol induces the activation of PKA, PKB, CREB, and Nrf2, and the expression of HO-1 and NQO1

We demonstrated that α-iso-cubebenol decreased 6-OHDA-induced SH-SY5Y cell death in a dose-dependent manner. Here, we carried out a series of experiments to study the mechanisms underlying the neuroprotective effects of α-iso-cubebenol against 6-OHDA-induced cell death. The PKA and PKB signaling pathways play a central role in neuronal cell survival. Therefore, we examined whether α-iso-cubebenol could induce the phosphorylation of PKA and PKB in SH-SY5Y cells. Cells were exposed to α-iso-cubebenol, total protein was harvested, and western blots were performed using the anti-phospho-PKA and -PKB antibodies. α-iso-cubebenol induced the phosphorylation of PKA and PKB in a dose-dependent manner (Fig. 5A). PKA and PKB pathways are involved in regulating the activation of CREB and Nrf2, which are key transcription factors with neuroprotective protective effects against various neurotoxins (Park et al., 2013; Baxter et al., 2011; Nakaso et al., 2008). Thus, we investigated the influence of α-iso-cubebenol on the activation of CREB and Nrf2. As shown in Fig. 5A, treatment with α-iso-cubebenol induced the phosphorylation of CREB and the nuclear translocation of Nrf2. To further determine their transcriptional activities, we transfected SH-SY5Y cells with CRE and ARE-LUC plasmid DNAs, which contain the luciferase gene driven by the CREB and the Nrf2 responsive element, respectively. Transfected SH-SY5Y cells were treated with α-iso-cubebenol, which induced a 5.2- and a 4.6-fold increase in CREB and Nrf2 promoter activity, respectively (Fig. 5B). The effect of α-iso-cubebenol on the expression level of ARE-dependent genes such as HO-1 and NQO1 proteins was then examined by western blotting. As shown in Fig. 5C, the level of HO-1 and NQO1 proteins were significantly increased by α-iso-cubebenol. Furthermore, HO-1 promoter reporter experiments showed that α-iso-cubebenol induced HO-1 promoter activity (Fig. 5D).

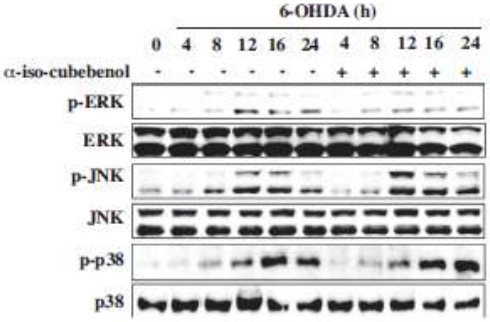

Fig. 4. Effects of α-iso-cubebenol on the 6-OHDA-induced phosphorylation of ERK, JNK, and p38 MAPKs. Cells were incubated with α-iso-cubebenol (20 μM) for 12 h, then stimulated with 6-OHDA (200 μM) for the indicated time. After incubation, cells were harvested and phosphorylated ERK, JNK, and p38 MAPKs levels were measured by western blot analysis using phospho-specific antibodies for ERK, JNK, and p38 MAPKs.

3.6. The neuroprotective effect of α-iso-cubebenol involves the CREB/Nrf2 pathway

In order to provide direct evidence of the involvement of the CREB/Nrf2 pathway in α-iso-cubebenol-mediated neuroprotection, we inhibited their activities using CREB and Nrf2 siRNAs. The efficiency of the CREB and Nrf2 siRNAs in knocking down CREB and Nrf2 was assayed by western blot. CREB and Nrf2 siRNAs significantly decreased the level of CREB and Nr2 in cells treated with α-iso-cubebenol (data not shown). We transfected SH-SY5Y cells with either the control, CREB, or Nrf2 siRNA for 48 h, followed by treatment with 20 μM of α-iso-cubebenol for an additional 12 h and then 200 μM of 6-OHDA for 24 h. In SH-SY5Y cells transfected with the control siRNA, α-iso-cubebenol inhibited 6-OHDA-induced neuronal cell death. However, α-iso-cubebenol was less effective in inhibiting the 6-OHDA-induced neuronal cell death in SH-SY5Y cells transfected with the CREB or Nrf2 siRNAs (Fig. 6A and B). Taken together, these data support the hypothesis that α-iso-cubebenol has robust neuroprotective effects and can potentially attenuate 6-OHDA-mediated neuronal cell death through activation of the CREB/Nrf2 signaling pathway.

4. Discussion

6-OHDA, MPP^+, and rotenone induce dopaminergic neuron cell death in vitro and are widely used as PD-mimicking agents. These neurotoxins selectively attack dopaminergic neurons using the cell death process related to naturally ongoing diseases (Bove and Perier, 2012). Our findings indicate that treatment with 6-OHDA induces the loss of mitochondrial metabolic activity (MTT assay) as well as the loss of membrane integrity (LDH release assay). However, α-iso-cubebenol effectively reduced 6-OHDA-, MPP^+-, and rotenone-induced neurotoxicity in SH-SY5Y cells (data not shown). The human-derived neuroblastoma SH-SY5Y cell line expresses some representative dopaminergic markers and has been extensively used as a model to test the effects of neurotoxins (Presgraves et al., 2004; Schneider et al., 2011). Therefore, the SH-SY5Y cell line is a suitable model to study the role of α-iso-cubebenol against 6-OHDA-mediated dopaminergic cell death. First, we demonstrated that the loss of mitochondrial metabolic activity (MTT assay) and membrane integrity (LDH release assay) in response to 6-OHDA was significantly decreased by pretreatment with α-iso-cubebenol in a concentration-dependent manner.

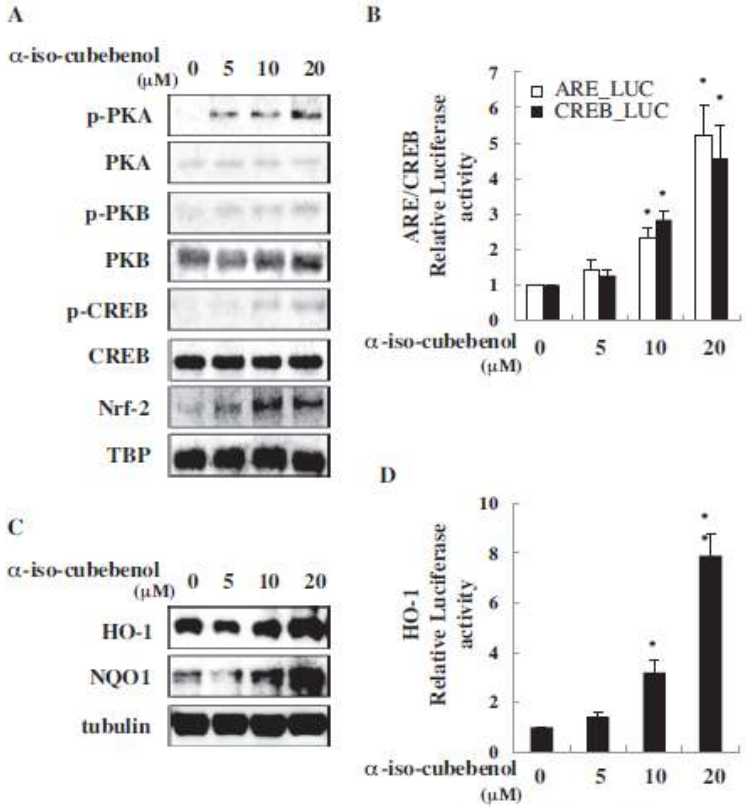

Fig. 5. Effects of α-iso-cubebenol on the activation of PKA, CREB, and Nrf2, and the expression of HO-1 and NQO1. (A) SH-SY5Y cells were incubated with α-iso-cubebenol for 4 h. p-PKA, PKA, p-PKB, PKB, p-CREB, and CREB expression, and nuclear localization of Nrf2 were determined by western blot. (B) Cells were transfected with the ARE- or CRE-luciferase constructs then treated with α-iso-cubebenol. Equal amounts of cell extract were assayed for dual-luciferase activity. Expression of the *Renilla* luciferase control was used to normalize ARE- or CRE-luciferase activity. (C) Cells were cultured with α-iso-cubebenol for 12 h, after which HO-1 and NQO-1 expression was determined by western blotting. (D) Cells were transfected with HO-1 a promoter-luciferase construct and equal amounts of cell extracts were assayed for dual luciferase activity. Each bar represents the mean ± SE from three independent experiments per group. *$P < 0.05$ vs. the control-treated group.

In addition, the TUNEL assay, which is a well-established measure of cellular apoptosis, indicated a decrease in apoptosis after treatment with α-iso-cubebenol.

6-OHDA-induced neuronal cell death is associated with intracellular ROS and calcium accumulation. In the central nervous system, ROS and calcium regulate neurotransmitters, excitation, mitochondrial dysfunction, endoplasmic reticulum stress, and apoptosis (Blum et al., 2001). Therefore, our data indicated that SH-SY5Y cells exposed to 6-OHDA presented increased levels of intracellular ROS and calcium. This increase was significantly inhibited by pretreatment with α-iso-cubebenol.

Mitochondria play a central role in regulating neuroprotection. The loss of mitochondria membrane potential further causes several changes in mitochondrial functions, which induce neuronal cell death (Schapira and Gegg, 2011). Our results showed that 6-OHDA induced mitochondria membrane potential loss. However, α-iso-cubebenol suppressed this 6-OHDA-induced effect. Dysfunction of mitochondria induced by 6-OHDA is regulated by various anti-and pro-apoptotic-related genes such as Bid, Bax, cytochorome *c*, and AIF. Following the loss of mitochondrial membrane potential, AIF is distributed in the cytosol and then translocated to the nucleus. Inhibition of AIF release from the mitochondria by pharmacological inhibitors has a significant neuroprotective effect in neurotoxin-induced cell injury (Gorman et al., 1998; Zhang et al., 2011). We have provided evidence that SH-SY5Y cell death occurs via apoptosis mediated by translocation of AIF from the mitochondria to the cytosol. Moreover, α-iso-cubebenol effectively inhibited the 6-OHDA-induced release of AIF from the mitochondria.

The role of the antioxidant-related genes HO-1 and NQO1 as well as the importance of the PKA/PKB/CREB/Nrf2 signaling pathway in neuroprotection remain unclear. Thus, we next investigated the effect of α-iso-cubebenol on HO-1 and NQO1 expression as well as on activation of the PKA/PKB/CREB/Nrf2 signaling pathway. PKA and PKB are important for several neuronal signaling pathways including cell survival, proliferation, and differentiation. CREB and Nrf2 are cAMP and redox-responsive transcription factors that prevent neurodegeneration through

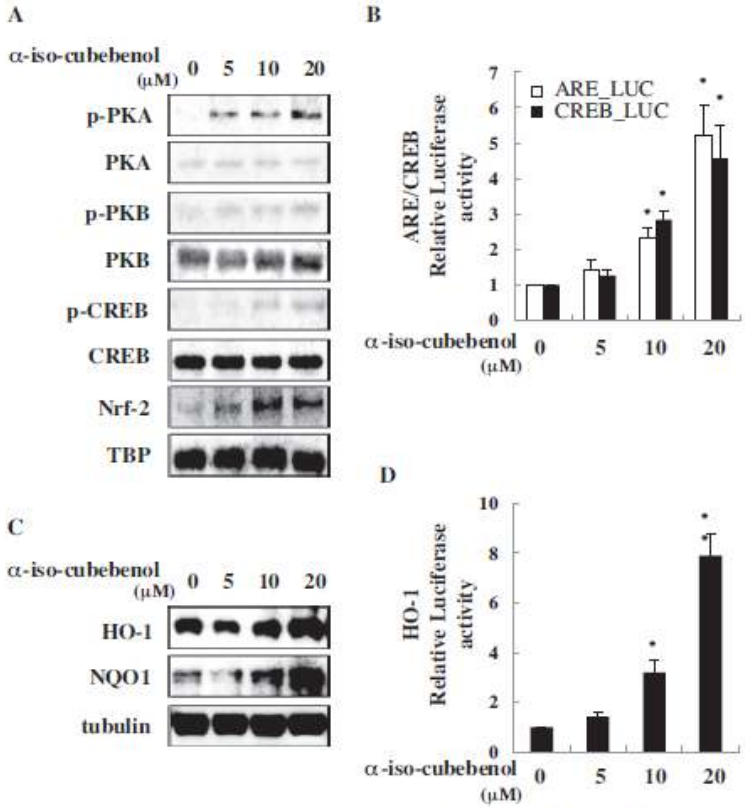

Fig. 5. Effects of α-iso-cubebenol on the activation of PKA, CREB, and Nrf2, and the expression of HO-1 and NQO1. (A) SH-SY5Y cells were incubated with α-iso-cubebenol for 4 h. p-PKA, PKA, p-PKB, PKB, p-CREB, and CREB expression, and nuclear localization of Nrf2 were determined by western blot. (B) Cells were transfected with the ARE- or CRE-luciferase constructs then treated with α-iso-cubebenol. Equal amounts of cell extract were assayed for dual-luciferase activity. Expression of the *Renilla* luciferase control was used to normalize ARE- or CRE-luciferase activity. (C) Cells were cultured with α-iso-cubebenol for 12 h, after which HO-1 and NQO-1 expression was determined by western blotting. (D) Cells were transfected with HO-1 a promoter-luciferase construct and equal amounts of cell extracts were assayed for dual luciferase activity. Each bar represents the mean ± SE from three independent experiments per group. *$P < 0.05$ vs. the control-treated group.

In addition, the TUNEL assay, which is a well-established measure of cellular apoptosis, indicated a decrease in apoptosis after treatment with α-iso-cubebenol.

6-OHDA-induced neuronal cell death is associated with intracellular ROS and calcium accumulation. In the central nervous system, ROS and calcium regulate neurotransmitters, excitation, mitochondrial dysfunction, endoplasmic reticulum stress, and apoptosis (Blum et al., 2001). Therefore, our data indicated that SH-SY5Y cells exposed to 6-OHDA presented increased levels of intracellular ROS and calcium. This increase was significantly inhibited by pretreatment with α-iso-cubebenol.

Mitochondria play a central role in regulating neuroprotection. The loss of mitochondria membrane potential further causes several changes in mitochondrial functions, which induce neuronal cell death (Schapira and Gegg, 2011). Our results showed that 6-OHDA induced mitochondria membrane potential loss. However, α-iso-cubebenol suppressed this 6-OHDA-induced effect. Dysfunction of mitochondria induced by 6-OHDA is regulated by various anti-and pro-apoptotic-related genes such as Bid, Bax, cytochorome *c*, and AIF. Following the loss of mitochondrial membrane potential, AIF is distributed in the cytosol and then translocated to the nucleus. Inhibition of AIF release from the mitochondria by pharmacological inhibitors has a significant neuroprotective effect in neurotoxin-induced cell injury (Gorman et al., 1998; Zhang et al., 2011). We have provided evidence that SH-SY5Y cell death occurs via apoptosis mediated by translocation of AIF from the mitochondria to the cytosol. Moreover, α-iso-cubebenol effectively inhibited the 6-OHDA-induced release of AIF from the mitochondria.

The role of the antioxidant-related genes HO-1 and NQO1 as well as the importance of the PKA/PKB/CREB/Nrf2 signaling pathway in neuroprotection remain unclear. Thus, we next investigated the effect of α-iso-cubebenol on HO-1 and NQO1 expression as well as on activation of the PKA/PKB/CREB/Nrf2 signaling pathway. PKA and PKB are important for several neuronal signaling pathways including cell survival, proliferation, and differentiation. CREB and Nrf2 are cAMP and redox-responsive transcription factors that prevent neurodegeneration through

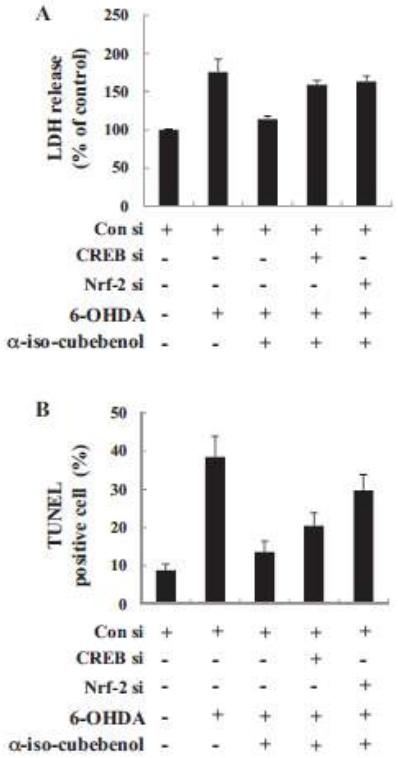

Fig. 6. Effects of CREB and Nrf2 disruption on the α-iso-cubebenol anti-apoptotic activity in 6-OHDA-treated SH-SY5Y cells. Cells were transfected with the control, CREB, and Nrf2 siRNA using the X-tremeGENE reagent according to the manufacturer's instructions. Cells were treated with 20 μM α-iso-cubebenol for 24 h and stimulated with 6-OHDA (200 μM) for 24 h, and the LDH release assay (A) and TUNEL assay (B) were performed.

inhibition of neuronal cell death. They bind to the DNA sequences of CREs and AREs, thereby regulating the transcription of neuroprotective genes (Park et al., 2013; Nakaso et al., 2008; Kawai et al., 2011). In the current study, activation of PKA and PKB as well as CREB and Nrf2 was significantly increased by pretreatment with α-iso-cubebenol. Nrf2 activation leads to the transcription of the HO-1 and NQO1 genes, which are involved in cellular homeostasis. The expression of HO-1 and NQO1, which are critical cytoprotective enzymes, is considered to be a protective response against cellular oxidative stress. Our results clearly indicated that α-iso-cubebenol induced HO-1 and NQO1 in SH-SY5Y cells. Furthermore, knockdown of CREB and Nrf2 by siRNA abolished α-iso-cubebenol-induced neuroprotection, indicating that CREB and Nrf2 may play an important role in mediating neuroprotection.

In conclusion, the present results suggest that α-iso-cubebenol, an active compound in *Schisandra chinensis*, effectively prevents 6-OHDA-induced neuronal cell death by inhibiting ROS and calcium accumulation. Mitochondrial dysfunction was also effectively suppressed by α-iso-cubebenol via inhibition of AIF translocation from the mitochondria to the cytosol. Furthermore, α-iso-cubebenol up-regulated the CREB and Nrf2 pathways and protected SH-SY5Y cells against 6-OHDA induced oxidative stress. Taken together, our results of the mechanisms underlying the neuroprotective effects of α-iso-cubebenol on 6-OHDA-induced cell death will provide additional insights into the molecular mechanisms of the effects of α-iso-cubebenol in clinical setting.

Conflict of interest

The authors declare that there are no conflicts of interest.

Transparency document

The Transparency document associated with this article can be found in the online version.

Acknowledgments

This research was supported by the Basic Science Research Program through the National Research Foundation of Korea (NRF) funded by the Ministry of Education, Science and Technology (2012R1A1A3010601). This research was supported by Bio-industry Technology Development Program (311054-03-3-HD120), Ministry for Food, Agriculture, Forestry and Fisheries, Republic of Korea.

References

Baxter PS, Martel MA, McMahon A, Kind PC, Hardingham GE. Pituitary adenylate cyclase-activating peptide induces long-lasting neuroprotection through the induction of activity-dependent signaling via the cyclic AMP response element-binding protein-regulated transcription co-activator 1. JNeurochem 2011;118:365–378.

Blum D, Torch S, Lambeng N, Nissou M, Benabid AL, Sadoul R, et al. Molecular pathways involved in the neurotoxicity of 6-OHDA, dopamine and MPTP: contribution to the apoptotic theory in Parkinson's disease. Prog Neurobiol 2001;65:135–72.

Bove J, Perier C. Neurotoxin-based models of Parkinson's disease. Neuroscience 2012;211:51–76.

Chen PC, Vargas MR, Pani AK, Smeyne RJ, Johnson DA, Kan YW, et al. Nrf2-mediated neuroprotection in the MPTP mouse model of Parkinson's disease: critical role for the astrocyte. Proc Natl Acad Sci U S A 2009;106:2933–8.

Cheng JC, Esparza S, Sandoval S, Shankar D, Fu C, Sakamoto KM. Potential role of CREB as a prognostic marker in acute myeloid leukemia. Future Oncol 2007;3:475–80.

Choi YW, Takamatsu S, Khan SI, Srinivas PV, Ferreira D, Zhao J, et al. Schisandrene, a dibenzocyclooctadiene lignan from *Schisandra chinensis*: structure-antioxidant activity relationships of dibenzocyclooctadiene lignans. J Nat Prod 2006;69:356–359.

Glinka Y, Gassen M, Youdim MB. Mechanism of 6-hydroxydopamine neurotoxicity. JNeural Transm Suppl 1997;50:55–66.

Glinka Y, Tipton KF, Youdim MB. Nature of inhibition of mitochondrial respiratory complex I by 6-hydroxydopamine. J Neurochem 1996;66:2004–10.

Gomez-Lazaro M, Galindo MF, Concannon CG, Segura MF, Fernandez-Gomez FJ, Llecha N, et al. 6-Hydroxydopamine activates the mitochondrial apoptosis pathway through p38 MAPK-mediated, p53-independent activation of Bax and PUMA. J Neurochem 2008;104:1599–612.

Gorman AM, Orrenius S, Ceccatelli S. Apoptosis in neuronal cells: role of caspases. Neuroreport 1998;9:849–55.

Guo LY, Hung TM, Bae KH, Shin EM, Zhou HY, Hong YN, et al. Anti-inflammatory effects of schisandrin isolated from the fruit of *Schisandra chinensis* Baill. Eur J Pharmacol 2008;591:293–9.

Hong SJ, Dawson TM, Dawson VL. Nuclear and mitochondrial conversations in cell death: PARP-1 and AIF signaling. Trends Pharmacol Sci 2004;25:259–64.

Innamorato NG, Rojo AI, Garcia-Yague AJ, Yamamoto M, de Ceballos ML, Cuadrado A. The transcription factor Nrf2 is a therapeutic target against brain inflammation. JImmunol 2008;181:680–9.

Katoh Y, Itoh K, Yoshida E, Miyagishi M, Fukamizu A, Yamamoto M. Two domains of Nrf2 cooperatively bind CBP, a CREB binding protein, and synergistically activate transcription. Genes Cells 2001;6:857–68.

Kawai Y, Garduno L, Theodore M, Yang J, Arinze IJ. Acetylation-deacetylation of the transcription factor Nrf2 (nuclear factor erythroid 2-related factor 2) regulates its transcriptional activity and nucleocytoplasmic localization. J Biol Chem 2011;286:7629–40.

Kim SJ, Min HY, Lee EJ, Kim YS, Bae K, Kang SS, et al. Growth inhibition and cell cycle arrest in the *G0/G1* by schizandrin, a dibenzocyclooctadiene lignan isolated from *Schisandra chinensis*, on T47D human breast cancer cells. Phytother Res 2010;24:193–7.

Identification of the responsible proteins for increased selenium bioavailability in the brain of transgenic rats overexpressing selenoprotein M

YONA KIM[1*], JUN SEO GOO[2*], IL YONG KIM[1], JI EUN KIM[2], MOON HWA KWAK[2], JUN GO[2], SUNBO SHIM[3], JIN TAE HONG[4], DAE YOUN HWANG[2] and JE KYUNG SEONG[1]

[1]Laboratory of Developmental Biology and Genomics, College of Veterinary Medicine, BK21 Program for Veterinary Science, Interdisciplinary Program for Bioinformatics and Program for Cancer Biology, Seoul National University, Seoul 151-742; [2]Department of Biomaterials Science, College of Natural Resources and Life Science, Life and Industry Convergence Research Institute, Pusan National University, Miryang, Gyeongsangnam-do 627-706; [3]Department of Laboratory Animal Resources, National Institute of Food and Drug Safety Evaluation, Korea FDA, Cheongwon, Chungcheongbuk-do 363-700; [4]College of Pharmacy, Chungbuk National University, Cheongju, Chungcheongbuk-do 361-763, Republic of Korea

Received March 25, 2014; Accepted September 9, 2014

DOI: 10.3892/ijmm.2014.1945

Abstract. The present study was conducted to investigate whether the high antioxidant activity induced by selenium (Sel) treatment and selenoprotein M (SelM) overexpression affected the protein profile of the brain cortex. To accomplish this, the changes in global protein expression were measured in transgenic (Tg) rats expressing human SelM (CMV/hSelM) and non-Tg rats using two-dimensional electrophoresis (2-DE). The results revealed that: i) CMV/hSelM Tg rats showed a high level of enzyme activity for antioxidant protein in the brain cortex compared to non-Tg rats; ii) the high activity of these enzymes induced a decrease in total antioxidant concentration and γ-secretase activity in CMV/hSelM Tg rats; iii) five proteins were upregulated and three were downregulated by SelM overexpression; iv) among the five upregulated proteins, two associated with creatine kinase B-type (B-CK) and E3 ubiquitin-protein ligase RING1 (RING finger protein 1) were further increased in the two groups following Sel treatment, whereas synaptotagmin-15 (SytXV), eukaryotic translation initiation factor 4H (eIF-4H) and lactate dehydrogenase B (LDH-B) were increased or decreased under the same conditions; v) the three downregulated proteins did not induce a significant change in expression following Sel treatment; and vi) the protein expression level alterations of the two selected spots (B-CK and SytXV) identified by 2-DE were extremely similar to the results from western blot analysis. Overall, the results of the present study provide primary novel biological evidence that new functional protein groups and individual proteins in the brain cortex of CMV/hSelM Tg rats are associated with Sel biology, including the response to Sel treatment and SelM overexpression.

Correspondence to: Professor Je Kyung Seong, Laboratory of Developmental Biology and Genomics, College of Veterinary Medicine, Seoul National University, 1 Gwanak-Ro, Gwanak-Gu, Seoul 151-742, Republic of Korea
E-mail: snumouse@snu.ac.kr

Professor Dae Youn Hwang, Department of Biomaterials Science, College of Natural Resources and Life Science, Life and Industry Convergence Research Institute, Pusan National University, 50 Cheonghak-ri, Samnangjin-eup, Miryang-si, Gyeongsangnam-do 627-706, Republic of Korea
E-mail: dyhwang@pusan.ac.kr

*Contributed equally

Key words: selenoprotein M, transgenic rat, protein profile, antioxidant, selenium

Introduction

Selenium (Sel) is an ubiquitous trace element in nature that has been shown to be essential to various aspects of human health (1). This trace element has also been shown to be required for normal growth and reproduction during spermatogenesis (2). Furthermore, Sel deficiency induces multiple diseases associated with oxidative damage, such as fatal cardiomyopathy, which is endemic in Keshan (China) (3), and muscular dystrophy in patients subjected to long-term unsupplemented parenteral nutrition (4). It is also well known that vitamin E can partially replace Sel deficiency (5,6). Sel exists naturally in organic (such as selenomethionine and selenocysteine) and inorganic forms (such as selenite, selenate and selenide) (7). However, these compounds require catabolizing into inorganic precursors prior to insertion into proteins, and the rare amino acid selenocysteine (Sec) is essential for the catalytic function of selenoenzymes (8). Sec, which is the 21st proteinogenic amino acid, was not initially recognized in the

classical genetic code as it is encoded by the UGA 'STOP' codon. For Sec insertion at UGA codons in the translation process, a specific RNA stem-loop structure is required. In eukaryotes, this loop resides in the 3'-untranslated region of the mRNA, known as the Sec-insertion-sequence (9). Sel has also been shown to be an essential part of mammalian enzymes, such as glutathione peroxidase (GPx), thyroid hormone deiodinase and thioredoxin reductase. Thus far, 25 genes encoding selenoproteins in the sequenced human genome have been identified (10). Selenoprotein M (SelM) was first reported as a 0.7-kb cDNA gene that encoded a new selenoprotein identified from the mammalian EST database. This gene has a 145-amino acid open reading frame beginning with an ATG codon in a favorable Kozak context and contains an in-frame TGA as the Sec codon. Furthermore, homologous proteins have been identified in the rat, zebra fish and other vertebrates, and Sec was conserved in these homologs (11). There have also been several functional studies of SelM. For example, the study by Müller *et al* (12) showed that this protein plays a major role in spicule formation in the demosponge *Suberites domuncula*. In addition, Hwang *et al* (13) indicated that SelM plays a suppressive or protective role in the pathology of patients with Alzheimer's disease (AD). However, there have been no studies for whether SelM overexpression could affect the changes in global gene expression in CMV/hSelM transgenic (Tg) rats following Sel treatment.

Sel is maintained at high levels in the brain, even upon prolonged dietary Sel deficiency (14). Changes in Sel concentration in the brain and blood have been detected in AD, Parkinson's disease (PD), multiple sclerosis and brain tumors. Several studies have shown that Sel treatment leads to reduced seizures, improved electroencephalogram recordings (15), protection against the depletion of striatal dopamine (16) and a reduction in the progression of neurodegeneration (17). Furthermore, several selenoproteins have been expressed in the brain. Among these proteins, GPx has been localized in glial cells, and its expression level was significantly upregulated in damaged areas in PD (18). High expression of selenoprotein P (SelP) was also observed in the olfactory bulb, hippocampus and frontal cortex (19). Genetically-engineered models, including Tg and knock-out models, can provide a platform to define the *in vivo* function of genes and to also study the molecular events responding to environmental changes (20). Previous studies using a knock-out model of SelP showed that it had the important function of Sel delivery into the brain tissue (21,22). Other selenoproteins, including selenoprotein W, thioredoxin reductase, 15-kDa selenoprotein and SelP, have also been detected in the brain. However, numerous questions regarding the roles of these proteins in neuronal function remain.

In the present study, the global change of gene expression affected by SelM overexpression and Sel treatment in the brain cortex was investigated. Two-dimensional electrophoresis (2-DE) analysis showed that eight proteins were significantly changed in CMV/hSelM Tg rats. These results indicated that the information isolated from SelM overexpression and Sel treatment may be useful for studying the association between antioxidant conditions and brain disease, which shows a higher level of oxidative stress condition in specific tissues.

Materials and methods

Maintenance and identification of CMV/hSelM Tg rats. The CMV/hSelM Tg rats used in the study, showing high antioxidant status in various tissues, were developed by microinjection of the CMV/hSelM recombinant gene into fertilized rat eggs (13). The animal protocol was reviewed and approved based on the ethical and scientific care procedures of the Korea Food and Drug Administration (KFDA)-Institutional Animal Care and Use Committee. All rats were maintained in an accredited KFDA animal facility in accordance with AAALAC International Animal Care policies (Accredited Unit-KFDA; unit No. 000996). The rats were provided a standard irradiated chow diet (Purina Mills Inc., St. Louis, MO, USA) *ad libitum* and maintained in a specified pathogen-free state under a strict light cycle (lights on at 06:00 h and off at 18:00 h). All the pedigrees were hemizygous for their transgenes.

Experimental design and Sel treatment. Sodium selenite ($NaSeO_3$) purchased from Sigma-Aldrich Co., (St. Louis, MO, USA) was dissolved in distilled water to a final concentration of 0.2 μmol/μl (23,24). Ten-week-old rats were randomly divided into two subgroups (n=6 per group). The first subgroup of the CMV/hSelM Tg and non-Tg rat groups each received a comparable volume of distilled water daily via intraperitoneal injection (vehicle-treated CMV/hSelM Tg and non-Tg groups), whereas rats in the second subgroup each received 5 μmol/kg body weight/day of sodium selenite via intraperitoneal injection for three weeks (Sel-treated CMV/hSelM Tg and non-Tg groups). At three weeks after Sel-solution injection, the animals were immediately euthanized using CO_2 gas, following which the cortex samples from their brains were prepared and stored in Eppendorf tubes at -70˚C until assayed.

Analysis of GPx and superoxide dismutase (SOD) activities and total oxidized products concentration. The levels of GPx and SOD in the brain cortex of CMV/hSelM Tg and non-Tg rats were detected by following the colorimetric assay procedure using Bioxytech SOD-525 and Bioxytech GPx-340 kits (OxisResearch™, Portland, OR, USA). The level of total oxidized products in the sera of CMV/hSelM Tg and non-Tg rats was detected using a Total Antioxidant Status kit (Randox Laboratories Ltd., Antrim, UK) as previously described (13).

γ-secretase activity analysis. The γ-secretase activity was detected with a γ-Secretase Activity kit (R&D System Inc., Minneapolis, MN, USA) using the manufacturer's instructions. Initially, cortex tissue was homogenized with a glass homogenizer in cold 1X extraction buffer to yield a final protein concentration of roughly 0.5-2.0 mg. These mixtures were incubated on ice for 10 min, after which they were centrifuged at 10,000 x g for 1 min to remove the unbroken fragments. The final supernatants collected from the centrifuged mixture were subsequently used for detection of secretase activity, and this process was carried out in the microplate provided by the manufacturer. To perform the enzyme reaction, 50 μl tissue lysate was added to each well, followed by 50 μl 2X reaction buffer and 5 μl substrate. The microplates were gently mixed and incubated in the dark at 37˚C for 1-2 h to induce an enzyme-substrate reaction. Final fluorescence produced by the

reaction was read on a fluorescent microplate reader using a filter that allowed EDANS excitation at between 335-355 nm.

Sample preparation for 2-DE. Analyses of global protein expression by 2-DE were performed according to the methods established by our laboratory in previous studies (25-27). The cortex samples isolated from the brain were homogenized in liquid nitrogen, following which the homogenized tissues were lysed in buffer [7 M urea, 2 M thiourea, 4% w/v CHAPS, 40 mM Tris and 100 mM dithioerythritol (DTE)]. The sample mixtures were subsequently centrifuged at 45,000 x g at 4˚C for 1 h, after which protein concentrations were determined by the Bradford protein assay (Bio-Rad, Hercules, CA, USA). In this process, a cortex sample was generated from a pool of the six animals in each group. The pooled samples were analyzed three times.

2-DE analysis. One-dimensional isoelectric focusing (IEF) was performed using 24 cm immobilized pH gradient (IPG) strips (GE Healthcare, Uppsala, Sweden) in a pH range of 3.0-10.0 (non-linear). Protein (1-mg) was loaded in a total volume of 450 μl, following which the samples were diluted with rehydration solution [7 M urea, 2 M thiourea, 4 % w/v CHAPS, 40 mM Tris, 100 mM DTE and 2% IPG buffer (pH 3.0-10.0)]. After rehydration for 13 h, the strips were focused at 30 V for 2 h, 100 V for 2 h, 200 V for 1 h, 500 V for 1 h, 1,000 V for 1 h and finally at 8,000 V for 22 h to obtain ~100,000 VHr (IPGphor; GE Healthcare). Once IEF was completed, the strips were equilibrated in 6 M urea containing 20% glycerol, 2% SDS and 0.01% bromophenol blue with 10 mM tributyl phosphine. Two-dimensional SDS-PAGE was performed using 8-18% linear gradient acrylamide gels on an EttanDalt system (GE Healthcare). Proteins were visualized by staining with Coomassie blue G-250 (Bio-Rad).

To analyze changes in protein expression between the types of rats according to SelM level, an average gel representing non-Tg rats was compared to an average gel representing the CMV/hSelM Tg rats. Only the filtered spots exceeding an intensity threshold of a 1.5 or 2-fold increase or decrease between non-Tg and CMV/hSleM Tg rats were studied further, whereas the threshold regulation factor for the significance level was set at $P \leq 0.05$. Furthermore, any spot showing a significant difference in expression between non-Tg and CMV/hSleM Tg rats was analyzed in all the rats to map changes in expression according to Sel-related factors. Finally, the spots showing significant changes in expression were subsequently identified by mass spectrometry.

Identification of protein spots. The stained gels were scanned with a GS800 densitometer (Bio-Rad) and analyzed using Image master™ (Swiss Institute of Bioinfomatics, Geneva, Switzerland). The spots were digested using trypsin, following which supernatant peptide mixtures were loaded onto a Poros R2 column (Applied Biosystems, Foster City, CA, USA) that had been washed with the following solutions: i) 70% acetonitrile in 5% formic acid; ii) 100% acetonitrile; and iii) 5% formic acid. Peptides were eluted using 5 μl of α-cyano-4-hydroxycinnamic acid and analyzed with a matrix-assisted laser desorption/ionization time-of-flight (MALDI-TOF) mass spectrometer (Voyager DE-PRO; Applied Biosystems). For protein identification, masses of peptides determined by MALDI-TOF were matched with theoretical peptides in the NCBI (http://www.ncbi.nih.gov/) database using the MASCOT (http://www.matrixscience.com) and ProFound programs (http://prowl.rockefeller.edu).

Western blot analysis. Total proteins prepared from a cortex sample of CMV/hSelM Tg and non-Tg rats were separated by electrophoresis on a 4-20% SDS-PAGE gel for 3 h and subsequently transferred to nitrocellulose membranes for 2 h at 40 V. Each membrane was incubated separately with anti-creatine kinase antibody (Abcam, Cambridge, UK), anti-synaptotagmin antibody (Santa Cruz Biotechnology, Inc., Santa Cruz, CA, USA), and anti-actin (Sigma-Aldrich) antibodies overnight at 4˚C. The membranes were incubated with horseradish peroxidase-conjugated goat anti-rabbit immunoglobulin G (Zymed Laboratories, Inc., South San Francisco, CA, USA) at a 1:1,000 dilution at room temperature for 2 h. The membrane blots were developed using a Chemiluminescence Reagent Plus kit (ECL; Amersham Pharmacia Biotech, Inc., Piscataway, NJ, USA).

Statistical analysis. Tests for significance between vehicle- and Sel-treated rats were performed using a one-way analysis of variance test of variance (SPSS for Windows, Release 10.10, Standard Version; SPSS, Inc., Chicago, IL, USA). Tests for significance between CMV/hSelM Tg and non-Tg rats were performed using a post-hoc test (SPSS for Windows, Release 10.10, Standard Version) of variance, and significance levels are provided throughout. All the values are reported as the mean ± standard deviation. $P<0.05$ was considered to indicate a statistically significant difference.

Results

Enhancement of SOD and GPX activity in the brain cortex of CMV/hSelM Tg rats. To confirm whether or not alteration of antioxidative conditions is induced by Sel treatment and SelM overexpression in the cortex region of rat brains, the activity of SOD and GPX was measured in the brain tissue of CMV/hSelM Tg and non-Tg rats using a detection kit containing a specific substrate. In the vehicle-treated group, SOD/GPX activity in the CMV/hSelM Tg rats showed a higher level of enzyme activity than that of the non-Tg rats, although they showed differing rates of increase (Fig. 1A and C). Following Sel treatment, the activity of these enzymes increased significantly in the CMV/hSelM Tg and non-Tg rats. However, the rate of increase in the CMV/hSelM Tg rats was greater than that of the non-Tg rats (Fig. 1A and C). These results indicate that SelM overexpression and Sel treatment induced an increase of antioxidant protection in the brain cortex from CMV/hSelM Tg rats.

Change in total oxidized products concentration in the brain of CMV/hSelM Tg rats. To determine whether or not enhancement of SOD and GPX activity was accompanied by a decreased level of oxidized products, the concentration of total oxidized products was determined in the serum of CMV/hSelM Tg and non-Tg rats following Sel treatment using an ELISA kit. For the vehicle-treated group, the concentration of total oxidized products at the basal level was significantly lower in the

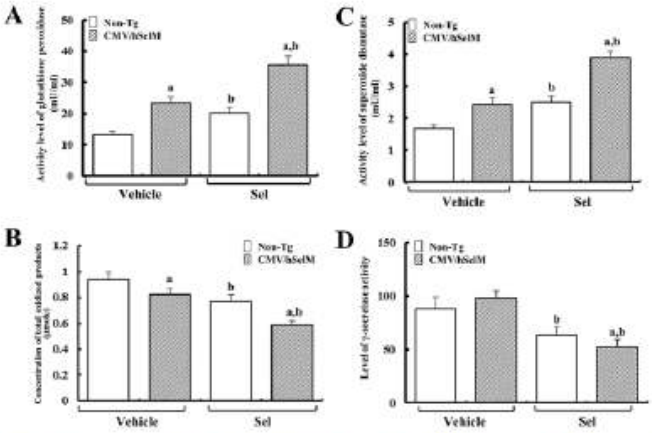

Figure 1. Effects of selenium (Sel) treatment and selenoprotein M (SelM)overexpression on (A) glutathione peroxidase (GPx) activity, (B) superoxide dismutase (SOD) activity, (C) concentration of total oxidized products and (D) γ-secretase activity in the brain cortex. The brains used in this assay were collected from CMV/hSelM Tg and Non-Tg rats following intraperitoneal injection of sodium selenite (5 μmole/kg body weight/day) for three weeks. Enzyme activity and total oxidized products were assayed in six rats per group by ELISA. The data represent the means ± standard deviation from three replicates. [a]Significant difference ($P<0.05$) when compared to non-Tg rats; [b]significant difference ($P<0.05$) when compared to the vehicle-treated group.

CMV/hSelM Tg rats compared to the non-Tg rats. Following Sel treatment, these levels decreased simultaneously in the CMV/hSelM Tg and non-Tg rats, although the concentration of total oxidized products in the CMV/hSelM Tg rats was consistently maintained at a low level compared to the non-Tg rats. In particular, the decreasing rate of total oxidized products concentration in the Sel-treated group was significantly greater compared to the vehicle-treated group (Fig. 1B). These results indicate that the overactivation of SOD and GPX induced by SelM overexpression and Sel treatment contributes to the increase in the functional activity for oxidized products protection in the brain cortex of CMV/hSelM rats.

Change of γ-secretase activity in the brain cortex of CMV/hSelM Tg rats. Furthermore, γ-secretase plays an important role in the production of Aβ-42 peptide in the pathogenesis of AD (28). To investigate the effects of Sel treatment and SelM overexpression on the physiological changes in neurodegenerative pathology, the activity of γ-secretase, a critical enzyme of Aβ-42 peptides production, was measured in the brains of CMV/hSelM Tg and non-Tg rats using a detection kit containing a specific substrate. For the vehicle-treated group, the activity of γ-secretase in the CMV/hSelM Tg rats was slightly higher compared to non-Tg rats, although this difference was not significant. However, following Sel treatment, these activities were significantly lower in the two groups of rats. Furthermore, the rate of decrease in γ-secretase activity in the CMV/hSelM Tg rats was higher compared to the non-Tg rats (Fig. 1D). These findings indicate that SelM overexpression and Sel treatment may lead to a decreased incidence of neurodegenerative disease in the brain cortex through the regulation of γ-secretase activity.

Proteome analysis of total proteins in brain cortex from of CMV/hSelM Tg rats. To characterize the changes in global protein expression in the brain cortex of CMV/hSelM Tg rats in response to the induced bioavailability of Sel treatment and SelM overexpression, whole proteins extracted from the brain cortex of 10-week old CMV/hSelM Tg and non-Tg rats were analyzed on analytic 2-DE gels. Computer analysis of gel images showed good matching in four analytical replicates, including vehicle-treated non-Tg, Sel-treated non-Tg, vehicle-treated CMV/hSelM Tg and Sel-treated CMV/hSelM Tg rats. The 2-DE protein maps of the samples from the four groups are shown in Fig. 2. Approximately 270 spots were detected in one gel from brain cortex. The spots that showed significantly different expression were selected for further analysis. Eight spots were identified as key proteins differentially expressed in four experimental groups. Furthermore, in the vehicle-treated group, eight spots were classified into two groups, including upregulated spots (five spots) and downregulated spots (three spots), according to their expression level in CMV/hSelM Tg rats. As shown in Table I, the five upregulated proteins included creatine kinase B-type (B-CK), synaptotagmin-15 (SytXV), E3 ubiquitin-protein ligase RING1 (RING1 finger protein 1), lactate dehydrogenase B (LDH-B) and eukaryotic translation initiation factor 4H (eIF-4H), whereas the three downregulated included centromere protein N (CENP-N), proteasome subunit K and dihydropyrimidinase-related protein 2 (DRP-2).

Following Sel treatment, the eight spots showed different patterns. The five-upregulated spots were classified into three groups according to their expression pattern. Two neighboring spots in the first group showed a marked increase in response to Sel treatment and were identified as B-CK and RING1 finger protein 1 (Fig. 3). The volume ratio of these two spots was significantly higher in the CMV/hSelM Tg rats compared to non-Tg rats. Following Sel treatment, these volumes were markedly increased in the two groups relative to the vehicle-treated group. Even though the volume of these

Table I. List of the differentially expressed proteins in the four experimental groups.

Spot no.	Protein name	Gene name	Accession no.	Sequence coverage, %	Mw, Da/pI	Mascot score	Vehicle		Selenium	
							Non-Tg	Tg[a]	Non-Tg[a]	Tg[a]
1	Creatine kinase B-type (EC 2.7.3.2) (Creatine kinase B chain) (B-CK)	Ckb	P07335	53	42698/5.39	124	1	3.07±0.31	2.19±0.18	3.87±0.25
2	E3 ubiquitin-protein ligase RING1 (EC 6.3.2.-) (Polycomb complex protein RING1) (RING finger protein 1)	Ring1	Q6MGB6	23	42634/5.54	30	1	2.72±0.18	2.98±0.21	3.62±0.28
3	Synaptotagmin-15 (Synaptotagmin XV) (SytXV)	Syt15	P59926	21	47562/8.45	32	1	1.66±0.12	2.37±0.18	1.25±0.11
4	L-lactate dehydrogenase B chain (EC 1.1.1.27) (LDH-B) (LDH heart subunit) (LDH-H)	Ldhb	P42123	14	36589/5.70	76	1	2.24±0.15	3.19±0.25	1.57±0.19
5	Eukaryotic translation initiation factor 4H (eIF-4H) (Williams-Beuren syndrome chromosomal region 1 protein homolog)	Eif4h	Q5XI72	51	27307/6.67	26	1	1.78±0.22	1.10±0.29	1.09±0.13
6	Proteasome subunit alpha type-3 (EC 3.4.25.1) (Proteasome component C8) (Proteasome subunit K) (Macropain subunit C8) (Multicatalytic endopeptidase complex subunit C8)	Psma3	P18422	58	28401/5.29	25	1	0.71±0.05	0.86±0.07	0.70±0.06
7	Centromere protein N (CENP-N)	Cenpn	Q5U2W4	31	39434/8.09	37	1	0.53±0.04	1.14±0.25	0.49±0.05
8	Dihydropyrimidinase-related protein 2 (DRP-2) (Turned on after division, 64 kDa protein) (TOAD-64) (Collapsin response mediator protein 2) (CRMP-2)	Dpysl2	P47942	32	62239/5.95	126	1	0.34±0.03	1.17±0.23	0.36±0.03

[a]Values in the last three columns on the right hand side are expressed as the relative value of the spot volume for the non-Tg vehicle group, which was defined as 1.

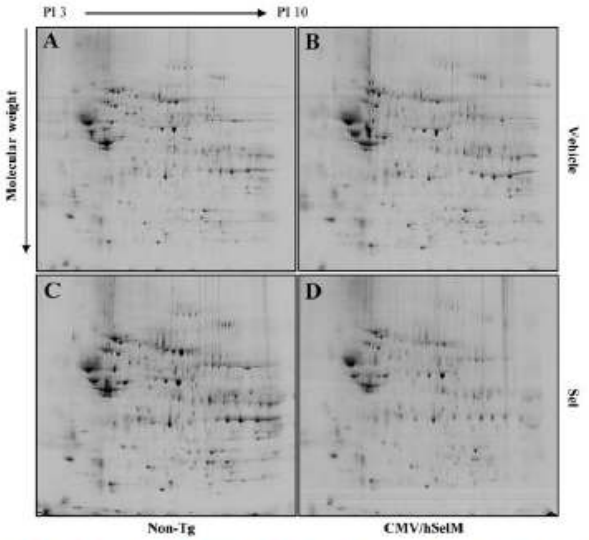

Figure 2. Two-dimensional electrophoresis (2-DE) protein patterns in the brain tissues from CMV/hSelM Tg and non-Tg rats. Analyses was of the brains cortex proteins by 2-DE. Cortex lysates (1 mg) from the rat brains of four groups; (A) vehicle-treated non-Tg, (B) selenium (Sel)-treated non-Tg, (C) vehicle-treated CMV/hSelM Tg and (D) Sel-treated CMV/hSelM Tg; were separated by one-dimensional isoelectric focusing (IEF) using 24 cm immobilized pH gradient strips with the pH range, 3.0-10.0 (non-linear). Second dimensional SDS-PAGE was then performed using 8-18% linear gradient acrylamide gels in an EttanDalt system. Protein spots were visualized by Coomassie blue G-250 staining.

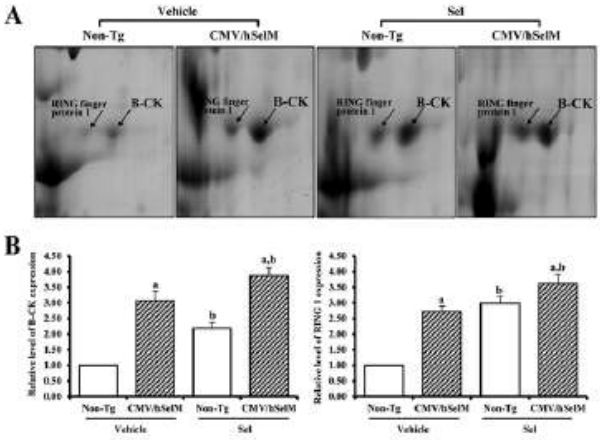

Figure 3. (A) Gel enlargement image and (B) relative expression level of RING finger protein 1 and creatine kinase B-type (B-CK) showing differential upregulation between cortex extracts from four experimental groups. Upregulated protein spots of RING finger protein 1 and B-CK were detected in the brain extracts from the four experimental groups. The spots differentially expressed on two-dimensional electrophoresis (2-DE) were further analyzed by a matrix-assisted laser desorption/ionization time-of-flight (MALDI-TOF) mass spectrometer. The data represent the means ± standard deviation of three replicates. [a]Significant difference ($P<0.05$) when compared to non-Tg rats; [b]significant difference ($P<0.05$) when compared to the vehicle-treated group.

two spots increased in the Sel-treated group, they remained at a higher level in the CMV/hSelM Tg rats compared to the non-Tg rats (Fig. 3). The next group consisted of two spots that showed moderate changes in SytXV and LDH-B (Table I). The spot identified as SytXV was expressed at higher levels in the CMV/hSelM Tg rats than non-Tg rats that had received

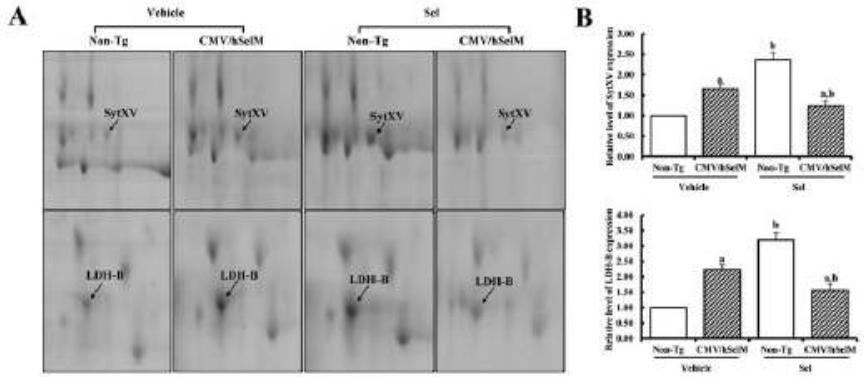

Figure 4. (A) Gel enlargement image and (B) relative expression level of synaptotagmin-15 (SytXV) and lactate dehydrogenase B (LDH-B) showing differential upregulation between cortex extracts from four experimental groups. Upregulated protein spots of SytXV and LDH-B were detected in the brain extracts from the four experimental groups. The spots differentially expressed on two-dimensional electrophoresis (2-DE) were further analyzed using a matrix-assisted laser desorption/ionization time-of-flight (MALDI-TOF) mass spectrometer. The data represent the means ± standard deviation from three replicates. [a]Significant difference ($P<0.05$) when compared to non-Tg rats; [b]significant difference ($P<0.05$) when compared to the vehicle-treated group.

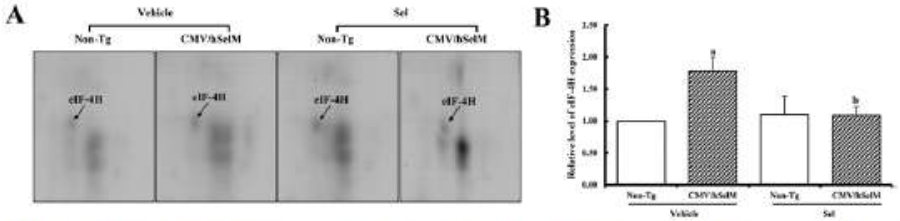

Figure 5. (A) Gel enlargement image and (B) relative expression level of eukaryotic translation initiation factor 4H (eIF-4H) showing differential up- or downregulation between cortex extracts from the four experimental groups. Up- or downregulated protein spots of eIF-4H were detected in the brain extracts from the four experimental groups. The spots differentially expressed on two-dimensional electrophoresis (2-DE) were further analyzed by a matrix-assisted laser desorption/ionization time-of-flight (MALDI-TOF) mass spectrometer. The data represent the means ± standard deviation from three replicates. [a]Significant difference ($P<0.05$) when compared to non-Tg rats; [b]significant difference ($P<0.05$) when compared to the vehicle-treated group.

vehicle treatment. Sel treatment induced an increase in spot volume in non-Tg rats, whereas it was significantly decreased in CMV/hSelM Tg rats (Fig. 4). The spot isolated as LDH-B showed a change similar to the spot of SytXV. However, the basic level of these spots was higher in the CMV/hSelM Tg rats compared to the non-Tg rats (Fig. 4). The third group was not affected by Sel treatment and was only induced by SelM overexpression. Spot eIF-4H showed a significantly higher level in CMV/hSelM Tg rats, but was significantly downregulated following Sel treatment, whereas it remained unchanged in the non-Tg rats (Fig. 5).

The group that showed downregulated SelM was further classified into two subgroups. One large spot known as proteasome subunit K belonged to the first subgroup. The volume of this spot was lower in CMV/hSelM Tg rats than non-Tg rats under vehicle-treated conditions. However, Sel treatment induced a decrease in the proteasome subunit K level in non-Tg rats, whereas it remained at a constant level in the CMV/hSelM Tg rats (Fig. 6). In the second subgroup, two spots identified as CENP-N and DRP-2 showed similar patterns under the two conditions (Table I), with a lower level being observed for CMV/hSelM Tg rats than non-Tg rats. These levels were not changed following Sel treatment in either group (Fig. 7).

Confirmation of B-CK and SytXV expression. Western blot analysis was conducted to validate the changes in the protein expression levels of the two selected spots (B-CK and SytXV) identified by 2-DE. As shown in Fig. 8, the expression of B-CK was significantly higher in the CMV/hSelM Tg rats than non-Tg rats. Following Sel treatment, its level increased further in the two groups, although its total expression pattern was maintained. In the case of SytXV, its expression level was higher in CMV/hSelM Tg rats compared to non-Tg rats under vehicle treatment conditions. However, expression of this protein increased significantly in response to Sel treatment in non-Tg rats, whereas CMV/hSelM rats showed no significant difference in expression. The expression pattern of the above proteins observed upon western blot analysis was extremely similar to that in the 2-DE gel image, indicating that the alteration of protein spots detected by 2-DE reflects changes

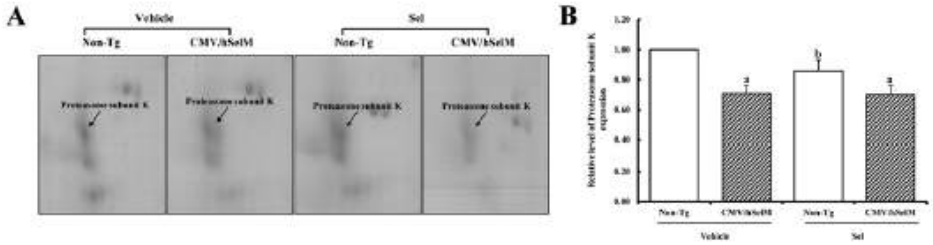

Figure 6. (A) Gel enlargement image and (B) relative expression level of proteasome subunit K showing differential downregulation between cortex extracts from four experimental groups. Downregulated protein spots of proteasome subunit K were detected in the brain extracts from the four experimental groups. The spots differentially expressed on two-dimensional electrophoresis (2-DE) were further analyzed by a matrix-assisted laser desorption/ionization time-of-flight (MALDI-TOF) mass spectrometer. The data represent the means ± standard deviation from three replicates. [a]Significant difference ($P<0.05$) when compared to non-Tg rats; [b]significant difference ($P<0.05$) when compared to the vehicle-treated group.

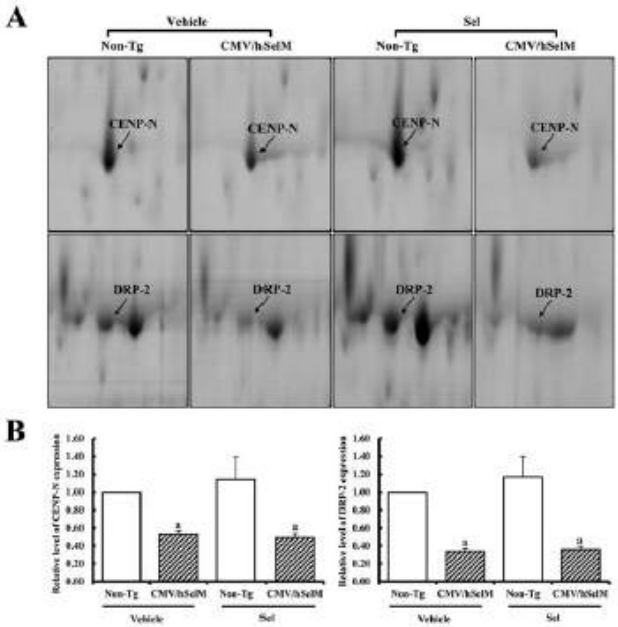

Figure 7. (A) Gel enlargement image and (B) relative expression level of CENP-N and DRP-2 showing differential downregulation between cortex extracts from four experimental groups. Downregulated protein spots of CENP-N and DRP-2 were detected in the brain extracts from the four experimental groups. The spots differentially expressed on two-dimensional electrophoresis (2-DE) were further analyzed by a matrix-assisted laser desorption/ionization time-of-flight (MALDI-TOF) mass spectrometer. The data represent the means ± standard deviation from three replicates. [a]Significant difference ($P<0.05$) when compared to non-Tg rats. CENP-N, centromere protein N; DRP-2, dihydropyrimidinase-related protein 2.

in protein expression in the brains of the CMV/hSelM Tg and non-Tg rats.

Discussion

Sel deficiency is associated with a variety of serious diseases, including infectious disease, cardiovascular disease, cancer and neurodegenerative disorders (7). Savaskan *et al* (29) provided direct evidence that Sel plays a pivotal role in neuronal susceptibility to excitotoxic lesions. The results of this study indicated that the neuroprotective effects of Sel are not directly mediated via the antioxidative effects of selenite, but require *de novo* protein synthesis. Therefore, Sel deficiency in the brain tissue leads to increased oxidative stress with subsequent NK-κB activation and neuronal cell death. Several studies reported that intracellular ETKs were activated by either sodium selenite, an inorganic salt known to activate ERK (30), or transfected with a constitutively active mutant of MEK1, an immediate upstream activator of ERKR (31,32). The present study investigated whether the high level of

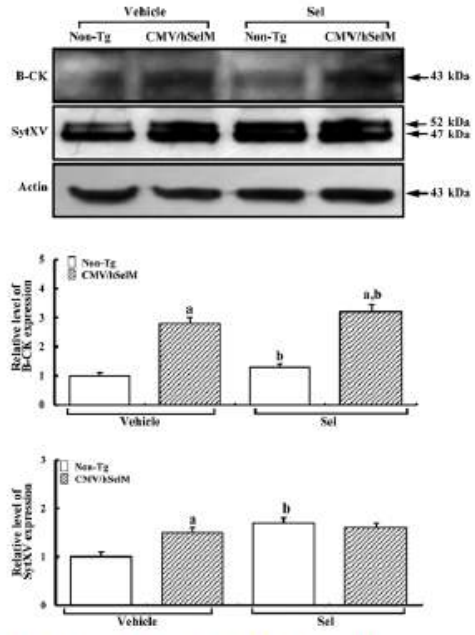

Figure 8. Conformation of creatine kinase B-type (B-CK) and synaptotagmin-15 (SytXV) expression in the brain cortex using western blot analysis. Tissue lysates were prepared from the brain tissue of vehicle-treated and selenium (Sel)-treated rats. Protein (50 μg per sample) were immunoblotted with the antibody for each protein. The expression level of B-CK and SytXV was detected with specific primary antibodies and horseradish peroxidase-conjugated goat anti-rabbit immunoglobulin G antibodies. The intensity of each protein was calculated using an imaging densitometer. The data represents the mean ± standard deviation from three replicates. [a]Significant difference ($P<0.05$) when compared to non-Tg rats; [b]significant difference ($P<0.05$) when compared to the vehicle-treated group.

antioxidants induced by Sel treatment and SelM overexpression affected the change in the cortex proteins of CMV/hSelM Tg and non-Tg rats. The CMV/hSelM Tg rats used in the study showed a higher level of antioxidant enzymes, such as SOD and GPX, compared to non-Tg rats. Additionally, the concentration of total oxidized products regulated by these enzymes was significantly decreased in the brain cortex of the CMV/hSelM Tg rats compared to non-Tg rats. These results indicate that the antioxidant condition was induced by Sel treatment and SelM overexpression in CMV/hSelM Tg rats. Furthermore, these findings are concordant with those of our previous study (13).

Aβ-42 peptide in the cortex of the brain is closely correlated with deposition at neuritic plaques in the pathogenesis of AD (28,33). The production of these peptides is tightly regulated by γ-secretase, which is composed of presenilin and four additional cofactors, nicastrin, Aph-1, Pen-2 and TMP-21, to create a multimeric protease complex (34,35). Thus far, limited studies investigating the correlation of Sel and γ-secretase have been conducted. The present study investigated whether the level of γ-secretase activity could be changed by Sel treatment and SelM overexpression in the brain of CMV/hSelM Tg rats. The results showed that the γ-secretase activity significantly decreased in response to Sel treatment. Therefore, the protein spot detected in the study may be correlated with the production of Aβ-42 peptides in CMV/hSelM Tg rats.

The study identified eight spots that were differentially expressed among four groups, which were vehicle-treated non-Tg, vehicle-treated CMV/hSelM Tg, Sel-treated non-Tg and Sel-treated CMV/hSelM Tg rats. Among these spots, creatine kinase was significantly upregulated in response to Sel treatment and SelM overexpression. B-CK, one of the creatine kinases, catalyzed the conversion of creatine to phosphocreatine, which was expressed in various tissue types (36). Generally, this enzyme is known as a buffering system of cellular ATP concentration and used as a marker of several diseases, including myocardial infarction, rhabdomyolysis, muscular dystrophy and renal failure (37). Decreased creatine kinase activity was recently reported to be tightly associated with neurodegenerative pathways in neurodegenerative diseases (38), ischemia (39) and other diseases (40,41). Creatine kinase and pyruvate kinase are crucial for energy homeostasis and antioxidant defense through inhibition of two enzyme activities (42). In the present study, the expression of B-CK was higher in CMV/hSelM Tg rats overexpressing SelM protein than non-Tg rats under vehicle-treated conditions. In addition, Sel treatment induced an increase of this enzyme expression in the two groups. Furthermore, this change pattern was observed in the spot identified as RING1. This enzyme, which is known as a Parkin, appeared to be part of the cell's defense against damage caused by environmental insults (43). This enzyme ubiquitinates itself and promotes its own degradation, and the impairment of ubiquitin ligase function may cause familial autosomal recessive PD. Furthermore, oxidative and nitrosative stress were closely associated with the ubiquitin ligase function of PD and the associated α-synucleinopathy (44).

SytXV and LDH-B showed similar protein change patterns on the 2-DE gels. Syt constitutes a family of membrane-trafficking proteins that are characterized by an N-terminal transmembrane region, a variable linker and two C-terminal domains (45,46). This protein is known as a Ca^{2+} sensor that regulates Ca^{2+}-dependent membrane trafficking, including endocrine exocytosis (47,48), synaptic vesicle exocytosis (49,50), plasma membrane repair (51,52) and acrosomal reaction (53). Several studies have also documented the correlation between neurotransmitter release and Syt function (54,55). However, limited studies of whether selenoprotein and Sel treatment were affected by SytXV expression have been conducted thus far. In the present study, the expression of this protein was significantly increased in response to SelM overexpression compared to non-Tg rats. However, in the CMV/hSelM Tg rats, Sel treatment did not induce a significant change in SytXV expression in the brain cortex. These results indicate that SelM overexpression could be affected by Ca^{2+}-dependent membrane trafficking through the regulation of Syt expression. Another spot was identified as LDH-B, which catalyzes the interconversion of pyruvate and lactate with concomitant interconversion of NADH and NAD^+ (56). Nazam Ansari *et al* (57) showed that serum lactate dehydrogenase and GPX were significantly lower in rats with ischemia. However, in the present study, LDH-B was increased

by SelM overexpression in CMV/hSelM Tg rats, but increased by Sel treatment in non-Tg rats, indicating that selenoprotein and Sel treatment are extremely important for normal brain function.

eIF-4H was the last member in the groups showing upregulated expression in response to SelM overexpression. This protein regulates protein synthesis through facilitating the binding of initiator tRNA to ribosomes (58). Several stress-responding genes induced by ultraviolet light, ER stress and reactive oxygen species were tightly regulated by eIF2. Furthermore, an abnormally high concentration of NO in the nervous system increases the eIF2α level of phosphorylated forms, thus suppressing protein synthesis in neurons (59). The eIF2α level of the phosphorylated form was also increased in hippocampal CA1 neurons following ischemia (60). In the present study, SelM overexpression induced increased eIF2α expression, but Sel treatment did not induce any change in either group.

The expression of CENP-N was extremely similar to that of DRP-2 upon 2-DE analysis. CENP-N was first reported as a member of three new human centromere proteins (CENP-M, CENP-N and CENP-T), which comprised a CENP-A nucleosome-associated complex (CENP-A NAC) (61). Additionally, disruption of CENP-A NAC by reduction of these three proteins induced a mitotic defect or significant mitotic delay in cells. However, there have been no studies of the correlation between CENP-N and antioxidant status. Therefore, to the best of our knowledge, the present study is the first to indicate that SelM overexpression led to a significant decrease in the expression of CENP-N.

DRP-2 is turned on following division of the 64-kDa protein or collapsing response mediator protein 2 (CRMP-2). This protein is highly expressed in the adult brain, is an important molecule in neurite outgrowth and axonal guidance, and plays a role in several neurological diseases, including AD, epilepsy and ischemia (62,63). Furthermore, a dramatic decrease of intact CRMP-2 was observed following maitotoxin treatment, *N*-methyl-D-asparatate treatment and ischemia induction, accompanied by the appearance of distinct breakdown products of CRMP-2 (63). The present study showed that SelM overexpression led to significant induction of the decrease of DRP-2 in CMV/hSelM Tg rats compared to non-Tg rats. These results indicate that SelM could be referred to as a regulator of DRP-2, although further study of the degradation process is necessary.

All the aforementioned results showed that SelM overexpression and Sel treatment play a crucial role in the regulation of brain function via modulation of eight associated proteins. In addition, our proteomic analysis allowed the verification of the change in protein patterns of brain antioxidant regulation. However, intensive study is required to define the role and detailed mechanism of SelM and Sel in the cortex region of the brain.

Acknowledgements

The authors wish to acknowledge the animal technicians, S.M. Choi (BS) and Ms. J.L. Song, for directing the Animal Facility and Care at the Division of Laboratory Animal Resources. The present study was supported by the grants from the KFDA. This study was supported by the Bio and Medical Technology Development Program of the National Research Foundation (NRF) funded by the Ministry of Science, ICT and Future Planning (2012M3A9B6055344), and also supported by Bio-industry Technology Development Program, Ministry of Agriculture, Food and Rural Affairs (311054-03-3-HD110) to Professor Je Kyung Seong.

References

1. Wilber CG: Toxicology of selenium: a review. Clin Toxicol 17: 171-230, 1980.
2. Smith AM and Picciano MF: Evidence for increased selenium requirement for the rat during pregnancy and lactation. J Nutr 116: 1068-1079, 1986.
3. Yang GQ, Chen JS, Wen ZM, Ge KY, Zhu LZ, Chen XC and Chen XS: The role of selenium in Keshan disease. Adv Nutr Res 6: 203-231, 1984.
4. van Rij AM, Thomson CD, McKenzie JM and Robinson MF: Selenium deficiency in total parenteral nutrition. Am J Clin Nutr 32: 2076-2085, 1979.
5. Schwarz K and Foltz CM: Selenium as an integral part of factor 3 against dietary necrotic liver degeneration. J Am Chem Soc 79: 3292-3293, 1957.
6. Reddy PG, Morill JL, Minocha HC and Stevenson JS: Vitamin E is immunostimulatory in calves. J Dairy Sci 70: 993-999, 1987.
7. Birringer M, Pilawa S and Flohé L: Trends in selenium biochemistry. Nat Prod Rep 19: 693-718, 2002.
8. Carlson BA, Novoselov SV, Kumaraswamy E, Lee BJ, Anver MR, Gladyshev VN and Hatfield DL: Specific excision of the selenocysteine tRNA[Ser]Sec (Trsp) gene in mouse liver demonstrates an essential role of selenoproteins in liver function. J Biol Chem 279: 8011-8017, 2004.
9. Berry MJ, Banu L, Chen YY, Mandel SJ, Kieffer JD, Harney JW and Larsen PR: Recognition of UGA as a selenocysteine codon in type I deiodinase requires sequences in the 3' untransalated region. Nature 353: 273-276, 1991.
10. Kryukov GV, Castellano S, Novoselov SV, Lobanov AV, Zehtab O, Guigó R and Gladyshev VN: Characterization of mammalian selenoproteomes. Science 300: 1439-1443, 2003.
11. Korotkov KV, Novoselov SV, Hatfield DL and Gladyshev VN: Mammalian selenoprotein in which selenocysteine (Sec) incorporation is supported by a new form of Sec insertion sequence element. Mol Cell Biol 22: 1402-1411, 2002.
12. Müller WE, Borejko A, Brandt D, *et al*: Selenium affects biosilica formation in the demosponge Suberites domuncula. Effect on gene expression and spicule formation. FEBS J 272: 3838-3852, 2005.
13. Hwang DY, Sin JS, Kim MS, *et al*: Overexpression of human selenoprotein M differentially regulates the concentrations of antioxidants and H_2O_2, the activity of antioxidant enzymes, and the composition of white blood cells in a transgenic rat. Int J Mol Med 21: 169-179, 2008.
14. Chen J and Berry MJ: Selenium and selenoproteins in the brain and brain diseases (Review). J Neurochem 86: 1-12, 2003.
15. Ramaekers VT, Calomme M, Vanden Berghe D and Makropoulos W: Selenium deficiency triggering intractable seizures. Neuropediatrics 25: 217-223, 1994.
16. Imam SZ, el-Yazal J, Newport GD, Itzhak Y, Cadet JL, Slikker W Jr and Ali SF: Methamphetamine-induced dopaminergic neurotoxicity: role of peroxynitrite and neuroprotective role of antioxidants and peroxynitrite decomposition catalysts. Ann NY Acad Sci 939: 366-380, 2001.
17. Zafar KS, Siddiqui A, Sayeed I, Ahmad M, Salim S and Islam F: Dose-dependent protective effect of selenium in rat model of Parkinson's disease: neurobehavioral and neurochemical evidences. J Neurochem 84: 438-446, 2003.
18. Takizawa S, Matsushima K, Shinohara Y, Ogawa S, Komatsu N, Utsunomiya H and Watanabe K: Immunohistochemical localization of glutathione peroxidase in infarcted human brain. J Neurol Sci 122: 66-73, 1994.
19. Saijoh K, Saito N, Lee MJ, Fujii M, Kobayashi T and Sumino K: Molecular cloning of cDNA encoding a bovine selenoprotein P-like protein containing 12 selenocysteines and a (His-Pro) rich domain insertion, and its regional expression. Brain Res Mol Brain Res 30: 301-311, 1995.
20. Kim IY, Shin JH and Seong JK: Mouse phenogenomics, toolbox for functional annotation of human genome. BMB Rep 43: 79-90, 2010.

Cell Reports
Report

Perturbation of NCOA6 Leads to Dilated Cardiomyopathy

Jae-il Roh,[1,2,13] Cheolho Cheong,[3,4,13] Young Hoon Sung,[1,2] Jeehyun Lee,[1,2] Jaewon Oh,[5] Beom Seob Lee,[6] Jong-Eun Lee,[7] Yong Song Gho,[8] Duk-Kyung Kim,[9] Chan Bae Park,[10] Ji Hyun Lee,[11] Jae Woon Lee,[12] Seok-Min Kang,[5,6,*] and Han-Woong Lee[1,2,*]

[1]Department of Biochemistry, College of Life Science and Biotechnology, Yonsei University, Seoul 120-749, South Korea
[2]Yonsei Laboratory Animal Research Center, Yonsei University, Seoul 120-749, South Korea
[3]Laboratory of Cellular Physiology and Immunology, Institut de Recherches Cliniques de Montréal, Montréal QC H2W 1R7, Canada
[4]Department of Microbiology, Infectiology and Immunology, Université de Montréal, Montreal QC H3T 1J4, Canada
[5]Cardiology Division, Severance Cardiovascular Hospital, Yonsei University College of Medicine, Seoul 120-752, South Korea
[6]Cardiovascular Research Institute, Yonsei University College of Medicine, Seoul 120-752, South Korea
[7]DNA Link, Inc., Songpa-Gu, Seoul 138-736, South Korea
[8]Department of Life Sciences, Pohang University of Science and Technology, Gyeongbuk 790-784, South Korea
[9]Cardiac and Vascular Center, Samsung Medical Center, Sungkyunkwan University School of Medicine, Suwon, Gyeonggi-do 440-746, South Korea
[10]Department of Physiology, Ajou University School of Medicine, Suwon 443-380, South Korea
[11]Department of Oral Biology, College of Dentistry, Yonsei University, Seoul 120-752, South Korea
[12]Department of Pediatrics, Oregon Health & Science University, Portland, OR 97239-3098, USA
[13]Co-first author
*Correspondence: smkang@yuhs.ac (S.-M.K.), hwl@yonsei.ac.kr (H.-W.L.)
http://dx.doi.org/10.1016/j.celrep.2014.07.027

SUMMARY

Dilated cardiomyopathy (DCM) is a progressive heart disease characterized by left ventricular dilation and contractile dysfunction. Although many candidate genes have been identified with mouse models, few of them have been shown to be associated with DCM in humans. Germline depletion of *Ncoa6*, a nuclear hormone receptor coactivator, leads to embryonic lethality and heart defects. However, it is unclear whether *Ncoa6* mutations cause heart diseases in adults. Here, we report that two independent mouse models of NCOA6 dysfunction develop severe DCM with impaired mitochondrial function and reduced activity of peroxisome proliferator-activated receptor δ (PPARδ), an NCOA6 target critical for normal heart function. Sequencing of NCOA6-coding regions revealed three independent nonsynonymous mutations present in 5 of 50 (10%) patients with idiopathic DCM (iDCM). These data suggest that malfunction of NCOA6 can cause DCM in humans.

INTRODUCTION

Dilated cardiomyopathy (DCM), characterized by cardiac enlargement and systolic dysfunction, is the most common form of cardiomyopathy, accounting for up to 30%–40% of all heart failure cases (Towbin and Bowles, 2002). Although DCM has diverse causes, approximately half of cases are idiopathic (iDCM). Clinical investigations have shown that approximately 40% of patients with iDCM exhibit the patterns of autosomal-dominant inheritance, implying that genes play an important role in DCM pathogenesis (Hershberger et al., 2010). Hence, the search for novel susceptibility loci is a major challenge in DCM research.

Nuclear receptor coactivator 6 (or NCOA6, also known as ASC-2, NRC, TRBP, PRIP, and RAP250) is ubiquitously expressed in diverse tissues including the heart and stimulates the transcriptional activity of various transcription factors and nuclear hormone receptors (NRs) by coordinating with cofactors (Mahajan and Samuels, 2008). NCOA6 possesses two LXXLL motifs required for interaction with NRs. The first LXXLL motif of NCOA6 can interact with almost all liganded NRs, whereas more restricted NRs can bind to the second LXXLL motif. In mice, germline mutation of *Ncoa6* induces growth retardation and developmental defects in the heart, liver, brain, and placenta, resulting in embryonic lethality between embryonic days 8.5 (E8.5) and 12.5 (Antonson et al., 2003; Kuang et al., 2002; Mahajan et al., 2004; Zhu et al., 2003). Overexpression of the dominant-negative version of the gene (*DN1*) incompletely suppresses endogenous NCOA6 activity, allowing mice to survive, but to develop several defects including cataract, atrial thrombosis, and hypertrophy at the later stage (Kim et al., 2002).

Peroxisome proliferator-activated receptors (PPARs) are the members of the NR superfamily that regulate fatty acid metabolism and mitochondrial function (Barger and Kelly, 2000; Wang et al., 2010). The transcriptional activity of *PPARs* is elevated or induced upon ligand binding and is regulated further by coactivators and corepressors (Guan et al., 2005; Viswakarma et al., 2010). PPARδ (also called PPARβ) is expressed at high levels in the heart and is essential for normal heart function (Cheng et al., 2004). In a mouse model, cardiomyocyte-specific

PPARδ knockout leads to DCM; however, whether an association between *PPARδ* polymorphisms and DCM exists in humans remains unknown.

RESULTS

Overexpression of *DN1* Causes DCM in Mice

Germline *Ncoa6* deficiency results in embryonic lethality with several developmental defects (Antonson et al., 2003; Kuang et al., 2002; Mahajan et al., 2004; Zhu et al., 2003). We produced transgenic (Tg) mouse lines overexpressing DN1 (849–929 residues containing an N-terminal LXXLL-1 motif of NCOA6, Figures S1A and S1B) that are able to reach adulthood, although these animals are prone to diverse defects (Kim et al., 2002). Among nine DN1-Tg lines, four founder mice (#71, #84, #87, and #104) expressed DN1 in their hearts (representative expression of DN1 is shown for founder #87 in Figure S1C). The progenies of founder #87 died prematurely at 20 weeks old (Figure S1D). Anatomical examination revealed cardiac enlargement and increased heart-to-body weight ratios with frequent pericardial effusion (Figures S1E–S1H). The progenies of founders #71, #84, and #104 exhibited similar phenotypes, which were absent in wild-type (WT) and mutant DN1-Tg mice in which the LXXLL-1 motif had been mutated to LXXAA (Kim et al., 2002). These phenotypes closely resembled those of DCM (Towbin and Bowles, 2002). Given that DN1 would be expected to compete with the binding of other coactivators for liganded NRs and multiorgan defects were found in DN1-Tg mice, it is unclear whether DN1 specifically blocks the activity of endogenous NCOA6 and causes DCM through cardiac cells only. For instance, we found multiple phenotypes such as fatty liver, thymic and spleen atrophy, lung hypoplasia, kidney hyperplasia, and brain defects in DN1-Tg mice (Kim et al., 2002).

Cardiomyocyte-Specific Ablation of NCOA6 Leads to DCM in Mice

To confirm the heart-specific function of NCOA6, we generated cardiomyocyte-specific *Ncoa6*-deficient (Δ/Δ) mice by employing floxed *Ncoa6* alleles (f/f) and a Cre recombinase transgene specific for differentiated cardiomyocytes under the control of the α-myosin heavy-chain promoter (*α-MHC-Cre*-Tg) (Agah et al., 1997; Zhu et al., 2003). Compared to control mice (f/f), NCOA6 mRNA and protein levels were significantly decreased in a heart-restrictive manner in Δ/Δ mice (Figures 1A and 1B). These mice demonstrated Mendelian inheritance and showed no significant cardiac developmental defects. Consistent with the phenotypes observed in DN1-Tg mice, Δ/Δ mice showed premature death, increased heart weight-to-body weight ratios, and cardiac dilatation (Figures 1C, 1D, and S2A–S2D). The increased heart weight was caused by atrial thrombi, whereas there was no alteration in the weight of the ventricle (Figure S2C). Histological examination of the hearts of Δ/Δ mice revealed common features of DCM, including enlarged ventricular cavities with thin walls and reactive myocardial fibrosis (Figures 1D, 1E, and S2D). Notably, *Ncoa6* heterozygous knockout mice (Δ/+) also exhibited the characteristics of DCM with late onset (Figures S2E–S2I), indicating that *Ncoa6* haploinsufficiency is sufficient to precipitate DCM in mice. Consistent with the previous reports by Agah et al. (1997) and Cheng et al. (2004), we could not find any significant differences of cardiac functions in *α-MHC-Cre*-Tg mice, compared to the f/f mice (data not shown). These results demonstrate that loss or insufficiency of NCOA6 function directly causes DCM.

Comparative transthoracic echocardiographic analysis revealed severe dilatation of the left ventricle (LV) and decreased contractility without a significant alteration in heart rate in Δ/Δ mice at 4 months of age (Figure 1F). Left ventricular end-systolic dimensions (LVESDs) and end-diastolic dimensions were enlarged 1.72- and 2.35-fold, respectively, compared to control mice (Figure 1G). Ejection fraction (EF) and fractional shortening, two direct measures of cardiac contractile function, were profoundly diminished compared to control mice (Figures 1H and S2J). Impaired cardiac function was also evident in Δ/+ and DN1-Tg mice (Figures S1I–S2L). Increased expression of cardiac hypertrophy markers, including atrial natriuretic peptide (*Anp*) and α- to *β-MHC* isoform switching (Reiser et al., 2001), were found in 12- and 20-week-old, but not 4-week-old, Δ/Δ mice (Figures S2M–S2O). Furthermore, the hearts of 12-week-old mice displayed hypertrophic phenotype (Figure S2P), suggesting that concentric hypertrophy transiently proceeds prior to the onset of DCM phenotype. Thus, *Ncoa6* defects progressively compromise overall cardiac function in mice.

Impaired Cardiac Ultrastructure and Mitochondrial Function in *NCOA6*-Deficient Mice

To examine potential mechanisms in the development of DCM, ultrastructural examination of cardiac tissues with transmission electron microscopy (TEM) was conducted and showed disarray of sarcomeres and mitochondria in the hearts of Δ/Δ mice (Figure 2A). The number of mitochondria was significantly decreased in the hearts of Δ/Δ mice (Figure 2B). In addition, reduced mitochondrial content was confirmed by measuring DNA, RNA, and respiratory chain protein levels, and impaired activity of mitochondrial complex II was evident in Δ/Δ and Δ/+ mice (Figures 2C–2F). These results suggest that NCOA6 is essential for the maintenance of normal mitochondrial function in cardiomyocytes.

NCOA6 Deficiency Impairs PPARδ Activity in Cardiomyocytes

Because PPARδ, one of the major targets of NCOA6, is crucial for mitochondrial biogenesis and cardiomyocyte-specific knockout of *Pparδ* causes spontaneous DCM in mice (Cheng et al., 2004; Wang et al., 2010), we hypothesized that depletion of NCOA6 alters PPARδ activity. To further explore the role of NCOA6 in PPARδ-mediated transactivation, we measured transcript levels of PPARδ targets in the mouse heart. Levels of key molecules involved in fatty acid oxidation (Cheng et al., 2004), such as *muscle-type carnitine palmitoyltransferase-1* (*Mcpt-1*), *Cd36*, *Fatp1*, *pyruvate dehydrogenase lipoamide kinase, isozyme 4* (*Pdk4*), and *uncoupling protein 3* (*Ucp3*), were considerably decreased even though no significant difference in *Pparδ* transcript levels was observed between Δ/Δ and f/f hearts (Figures 3A–3C). Similar to cardiomyocyte-specific knockout of *Pparδ* (Cheng et al., 2004), Δ/Δ mouse showed cardiac lipid accumulation (Figure S3A). Collectively, these data suggest

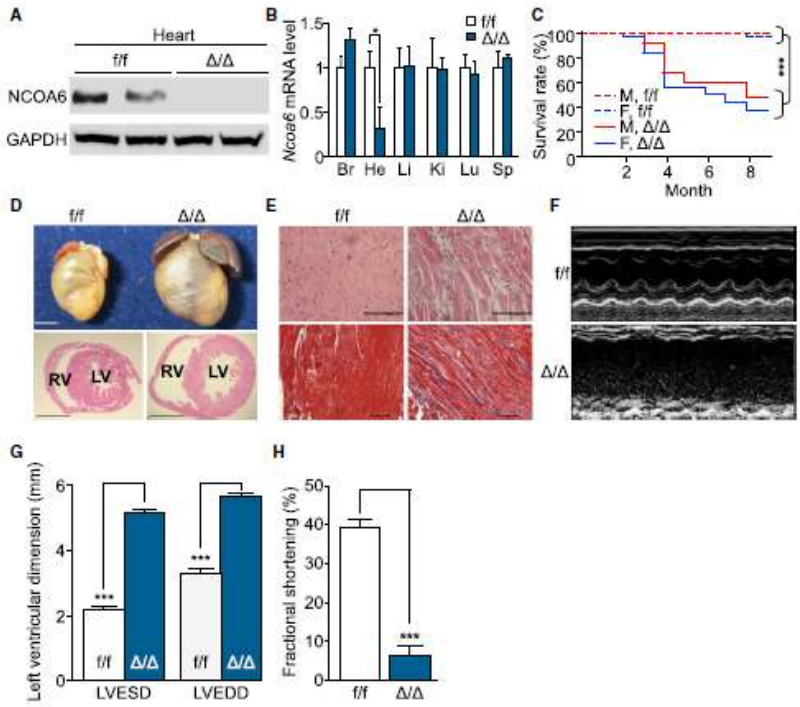

Figure 1. Premature Death and Impaired Cardiac Function in Cardiomyocyte-Specific *Ncoa6* Knockout Mice

(A) Western blot analysis of NCOA6 in the hearts of 1-month-old f/f and Δ/Δ male mice. Glyceraldehyde 3-phosphate dehydrogenase (GAPDH) was used as a loading control.

(B) Real-time quantitative PCR analysis of *Ncoa6* mRNA in various organs of 1-month-old f/f and Δ/Δ male mice. Br, brain; He, heart; Li, liver; Ki, kidney; Lu, lung; Sp, spleen. *Ncoa6* mRNA levels were normalized to those of *Gapdh*. Graphs show mean ± SD. $^{*}p < 0.05$.

(C) Kaplan-Meier survival curves of f/f (male, n = 34; female, n = 34) and Δ/Δ (male, n = 21; female, n = 39) mice. Genders and genotypes are labeled inside the plot. M, male; F, female. $^{***}p < 0.001$.

(D) Gross morphology (top) and histological examinations (bottom; hematoxylin and eosin staining [H&E]) of hearts from 4-month-old female f/f and Δ/Δ mice. RV, right ventricle. Scale bars, 2.5 mm.

(E) H&E (top) and Masson's trichrome staining (bottom) of LVs from 4-month-old female mice. Scale bars, 100 μm.

(F–H) Representative profiles of M-mode echocardiographic analyses (F) and quantitative representations of LVESD and left ventricular end-diastolic dimension (LVEDD) (G) and percent fractional shortening (H) of f/f (male, n = 3; female, n = 4) and Δ/Δ (male, n = 3; female, n = 3) mice. Graphs show mean ± SD. $^{**}p < 0.001$. See also Figures S1 and S2.

that *NCOA6* deficiency results in dysfunctional activity of PPARδ and fatty acid metabolism. Interestingly, increased expressions of estrogen receptor alpha (ERα) and its target genes were found in the Δ/Δ mouse hearts (Figures S3B–S3D).

We also found that Cre-mediated *Ncoa6* deficiency attenuated the induction of PPARδ targets by the selective PPARδ agonist GW501516 (GW) in neonatal primary cardiomyocytes (Figures 3D–3G). In addition, in the AC16 human cardiomyocyte cell line, small hairpin RNA (shRNA)-mediated NCOA6 knockdown (Figures 3H and 3I) reduced GW-induced activation of PPARδ and its target genes (Figures 3J–3M), indicating that PPARδ requires NCOA6 for optimal transactivation of its target genes.

Nonsynonymous Mutations of *NCOA6* in Patients with iDCM

To find the relevance of NCOA6-mediated DCM pathogenesis to human iDCM, we screened the entire *NCOA6*-coding sequence in patients with iDCM and identified four nonsynonymous substitutions in 8 out of 50 patients with iDCM (c.1038C > G, P239R;

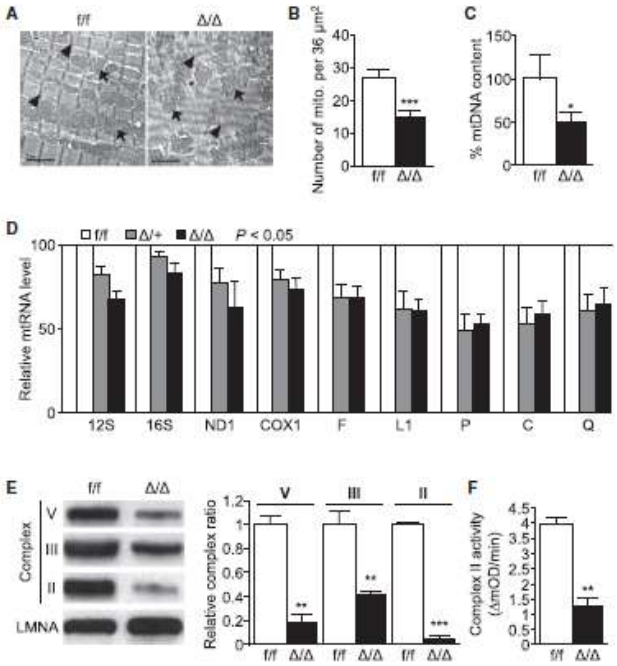

Figure 2. Cardiomyocyte-Specific *Ncoa6* Deficiency Impairs Cardiac Ultrastructures and Mitochondrial Function in Mice

(A) TEM analysis of LVs from 3-month-old f/f and Δ/Δ female mice. Scale bars, 2 μm. Arrowheads point to Z discs; arrows point to mitochondria.

(B and C) Quantification of the number of mitochondria (mito.) per 36 μm^2 calculated from three independent TEM images (B) and mtDNA contents (C) by Southern blot analyses in the hearts of 3-month-old male and female mouse ventricles ($n = 3$ for each genotype). Graphs show mean ± SD. $^*p < 0.05$; $^{***}p < 0.001$.

(D) Analyses of mitochondrial rRNAs (12S and 16S), mRNAs (*ND1* and *COX1*), and tRNAs (F, L1, P, C, and Q) by northern blot. $p < 0.05$ for all mitochondrial RNAs (mtRNAs). LVs of 3- to 5-month-old male and female mice ($n = 3$ for each genotype) were used.

(E) Analysis of mitochondrial respiratory chain complexes II, III, and V by western blot (left) and its quantitative ratios (right) of each complex to lamin A (LMNA). LVs of 3- to 5-month-old male and female mice ($n = 3$ for each genotype) were used. LMNA was used as a loading control. Graphs show mean ± SD. $^{**}p < 0.01$; $^{**}p < 0.001$.

(F) Analysis of mitochondrial complex II activity in 2- to 3-month-old mice (male, $n = 3$; female, $n = 4$ for each genotype). mOD, mitochondrial optical density. Graphs show mean ± SD. $^*p < 0.01$.

c.2430G > A, G703E; c.2618A > T, M766L; and c.3848A > G, T1176A). P239R was found in both patients without DCM and patients with iDCM, indicating that this is not a DCM-causing mutation. Rather, it appears to be a SNP that is specific to the Korean population. This SNP is not found among American populations (Table S1) (Fu et al., 2013). G703E and M766L mutations were found in one patient each, and three patients were harboring the T1176A mutation (total 10%; Table S1). These 3 mutations were absent in 403 Korean healthy subjects, and only 1 subject showed T1176A mutation among the 6,502 American populations (Figures 4A and 4B; Table S1) (Fu et al., 2013), suggesting that 3 variants are potent DCM-related mutations in humans. G703E and T1176A were located in regions of the *NCOA6* gene that are highly conserved across species (Figure 4C), whereas *Macaca mulatta* encodes leucine rather than methionine at human M766 position, suggesting that M766L substitution might not be harmful. All five patients possessed one WT allele.

The effects of each *NCOA6* mutation on the protein conformation were estimated with the protein structure-prediction software (Buchan et al., 2010; Cheng et al., 2005). The G703E substitution appeared to induce remarkable structural deformations by transforming coiled-coil and β sheet structures into an α helix (Figure S4A). Furthermore, in silico evaluation with PolyPhen-2 and SIFT software showed a potentially deleterious effect of G703E on NCOA6 function: PolyPhen score of 0.999; SIFT score of 0.006 (Adzhubei et al., 2010; Ng and Henikoff, 2003). Although M766L and T1176A substitutions were predicted to induce no structural change and be benign (PolyPhen-2 score of 0 in both, and SIFT score of 0.039 and 0.289 in M766L and T1176A, respectively), we could not exclude the possibility that M766L and T1176A substitutions are also deleterious for NCOA6 functions. T1176A transcript level was similar to those of the *NCOA6* WT and its other mutants, but its protein level was significantly low (Figures S4B and S4C), though its mechanism is inconclusive.

Because depletion of *Ncoa6* leads to decreased transcriptional activity of PPARδ in mice, we examined whether NCOA6 variants alter the activity PPARδ. In fact, overexpression of G703E and T1176A significantly suppressed the activation of a PPARδ and its targets including *CD36* and *FATP1* in the AC16 parental and *NCOA6* knockdown cells upon the treatment with GW (Figures 4D–4F and S4D). However, no remarkable difference was observed between WT and M766L mutant NCOA6, implying that M766L may not be a pathogenic mutation for DCM, though further investigation is required to clarify its physiological effect. Altogether, these data suggest that two substitutions (G703E and T1176A, if M766L is not) perturb NCOA6-PPAR signaling via distinct mechanisms: G703E causes structural and functional defects, whereas T1176A reduces the expression of PPARδ targets possibly by destabilizing NCOA6 proteins.

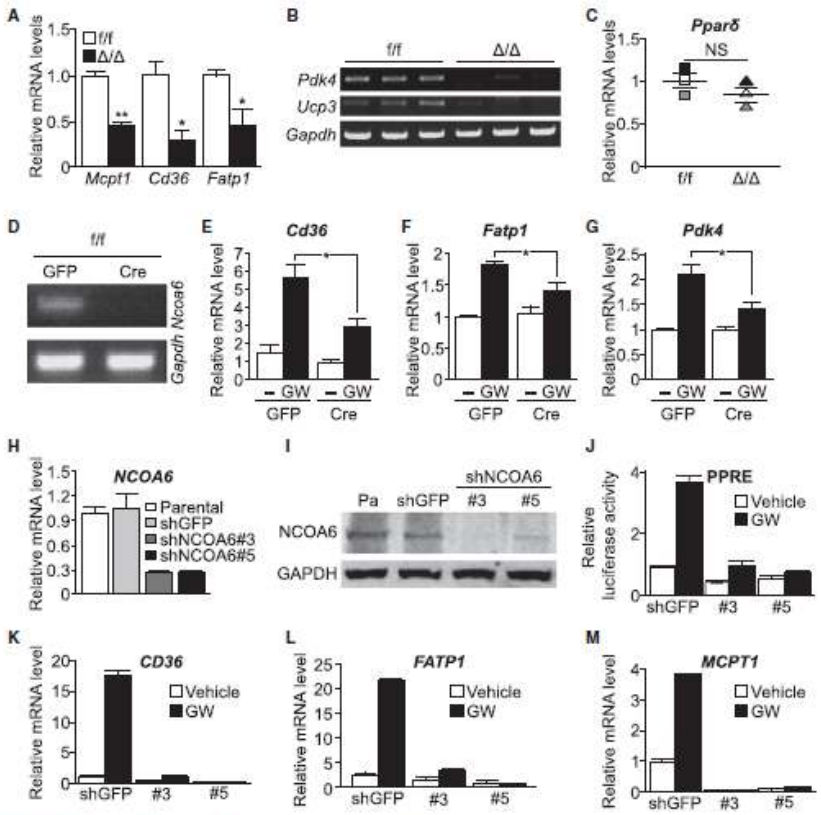

Figure 3. NCOA6 Is Required for Normal Transcriptional Activity of PPARδ

(A and B) Transcript levels of PPARδ targets in the LVs of f/f (white; male, n = 1; female, n = 2) and Δ/Δ (black; male, n = 1; female, n = 2) mice. Graphs show mean ± SD. *$p < 0.05$; **$p < 0.01$.

(C) mRNA levels of *PPARδ* in the hearts of f/f and Δ/Δ mice (n = 3 per each genotype). *Gapdh* was used as a loading control. NS, not statistically significant.

(D) Semiquantitative PCR analyses of *Ncoa6* in primary cardiomyocytes, transduced with lentivirus encoding GFP or Cre constructs, isolated from the f/f mouse heart.

(E–G) Transcript levels of *Cd36* (E), *Fatp1* (F), and *Pdk4* (G) in f/f primary cardiomyocytes containing GFP or Cre constructs. Treatment with GW lasted 48 hr. Graphs show mean ± SD. *$p < 0.05$.

(H–M) Transcript and protein levels of NCOA6 were examined by real-time quantitative PCR (H) and western blot (I). Parental (Pa), no transfection; shGFP, shRNA against *GFP*; shNCOA6 #3 and #5, independent shRNA constructs against *NCOA6*. (J) Relative PPAR response element (PPRE)-luciferase activity. Treatment with GW lasted 24 hr. (K–M) Transcript levels of *CD36* (K), *FATP1* (L), and *MCPT-1* (M) were measured by real-time quantitative PCR analyses after treatment with GW for 48 hr. Graphs show mean ± SD.

See also Figure S3.

DISCUSSION

Ncoa6 deficiency reduces the number of mitochondria in cardiac tissue. Cardiac abnormality of mitochondrial function is closely associated with DCM pathogenesis (Marin-Garcia et al., 1995). In addition, impaired expression of *Ncoa6* has been found in muscle fibers with a dysfunctional electron transport system (Herbst et al., 2013). Thus, *Ncoa6* mutations appear to induce a loss of or suppress biogenesis of mitochondria in the heart. NCOA6 is a critical component of the steady-state

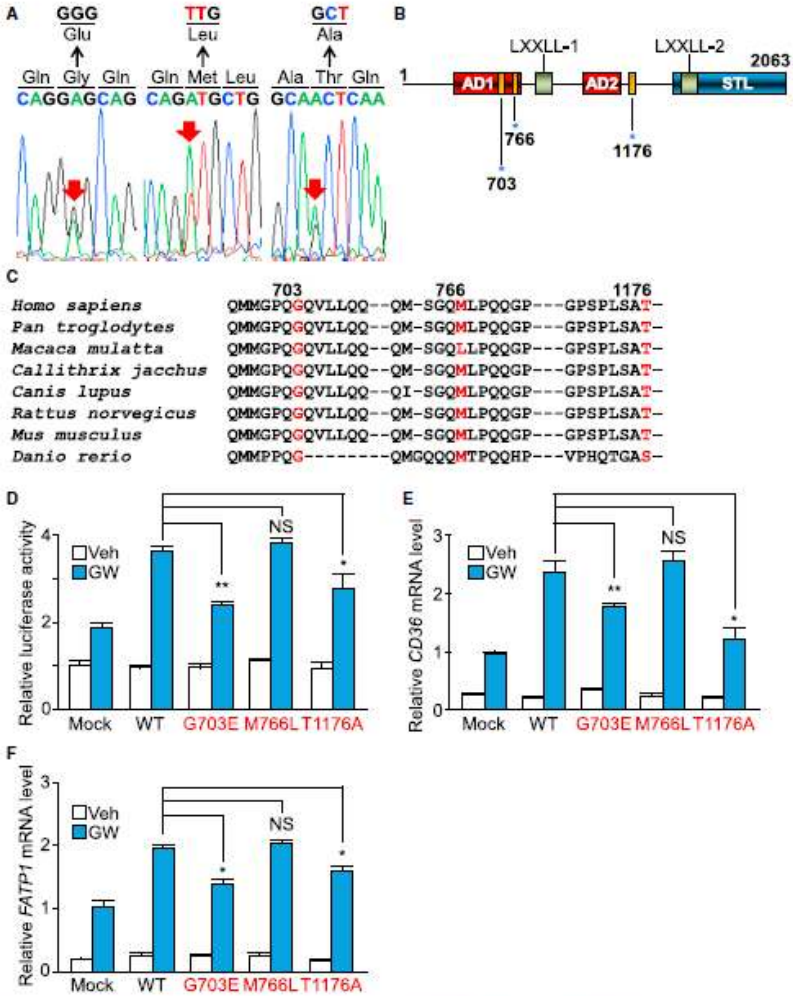

Figure 4. Nonsynonymous Mutations of *NCOA6* in Human Patients with iDCM Result in Impaired PPARδ Activity

(A) DNA sequences of *NCOA6* exons that were obtained from patients with IDCM. Red arrows indicate mutation sites. Glu, glutamate; Leu, leucine; Ala, alanine; Gln, glutamine; Gly, glycine; Met, methionine; Thr, threonine.

(B) Schematic representation of the human NCOA6 protein. AD, activation domain; STL, serine, threonine, and leucine-rich region. Blue asterisks indicate mutation sites.

(C) NCOA6 amino acid sequence alignment across eight species. Numerals indicate the positions of the amino acid mutations (red) in patients.

(D–F) Relative luciferase activity of PPRE (D) and gene expression levels of *CD36* (E) and *FATP1* (F) in WT and mutant *NCOA6*-transfected AC16 cells with or without treatment with GW for 48 hr. Graphs show the mean of triplicate experiments ± SD. NS, not statistically significant; Veh, vehicle. $^{*}p < 0.05$; $^{**}p < 0.01$.

See also Figure S4 and Table S1.

ASC-2 complex (ASCOM), which is essential for proper NR transactivation (Mahajan and Samuels, 2008). Because NCOA6 stimulates NR transactivation activity, it is reasonable to expect altered downstream signaling of NRs to play a role in the mechanism for DCM. Here, we provide the potent evidence linking abnormal NR signaling to human DCM pathogenesis. Consistent with previous studies reviewed by Mahajan and Samuels (2008), our results indicate that depletion of *NCOA6* expression results in remarkably reduced PPARδ activity both in vitro and in vivo.

Germline loss of *Ncoa6* leads to embryonic lethality with multiple organ dysfunction including the placenta (Antonson et al., 2003; Kuang et al., 2002; Zhu et al., 2003). The homozygous null mutation of *Ncoa6* precipitates cardiac developmental abnormalities at E10.5, suggesting that NCOA6 might still be essential for early cardiac development before this stage (Kuang et al., 2002). Because α-MHC-Cre starts to function at E14.5, α-MHC-Cre-mediated depletion of *Ncoa6* might not be sufficient to cause early cardiac developmental defects.

It appears that *NCOA6* mutations may disrupt diverse NR transactivation via an effect on ASCOM. In fact, another observation suggests that NR pathways other than PPARδ may be affected by *NCOA6* mutations (Mahajan and Samuels, 2008). Our findings imply that additional NRs might be influenced by NCOA6 impairment. In support of these findings, it has been shown that mutations in mixed-lineage leukemia (MLL) 2/4 and tryptophan (W)-aspartic acid (D) repeat domain (WDR) 5, which are also components of ASCOM, are likely to be involved in congenital heart disease (Zaidi et al., 2013). This evidence indicates that *Ncoa6* deficiency significantly alters the activity of the NRs, resulting in DCM.

A recent study in mice revealed that NCOA6 promotes ubiquitination-mediated degradation of ERα, whereas *Ncoa6* deficiency causes ERα accumulation in uterine stromal cells during the preimplantation period (Kawagoe et al., 2012). Consistent with these findings, we observed that the expression of ERα and its target genes was significantly increased in *Ncoa6* Δ/Δ mice prior to DCM pathogenesis. Interestingly, it is common for ERα expression to increase in patients with end-stage DCM (Mahmoodzadeh et al., 2006). Based on these lines of evidence, we hypothesized that the expression and/or function of *NCOA6* may be suppressed prior to the onset of clinical DCM manifestations, possibly accelerating the progression of the disease. Taken together, our findings will manifest stepping forward to a more accurate diagnosis of human DCM.

EXPERIMENTAL PROCEDURES

Animals

All animal experiments were performed in accordance with Korean Food and Drug Administration guidelines. Protocols were reviewed and approved by the Institutional Animal Care and Use Committee of the Yonsei University (YLARC 2008-0014). Mice that had been backcrossed to the FVB/NTac strain for at least nine generations were used and maintained in the specific pathogen-free facility of the Yonsei Laboratory Animal Research Center.

Primary Cardiomyocyte Culture

Primary cardiomyocytes were isolated as previously described by Crone et al. (2002).

Human Genomic DNA Mutation Analysis

Each subject was provided with written informed consent to participate in the study according to the guidelines of the institutional review board (4-2007-0234). Exon scanning of all *NCOA6* (NM_014071)-coding regions and splice junction sites was performed by direct sequencing.

Echocardiogram

Echocardiography was performed with the echocardiographic system (Vivid 7; GE Medical Systems) equipped with a 12 MHz transducer. Mice with shaved chests were anesthetized with isoflurane (Hana Pharmaceutical) and placed on a platform. End-systolic and end-diastolic dimensions were measured using M-mode echocardiogram imaging that was obtained at the papillary muscle level for the measurement of LV wall thickness and LV dimensions. We captured these images over more than ten cardiac cycles, and the data shown are averages from at least three cardiac cycles per image acquisition. These procedures were performed at least three times, and average values were determined for each mouse.

Statistical Analyses

Statistical significance was determined using the two-tailed Student's t test. Data were analyzed with GraphPad Prism (GraphPad Software). p values less than 0.05 were considered statistically significant.

SUPPLEMENTAL INFORMATION

Supplemental Information includes Supplemental Experimental Procedures, four figures, and one table and can be found with this article online at http://dx.doi.org/10.1016/j.celrep.2014.07.027.

AUTHOR CONTRIBUTIONS

J.-I.R., C.C., and J.L. performed in vitro and in vivo experiments; J.O., D.-K.K., B.S.L., and S.-M.K. performed cardiac phenotyping; C.B.P. performed mitochondria-related experiments; J.-E.L. and J.H.L. analyzed human mutations; Y.S.G. performed TEM analysis; J.-I.R., C.C., Y.H.S., J.W.L., and H.-W.L. wrote the manuscript. H.-W.L. designed and supervised the project.

ACKNOWLEDGMENTS

This work was supported by the National Research Foundation (NRF) funded by the Ministry of Education, Science and Technology of the Korean government (2009-0081177, 2010-0020878, and 2012R1A1A2009607); the Bio-Industry Technology Development Program, MAFRA (311054232-HD1102), Korea; a Korean Healthcare Technology R&D Project from the Ministry of Health and Welfare (A085136); a grant (14182MFDS978) from the Korean Ministry of Food and Drug Safety in 2014; by the Canadian Institutes of Health Research (CIHR; MOP-125933); and the Canada and NRF of Korea (GRN-2013S1A2A2035348). C.C. is a Chercheur-Boursier Junior of Fonds de recherché du Québec-Santé and CIHR New Investigator awardee, and J.W.L. is supported by the NIH (DK064678).

Received: February 3, 2014
Revised: May 31, 2014
Accepted: July 15, 2014
Published: August 14, 2014

REFERENCES

Adzhubei, I.A., Schmidt, S., Peshkin, L., Ramensky, V.E., Gerasimova, A., Bork, P., Kondrashov, A.S., and Sunyaev, S.R. (2010). A method and server for predicting damaging missense mutations. Nat. Methods *7*, 248–249.

Agah, R., Frenkel, P.A., French, B.A., Michael, L.H., Overbeek, P.A., and Schneider, M.D. (1997). Gene recombination in postmitotic cells. Targeted expression of Cre recombinase provokes cardiac-restricted, site-specific rearrangement in adult ventricular muscle in vivo. J. Clin. Invest. *100*, 169–179.

Lab Anim Res 2014: 30(2), 45-53
http://dx.doi.org/10.5625/lar.2014.30.2.45

Laboratory Animal Research
http://submission.kalas.or.kr

Proteomic analysis of domestic pig pancreas during development using two-dimensional electrophoresis and matrix-assisted laser desorption/ionization-time of flight mass spectrometry

Ji Ye Ahn[1], Il Yong Kim[1], Sae Jin Oh[1], Hye Sook Hwang[1], Sun Shin Yi[2], Yo Na Kim[1], Jae Hoon Shin[1], Yeo Sung Yoon[1], Je Kyung Seong[1]*

[1]Laboratory of Developmental Biology and Genetics, College of Veterinary Medicine, BK21Plus Program for Creative Veterinary Science Research, BIO-MAX institute, Seoul National University, Seoul, Korea
[2]Department of Biomedical Laboratory Science, College of Biomedical Science, Soonchunhyang University, Asan, Korea

Pig pancreas may be a therapeutic resource for human diabetic patients. However, this potential is hindered by a lack of knowledge of the molecular events of pig pancreas development. In this study, the embryonic day 60, neonate and 6-month protein profiles of pig pancreas were ascertained at using two-dimensional gel electrophoresis and matrix assisted laser desorption/ionization-time of flight mass spectrometry. Twenty four proteins were differentially expressed during pig pancreas development. Among them, 12 spots increased and 7 spots decreased according to development. The expression of 5 protein were highest at birth. Expression of digestive enzymes including trypsin, pancreatic triacylglycerol lipase and pancreatic alpha-amylase was elevated in adults, whereas chymotrypsins were highly expressed in neonates. Proteins that were abundantly expressed during gestation were alpha-1-antitrypsin, alpha-fetoprotein and transferrins. Taken together, we found out that several proteins were significantly up- or down- regulated from pig pancreas based on developmental stage. This study will provide basis for understanding development of pig pancreas.

Keywords: Domestic pig, pancreas, development, 2-DE proteomics, MALDI-TOF

Received 20 February 2014; Revised version received 19 March 2014; Accepted 26 March 2014

The pancreas is a complex gland having both exocrine and endocrine activities. The exocrine pancreas in the mature animal synthesizes and stores digestive enzymes to release after ingestion of a meal that induces neural and hormonal stimulation [1]. The endocrine pancreas contains five major cell types, which produce insulin (B cells), glucagon (A cells), somatostatin (D cells), pancreatic polypeptide (PP cells) and ghrelin, which is a novel growth hormone-releasing peptide (ghrelin cells). B cells may also express islet amyloid polypeptide (IAPP), another member of the insulin family of proteins, insulin-like growth factor-II (IGF-II) and pituitary adenylate cyclase activating polypeptide (PACAP) [2].

The pancreas releases these various enzymes and hormones to digest foods and maintain glucose homeostasis. If pancreas is damaged, the aftermath can be serious. Two examples are diabetes mellitus and pancreatic adenocarcinoma. Diabetes mellitus is a chronic metabolic disorder resulting from defects in insulin secretion or function. The global prevalence of diabetes was estimated as 2.8% in 2000 and is predicted to grow to 4.4% by 2030. The total number of diabetics is projected to rise from 171 million in 2000 to 366 million in 2030 due to population growth, aging, urbanization and increasing prevalence of obesity and physical inactivity [3]. Pancreatic adenocarcinoma is the

*Corresponding author: Je Kyung Seong, Laboratory of Developmental Biology and Genetics, College of Veterinary Medicine, BK21Plus Program for Creative Veterinary Science Research, BIO-MAX institute, Seoul National University, Seoul 151-742, Korea
Tel: +82-2-883-8395; Fax: +82-2-875-8395; E-mail: snumouse@snu.ac.kr

fourth leading cause of cancer deaths in the United States and its prognosis is usually dismal [1].

Preventive and effective treatments of pancreas-related diseases including diabetes mellitus, pancreatitis and pancreatic cancer require knowledge of the biology and molecular characteristics of the pancreas. Better understanding of pancreatic development and regeneration will provide valuable information about the identification of molecular markers involved in the pathogenesis of pancreatic cancer. As well, marker identification can be useful for islet cell transplantation, which is being explored as a treatment for diabetes.

Few proteomic studies have been done using human pancreatic tissues to elucidate the mechanisms of diabetes mellitus and pancreatic cancers because of difficulty in preparing human samples [4-7]. Instead, *in vivo* experiments have mainly used animal models. Several studies have contributed to the understanding of the molecular network governing developing pancreas in mouse and rat models [8,9].

The pig has become an attractive subject of study because of its potential use for xenotransplantation [10]. Nonhuman primate, such as apes and monkeys, more closely resemble humans anatomically and physiologically than do pigs. Nonetheless, xenotransplantation using nonhuman primates as xenograft donors is unlikely primarily because of the infectious risks to human patients and their contacts. Pigs produce large litters (up to 10 littermates), have a short gestation time (4 months), are somewhat similar to humans anatomically and physiologically, are available in large numbers (an estimated 90 million pigs are raised for human consumption yearly in the United States) and have a long history of providing medicinal products (skin, insulin, cardiac prostheses, clotting factors) for humans. For these reasons, the pig has become the most likely candidate for consideration as an organ donor [11-14]. Hindering this potential, the development of pig pancreas is not well understood.

In this study we investigated changes in the proteomic profile during pig pancreas development in embryonic day 60 (E60), neonatal and 6-month-old pigs using two-dimensional gel electrophoresis (2-DE) and matrix-assisted laser desorption/ionization-time of flight mass spectrometry (MALDI-TOF MS).

Materials and Methods

Pancreas protein extraction

Pancreas of E60 (n=4), neonate (n=3), 6-month-old male pigs (n=3) were removed immediately after sacrifice and stored in liquid nitrogen until used. Frozen pancreas tissues were homogenized in 400 µl lysis buffer (7 M urea, 2 M thiourea, 2% w/v CHAPS, 2% Pharmalyte pH3-10, 100 mM DTE). After centrifugation (50,000 rpm at 4℃ for 1 h) the supernatant was extracted and complete protease inhibitor cocktail (Roche Applied Science, Basel, Germany), DNase I (2.5 mg/mL; Roche Applied Science) and RNase (2.5 mg/mL; Roche Applied Science) were added. The protein concentration was measured by spectrophotometry using Bio-Rad Protein Assay (Bio-Rad Laboratories, Hercules, CA, USA) based on the Bradford method. Because urea, thiourea, CHAPS and other constituents of the sample/lysis buffer can interfere with the protein estimation, the standard curve was generated using bovine serum albumin (BSA) at concentrations of 0, 2, 5, 7 and 10 mg/mL. In this process, pancreas sample was made from a pool of each of the 3~4 animals in each group, and each pooled sample was run 3 times.

2-DE

2-DE was performed as previously described [15]. One milligram quantities of protein were diluted in the sample buffer with 2% IPG buffer up to 450 µL. Samples were added to pH 3-10, nonlinear, 24 cm IPG strips (Amersham Pharmacia Biotech, Piscataway, NJ, USA) and covered with mineral oil. After rehydration for 16 h at 20℃, isoelectric focusing was carried out in eight steps under step-n-hold mode as follows: (S1) 30 V, 2 h; (S2) 100 V, 2 h; (S3) 200 V, 1 h; (S4) 500 V, 1 h; (S5) 1,000 V, 1 h; (S6) gradient, 8,000 V, 1 h; (S7) gradient, 100,000 V, 1 h and (S8) 20,000 VHrs. The total voltage applied was 129,960 Vh (IPGphore Isoelectric Focusing Unit: Amersham Pharmacia Biotech). The IPG strips were equilibrated in buffer containing 6 M urea, 20% glycerol, 1.5 M Tris-HCl, pH 8.8, 2.5% acrylamide and Tributyl phosphine (Fluka, Buchs SG, Switzerland). After equilibration, SDS-PAGE was performed by 8-18% gradient gel without stacking gel via the Ettan Dalt system (Amersham Pharmacia Biotech). 2-DE was carried

out overnight at 4 W per gel at 20°C. After finishing 2-DE, the proteins on gels were fixed with protein fixing solution (40% methanol, 5% phosphoric acid) for 2 h and then stained using Coomassie G-250 (Bio-Rad) for 3 h. To remove extra dye in gels, the gels were washed with distilled water.

Protein visualization and image analysis

The stained gels were scanned using a GS-800 calibrated densitometer (Bio-Rad) and spot analysis was performed with the ImageMaster™ 2D platinum software version 5.0 (Amersham Pharmacia Biotech). The digitalized 2-DE gel images were compared by matching using Image master 5.0 (Amersham Biosciences, Piscataway, NJ, USA).

In-gel digestion and protein identification by MALDI-TOF MS

Spots of interest on the 2-DE gel were excised, cut into small pieces and digested with 12.5 ng/μL trypsin (Promega, Madison, WI, USA) in 50 mM ammonium bicarbonate (pH 8.0), as previously described [16]. The preparation procedures for MALDI-TOF MS used reversed-phase columns as previously described [17]. The tryptic peptides were passed through a POROS 50 R2 column (Applied Biosystems, Forster City, CA, USA). After washing the column with 70% acetonitrile in 5% formic acid, 100% acetonitrile and 5% formic acid, peptides were loaded into column and washed with 5% formic acid. The peptides were eluted with 10 mg/mL a-cyano-4-hydroxy-cinnamic acid (Sigma-Aldrich, St. Louis, MO, USA) containing solution and elutes were dropped on a MALDI sample plate [18]. Mass analyses were performed using a Voyger-DE PRO MALDI-TOF MS apparatus (Applied Biosystems, Franklin Lakes, NJ, USA), equipped with a 337 nm nitrogen laser. This machine was operated at an accelerating voltage of 20 K, positive ion reflection mode, voltage grid of 74.5%, guide wire voltage of 0% and a delay time of 110 ns. The spectra were externally calibrated using a standard peptide mixture containing angiotensin I, 1,296.68 [M+H]; Glu-Hibrinopeptide B, 1,570.67 [M+H]; ACTH (clip18-39), 2,465.19[M+H]). The proteins were identified by Swiss-Prot and MSDB protein database using MS-FIT (Protein Prospector; UCSF, San Francisco, CA, USA). All the cases of search were analyzed with a 100 ppm mass tolerance and 1 miss cleavage.

Results

Protein identification and analysis during pancreas developmental stages

To analyze the changes in the proteome profile during pig pancreas development, the pancreas of E60, neonate, and 6 month-old pigs were used. Pancreatic tissue was processed for 2-D electrophoresis to isolate the candidate proteins that were differentially expressed during development. The change of protein expression was

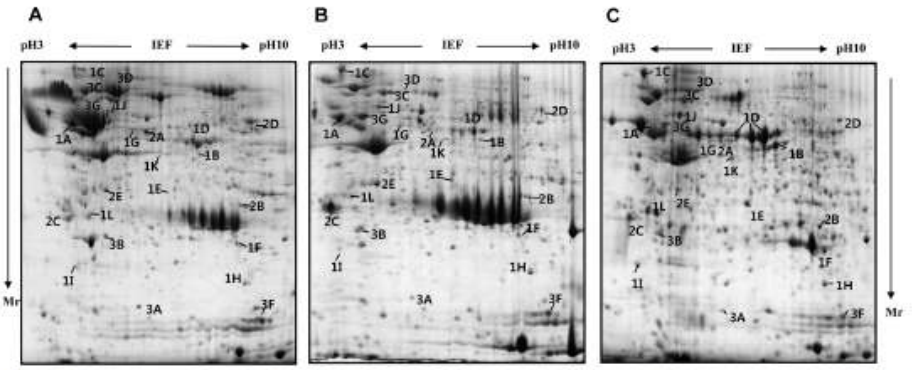

Figure 1. Representative Coomassie blue stained 2-DE gels of pig pancreas based on developmental stages. The proteins (1 mg) were separated on a 24 cm, pH 3-10 nonlinear strip, followed by an 8-18% gradient SDS-PAGE. Proteins were detected by Coomassie blue staining on the 2-DE images of the master gel. The proteins identified are designated with their accession numbers. (A) E60, (B) neonate, (C) adult pig pancreas. The symbol at (C) indicates development group number (1, 2 and 3) and alphabet order in Table 1. Mr indicates molecular weight of proteins.

Table 1. Proteins identified by MALDI-TOF MS and classified into three groups depending on the expression pattern during pig pancreas development

No.	Proteins identified	Expression Pattern*	Accession no.	Coverage %	Mr/pI	Species	Score
1. Up-regulated proteins in adult							
A	Protein disulfide-isomerase precursor		P07237	17%	57081/ 4.76	HUMAN	69
B	Glycine amidinotransferase		P50441	25%	44160/ 6.17	PIG	89
C	Endoplasmin precursor		Q29092	27%	92413/4.75	PIG	166
D	Pancreatic alpha-amylase precursor		P00690	21%	57050/6.51	PIG	106
E	MHC class II antigen		Q8MHP1	17%	30569/ 6.31	BOVINE	33
F	Trypsin precursor		P00761		24.409	HUMAN	40
G	Pancreatic triacylglycerol lipase		P00591	16%	50053/5.73	PIG	42
H	Phosphatidylethanolamine-binding protein		Q5R4R0	32%	20955/8.18	PONPY	43
I	Translationally-controlled tumor protein		P61288	33%	19583/4.84	PIG	106
J	60 kDa heat shock protein		P10809	18%	61016/5.70	HUMAN	88
K	Hypothetical protein FLJ39175		Q8N8N1	26%	30977/5.69	HUMAN	49
L	Laminin receptor		Q4GWZ2	27%	32907/4.80	PIG	81
2. Up-regulated proteins in neonate							
A	keratin, 53K type II cytoskeletal		A25004	29%	42369/ 5.13	BOVINE	136
B	Chymotrypsinogen 2		Q9W7Q3		25.666	BOVINE	
C	14-3-3 protein		P62261	19%	29155/4.63	BOVINE	32
D	Pyruvate kinase (EC 2.7.1.40) isozyme M2		A26186	24%	57744/7.15	Rat	108
E	Spermidine synthase (EC 2.5.1.16)		A32610	11%	33803/5.30	HUMAN	74
3. Up-regulated proteins in E60							
A	Stathmin (Phosphoprotein p19)		P16949	18%	17161/5.77	HUMAN	45
B	Apolipoprotein A-I precursor		P18648	24%	30307/ 5.48	PIG	90
C	Alpha-fetoprotein		Q8MJ76	16%	68580/5.47	PIG	74
D	Transferrin		S01384	16%	76918/6.93	PIG	89
E	F25B3.3 kinase like protein (Fragment)		O09004	22%	29241/6.50	MOUSE	40
F	Peptidyl-prolyl cis-trans isomerase A		P62936	43%	17727/8.37	PIG	88
G	Alpha-1-antitrypsin precursor		P50447	30%	47164/5.54	PIG	154

*The expression pattern represent protein expression level at each development stage (E60→neonate→adult).

detected in each of the Coomassie blue stained gels using computer-assisted image analysis. At each respective developmental stage, a total of 467, 402 and 557 spots were detected from each gel (Figure 1). Among them, 24

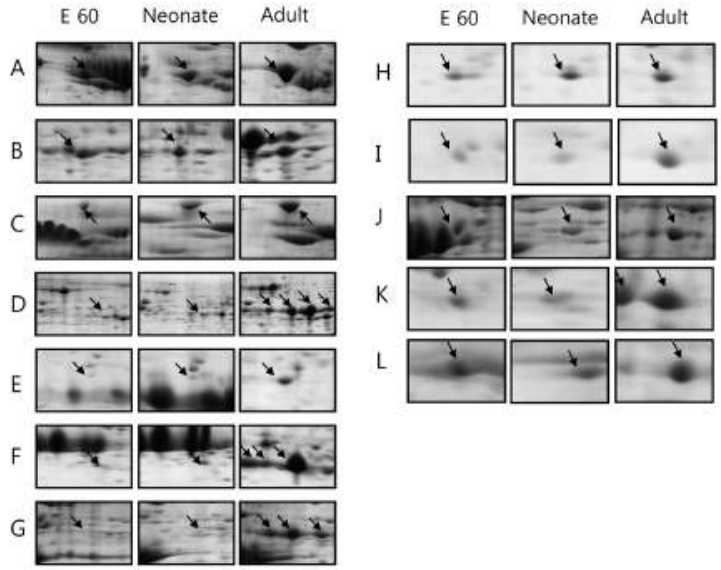

Figure 2. 2-DE gel enlargements showing proteins that are highly expressed in the adult stage. Various zymogens (pancreatic alpha-amylase precursor, trypsin precursor and pancreatic triacylglycerol lipase) and protein synthesis related proteins (protein disulfide-isomerase precursor, endoplasmin precursor, 60 kDa heat shock protein and phosphatidylethanolamine-binding protein) are up-regulated. The proteins of interest are indicated by arrows. These proteins were identified by MALDI-TOF MS (A. protein disulfide-isomerase precursor, B. glycine amidinotransferase, C. endoplasmin precursor, D. pancreatic alpha-amylase precursor, E. MHC class II antigen, F. trypsin precursor, G. pancreatic triacylglycerol lipase, H. phosphatidylethanolamine-binding protein, I. translationally-controlled tumor protein, J. 60 kDa heat shock protein, K. hypothetical protein FLJ39175, and L. laminin receptor).

proteins showed marked changes in expression. Twelve spots increased, while 7 spots decreased. The expression level of 5 spots was highest at birth. Twenty four differentially expressed proteins were identified by MALDI-TOF MS and MASCOT (Table 1). Changes in protein expression patterns were visualized in gels.

Up-regulated proteins in adult

The amount of protein disulfide-isomerase precursor, endoplasmic precursor, glycine aminotransferase and heat shock protein increased gradually during the development from fetus to adult pig (Figure 2). Their increase suggests that gradual increase in body mass and food uptake of animal results in higher protein content of these proteins for making the necessary quantities of digestive enzymes and hormones. In addition, digestive enzyme precursors, such as pancreatic alpha-amylase precursor, trypsin precursor and pancreatic triacylglycerol lipase, were stage-specific proteins dominantly expressed in adult pig pancreas. Immune-mediated MHC class II antigen was expressed in large quantities in the adult pancreas.

Up-regulated neonatal proteins

Expression of 5 proteins were up-regulated at the time of birth: chymotrypsinogen 2, pyruvate kinase isozyme M2, spermidine synthase and 14-3-3 protein (Figure 3). Among them, the change in expression pattern of chymotrypsinogen 2 was especially pronounced. However, although chymotrypsinogen 2 was rarely expressed in adult pig pancreas, it occupied at least 20% of entire pancreas proteins in fetus and neonate, especially neonates. The specific activity of chymotrypsin increased until birth and then declined precipitously, consistent with prior reports [19,20].The activities of other zymogens (amylase, lipase and elastase) were low in the fetus and steadily increased after birth.

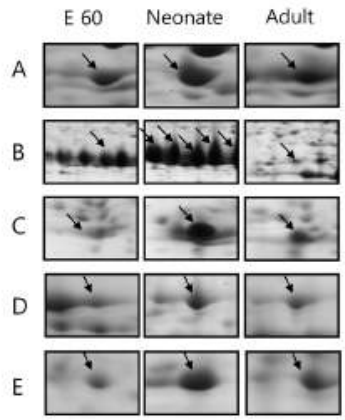

Figure 3. 2-DE gel enlargements showing the proteins especially expressed in the neonatal stage. Chymotrypsinogen 2 and 14-3-3 protein are significantly up-regulated at birth. The proteins of interest are indicated by arrows. These proteins were identified by MALDI-TOF MS (A. keratin, 53K type II cytoskeletal, B. chymotrypsinogen 2, C. 14-3-3 protein, D. pyruvate kinase (EC 2.7.1.40) isozyme M2, E. spermidine synthase (EC 2.5.1.16)).

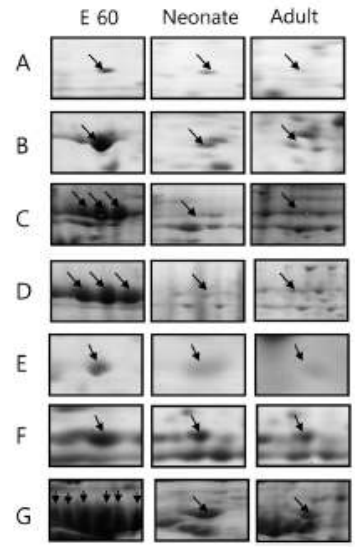

Figure 4. 2-DE gel enlargements showing the proteins especially more expressed in the embryonic stage. Apolipoprotein A-I precursor, alpha-fetoprotein, transferrin and alpha-1-antitrypsin precursor are markedly expressed in fetal developing pancreas. The proteins of interest are indicated by arrows. These proteins were identified by MALDI-TOF MS (A. stathmin (Phosphoprotein p19), B. apolipoprotein A-I precursor, C. alpha-fetoprotein, D. transferrin. E. F25B3.3 kinase like protein (Fragment), F. peptidyl-prolyl cis-trans isomerase A, G. alpha-1-antitrypsin precursor).

Up-regulated fetal proteins

Expression of 7 spots was significantly increased in fetal pigs compared to neonate and adult stages (Figure 4). Apolipoprotein precursor, alpha-fetoprotein, transferring and alpha –1-antitrypsin precursor were strong markers of developing pancreas. They were difficult to detect in the developed pancreas.

Classification by function

The 24 identified proteins were classified by their functions based on a search at http://harvester.embl.de (Table 2). The functions included glucose or lipid metabolism (n=5), transport of ions like Fe and Ni, or lipid (n=4), maintenance of intracellular structure and cell-to-cell adhesion (n=2), protein folding (n=4), protein synthesis (n=2), anti-proteases (n=2), regulators of signal transduction or insulin sensitivity (n=2), inhibit of apoptosis and induce proliferation (n=2) and immune system related (n=1).

Discussion

Pancreas obtained prior to birth (E60), at the end of pregnancy (neonate) and at adulthood (6 months of age) were analyzed to reveal proteins that were differentially expressed during pig pancreas development. Using 2D proteomics, proteins were resolved and were identified using MALDI-TOF and MASCOT database. We identified 462, 402 and 557 proteins at E60, neonate and 6-month-old adult pig, respectively. Among those identified proteins, 24 proteins showed pronounced differences in protein expression level at each developmental stage. The fetus and the neonatal pig pancreas had similar protein expression patterns on 2-DE gels, while the adult pig pancreas had a significantly different pattern. In the adult pig, digestive enzymes, such as pancreatic alpha-amylase precursor, trypsin precursor, pancreatic triacylglycerol lipase, protein disulfide-isomerase precursor, endoplasmin precursor and glycine amidinotransferase, which are associated with protein synthesis and formation of tertiary structure, consisted most of the dramatically up-regulated proteins on the 2-DE map.

Table 2. Classification of identified pig pancreas proteins by biological functions

Functional category	Proteins
Metabolism	Pancreatic alpha-amylase precursor Pancreatic triacylglycerol lipase Pyruvate kinase (EC 2.7.1.40) isozyme M2 Chymotrypsinogen A Trypsinogen
Transport	Hypothetical protein FLJ39175 Apolipoprotein A-I precursor Alpha fetoprotein Transferrin
Cell structure	Keratin, 53K type II cytoskeletal Laminin receptor
Protein folding	Protein disulfide isomerase Endoplasmin precursor 60 kDa Heat shock protein Peptidyl-prolyl cis-trans isomerase A
Protein biosynthesis	Glycine amidinotransferase (creatine biosynthesis) Spermidine synthase (EC 2.5.1.16)
Inhibition	Phosphatidylethanolamine-binding protein Alpha-1-antitrypsin precursor
Regulation	14-3-3 Protein epsilon (insulin sensitivity) BTB/POZ domain containing protein 1(transcription regulation)
Cell cycle	Translationally-controlled tumor protein (inhibit apoptosis) Stathmin (Phosphoprotein p19)
Immune response	MHC class II antigen

Comparing protein expression levels in the E60 and the neonatal pig (Figure 1), proteins in the fetal pig were more acidic and high in molecular weights. These included stathmin, apolipoprotein A-I precursor, alpha-fetoprotein, transferrin, peptidyl-prolyl cis-trans isomerase A (cyclophilin A) and alpha-1-antitrypsin precursor. These proteins gradually decreased during pancreas development. Stathmin is the tubulin-binding protein but a neuroproteomic search identified it as a novel Cdk5 substrate. Stathmin is phosphorylated by Cdk5 [21] and is involved in cancer development [22,23]. Stathmin gene overexpression is important in the maintenance of the malignant phenotype in tumor cells, and the blocking efficacy and tumor specificity of this target has been addressed in clinical trials [24]. Small interfering RNA-induced repression of stathmin decreases cell proliferation, viability and clonogenicity in mutant p53 tumor cell lines [25]. Although the relationship between stathmin and cell development is unclear, since stathmin is associated with aberrant cell proliferation, it is expected that stathmin contributes to cell development in some manner.

Apolipoprotein A-I (apoA-I) is the major lipoprotein component of high-density lipoprotein, and plays an important role in reverse cholesterol transport [26]. It also is an anti-inflammatory and anti-atherosclerosis molecule and functions as a potent inhibitor of dendritic cell differentiation and maturation [27]. Apo A-I has two major sites of synthesis: the intestine and the liver. Apo A-I is expressed in the pancreas and 12% of the liver [28]. Presently, its expression decreased gradually according to the developmental stage, which may be due to lack of cell type specification during early development because liver and pancreas have the same developmental origin. In addition, the liver controls lipid metabolism and repression of inflammatory response, which may contribute to the development of the pancreas (although there is scant evidence in support of this).

The liver and yolk sac of fetuses the principle sites of alpha-fetoprotein (AFP) synthesis in ontogenesis, and the dynamics of AFP in ontogenesis from the early embryonic period through mid-pregnancy to pregnancy termination to AFP shut-down in early postnatal period [29]. AFP plays an important role in regulation of immune system, which is associated with repression on the immune system, such as decrease in natural killer cell activity [30], induction of T suppressor cells [31,32], repression of mitogenic response of PHA and Con A [33-36], restriction on T cell differentiation to Ia determinants [37], decrease in phagocytic activity of

macrophage [38,39] and decrease in macrophage Ia expression level [40-42].

Transferrin, a 76-80 kDa glycoprotein, is responsible for the transport of iron to cells within both the fetal and maternal systems [43]. It is not only the transporter of iron but also has activities of growth factor and repressing reactive oxygen species production [44]. The concentration of AFP, alpha 1-antitrypsin and transferrin in serum increases with age until 40-50 days of gestation and then decreases progressively at birth in pigs [45].

Cyclophilin A (CyP-A) is a soluble cytoplasmic immunophilin involved in T cell differentiation and proliferation. A role for CyP-A in neuronal differentiation has been implied [46]. Alpha-1- antitrypsin (α1-AT) acts as a suicide inhibitor of a wide range of serine proteases. In normal humans, more than 2 g of α1-AT protein is synthesized daily, resulting in a serum concentration of about 2 mg/mL. The primary function of α1-AT protein is inhibition of neutrophil elastase, which may protect from excessive tissue damage [47]. In addition to its well established role of neutralizing elastase activity, in cell lines of both mesenchymal and epithelial origin, α1-AT can enhance DNA synthesis and cell proliferation particularly when insulin is present [46]. The highest amounts of α1-AT were clearly present in the fetal sheep liver, regardless of the stage of gestation. The decline in hepatic α1-AT in term and neonatal animals occurs at a time when the plasma levels of glucocorticoids markedly suggesting that the natural increase in cortisol during late gestation in the sheep fetus may be responsible for this decline in the abundance of hepatic alpha-1-antitrypsin. It may influence the ability of fetus to control proteinases at the fetal maternal interface and influence events leading to parturition, and/or the ultimate demise of the placenta [49].

Disruptions in pancreatic functions cause indigestion problems and altered glucose homeostasis, which can prelude the development of diabetes mellitus, pancreatic cancer and pancreatitis. The pig pancreas is an important resource of xenotransplantation for human diabetic patients, but little is known about its developmental stage at the molecular level. We presented proteomic alterations in pig pancreas by analyzing the changes in protein expression level during development. This study will provide basis for rudimentary understanding development of pig pancreas at the molecular level.

Acknowledgments

This work was supported by the grants from the Ministry of Agriculture, Food and Rural Affairs (311054-03-2-HD110) and Ministry of Science, ICT and Future Planning (2013M3A9D5072550), Korea to Prof. Je Kyung Seong.

References

1. Rao MS, Reddy JK. Pancreatic stem cells: differentiation options. Stem Cell Rev 2005; 1(3): 265-271.
2. Portela-Gomes GM1, Hacker GW, Weitgasser R. Neuroendocrine cell markers for pancreatic islets and tumors. Appl Immunohistochem Mol Morphol 2004; 12(3): 183-192.
3. Wild S, Roglic G, Green A, Sicree R, King H. Global prevalence of diabetes: estimates for the year 2000 and projections for 2030. Diabetes Care 2004; 27(5): 1047-1053.
4. Herber S, Grus FH, Sabuncuo P, Augustin AJ. Two-dimensional analysis of tear protein patterns of diabetic patients. Electrophoresis 2001; 22(9): 1838-1844.
5. Sabek OM, Marshall DR, Penmetsa R, Scarborough O, Gaber AO. Examination of gene expression profile of functional human pancreatic islets after 2-week culture. Transplant Proc 2006; 38(10): 3678-3679.
6. Lee EJ, Gusev Y, Jiang J, Nuovo GJ, Lerner MR, Frankel WL, Morgan DL, Postier RG, Brackett DJ, Schmittgen TD. Expression profiling identifies microRNA signature in pancreatic cancer. Int J Cancer 2007; 120(5): 1046-1054.
7. Hojlund K, Wrzesinski K, Larsen PM, Fey SJ, Roepstorff P, Handberg A, Dela F, Vinten J, McCormack JG, Reynet C, Beck-Nielsen H. Proteome analysis reveals phosphorylation of ATP synthase beta -subunit in human skeletal muscle and proteins with potential roles in type 2 diabetes. J Biol Chem 2003; 278(12): 10436-10442.
8. Qiu L, List EO, Kopchick JJ. Differentially expressed proteins in the pancreas of diet-induced diabetic mice. Mol Cell Proteomics 2005; 4(9): 1311-1318.
9. Silva D, Petrovsky N. Identification of key beta cell gene signaling pathways involved in type 1 diabetes. Ann N Y Acad Sci 2004; 1037(1): 203-207.
10. Ibrahim Z, Busch J, Awwad M, Wagner R, Wells K, Cooper DK. Selected physiologic compatibilities and incompatibilities between human and porcine organ systems. Xenotransplantation 2006; 13(6): 488-499.
11. Levy MF. Animal organs for human transplantation: how close are we? Proc (Bayl Univ Med Cent) 2000; 13(1): 3-6.
12. Starzl TE, Fung J, Tzakis A, Todo S, Demetris AJ, Marino IR, Doyle H, Zeevi A, Warty V, Michaels M, Kusne S, Rudert WA, Trucco M. Baboon-to-human liver transplantation. Lancet. 1993; 341(8837): 65-71.
13. Levy MF, Crippin J, Sutton S, Netto G, McCormack J, Curiel T, Goldstein RM, Newman JT, Gonwa TA, Banchereau J, Diamond LE, Byrne G, Logan J, Klintmalm GB. Liver allotransplantation after extracorporeal hepatic support with transgenic (hCD55/hCD59) porcine livers: clinical results and lack of pig-to-human transmission of the porcine endogenous retrovirus. Transplantation 2000; 69(2): 272-280.
14. Paradis K, Langford G, Long Z, Heneine W, Sandstrom P, Switzer WM, Chapman LE, Lockey C, Onions D, Otto E. Search for cross-species transmission of porcine endogenous retrovirus in patients treated with living pig tissue. The XEN 111 Study Group.

Lab Anim Res 2014: 30(1), 1-7
http://dx.doi.org/10.5625/lar.2014.30.1.1

Laboratory Animal Research
http://submission.kalas.or.kr

Proteomic analysis of pancreas in miniature pigs according to developmental stages using two-dimensional electrophoresis and matrix-assisted laser desorption/ionization-time of flight mass spectrometry

Sun Shin Yi[1], Il Yong Kim[2], Sae Jin Oh[3], Hye Jung Yeom[4], Su Cheong Yeom[5], Seung Yong Hwang[6], Je Kyung Seong[2]*

[1]*Department of Biomedical Laboratory Science, College of Biomedical Sciences, Soonchunhyang University, Asan, Korea*
[2]*Laboratory of Developmental Biology and Genetics, College of Veterinary Medicine, BK21 Plus Program for Creative Science Research, BIO-MAX institute, Seoul National University, Seoul, Korea*
[3]*Department of Pathology and Laboratory of Immune Regulation, College of Medicine, Seoul National University, Seoul, Korea*
[4]*Transitional Research Institute, College of Medicine, Seoul National University, Seoul, Korea*
[5]*Biomedical Center for Animal Resource and Development, BIO-MAX Institute, Seoul National University, Seoul, Korea*
[6]*Department of Biochemistry, Hanyang University, Ansan, Korea*

Organ transplantation is limited by the shortage of human organs. Many studies have sought to overcome this hurdle by using animal organs. Porcine organs, especially from miniature pigs, have been used for organ xenotransplantation rather than nonhuman primates. While the molecular profiling for transplantation is well known in humans and rodents, the situation for pigs is almost completely unknown. The present study examined protein regulation of the developing stages of the pancreatic proteome (4 day-old miniature neonate, 19 day-old miniature piglet, and 14 month-old miniature adult pigs) using two-dimensional gel electrophoresis and matrix assisted laser desorption/ionization-time of flight mass spectrometry. Thirteen different expressed spots were observed and nine were identified. The data presented within this study provides critical direction relating to the development of pancreas of miniature pigs, which will assist future proteome analysis of the pancreas, and advance our understanding of the hurdles facing xenotransplantation.

Key words: Human organ, pancreas, miniature pig, proteome, 2-DE MALDI-TOF

Received 21 September 2013; Revised version received 11 January 2014; Accepted 21 January 2014

The increasing shortage of human donor organs has provoked interest in the possible use of animal organs for transplantation into humans [1-3]. Organ transplants from nonhuman primates have been studied as replacements for human organs. However, using organs of nonhuman primates can be dangerous, and their organs can be too small for transplanatation into adult humans [1]. Pigs are the most likely candidate for xenotransplantation [4,5]. Moreover, as a potential xenotransplantation source, pigs have to be managed under conditions of stringent bioexclusion. Miniature pigs produced by a selective breeding system are recommended [6,7].

Miniature pigs have many physiological similarities with humans and provide some breeding and manipulation advantages compared to non-human primates [8]. The organs commonly used from miniature pigs are the heart, kidney, liver and pancreas. The pancreas controls endocrine, exocrine and glucose metabolism through the creation of insulin. Porcine pancreatic tissue can be a

*Corresponding author: Je-Kyung Seong, Laboratory of Developmental Biology and Genetics, College of VeterinaryMedicine, BK21 Program for Veterinary Science, BIO-MAX institute, Seoul National University, Seoul 151-742, Korea
Tel: +82-2-883-8395; Fax: +82-2-875-8395; E-mail: snumouse@snu.ac.kr

good resource of transplantation therapy for human diabetic patients [9-11]. Transplantation of porcine pancreatic islets into non-human primates or other species has been documented [12-14]. However, the characteristics of pancreatic protein expression in pigs are ill-understood, while the expression of pancreatic proteins in humans and rodents is better defined.

Presently, pancreatic protein expression was examined chronologically using a miniature neonate pig (4-day-old), miniature piglet (19-day-old) and miniature adult pig (14-months-old). Proteins that were differentially expressed during development were revealed by two-dimensional electrophoresis (2-DE) and matrix assisted laser desorption/ionization-time of flight mass spectrometry (MALDI-TOF MS). While the repository of identified porcine proteins in Swiss-Prot and NCBI databases are relatively scant, these sources were used presently to help identify the differentially expressed proteins. The data should aid future proteome analyses.

Materials and Methods

Laboratory animals

The miniature pigs were housed in the air barrier facility of the Center for Animal Resource Development at Seoul National University. Three pigs (male 4-old-, 19-day- and 14-month-old miniature pig) having different ages and developmental stages were used. They were conditioned in the same room at 24±2℃ with a 12/12 (light/dark) cycle. Air and water were filtered, and all equipment and food were sterilized before use. This study was approved as an animal use protocol by the Institutional Animal Care and Use Committee at SNU (SNU-IACUC approval number: SNU-060613-5). Intramuscular anesthesia was achieved using a mixture of 2 mL ketamine · HCl (50 mg/mL/kg), 1 mL xylazin (2.3 mg/mL/kg) and 1 mL atropine sulfate (0.5 mg/mL/10 kg) during every painful/stressful procedure. The abdomen of each pig was shaved and disinfected with polyvinylpyrrolidone-iodine. The animals were immobilized on a surgical plane-table by adhesive ties. A median laparotomy was performed. The pancreas from the animals were nipped off aseptically and stored in liquid nitrogen while being transported to the laboratory.

Sample preparation for 2DE

The pancreas of each pig (one miniature pig for each age stage, respectively)was removed immediately after sacrifice and stored at −70℃ until used. In briefly, the peritoneal of the miniature pigs under the anesthesia were pre-chilled by filling of large quantity of ice before removing the pancreas. The pancreas was collected from the distal end of normal pancreas immediately from the animals and snap-frozen in liquid nitrogen, and stored at stored at −70℃. The frozen pancreas tissues (1 g) in a mortar were grounded to powder under the constant addition of liquid nitrogen. The powder is normally suspended in 900 μL lysis buffer (7 M urea, 2 M thiourea, 2% w/v CHAPS, 2% pharmalyte pH3-10, 100 mM DTE). Samples were centrifuged at 50,000 rpm at 4℃ for 1 h. The supernatant was carefully removed and immediately frozen at −70℃.

2DE

2D-polyacrylamide gel electrophoresis (PAGE) was performed as previously described [15]. Aliquots containing 1 mg total protein were diluted in lysis buffer to a total volume of 450 μL. The samples were applied to a 240 mm, immobilized, nonlinear pH 3-10 IPG Drystrip (Amersham Pharmacia Biotech, Piscataway, NJ, USA), which was rehydrated for at least 12 h. After rehydration, the strips were focused at 30 V for 3 h, 100 V for 1 h, 200 V for 1 h, 500 V for 1 h, 1,000 V for 1 h and finally at 8,000 V for 11 h to obtain approximately 90,000 Vh (Ettan™ IPGphor™ II IEF systems; Amersham Pharmacia Biotech). Once isoelectric focusing was completed, the strips were equilibrated in 6 M urea containing 20% v/v glycerol, 2% w/v sodium dodecyl sulfate (SDS) and 0.01% w/v BPB with 10 mM tributyl phosphine (Flukachemie, Buchs, Switzerland). SDS-PAGE was performed using an 8-18% separating gel without a stacking gel using the Ettan Dalt system (Amersham Pharmacia Biotech) twice per each aged-group for the confirmation of separated gel-spot trends. The second dimension electrophoresis was carried out overnight at 3 W/gel at 20℃. The gels were stained with Coomassie G-250 (Bio-Rad Laboratories, Hercules, CA, USA).

Protein visualization and image analysis

The gels were stained with Coomassie G-250 (Bio-Rad) as previously described [12]. The stained gels were scanned using a GS 800 photometer (Bio-Rad) and analyzed with the ImageMaster™ 2D Platinum Software version 5.0 (GeneBio, Geneva, Switzerland). The digitalized 2DE gel images were compared by a matching method

(Image master 5.0; Amersham Biosciences). Differentially expressed spots (>3-fold and <1/3-fold) were analyzed and annotated.

In-gel digestion

The spots were cut into smaller pieces and digested using 12.5 ng/μL trypsin (Promega, Madison, WI, USA) in 50 mM ammonium bicarbonate, pH 8.0, as previously described [16]. For MALDI-TOF MS analysis, the tryptic peptides were concentrated on a POROS 50 R2 column (Applied BioSystems, Foster City, CA, USA). After subsequent washing steps of column with 70% acetonitrile (can) in 5% FA, 100% can and 5% FA, the samples were loaded into a POROS 50 R2 column and washed with 5% FA. The sample was eluted with 2 μL of matrix solution consisting of 10 mg/mL α-cyano-4-hydroxy-cinnamic acid (Sigma-Aldrich, St. Louis, MO, USA) and then dropped onto a MALDI sample plate [24].

Protein identification by MALDI-TOF

MALDI-TOF MS was performed using a Voyager DE-PRO spectrometer (Applied Biosystems) equipped with a 337 nm nitrogen laser. The instrument was operated at an accelerating voltage of 20 kV, positive ion reflection mode, voltage grid 74.5%, guide wire voltage 0% and delay-time of 120 ns. The spectra were internally calibrated using the trypsin autolysis products (842.51 [M+H] and 2211.11 [M+H]), and searching in Swiss-Prot identified the proteins and NCBI database using Mascot (Matrix Science, London, UK). Monoisotopic peaks [MH+] were selected and all the searches were analyzed with a 50 ppm mass tolerance.

Results

Protein identification by MS

Porcine pancreatic proteins that were differentially expressed were identified and compared according to the developmental stage. Pancreatic proteins were extracted and analyzed by 2DE. After the resolved proteins were visualized by Coomassie blue staining, 2-DE was repeated in three independent experiments for the three pairs of matched samples (Figure 1). For each sample, the three gels with the best resolution were selected for analysis. Spot intensities were analyzed using Image Master™ software (Geneva Bioinformatics, S.A, Geneva, Switzerland). Among the 289 protein spots detected, 13 differentially expressed spots were identified. The protein spots up-regulated more than 3-fold or down-regulated less than 1/3-fold down-regulation were selected, excised from the gels and digested. Peptide fingerprinting was accomplished by MALDI-TOF MS. Peptide mass data were identified by Mascot. Thirteen differentially expressed protein spots were evident. Of these, nine were identified (Table 1) and their functions established based on a search at http://www.ebi.ac.uk/ego (Table 1).

Classification of the identified proteins

The increased and decreased intensities of the selected spots were ascertained chronologically by comparison of

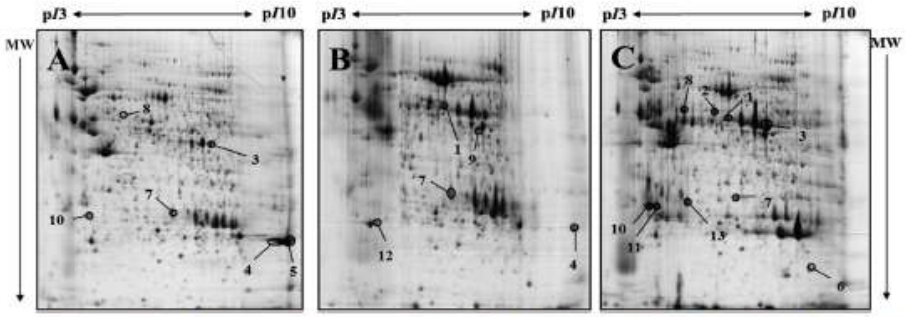

Figure 1. Representative 2-DE gels of pancreas of 4-day-old, 19-day-old and 14-month-old miniature pigs by developmental stages, visualized by Commassie blue staining. Samples of 1mg protein were separated on pH3-10 non-linear IPG strip (24cm) following by 8-18% gradient SDS-PAGE in the second dimension. Proteins were detected by Coomassie brilliant blue G-250 and compared using ImageMaster™ 2D Platinum Software version 5.0. A: 2-DE gel of 4-day old miniature pig(neonate), B: 2-DE gel of 19-day old miniature pig, C: 2-DE gel of 14-month old miniature pig. The closed circles indicate 13 differentially expressed protein spots in the 4-day-old miniature neonate pig, 19-day-old miniature piglet and 14-month-old miniature adult pig.

Table 1. Proteins of miniature pig pancreas 2-D gels, which were identified by peptide mass fingerprinting using MALDI-TOF MS

Spot No.	Name	Accession No.	Sequence Coverage (%)	MW (Da)/pI	Score	Expect	Species	Database
1	Unknown	-	-	-	-	-	-	-
2	Pancreatic triacylglycerol lipase	P00591	16%	50053/5.73	51	0.72	Pig	Swissprot
3	Pancreatic alpha amylase precursor	P00690	31%	57050/6.51	132	6.10E-09	Pig	Swissprot
4	Hemoglobin alpha-subunit	P01965	58%	15030/8.76	99	1.20E-05	Pig	Swissprot
5	Hemoglobin alpha-subunit	P01965	58%	15030/8.76	109	1.20E-06	Pig	Swissprot
6	Tyrosine-rich protein 1 precursor	Q8VIH7	13%-	18051/8.94-	20	9.3E+02	mouse	Swissprot
7	Unknown	-	-	-	-	-	-	-
8	Interleukin-1 receptor type I precursor	Q02955	11%	66715/6.12	30	1.00E-02	Rat	Swissprot
9	Alpha-enolase (2-phospho-D-glycerate hydro-lyase)	Q9XSJ4	21%-	47116/6.43	84	0.0004	Bovine	Swissprot
10	Unknown	-	-	-	-	-	-	-
11	Bisphosphoglycerate mutase	P07738	21%	29855/6.10	29	1.3e+02	Human	Swissprot-
12	Unknown	-	-	-	-	-	-	-
13	High mobility group protein B2	P17741	18%	23987/7.10	36	25	pig	Swissprot

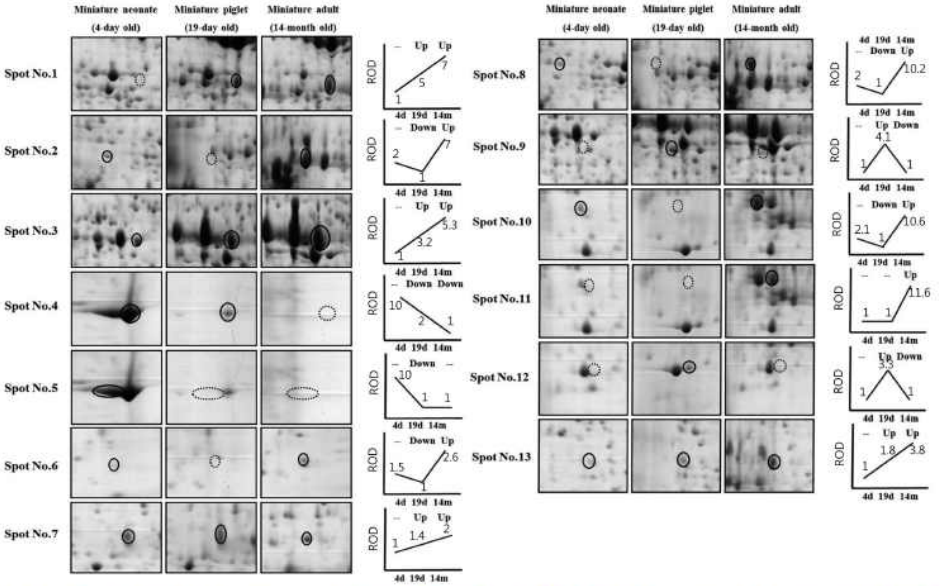

Figure 2. Two-DE images of alterative spots of pancreas according to developmental stage. The circles indicate differentially expressed protein spots and the dot circles show down-expressed patterns. The expression patterns of the different three stages are presented as simple line graphs. Relative optical (ROD) are indicated as relative numbers under the lines compared with the lowest protein optical density (the lowest optical density is made as an '1') of each spot.

the miniature pigs from the neonate stage to adulthood (Figure 2). The expression of pancreatic triacylglycerol lipase (spot 2), tyrosine-rich protein 1 precursor (spot 6) and interleukin-1 receptor type Iprecursor (spot 8) were down- and up-regulated. Although spot 10 displayed a similar intensity, correct identification was not achieved. Pancreatic alpha amylase precursor (spot 3) and high mobility group protein B2 (spot 13) were both up-regulated. Spots 1 and 7 displayed similar intensity patterns, but correct identification was again not achieved. Hemoglobin alpha-subunit spots (spots 4 and 5) were shown side-by-side; the spot intensities were variable, being either both down-regulated or down-regulated and unchanged, respectively. Bisphosphoglyceratemutase (2, 3-bisphosphoglycrerate mutase; spot 11) expression was either unchanged or up-regulated. The expression of alpha-enolase (2-phospho-D-glyceratehydro-lyase; spot 9) and spot no. 12 was up-regulated and down-regulated, respectively. Spot 12, which showed similar spot intensity, was not identified correctly.

Discussion

This study is, to our knowledge, the first report of protein expression of pancreas in miniature pigs according to the developmental stage. Although xenotransplantation of pancreas using pathogen-free miniature pigs has been explored for a few decades, few studies have examined the proteome of the whole pancreas of miniature pigs at the chronological developmental stages (in this study, neonate, 19-day old and 14-month old miniature pigs). A comprehensive understanding of protein expressional alteration in the pancreas can provide useful biological and clinical information. About 300 proteins with isoelectric points of 3-10 and molecular weight of 10-100 kDa were detected. Of 289 spots, 13 were significantly changed during development; of these, nine spots were functionally identified. Of these identified proteins, few were directly related with pancreas functions. For instance, pancreatic triacylglycerol lipase is required for efficient dietary triglyceride digestion [18,19]. Although this enzyme may play a role in fat metabolism, its expression varies developmentally and by tissue [19]. Pancreatic alpha amylase precursor is found in the pancreas and salivary gland [20]. Alpha-amylase is a typical secretory protein that is subject to glycosylation machinery during its biosynthesis [21,22]. The glycosylation is preceded by proteolytic processing during the biosynthesis of the alpha-amylase molecule [23]. The mammalian interleukin-1 receptor type 1-Toll-like receptor superfamily has important roles in innate immunity, inflammatory responses, stress response and fatal immune disorders [24-27], and it undergoes intramembrane proteolytic processing [28]. Several studies have reported the relationship of interleukin-1 receptor type 1 with pancreatitis [29-31]. In addition, inflammation in type 2 diabetes has been linked to interleukin-1 receptor type 1 [30]. Alpha-enolase is a 48-kDa protein that is crucial in the glycolytic pathway [32], where it catalyzes the formation of phosphoenolpyruvate from 2-phosphoglycerate, the second of the two high energy intermediates that generate ATP in glycolysis [33].

Despite the numerous studies of xenotransplantation between pigs and humans for considerable times, the proteomic alterations of various organs during development, whether or not these changes are critical in the particular developmental stage, has not been considered. Additionally, data concerning the proteome of porcine pancreatic tissue are scant [5], with no attempt to investigate the transplantation-relevant proteomic expressional relationships and differences between human and miniature pigs.

Knowledge of the alteration of the protein complement would provide valuable information to overcome the problems posed by the immunologic barrier, microbiologic differences and xenospecies, which presently hinder xenotransplantation. From the present data, the pancreactic proteomic alterations in the developmental stages appear to contain several enzymatic activities and immune responses, and have hematological relevance. Although the scope of the data was hindered by technical problems, the data provides the first reference of the protein expression during pancreas development, which will be useful in further proteome analyses of the porcine pancreas with respect to xenotransplantation.

Acknowledgments

This work was supported by the grants from the Bio-Industry Technology Development Program Ministry of Agriculture, Food and Rural Affairs, Korea to Prof. Je Kyung Seong (311054-03-2HD110), and this work was also supported by Soonchunhyang University Research Fund to Prof. Sun Shin Yi.

References

1. Cooper DK, Gollackner B, Sachs DH. Will the pig solve the transplantation backlog? Annu Rev Med 2002; 53: 133-147.
2. Platt JL. Physiologic barriers to xenotransplantation. Transplant Proc 2000; 32(7): 1547-1548.
3. Ryu JM, Kim DH, Lee MY, Lee SH, Park JH, Yun SP, Jang MW, Kim SH, Rho GJ, Han HJ. Imaging evaluation of the liver using multi-detector row computed tomography in micropigs as potential living liver donors. J Vet Sci 2009; 10(2): 93-98.
4. Ibrahim Z, Busch J, Awwad M, Wagner R, Wells K, Cooper DK. Selected physiologic compatibilities and incompatibilities between human and porcine organ systems. Xenotransplantation 2006; 13(6), 488-499.
5. Tucker A, Belcher C, Moloo B, Bell J, Mazzulli T, Humar A, Hughes A, McArdle P, Talbot A. The production of transgenic pigs for potential use in clinical xenotransplantation: baseline clinical pathology and organ size studies. Xenotransplantation 2002; 9(3): 203-208.
6. Ando A, Ota M, Sada M, Katsuyama Y, Goto R, Shigenari A, Kawata H, Anzai T, Iwanaga T, Miyoshi Y, Fujimura N, Inoko H. Rapid assignment of the swine major histocompatibility complex (SLA) class I and II genotypes in Clawn miniature swine using PCR-SSP and PCR-RFLP methods. Xenotransplantation 2005; 12(2): 121-126.
7. Park CG, Kim JS, Shin JS, Kim YH, Kim SJ. Current Status and Future Perspectives of xenotransplantation. J Korean SocTranplant 2009; 23(3): 203-213.
8. Vodicka P, Smetana K Jr, Dvoránková B, Emerick T, Xu YZ, Ourednik J, Ourednik V, Motlik J. The miniature pig as an animal model in biomedical research. Ann N Y Acad Sci 2005; 1049: 161-171.
9. Choi JS, Cho YK, Y oon SH, Kwon SO, Koo DB, Yu K. Proteomic analysis of porcine pancreas development. BMB Rep 2009; 42(10): 661-666.
10. Han HJ, Kang SS, Park SH. Tissue specific expression of lipid metabolism related molecules in digestive organs of miniature pigs. Lab Anim Res 2010; 26(3): 273-278.
11. Lee MS, Song KD, Yang HJ, Solis CD, Kim SH, Lee WK. Development of a type II diabetic mellitus animal model using Micropig®. Lab Anim Res 2012; 28(3): 205-208.
12. Cozzi E, Bosio E. Islet xenotransplantation: current status of preclinical studies in the pig-to-nonhuman primate model. Curr Opin Organ Transplant 2008; 13(2): 155-158.
13. Marigliano M, Bertera S, Grupillo M, Trucco M, Bottino R. Pig-to-nonhuman primates pancreatic islet xenotransplantation: an overview. Curr Diab Rep 2011; 11(5): 402-412.
14. Rood PP, Buhler LH, Bottino R, Trucco M, Cooper DK. Pig-to-nonhuman primate islet xenotransplantation: a review of current problems. Cell Transplant 2006; 15(2): 89-104.
15. Steiner S, Anderson NL. Pharmaceutical proteomics. Ann N Y Acad Sci 2000; 919: 48-51.
16. Görg A, Obermaier C, Boguth G, Harder A, Scheibe B, Wildgruber R, Weiss W. The current state of two-dimensional electrophoresis with immobilized pH gradients. Electrophoresis 2000; 21(6): 1037-1053.
17. Shevchenko A, Wilm M, Vorm O, Mann M. Mass spectrometric sequencing of proteins silver-stained polyacrylamide gels. Anal Chem 1996; 68(5): 850-858.
18. Lewe ME. The triglyceride lipases of the pancreas. J Lipid Res 2002; 43(12): 2007-2016.
19. Mahan JT, Heda GD, Rao RH, Mansbach CM 2nd. The intestine expresses pancreatic triacylglycerol lipase: regulation by dietary lipid. Am J Physiol Gastrointest Liver Physiol 2001; 280(6): G1187-1196.
20. Hagenbüchle O, Bovey R, Young RA. Tissue-specific expression of mouse-alpha-amylase genes: nucleotide sequence of isoenzyme mRNAs from pancreas and salivary gland. Cell 1980; 21(1): 179-187.
21. Doyon Y, Home W, Daull P, LeBel D. Effect of C-domain N-glycosylation and deletion on rat pancreatic alpha-amylase secretion and activity. Biochem J 2002; 362(Pt 1): 259-264.
22. Miyata S, Akazawa T. Biosynthesis of rice seed alpha-amylase: proteolytic processing and glycosylation of precursor polypeptides by microsomes. J Cell Biol 1983; 96(3): 802-806.
23. Miyata S, Akazawa T. alpha-Amylase biosynthesis: evidence for temporal sequence of NH2-terminal peptide cleavage and protein glycosylation. Proc Natl Acad Sci USA 1982; 79(21): 6566-6568.
24. Akira S, Takeda K. Toll-like receptor signalling. Nat Rev Immunol 2004; 4(7): 499-511.
25. Creagh EM, O'Neill LA. TLRs, NLRs and RLRs: a trinity of pathogen sensors that co-operate in innate immunity. Trends Immunol 2006; 27(8): 352-357.
26. Subramaniam S, Stansberg C, Cunningham C. The interleukin 1 receptor family. Dev Comp Immunol 2004; 28(5): 415-428.
27. Takeda K, Akira S. Toll-like receptors in innate immunity. Int Immunol 2005; 17(1), 1-14.
28. Elzinga BM, Twomey C, Powell JC, Harte F, McCarthy JV. Interleukin-1 receptor type 1 is a substrate for gamma-secretase-dependent regulated intramembrane proteolysis. J Biol Chem 2009; 284(3): 1394-1409.
29. Abcouwer SF, Norman J, Fink G, Carter G, Lustig RJ, Souba WW. Tissue-specific regulation of glutamine synthetase gene expression in acute pancreatitis is confirmed by using interleukin-1 receptor knockout mice. Surgery 1996; 120(2): 255-263.
30. Chentouf M, Dubois G, Jahannaut C, Castex F, Lajoix AD, Gross R, Peraldi-Roux S. Excessive food intake, obesity and inflammation process in Zucker fa/fa rat pancreatic islets. PLoS One 2011; 6(8): e22954.
31. Fink GW, Norman JG. Specific changes in the pancreatic expression of the interleukin 1 family of genes during experimental acute pancreatitis. Cytokine 1997; 9(12): 1023-1027.
32. Subramanian A, Miller DM. Structural analysis of alpha-enolase. Mapping the functional domains involved in down-regulation of the c-myc protooncogene. J Biol Chem 2000; 275(8): 5958-5965.
33. Wold, F. (1971) The Enzymes; (Boyer, P.D., ed) 3rd Ed. 5, pp. 499-508, Academic Press, New York, USA.

4. 비임상시험 데이터

<자초추출물의 조제물 중 Acetylshikonin의 농도분석법 중 validation 및 안정성 확인시험>

Table 1. System suitability

Concentration of standard solution (μg/mL)	Classification	No.1	No.2	No.3	No.4	No.5	No.6	Mean	SD	CV (%)
20	Peak area	100.09	98.08	99.08	99.24	99.07	100.23	99.30	0.79	0.80
	RT	16.99	17.01	17.00	16.99	16.99	16.99	17.00	0.01	0.06

Table 2. Accuracy of calibration curve

(A) Day 0

Concentration of standard solution (μg/mL)	Peak area	Measured concentration (μg/mL)	Accuracy (%)
5	21.07	5.440	108.80
10	48.46	10.26	102.60
20	98.95	19.13	95.65
50	274.99	50.09	100.18
100	559.31	100.1	100.10

y= 5.6872x – 9.8686, r = 0.9999

(B) Day 7

Concentration of standard solution (μg/mL)	Peak area	Measured concentration (μg/mL)	Accuracy (%)
5	26.53	5.199	103.98
10	56.70	10.06	100.60
20	114.62	19.38	96.90
50	308.10	50.52	101.04
100	614.60	99.85	99.85

y= 6.2131x – 5.7732, r = 0.9999

Table 3. Accuracy and precision of intra-day variation

Concentration of dosing formulation (mg/mL)	[1)]Actual concentrations of Acetylshikonin (mg/mL)	Measured concentration (mg/mL)			Mean (mg/mL)	SD	CV (%)	Accuracy (%)
		No.1	No.2	No.3				
10	2.334	2.419	2.419	2.386	2.408	0.019	0.79	103.17
400	93.36	92.58	93.32	88.81	91.57	2.42	2.64	98.08

[1)]Actual concentrations of Acetylshikonin = Concentrations of dosing formulation × Acetylshikonin of content (23.34%)

Table 4. Stability of stock solution

(A) Day 0

Time (hr)	Concentration of Standard solution (μg/mL)	Measured concentration (μg/mL)			Mean (μg/mL)	SD	CV (%)	Accuracy (%)
		No.1	No.2	No.3				
4	20	20.12	20.13	20.25	20.17	0.07	0.35	100.85

(B) Day 7

Time (Day)	Concentration of Standard solution (μg/mL)	Measured concentration (μg/mL)			Mean (μg/mL)	SD	CV (%)	Accuracy (%)
		No.1	No.2	No.3				
7	20	18.18	18.26	18.30	18.25	0.06	0.33	91.25

Table 5. Stability of treated samples in the autosampler

Time (hr)	Concentration of dosing formulation (mg/mL)	[1)]Actual concentrations of Acetylshikonin (mg/mL)	Measured concentration (mg/mL)			Mean (mg/mL)	SD	CV (%)	Accuracy (%)	Variation (%)
			No.1	No.2	No.3					
0	10	2.334	2.419	2.419	2.386	2.408	0.019	0.79	103.17	-
	400	93.36	92.58	93.32	88.81	91.57	2.42	2.64	98.08	-
20	10	2.334	2.520	2.530	2.490	2.513	0.021	0.84	107.67	4.36
	400	93.36	98.70	99.78	94.30	97.59	2.90	2.97	104.53	6.57

[1)]Actual concentrations of Acetylshikonin = Concentrations of dosing formulation × Acetylshikonin of content (23.34%)

Table 6. Homogeneity of the dosing formulations

Concentration of dosing formulation (mg/mL)	[1)]Actual concentrations of Acetylshikonin (mg/mL)		Measured concentration (mg/mL)			Mean (mg/mL)	SD	CV (%)	Accuracy (%)
			No.1	No.2	No.3				
10	2.334	Upper	2.350	2.384	2.370	2.372	0.035	1.48	101.63
		Middle	2.419	2.419	2.386				
		Lower	2.319	2.374	2.331				
400	93.36	Upper	93.87	97.24	97.05	95.16	3.20	3.36	101.93
		Middle	92.58	93.32	88.81				
		Lower	97.92	97.45	98.22				

[1)]Actual concentrations of Acetylshikonin = Concentrations of dosing formulation × Acetylshikonin of content (23.34%)

Table 7. Stability of the dosing formulations for 4 hours at room temperature

Time (hr)	Concentration of dosing formulation (mg/mL)	[1)]Actual concentrations of Acetylshikonin (mg/mL)	Measured concentration (mg/mL)			Mean (mg/mL)	SD	CV (%)	Accuracy (%)	Variation (%)
			No.1	No.2	No.3					
0	10	2.334	2.419	2.419	2.386	2.408	0.019	0.79	103.17	-
	400	93.36	92.58	93.32	88.81	91.57	2.42	2.64	98.08	-
4	10	2.334	2.419	2.086	2.136	2.214	0.180	8.13	94.86	-8.06
	400	93.36	78.77	91.02	89.19	86.33	6.61	7.66	92.47	-5.72

[1)]Actual concentrations of Acetylshikonin = Concentrations of dosing formulation × Acetylshikonin of content (23.34%)

Table 8. Stability of the dosing formulations for 7 days under refrigeration

Time (Day)	Concentrations of dosing formulation (mg/mL)	[1)]Actual concentrations of Acetylshikonin (mg/mL)	Measured concentration (mg/mL)			Mean (mg/mL)	SD	CV (%)	Accuracy (%)	Variation (%)
			No.1	No.2	No.3					
0	10	2.334	2.419	2.419	2.386	2.408	0.019	0.79	103.17	-
	400	93.36	92.58	93.32	88.81	91.57	2.42	2.64	98.08	-
7	10	2.334	2.168	2.159	2.170	2.166	0.006	0.28	92.80	-10.05
	400	93.36	80.19	84.46	88.92	84.52	4.37	5.17	90.53	-7.70

[1)]Actual concentrations of Acetylshikonin = Concentrations of dosing formulation × Acetylshikonin of content (23.34%)

Table 9. Accuracy and precision of QC sample

(A) Day 0

Concentration of QC sample (μg/mL)	Measured concentration (μg/mL)			Mean (μg/mL)	SD	CV (%)	Accuracy (%)
	No.1	No.2	No.3				
20	19.40	19.21	19.20	19.27	0.11	0.57	96.35

(B) Day 7

Concentration of QC sample (μg/mL)	Measured concentration (μg/mL)			Mean (μg/mL)	SD	CV (%)	Accuracy (%)
	No.1	No.2	No.3				
20	20.35	20.43	20.35	20.38	0.05	0.25	101.90

<자초추출물의 랫드를 이용한 단회 경구투여 독성시험>

Table 1. Summary of Mortality

Sex	Group / Dose (mg/kg)	No. of animals	Days after dosing															Mortality (dead/total)
			0	1	2	3	4	5	6	7	8	9	10	11	12	13	14	
Male	G1 0	5	0	0	0	0	0	0	0	0	0	0	0	0	0	0	0	0% (0/5)
	G2 500	5	0	0	0	0	0	0	0	0	0	0	0	0	0	0	0	0% (0/5)
	G3 1,000	5	0	0	0	0	0	0	0	0	0	0	0	0	0	0	0	0% (0/5)
	G4 2,000	5	0	0	0	0	0	0	0	0	0	0	0	0	0	0	0	0% (0/5)
Female	G1 0	5	0	0	0	0	0	0	0	0	0	0	0	0	0	0	0	0% (0/5)
	G2 500	5	0	0	0	0	0	0	0	0	0	0	0	0	0	0	0	0% (0/5)
	G3 1,000	5	0	0	0	0	0	0	0	0	0	0	0	0	0	0	0	0% (0/5)
	G4 2,000	5	0	0	0	0	0	0	0	0	0	0	0	0	0	0	0	0% (0/5)

Table 2. Summary of Clinical Signs

Sex	Group / Dose (mg/kg)	No. of animals	Clinical signs	Hours (Day 0) after dosing				
				0.5	1	2	4	6
Male	G1 0	5	NOA	5	5	5	5	5
	G2 500	5	NOA	5	5	5	3	4
			Mucous stool (black)				2	
			Soft stool (black)				2	
			Soiled perineal region				1	1
	G3 1,000	5	NOA	5	5	3	4	4
			Diarrhea (black)			2	1	
			Soft stool (black)			2		1
			Soiled perineal region			2	1	
			Mucous stool (black)				1	1
	G4 2,000	5	NOA	2	5	1	2	3
			Salivation	3				
			Soft stool (black)			4		2
			Soiled perineal region			3	3	
			Mucous stool (black)				1	2
Female	G1 0	5	NOA	5	5	5	3	5
			Mucous stool				2	
	G2 500	5	NOA	5	5	4	5	5
			Diarrhea (black)			1		
	G3 1,000	5	NOA	5	5	3	3	3
			Diarrhea (black)			2		
			Soft stool (black)			2		2
			Mucous stool (black)				2	2
			Soiled perineal region				1	
	G4 2,000	5	NOA	3	5	3	1	4
			Salivation	2				
			Soft stool (black)			2	1	1
			Soiled perineal region			2	2	
			Diarrhea (black)			2		
			Mucous stool (black)				3	1

NOA: No Observable Abnormality

Table 2. (Continued)

Sex	Group / Dose (mg/kg)	No. of animals	Clinical signs	Days after dosing													
				1	2	3	4	5	6	7	8	9	10	11	12	13	14
Male	G1 0	5	NOA	5	5	5	5	5	5	5	5	5	5	5	5	5	5
	G2 500	5	NOA				4	5	5	5	5	5	5	5	5	5	5
			Compound-colored stool (black)	5	5	5	1										
			Soft stool (black)	1													
			Decrease of fecal volume	2													
	G3 1,000	5	NOA					4	5	5	5	5	5	5	5	5	5
			Compound-colored stool (black)	5	5	5	5	1									
			Diarrhea (black)	3													
			Soft stool (black)	1	1												
			Soiled perineal region	3	1												
			Chromaturia (color of the test substance)		2	1											
	G4 2,000	5	NOA						4	5	5	5	5	5	5	5	5
			Compound-colored stool (black)	4	5	5	5	5	1								
			Diarrhea (black)	5	1												
			Soft stool (black)	5													
			Soiled perineal region	4	4	1											
			Decrease in food intake		1												
			Chromaturia (color of the test substance)		5	5											
			Decrease of fecal volume		1												

NOA: No Observable Abnormality

Table 2. (Continued)

Sex	Group / Dose (mg/kg)	No. of animals	Clinical signs	Days after dosing													
				1	2	3	4	5	6	7	8	9	10	11	12	13	14
Female	G1 0	5	NOA	5	5	5	5	5	5	5	5	5	5	5	5	5	5
	G2 500	5	NOA				5	5	5	5	5	5	5	5	5	5	5
			Compound-colored stool (black)	4	5	5											
			Diarrhea (black)	2													
			Soiled perineal region	2													
	G3 1,000	5	NOA				1	5	5	5	5	5	5	5	5	5	5
			Compound-colored stool (black)	5	5	5	4										
			Diarrhea (black)	2													
			Chromaturia (color of the test substance)		1												
	G4 2,000	5	NOA						2	5	5	5	5	5	5	5	5
			Compound-colored stool (black)	4	5	5	5	5	3								
			Diarrhea (black)	3	1												
			Soiled perineal region	3	3												
			Soft stool (black)		1												
			Decrease of fecal volume		1												
			Chromaturia (color of the test substance)			1											

NOA: No Observable Abnormality

Table 3. Mean Body Weights

(g)

Sex	Group / Dose (mg/kg)		Days after dosing 0	1	3	7	14	Gain 0 ~ 14
Male	G1	Mean	163.1	183.5	207.8	247.2	312.5	149.4
	0	S.D.	4.9	4.5	4.3	7.1	17.2	19.5
		N	5	5	5	5	5	5
	G2	Mean	163.4	167.2 **	183.5 **	231.4 *	307.0	143.7
	500	S.D.	4.0	6.6	2.8	5.8	13.2	11.0
		N	5	5	5	5	5	5
	G3	Mean	162.3	164.7 **	171.9 **	216.2 **	287.5	125.2
	1,000	S.D.	5.4	7.7	9.4	9.2	15.2	12.7
		N	5	5	5	5	5	5
	G4	Mean	163.0	160.0 **	162.2 **	209.2 **	284.4 *	121.4
	2,000	S.D.	5.4	7.4	7.7	10.3	17.5	17.1
		N	5	5	5	5	5	5
Female	G1	Mean	143.9	159.5	170.0	186.4	214.3	70.4
	0	S.D.	1.7	0.8	4.2	7.3	12.5	11.8
		N	5	5	5	5	5	5
	G2	Mean	142.8	150.9 *	163.6	182.8	211.0	68.1
	500	S.D.	5.0	6.4	5.0	12.9	13.1	11.6
		N	5	5	5	5	5	5
	G3	Mean	141.8	145.1 *	155.7 **	182.6	213.6	71.9
	1,000	S.D.	3.9	2.4	6.7	6.0	9.5	8.5
		N	5	5	5	5	5	5
	G4	Mean	141.5	141.7 *	147.3 **	175.8	206.2	64.7
	2,000	S.D.	6.5	7.5	6.1	10.5	11.0	5.0
		N	5	5	5	5	5	5

Significantly different from control by Dunnett's t-test: * $p<0.05$, ** $p<0.01$.

<자초추출물의 랫드를 이용한 2주반복 경구투여 및 용량결정(DRF)시험>

Table 1. Summary of clinical signs

Sex: Male

Group / Dose (mg/kg)	No. of animals	Clinical sign	No. of animals affected
G2	5	Compound-colored stool (black)	5
100		Salivation (after dosing)	4
		Salivation (before dosing)	2
		Piloerection	1
G3	5	Compound-colored stool (black)	5
300		Piloerection	4
		Salivation (after dosing)	4
		Compound-colored stool (violet)	2
		Abdominal distention	1
		Chromaturia (pale brown)	1
		Coloring of fur (tail)	1
		Salivation (before dosing)	1
		Decrease in food intake	1
		Decrease in locomotor activity	1
		Decrease of fecal volume	1
		Mucous stool	1
		Dyspnea	1
		Hypothermia	1
		Irregular respiration	1
		Dorsal position	1
		Death	1
G4	5	Chromaturia (pale brown)	5
1,000		Compound-colored stool (black)	5
		Compound-colored stool (red)	5
		Irregular respiration	5
		Mucous stool	5
		Piloerection	5
		Salivation (after dosing)	5
		Salivation (before dosing)	5
		Coloring of fur (anogenital region)	4
		Coloring of fur (tail)	4
		Coloring of fur (whole body)	3
		Coloring of fur (foot pad, hindlimb)	2
		Staining around mouth	2
		Abdominal distention	1
		Coloring of fur (abdomen)	1
		Coloring of fur (foot pad, forelimb)	1
		Decrease in food intake	1
		Decrease of fecal volume	1
		Dyspnea	1
		Hypothermia	1

Table 1. (Continued)

Sex: Female

Group / Dose (mg/kg)	No. of animals	Clinical sign	No. of animals affected
G2	5	Compound-colored stool (black)	5
100		Salivation (after dosing)	3
		Salivation (before dosing)	1
		Piloerection	1
G3	5	Chromaturia (pale brown)	1
300		Compound-colored stool (violet)	1
		Compound-colored stool (black)	5
		Mucous stool	1
		Piloerection	1
		Salivation (after dosing)	5
		Salivation (before dosing)	3
G4	5	Abdominal distention	1
1,000		Chromaturia (pale brown)	5
		Coloring of fur (anogenital region)	5
		Coloring of fur (face)	1
		Coloring of fur (foot pad, forelimb)	1
		Coloring of fur (tail)	2
		Coloring of fur (whole body)	1
		Compound-colored stool (red)	5
		Compound-colored stool (violet)	1
		Compound-colored stool (black)	5
		Decrease in food intake	2
		Decrease in locomotor activity	1
		Decrease of fecal volume	2
		Dyspnea	2
		Hypothermia	2
		Irregular respiration	5
		Lying on side	2
		Mucous stool	5
		Piloerection	5
		Salivation (after dosing)	5
		Salivation (before dosing)	3
		Staining around mouth	1
		Crawing position	1
		Death	2

Table 1. (Continued)

Sex: Male

Group / Dose (mg/kg)	No. of animals	Clinical sign	Day													
			1	2	3	4	5	6	7	8	9	10	11	12	13	14
G1 0	5	NOA	5	5	5	5	5	5	5	5	5	5	5	5	5	5
G2 100	5	NOA	5													
		Compound-colored stool (black)		5	5	5	5	5	5	5	5	5	5	5	5	5
		Salivation (after dosing)					1					1	4	1	1	3
		Salivation (before dosing)							1			1				
		Piloerection											1	1	1	
G3 300	5	NOA	5													
		Compound-colored stool (black)		5	5	5	5	5	5	5	5	5	5	5	5	5
		Compound-colored stool (violet)				2										
		Salivation (after dosing)					2	1	1		1	1	2	2	3	3
		Irregular respiration					1	1					1			
		Hypothermia					1									
		Decrease in locomotor activity					1									
		Decrease in food intake							1	1				1	1	1
		Dyspnea							1					1	1	
		Decrease fecal volume							1	1				1	1	1
		Chromaturia (pale brown)							1	1				1	1	1
		Piloerection								1	1	1	2	4	2	1
		Abdominal distention												1	1	
		Salivation (before dosing)													1	1
		Mucous stool													1	
		Coloring of fur (tail)													1	
		Dorsal position														1
		Death														1
G4 1,000	5	NOA	5													
		Chromaturia (pale brown)		4	5	4	4	3	1	1	1	1	1	2	3	2
		Compound-colored stool (black)		5	5	5	5	5	5	5	5	5	5	5	5	5
		Irregular respiration		2	2	2	2	2	1	1	3	2	3	4	2	1
		Salivation (after dosing)		4	4	5	4	5	5	4	5	5	5	5	4	4
		Compound-colored stool (red)			5	5	1	1								
		Mucous stool			5	4	1	1	1			1	1		1	
		Coloring of fur (whole body)			3	3	3	3		1	1	1	1	1	1	1
		Coloring of fur (anogenital region)			1	2	2	1	3	2	3	2	1	2	1	1
		Coloring of fur (tail)				2	2	2	4	4	4	3	3	4	4	4
		Piloerection					1	2	3	3	3	4	4	5	4	4
		Staining around mouth					2									
		Coloring of fur (foot pad, forelimb)					1									
		Coloring of fur (foot pad, hindlimb)					1		1	1						
		Salivation (before dosing)							2	2	3	2	2	3	2	1
		Coloring of fur (abdomen)							1							
		Decrease in food intake								1	1	1			1	
		Dyspnea								1		1				
		Hypothermia								1	1	1	1	1	1	1
		Decrease fecal volume								1	1	1	1		1	
		Abdominal distention													1	1

NOA: No Observable Abnormality

Table 1. (Continued)

Sex: Female

Group / Dose (mg/kg)	No. of animals	Clinical sign	Day													
			1	2	3	4	5	6	7	8	9	10	11	12	13	14
G1 0	5	NOA	5	5	5	5	5	5	5	5	5	5	5	5	5	5
G2 100	5	NOA	5													
		Compound-colored stool (black)		5	5	5	5	5	5	5	5	5	5	5	5	5
		Salivation (after dosing)					3	1					2	2	1	2
		Salivation (before dosing)									1		1	1	1	1
		Piloerection												1		
G3 300	5	NOA	5													
		Compound-colored stool (black)		5	5	5	5	5	5	5	5	5	5	5	5	5
		Mucous stool				1		1								
		Compound-colored stool (violet)				1										
		Salivation (after dosing)					1	1			1	1	5	1	2	3
		Chromaturia (pale brown)					1									
		Salivation (before dosing)							1	2	2	1	1	1	2	1
		Piloerection													1	
G4 1,000	5	NOA	5													
		Compound-colored stool (black)		5	5	4	5	5	5	5	5	5	5	3	3	3
		Chromaturia (pale brown)		2	5	5		1		1			1		1	1
		Irregular respiration		2		1	2	2	1	1		2		2		
		Salivation (after dosing)		2		5	2	4	3	4	4	4	3	3	3	3
		Coloring of fur (anogenital region)			4	4	3	3	2	2	2	2	2	2	1	1
		Compound-colored stool (red)			5	5	1			1						
		Mucous stool			4	3	1	1		1	1					
		Coloring of fur (tail)				1	2	1	1	1	1	1	1	1	2	2
		Coloring of fur (face)				1										
		Piloerection					2	2	3	3	3	3	4	1	2	1
		Staining around mouth					1									
		Coloring of fur (foot pad, forelimb)					1									
		Coloring of fur (whole body)						1	1	1		1				
		Compound-colored stool (violet)						1								
		Salivation (before dosing)							1	2	1				1	1
		Dyspnea							1	1	1		1			
		Decrease in food intake								1			2			
		Decrease in locomotor activity								1						
		Hypothermia								1	1	1	1			
		Decrease fecal volume								1	1		2			
		Abdominal distention											1			
		Lying on side											2			
		Crawing position											1			
		Death											2			

NOA: No Observable Abnormality

Table 2. Mean Body Weights

Sex: Male						(g)
Group / Dose (mg/kg)		Day 1	4	8	11	14
G1 0	Mean	203.4	231.7	268.4	297.3	323.6
	S.D.	6.1	10.8	12.9	17.6	21.0
	N	5	5	5	5	5
G2 100	Mean	202.3	227.7	263.5	293.5	320.9
	S.D.	6.8	6.7	9.9	9.2	14.7
	N	5	5	5	5	5
G3 300	Mean	202.7	206.8	230.5 **	252.0 *	292.5
	S.D.	7.8	9.9	31.3	37.8	15.5
	N	5	5	5	5	4
G4 1,000	Mean	201.4	182.5 **	195.8 **	207.7 **	225.3 *
	S.D.	8.0	5.8	19.6	35.5	53.0
	N	5	5	5	5	5

Sex: Female						(g)
Group / Dose (mg/kg)		Day 1	4	8	11	14
G1 0	Mean	152.5	166.1	180.4	188.9	199.6
	S.D.	5.6	5.2	4.1	6.5	9.3
	N	5	5	5	5	5
G2 100	Mean	155.9	162.2	178.0	190.5	200.6
	S.D.	10.0	9.9	9.6	11.1	12.2
	N	5	5	5	5	5
G3 300	Mean	151.8	154.9 *	171.5	180.7	189.9
	S.D.	3.5	4.2	6.2	7.6	8.9
	N	5	5	5	5	5
G4 1,000	Mean	151.3	142.7 **	144.8 *	145.7 **	176.5 *
	S.D.	1.6	6.0	18.2	23.5	8.9
	N	5	5	5	5	3

Significantly different from control by Dunnett's t-test: * $p<0.05$, ** $p<0.01$.

Table 3. Mean Food Consumption

Sex: Male				(g/day)
Group / Dose (mg/kg)		Week 0	1	2
G1 0	Mean	27.5	27.1	29.0
	S.D.	2.2	2.3	3.1
	N	5	5	5
G2 100	Mean	28.6	26.4	31.8
	S.D.	1.6	1.3	5.0
	N	5	5	5
G3 300	Mean	29.5	20.6 **	30.1
	S.D.	1.6	4.9	3.8
	N	5	5	4
G4 1,000	Mean	30.5	14.6 **	21.9
	S.D.	3.7	2.0	7.5
	N	5	5	5

Sex: Female				(g/day)
Group / Dose (mg/kg)		Week 0	1	2
G1 0	Mean	20.3	19.7	20.7
	S.D.	2.6	0.8	3.1
	N	5	5	5
G2 100	Mean	21.6	18.1	20.2
	S.D.	1.9	1.7	1.8
	N	5	5	5
G3 300	Mean	19.3	16.6 *	21.4
	S.D.	1.3	1.4	5.0
	N	5	5	5
G4 1,000	Mean	19.4	11.7 **	18.6
	S.D.	2.4	1.8	5.7
	N	5	5	3

Significantly different from control by Dunnett's t-test: * $p<0.05$, ** $p<0.01$.

<자초추출물의 랫드를 이용한 4주 반복 경구투여 독성시험 및 2주 회복시험>

Table 1-1. Summary of Clinical Signs (Dosing period)

Sex: Male

Group / Dose (mg/kg/day)	No. of animals	Clinical sign	Day													
			1	2	3	4	5	6	7	8	9	10	11	12	13	14
G1	15	NOA	15	15	15	15	15	15	15	15	15	15	15	15	15	15
0																
G2	10	NOA	10	1	4	1	5	5	5	6	4	2	2	2	3	3
25		Compound-colored stool (black)		9	5	8	4	4	4	3	5	7	7	7	6	6
		Death			1											
		Lying on side			1											
G3	10	NOA	10													
100		Compound-colored stool (black)		10	10	10	10	10	10	10	10	10	10	10	10	10
G4	15	NOA	15													
400		Compound-colored stool (black)		15	15	15	15	15	15	15	15	15	15	15	15	15
		Irregular respiration		2	2	2	1									
		Salivation (after dosing)			7	6	1	1			1	6	6	6	5	8
		Salivation (before dosing)										3	1	2	2	5

Group / Dose (mg/kg/day)	No. of animals	Clinical sign	Day													
			15	16	17	18	19	20	21	22	23	24	25	26	27	28
G1	15	NOA	15	15	15	15	15	15	15	15	15	15	15	15	15	15
0																
G2	9	NOA	4	4	4	2	3	3	3	3	2	3	4	4	4	4
25		Compound-colored stool (black)	5	5	5	7	6	6	6	6	7	6	5	5	5	5
G3	10	Compound-colored stool (black)	10	10	10	10	10	10	10	10	10	10	10	10	10	10
100		Salivation (after dosing)			4	3	2	3	3	3	2	2	1	1	1	1
		Salivation (before dosing)			1					1	1	2	2	2	2	2
G4	10	Compound-colored stool (black)	15	15	15	15	15	15	15	15	15	15	15	15	15	15
400		Salivation (after dosing)	8	7	5	8	8	9	9	7	8	8	8	8	8	8
		Salivation (before dosing)	5	5	3	5	5	6	6	3	4	4	5	5	5	5
		Chromaturia (pale brown)												1	1	3

NOA: No Observable Abnormality

Table 1-1. (Continued)

Sex: Female

Group / Dose (mg/kg/day)	No. of animals	Clinical sign	Day													
			1	2	3	4	5	6	7	8	9	10	11	12	13	14
G1	15	NOA	15	15	15	15	15	15	15	15	15	15	15	15	15	15
0																
G2	10	NOA	10	2	2	2	2				3	2	2	2	2	2
25		Compound-colored stool (black)		8	8	8	8	10	10	10	7	8	8	8	8	8
G3	10	NOA	10													
100		Compound-colored stool (black)		10	10	10	10	10	10	10	10	10	10	10	10	10
G4	10	NOA	15													
400		Compound-colored stool (black)		15	15	15	15	15	15	15	15	15	15	15	15	15
		Irregular respiration		4	4											
		Salivation (after dosing)		5	5	1	1	1	2	3	7	6	5	5	4	4
		Salivation (before dosing)									5	4	4	3	2	2

Group / Dose (mg/kg/day)	No. of animals	Clinical sign	Day													
			15	16	17	18	19	20	21	22	23	24	25	26	27	28
G1	15	NOA	15	15	15	15	15	15	15	15	15	15	15	15	15	15
0																
G2	10	NOA	4	2	3	3	3	3	5	5	2	4	4	5	5	5
25		Compound-colored stool (black)	6	8	7	7	7	7	5	5	8	6	6	5	5	5
G3	10	Compound-colored stool (black)	10	10	10	10	10	10	10	10	10	10	10	10	10	10
100		Salivation (before dosing)		1	1					1						
		Salivation (after dosing)								1						
G4	10	Compound-colored stool (black)	15	15	15	15	15	15	15	15	15	15	15	15	15	15
400		Salivation (after dosing)	4	2	4	3	3	3	3	1				1	1	1
		Salivation (before dosing)	1	2	2	2	2	2	2	2		2	2	3	3	2
		Chromaturia (pale brown)											1	1	5	5

NOA: No Observable Abnormality

Table 1-2. Summary of Clinical Signs (Recovery period)

Sex: Male

Group / Dose (mg/kg/day)	No. of animals	Clinical sign	Day													
			29	30	31	32	33	34	35	36	37	38	39	40	41	42
G1	5	NOA	5	5	5	5	5	5	5	5	5	5	5	5	5	5
0																
G4	5	Compound-colored stool (black)	5	5	2											
400		NOA			3	5	5	5	5	5	5	5	5	5	5	5

Sex: Female

Group / Dose (mg/kg/day)	No. of animals	Clinical sign	Day													
			29	30	31	32	33	34	35	36	37	38	39	40	41	42
G1	5	NOA	5	5	5	5	5	5	5	5	5	5	5	5	5	5
0																
G4	5	Compound-colored stool (black)	5	5												
400		NOA			5	5	5	5	5	5	5	5	5	5	5	5

NOA: No Observable Abnormality

Table 2. Mean Body weights

Sex Male (g)

Group / Dose (mg/kg/day)		Week							
		Dosing period					Recovery period		
		0	1	2	3	4	4	5	6
G1	Mean	203.7	269.5	331.0	380.9	410.8	422.0	466.1	484.3
0	S.D.	4.9	7.8	11.5	17.2	22.7	19.4	24.5	24.5
	N	15	15	15	15	15	5	5	5
G2	Mean	202.8	261.8	317.6	363.6	394.9			
25	S.D.	4.7	13.5	24.5	32.7	40.2			
	N	10	9	9	9	9			
G3	Mean	202.0	265.4	324.6	367.3	403.4			
100	S.D.	4.8	8.9	18.1	26.8	30.5			
	N	10	10	10	10	10			
G4	Mean	203.4	239.6 ##	298.5 **	342.1 **	369.8 **	367.2 ^^	416.7 ^	442.4 ^
400	S.D.	6.7	18.8	14.3	21.6	23.1	21.5	24.2	26.0
	N	15	15	15	15	15	5	5	5

Sex Female (g)

Group / Dose (mg/kg/day)		Week							
		Dosing period					Recovery period		
		0	1	2	3	4	4	5	6
G1	Mean	164.0	187.0	205.8	224.7	232.6	238.3	253.6	262.3
0	S.D.	5.5	10.0	15.2	17.4	20.6	24.9	32.7	26.2
	N	15	15	15	15	15	5	5	5
G2	Mean	163.4	189.8	215.0	233.0	244.0			
25	S.D.	5.0	6.2	6.2	7.6	8.2			
	N	10	10	10	10	10			
G3	Mean	165.3	188.5	203.9	225.0	237.8			
100	S.D.	5.8	10.2	17.9	22.3	26.8			
	N	10	10	10	10	10			
G4	Mean	164.2	185.5	211.1	230.6	243.7	251.5	261.2	267.6
400	S.D.	4.7	6.9	11.7	15.2	17.6	21.8	26.9	26.0
	N	15	15	15	15	15	5	5	5

Significantly different from control by Dunnett's t-test: ** $p<0.01$.
Significantly different from control by Steel test: ## $p<0.01$.
Significantly different from control by Student t-test: ^ $p<0.05$, ^^ $p<0.01$.

Table 3. Mean Food Consumption

Sex Male (g/day)

Group / Dose (mg/kg/day)		Week 0	1	2	3	4	5	6
		Dosing period					Recovery period	
G1 0	Mean	27.9	28.4	31.5	32.5	31.9	35.5	35.1
	S.D.	1.8	1.9	2.2	2.2	2.9	2.5	2.8
	N	15	15	15	15	15	5	5
G2 25	Mean	27.4	27.0	28.2 *	29.0 *	28.8		
	S.D.	1.3	1.9	3.3	3.2	3.4		
	N	10	9	9	9	9		
G3 100	Mean	27.2	27.0	29.4	29.8	30.1		
	S.D.	2.0	1.5	2.2	3.1	2.6		
	N	10	10	10	10	10		
G4 400	Mean	27.5	21.9 ##	29.2	32.4	31.1	33.0	33.1
	S.D.	2.1	3.7	2.6	3.9	3.8	1.9	1.5
	N	15	15	15	15	15	5	5

Sex Female (g/day)

Group / Dose (mg/kg/day)		Week 0	1	2	3	4	5	6
		Dosing period					Recovery period	
G1 0	Mean	20.8	18.8	20.0	20.4	20.2	23.9	22.2
	S.D.	2.6	1.8	2.3	2.3	2.8	4.4	2.7
	N	15	15	15	15	15	5	5
G2 25	Mean	20.0	19.0	20.2	20.2	20.4		
	S.D.	2.7	1.1	1.2	1.4	1.4		
	N	10	10	10	10	10		
G3 100	Mean	20.4	17.6	18.5	20.5	20.8		
	S.D.	1.9	2.0	2.4	4.7	5.2		
	N	10	10	10	10	10		
G4 400	Mean	20.1	16.8 **	20.7	21.5	22.1	24.9	23.6
	S.D.	2.4	1.6	2.3	2.9	2.4	4.0	3.3
	N	15	15	15	15	15	5	5

Significantly different from control by Dunnett's t-test: *p<0.05, ** p<0.01.
Significantly different from control by Steel test: ## p<0.01.

Table 4-1. Summary of Ophthalmological Examination (Main group)

Sex Male

Group / Dose (mg/kg/day)	No. of animals	Findings	Right eye: Pupil light reflex	Right eye: Anterior segment	Right eye: Trans-parent media	Right eye: Fundus	Left eye: Pupil light reflex	Left eye: Anterior segment	Left eye: Trans-parent media	Left eye: Fundus
G1 0	5	Normal	5	5	5	5	5	5	5	5
G2 25	5	Normal	5	5	5	5	5	5	5	5
G3 100	5	Normal	5	5	5	5	5	5	5	5
G4 400	5	Normal	5	5	5	5	5	5	5	5

Sex Female

Group / Dose (mg/kg/day)	No. of animals	Findings	Right eye: Pupil light reflex	Right eye: Anterior segment	Right eye: Trans-parent media	Right eye: Fundus	Left eye: Pupil light reflex	Left eye: Anterior segment	Left eye: Trans-parent media	Left eye: Fundus
G1 0	5	Normal	5	5	5	5	5	5	5	5
G2 25	5	Normal	5	5	5	5	5	5	5	5
G3 100	5	Normal	5	5	5	5	5	5	5	5
G4 400	5	Normal	5	5	5	5	5	5	5	5

Table 4-2. Summary of Ophthalmological Examination (Recovery group)

Sex Male

Group / Dose (mg/kg/day)	No. of animals	Findings	Right eye				Left eye			
			Pupil light reflex	Anterior segment	Trans-parent media	Fundus	Pupil light reflex	Anterior segment	Trans-parent media	Fundus
G1 0	5	Normal	5	5	5	5	5	5	5	5
G4 400	5	Normal	5	5	5	5	5	5	5	5

Sex Female

Group / Dose (mg/kg/day)	No. of animals	Findings	Right eye				Left eye			
			Pupil light reflex	Anterior segment	Trans-parent media	Fundus	Pupil light reflex	Anterior segment	Trans-parent media	Fundus
G1 0	5	Normal	5	5	5	5	5	5	5	5
G4 400	5	Normal	5	5	5	5	5	5	5	5

<자조추출물의 비글견을 이용한 단회 경구투여 용량증가 독성시험>

Table 1. Clinical Signs

Sex : male

Group /Dose (mg/kg)	Animal ID	Day																																		
		0*					1	2	3	4*					5	6	7	8*					9	10	11	12	13	14	15	16	17	18	19	20	21
		0.5 hr	1 hr	2 hr	4 hr	6 hr				0.5 hr	1 hr	2 hr	4 hr	6 hr				0.5 hr	1 hr	2 hr	4 hr	6 hr														
G1 0→0→0	1101	-	-	-	-	-	-	-	-	-	-	-	-	-	-	-	-	-	-	-	-	-	-	-	-	-	-	-	-	-	-	-	-	-	-	-
G2 500→1,000 →2,000	1201	-	-	C,D	C,D	-	-	-	-	-	-	C,D	-	C,D	C	-	-	C,D	-	C,D	C,D,V	-	C	-	-	-	-	-	-	-	-	-	-	-	-	-
	1202	-	-	-	C,D	-	C	-	-	V	C,D	-	-	C,D,V	C	-	-	-	C,D	C,D	C,D,V	-	C	-	-	-	-	-	-	-	-	-	-	-	-	-

Sex : female

Group /Dose (mg/kg)	Animal ID	Day																																		
		0*					1	2	3	4*					5	6	7	8*					9	10	11	12	13	14	15	16	17	18	19	20	21
		0.5 hr	1 hr	2 hr	4 hr	6 hr				0.5 hr	1 hr	2 hr	4 hr	6 hr				0.5 hr	1 hr	2 hr	4 hr	6 hr														
G1 0→0→0	2101	-	-	-	-	-	-	-	-	-	-	-	-	-	-	-	-	-	-	-	-	-	-	-	-	-	-	-	-	-	-	-	-	-	-	-
G2 500→1,000 →2,000	2201	C,D	-	-	C,D	C,D	-	-	-	-	-	-	C,D	-	C	-	-	C,D	-	C,D	C,D	-	C	-	-	-	-	-	-	-	-	-	-	-	-	-
	2202	-	C,D	-	C,D	C,D	-	-	-	-	-	-	C,D	-	C	-	-	V	-	-	-	C,D	C,D	-	-	-	-	-	-	-	-	-	-	-	-	-

*: dosing day -: no abnormal findings, C: compound colored stool, D: diarrhea, V: vomiting

Table 2. Body Weights

Sex : male

Group /Dose (mg/kg)	Animal ID	Day (kg)										
		0*	1	3	4*	5	7	8*	9	11	15	21
G1	1101	7.20	7.05	7.25	7.16	7.22	7.21	7.21	7.12	7.22	7.38	7.24
0→0→0	N	1	1	1	1	1	1	1	1	1	1	1
G2	1201	7.98	8.00	8.03	8.11	8.19	8.09	8.13	8.13	8.16	8.35	8.36
500→1,000	1202	8.08	7.93	8.01	7.93	8.11	8.29	8.29	8.27	8.33	8.54	8.76
→2,000	Mean	8.03	7.97	8.02	8.02	8.15	8.19	8.21	8.20	8.25	8.45	8.56
	S.D.	0.07	0.05	0.01	0.13	0.06	0.14	0.11	0.10	0.12	0.13	0.28
	N	2	2	2	2	2	2	2	2	2	2	2

Sex : female

Group /Dose (mg/kg)	Animal ID	Day (kg)										
		0*	1	3	4*	5	7	8*	9	11	15	21
G1	2101	6.34	6.26	6.19	6.35	6.47	6.34	6.33	6.41	6.59	6.53	6.70
0→0→0	N	1	1	1	1	1	1	1	1	1	1	1
G2	2201	7.24	7.23	7.20	7.14	7.37	7.26	7.33	7.54	7.40	7.50	7.65
500→1,000	2202	6.82	6.84	6.80	6.76	6.96	6.75	6.78	6.97	6.76	6.84	6.92
→2,000	Mean	7.03	7.04	7.00	6.95	7.17	7.01	7.06	7.26	7.08	7.17	7.29
	S.D.	0.30	0.28	0.28	0.27	0.29	0.36	0.39	0.40	0.45	0.47	0.52
	N	2	2	2	2	2	2	2	2	2	2	2

* : dosing day.

Table 3. Necropsy Findings

Sex	Group / Dose (mg/kg)	Animal ID	Organ	Findings	Day of sacrifice
Male	G1 0→0→0	1101	All	Unremarkable findings	22
	G2 500→1,000→2,000	1201	All	Unremarkable findings	22
		1202	All	Unremarkable findings	22
Female	G1 0→0→0	2101	All	Unremarkable findings	22
	G2 500→1,000→2,000	2201	All	Unremarkable findings	22
		2202	All	Unremarkable findings	22

<자초추출물의 비글견을 이용한 2주 반복 경구투여 용량결정시험>

Table 1. Clinical Signs

Sex : Male

Group /Dose (mg/kg)	Animal ID	Clinicla sign	Day of dosing													
			0	1	2	3	4	5	6	7	8	9	10	11	12	13
G1	1101		-	-	-	-	-	-	-	-	-	-	-	-	-	-
0	1102		-	-	-	-	-	-	-	-	-	-	-	-	-	-
G2	1201	Compound colored stool	+	+	+	-	+	+	+	+	+	+	+	+	+	+
100		Diarrhea	+	+	+	-	+	-	-	+	+	-	+	-	+	+
		Soft stool	-	-	-	-	+	+	+	-	-	-	-	-	-	+
		Vomiting	-	-	-	-	+	-	-	-	+	-	-	+	-	+
	1202	Compound colored stool	+	+	+	+	+	+	+	+	+	+	+	+	+	+
		Diarrhea	+	-	-	-	+	-	-	+	+	+	+	-	-	+
		Soft stool	-	+	+	-	-	-	-	-	-	-	-	-	+	-
		Vomiting	+	-	-	-	+	-	-	+	-	-	-	+	-	-
G3	1301	Compound colored stool	+	+	+	+	-	+	+	+	+	+	+	+	-	+
300		Diarrhea	+	+	+	+	-	+	-	+	+	+	-	+	-	+
		Soft stool	-	-	+	-	-	+	+	+	-	-	-	+	-	-
		Vomiting	-	-	-	-	-	-	-	+	-	-	+	-	+	-
	1302	Compound colored stool	-	+	+	+	+	+	+	+	+	+	+	+	+	+
		Diarrhea	-	-	+	+	+	+	+	+	+	+	+	+	-	+
		Soft stool	-	+	-	-	-	+	-	+	-	-	-	-	+	-
		Vomiting	-	-	-	-	-	-	-	-	-	-	+	-	-	-
G4	1401	Compound colored stool	+	+	+	+	+	+	+	+	+	-	+	+	+	+
500		Diarrhea	+	+	+	+	+	+	+	-	-	-	-	+	+	+
		Salivation	-	-	-	-	-	+	-	-	-	-	+	+	+	+
		Soft stool	-	+	-	-	-	-	-	+	+	-	-	-	-	-
		Vomiting	+	+	-	+	-	-	-	+	-	+	+	-	-	-
	1402	Compound colored stool	+	-	+	+	+	+	+	+	+	-	+	+	+	+
		Diarrhea	+	-	+	+	+	+	+	-	+	-	+	+	-	-
		Salivation	-	-	+	+	+	+	+	+	+	+	+	+	+	+
		Soft stool	-	-	+	-	-	-	-	+	-	-	-	+	+	-
		Vomiting	+	+	+	+	-	-	+	-	-	-	-	-	+	-

- : No observable abnormality, + : Observable abnormality.

Table 1. (continued)

Sex : Female

Group /Dose (mg/kg)	Animal ID	Clinicla sign	Day of dosing													
			0	1	2	3	4	5	6	7	8	9	10	11	12	13
G1	2101		-	-	-	-	-	-	-	-	-	-	-	-	-	-
0	2102		-	-	-	-	-	-	-	-	-	-	-	-	-	-
G2	2201	Compound colored stool	+	+	+	+	+	+	+	+	-	+	+	+	+	+
100		Diarrhea	+	-	+	+	+	+	-	-	-	+	+	-	-	-
		Soft stool	-	+	-	-	-	+	+	-	-	-	-	+	+	+
		Vomiting	-	+	-	-	-	-	-	-	+	+	+	+	-	-
	2202	Compound colored stool	+	+	+	-	+	+	+	+	+	-	+	+	+	+
		Diarrhea	-	+	+	-	+	-	+	+	+	-	+	+	+	+
		Soft stool	-	+	-	-	-	+	-	+	-	-	-	-	-	-
		Vomiting	+	-	-	+	-	-	-	-	-	-	-	-	-	-
G3	2301	Compound colored stool	+	+	+	+	+	+	+	+	+	+	+	+	+	+
300		Diarrhea	+	+	+	+	+	-	+	-	+	-	+	+	+	+
		Soft stool	-	-	-	-	-	+	-	-	-	-	-	+	-	-
		Vomiting	+	+	-	-	-	+	-	-	-	+	-	-	-	-
	2302	Compound colored stool	+	+	-	+	+	+	+	+	+	+	+	+	+	+
		Diarrhea	+	+	-	+	+	+	+	+	+	+	+	+	+	+
		Soft stool	-	-	-	-	-	+	-	-	-	-	-	-	-	-
		Vomiting	+	-	-	+	+	-	-	-	+	-	-	-	-	+
G4	2401	Compound colored stool	+	-	+	+	+	+	+	+	+	+	+	+	+	+
500		Diarrhea	+	-	+	-	+	-	+	-	+	+	+	-	+	+
		Salivation	-	-	-	-	-	+	+	+	+	+	+	+	+	+
		Soft stool	-	-	+	-	+	-	-	+	+	-	-	+	+	-
		Vomiting	+	-	-	-	-	-	-	-	-	-	-	-	-	+
	2402	Compound colored stool	+	+	+	+	+	+	+	+	+	+	+	+	+	+
		Diarrhea	+	+	+	+	+	+	-	+	+	+	+	+	+	+
		Soft stool	-	-	-	+	-	-	-	-	+	-	-	+	-	-
		Vomiting	+	+	-	-	+	-	+	+	-	-	-	-	-	-

- : No observable abnormality, + : Observable abnormality.

Table 2. Body Weights

Sex	Group /Dose (mg/kg)	Animal ID	Day (kg)				
			0	3	7	10	13
Male	G1	1101	6.00	5.99	6.10	6.24	6.40
	0	1102	6.37	6.51	6.66	6.84	6.94
		Mean	**6.19**	**6.25**	**6.38**	**6.54**	**6.67**
		S.D.	**0.26**	**0.37**	**0.40**	**0.42**	**0.38**
		N	2	2	2	2	2
	G2	1201	5.93	6.13	6.06	6.20	6.36
	100	1202	6.00	6.21	6.42	6.54	6.72
		Mean	**5.97**	**6.17**	**6.24**	**6.37**	**6.54**
		S.D.	**0.05**	**0.06**	**0.25**	**0.24**	**0.25**
		N	2	2	2	2	2
	G3	1301	6.00	6.21	6.14	6.48	6.39
	300	1302	6.15	6.35	6.41	6.42	6.40
		Mean	**6.08**	**6.28**	**6.28**	**6.45**	**6.40**
		S.D.	**0.11**	**0.10**	**0.19**	**0.04**	**0.01**
		N	2	2	2	2	2
	G4	1401	5.89	5.87	6.03	6.00	6.13
	500	1402	6.58	6.77	6.75	6.92	6.94
		Mean	**6.24**	**6.32**	**6.39**	**6.46**	**6.54**
		S.D.	**0.49**	**0.64**	**0.51**	**0.65**	**0.57**
		N	2	2	2	2	2
Female	G1	2101	5.09	5.09	5.31	5.49	5.51
	0	2102	5.73	5.86	6.00	6.04	6.10
		Mean	**5.41**	**5.48**	**5.66**	**5.77**	**5.81**
		S.D.	**0.45**	**0.54**	**0.49**	**0.39**	**0.42**
		N	2	2	2	2	2
	G2	2201	5.23	5.42	5.43	5.59	5.63
	100	2202	5.79	5.73	5.66	5.76	5.76
		Mean	**5.51**	**5.58**	**5.55**	**5.68**	**5.70**
		S.D.	**0.40**	**0.22**	**0.16**	**0.12**	**0.09**
		N	2	2	2	2	2
	G3	2301	5.42	5.46	5.42	5.46	5.61
	300	2302	5.44	5.49	5.43	5.43	5.59
		Mean	**5.43**	**5.48**	**5.43**	**5.45**	**5.60**
		S.D.	**0.01**	**0.02**	**0.01**	**0.02**	**0.01**
		N	2	2	2	2	2
	G4	2401	5.12	5.36	5.48	5.38	5.57
	500	2402	5.82	5.75	5.87	6.02	6.00
		Mean	**5.47**	**5.56**	**5.68**	**5.70**	**5.79**
		S.D.	**0.49**	**0.28**	**0.28**	**0.45**	**0.30**
		N	2	2	2	2	2

Table 3. Food Consumptions

Sex	Group /Dose (mg/kg)	Animal ID	Week (g/day)		
			0	1	2
Male	G1	1101	250	196	250
	0	1102	250	250	250
		Mean	**250**	**223**	**250**
		S.D.	**0**	**38**	**0**
		N	**2**	**2**	**2**
	G2	1201	250	111	209
	100	1202	250	215	250
		Mean	**250**	**163**	**230**
		S.D.	**0**	**74**	**29**
		N	**2**	**2**	**2**
	G3	1301	250	78	250
	300	1302	250	250	250
		Mean	**250**	**164**	**250**
		S.D.	**0**	**122**	**0**
		N	**2**	**2**	**2**
	G4	1401	235	250	250
	500	1402	250	250	250
		Mean	**243**	**250**	**250**
		S.D.	**11**	**0**	**0**
		N	**2**	**2**	**2**
Female	G1	2101	250	216	180
	0	2102	228	250	141
		Mean	**239**	**233**	**161**
		S.D.	**16**	**24**	**28**
		N	**2**	**2**	**2**
	G2	2201	231	193	219
	100	2202	250	109	164
		Mean	**241**	**151**	**192**
		S.D.	**13**	**59**	**39**
		N	**2**	**2**	**2**
	G3	2301	213	161	166
	300	2302	184	208	196
		Mean	**199**	**185**	**181**
		S.D.	**21**	**33**	**21**
		N	**2**	**2**	**2**
	G4	2401	250	222	170
	500	2402	250	250	250
		Mean	**250**	**236**	**210**
		S.D.	**0**	**20**	**57**
		N	**2**	**2**	**2**

Table 4-1. Urinalysis Result of Pre-dosing

Sex : Male

Group		G1		G2		G3		G4	
Dose (mg/kg)		0		100		300		500	
Animal ID		1101	1102	1201	1202	1301	1302	1401	1402
Color	Pale yellow		V						
	Yellow	V		V	V	V	V	V	V
Specific gravity	-	1.024	1.010	1.015	1.023	1.025	1.010	1.025	1.020
pH	5								
	6								
	6.5	V							
	7								
	8		V		V	V			
	9			V			V	V	V
Protein (mg/dL)	-	V	V	V	V	V	V	V	V
	25								
	75								
Glucose (mg/dL)	-	V	V	V	V	V	V	V	V
	50								
Ketone body (mg/dL)	-	V	V	V	V	V	V	V	V
	5								
	15								
Bilirubin (mg/dL)	-	V	V	V	V	V	V	V	V
	1								
	3								
Erythrocyte (Ery/μL)	-	V	V	V	V	V		V	V
	10								
	25								
	50								
	150								
	250						V		
Cast†	0	V	V	V	V	V	V	V	V
	1~5								
	6~10								
	>10								
Epithelia Cell†	0	V	V	V	V	V	V	V	V
	1~5								
	6~10								
	>10								

† : number of counts in 20 visual fields, 400×.

Table 4-1. (continued)

Sex : Female

Group		G1		G2		G3		G4	
Dose (mg/kg)		0		100		300		500	
Animal ID		2101	2102	2201	2202	2301	2302	2401	2402
Color	Pale yellow								
	Yellow	V	V	V	V	V	V	V	V
Specific gravity	-	1.016	1.025	1.019	1.022	1.019	1.025	1.026	1.018
pH	5								
	6			V					
	6.5	V							
	7							V	
	8				V				
	9		V			V	V		V
Protein (mg/dL)	-	V	V	V	V	V	V	V	V
	25								
	75								
Glucose (mg/dL)	-	V	V	V	V	V	V	V	V
	50								
Ketone body (mg/dL)	-	V	V	V	V	V	V	V	V
	5								
	15								
Bilirubin (mg/dL)	-	V	V	V	V	V	V	V	V
	1								
	3								
Erythrocyte (Ery/μL)	-		V	V	V	V	V	V	V
	10								
	25								
	50	V							
	150								
	250								
Cast†	0	V	V	V	V	V	V	V	V
	1~5								
	6~10								
	>10								
Epithelia Cell†	0	V	V	V	V	V	V	V	V
	1~5								
	6~10								
	>10								

† : number of counts in 20 visual fields, 400×.

Table 4-2. Urinalysis Result at Week 2 of Dosing

Sex : Male

Group		G1		G2		G3		G4	
Dose (mg/kg)		0		100		300		500	
Animal ID		1101	1102	1201	1202	1301	1302	1401	1402
Color	Pale yellow	V	V						
	Yellow			V	V	V	V	V	V
Specific gravity	-	1.013	1.010	1.019	1.022	1.022	1.020	1.035	1.047
pH	5								
	6				V				V
	6.5								
	7								
	8								
	9	V	V	V		V	V	V	
Protein (mg/dL)	-	V	V	V	V	V	V		
	25							V	V
	75								
Glucose (mg/dL)	-	V	V	V	V	V	V	V	V
	50								
Ketone body (mg/dL)	-	V	V	V	V	V	V	V	V
	5								
	15								
Bilirubin (mg/dL)	-	V	V	V	V	V	V	V	V
	1								
	3								
Erythrocyte (Ery/μL)	-	V	V	V	V	V	V	V	V
	10								
	25								
	50								
	150								
	250								
Cast†	0	V	V	V	V	V	V	V	V
	1~5								
	6~10								
	>10								
Epithelia Cell†	0	V	V	V	V	V	V	V	V
	1~5								
	6~10								
	>10								

† : number of counts in 20 visual fields, 400×.

Table 4-2. (continued)

Sex : Female

Group		G1		G2		G3		G4	
Dose (mg/kg)		0		100		300		500	
Animal ID		2101	2102	2201	2202	2301	2302	2401	2402
Color	Pale yellow								
	Yellow	V	V	V	V	V	V	V	V
Specific gravity	-	1.021	1.044	1.018	1.048	1.040	1.047	1.025	1.024
pH	5								
	6							V	
	6.5								
	7								
	8			V			V		
	9	V	V		V	V			V
Protein (mg/dL)	-	V	V						V
	25			V	V	V	V	V	
	75								
Glucose (mg/dL)	-	V	V	V	V	V	V	V	V
	50								
Ketone body (mg/dL)	-	V	V	V	V	V	V	V	V
	5								
	15								
Bilirubin (mg/dL)	-	V	V	V	V	V	V	V	V
	1								
	3								
Erythrocyte (Ery/μL)	-	V	V	V	V	V	V	V	V
	10								
	25								
	50								
	150								
	250								
Cast†	0	V	V	V	V	V	V	V	V
	1~5								
	6~10								
	>10								
Epithelia Cell†	0	V	V	V	V	V	V	V	V
	1~5								
	6~10								
	>10								

† : number of counts in 20 visual fields, 400×.

<자초추출물의 비글견을 이용한 4주 반복 경구투여 독성시험, 2주 회복시험 및 독성동태시험>

Table 1. Summary of Clinical Signs

Ses	Group /Dose (mg/kg/day)	Animal ID	Dosing for 4-week						Recovery for 2-week		
			Salivation	Compound-colored stool	Diarrhea	Mucous stool	Soft stool	Vomiting	Compound-colored stool	Diarrhea	Soft stool
Male	G1 0	1101	0	0	0	0	1	0			
		1102	0	0	0	0	3	0			
		1103	0	0	0	0	0	0			
		1104	0	0	1	0	3	0	0	0	0
		1105	0	0	0	0	4	0	0	0	0
	G2 30	1201	12	19	8	1	11	5			
		1202	0	18	18	0	6	10			
		1203	20	18	6	0	8	5			
	G3 100	1301	0	27	26	0	2	2			
		1302	16	27	23	0	3	4			
		1303	0	27	19	0	6	0			
	G4 300	1401	3	27	25	0	2	4			
		1402	23	28	23	0	3	6			
		1403	1	27	20	0	4	6			
		1404	3	24	11	0	8	13	1	0	1
		1405	8	25	12	1	8	2	0	0	0
Female	G1 0	2101	0	0	0	0	0	0			
		2102	0	0	0	0	2	0			
		2103	0	0	0	0	0	0			
		2104	0	0	1	0	1	0	0	0	0
		2105	0	0	0	0	0	0	0	0	0
	G2 30	2201	11	16	5	0	11	5			
		2202	0	13	3	0	7	8			
		2203	9	16	11	0	6	2			
	G3 100	2301	2	27	15	0	12	4			
		2302	1	22	16	0	4	9			
		2303	1	27	20	0	7	3			
	G4 300	2401	9	26	18	0	3	13			
		2402	14	28	17	0	8	2			
		2403	20	25	14	0	8	8			
		2404	16	26	19	0	5	9	1	1	0
		2405	0	27	20	0	4	3	1	0	1

Values are total number of days with findings.

Table 2. Mean Body Weights

Sex	Group /Dose (mg/kg/day)		Week of dosing (kg)					Week of recovery (kg)	
			0	1	2	3	4	5	6
Male	G1 0	Mean	8.21	8.46	8.66	8.92	9.09	9.24	9.39
		S.D.	0.25	0.25	0.26	0.35	0.31	0.49	0.47
		N	5	5	5	5	5	2	2
	G2 30	Mean	8.11	8.30	8.43	8.61	8.70		
		S.D.	0.22	0.20	0.25	0.25	0.20		
		N	3	3	3	3	3		
	G3 100	Mean	8.11	8.36	8.57	8.75	8.90		
		S.D.	0.39	0.40	0.44	0.55	0.61		
		N	3	3	3	3	3		
	G4 300	Mean	8.13	8.25	8.35	8.44	8.54	8.54	8.70
		S.D.	0.45	0.36	0.40	0.44	0.38	0.40	0.46
		N	5	5	5	5	5	2	2
Female	G1 0	Mean	7.13	7.39	7.55	7.79	7.88	8.25	8.54
		S.D.	0.65	0.73	0.67	0.67	0.51	0.72	0.54
		N	5	5	5	5	5	2	2
	G2 30	Mean	7.19	7.26	7.44	7.71	7.67		
		S.D.	0.43	0.30	0.31	0.27	0.22		
		N	3	3	3	3	3		
	G3 100	Mean	7.23	7.25	7.38	7.56	7.67		
		S.D.	0.36	0.32	0.28	0.33	0.21		
		N	3	3	3	3	3		
	G4 300	Mean	7.27	7.36	7.41	7.43	7.38	7.43	7.66
		S.D.	0.74	0.80	0.77	0.93	0.92	1.09	1.00
		N	5	5	5	5	5	2	2

Table 3. Mean Food Consumptions

Sex	Group /Dose (mg/kg/day)		Week of dosing (g/day)					Week of recovery (g/day)	
			0	1	2	3	4	5	6
Male	G1 0	Mean	250	250	250	239	237	250	250
		S.D.	0	0	0	24	30	0	0
		N	5	5	5	5	5	2	2
	G2 30	Mean	250	250	250	250	250		
		S.D.	0	0	0	0	0		
		N	3	3	3	3	3		
	G3 100	Mean	250	250	250	250	250		
		S.D.	0	0	0	0	0		
		N	3	3	3	3	3		
	G4 300	Mean	250	250	250	223	227	250	250
		S.D.	0	0	0	61	52	0	0
		N	5	5	5	5	5	2	2
Female	G1 0	Mean	250	245	250	250	250	176	250
		S.D.	0	11	0	0	0	105	0
		N	5	5	5	5	5	2	2
	G2 30	Mean	250	237	250	250	250		
		S.D.	0	23	0	0	0		
		N	3	3	3	3	3		
	G3 100	Mean	250	207	250	250	231		
		S.D.	0	75	0	0	33		
		N	3	3	3	3	3		
	G4 300	Mean	242	227	238	223	250	250	250
		S.D.	17	32	27	59	0	0	0
		N	5	5	5	5	5	2	2

<자초추출물의 세균을 이용한 복귀돌연변이시험>

Table 1. The Number of Revertant Colonies per Plate in Absence Metabolic Activation (Dose Range Finding Study)

Strain	Test item	Dose level (μg/plate)	Individual revertant colony counts	Mean
TA98	Dimethyl sulfoxide	0	19 , 18	19
	Test Substacne	4.88	15 , 15	15
		19.5	15 , 13	14
		78.1	12* , 9*	11
		313	5* , 3*	4
		1,250†	0* , 0*	0
		5,000†	0* , 0*	0
	2-Nitrofluorene (2-NF)	5.0	622 , 515	569
TA100	Dimethyl sulfoxide	0	62 , 58	60
	Test Substacne	4.88	51 , 54	53
		19.5	31* , 34*	33
		78.1	0* , 0*	0
		313	0* , 0*	0
		1,250†	0* , 0*	0
		5,000†	0* , 0*	0
	Sodium azide (SA)	1.5	583 , 546	565
TA1535	Dimethyl sulfoxide	0	6 , 7	7
	Test Substacne	4.88	9 , 9	9
		19.5	4* , 6*	5
		78.1	2* , 0*	1
		313	0* , 0*	0
		1,250†	0* , 0*	0
		5,000†	0* , 0*	0
	Sodium azide (SA)	1.5	425 , 516	471
TA1537	Dimethyl sulfoxide	0	4 , 3	4
	Test Substacne	4.88	6 , 5	6
		19.5	2* , 5*	4
		78.1	0* , 0*	0
		313	0* , 0*	0
		1,250†	0* , 0*	0
		5,000†	0* , 0*	0
	9-Aminoacridine (9-AA)	80.0	232 , 296	264
WP2*uvrA* (pKM101)	Dimethyl sulfoxide	0	81 , 87	84
	Test Substacne	4.88	84 , 106	95
		19.5	94 , 96	95
		78.1	96 , 95	96
		313	55 , 53	54
		1,250†	36* , 49*	43
		5,000†	6* , 4*	5
	2-(2-furyl)-3-(5-nitro-2-furyl)acrylamide (AF2)	0.005	600 , 505	553

*: Indicated growth inhibition

†: Precipitation

Table 2. The Number of Revertant Colonies per Plate in Presence Metabolic Activation (Dose Range Finding Study)

Strain	Test item	Dose level (μg/plate)	Individual revertant colony counts	Mean
TA98	Dimethyl sulfoxide	0	22, 32	27
	Test Substacne	4.88	28, 21	25
		19.5	29, 25	27
		78.1	21, 23	22
		313	25, 23	24
		1,250†	15, 25	20
		5,000†	14, 18	16
	2-Aminoanthracene (2-AA)	1.0	233, 251	242
TA100	Dimethyl sulfoxide	0	87, 88	88
	Test Substacne	4.88	64, 59	62
		19.5	68, 54	61
		78.1	55, 65	60
		313	74, 69	72
		1,250†	62*, 63*	63
		5,000†	50*, 45*	48
	2-Aminoanthracene (2-AA)	2.0	293, 259	276
TA1535	Dimethyl sulfoxide	0	9, 10	10
	Test Substacne	4.88	10, 8	9
		19.5	7, 6	7
		78.1	6, 8	7
		313	9, 8	9
		1,250†	4, 8	6
		5,000†	7, 9	8
	2-Aminoanthracene (2-AA)	3.0	115, 132	124
TA1537	Dimethyl sulfoxide	0	9, 10	10
	Test Substacne	4.88	13, 8	11
		19.5	8, 7	8
		78.1	8, 9	9
		313	12, 7	10
		1,250†	2*, 4*	3
		5,000†	5*, 6*	6
	2-Aminoanthracene (2-AA)	3.0	144, 112	128
WP2*uvrA* (pKM101)	Dimethyl sulfoxide	0	104, 107	106
	Test Substacne	4.88	106, 108	107
		19.5	118, 107	113
		78.1	129, 99	114
		313	109, 111	110
		1,250†	135, 124	130
		5,000†	127, 118	123
	2-Aminoanthracene (2-AA)	2.0	405, 432	419

*: Indicated growth inhibition

†: Precipitation

Table 3. The Number of Revertant Colonies per Plate in Absence Metabolic Activation (Main Study)

Strain	Test item	Dose level (μg/plate)	Individual revertant colony counts	Mean	S.D.
TA98	Dimethyl sulfoxide	0	11 , 8 , 11	10	2
	Test Substacne	2.44	11 , 12 , 10	11	1
		4.88	11 , 11 , 14	12	2
		9.77	15 , 16 , 15	15	1
		19.5	15 , 12 , 14	14	2
		39.1	12* , 13* , 13*	13	1
		78.1	17* , 10* , 13*	13	4
	2-Nitrofluorene (2-NF)	5.0	437 , 430 , 569	479	78
TA100	Dimethyl sulfoxide	0	48 , 46 , 66	53	11
	Test Substacne	0.610	53 , 62 , 70	62	9
		1.22	55 , 52 , 58	55	3
		2.44	73 , 58 , 48	60	13
		4.88	57 , 65 , 54	59	6
		9.77	51* , 49* , 49*	50	1
		19.5	51* , 52* , 40*	48	7
	Sodium azide (SA)	1.5	515 , 478 , 489	494	19
TA1535	Dimethyl sulfoxide	0	8 , 5 , 7	7	2
	Test Substacne	0.610	8 , 5 , 7	7	2
		1.22	7 , 6 , 8	7	1
		2.44	8 , 6 , 6	7	1
		4.88	6 , 7 , 7	7	1
		9.77	6* , 8* , 5*	6	2
		19.5	5* , 5* , 6*	5	1
	Sodium azide (SA)	1.5	427 , 363 , 340	377	45
TA1537	Dimethyl sulfoxide	0	6 , 8 , 5	6	2
	Test Substacne	0.610	6 , 6 , 3	5	2
		1.22	6 , 4 , 4	5	1
		2.44	7 , 7 , 8	7	1
		4.88	10 , 6 , 6	7	2
		9.77	8 , 9 , 8	8	1
		19.5	6* , 5* , 5*	5	1
	9-Aminoacridine (9-AA)	80.0	291 , 373 , 317	327	42
WP2*uvrA* (pKM101)	Dimethyl sulfoxide	0	95 , 87 , 102	95	8
	Test Substacne	39.1	62 , 77 , 86	75	12
		78.1	63 , 82 , 78	74	10
		156	69 , 63 , 65	66	3
		313	62 , 58 , 80	67	12
		625†	70 , 53 , 60	61	9
		1,250†	25* , 23* , 28*	25	3
	2-(2-furyl)-3-(5-nitro-2-furyl)acrylamide (AF2)	0.005	481 , 450 , 442	458	21

S.D.: Standard Deviation

*: Indicated growth inhibition

†: Precipitation

Table 4. The Number of Revertant Colonies per Plate in Presence Metabolic Activation (Main Study)

Strain	Test item	Dose level (μg/plate)	Individual revertant colony counts	Mean	S.D.
TA98	Dimethyl sulfoxide	0	23 , 25 , 23	24	1
	Test Substacne	313	16 , 20 , 22	19	3
		625†	23 , 22 , 15	20	4
		1,250†	25 , 18 , 19	21	4
		2,500†	25 , 18 , 20	21	4
		5,000†	23 , 15 , 14	17	5
	2-Aminoanthracene (2-AA)	1.0	212 , 228 , 178	206	26
TA100	Dimethyl sulfoxide	0	55 , 78 , 76	70	13
	Test Substacne	39.1	74 , 65 , 73	71	5
		78.1	55 , 56 , 73	61	10
		156	68 , 66 , 60	65	4
		313	74 , 70 , 82	75	6
		625†	72 , 79 , 66	72	7
		1,250†	69* , 75* , 60*	68	8
	2-Aminoanthracene (2-AA)	2.0	440 , 446 , 371	419	42
TA1535	Dimethyl sulfoxide	0	6 , 4 , 8	6	2
	Test Substacne	313	6 , 10 , 5	7	3
		625†	3 , 7 , 5	5	2
		1,250†	4 , 5 , 7	5	2
		2,500†	8 , 7 , 9	8	1
		5,000†	5 , 5 , 4	5	1
	2-Aminoanthracene (2-AA)	3.0	51 , 60 , 77	63	13
TA1537	Dimethyl sulfoxide	0	13 , 13 , 17	14	2
	Test Substacne	39.1	14 , 11 , 14	13	2
		78.1	11 , 16 , 15	14	3
		156	12 , 11 , 11	11	1
		313	10 , 11 , 15	12	3
		625†	10 , 18 , 10	13	5
		1,250†	14* , 10* , 11*	12	2
	2-Aminoanthracene (2-AA)	3.0	100 , 134 , 103	112	19
WP2*uvrA* (pKM101)	Dimethyl sulfoxide	0	102 , 102 , 87	97	9
	Test Substacne	313	86 , 74 , 90	83	8
		625†	81 , 90 , 86	86	5
		1,250†	103 , 81 , 86	90	12
		2,500†	83 , 73 , 101	86	14
		5,000†	89 , 94 , 73	85	11
	2-Aminoanthracene (2-AA)	2.0	298 , 281 , 336	305	28

S.D.: Standard Deviation

*: Indicated growth inhibition

†: Precipitation

Table 5. Historical Control Data

Historical negative control values of revertant colonies

Strain	S9 mix	N	Mean ± S.D.	Range	
				Lower	Upper
TA100	-	108	76.4 ± 13.8	42.7	110.0
	+	108	88.8 ± 14.6	50.7	126.9
TA1535	-	108	10.0 ± 2.2	3.9	16.1
	+	108	8.8 ± 2.0	3.0	14.7
WP2*uvrA* (pKM101)	-	108	116.7 ± 21.9	57.4	176.0
	+	108	137.5 ± 20.5	79.3	195.6
TA98	-	108	16.6 ± 3.6	5.7	27.5
	+	108	23.6 ± 4.1	13.0	34.1
TA1537	-	108	6.4 ± 1.7	1.5	11.3
	+	108	11.5 ± 2.5	4.7	18.2

Historical positive control values of revertant colonies

Strain	S9 mix	Positive control	Dose (μg/plate)	N	Mean ± S.D.	Range	
						Lower	Upper
TA100	-	SA	1.5	108	476.5 ± 82.8	283.7	669.4
	+	2-AA	2.0	97	425.1 ± 112.6	124.7	725.5
TA1535	-	SA	1.5	108	451.9 ± 77.1	255.4	648.5
	+	2-AA	3.0	108	128.2 ± 31.1	50.9	205.5
WP2*uvrA* (pKM101)	-	AF2	0.005	108	776.2 ± 152.8	362.0	1190.4
	+	2-AA	2.0	108	397.5 ± 75.6	179.3	615.8
TA98	-	2-NF	5.0	108	529.3 ± 109.3	245.4	813.1
	+	2-AA	1.0	103	265.6 ± 49.9	130.0	401.2
TA1537	-	9-AA	80.0	108	315.9 ± 111.1	38.6	593.2
	+	2-AA	3.0	97	129.7 ± 34.8	42.0	217.3

Negative control : Water for injection, Dimethyl sulfoxide, Acetone, 0.5% methyl cellulose 1,500cP solution, 0.5% carboxymethylcellulose sodium salt solution

SA : Sodium azide

2-AA : 2-Aminoanthracene

AF2 : 2-(2-furyl)-3-(5-nitro-2-furyl)acrylamide

2-NF : 2-Nitrofluorene

9-AA : 9-Aminoacridine

The above historical control values were obtained from the data pooled from May 1, 2011 to May 31, 2012

The range was calculated by the control limit of X derived from $\overline{X}$-$\overline{R}$-Rs value.

<자초추출물의 포유류 배양세포를 이용한 염색체이상시험>

Table 1. Summary of Growth Inhibition Study

Test substance	Dose (μg/mL)	S9 mix	Trt-Rec Time (hr)	Growth of cells (OD) (Mean±S.D.)	Growth rate (%)
Tetrahydrofuran	0	-	6-18	1.142 ± 0.028	100
Test Substance	5	-	6-18	0.560 ± 0.058	49.0
	10	-	6-18	0.201 ± 0.087	17.6
	50	-	6-18	0.092 ± 0.004	8.06
	100	-	6-18	0.095 ± 0.005	8.32
	250	-	6-18	0.121 ± 0.006	10.6
	500†	-	6-18	0.146 ± 0.017	12.8
	1,000†	-	6-18	0.144 ± 0.013	12.6
	2,500†	-	6-18	0.155 ± 0.015	13.6
	5,000†	-	6-18	0.181 ± 0.041	15.8
Tetrahydrofuran	0	+	6-18	0.935 ± 0.023	100
Test Substance	5	+	6-18	0.910 ± 0.055	97.3
	10	+	6-18	0.932 ± 0.065	99.7
	50	+	6-18	0.850 ± 0.047	90.9
	100	+	6-18	0.276 ± 0.035	29.5
	250†	+	6-18	0.137 ± 0.008	14.7
	500†	+	6-18	0.237 ± 0.031	25.3
	1,000†	+	6-18	0.209 ± 0.021	22.4
	2,500†	+	6-18	0.335 ± 0.039	35.8
	5,000†	+	6-18	0.230 ± 0.010	24.6
Tetrahydrofuran	0	-	24-0	1.150 ± 0.155	100
Test Substance	5	-	24-0	0.751 ± 0.112	65.3
	10	-	24-0	0.237 ± 0.045	20.6
	50	-	24-0	0.096 ± 0.004	8.35
	100	-	24-0	0.102 ± 0.005	8.87
	250	-	24-0	0.138 ± 0.012	12.0
	500†	-	24-0	0.150 ± 0.024	13.0
	1,000†	-	24-0	0.178 ± 0.024	15.5
	2,500†	-	24-0	0.229 ± 0.038	19.9
	5,000†	-	24-0	0.353 ± 0.101	30.7

Trt-Rec time : Treatment-Recovery times

S.D.:Standard deviation

† : Precipitation

Table 2. Summary of Main Study

Test substance	Dose (μg/mL)	S9 mix	Trt-Rec Time (hr)	No. of cell analyzed	Number of cells with structural aberrations						gap (%)	Number of cells with numerical aberrations			TR value
					ctb	csb	cte	cse	frg	total (%)		end	pol	total (%)	
Tetrahydrofuran	0	-	6-18	100/100	0/0	0/0	0/0	0/0	0/0	0 (0.0)	0 (0.0)	0/0	0/0	0 (0.0)	-
Test Substance	0.625	-	6-18	100/100	1/0	0/0	0/1	0/0	0/0	2 (1.0)	0 (0.0)	0/0	2/0	2 (1.0)	-
	1.25	-	6-18	100/100	0/0	0/0	0/0	0/0	0/0	0 (0.0)	0 (0.0)	0/0	2/1	3 (1.5)	-
	2.50	-	6-18	100/100	2/1	0/0	2/0	0/0	0/0	4 (2.0)	0 (0.0)	0/0	3/1	4 (2.0)	-
	5.00	-	6-18	toxic											-
MMC	0.05	-	6-18	100/100	4/1	0/0	12/21	1/0	0/0	37* (18.5)	0 (0.0)	0/0	1/0	1 (0.5)	330,000
Tetrahydrofuran	0	+	6-18	100/100	0/0	0/0	0/0	0/0	0/0	0 (0.0)	0 (0.0)	0/0	0/0	0 (0.0)	-
Test Substance	10.5	+	6-18	100/100	1/0	0/0	0/0	0/0	0/0	1 (0.5)	0 (0.0)	0/0	0/1	1 (0.5)	-
	21.0	+	6-18	100/100	1/0	0/0	1/2	0/0	0/0	4 (2.0)	1 (0.5)	0/0	4/4	8# (4.0)	-
	42.0	+	6-18	100/100	5/8	0/0	9/11	0/0	0/0	32## (16.0)	0 (0.0)	0/0	2/3	5 (2.5)	238
	84.0	+	6-18	toxic											-
B[a]P	20	+	6-18	100/100	2/0	1/0	10/12	0/0	0/0	25* (12.5)	1 (0.5)	1/0	0/0	1 (0.5)	550
Tetrahydrofuran	0	-	24-0	not observed[1)]											
Test Substance	0.875	-	24-0												
	1.75	-	24-0												
	3.50	-	24-0												
	7.00	-	24-0												
MMC	0.05	-	24-0												

D_{20}=0.057 mg/mL (S9+, 6+18hr), TR value=238 (S9+, 6+18hr)

Aberration; gap: chromatid and chromosome gap, ctb: chromatid break, cte: chromatid exchange, csb: chromosome break, cse: chromosome exchange, frg: fragmentation, end: endoreduplication, pol: polyploidy

MMC: Mitomycin C, B[a]P: Benzo[a]pyrene

Trt-Rec time : Treatment-Recovery times

Significant difference from negative control by fisher's exact test : * $p<0.05$

Significant difference from negative control by Cochran-Armitage trend test : ## $p<0.01$, # $p<0.05$

1) : Since the result of the short time treatment with metabolic activation was positive, slides in the continuous treatment without metabolic activation was not evident.

Table 3. Historical Control Data

Historical control values of structural aberrations

Group	S9 mix	Time of exposure (hr)	N	Structural aberration cells without gap (%) (Mean±S.D.)			Range (%)	
							MIN	MAX
Negative	-	6-18	113	0.1	±	0.3	0	<5
	+	6-18	113	0.2	±	0.4	0	<5
	-	24-0	102	0.2	±	0.3	0	<5
Positive	-	6-18[a)]	113	19.3	±	5.0	<10	34*
	+	6-18[b)]	113	20.8	±	5.8	<10	38*
	-	24-0[a)]	102	19.4	±	5.8	<10	37*

Historical control values of numerical aberration

Group	S9 mix	Time of exposure (hr)	N	Numerical aberration cells (%) (Mean±S.D.)			Range(%)	
							MIN	MAX
Negative	-	6-18	113	0.1	±	0.3	0	<5
	+	6-18	113	0.1	±	0.3	0	<5
	-	24-0	103	0.1	±	0.3	0	<5

Negative control : Water for injection, Dimethyl sulfoxide, Acetone, 0.5% methyl cellulose 1500cP solution, 0.5% carboxymethylcellulose sodium salt solution, Tetrahydrofuran etc.

a : Mitomycin C (0.05 μg/mL)

b : Benzo[a]pyrene (20 μg/mL)

N : The total number of chromosome aberration test

The above historical control values were obtained from the data pooled from Jan. 1, 2011 to May 31, 2012.

*: The range was calculated by the control limit from Mean ± 3S.D.

<자초추출물의 마우스를 이용한 소핵시험>

Table 1. Clinical Signs (Dose Range Finding Study)

Test substance	Dose (mg/kg)	Route	No. of animals	Clinical signs	Hours after treatment				
					0	2	24	48	72
Test substance	125	P.O.	3	NAD	3	3	3	3	3
	250	P.O.	3	NAD	3	3	0	0	3
				A	0	0	3	3	0
	500	P.O.	3	NAD	3	3	0	0	3
				A	0	0	3	3	0
				B	0	0	1	0	0
	1,000	P.O.	3	NAD	3	0	0	0	0
				A	0	3	3	3	3
				B	0	0	1	1	0
	2,000	P.O.	3	NAD	3	0	0	0	0
				A	0	3	3	3	3
				B	0	0	2	3	2

NAD : No Abnormalities Detected
P.O. : Per Os
A : Compound-colored stool
B : Soiled perineal region

Table 2. Clinical Signs (Sampling Time Determining Study)

Test substance	Dose (mg/kg)	Route	No. of animals	Clinical signs	Hours after treatment				
					0	2	24	48	72
Test substance	2,000	P.O.	3	NAD	3	0	0	-	-
				A	0	3	3	-	-
				B	0	0	3	-	-
	2,000	P.O.	3	NAD	3	0	0	0	-
				A	0	3	3	3	-
				B	0	0	2	1	-
	2,000	P.O.	3	NAD	3	0	0	0	0
				A	0	3	3	2	2
				B	0	1	3	0	0
				C	0	0	1	0	0
				D	0	0	0	1	0

NAD : No Abnormalities Detected
P.O. : Per Os
A : Compound-colored stool
B : Soiled perineal region
C : Decrease in locomotor activity
D : Death

Table 3. Results (Sampling Time Determining Study)

Test substance	Dose (mg/kg)	Route	Hours after administration	Animal ID	Counted PCE : NCE	PCE/ (PCE+NCE)	MNPCE/ PCE
Test substance	2,000	P.O.	24	B1101	198 : 302	0.396	3 / 2000
				B1102	210 : 290	0.420	2 / 2000
				B1103	268 : 232	0.536	2 / 2000
				Total	- : -	-	7 / 6000
				Mean±S.D.	- : -	0.451 ± 0.075	2.3 ± 0.6
			48	B1201	282 : 218	0.564	1 / 2000
				B1202	48 : 452	0.096	1 / 2000
				B1203	232 : 268	0.464	3 / 2000
				Total	- : -	-	5 / 6000
				Mean±S.D.	- : -	0.375 ± 0.246	1.7 ± 1.2
			72	B1301	184 : 316	0.368	0 / 2000
				B1302	197 : 303	0.394	0 / 2000
				B1303	- : -	-	- / -
				Total	- : -	-	0 / 4000
				Mean±S.D.	- : -	0.381 ± 0.018	0.0 ± 0.0

P.O.: Per Os
S.D.: Standard Deviation
MNPCE: Micronucleated polychromatic erythrocyte
PCE: Polychromatic erythrocyte
NCE: Normochromatic erythrocyte
- : No data

Table 4. Clinical Sings (Main Study)

Group		Dose (mg/kg)	Route	No. of animals	Clinical signs	Hours after treatment		
						0	2	24
Negative control	Corn oil	0	P.O.	5	NAD	5	5	5
Test substance	Test substance	500	P.O.	5	NAD	5	5	0
					A	0	0	5
					B	0	0	2
		1,000	P.O.	5	NAD	5	0	0
					A	0	5	5
					B	0	0	4
		2,000	P.O.	5	NAD	5	0	0
					A	0	5	5
					B	0	0	5
Positive control	MMC	2	I.P.	5	NAD	5	5	5

P.O.: Per Os
I.P.: Intraperitoneal
MMC : Mitomycin C
NAD : No Abnormalities Detected
A : Compound-colored stool
B : Soiled perineal region

Table 5. Body Weights (Main Study)

Group		Dose (mg/kg)	Route	Hours after administration	Animal ID	Body weight (g) at the time of	
						Administration	Sacrifice
Negative control	Corn oil	0	P.O.	24	1101	33.8	32.2
					1102	32.6	31.8
					1103	32.4	31.8
					1104	31.1	30.6
					1105	31.0	30.4
					Mean±S.D.	32.2 ± 1.2	31.4 ± 0.8
Test substance	Test substance	500	P.O.	24	1201	33.7	33.0
					1202	32.8	31.1
					1203	32.2	31.3
					1204	31.2	30.9
					1205	30.9	30.0
					Mean±S.D.	32.1 ± 1.1	31.3 ± 1.1
		1,000	P.O.	24	1301	33.6	31.4
					1302	33.0	30.2
					1303	32.2	31.3
					1304	31.2	29.9
					1305	30.7	29.7
					Mean±S.D.	32.1 ± 1.2	30.5 ± 0.8
		2,000	P.O.	24	1401	33.4	30.5
					1402	33.1	31.1
					1403	31.7	29.3
					1404	31.4	29.3
					1405	29.8	27.2
					Mean±S.D.	31.9 ± 1.4	29.5 ± 1.5
Positive control	MMC	2	I.P.	24	1501	33.2	31.7
					1502	33.1	32.1
					1503	31.6	30.8
					1504	31.5	29.9
					1505	29.8	29.6
					Mean±S.D.	31.9 ± 1.4	30.8 ± 1.1

P.O.:Per Os

I.P. : Intraperitoneal

MMC : Mitomycin C

S.D. : Standard Deviation

Table 6. Results (Main Study)

Groups		Dose (mg/kg)	Route	Hours after administration	Animal ID	Counted PCE : NCE	PCE/ (PCE+NCE)	MNPCE/ PCE
Negative control	Corn oil	0	P.O.	24	1101	148 : 352	0.296	0 / 2000
					1102	138 : 362	0.276	0 / 2000
					1103	134 : 366	0.268	0 / 2000
					1104	129 : 371	0.258	2 / 2000
					1105	141 : 359	0.282	0 / 2000
					Total	- : -	-	2 / 10000
					Mean±S.D.	- : -	0.276 ± 0.014	0.4 ± 0.9
Test Substacne		0	P.O.	24	1201	101 : 399	0.202	0 / 2000
					1202	141 : 359	0.282	2 / 2000
					1203	172 : 328	0.344	0 / 2000
					1204	156 : 344	0.312	0 / 2000
					1205	130 : 370	0.260	1 / 2000
					Total	- : -	-	3 / 10000
					Mean±S.D.	- : -	0.280 ± 0.054	0.6 ± 0.9
		500	P.O.	24	1301	129 : 371	0.258	0 / 2000
					1302	71 : 429	0.142	0 / 2000
					1303	164 : 336	0.328	3 / 2000
					1304	151 : 349	0.302	2 / 2000
					1305	112 : 388	0.224	1 / 2000
					Total	- : -	-	6 / 10000
					Mean±S.D.	- : -	0.251 ± 0.073	1.2 ± 1.3
		1,000	P.O.	24	1401	129 : 371	0.258	0 / 2000
					1402	163 : 337	0.326	1 / 2000
					1403	163 : 337	0.326	0 / 2000
					1404	115 : 385	0.230	1 / 2000
					1405	143 : 357	0.286	1 / 2000
					Total	- : -	-	3 / 10000
					Mean±S.D.	- : -	0.285 ± 0.042	0.6 ± 0.5
Positive control	MMC	2	I.P.	24	1501	131 : 369	0.262	72 / 2000
					1502	166 : 334	0.332	65 / 2000
					1503	179 : 321	0.358	57 / 2000
					1504	128 : 372	0.256	48 / 2000
					1505	167 : 333	0.334	52 / 2000
					Total	- : -	-	294† / 10000
					Mean±S.D.	- : -	0.308 ± 0.046	58.8 ± 9.7

P.O.: Per Os
I.P. : Intraperitoneal
MNPCE : Micronucleated polychromatic erythrocyte
PCE : Polychromatic erythrocyte
NCE : Normochromatic erythrocyte
MMC : Mitomycin C
S.D. : Standard Deviation
Significant difference from negative control by Kastendaum & Bowman : † $p<0.05$

Table 7. Historical Control Data

Historical control values of micronucleated polychromatic erythrocytes(MNPCE)

Group	Dose (mg/kg)	n	MNPCE/2000PCE Mean±S.D.			Range (MNPCE/2000PCE)	
						MIN	MAX
Negative control	0	103	0.6	±	0.50	0	1.8
Positive control	2	103	126.2	±	31.44	47.6	204.8

Historical control values of ratio of polychromatic erythrocytes(PCE) to total erythrocytes

Group	Dose (mg/kg)	n	PCE/NCE+PCE Mean±S.D.			Range (PCE/NCE+PCE)	
						MIN	MAX
Negative control	0	103	0.372	±	0.041	0.270	0.473
Positive control	2	103	0.343	±	0.045	0.231	0.455

Negative control : Including water for injection, normal saline injection, olive oil, corn oil,
0.5% methyl cellulose 1,500cP solution, 0.5% CMC-Na solution, DMSO, PBS *etc*.

Positive control : Mitomycin C (2 mg/kg, I.P., single administration)

The above historical control values were obtained from the data pooled from Jan. 15, 2009 to May 30, 2012.

The range was calculated by the control limit from Mean ± 2.5S.D.

<자초추출물의 토끼를 이용한 피부자극시험>

Table 1. Clinical Signs

Test group	Animal ID	Day			
		0	1	2	3
G1 Test substance	1101	-	-	-	-
	1102	-	-	-	-
	1103	-	-	-	-
	1104	-	-	-	-
	1105	-	-	-	-
	1106	-	-	-	-

- : No Observable Abnormality

Table 2. Body Weights

(kg)

Test group	Animal ID	Day		Gain
		0	3	
G1 Test substance	1101	2.15	2.26	0.11
	1102	2.21	2.30	0.09
	1103	2.20	2.30	0.10
	1104	2.16	2.28	0.12
	1105	2.18	2.27	0.09
	1106	2.19	2.28	0.09
	Mean	2.18	2.28	0.10
	S.D.	0.02	0.02	0.01
	No. of animals	6	6	6

Table 3. Skin Irritation Scores

Applied area	Animal ID	Score of erythema and eschar/edema					
		Intervals (hours)					
		24		(48)		72	
		Intact	Abraded	Intact	Abraded	Intact	Abraded
100% Test substance	1101	- / 4	- / 4	(- / 4)	(- / 4)	- / 4	- / 4
	1102	- / 4	- / 4	(- / 4)	(- / 4)	- / 4	- / 4
	1103	- / 4	- / 4	(- / 4)	(- / 4)	- / 4	- / 4
	1104	- / 4	- / 4	(- / 4)	(- / 4)	- / 4	- / 4
	1105	- / 4	- / 4	(- / 4)	(- / 4)	- / 4	- / 4
	1106	- / 4	- / 4	(- / 4)	(- / 4)	- / 4	- / 4
	Total score	-	-	(-)	(-)	-	-
	Mean score	-		(-)		-	
	P.I.I.[a)]	*-					
Only patch	1101	0 / 0	0 / 0	(0 / 0)	(0 / 0)	0 / 0	0 / 0
	1102	0 / 0	0 / 0	(0 / 0)	(0 / 0)	0 / 0	0 / 0
	1103	0 / 0	0 / 0	(0 / 0)	(0 / 0)	0 / 0	0 / 0
	1104	0 / 0	0 / 0	(0 / 0)	(0 / 0)	0 / 0	0 / 0
	1105	0 / 0	0 / 0	(0 / 0)	(0 / 0)	0 / 0	0 / 0
	1106	0 / 0	0 / 0	(0 / 0)	(0 / 0)	0 / 0	0 / 0
	Total score	0	0	(0)	(0)	0	0
	Mean score	0		(0)		0	
	P.I.I.[a)]	0					

hours : Observation after application

a: P.I.I. (primary skin irritation index) = $\frac{\text{Summation mean score of 24 and 72 hours}}{\text{Intervals (2) x Test site (2)}}$

( ) = Total values not used for calculation of P.I.I.

- : The erythema was not possible to observe because of severe skin coloring with the test substance.

* The P.I.I. could not calculated because of erythema.

<자초추출물의 토끼를 이용한 안점막자극시험>

Table 1. Summary of Clinical Signs

Test group	Clinical signs	Day												
		0	1	2	3	4	5	6	7	8	9	10	11	12	13
G1 Unwashed	No. of animals	6	6	6	6	6	6	6	6	6	6	6	6	6	6
	NOA	6	6	6	6	6	6	6	6	6	6	6	6	6	6
G2 Washed	No. of animals	3	3	3	3	3	3	3	3						
	NOA	3	3	3	3	3	3	3	3						

NOA : No Observable Abnormality

Table 2. Mean Body Weights

(kg)

Test group		Day			Gain
		0	7	13	
G1 Unwashed	Mean	2.11		2.39	0.28
	S.D.	0.07		0.06	0.03
	No. of anim	6		6	6
G2 Washed	Mean	2.20	2.37		0.17
	S.D.	0.06	0.06		0.02
	No. of anim	3	3		3

Table 3. Summary of Eye Irritation Scores

Test group (Conc.)	No. of animals	M.I.O.I. Intervals (Day) 1	2	3	4	7	I.A.O.I.
G1 Unwashed (100%)	6	12.7	10.3	10.3	10.0	6.0	12.7
G2 Washed (100%)	3	6.0	4.0	4.0	4.0	0.0	6.0

Day : Observation after application

M.I.O.I.: Mean Index of Ocular Irritation

I.A.O.I.: Index of Acute Ocular Irritaiton (The maximum value of M.I.O.I. during the observation time)

Conc. : Concentration

Table 3. (Continued)

Test group (Conc.)	No. of animals	M.I.O.I. Intervals (Day) 10	13
G1 Unwashed (100%)	6	6.0	0.0

Day : Observation after application

M.I.O.I.: Mean Index of Ocular Irritation

Conc. : Concentration

<자초추출물의 기니픽을 이용한 항원성 평가>

Table 1. Summary of Clinical Signs

Test group /Dose (mg/kg)	Clinical signs	Day																											
		0	1	2	3	4	5	6	7	8	9	10	11	12	13	14	15	16	17	18	19	20	21	22	23	24	25	26	27	28	29
G1 /0	No. of animals	5	5	5	5	5	5	5	5	5	5	5	5	5	5	5	5	5	5	5	5	5	5	5	5	5	5	5	5	5	5
	NOA	5	5	5	5	5	5	5	5	5	5	5	5	5	5	5	5	5	5	5	5	5	5	5	5	5	5	5	5	5	5
G2 /25	No. of animals	5	5	5	5	5	5	5	5	5	5	5	5	5	5	5	5	5	5	5	5	5	5	5	5	5	5	5	5	5	5
	NOA	5	5	5	5	5	5	5	5	5	5	5	5	5	5	5	5	5	5	5	5	5	5	5	5	5	5	5	5	5	5
G3 /200	No. of animals	5	5	5	5	5	5	5	5	5	5	5	5	5	5	5	5	5	5	5	5	5	5	5	5	5	5	5	5	5	5
	NOA	5	5	5	5	5	5	5	5	5	5	5	5	5	5	5	5	5	5	5	5	5	5	5	5	5	5	5	5	5	5
G4 /200-FCA	No. of animals	5	5	5	5	5	5	5	5	5	5	5	5	5	5	5	5	5	5	5	5	5	5	5	5	5	5	5	5	5	5
	NOA	5	5	5	5	5	5	5	5	5	5	5	5	5	5	5	5	5	5	5	5	5	5	5	5	5	5	5	5	5	5
G5 /5-FCA (OVA)	No. of animals	5	5	5	5	5	5	5	5	5	5	5	5	5	5	5	5	5	5	5	5	5	5	5	5	5	5	5	5	5	5
	NOA	5	5	5	5	5	5	5	5	5	5	5	5	5	5	5	5	5	5	5	5	5	5	5	5	5	5	5	5	5	5

NOA : No Observable Abnormality
FCA : Freund's Complete Adjuvant
OVA : Ovalbumin

Table 2. Mean Body Weights

(g)

Test group /Dose (mg/kg)		Day					Gain
		0	7	14	21	29	
G1 /0	Mean	369	417	468	524	596	227
	S.D.	20	20	38	39	38	21
	No. of animal	5	5	5	5	5	5
G2 /25	Mean	364	417	485	536	598	233
	S.D.	7	14	20	35	32	36
	No. of animal	5	5	5	5	5	5
G3 /200	Mean	367	413	476	532	617	251
	S.D.	11	22	42	48	47	42
	No. of animal	5	5	5	5	5	5
G4 /200-FCA	Mean	369	403	445	485	521	152
	S.D.	9	12	15	13	10	7
	No. of animal	5	5	5	5	5	5
G5 /5-FCA (OVA)	Mean	366	421	456	484	540	174
	S.D.	16	21	29	36	35	34
	No. of animal	5	5	5	5	5	5

FCA : Freund's Complete Adjuvant

OVA : Ovalbumin

Table 3. Summary of Passive Cutaneous Anaphylaxis (PCA) Reaction

Group		Test item	N	Dilution factor of antiserum										
Induction /Dose (mg/kg)	Challenge /Dose (mg/kg)			×10	×20	×40	×80	×160	×320	×640	×1280	×2560	×5120	Saline
G1 /0	G6 /0	Corn oil	10	0	0	0	0	0	0	0	0	0	0	0
G2 /25	G7 /2.5	Test substance	10	0	0	0	0	0	0	0	0	0	0	0
G3 /200	G8 /2.5	Test substance	10	0	0	0	0	0	0	0	0	0	0	0
G4 /200-FCA	G9 /2.5	Test substance	10	0	0	0	0	0	0	0	0	0	0	0
G5 /5-FCA (OVA)	G10 /10 (OVA)	OVA	10	10	10	10	10	10	10	10	10	10	10	0

FCA : Freund's Complete Adjuvant

OVA : Ovalbumin

N : No. of animals

Table 4. Summary of Active Systemic Anaphylaxis (ASA) Reaction

Symptoms	Group	G1	G2	G3	G4	G5
	Test item	Corn oil	Test substance	Test substance	Test substance	OVA
	Induction dose (mg/kg)	0	25	200	200-FCA	5-FCA
	Challenge dose (mg/kg)	0	2.5	2.5	2.5	10
	No. of animals	5	5	5	5	5
Restlessness		0	0	0	0	0
Piloerection		0	0	0	0	0
Tremor		0	0	0	0	0
Rubbing or licking nose		0	0	0	0	0
Sneezing		0	0	0	0	0
Coughing		0	0	0	0	0
Hyperpnea		0	0	0	0	5
Urination		4	3	3	4	5
Evacuation		3	5	3	3	5
Lacrimation		0	0	0	0	0
Dyspnea		0	0	0	0	5
Rhonchus		0	0	0	0	1
Cyanosis		0	0	0	0	0
Staggering gait		0	0	0	0	5
Jumping		0	0	0	0	0
Gasping and writhing		0	0	0	0	3
Convulsion		0	0	0	0	5
Side position		0	0	0	0	5
Cheyne-Stokes respiration		0	0	0	0	5
Death		0	0	0	0	5

FCA : Freund's Complete Adjuvant
OVA : Ovalbumin

<자초추출물의 랫드를 이용한 4주 반복 경구투여 독성동태시험>

Sex	Group / Dose (mg/kg)	Phase	Toxicokinetic parameters			
			AUC_{last} (ng·hr/mL)	C_{max} (ng/mL)	T_{max} (hr)	$t_{1/2}$ (hr)
Male	G2 /	Day 1	376.79	41.80	0.50	7.42
	25	Day 28	722.05	60.90	3.00	15.60
	G3 /	Day 1	1,042.90	123.00	0.50	11.49
	100	Day 28	2,018.40	146.00	3.00	14.24
	G4 /	Day 1	1,198.80	145.00	0.50	43.29
	400	Day 28	5,008.25	360.00	0.50	14.42
Female	G2 /	Day 1	310.06	35.40	0.50	5.48
	25	Day 28	580.33	53.10	3.00	24.76
	G3 /	Day 1	710.13	55.40	0.50	11.05
	100	Day 28	1,677.03	127.00	1.00	13.85
	G4 /	Day 1	1,410.68	106.00	0.50	-
	400	Day 28	4,595.75	400.00	3.00	14.99

-: $t_{1/2}$ was not calculated because of less than 3 points for calculation.

<LC/MS/MS를 이용한 랫드 혈장 중acetylshikonin의 분석법 Validation>

Table 1. System suitability for the determination of Acetylshikonin in stabilized rat plasma

Analytical date	Classification		No. 1	No. 2	No. 3	No. 4	No. 5	Mean ± SD	Precision (%)
Jul. 03, 2013	Peak area ratio		0.01263	0.01369	0.01328	0.01206	0.01276	0.01288 ± 0.00063	4.9
	Retention time (min)	Analyte	3.70	3.70	3.70	3.71	3.70	3.70 ± 0.00	0.1
		Emodin	3.46	3.46	3.46	3.47	3.46	3.46 ± 0.00	0.1
Jul. 04, 2013	Peak area ratio		0.01550	0.01930	0.01597	0.01698	0.01689	0.01693 ± 0.00147	8.7
	Retention time (min)	Analyte	3.71	3.70	3.70	3.70	3.70	3.70 ± 0.00	0.1
		Emodin	3.49	3.48	3.48	3.48	3.48	3.48 ± 0.00	0.1
Jul. 08, 2013	Peak area ratio		0.01878	0.02114	0.02004	0.02176	0.02058	0.02046 ± 0.00114	5.6
	Retention time (min)	Analyte	3.70	3.71	3.70	3.70	3.70	3.70 ± 0.00	0.1
		Emodin	3.49	3.48	3.48	3.48	3.48	3.48 ± 0.00	0.1
Jul. 09, 2013	Peak area ratio		0.02575	0.02655	0.02233	0.02247	0.02488	0.02440 ± 0.00192	7.9
	Retention time (min)	Analyte	3.68	3.68	3.68	3.68	3.68	3.68 ± 0.00	0.0
		Emodin	3.44	3.44	3.45	3.44	3.44	3.44 ± 0.00	0.1
Jul. 10, 2013	Peak area ratio		0.01412	0.01602	0.01314	0.01476	0.01425	0.01446 ± 0.00105	7.3
	Retention time (min)	Analyte	3.71	3.71	3.71	3.71	3.71	3.71 ± 0.00	0.0
		Emodin	3.49	3.49	3.48	3.49	3.49	3.49 ± 0.00	0.1
Jul. 11, 2013	Peak area ratio		0.01618	0.01872	0.01499	0.01473	0.01639	0.01620 ± 0.00158	9.8
	Retention time (min)	Analyte	3.71	3.71	3.71	3.71	3.70	3.71 ± 0.00	0.1
		Emodin	3.49	3.49	3.49	3.49	3.49	3.49 ± 0.00	0.0
Jul. 18, 2013	Peak area ratio		0.02007	0.02069	0.02126	0.02083	0.01957	0.02048 ± 0.00067	3.2
	Retention time (min)	Analyte	3.74	3.73	3.72	3.73	3.72	3.73 ± 0.01	0.2
		Emodin	3.51	3.51	3.51	3.51	3.51	3.51 ± 0.00	0.0
Jul. 24, 2013	Peak area ratio		0.01783	0.02113	0.01744	0.01735	0.01806	0.01836 ± 0.00157	8.6
	Retention time (min)	Analyte	3.72	3.72	3.72	3.73	3.72	3.72 ± 0.00	0.1
		Emodin	3.50	3.49	3.50	3.50	3.50	3.50 ± 0.00	0.1
Jul. 25, 2013	Peak area ratio		0.01612	0.01726	0.01549	0.01628	0.01564	0.01616 ± 0.00070	4.3
	Retention time (min)	Analyte	3.72	3.71	3.72	3.71	3.71	3.71 ± 0.01	0.1
		Emodin	3.50	3.49	3.50	3.50	3.49	3.50 ± 0.01	0.2
Jul. 26, 2013	Peak area ratio		0.01739	0.01875	0.01674	0.01583	0.01600	0.01694 ± 0.00119	7.0
	Retention time (min)	Analyte	3.73	3.72	3.72	3.72	3.72	3.72 ± 0.00	0.1
		Emodin	3.50	3.50	3.50	3.49	3.49	3.50 ± 0.01	0.2
Jul. 29, 2013	Peak area ratio		0.01900	0.01943	0.01772	0.01946	0.02022	0.01917 ± 0.00092	4.8
	Retention time (min)	Analyte	3.72	3.72	3.72	3.72	3.72	3.72 ± 0.00	0.0
		Emodin	3.50	3.50	3.50	3.50	3.50	3.50 ± 0.00	0.0

Peak area ratio = (Peak area of reference standard) / (Peak area of internal reference standard).

Precision (%) = (Standard deviation (SD) / Mean) × 100.

Analyte: Acetylshikonin-derivatized.

Table 1. (Continued)

Analytical date	Classification		No. 1	No. 2	No. 3	No. 4	No. 5	Mean ± SD	Precision (%)
Jul. 30, 2013	Peak area ratio		0.02351	0.02160	0.02324	0.02220	0.02256	0.02262 ± 0.00077	3.4
	Retention time (min)	Analyte	3.71	3.72	3.72	3.72	3.71	3.72 ± 0.01	0.1
		Emodin	3.49	3.49	3.50	3.49	3.49	3.49 ± 0.00	0.1
Aug. 01, 2013	Peak area ratio		0.01537	0.01763	0.01585	0.01685	0.01358	0.01586 ± 0.00155	9.7
	Retention time (min)	Analyte	3.70	3.72	3.72	3.71	3.70	3.71 ± 0.01	0.3
		Emodin	3.47	3.49	3.49	3.48	3.49	3.48 ± 0.01	0.3
Aug. 06, 2013	Peak area ratio		0.02423	0.02712	0.02290	0.02380	0.02444	0.02450 ± 0.00158	6.5
	Retention time (min)	Analyte	3.72	3.73	3.72	3.72	3.73	3.72 ± 0.01	0.1
		Emodin	3.50	3.50	3.50	3.50	3.51	3.50 ± 0.00	0.1
Aug. 07, 2013	Peak area ratio		0.01309	0.01307	0.01321	0.01316	0.01197	0.01290 ± 0.00052	4.1
	Retention time (min)	Analyte	3.72	3.72	3.72	3.73	3.74	3.73 ± 0.01	0.2
		Emodin	3.50	3.51	3.51	3.51	3.51	3.51 ± 0.00	0.1
Aug. 08, 2013	Peak area ratio		0.01262	0.01233	0.01340	0.01291	0.01358	0.01297 ± 0.00052	4.0
	Retention time (min)	Analyte	3.72	3.72	3.72	3.72	3.72	3.72 ± 0.00	0.0
		Emodin	3.50	3.50	3.50	3.50	3.50	3.50 ± 0.00	0.0
Aug. 26, 2013	Peak area ratio		0.005992	0.006199	0.006670	0.006033	0.006632	0.006305 ± 0.000325	5.2
	Retention time (min)	Analyte	3.71	3.71	3.70	3.71	3.71	3.71 ± 0.00	0.1
		Emodin	3.49	3.48	3.48	3.49	3.49	3.49 ± 0.01	0.2
Aug. 29, 2013	Peak area ratio		0.01499	0.01433	0.01319	0.01242	0.01282	0.01355 ± 0.00107	7.9
	Retention time (min)	Analyte	3.72	3.72	3.74	3.72	3.71	3.72 ± 0.01	0.3
		Emodin	3.49	3.49	3.49	3.50	3.49	3.49 ± 0.00	0.1

Peak area ratio = (Peak area of reference standard) / (Peak area of internal reference standard).

Precision (%) = (Standard deviation (SD) / Mean) × 100.

Analyte: Acetylshikonin-derivatized.

Table 2. Carryover effect for the determination of Acetylshikonin in stabilized rat plasma

Analytical date	Analyte	No.	Peak area of blank sample	Peak area of LLOQ	Carryover effect (%)
Jul. 03, 2013	Acetylshikonin derivatized	1	0	4693	0.0
		2	0		0.0
		3	0		0.0
	Emodin	1	0	423334	0.0
		2	0		0.0
		3	0		0.0
Jul. 04, 2013	Acetylshikonin derivatized	1	147	5313	2.8
		2	0		0.0
		3	0		0.0
	Emodin	1	0	420581	0.0
		2	0		0.0
		3	0		0.0
Jul. 08, 2013	Acetylshikonin derivatized	1	637	5332	11.9
		2	0		0.0
		3	0		0.0
	Emodin	1	0	239122	0.0
		2	0		0.0
		3	0		0.0
Jul. 09, 2013	Acetylshikonin derivatized	1	0	6434	0.0
		2	0		0.0
		3	0		0.0
	Emodin	1	0	322218	0.0
		2	0		0.0
		3	0		0.0
Jul. 10, 2013	Acetylshikonin derivatized	1	0	6252	0.0
		2	0		0.0
		3	0		0.0
	Emodin	1	0	412723	0.0
		2	0		0.0
		3	0		0.0
Jul. 11, 2013	Acetylshikonin derivatized	1	540	7038	7.7
		2	0		0.0
		3	0		0.0
	Emodin	1	0	430029	0.0
		2	0		0.0
		3	0		0.0

Carryover effect (%) = (Peak area of blank sample)/ (Peak area of LLOQ sample) × 100.

Table 2. (Continued)

Analytical date	Analyte	No.	Peak area of blank sample	Peak area of LLOQ	Carryover effect (%)
Jul. 18, 2013	Acetylshikonin derivatized	1	0	8131	0.0
		2	0		0.0
		3	0		0.0
	Emodin	1	0	450015	0.0
		2	0		0.0
		3	0		0.0
Jul. 24, 2013	Acetylshikonin derivatized	1	0	8642	0.0
		2	0		0.0
		3	0		0.0
	Emodin	1	0	443767	0.0
		2	0		0.0
		3	0		0.0
Jul. 25, 2013	Acetylshikonin derivatized	1	0	8924	0.0
		2	0		0.0
		3	0		0.0
	Emodin	1	0	630226	0.0
		2	0		0.0
		3	0		0.0
Jul. 26, 2013	Acetylshikonin derivatized	1	135	7194	1.5
		2	0		0.0
		3	0		0.0
	Emodin	1	0	485436	0.0
		2	0		0.0
		3	0		0.0
Jul. 29, 2013	Acetylshikonin derivatized	1	756	9071	10.5
		2	0		0.0
		3	0		0.0
	Emodin	1	0	474713	0.0
		2	0		0.0
		3	0		0.0
Jul. 30, 2013	Acetylshikonin derivatized	1	877	8801	9.7
		2	0		0.0
		3	0		0.0
	Emodin	1	0	398038	0.0
		2	0		0.0
		3	0		0.0

Carryover effect (%) = (Peak area of blank sample)/ (Peak area of LLOQ sample) × 100.

Table 2. (Continued)

Analytical date	Analyte	No.	Peak area of blank sample	Peak area of LLOQ	Carryover effect (%)
Aug. 01, 2013	Acetylshikonin derivatized	1	0	4972	0.0
		2	0		0.0
		3	0		0.0
	Emodin	1	0	472901	0.0
		2	0		0.0
		3	0		0.0
Aug. 06, 2013	Acetylshikonin derivatized	1	239	5094	4.7
		2	0		0.0
		3	0		0.0
	Emodin	1	0	222193	0.0
		2	0		0.0
		3	0		0.0
Aug. 07, 2013	Acetylshikonin derivatized	1	0	5473	0.0
		2	0		0.0
		3	0		0.0
	Emodin	1	0	303242	0.0
		2	0		0.0
		3	0		0.0
Aug. 08, 2013	Acetylshikonin derivatized	1	0	5102	0.0
		2	0		0.0
		3	0		0.0
	Emodin	1	0	420149	0.0
		2	0		0.0
		3	0		0.0
Aug. 26, 2013	Acetylshikonin derivatized	1	0	7961	0.0
		2	0		0.0
		3	413		5.2
	Emodin	1	215	1116642	0.0
		2	0		0.0
		3	2281		0.2
Aug. 29, 2013	Acetylshikonin derivatized	1	0	3361	0.0
		2	0		0.0
		3	0		0.0
	Emodin	1	0	239881	0.0
		2	0		0.0
		3	0		0.0

Carryover effect (%) = (Peak area of blank sample)/ (Peak area of LLOQ sample) × 100.

Table 3. Selectivity for the determination of Acetylshikonin in stabilized rat plasma
[Analytical date: Jul. 03, 2013]

Analyte	Sex	Lot No.	Peak area of blank sample	Peak area of LLOQ	Selectivity (%)
Acetylshikonin derivatized	Male	RMP130418001	0	5263	0.0
		RMP130418002	0	5077	0.0
		RMP130418003	0	4384	0.0
	Female	RFP130418001	0	4630	0.0
		RFP130418002	0	4242	0.0
		RFP130418003	0	5556	0.0
Emodin	Male	RMP130418001	0	398776	0.0
		RMP130418002	0	283500	0.0
		RMP130418003	0	318129	0.0
	Female	RFP130418001	0	341763	0.0
		RFP130418002	0	319919	0.0
		RFP130418003	0	372927	0.0

Selectivity (%) =(Peak area of blank sample)/ (Peak area of LLOQ sample) × 100.

Table 4. Matrix effect for the determination of Acetylshikonin in stabilized rat plasma
[Analytical date: Jul. 03, 2013]

Analyte	Theoretical concentration (ng/mL)	Sex	Lot No.	Determined concentration† (ng/mL)	Mean ± SD (ng/mL)	Accuracy (%)	Precision (%)
Acetylshikonin	5.00	Male	RMP130418001	5.74	6.11 ± 0.54	122.2	8.9
			RMP130418002	7.15			
			RMP130418003	5.92			
		Female	RFP130418001	5.85			
			RFP130418002	5.76			
			RFP130418003	6.25			

Accuracy (%) = (Determined concentration / Theoretical concentration) × 100.

Precision (%) = (Standard deviation (SD) / Mean) × 100.

Table 5. Calibration curves (weighting: $1/X^2$) for the determination of Acetylshikonin in stabilized rat plasma

Analytical date	Theoretical concentration (ng/mL)	Peak area			Determined concentration (ng/mL)	Accuracy (%)
		Analyte	Emodin	Ratio		
Jul. 03, 2013	Blank	0	0	0.000	-	-
	Zero	0	383429	0.000	-	-
	5.00	4693	423334	0.01109	5.11	102.3
	10.0	11044	399835	0.02762	10.0	100.4
	20.0	24750	497007	0.04980	16.6	83.2
	50.0	65330	363306	0.1798	55.4	110.7
	100	126271	337806	0.3738	113	113.1
	200	236334	359965	0.6565	197	98.7
	500	663175	366580	1.809	541	108.1
	900	1176679	380882	3.089	922	102.4
	1,000	1144495	422112	2.711	809	80.9
y = 0.00336x - 0.00609		r = 0.9919				
Jul. 04, 2013	Blank	0	0	0.000	-	-
	Zero	0	452974	0.000	-	-
	5.00	5313	420581	0.01263	5.05	101.0
	10.0	11777	419657	0.02806	9.83	98.3
	20.0	22843	393763	0.05801	19.1	95.5
	50.0	67245	384081	0.1751	55.3	110.6
	100	130087	392947	0.3311	104	103.6
	200	234486	412771	0.5681	177	88.5
	500	639409	561181	1.139	354	-†
	900	1119654	376035	2.978	923	102.5
	1,000	1130139	462248	2.445	758	-††
y = 0.00323x - 0.00369		r = 0.9966				
Jul. 08, 2013	Blank	0	0	0.000	-	-
	Zero	0	208163	0.000	-	-
	5.00	5332	239122	0.02230	4.96	99.1
	10.0	11061	248454	0.04452	10.1	101.4
	20.0	22020	252343	0.08726	20.1	100.5
	50.0	60299	277509	0.2173	50.4	100.8
	100	108072	251445	0.4298	100	100.0
	200	213247	253596	0.8409	196	97.9
	500	518205	234839	2.207	514	102.9
	900	978854	251401	3.894	908	100.9
	1,000	1073371	259289	4.140	965	96.5
y = 0.00429x + 0.00104		r = 0.9998				

†: This accuracy of this point did not meet the acceptance criteria.

††: The accuracy of ULOQ in the calibration samples did not meet the acceptance criteria. Although the results of calibration curve did not meet the acceptance criteria, the results of the batch were adopted because all QC samples could be detemined by the calbration curve excluding ULOQ.

Accuracy was calculated from Analyst 1.5.2 software program.

Table 5. (Continued)

Analytical date	Theoretical concentration (ng/mL)	Peak area			Determined concentration (ng/mL)	Accuracy (%)
		Acetylshikonin	Emodin	Ratio		
Jul. 09, 2013	Blank	0	0	0.000	-	-
	Zero	0	262856	0.000	-	-
	5.00	6434	322218	0.01997	4.94	98.8
	10.0	14097	363938	0.03873	10.6	105.5
	20.0	28840	311010	0.09273	26.7	-[†]
	50.0	74055	491019	0.1508	44.1	88.2
	100	157110	538178	0.2919	86.3	86.3
	200	271977	366990	0.7411	221	110.3
	500	681189	390535	1.744	521	104.2
	900	1089526	396038	2.751	822	91.3
	1,000	1443338	374028	3.859	1150	115.4
y = 0.00334x + 0.00346		r = 0.9931				
Jul. 10, 2013	Blank	0	0	0.000	-	-
	Zero	0	378410	0.000	-	-
	5.00	6252	412723	0.01515	4.84	96.7
	10.0	15686	450851	0.03479	10.6	106.5
	20.0	28082	425585	0.06599	19.9	99.4
	50.0	81196	527337	0.1540	45.9	91.8
	100	167169	423797	0.3945	117	117.0
	200	304913	393409	0.7751	230	114.8
	500	865150	600759	1.440	426	85.2
	900	1364327	518197	2.633	779	86.6
	1,000	1519947	440518	3.450	1020	102.1
y = 0.00338x - 0.00121		r = 0.9917				
Jul. 11, 2013	Blank	0	0	0.000	-	-
	Zero	0	403625	0.000	-	-
	5.00	7038	430029	0.01637	5.11	102.1
	10.0	12942	394737	0.03279	10.0	100.1
	20.0	25318	421105	0.06012	18.2	90.9
	50.0	65815	414849	0.1586	47.6	95.3
	100	144223	409783	0.3519	105	105.4
	200	305955	413785	0.7394	221	110.6
	500	665620	391223	1.701	509	101.7
	900	1103801	360552	3.061	915	101.7
	1,000	1337191	433973	3.081	921	92.1
y = 0.00335x - 0.000723		r = 0.9974				

[†]: This accuracy of this point did not meet the acceptance criteria.

Accuracy was calculated from Analyst 1.5.2 software program.

Table 5. (Continued)

Analytical date	Theoretical concentration (ng/mL)	Peak area			Determined concentration (ng/mL)	Accuracy (%)
		Acetylshikonin	Emodin	Ratio		
Jul. 18, 2013	Blank	0	0	0.000	-	-
	Zero	0	426589	0.000	-	-
	5.00	8131	450015	0.01807	4.94	98.8
	10.0	16111	440420	0.03658	9.75	97.5
	20.0	35663	438777	0.08128	21.4	106.8
	50.0	95969	446574	0.2149	56.1	112.1
	100	191632	587531	0.3262	85.0	85.0
	200	385326	449150	0.8579	223	111.5
	500	890545	430863	2.067	537	107.4
	900	1451434	465785	3.116	810	90.0
	1,000	1638049	468399	3.497	909	90.9
y = 0.00385x - 0.000956		r = 0.9936				
Jul. 24, 2013	Blank	0	0	0.000	-	-
	Zero	0	560951	0.000	-	-
	5.00	8642	443767	0.01947	5.00	99.9
	10.0	19979	460829	0.04335	10.8	108.4
	20.0	38853	586639	0.06623	16.4	82.1
	50.0	107972	510631	0.2114	51.9	103.9
	100	238200	451796	0.5272	129	-†
	200	447067	572141	0.7814	191	95.7
	500	1081432	483048	2.239	548	109.5
	900	1835197	486793	3.770	922	102.5
	1,000	2040098	508917	4.009	981	98.1
y = 0.00409x - 0.000953		r = 0.9951				
Jul. 25, 2013	Blank	0	0	0.000	-	-
	Zero	0	546228	0.000	-	-
	5.00	8924	630226	0.01416	5.04	100.8
	10.0	18221	638591	0.02853	9.49	94.9
	20.0	38203	577400	0.06616	21.1	105.6
	50.0	105112	612373	0.1716	53.7	107.5
	100	166915	579408	0.2881	89.8	89.8
	200	402284	586663	0.6857	213	106.4
	500	960979	606763	1.584	490	98.1
	900	1658154	631617	2.625	813	90.3
	1,000	1902378	551712	3.448	1070	106.7
y = 0.00323x - 0.00214		r = 0.9967				

†: This accuracy of this point did not meet the acceptance criteria.

Accuracy was calculated from Analyst 1.5.2 software program.

Table 5. (Continued)

Analytical date	Theoretical concentration (ng/mL)	Peak area			Determined concentration (ng/mL)	Accuracy (%)
		Acetylshikonin	Emodin	Ratio		
Jul. 26, 2013	Blank	0	0	0.000	-	-
	Zero	0	415467	0.000	-	-
	5.00	7194	485436	0.01482	5.18	103.5
	10.0	16189	585658	0.02764	8.46	84.6
	20.0	34513	423243	0.08155	22.3	111.3
	50.0	93443	442566	0.2111	55.4	110.9
	100	189129	471942	0.4007	104	104.0
	200	391208	472357	0.8282	213	106.7
	500	916204	480603	1.906	489	97.9
	900	1499230	466235	3.216	825	91.6
	1,000	1650588	473122	3.489	895	89.5
y = 0.00391x - 0.00540		r = 0.9940				
Jul. 29, 2013	Blank	0	0	0.000	-	-
	Zero	0	497968	0.000	-	-
	5.00	9071	474713	0.01911	4.81	96.2
	10.0	22485	498650	0.04509	10.3	102.7
	20.0	46720	491694	0.09502	20.8	103.8
	50.0	124495	482578	0.2580	55.0	110.0
	100	247904	491046	0.5048	107	106.9
	200	518988	482996	1.075	227	113.3
	500	1067534	495911	2.153	453	90.7
	900	1675741	472560	3.546	746	82.9
	1,000	2228788	502410	4.436	933	93.3
y = 0.00476x - 0.00378		r = 0.9937				
Jul. 30, 2013	Blank	0	0	0.000	-	-
	Zero	0	446603	0.000	-	-
	5.00	8801	398038	0.02211	4.97	99.3
	10.0	19636	444159	0.04421	9.69	96.9
	20.0	47161	501644	0.09401	20.3	101.6
	50.0	108279	419610	0.2580	55.4	110.7
	100	238790	432871	0.5516	118	118.1
	200	405252	434972	0.9317	199	99.6
	500	1031727	438602	2.352	503	100.5
	900	1578614	465683	3.390	724	80.5
	1,000	1950331	449151	4.342	928	92.8
y = 0.00468x - 0.00114		r = 0.9929				

Accuracy was calculated from Analyst 1.5.2 software program.

Table 5. (Continued)

Analytical date	Theoretical concentration (ng/mL)	Peak area			Determined concentration (ng/mL)	Accuracy (%)
		Acetylshikonin	Emodin	Ratio		
Aug. 01, 2013	Blank	0	0	0.000	-	-
	Zero	0	454380	0.000	-	-
	5.00	4972	472901	0.01051	4.88	97.6
	10.0	11581	465560	0.02488	10.5	105.1
	20.0	24537	506302	0.04846	19.7	98.7
	50.0	65321	511068	0.1278	50.8	101.6
	100	127247	525293	0.2422	95.6	95.6
	200	283451	500686	0.5661	222	111.2
	500	624514	508200	1.229	482	96.4
	900	1132370	488560	2.318	909	100.9
	1,000	1137527	481053	2.365	927	92.7
y = 0.00255x - 0.00195		r = 0.9980				
Aug. 06, 2013	Blank	0	0	0.000	-	-
	Zero	0	207761	0.000	-	-
	5.00	5094	222193	0.02293	4.87	97.4
	10.0	11828	229067	0.05163	10.1	101.3
	20.0	24992	225573	0.1108	21.0	104.8
	50.0	57639	203607	0.2831	52.5	105.0
	100	121795	211914	0.5747	106	105.9
	200	237447	213817	1.111	204	102.0
	500	623265	236696	2.633	483	96.5
	900	1113880	228598	4.873	893	99.2
	1,000	1168528	243159	4.806	880	88.0
y = 0.00546x - 0.00369		r = 0.9980				
Aug. 07, 2013	Blank	0	0	0.000	-	-
	Zero	0	387186	0.000	-	-
	5.00	5473	303242	0.01805	5.10	101.9
	10.0	13309	429840	0.03096	9.41	94.1
	20.0	25366	406243	0.06244	19.9	99.7
	50.0	68128	422196	0.1614	53.0	106.0
	100	138774	422684	0.3283	109	108.8
	200	256062	404270	0.6334	211	105.4
	500	630026	418784	1.504	502	100.4
	900	1095979	426489	2.570	858	95.3
	1,000	1075475	405706	2.651	885	88.5
y = 0.00299x + 0.00280		r = 0.9973				

Accuracy was calculated from Analyst 1.5.2 software program.

Table 5. (Continued)

Analytical date	Theoretical concentration (ng/mL)	Peak area			Determined concentration (ng/mL)	Accuracy (%)
		Analyte	Emodin	Ratio		
Aug. 08, 2013	Blank	0	0	0.000	-	-
	Zero	0	421602	0.000	-	-
	5.00	5102	420149	0.01214	4.91	98.1
	10.0	11441	427842	0.02674	10.2	102.1
	20.0	22918	436078	0.05255	19.6	97.9
	50.0	60947	403023	0.1512	55.4	110.8
	100	121505	416920	0.2914	106	106.3
	200	234767	406083	0.5781	210	105.2
	500	525673	416104	1.263	459	91.8
	900	857291	393348	2.179	791	87.9
	1,000	834675	400019	2.087	758	-††
y = 0.00276x - 0.00138		r = 0.9961				
Aug. 26, 2013	Blank	0	0	0.000	-	-
	Zero	0	1258266	0.000	-	-
	5.00	7961	1116642	0.007129	4.94	98.7
	10.0	15435	1189122	0.01298	9.68	96.8
	20.0	32420	1202830	0.02695	21.0	105.0
	50.0	84930	1184266	0.07172	57.3	114.5
	100	168757	1291402	0.1307	105	105.0
	200	311525	1638482	0.1901	153	-†
	500	792188	1182156	0.6701	542	108.4
	900	1236479	1236847	0.9997	809	89.9
	1,000	1458362	1446254	1.008	816	81.6
y = 0.00123x + 0.00104		r = 0.9926				
Aug. 29, 2013	Blank	0	0	0.000	-	-
	Zero	0	262879	0.000	-	-
	5.00	3361	239881	0.01401	4.56	91.2
	10.0	7807	203799	0.03831	11.9	118.6
	20.0	15804	255012	0.06197	19.0	94.9
	50.0	41433	243159	0.1704	51.6	103.1
	100	93058	258642	0.3598	109	108.5
	200	140985	199870	0.7054	212	106.2
	500	431213	248532	1.735	522	104.4
	900	623018	243429	2.559	770	85.5
	1,000	673601	231468	2.910	875	87.5
y = 0.00333x - 0.00115		r = 0.9923				

†: This accuracy of this point did not meet the acceptance criteria.

††: The accuracy of ULOQ in the calibration samples did not meet the acceptance criteria. Although the results of calibration curve did not meet the acceptance criteria, the results of the batch were adopted because all QC samples could be detemined by the calbration curve excluding ULOQ.

Accuracy was calculated from Analyst 1.5.2 software program.

Table 6. Reproducibility for the determination of Acetylshikonin in stabilized rat plasma

Theoretical concentration (ng/mL)	Analytical date	Determined concentration (ng/mL)	Intra reproducibility			Inter reproducibility		
			Mean ± SD (ng/mL)	Accuracy (%)	Precision (%)	Mean ± SD (ng/mL)	Accuracy (%)	Precision (%)
5.00	Jul. 04, 2013	6.19	5.90 ± 0.54	118.0	9.1	5.36 ± 0.81	107.1	15.2
		6.61						
		5.92						
		5.25						
		5.53						
	Jul. 10, 2013	4.34	4.87 ± 1.02	97.4	20.9			
		6.61						
		4.93						
		4.31						
		4.15						
	Jul. 11, 2013	5.13	5.43 ± 0.80	108.6	14.6			
		6.68						
		5.73						
		4.75						
		4.86						
	Aug. 26, 2013	4.37	4.71 ± 0.36	94.2	7.7			
		4.46						
		4.81						
		4.62						
		5.28						
	Aug. 29, 2013	5.52	5.87 ± 0.59	117.4	10.1			
		6.88						
		5.73						
		5.37						
		5.86						
15.0	Jul. 04, 2013	18.4	17.1 ± 1.2	113.7	6.8	16.4 ± 1.1	109.3	6.9
		17.5						
		15.2						
		17.1						
		17.1						
	Jul. 10, 2013	17.5	16.4 ± 1.4	109.1	8.6			
		17.2						
		16.9						
		14.0						
		16.2						
	Jul. 11, 2013	14.7	15.3 ± 0.8	101.7	5.3			
		16.4						
		15.6						
		15.3						
		14.3						
	Aug. 26, 2013	16.2	16.6 ± 0.7	110.4	4.2			
		16.2						
		17.6						
		16.9						
		15.9						
	Aug. 29, 2013	15.6	16.7 ± 0.9	111.3	5.3			
		18.0						
		16.7						
		16.3						
		16.9						

Accuracy (%) = (Mean of the determined concentration / theoretical concentration) × 100.

Precision (%) = (Standard deviation (SD) / Mean) × 100.

Table 6. (Continued)

Theoretical concentration (ng/mL)	Analytical date	Determined concentration (ng/mL)	Intra reproducibility			Inter reproducibility		
			Mean ± SD (ng/mL)	Accuracy (%)	Precision (%)	Mean ± SD (ng/mL)	Accuracy (%)	Precision (%)
300	Jul. 04, 2013	318	286 ± 20	95.2	7.0	314 ± 40	104.8	12.7
		283						
		263						
		279						
		285						
	Jul. 10, 2013	289	322 ± 21	107.2	6.4			
		345						
		319						
		330						
		325						
	Jul. 11, 2013	273	267 ± 18	89.0	6.8			
		261						
		238						
		281						
		282						
	Aug. 26, 2013	382	360 ± 26	120.0	7.1			
		393						
		347						
		337						
		341						
	Aug. 29, 2013	338	338 ± 23	112.7	6.8			
		372						
		307						
		336						
		338						
750	Jul. 04, 2013	608	666 ± 55	88.8	8.2	748 ± 89	99.7	11.9
		625						
		653						
		735						
		710						
	Jul. 10, 2013	947	881 ± 83	117.5	9.4			
		770						
		878						
		975						
		835						
	Jul. 11, 2013	771	707 ± 37	94.3	5.2			
		688						
		706						
		688						
		683						
	Aug. 26, 2013	766	757 ± 13	101.0	1.7			
		768						
		737						
		752						
		763						
	Aug. 29, 2013	801	728 ± 54	97.0	7.5			
		731						
		757						
		670						
		680						

Accuracy (%) = (Mean of the determined concentration / theoretical concentration) × 100.

Precision (%) = (Standard deviation (SD) / Mean) × 100.

Table 7. Reproducibility for the determination of Acetylshikonin in stabilized rat plasma containing unacceptable data

Theoretical concentration (ng/mL)	Analytical date	Determined concentration (ng/mL)	Intra reproducibility			Inter reproducibility		
			Mean ± SD (ng/mL)	Accuracy (%)	Precision (%)	Mean ± SD (ng/mL)	Accuracy (%)	Precision (%)
5.00	Jul. 04, 2013	6.19	5.90 ± 0.54	118.0	9.1	5.23 ± 0.77	104.6	14.8
		6.61				(104.6 ± 15.5%)		
		5.92						
		5.25						
		5.53						
	Jul. 08, 2013	4.64	4.31 ± 0.45	86.3	10.4			
		4.32						
		4.39						
		4.66						
		3.56						
	Jul. 09, 2013	5.19	5.48 ± 0.58	109.6	10.5			
		4.59						
		5.86						
		5.90						
		5.85						
	Jul. 10, 2013	4.34	4.87 ± 1.02	97.4	20.9			
		6.61						
		4.93						
		4.31						
		4.15						
	Jul. 11, 2013	5.13	5.43 ± 0.80	108.6	14.6			
		6.68						
		5.73						
		4.75						
		4.86						
	Jul. 18, 2013	5.16	5.26 ± 0.35	105.2	6.6			
		5.20						
		5.56						
		5.62						
		4.76						
	Aug. 26, 2013	4.37	4.71 ± 0.36	94.2	7.7			
		4.46						
		4.81						
		4.62						
		5.28						
	Aug. 29, 2013	5.52	5.87 ± 0.59	117.4	10.1			
		6.88						
		5.73						
		5.37						
		5.86						

Accuracy (%) = (Mean of the determined concentration / theoretical concentration) × 100.
Precision (%) = (Standard deviation (SD) / Mean) × 100.

Table 7. (Continued)

Theoretical concentration (ng/mL)	Analytical date	Determined concentration (ng/mL)	Intra reproducibility			Inter reproducibility		
			Mean ± SD (ng/mL)	Accuracy (%)	Precision (%)	Mean ± SD (ng/mL)	Accuracy (%)	Precision (%)
15.0	Jul. 04, 2013	18.4	17.1 ± 1.2	113.7	6.8	16.1 ± 1.9 (107.1 ± 12.4%)	107.1	11.6
		17.5						
		15.2						
		17.1						
		17.1						
	Jul. 08, 2013	9.39	13.5 ± 2.6	90.1	19.3			
		15.3						
		15.8						
		14.5						
		12.6						
	Jul. 09, 2013	14.4	17.9 ± 2.2	119.1	12.4			
		19.1						
		17.1						
		20.1						
		18.6						
	Jul. 10, 2013	17.5	16.4 ± 1.4	109.1	8.6			
		17.2						
		16.9						
		14.0						
		16.2						
	Jul. 11, 2013	14.7	15.3 ± 0.8	101.7	5.3			
		16.4						
		15.6						
		15.3						
		14.3						
	Jul. 18, 2013	14.5	15.2 ± 0.9	101.5	5.9			
		16.3						
		16.1						
		14.7						
		14.5						
	Aug. 26, 2013	16.2	16.6 ± 0.7	110.4	4.2			
		16.2						
		17.6						
		16.9						
		15.9						
	Aug. 29, 2013	15.6	16.7 ± 0.9	111.3	5.3			
		18.0						
		16.7						
		16.3						
		16.9						

Accuracy (%) = (Mean of the determined concentration / theoretical concentration) × 100.
Precision (%) = (Standard deviation (SD) / Mean) × 100.

Table 7. (Continued)

Theoretical concentration (ng/mL)	Analytical date	Determined concentration (ng/mL)	Intra reproducibility			Inter reproducibility		
			Mean ± SD (ng/mL)	Accuracy (%)	Precision (%)	Mean ± SD (ng/mL)	Accuracy (%)	Precision (%)
300	Jul. 04, 2013	318	286 ± 20	95.2	7.0	319 ± 57 (106.4 ± 18.9%)	106.4	17.8
		283						
		263						
		279						
		285						
	Jul. 08, 2013	203	270 ± 52	89.9	19.2			
		253						
		347						
		270						
		276						
	Jul. 09, 2013	474	421 ± 36	140.5	8.6			
		431						
		423						
		403						
		376						
	Jul. 10, 2013	289	322 ± 21	107.2	6.4			
		345						
		319						
		330						
		325						
	Jul. 11, 2013	273	267 ± 18	89.0	6.8			
		261						
		238						
		281						
		282						
	Jul. 18, 2013	314	289 ± 20	96.3	6.9			
		305						
		283						
		277						
		266						
	Aug. 26, 2013	382	360 ± 26	120.0	7.1			
		393						
		347						
		337						
		341						
	Aug. 26, 2013	338	338 ± 23	112.7	6.8			
		372						
		307						
		336						
		338						

Accuracy (%) = (Mean of the determined concentration / theoretical concentration) × 100.
Precision (%) = (Standard deviation (SD) / Mean) × 100.

Table 7. (Continued)

Theoretical concentration (ng/mL)	Analytical date	Determined concentration (ng/mL)	Intra reproducibility			Inter reproducibility		
			Mean ± SD (ng/mL)	Accuracy (%)	Precision (%)	Mean ± SD (ng/mL)	Accuracy (%)	Precision (%)
750	Jul. 04, 2013	608	666 ± 55	88.8	8.2	710 ± 139 (94.7 ± 18.5%)	94.7	19.5
		625						
		653						
		735						
		710						
	Jul. 08, 2013	436	501 ± 50	66.8	10.0			
		469						
		501						
		539						
		559						
	Jul. 09, 2013	818	876 ± 82	116.8	9.4			
		948						
		761						
		938						
		914						
	Jul. 10, 2013	947	881 ± 83	117.5	9.4			
		770						
		878						
		975						
		835						
	Jul. 11, 2013	771	707 ± 37	94.3	5.2			
		688						
		706						
		688						
		683						
	Jul. 18, 2013	584	567 ± 85	75.6	15.0			
		649						
		427						
		614						
		562						
	Aug. 26, 2013	766	757 ± 13	101.0	1.7			
		768						
		737						
		752						
		763						
	Aug. 29, 2013	801	728 ± 54	97.0	7.5			
		731						
		757						
		670						
		680						

Accuracy (%) = (Mean of the determined concentration / theoretical concentration) × 100.
Precision (%) = (Standard deviation (SD) / Mean) × 100.

Table 8. Dilution reproducibility for the determination of Acetylshikonin in stabilized rat plasma
[Analytical date: Jul. 08, 2013]

Analyte	Theoretical concentration (ng/mL)	Dilution factor	No.	Determined concentration (ng/mL)	Mean ± SD (ng/mL)	Accuracy (%)	Precision (%)
Acetylshikonin	2,000	10	1	1,750	2,090 ± 244	104.4	11.7
			2	2,280			
			3	1,930			
			4	2,330			
			5	2,150			

Accuracy (%) = (Mean of the determined concentration / theoretical concentration) × 100.
Precision (%) = (Standard deviation (SD) / Mean) × 100.

Table 9. Stability for the determination of Acetylshikonin in stabilized rat plasma

Theoretical concentration (ng/mL)	Analytical date	Classification	Determined concentration (ng/mL)	Mean ± SD (ng/mL)	Accuracy (%)	Precision (%)
15.0	Aug. 06, 2013	Initial	13.5	14.4 ± 0.8	96.1	5.6
			14.8			
			15.2			
			15.0			
			13.6			
	Aug. 07, 2013	On ice	14.6	13.7 ± 0.8	91.1	6.0
			13.3			
		0.5 hrs	13.1			
	Aug. 07, 2013	On ice	13.2	14.2 ± 0.9	94.7	6.1
			14.6			
		1 hr	14.8			
	Aug. 07, 2013	Room tempreture	13.1	13.4 ± 0.6	89.1	4.8
		1hr	14.1			
		after derivatization	12.9			
	Jul. 25, 2013	Initial	16.2	15.6 ± 2.2	103.7	13.8
			18.5			
			13.2			
			16.2			
			13.7			
	Jul. 30, 2013	Freezer	13.7	13.8 ± 0.7	91.8	5.1
		(-70℃)	14.5			
		5 days	13.1			
	Aug. 01, 2013	Freezer	14.8	16.6 ± 3.2	110.9	19.1
		(-70℃)	20.3			
		7 days	14.8			
	Aug. 08, 2013	Freezer	14.6	15.8 ± 1.0	105.1	6.4
		(-70℃)	16.4			
		14 days	16.3			
	Aug. 26, 2013	Freezer	12.9	13.1 ± 0.9	87.6	6.7
		(-70℃)	14.1			
		32 days	12.4			
	Jul. 26, 2013	Freeze-thaw	15.7	15.9 ± 1.2	106.0	7.6
		1 cycle	17.2			
		(-70℃)	14.8			
	Jul. 09, 2013	Initial	14.4	17.9 ± 2.2	119.1	12.4
			19.1			
			17.1			
			20.1			
			18.6			
	Jul. 10, 2013	Extracted samples	11.2	14.2 ± 4.1	94.4	28.7
		in autosampler (10℃)	18.8			
		24 hrs	12.5			
	Jul. 11, 2013	Extracted samples	11.2	15.1 ± 4.2	100.9	27.9
		in autosampler (10℃)	19.6			
		48 hrs	14.6			

Accuracy (%) = (Mean of the determined concentration / theoretical concentration) × 100.

Precision (%) = (Standard deviation (SD) / Mean) × 100.

Table 9. (Continued)

Theoretical concentration (ng/mL)	Analytical date	Classification	Determined concentration (ng/mL)	Mean ± SD (ng/mL)	Accuracy (%)	Precision (%)
750	Aug. 06, 2013	Initial	686	696 ± 20	92.8	2.9
			711			
			666			
			712			
			706			
	Aug. 07, 2013	On ice	760	768 ± 8	102.4	1.0
			776			
		0.5 hrs	767			
	Aug. 07, 2013	On ice	740	737 ± 17	98.3	2.3
			719			
		1 hr	752			
	Aug. 07, 2013	Room tempreture	730	707 ± 21	94.2	2.9
		1hr	699			
		after derivatization	691			
	Jul. 25, 2013	Initial	778	711 ± 82	94.8	11.5
			779			
			752			
			613			
			632			
	Jul. 30, 2013	Freezer	587	627 ± 45	83.6	7.1
		(-70℃)	675			
		5 days	618			
	Aug. 01, 2013	Freezer	649	645 ± 19	86.0	3.0
		(-70℃)	662			
		7 days	624			
	Aug. 08, 2013	Freezer	798	737 ± 54	98.3	7.4
		(-70℃)	719			
		14 days	694			
	Aug. 26, 2013	Freezer	660	665 ± 6	88.7	0.8
		(-70℃)	671			
		32 days	665			
	Jul. 26, 2013	Freeze-thaw	715	673 ± 85	89.7	12.6
		1 cycle	728			
		(-70℃)	575			
	Jul. 09, 2013	Initial	818	876 ± 82	116.8	9.4
			948			
			761			
			938			
			914			
	Jul. 10, 2013	Extracted samples	624	625 ± 52	83.4	8.3
		in autosampler (10℃)	678			
		24 hrs	574			
	Jul. 11, 2013	Extracted samples	651	658 ± 45	87.8	6.9
		in autosampler (10℃)	707			
		48 hrs	617			

Accuracy (%) = (Mean of the determined concentration / theoretical concentration) × 100.
Precision (%) = (Standard deviation (SD) / Mean) × 100.

Table 10. Stability of Acetylshikonin and Emodin in the stock solutions

Analyte: Acetylshikonin

Analytical date	Preparation date	Classification	Peak area			Mean	Residual ratio (%)
			Acetylshikonin (A)	Emodin (B)	Ratio (A/B)		
Jul. 22, 2013	Jul. 22, 2013	Control	950933	507366	1.874	1.918	-
			981248	511261	1.919		
			1006332	513623	1.959		
	Jul. 22, 2013	Room temperature 2 hrs	1025000	538939	1.902	1.952	101.8
			1008349	528296	1.909		
			1037818	507392	2.045		
	Jul. 02, 2013	Refrigerator 20 days	836611	512048	1.634	1.760	91.8
			884610	484564	1.826		
			954573	524332	1.821		

Residual ratio (%) = (Mean peak area ratio of sample after storage / Mean peak area ratio of sample immediately after preparation) × 100.

Analyte: Emodin

Analytical date	Preparation date	Classification	Peak area			Mean	Residual ratio (%)
			Acetylshikonin (A)	Emodin (B)	Ratio (B/A)		
Jul. 22, 2013	Jul. 22, 2013	Control	950933	507366	0.5335	0.522	-
			981248	511261	0.5210		
			1006332	513623	0.5104		
	Jul. 22, 2013	Room temperature 2 hrs	1010457	549778	0.5441	0.583	111.8
			1002651	545726	0.5443		
			689172	455438	0.6608		
	Jul. 02, 2013	Refrigerator 20 days	1049621	550018	0.5240	0.520	99.7
			1067087	596602	0.5591		
			1089509	520530	0.4778		

Residual ratio (%) = (Mean peak area ratio of sample after storage / Mean peak area ratio of sample immediately after preparation) × 100.

<LC/MS/MS를 이용한 비글견 혈장 중acetylshikonin의 분석법 Validation>

Table 1. System suitability for the determination of Acetylshikonin in stabilized dog plasma

Analytical date	Classification		No. 1	No. 2	No. 3	No. 4	No. 5	Mean ± SD	Precision (%)
Sep. 06, 2013	Peak area ratio		0.03091	0.03145	0.03278	0.03445	0.03363	0.03264 ± 0.00147	4.5
	Retention time (min)	Analyte	3.72	3.74	3.72	3.70	3.69	3.71 ± 0.02	0.5
		Emodin	3.49	3.49	3.48	3.48	3.48	3.48 ± 0.01	0.2
Sep. 10, 2013	Peak area ratio		0.04425	0.04751	0.04284	0.04222	0.04820	0.04500 ± 0.00272	6.0
	Retention time (min)	Analyte	3.72	3.72	3.72	3.71	3.72	3.72 ± 0.00	0.1
		Emodin	3.50	3.50	3.50	3.50	3.51	3.50 ± 0.00	0.1
Sep. 11, 2013	Peak area ratio		0.03675	0.03328	0.03512	0.03336	0.03705	0.03511 ± 0.00179	5.1
	Retention time (min)	Analyte	3.72	3.73	3.72	3.71	3.72	3.72 ± 0.01	0.2
		Emodin	3.49	3.50	3.50	3.49	3.50	3.50 ± 0.01	0.2
Sep. 13, 2013	Peak area ratio		0.04111	0.04017	0.04260	0.04339	0.04186	0.04183 ± 0.00126	3.0
	Retention time (min)	Analyte	3.74	3.73	3.73	3.72	3.76	3.74 ± 0.02	0.4
		Emodin	3.51	3.49	3.49	3.50	3.50	3.50 ± 0.01	0.2
Sep. 14, 2013	Peak area ratio		0.04030	0.03994	0.04154	0.03932	0.04358	0.04094 ± 0.00169	4.1
	Retention time (min)	Analyte	3.74	3.74	3.74	3.73	3.74	3.74 ± 0.00	0.1
		Emodin	3.50	3.51	3.51	3.51	3.51	3.51 ± 0.00	0.1
Sep. 25, 2013	Peak area ratio		0.04647	0.04484	0.04556	0.04654	0.04187	0.04506 ± 0.00191	4.2
	Retention time (min)	Analyte	3.72	3.73	3.73	3.74	3.74	3.73 ± 0.01	0.2
		Emodin	3.51	3.52	3.52	3.52	3.52	3.52 ± 0.00	0.1
Oct. 13, 2013	Peak area ratio		0.01597	0.01695	0.01518	0.01481	0.01605	0.01579 ± 0.00083	5.3
	Retention time (min)	Analyte	3.69	3.70	3.70	3.69	3.69	3.69 ± 0.01	0.1
		Emodin	3.46	3.46	3.47	3.47	3.46	3.46 ± 0.01	0.2
Oct. 24, 2013	Peak area ratio		0.02373	0.02137	0.02115	0.02207	0.02372	0.02241 ± 0.00125	5.6
	Retention time (min)	Analyte	3.68	3.69	3.69	3.69	3.69	3.69 ± 0.00	0.1
		Emodin	3.47	3.47	3.47	3.47	3.48	3.47 ± 0.00	0.1

Peak area ratio = (Peak area of reference standard) / (Peak area of internal reference standard).

Precision (%) = (Standard deviation (SD) / Mean) × 100.

Analyte: Acetylshikonin derivatized.

Table 2. Carryover effect for the determination of Acetylshikonin in stabilized dog plasma

Analytical date	Analyte	No.	Peak area of blank sample	Peak area of LLOQ	Carryover effect (%)
Sep. 06, 2013	Acetylshikonin derivatized	1	0	6052	0.0
		2	0		0.0
		3	0		0.0
	Emodin	1	0	179723	0.0
		2	0		0.0
		3	0		0.0
Sep. 10, 2013	Acetylshikonin derivatized	1	0	4971	0.0
		2	0		0.0
		3	0		0.0
	Emodin	1	0	174666	0.0
		2	0		0.0
		3	0		0.0
Sep. 11, 2013	Acetylshikonin derivatized	1	0	6995	0.0
		2	0		0.0
		3	0		0.0
	Emodin	1	0	175632	0.0
		2	0		0.0
		3	0		0.0
Sep. 13, 2013	Acetylshikonin derivatized	1	0	7862	0.0
		2	0		0.0
		3	0		0.0
	Emodin	1	0	198389	0.0
		2	0		0.0
		3	0		0.0
Sep. 14, 2013	Acetylshikonin derivatized	1	357	8325	4.3
		2	0		0.0
		3	0		0.0
	Emodin	1	0	203263	0.0
		2	0		0.0
		3	0		0.0
Sep. 25, 2013	Acetylshikonin derivatized	1	0	8633	0.0
		2	0		0.0
		3	0		0.0
	Emodin	1	0	223216	0.0
		2	0		0.0
		3	0		0.0
Oct. 13, 2013	Acetylshikonin derivatized	1	0	4905	0.0
		2	0		0.0
		3	0		0.0
	Emodin	1	0	248670	0.0
		2	0		0.0
		3	0		0.0
Oct. 24, 2013	Acetylshikonin derivatized	1	0	4557	0.0
		2	0		0.0
		3	0		0.0
	Emodin	1	0	208540	0.0
		2	0		0.0
		3	0		0.0

Carryover effect (%) = (Peak area of blank sample)/ (Peak area of LLOQ sample) × 100.

Table 3. Selectivity for the determination of Acetylshikonin in stabilized dog plasma
[Analytical date: Sep. 10, 2013]

Analyte	Sex	Lot No.	Peak area of blank sample	Peak area of LLOQ	Selectivity (%)
Acetylshikonin derivatized	Male	DMP130327001	0	4767	0.0
		DMP130327002	0	4630	0.0
		DMP130327003	0	4611	0.0
	Female	DFP130327001	0	5242	0.0
		DFP130327002	0	3519	0.0
		DFP130327003	0	3685	0.0
Emodin	Male	DMP130327001	0	124861	0.0
		DMP130327002	0	213376	0.0
		DMP130327003	0	153839	0.0
	Female	DFP130327001	0	161253	0.0
		DFP130327002	0	210496	0.0
		DFP130327003	0	199841	0.0

Selectivity (%) =(Peak area of blank sample)/ (Peak area of LLOQ sample) × 100.

Table 4. Matrix effect for the determination of Acetylshikonin in stabilized dog plasma

Analyte	Theoretical concentration (ng/mL)	Sex	Analytical date	Lot No.	Determined concentration (ng/mL)	Mean ± SD (ng/mL)	Accuracy (%)	Precision (%)
Acetylshikonin	5.00	Male	Sep. 10, 2013	DMP130327001	6.41	4.55 ± 1.12	90.9	24.5
				DMP130327002	3.65			
				DMP130327003	5.03			
			Sep. 25, 2013	DMP130326001	6.21			
				DMP130326002	4.88			
				DMP130326003	4.85			
			Oct. 13, 2013	DMP130320001	5.32			
				DMP130320002	6.19			
				DMP130320003	4.10			
		Female	Sep. 10, 2013	DFP130327001	5.46			
				DFP130327002	2.82			
				DFP130327003	3.11			
			Sep. 25, 2013	DFP130326001	3.26			
				DFP130326002	4.50			
				DFP130326003	3.54			
			Oct. 13, 2013	DFP130320001	3.35			
				DFP130320002	4.26			
				DFP130320003	4.89			

Accuracy (%) = (Determined concentration / Theoretical concentration) × 100.

Precision (%) = (Standard deviation (SD) / Mean) × 100.

Table 5. Calibration curves (weighting: $1/X^2$) for the determination of Acetylshikonin in stabilized dog plasma

Analytical date	Theoretical concentration (ng/mL)	Peak area			Determined concentration (ng/mL)	Accuracy (%)
		Analyte	Emodin	Ratio		
Sep. 06, 2013	Blank	0	0	0.000	-	-
	Zero	0	159721	0.000	-	-
	5.00	6052	179723	0.03367	5.02	100.5
	10.0	12269	169378	0.07244	10.1	100.6
	20.0	26489	187435	0.1413	19.0	95.0
	50.0	69096	176686	0.3911	51.4	102.8
	100	131607	169177	0.7779	102	101.6
	200	284580	172616	1.649	215	107.3
	500	635170	168007	3.781	491	98.3
	900	1215317	173817	6.992	908	100.9
	1,000	1298453	181514	7.153	929	92.9
y = 0.00770x -0.00502		r = 0.9988				
Sep. 10, 2013	Blank	0	0	0.000	-	-
	Zero	0	172738	0.000	-	-
	5.00	4971	174666	0.02846	4.78	95.6
	10.0	9711	157374	0.06171	10.3	103.4
	20.0	21123	163037	0.1296	21.7	108.4
	50.0	49728	158867	0.3130	52.4	104.7
	100	96440	154235	0.6253	105	104.6
	200	201134	171057	1.176	197	98.3
	500	528298	174598	3.026	506	101.2
	900	865993	175913	4.923	823	91.4
	1,000	919956	166492	5.526	924	92.4
y = 0.00598x -0.000137		r = 0.9977				
Sep. 11, 2013	Blank	0	0	0.000	-	-
	Zero	0	183492	0.000	-	-
	5.00	6995	175632	0.03983	4.90	98.0
	10.0	15637	184561	0.08472	10.2	102.2
	20.0	32138	182881	0.1757	21.0	105.0
	50.0	76633	188820	0.4059	48.3	96.5
	100	168950	199998	0.8448	100	100.3
	200	304506	177099	1.719	204	101.9
	500	684058	169669	4.032	478	95.6
	900	1273824	158632	8.030	951	105.7
	1,000	1347300	168248	8.008	949	94.9
y = 0.00844x -0.00153		r = 0.9990				

Accuracy was calculated from Analyst 1.5.2 software program.

Analyte: Acetylshikonin derivatized.

Table 5. (Continued)

Analytical date	Theoretical concentration (ng/mL)	Peak area			Determined concentration (ng/mL)	Accuracy (%)
		Analyte	Emodin	Ratio		
Sep. 13, 2013	Blank	0	0	0.000	-	-
	Zero	0	203116	0.000	-	-
	5.00	7862	198389	0.03963	4.86	97.2
	10.0	16707	293646	0.05689	6.86	-†
	20.0	36848	204193	0.1805	21.2	105.8
	50.0	101601	208442	0.4874	56.7	113.3
	100	198091	221395	0.8947	104	103.8
	200	364349	211405	1.723	200	99.8
	500	844995	221043	3.823	443	88.5
	900	1468930	198429	7.403	857	95.2
	1,000	1472841	177007	8.321	963	96.3
y = 0.00864x -0.00237		r = 0.9967				
Sep. 14, 2013	Blank	0	0	0.000	-	-
	Zero	0	217425	0.000	-	-
	5.00	8325	203263	0.04095	4.76	95.3
	10.0	16452	189930	0.08662	10.2	101.6
	20.0	34183	175504	0.1948	22.9	114.7
	50.0	93295	176769	0.5278	62.3	-†
	100	164535	174955	0.9404	111	111.1
	200	346847	229198	1.513	179	89.4
	500	813513	188369	4.319	511	102.1
	900	1308040	178851	7.314	865	96.1
	1,000	1525633	201112	7.586	897	89.7
y = 0.00846x +0.000665		r = 0.9945				
Sep. 25, 2013	Blank	0	0	0.000	-	-
	Zero	0	226414	0.000	-	-
	5.00	8633	223216	0.03868	4.72	94.4
	10.0	19581	209571	0.09343	10.7	107.4
	20.0	38816	205894	0.1885	21.2	106.0
	50.0	98883	200588	0.4930	54.7	109.3
	100	195149	242078	0.8061	89.1	89.1
	200	381304	203720	1.872	206	103.1
	500	908656	195381	4.651	512	102.3
	900	1355861	218284	6.211	683	-†
	1,000	1530748	190442	8.038	884	88.4
y = 0.00910x -0.00425		r = 0.9954				

†: This accuracy of this point did not meet the acceptance criteria.

Accuracy was calculated from Analyst 1.5.2 software program.

Analyte: Acetylshikonin derivatized.

Table 5. (Continued)

Analytical date	Theoretical concentration (ng/mL)	Peak area			Determined concentration (ng/mL)	Accuracy (%)
		Analyte	Emodin	Ratio		
Oct. 13, 2013	Blank	0	0	0.000	-	-
	Zero	0	254571	0.000	-	-
	5.00	4905	248670	0.01973	4.70	94.0
	10.0	11188	231661	0.04829	11.2	111.5
	20.0	23702	276343	0.08577	19.6	98.1
	50.0	55473	240387	0.2308	52.4	104.8
	100	115931	250935	0.4620	105	104.6
	200	231453	253337	0.9136	207	103.3
	500	516424	232478	2.221	502	100.4
	900	854815	299079	2.858	646	-†
	1,000	884917	240216	3.684	832	83.2
y = 0.00443x -0.00108		r = 0.9951				
Oct. 24, 2013	Blank	0	0	0.000	-	-
	Zero	0	192650	0.000	-	-
	5.00	4557	208540	0.02185	5.07	101.4
	10.0	6366	190702	0.03338	9.35	93.5
	20.0	12940	210893	0.06136	19.8	98.8
	50.0	33513	201858	0.1660	58.6	117.3
	100	62315	207492	0.3003	109	108.6
	200	116626	200436	0.5819	213	106.6
	500	296059	217744	1.360	502	100.5
	900	482598	212451	2.272	841	93.5
	1,000	507567	234963	2.160	800	80.0
y = 0.00269x +0.00822		r = 0.9927				

†: This accuracy of this point did not meet the acceptance criteria.

Accuracy was calculated from Analyst 1.5.2 software program.

Analyte: Acetylshikonin derivatized.

Table 6. Reproducibility for the determination of Acetylshikonin in stabilized dog plasma

Theoretical concentration (ng/mL)	Analytical date	Determined concentration (ng/mL)	Intra reproducibility			Inter reproducibility		
			Mean ± SD (ng/mL)	Accuracy (%)	Precision (%)	Mean ± SD (ng/mL)	Accuracy (%)	Precision (%)
5.00	Sep. 06, 2013	6.00	6.11 ± 0.27	122.3	4.5	5.34 ± 0.64	106.8	12.0
		6.03						
		6.27						
		5.78						
		6.49						
	Sep. 10, 2013	4.61	4.69 ± 0.27	93.8	5.7			
		4.89						
		4.41						
		5.04						
		4.50						
	Sep. 11, 2013	5.24	4.88 ± 0.55	97.6	11.3			
		5.30						
		5.29						
		4.36						
		4.20						
	Sep. 13, 2013	6.14	5.59 ± 0.39	111.8	6.9			
		5.70						
		5.13						
		5.32						
		5.65						
	Sep. 14, 2013	5.45	5.43 ± 0.47	108.7	8.7			
		5.77						
		5.55						
		4.63						
		5.77						
15.0	Sep. 06, 2013	17.7	17.7 ± 1.0	118.0	5.4	16.5 ± 1.4	109.8	8.2
		17.7						
		19.2						
		16.6						
		17.3						
	Sep. 10, 2013	17.4	16.6 ± 0.7	110.8	4.3			
		17.2						
		16.4						
		15.6						
		16.5						
	Sep. 11, 2013	13.0	14.5 ± 0.9	96.9	6.0			
		14.7						
		14.9						
		15.1						
		15.0						
	Sep. 13, 2013	18.0	16.6 ± 1.1	110.4	6.5			
		17.4						
		16.0						
		15.7						
		15.7						
	Sep. 14, 2013	16.8	17.0 ± 0.9	113.1	5.3			
		17.6						
		17.2						
		15.5						
		17.7						

Accuracy (%) = (Mean of the determined concentration / theoretical concentration) × 100.

Precision (%) = (Standard deviation (SD) / Mean) × 100.

Table 6. (Continued)

Theoretical concentration (ng/mL)	Analytical date	Determined concentration (ng/mL)	Intra reproducibility			Inter reproducibility		
			Mean ± SD (ng/mL)	Accuracy (%)	Precision (%)	Mean ± SD (ng/mL)	Accuracy (%)	Precision (%)
300	Sep. 06, 2013	347	350 ± 38	116.5	11.0	312 ± 30	104.0	9.7
		328						
		348						
		312						
		413						
	Sep. 10, 2013	323	308 ± 16	102.7	5.3			
		314						
		290						
		291						
		322						
	Sep. 11, 2013	271	280 ± 8	93.5	2.9			
		288						
		287						
		272						
		284						
	Sep. 13, 2013	285	305 ± 14	101.7	4.5			
		315						
		319						
		299						
		308						
	Sep. 14, 2013	318	317 ± 19	105.5	5.9			
		329						
		320						
		331						
		285						
750	Sep. 06, 2013	801	744 ± 42	99.1	5.6	684 ± 47	91.2	6.8
		732						
		754						
		685						
		746						
	Sep. 10, 2013	673	668 ± 13	89.1	1.9			
		653						
		659						
		686						
		670						
	Sep. 11, 2013	670	652 ± 18	86.9	2.8			
		636						
		638						
		642						
		673						
	Sep. 13, 2013	678	659 ± 43	87.9	6.5			
		698						
		674						
		586						
		661						
	Sep. 14, 2013	708	697 ± 44	93.0	6.3			
		741						
		734						
		663						
		640						

Accuracy (%) = (Mean of the determined concentration / theoretical concentration) × 100.
Precision (%) = (Standard deviation (SD) / Mean) × 100.

Table 7. Dilution reproducibility for the determination of Acetylshikonin in stabilized dog plasma
[Analytical date: Sep. 25, 2013]

Analyte	Theoretical concentration (ng/mL)	Dilution factor	No.	Determined concentration (ng/mL)	Mean ± SD (ng/mL)	Accuracy (%)	Precision (%)
Acetylshikonin	2,000	10	1	2,120	2,070 ± 82	103.5	4.0
			2	1,950			
			3	2,020			
			4	2,120			
			5	2,140			

Accuracy (%) = (Mean of the determined concentration / theoretical concentration) × 100.
Precision (%) = (Standard deviation (SD) / Mean) × 100.

Table 8. Stability for the determination of Acetylshikonin in stabilized dog plasma

Theoretical concentration (ng/mL)	Analytical date	Classification	Determined concentration (ng/mL)	Mean	± SD (ng/mL)	Accuracy (%)	Precision (%)
15.0	Sep. 11, 2013	Initial	13.0	14.5	0.9	96.9	6.0
			14.7				
			14.9				
			15.1				
			15.0				
	Sep. 14, 2013	On ice	14.9	14.6	0.7	97.1	4.6
		2 hrs	13.8				
			15.0				
	Sep. 13, 2013	Extracted samples	14.9	16.5	1.4	109.8	8.3
		in autosampler (10℃)	17.1				
		47 hrs	17.4				
	Sep. 14, 2013	Extracted samples	17.9	17.9	0.7	119.3	3.9
		in autosampler (10℃)	17.2				
		71 hrs	18.6				
	Sep. 13, 2013	Freeze-thaw	15.8	14.7	1.7	98.0	11.2
		1 cycles	12.8				
		(-80℃)	15.5				
	Sep. 25, 2013	Deep freezer	16.8	17.5	0.6	116.9	3.7
		(-80℃)	17.8				
		2 weeks (14 days)	18.0				
	Oct. 24, 2013	Deep freezer †	19.0	17.6	1.3	117.6	7.2
		(-80℃)	17.4				
		1 month (42 days)	16.5				

Accuracy (%) = (Mean of the determined concentration / theoretical concentration) × 100.

Precision (%) = (Standard deviation (SD) / Mean) × 100.

†: The stability samples were pretreated on Oct. 23, 2013.

Table 8. (Continued)

Theoretical concentration (ng/mL)	Analytical date	Classification	Determined concentration (ng/mL)	Mean	± SD (ng/mL)	Accuracy (%)	Precision (%)
750	Sep. 11, 2013	Initial	670	652	18	86.9	2.8
			636				
			638				
			642				
			673				
	Sep. 14, 2013	On ice	660	635	22	84.7	3.4
		2 hrs	626				
			620				
	Sep. 13, 2013	Extracted samples	798	778	24	103.7	3.1
		in autosampler (10℃)	785				
		47 hrs	751				
	Sep. 14, 2013	Extracted samples	799	797	22	106.3	2.8
		in autosampler (10℃)	818				
		71 hrs	774				
	Sep. 13, 2013	Freeze-thaw	717	709	8	94.5	1.1
		1 cycles	701				
		(-80℃)	708				
	Sep. 25, 2013	Deep freezer	791	781	46	104.1	5.9
		(-80℃)	730				
		2 weeks (14 days)	821				
	Oct. 24, 2013	Deep freezer †	806	881	65	117.4	7.4
		(-80℃)	928				
		1 month (42 days)	908				

Accuracy (%) = (Mean of the determined concentration / theoretical concentration) × 100.

Precision (%) = (Standard deviation (SD) / Mean) × 100.

†: The stability samples were pretreated on Oct. 23, 2013.

<자초추출물의 랫드를 이용한 4주 반복 경구투여 독성동태시험에서 채취된 랫드 혈장 중 아세틸시코닌의 농도 측정>

Table 1. System suitability for the determination of acetylshikonin in rat plasma

Analytical date	Classification		No. 1	No. 2	No. 3	No. 4	No. 5	Mean ± SD	Precision (%)
Aug. 13, 2013	Peak area ratio		0.01933	0.02104	0.01984	0.02047	0.02040	0.02022 ± 0.00065	3.2
	Retention time (min)	Analyte	3.72	3.72	3.72	3.73	3.73	3.72 ± 0.01	0.1
		Emodin	3.50	3.50	3.50	3.50	3.51	3.50 ± 0.00	0.1
Aug. 22, 2013	Peak area ratio		0.02144	0.02465	0.02047	0.02454	0.02014	0.02225 ± 0.00220	9.9
	Retention time (min)	Analyte	3.70	3.70	3.70	3.70	3.70	3.70 ± 0.00	0.0
		Emodin	3.48	3.48	3.48	3.48	3.47	3.48 ± 0.00	0.1
Aug. 23, 2013	Peak area ratio		0.03429	0.03195	0.03336	0.03282	0.03183	0.03285 ± 0.00102	3.1
	Retention time (min)	Analyte	3.73	3.73	3.71	3.71	3.71	3.72 ± 0.01	0.3
		Emodin	3.50	3.49	3.50	3.49	3.49	3.49 ± 0.01	0.2
Aug. 27, 2013	Peak area ratio		0.01329	0.01459	0.01625	0.01392	0.01444	0.01450 ± 0.00110	7.6
	Retention time (min)	Analyte	3.70	3.70	3.70	3.71	3.71	3.70 ± 0.01	0.1
		Emodin	3.47	3.48	3.48	3.48	3.48	3.48 ± 0.00	0.1
Aug. 28, 2013	Peak area ratio		0.01378	0.01351	0.01307	0.01428	0.01295	0.01352 ± 0.00054	4.0
	Retention time (min)	Analyte	3.72	3.71	3.71	3.72	3.70	3.71 ± 0.01	0.2
		Emodin	3.49	3.49	3.49	3.49	3.48	3.49 ± 0.00	0.1
Sep. 10, 2013	Peak area ratio		0.03513	0.03347	0.03215	0.03312	0.03379	0.03353 ± 0.00108	3.2
	Retention time (min)	Analyte	3.72	3.74	3.74	3.71	3.72	3.73 ± 0.01	0.4
		Emodin	3.47	3.48	3.47	3.47	3.47	3.47 ± 0.00	0.1
Sep. 26, 2013	Peak area ratio		0.02952	0.02442	0.02583	0.02806	0.02766	0.02710 ± 0.00199	7.4
	Retention time (min)	Analyte	3.72	3.73	3.73	3.72	3.72	3.72 ± 0.01	0.1
		Emodin	3.50	3.51	3.51	3.50	3.50	3.50 ± 0.01	0.2
Sep. 27, 2013	Peak area ratio		0.02548	0.02459	0.02150	0.02641	0.02800	0.02520 ± 0.00242	9.6
	Retention time (min)	Analyte	3.73	3.72	3.73	3.73	3.73	3.73 ± 0.00	0.1
		Emodin	3.51	3.52	3.51	3.52	3.51	3.51 ± 0.01	0.2
Oct. 01, 2013	Peak area ratio		0.02232	0.02277	0.02359	0.02433	0.02445	0.02349 ± 0.00094	4.0
	Retention time (min)	Analyte	3.72	3.72	3.71	3.72	3.71	3.72 ± 0.01	0.1
		Emodin	3.50	3.50	3.50	3.50	3.50	3.50 ± 0.00	0.0

Peak area ratio = Peak area of analyte / Peak area of internal reference standard.

Precision (%) = (Standard deviation (SD) / Mean) × 100.

Analyte: Acetylshikonin dedrivatized.

Table 2. Calibration curves (weighting: $1/X^2$) for the determination of acetylshikonin in rat plasma

Analytical date	Nominal concentration (ng/mL)	Peak area			Measured concentration (ng/mL)	Accuracy (%)
		Analyte	Emodin	Ratio		
Aug. 13, 2013	Blank	0	0	0	-	-
	Zero	0	253886	0	-	-
	5.00	5075	250781	0.02024	4.80	95.9
	10.0	10862	245269	0.04429	10.2	101.6
	20.0	23434	230856	0.1015	22.9	114.6
	50.0	53158	246746	0.2154	48.3	96.6
	100	113042	256449	0.4408	98.6	98.6
	200	238541	257098	0.9278	207	103.6
	500	560759	244687	2.292	511	102.3
	900	880838	235903	3.734	833	92.5
	1,000	924641	218745	4.227	943	94.3
y = 0.00448x - 0.00127		r = 0.9972				
Aug. 22, 2013	Blank	0	0	0	-	-
	Zero	0	115614	0	-	-
	5.00	2492	115671	0.02155	4.43	88.5
	10.0	6900	106674	0.06468	11.9	119.4
	20.0	13463	115671	0.1164	20.9	104.7
	50.0	36333	124101	0.2928	51.6	103.3
	100	72513	120927	0.5996	105	105.1
	200	145038	118639	1.223	214	106.8
	500	370911	126826	2.925	510	102.0
	900	523251	118978	4.398	766	85.1
	1,000	591212	120949	4.888	852	85.2
y = 0.00574x - 0.00388		r = 0.9915				
Aug. 23, 2013	Blank	0	0	0	-	-
	Zero	0	87278	0	-	-
	5.00	3189	94061	0.03390	4.80	96.0
	10.0	6587	91097	0.07230	10.2	102.3
	20.0	15878	103101	0.1540	21.8	109.0
	50.0	38711	100209	0.3863	54.7	109.3
	100	85437	94372	0.9053	128	128.1†
	200	165146	133884	1.233	175	87.3
	500	378016	98033	3.856	546	109.1
	900	601151	101714	5.910	836	92.9
	1,000	649431	97595	6.654	942	94.2
y = 0.00707x - 0.0000141		r = 0.9951				

Accuracy was calculated using Analyst 1.5.2 software program.

Analyte: Acetylshikonin derivatized.

†: The accuracy of this point did not meet the acceptance criteria.

Table 2. (Continued)

Analytical date	Nominal concentration (ng/mL)	Peak area			Measured concentration (ng/mL)	Accuracy (%)
		Analyte	Emodin	Ratio		
Aug. 27, 2013	Blank	0	0	0	-	-
	Zero	0	293137	0	-	-
	5.00	4059	274052	0.01481	4.86	97.2
	10.0	9856	331056	0.02977	9.87	98.7
	20.0	19229	294012	0.06540	21.8	109.1
	50.0	48865	306457	0.1594	53.3	106.7
	100	102580	308440	0.3326	111	111.3
	200	193716	302817	0.6397	214	107.1
	500	450780	322632	1.397	468	93.6
	900	781009	314979	2.480	831	92.3
	1,000	822324	328027	2.507	840	84.0
y = 0.00298x + 0.000315		r = 0.9946				
Aug. 28, 2013	Blank	0	0	0	-	-
	Zero	0	273047	0	-	-
	5.00	3569	285521	0.01250	4.74	94.8
	10.0	8036	271688	0.02958	10.2	102.5
	20.0	19260	284225	0.06776	22.6	112.8
	50.0	48153	294236	0.1637	53.5	106.9
	100	98847	306303	0.3227	105	104.7
	200	202775	332016	0.6107	198	98.8
	500	457474	324437	1.410	455	91.0
	900	803007	325424	2.468	796	88.4
	1,000	867359	279498	3.103	1000	100.1
y = 0.00310x - 0.00221		r = 0.9961				
Sep. 10, 2013	Blank	0	0	0	-	-
	Zero	0	169169	0	-	-
	5.00	5317	157637	0.03373	4.89	97.9
	10.0	11235	161023	0.06977	10.1	101.0
	20.0	21855	155061	0.1409	20.4	101.9
	50.0	61907	159018	0.3893	56.3	112.5
	100	110476	161033	0.6860	99.1	99.1
	200	220484	160303	1.375	199	99.4
	500	555356	160367	3.463	500	100.1
	900	912807	157858	5.782	836	92.8
	1,000	1098245	166659	6.590	952	95.2
y = 0.00692x - 0.000140		r = 0.9980				

Accuracy was calculated using Analyst 1.5.2 software program.

Analyte: Acetylshikonin derivatized.

Table 2. (Continued)

Analytical date	Nominal concentration (ng/mL)	Peak area			Measured concentration (ng/mL)	Accuracy (%)
		Analyte	Emidin	Ratio		
Sep. 26, 2013	Blank	0	0	0	-	-
	Zero	0	157779	0	-	-
	5.00	4498	164353	0.02737	4.76	95.3
	10.0	9933	156659	0.06340	10.6	105.9
	20.0	19373	156536	0.1238	20.4	101.8
	50.0	51235	156417	0.3276	53.3	106.7
	100	105180	153513	0.6852	111	111.2
	200	206648	150684	1.371	222	111.1
	500	460102	159224	2.890	468	93.6
	900	747330	148514	5.032	814	90.5
	1,000	798858	154000	5.187	840	84.0
y = 0.00618x - 0.00208		r = 0.9940				
Sep. 27, 2013	Blank	0	0	0	-	-
	Zero	0	170370	0	-	-
	5.00	4323	139438	0.03101	4.96	99.1
	10.0	9390	160673	0.05844	9.80	98.0
	20.0	18895	159004	0.11880	20.5	102.4
	50.0	48792	158771	0.3073	53.8	107.5
	100	97492	158860	0.6137	108	107.9
	200	201524	160451	1.2560	221	110.7
	500	460641	168479	2.734	482	96.5
	900	741186	163050	4.546	803	89.2
	1,000	800649	159329	5.025	887	88.7
y = 0.00566x + 0.00295		r = 0.9960				
Oct. 01, 2013	Blank	0	0	0	-	-
	Zero	0	170084	0	-	-
	5.00	3247	171955	0.01888	4.66	93.1
	10.0	7722	176258	0.04381	10.7	106.8
	20.0	15062	172523	0.08730	21.2	106.0
	50.0	40799	172549	0.2365	57.3	114.5
	100	81608	179812	0.4538	110	109.8
	200	161304	176422	0.9143	221	110.6
	500	328915	181773	1.809	438	87.5
	900	572004	183787	3.112	753	83.6
	1,000	628569	172745	3.639	880	88.0
y = 0.00414x - 0.00221		r = 0.9910				

Accuracy was calculated using Analyst 1.5.2 software program.
Analyte: Acetylshikonin derivatized.

Table 3. Quality control for the determination of acetylshikonin in rat plasma

Analytical date	Nominal concentration (ng/mL)	Peak area			Measured concentration (ng/mL)	Accuracy (%)
		Analyte	Emodin	Ratio		
Aug. 22, 2013	15.0	9350	100750	0.09280	16.8	112.2
	300	241378	110804	2.178	380	126.6
	750	423092	114845	3.684	642	85.6
	15.0	8823	98553	0.08952	16.3	108.4
	300	261247	99287	2.631	459	152.9†
	750	442910	103344	4.286	747	99.6
Aug. 23, 2013	15.0	13768	117599	0.1171	16.6	110.4
	300	300124	101960	2.944	416	138.8†
	750	666800	114559	5.821	824	109.8
	15.0	13672	126967	0.1077	15.2	101.6
	300	285643	106667	2.678	379	126.3
	750	716647	148333	4.831	684	91.1
Aug. 27, 2013	15.0	17296	339826	0.05090	17.0	113.0
	300	327101	282302	1.159	388	129.4
	750	678151	310768	2.182	731	97.5
	15.0	16424	264696	0.06205	20.7	137.9†
	300	304836	258706	1.178	395	131.6†
	750	631048	267769	2.357	790	105.3
Aug. 28, 2013	15.0	11616	312355	0.03719	12.7	84.7
	300	276081	308267	0.8956	289	96.4
	750	587233	276735	2.122	685	91.3
	15.0	12055	275763	0.04372	14.8	98.7
	300	273258	275353	0.9924	321	106.8
	750	647135	314983	2.055	663	88.4

Accuracy was calculated using Analyst 1.5.2 software program.

Analyte: Acetylshikonin derivatized.

†: The accuracy of QC sample did not meet the acceptance criteria.

Table 3. (Continued)

Analytical date	Nominal concentration (ng/mL)	Peak area			Measured concentration (ng/mL)	Accuracy (%)
		Analyte	Emodin	Ratio		
Sep. 26, 2013	15.0	17286	160250	0.1079	17.8	118.6
	300	291471	163408	1.784	289	96.3
	750	625027	182020	3.434	556	74.1
	15.0	16328	155198	0.1052	17.4	115.7
	300	290687	178170	1.632	264	88.1
	750	697844	159606	4.372	708	94.4
Sep. 27, 2013	15.00	13262	185409	0.07153	12.1	80.8
	300	289880	180841	1.603	283	94.2
	750	601876	184189	3.268	577	76.9
	15.0	14493	149167	0.0972	16.6	111.0
	300	286954	152739	1.879	331	110.5
	750	570352	146990	3.880	685	91.3
Oct. 01, 2013	15.0	11362	179925	0.06315	15.4	102.4
	300	228357	175929	1.298	314	104.6
	750	530475	175030	3.031	733	97.7
	15.0	10157	189168	0.05369	13.1	87.2
	300	256255	197455	1.298	314	104.6
	750	551313	202863	2.718	657	87.6

Accuracy was calculated using Analyst 1.5.2 software program.
Analyte: Acetylshikonin derivatized.

Table 4. Concentration of acetylshikonin in rat plasma of individual test sample on Day 1

Sex Male

Group / Dose (mg/kg)	Time (hr) / Animal ID	Plasma concentration (ng/mL)							
		0	0.5	1	3	5	8	12	24
G1 / 0	1101			BQL					
	1102			BQL					
	1103			BQL					
	Mean			-					
	SD			-					
G2 / 25	1201 / 1204	BQL	39.4	35.3	36.6	20.0	16.3	11.1	5.87
	1202 / 1205	BQL	44.1	41.2	39.9	24.4	21.0	12.1	6.16
	1203 / 1206	BQL	41.8	31.1	27.6	23.7	20.3	11.9	BQL
	Mean	-	41.8	35.9	34.7	22.7	19.2	11.7	4.01
	SD	-	2.4	5.1	6.4	2.4	2.5	0.5	3.48
G3 / 100	1301 / 1304	BQL	145	115	79.2	67.0	55.4	44.9	20.0
	1302 / 1305	BQL	166	142	59.6	59.2	48.8	29.1	14.4
	1303 / 1306	BQL	59.1	59.3	55.2	50.1	47.4	32.9	21.8
	Mean	-	123	105	64.7	58.8	50.5	35.6	18.7
	SD	-	57	42	12.8	8.5	4.3	8.2	3.9
G4 / 400	1401 / 1404	BQL	124	147	67.1	34.6	37.6	22.2	67.2
	1402 / 1405	BQL	179	61.6	52.0	42.7	55.7	34.7	57.3
	1403 / 1406	BQL	132	131	46.7	35.7	67.6	39.0	43.8
	Mean	-	145	113	55.3	37.7	53.6	32.0	56.1
	SD	-	30	45	10.6	4.4	15.1	8.7	11.7

BQL: Below the Quantification Limit (< 5.00 ng/mL).
- : Not calculated.

Table 4. (Continued)

Sex Female

Group / Dose (mg/kg/day)	Time (hr) / Animal ID	Plasma concentration (ng/mL) 0	0.5	1	3	5	8	12	24
G1 / 0	2101			BQL					
	2102			BQL					
	2103			BQL					
	Mean			-					
	SD			-					
G2 / 25	2201 / 2204	BQL	36.8	25.0	24.1	18.3	16.8	11.4	BQL
	2202 / 2205	BQL	30.2	52.1	29.7	22.5	15.9	13.3	5.05
	2203 / 2206	BQL	39.3	26.9	16.8	20.3	9.98	9.50	BQL
	Mean	-	35.4	34.7	23.5	20.4	14.2	11.4	1.68
	SD	-	4.7	15.1	6.5	2.1	3.7	1.9	2.92
G3 / 100	2301 / 2304	BQL	61.2	53.4	53.4	27.2	45.6	31.6	14.7
	2302 / 2305	BQL	62.9	55.2	40.8	29.4	40.7	19.6	12.6
	2303 / 2306	BQL	42.1	42.9	28.6	26.9	38.4	36.4	17.0
	Mean	-	55.4	50.5	40.9	27.8	41.6	29.2	14.8
	SD	-	11.5	6.6	12.4	1.4	3.7	8.7	2.2
G4 / 400	2401 / 2404	BQL	62.6	88.3	26.6	51.4	55.0	68.1	74.3
	2402 / 2405	BQL	124	76.2	35.0	49.0	29.4	44.2	55.5
	2403 / 2406	BQL	130	116	49.7	42.7	34.7	82.1	65.1
	Mean	-	106	93.5	37.1	47.7	39.7	64.8	65.0
	SD	-	37	20.4	11.7	4.5	13.5	19.2	9.4

BQL: Below the Quantification Limit (< 5.00 ng/mL).

- : Not calculated.

Table 5. Concentration of acetylshikonin in rat plasma of individual test sample on Day 28

Sex Male

Group / Dose (mg/kg/day)	Time (hr) / Animal ID	Plasma concentration (ng/mL) 0	0.5	1	3	5	8	12	24
G1 / 0	1101			BQL					
	1102			BQL					
	1103			BQL					
	Mean			-					
	SD			-					
G2 / 25	1201 / 1204	16.5	40.6	49.0	54.6	46.6	39.7	27.1	16.9
	1202 / 1205	11.3	27.7	54.8	67.3	36.6	36.3	19.7	15.3
	1203 / 1206	12.3	47.8	43.7	60.7	37.0	39.1	19.0	20.9
	Mean	13.4	38.7	49.2	60.9	40.1	38.4	21.9	17.7
	SD	2.8	10.2	5.6	6.4	5.7	1.8	4.5	2.9
G3 / 100	1301 / 1304	37.7	118	107	133	119	92.9	81.3	45.3
	1302 / 1305	36.3	91.9	235	166	97.6	103	75.4	38.3
	1303 / 1306	50.9	122	83.2	140	154	75.4	70.6	41.4
	Mean	41.6	111	142	146	124	90.4	75.8	41.7
	SD	8.1	16	82	17	28	14.0	5.4	3.5
G4 / 400	1401 / 1404	89.3	338	297	447	257	275	157	127
	1402 / 1405	136	299	320	334	316	246	199	112
	1403 / 1406	106	443	219	256	238	290	171	127
	Mean	110	360	279	346	270	270	176	122
	SD	24	74	53	96	41	22	21	9

BQL: Below the Quantification Limit (< 5.00 ng/mL).

- : Not calculated.

Table 5. (Continued)

Sex: Female

Group / Dose (mg/kg/day)	Time (hr) / Animal ID	Plasma concentration (ng/mL) 0	0.5	1	3	5	8	12	24
G1 / 0	2101			BQL					
	2102			BQL					
	2103			BQL					
	Mean			-					
	SD			-					
G2 / 25	2201 / 2204	14.6	20.1	27.3	43.5	38.2	24.7	20.9	15.8
	2202 / 2205	10.4	32.8	24.5	52.9	43.4	25.2	19.8	11.9
	2203 / 2206	12.1	31.3	34.2	62.9	38.6	17.1	18.5	15.0
	Mean	12.4	28.1	28.7	53.1	40.1	22.3	19.7	14.2
	SD	2.1	6.9	5.0	9.7	2.9	4.5	1.2	2.1
G3 / 100	2301 / 2304	38.9	83.0	129	133	111	84.0	69.3	34.8
	2302 / 2305	39.9	108	159	110	102	66.1	69.6	32.9
	2303 / 2306	39.6	101	94.1	112	123	78.3	39.3	33.3
	Mean	39.5	97.3	127	118	112	76.1	59.4	33.7
	SD	0.5	12.9	32	13	11	9.1	17.4	1.0
G4 / 400	2401 / 2404	80.2	140	254	512	195	273	38.4	115
	2402 / 2405	133	331	270	350	259	234	216	94.2
	2403 / 2406	99.1	526	511	338	280	200	159	105
	Mean	104	332	345	400	245	236	138	105
	SD	27	193	144	97	44	37	91	10

BQL: Below the Quantification Limit (< 5.00 ng/mL).

- : Not calculated.

Table 6. Parallel quality control for the determination of acetylshikonin in rat plasma

Analytical date	Nominal concentration (ng/mL)	Peak area: Analyte	Emodin	Ratio	Measured concentration (ng/mL)	Mean	±	SD	Accuracy (%)	Precision (%)
Aug. 13, 2013	15	16100	235230	0.06844	15.5	15.5	±	1.6	103.3	10.3
		17428	231337	0.07533	17.1					
		16727	274653	0.06090	13.9					
	750	685887	223173	3.073	686	706.0	±	25.0	94.1	3.5
		697892	223015	3.129	698					
		704271	214152	3.289	734					
Sep. 10, 2013	15	17031	160997	0.1058	15.3	15.1	±	0.2	100.9	1.4
	15	19112	186102	0.1027	14.9					
	15	18738	177863	0.1054	15.2					
	750	765986	178321	4.296	621	645.7	±	25.5	86.1	4.0
	750	752113	161639	4.653	672					
	750	802740	180191	4.455	644					

Analyte: Acetylshikonin dedrivatized.

Table 7. Reassay summary for the determination of acetylshikonin in rat plasma of individual test sample

Phase	Sex	Group	Dose (mg/kg)	Animal ID	Time (hr)	Measured concentration (ng/mL)		Reassay reason
						Original	Reassay	
Day 1	Male	G1	0	1101	1	-	BQL	a)
Day 1	Male	G1	0	1102	1	-	BQL	a)
Day 1	Male	G1	0	1103	1	-	BQL	a)
Day 1	Male	G2	25	1201	0	-	BQL	a)
Day 1	Male	G2	25	1201	0	-	BQL	a)
Day 1	Male	G2	25	1201	0	-	BQL	a)
Day 1	Male	G3	100	1301	0	-	BQL	a)
Day 1	Male	G3	100	1302	0	-	BQL	a)
Day 1	Male	G3	100	1303	0	-	BQL	a)
Day 1	Male	G4	400	1401	0	-	BQL	a)
Day 1	Male	G4	400	1402	0	-	BQL	a)
Day 1	Male	G4	400	1403	0	-	BQL	a)
Day 1	Female	G1	0	2101	1	-	BQL	a)
Day 1	Female	G1	0	2102	1	-	BQL	a)
Day 1	Female	G1	0	2103	1	-	BQL	a)
Day 1	Female	G2	25	2201	0	-	BQL	a)
Day 1	Female	G2	25	2202	0	-	BQL	a)
Day 1	Female	G2	25	2203	0	-	BQL	a)
Day 1	Female	G3	100	2301	0	-	BQL	a)
Day 1	Female	G3	100	2302	0	-	BQL	a)
Day 1	Female	G3	100	2303	0	-	BQL	a)
Day 1	Female	G4	400	2401	0	-	BQL	a)
Day 1	Female	G4	400	2402	0	-	BQL	a)
Day 1	Female	G4	400	2403	0	-	BQL	a)

-: Not acceptable data.

BQL: Below the Quantification Limit (< 5.00 ng/mL).

a) Because a miss or improper operation was made during the pretreatment of the test samples.

Table 7. (Continued)

Phase	Sex	Group	Dose (mg/kg)	Animal ID	Time (hr)	Measured concentration (ng/mL)		Reassay reason
						Original	Reassay	
Day 28	Male	G4	400	1401	0	-	89.3	b)
Day 28	Male	G4	400	1404	0.5	-	338	b)
Day 28	Male	G4	400	1401	1	-	297	b)
Day 28	Male	G4	400	1404	3	-	447	b)
Day 28	Male	G4	400	1401	5	-	257	b)
Day 28	Male	G4	400	1404	8	-	275	b)
Day 28	Male	G4	400	1401	12	-	157	b)
Day 28	Male	G4	400	1404	24	-	127	b)
Day 28	Male	G4	400	1402	0	-	136	b)
Day 28	Male	G4	400	1405	0.5	-	299	b)
Day 28	Male	G4	400	1402	1	-	320	b)
Day 28	Male	G4	400	1405	3	-	334	b)
Day 28	Male	G4	400	1402	5	-	316	b)
Day 28	Male	G4	400	1405	8	-	246	b)
Day 28	Male	G4	400	1402	12	-	199	b)
Day 28	Male	G4	400	1405	24	-	112	b)
Day 28	Male	G4	400	1403	0	-	106	b)
Day 28	Male	G4	400	1406	0.5	-	443	b)
Day 28	Male	G4	400	1403	1	-	219	b)
Day 28	Male	G4	400	1406	3	-	256	b)
Day 28	Male	G4	400	1403	5	-	238	b)
Day 28	Male	G4	400	1406	8	-	290	b)
Day 28	Male	G4	400	1403	12	-	171	b)
Day 28	Male	G4	400	1406	24	-	127	b)
Day 28	Female	G4	400	2401	0	-	80.2	b)
Day 28	Female	G4	400	2404	0.5	-	140	b)
Day 28	Female	G4	400	2401	1	-	254	b)
Day 28	Female	G4	400	2404	3	-	512	b)
Day 28	Female	G4	400	2401	5	-	195	b)
Day 28	Female	G4	400	2404	8	-	273	b)
Day 28	Female	G4	400	2401	12	-	38.4	b)
Day 28	Female	G4	400	2404	24	-	115	b)
Day 28	Female	G4	400	2402	0	-	133	b)
Day 28	Female	G4	400	2405	0.5	-	331	b)
Day 28	Female	G4	400	2402	1	-	270	b)
Day 28	Female	G4	400	2405	3	-	350	b)
Day 28	Female	G4	400	2402	5	-	259	b)
Day 28	Female	G4	400	2405	8	-	234	b)
Day 28	Female	G4	400	2402	12	-	216	b)
Day 28	Female	G4	400	2405	24	-	94.2	b)
Day 28	Female	G4	400	2403	0	-	99.1	b)
Day 28	Female	G4	400	2406	0.5	-	526	b)
Day 28	Female	G4	400	2403	1	-	511	b)
Day 28	Female	G4	400	2406	3	-	338	b)
Day 28	Female	G4	400	2403	5	-	280	b)
Day 28	Female	G4	400	2406	8	-	200	b)
Day 28	Female	G4	400	2403	12	-	159	b)
Day 28	Female	G4	400	2406	24	-	105	b)

-: Not acceptable data.

b) Because the IS peak area was variable and re-injection was conducted after equilibration.

Table 8. Toxicokinetic parameters of acetylshikonin after oral administration in rat

Sex	Group / Dose (mg/kg)	Phase	Toxicokinetic parameters			
			AUC_{last} (ng·hr/mL)	C_{max} (ng/mL)	T_{max} (hr)	$t_{1/2}$ (hr)
Male	G2 /	Day 1	376.79	41.80	0.50	7.42
	25	Day 28	722.05	60.90	3.00	15.60
	G3 /	Day 1	1,042.90	123.00	0.50	11.49
	100	Day 28	2,018.40	146.00	3.00	14.24
	G4 /	Day 1	1,198.80	145.00	0.50	43.29
	400	Day 28	5,008.25	360.00	0.50	14.42
Female	G2 /	Day 1	310.06	35.40	0.50	5.48
	25	Day 28	580.33	53.10	3.00	24.76
	G3 /	Day 1	710.13	55.40	0.50	11.05
	100	Day 28	1,677.03	127.00	1.00	13.85
	G4 /	Day 1	1,410.68	106.00	0.50	-
	400	Day 28	4,595.75	400.00	3.00	14.99

-: $t_{1/2}$ was not calculated because of less than 3 points for calculation.

<자초추출물의 비글견을 이용한 4주 반복 경구투여 독성시험, 2주회복시험 및 독성동태시험에서 채취된 비글견 혈장 중 아세틸시코닌의 농도 측정>

Table 1. System suitability for the determination of acetylshikonin in dog plasma

Analytical date	Classification		No. 1	No. 2	No. 3	No. 4	No. 5	Mean ± SD	Precision (%)
Oct. 10, 2013	Peak area ratio		0.02508	0.02468	0.02551	0.02506	0.02790	0.02565 ± 0.00129	5.0
	Retention time (min)	Analyte	3.69	3.69	3.70	3.68	3.68	3.69 ± 0.01	0.2
		Emodin	3.47	3.47	3.47	3.47	3.46	3.47 ± 0.00	0.1
Nov. 04, 2013	Peak area ratio		0.01672	0.01556	0.01568	0.01393	0.01801	0.01598 ± 0.00151	9.5
	Retention time (min)	Analyte	3.73	3.72	3.74	3.72	3.72	3.73 ± 0.01	0.2
		Emodin	3.51	3.51	3.51	3.50	3.51	3.51 ± 0.00	0.1
Nov. 05, 2013	Peak area ratio		0.01122	0.01218	0.01279	0.01179	0.01177	0.01195 ± 0.00058	4.9
	Retention time (min)	Analyte	3.70	3.70	3.71	3.71	3.72	3.71 ± 0.01	0.2
		Emodin	3.50	3.49	3.49	3.49	3.50	3.49 ± 0.01	0.2
Nov. 13, 2013	Peak area ratio		0.01557	0.01744	0.01654	0.01863	0.01742	0.01712 ± 0.00114	6.7
	Retention time (min)	Analyte	3.80	3.78	3.79	3.78	3.80	3.79 ± 0.01	0.3
		Emodin	3.57	3.56	3.57	3.56	3.57	3.57 ± 0.01	0.2
Nov. 27, 2013	Peak area ratio		0.03340	0.02880	0.02859	0.02974	0.03101	0.03031 ± 0.00197	6.5
	Retention time (min)	Analyte	3.80	3.80	3.80	3.81	3.81	3.80 ± 0.01	0.1
		Emodin	3.58	3.58	3.58	3.58	3.58	3.58 ± 0.00	0.0
Nov. 28, 2013	Peak area ratio		0.02814	0.02627	0.02633	0.02777	0.02374	0.02645 ± 0.00173	6.5
	Retention time (min)	Analyte	3.79	3.80	3.79	3.79	3.80	3.79 ± 0.01	0.1
		Emodin	3.56	3.57	3.57	3.56	3.57	3.57 ± 0.01	0.2
Nov. 29, 2013	Peak area ratio		0.01910	0.02018	0.01979	0.02372	0.02032	0.02062 ± 0.00180	8.7
	Retention time (min)	Analyte	3.78	3.77	3.78	3.78	3.78	3.78 ± 0.00	0.1
		Emodin	3.55	3.55	3.55	3.55	3.56	3.55 ± 0.00	0.1

Peak area ratio = Peak area of analyte / Peak area of internal reference standard.
Precision (%) = (Standard deviation (SD) / Mean) × 100.
Analyte: Acetylshikonin derivatized.

Table 2. Calibration curves (weighting: $1/X^2$) for the determination of acetylshikonin in dog plasma

Analytical date	Theoretical concentration (ng/mL)	Peak area			Determined concentration (ng/mL)	Accuracy (%)
		Analyte	Emodin	Ratio		
Oct. 10, 2013	Blank	0	0	0	-	-
	Zero	0	212743	0	-	-
	5.00	4502	206802	0.02177	4.74	94.7
	10.0	10754	222529	0.04833	9.90	99.0
	20.0	28845	242269	0.1191	23.7	118.0
	50.0	67437	222041	0.3037	59.6	119.0
	100	90950	204066	0.4457	87.2	87.2
	200	220123	214681	1.025	200	100.0
	500	563689	225494	2.500	487	97.4
	900	811157	193267	4.197	817	90.8
	1,000	1072677	224221	4.784	932	93.2
y = 0.00514x - 0.00256		r = 0.9917				
Nov. 04, 2013	Blank	0	0	0	-	-
	Zero	0	36533	0	-	-
	5.00	709	49013	0.01447	4.85	97.0
	10.0	1502	46582	0.03224	10.5	105.4
	20.0	2928	49573	0.05907	19.1	95.6
	50.0	7886	48089	0.1640	52.7	105.4
	100	17349	47260	0.3671	118	117.6
	200	31507	48755	0.6462	207	103.5
	500	82544	49821	1.657	530	106.0
	900	115928	49039	2.364	756	84.0
	1,000	133971	50101	2.674	855	85.5
y = 0.00313x - 0.000700		r = 0.9927				
Nov. 05, 2013	Blank	0	0	0	-	-
	Zero	0	44279	0	-	-
	5.00	612	43893	0.01394	5.27	105.3
	10.0	769	30743	0.02500	8.97	89.7
	20.0	1491	27511	0.05418	18.7	93.7
	50.0	5304	32163	0.1649	55.8	111.6
	100	13033	41533	0.3138	106	105.6
	200	24342	42611	0.5713	192	95.9
	500	62384	38866	1.605	538	107.6
	900	111194	38714	2.872	962	106.9
	1,000	111739	44783	2.495	836	83.6
y = 0.00299x - 0.00180		r = 0.9941				

Accuracy was calculated using Analyst 1.5.2 software program.

Analyte: Acetylshikonin derivatized.

Table 2. (Continued)

Analytical date	Theoretical concentration (ng/mL)	Peak area			Determined concentration (ng/mL)	Accuracy (%)
		Analyte	Emodin	Ratio		
Nov. 13, 2013	Blank	0	0	0	-	-
	Zero	0	151965	0	-	-
	5.00	2454	144469	0.01698	4.97	99.4
	10.0	6327	165596	0.03820	10.0	100.4
	20.0	12975	163774	0.07923	19.8	99.1
	50.0	34406	161990	0.2124	51.6	103.2
	100	71293	160137	0.4452	107	107.2
	200	135008	162540	0.8306	199	99.6
	500	316728	159990	1.980	473	94.7
	900	597496	161683	3.695	883	98.1
	1,000	636891	154704	4.117	983	98.3
y = 0.00419x - 0.00385		r = 0.9992				
Nov. 27, 2013	Blank	0	0	0	-	-
	Zero	0	115378	0	-	-
	5.00	3526	119714	0.02946	4.71	94.2
	10.0	7288	116514	0.06255	10.3	102.5
	20.0	15484	114031	0.1358	22.5	112.6
	50.0	41769	125132	0.3338	55.7	111.4
	100	82697	127617	0.6480	108	108.3
	200	160357	132946	1.206	202	100.9
	500	381601	133058	2.868	480	96.0
	900	617520	129431	4.771	799	88.8
	1,000	679660	133547	5.089	852	85.2
y = 0.00597x + 0.00135		r = 0.9939				
Nov. 28, 2013	Blank	0	0	0	-	-
	Zero	0	113403	0	-	-
	5.00	2832	115935	0.02443	4.71	94.2
	10.0	6888	120626	0.05711	10.9	109.0
	20.0	15346	117977	0.1301	24.7	123.6↑
	50.0	35706	119891	0.2978	56.5	112.9
	100	64293	119603	0.5376	102	101.9
	200	131605	121798	1.081	205	102.3
	500	332106	124918	2.659	503	100.7
	900	545966	125872	4.337	821	91.3
	1,000	598188	129008	4.637	878	87.8
y = 0.00528x - 0.000440		r = 0.9955				

Accuracy was calculated using Analyst 1.5.2 software program.
Analyte: Acetylshikonin derivatized.
↑: The accuracy of this point did not meet the acceptance criteria.

Table 2. (Continued)

Analytical date	Theoretical concentration (ng/mL)	Peak area			Determined concentration (ng/mL)	Accuracy (%)
		Analyte	Emodin	Ratio		
Nov. 29, 2013	Blank	0	0	0	-	-
	Zero	0	144111	0	-	-
	5.00	3653	152622	0.02394	4.78	95.6
	10.0	6710	145081	0.04625	9.85	98.5
	20.0	15334	145308	0.1055	23.3	116.6
	50.0	37609	155754	0.2415	54.2	108.5
	100	57735	129563	0.4456	101	100.6
	200	149648	154741	0.9671	219	109.6
	500	318983	149599	2.132	484	96.8
	900	537489	152999	3.513	798	88.6
	1,000	585289	156216	3.747	851	85.1
y = 0.00440x + 0.00290		r = 0.9934				

Accuracy was calculated using Analyst 1.5.2 software program.
Analyte: Acetylshikonin derivatized.

Table 3. Quality control for the determination of acetylshikonin in dog plasma

Analytical date	Theoretical concentration (ng/mL)	Peak area			Determined concentration (ng/mL)	Accuracy (%)
		Analyte	Emodin	Ratio		
Nov. 04, 2013	15.0	2084	45853	0.04544	14.8	98.4
	300	43209	46319	0.9329	299	99.5
	750	94524	50257	1.881	602	80.2
	15.0	2166	39683	0.05458	17.7	117.9
	300	35719	39238	0.9103	291	97.1
	750	76573	36121	2.120	678	90.4
Nov. 05, 2013	15.0	1793	44518	0.04028	14.1	93.9
	300	37168	41896	0.8871	298	99.2
	750	80530	38812	2.075	695	92.7
	15.0	1829	32112	0.05696	19.7	131.1†
	300	32088	40550	0.7913	266	88.5
	750	80084	33818	2.368	793	105.8
Nov. 13, 2013	15.0	9720	153527	0.06331	16.0	106.8
	300	218621	150628	1.451	347	115.8
	750	490865	158545	3.096	740	98.6
	15.0	9221	133231	0.06921	17.4	116.2
	300	203447	133021	1.529	366	122.0†
	750	448148	140836	3.182	760	101.4
Nov. 27, 2013	15.0	12482	123353	0.1012	16.7	111.5
	300	240192	128345	1.871	313	104.4
	750	520899	130586	3.989	668	89.1
	15.0	12455	127347	0.09780	16.2	107.7
	300	232720	130867	1.778	298	99.2
	750	518989	134851	3.849	644	85.9
Nov. 28, 2013	15.0	10366	116912	0.08867	16.9	112.5
	300	206090	123197	1.673	317	105.6
	750	466683	126502	3.689	699	93.1
	15.0	10661	123172	0.08656	16.5	109.8
	300	193198	119866	1.612	305	101.7
	750	422578	126178	3.349	634	84.6
Nov. 29, 2013	15.0	11899	159665	0.07452	16.3	108.5
	300	198652	155947	1.274	289	96.3
	750	474027	155446	3.049	692	92.3
	15.0	9661	153428	0.06297	13.7	91.0
	300	149965	112164	1.337	303	101.1
	750	429036	155216	2.764	628	83.7

Accuracy was calculated using Analyst 1.5.2 software program.
Analyte: Acetylshikonin derivatized.
†: The accuracy of QC sample did not meet the acceptance criteria.

Table 4. Concentration of acetylshikonin in dog plasma of individual test sample on Day 1

Sex: Male

Group / Dose (mg/kg/day)	Time (hr) / Animal ID	Final concentration (ng/mL)									
		0	0.25	0.5	0.75	1	2	4	6	10	24
G1 / 0	1101					BQL					
	1102					BQL					
	1103					BQL					
	Mean					-					
	SD					-					
G2 / 30	1201	BQL	12.1	17.6	12.8	14.2	9.57	BQL	BQL	BQL	BQL
	1202	BQL	23.4	34.1	36.6	13.5	26.9	10.9	9.34	23.4	BQL
	1203	BQL	13.9	37.2	39.8	29.6	17.6	13.4	6.53	BQL	BQL
	Mean	-	16.5	29.6	29.7	19.1	18.0	8.10	5.29	7.80	-
	SD	-	6.1	10.5	14.8	9.1	8.7	7.13	4.79	13.51	-
G3 / 100	1301	BQL	BQL	24.3	30.1	29.8	25.4	20.4	13.5	7.15	BQL
	1302	BQL	19.7	27.4	27.7	20.3	15.9	8.22	BQL	BQL	BQL
	1303	BQL	BQL	25.6	54.7	50.2	48.7	29.5	35.4	22.4	8.61
	Mean	-	6.57	25.8	37.5	33.4	30.0	19.4	16.3	9.85	2.87
	SD	-	11.37	1.6	14.9	15.3	16.9	10.7	17.9	11.44	4.97
G4 / 300	1401	BQL	BQL	20.4	27.4	35.9	37.7	19.4	12.6	8.41	BQL
	1402	BQL	25.2	41.6	31.9	25.5	7.04	12.4	7.85	5.17	BQL
	1403	BQL	26.5	32.9	28.4	24.5	10.7	15.3	8.51	5.86	BQL
	Mean	-	17.2	31.6	29.2	28.6	18.5	15.7	9.65	6.48	-
	SD	-	14.9	10.7	2.4	6.3	16.7	3.5	2.57	1.71	-

BQL: Below the Quantification Limit (< 5.00 ng/mL).
- : Not calculated.

Table 4. (Continued)

Sex: Female

Group / Dose (mg/kg/day)	Time (hr) / Animal ID	Final concentration (ng/mL) 0	0.25	0.5	0.75	1	2	4	6	10	24
G1 / 0	2101					BQL					
	2102					BQL					
	2103					BQL					
	Mean					-					
	SD					-					
G2 / 30	2201	BQL	17.8	33.8	28.6	34.0	24.3	37.8	34.1	26.5	6.64
	2202	BQL	BQL	BQL	BQL	5.79	102	76.7	65.8	34.2	BQL
	2203	BQL	BQL	17.8	38.6	35.2	33.0	42.3	31.1	10.0	5.33
	Mean	-	5.93	17.2	22.4	25.0	53.1	52.3	43.7	23.6	3.99
	SD	-	10.28	16.9	20.0	16.6	42.6	21.3	19.2	12.4	3.52
G3 / 100	2301	BQL	BQL	14.7	17.1	23.2	54.9	57.2	44.7	32.5	13.4
	2302	BQL	34.6	32.1	24.4	25.3	25.3	14.0	8.28	BQL	7.45
	2303	BQL	30.0	39.6	22.9	21.9	26.7	19.1	7.63	5.18	BQL
	Mean	-	21.5	28.8	21.5	23.5	35.6	30.1	20.2	12.6	6.95
	SD	-	18.8	12.8	3.9	1.7	16.7	23.6	21.2	17.5	6.71
G4 / 300	2401	BQL	51.3	50.2	6.41	47.8	55.0	45.7	30.5	21.4	8.16
	2402	BQL	BQL	43.7	63.2	73.3	49.6	32.5	22.0	12.7	5.50
	2403	BQL	40.3	20.4	27.4	20.1	27.7	6.17	BQL	BQL	BQL
	Mean	-	30.5	38.1	32.3	47.1	44.1	28.1	17.5	11.4	4.55
	SD	-	27.0	15.7	28.7	26.6	14.5	20.1	15.7	10.8	4.16

BQL: Below the Quantification Limit (< 5.00 ng/mL).
- : Not calculated.

Table 5. Concentration of acetylshikonin in dog plasma of individual test sample on Day 28

Sex: Male

Group / Dose (mg/kg/day)	Time (hr) / Animal ID	Final concentration (ng/mL) 0	0.25	0.5	0.75	1	2	4	6	10	24
G1 / 0	1101					BQL					
	1102					BQL					
	1103					BQL					
	Mean					-					
	SD					-					
G2 / 30	1201	7.55	17.0	28.4	29.1	35.7	37.5	27.9	18.7	12.5	6.73
	1202	8.33	32.6	41.6	34.2	33.5	22.3	18.0	12.1	20.7	7.40
	1203	6.84	19.7	26.4	24.9	29.2	48.0	41.5	28.6	16.7	6.95
	Mean	7.57	23.1	32.1	29.4	32.8	35.9	29.1	19.8	16.6	7.03
	SD	0.75	8.3	8.3	4.7	3.3	12.9	11.8	8.3	4.1	0.34
G3 / 100	1301	33.7	48.2	81.4	97.0	118	76.8	87.9	91.2	76.1	28.5
	1302	5.19	28.2	35.5	34.8	34.2	24.2	16.1	13.0	8.99	5.64
	1303	36.0	70.1	91.7	102	111	106	95.0	69.7	91.4	32.5
	Mean	25.0	48.8	69.5	77.9	87.7	69.0	66.3	58.0	58.8	22.2
	SD	17.2	21.0	29.9	37.4	46.5	41.5	43.6	40.4	43.8	14.5
G4 / 300	1401	25.9	31.7	63.6	97.6	67.8	151	79.9	81.3	53.1	19.3
	1402	33.0	37.1	51.7	67.6	130	64.8	93.4	79.8	69.9	23.7
	1403	36.2	80.7	98.0	107	131	147	74.4	63.6	60.8	34.0
	Mean	31.7	49.8	71.1	90.7	110	121	82.6	74.9	61.3	25.7
	SD	5.3	26.9	24.0	20.6	36	49	9.8	9.8	8.4	7.5

BQL: Below the Quantification Limit (< 5.00 ng/mL).
- : Not calculated.

Table 5. (Continued)

Sex: Female

Group / Dose (mg/kg/day)	Time (hr) / Animal ID	Final concentration (ng/mL) 0	0.25	0.5	0.75	1	2	4	6	10	24
G1 / 0	2101					BQL					
	2102					BQL					
	2103					BQL					
	Mean					-					
	SD					-					
G2 / 30	2201	9.22	29.1	29.6	30.1	31.1	23.5	17.6	11.1	19.5	BQL
	2202	5.19	9.15	11.5	13.0	12.7	60.7	36.2	42.0	31.8	9.14
	2203	10.5	9.06	9.54	26.5	26.3	29.4	42.2	29.1	23.7	8.34
	Mean	8.30	15.8	16.9	23.2	23.4	37.9	32.0	27.4	25.0	5.83
	SD	2.77	11.5	11.1	9.0	9.5	20.0	12.8	15.5	6.3	5.06
G3 / 100	2301	43.3	60.1	64.9	75.9	82.6	77.9	91.3	66.8	83.8	34.1
	2302	22.2	26.2	60.3	72.1	74.5	82.6	55.3	67.5	55.5	24.1
	2303	13.3	32.0	49.9	72.3	51.7	41.2	32.5	23.1	31.8	17.2
	Mean	26.3	39.4	58.4	73.4	69.6	67.2	59.7	52.5	57.0	25.1
	SD	15.4	18.1	7.7	2.1	16.0	22.7	29.6	25.4	26.0	8.5
G4 / 300	2401	35.5	101	91.2	95.6	79.7	104	88.8	55.2	60.9	32.6
	2402	40.0	71.5	159	153	127	88.5	84.2	60.4	54.9	29.9
	2403	20.9	51.1	50.0	75.6	83.2	97.3	85.0	49.8	52.7	26.4
	Mean	32.1	74.5	100	108	96.6	96.6	86.0	55.1	56.2	29.6
	SD	10.0	25.1	55	40	26.4	7.8	2.5	5.3	4.2	3.1

BQL: Below the Quantification Limit (< 5.00 ng/mL).
- : Not calculated.

Table 6. Parallel quality control for the determination of acetylshikonin in dog plasma

Analytical date	Theoretical concentration (ng/mL)	Peak area Analyte	Emodin	Ratio	Determined concentration (ng/mL)	Mean	± (%)	SD	Accuracy (%)	Precision (%)
Oct. 10, 2013	15.0	14267	202436	0.07047	14.2	14.4	±	0.9	96.0	6.4
		13342	198070	0.06736	13.6					
		13760	179600	0.07661	15.4					
	750	729080	210120	3.470	676	619	±	67	82.5	10.8
		669656	205053	3.266	636					
		518347	183326	2.797	545					
Nov. 13, 2013	15.0	10267	151852	0.06761	17.1	18.4	±	1.2	122.9	6.3
		11274	147430	0.07647	19.2					
		10104	133733	0.07556	19.0					
	750	483067	153524	3.147	752	760	±	11	101.4	1.5
		496018	156766	3.164	756					
		507416	156784	3.236	773					

Analyte: Acetylshikonin dederivatized.

Table 7. Reassay summary for the determination of acetylshikonin in dog plasma of individual test sample

Phase	Sex	Group	Dose (mg/kg/day)	Animal ID	Time (hr)	Measured concentration (ng/mL)		Note
						Original	Reassay	
Day1	Male	G4	300	1401	0	-	BQL	a)
Day1	Male	G4	300	1401	0.25	-	BQL	a)
Day1	Male	G4	300	1401	0.5	-	20.4	a)
Day1	Male	G4	300	1401	0.75	-	27.4	a)
Day1	Male	G4	300	1401	1	-	35.9	a)
Day1	Male	G4	300	1401	2	-	37.7	a)
Day1	Male	G4	300	1401	4	-	19.4	a)
Day1	Male	G4	300	1401	6	-	12.6	a)
Day1	Male	G4	300	1401	10	-	8.41	a)
Day1	Male	G4	300	1401	24	-	BQL	a)
Day1	Male	G4	300	1402	0	-	BQL	a)
Day1	Male	G4	300	1402	0.25	-	25.2	a)
Day1	Male	G4	300	1402	0.5	-	41.6	a)
Day1	Male	G4	300	1402	0.75	-	31.9	a)
Day1	Male	G4	300	1402	1	-	25.5	a)
Day1	Male	G4	300	1402	2	-	7.04	a)
Day1	Male	G4	300	1402	4	-	12.4	a)
Day1	Male	G4	300	1402	6	-	7.85	a)
Day1	Male	G4	300	1402	10	-	5.17	a)
Day1	Male	G4	300	1402	24	-	BQL	a)
Day1	Male	G4	300	1403	0	-	BQL	a)
Day1	Male	G4	300	1403	0.25	-	26.5	a)
Day1	Male	G4	300	1403	0.5	-	32.9	a)
Day1	Male	G4	300	1403	0.75	-	28.4	a)
Day1	Male	G4	300	1403	1	-	24.5	a)
Day1	Male	G4	300	1403	2	-	10.7	a)
Day1	Male	G4	300	1403	4	-	15.3	a)
Day1	Male	G4	300	1403	6	-	8.51	a)
Day1	Male	G4	300	1403	10	-	5.86	a)
Day1	Male	G4	300	1403	24	-	BQL	a)

-: The measured concentrations were rejected because the results of QC samples did not meet the acceptance criteria.

BQL: Below the Quantification Limit (< 5.00 ng/mL).

a) The results of QC samples did not meet the acceptance criteria.

Table 7. (Continued)

Phase	Sex	Group	Dose (mg/kg/day)	Animal ID	Time (hr)	Measured concentration (ng/mL)		Note
						Original	Reassay	
Day1	Female	G4	300	2401	0	-	BQL	a)
Day1	Female	G4	300	2401	0.25	-	51.3	a)
Day1	Female	G4	300	2401	0.5	-	50.2	a)
Day1	Female	G4	300	2401	0.75	-	6.41	a)
Day1	Female	G4	300	2401	1	-	47.8	a)
Day1	Female	G4	300	2401	2	-	55.0	a)
Day1	Female	G4	300	2401	4	-	45.7	a)
Day1	Female	G4	300	2401	6	-	30.5	a)
Day1	Female	G4	300	2401	10	-	21.4	a)
Day1	Female	G4	300	2401	24	-	8.16	a)
Day1	Female	G4	300	2402	0	-	BQL	a)
Day1	Female	G4	300	2402	0.25	-	BQL	a)
Day1	Female	G4	300	2402	0.5	-	43.7	a)
Day1	Female	G4	300	2402	0.75	-	63.2	a)
Day1	Female	G4	300	2402	1	-	73.3	a)
Day1	Female	G4	300	2402	2	-	49.6	a)
Day1	Female	G4	300	2402	4	-	32.5	a)
Day1	Female	G4	300	2402	6	-	22.0	a)
Day1	Female	G4	300	2402	10	-	12.7	a)
Day1	Female	G4	300	2402	24	-	5.50	a)
Day1	Female	G4	300	2403	0	-	BQL	a)
Day1	Female	G4	300	2403	0.25	-	40.3	a)
Day1	Female	G4	300	2403	0.5	-	20.4	a)
Day1	Female	G4	300	2403	0.75	-	27.4	a)
Day1	Female	G4	300	2403	1	-	20.1	a)
Day1	Female	G4	300	2403	2	-	27.7	a)
Day1	Female	G4	300	2403	4	-	6.17	a)
Day1	Female	G4	300	2403	6	-	BQL	a)
Day1	Female	G4	300	2403	10	-	BQL	a)
Day1	Female	G4	300	2403	24	-	BQL	a)

—: The measured concentrations were rejected because the results of QC samples did not meet the acceptance criteria.

BQL: Below the Quantification Limit (< 5.00 ng/mL).

a) The results of QC samples did not meet the acceptance criteria.

Table 8. Toxicokinetic parameters of acetylshikonin after oral administration in dog on Day 1

Sex	Dose (mg/kg)	Animal ID	Toxicokinetic parameters			
			AUC_{last} (ng·hr/mL)	C_{max} (ng/mL)	T_{max} (hr)	$t_{1/2}$ (hr)
Male	30	1201	24.29	17.60	0.50	2.49
		1202	168.93	36.60	0.75	-
		1203	100.96	39.80	0.75	2.49
		Mean	98.06	31.33	0.67	2.49
		SD	72.37	12.00	0.14	0.01
	100	1301	165.93	30.10	0.75	4.34
		1302	63.46	27.70	0.75	2.27
		1303	551.57	54.70	0.75	9.14
		Mean	260.32	37.50	0.75	5.25
		SD	257.38	14.94	0.00	3.52
	300	1401	184.36	37.70	2.00	5.18
		1402	109.86	41.60	0.50	4.95
		1403	121.16	32.90	0.50	4.61
		Mean	138.46	37.40	1.00	4.91
		SD	40.15	4.36	0.87	0.29
Female	30	2201	540.63	37.80	4.00	7.45
		2202	575.82	102.00	2.00	5.00
		2203	390.81	42.30	4.00	8.24
		Mean	502.42	60.70	3.33	6.90
		SD	98.25	35.84	1.15	1.69
	100	2301	739.60	57.20	4.00	10.51
		2302	181.53	34.60	0.25	12.58
		2303	148.31	39.60	0.50	3.23
		Mean	356.48	43.80	1.58	8.77
		SD	332.21	11.87	2.10	4.91
	300	2401	571.97	55.00	2.00	9.61
		2402	430.74	73.30	1.00	9.56
		2403	82.31	40.30	0.25	1.63
		Mean	361.67	56.20	1.08	6.93
		SD	252.03	16.53	0.88	4.59

-: $t_{1/2}$ was not calculated because of less than 3 points for calculation.

Table 9. Toxicokinetic parameters of acetylshikonin after oral administration in dog on Day 28

Sex	Dose (mg/kg)	Animal ID	Toxicokinetic parameters			
			AUC_{last} (ng·hr/mL)	C_{max} (ng/mL)	T_{max} (hr)	$t_{1/2}$ (hr)
Male	30	1201	369.64	37.50	2.00	12.96
		1202	392.93	41.60	0.50	12.27
		1203	476.61	48.00	2.00	9.31
		Mean	413.06	42.37	1.50	11.51
		SD	56.25	5.29	0.87	2.58
	100	1301	1583.61	118.00	1.00	10.49
		1302	274.54	35.50	0.50	14.11
		1303	1748.03	111.00	1.00	13.63
		Mean	1,202.06	88.17	0.83	12.74
		SD	807.45	45.74	0.29	1.97
	300	1401	1337.04	151.00	2.00	8.90
		1402	1442.88	130.00	1.00	10.10
		1403	1503.13	147.00	2.00	18.40
		Mean	1,427.68	142.67	1.67	12.46
		SD	84.08	11.15	0.58	5.17
Female	30	2201	185.54	31.10	1.00	31.06
		2202	656.63	60.70	2.00	8.07
		2203	516.51	42.20	4.00	9.79
		Mean	452.89	44.67	2.33	16.31
		SD	241.90	14.95	1.53	12.81
	100	2301	1600.01	91.30	4.00	15.62
		2302	1194.19	82.60	2.00	11.98
		2303	675.23	72.30	0.75	17.73
		Mean	1,156.48	82.07	2.25	15.11
		SD	463.55	9.51	1.64	2.91
	300	2401	1401.70	104.00	2.00	16.46
		2402	1366.00	159.00	0.50	17.24
		2403	1223.24	97.30	2.00	17.80
		Mean	1,330.31	120.10	1.50	17.17
		SD	94.43	33.85	0.87	0.67

Table 10. Summary of toxicokinetic parameters of acetylshikonin after oral administration in dog

Sex	Group / Dose (mg/kg)	Phase	Toxicokinetic parameters			
			AUC_{last} (ng·hr/mL)	C_{max} (ng/mL)	T_{max} (hr)	$t_{1/2}$ (hr)
Male	G2	Day 1	98.06	31.33	0.67	2.49
	30	Day 28	413.06	42.37	1.50	11.51
	G3	Day 1	260.32	37.50	0.75	5.25
	100	Day 28	1202.06	88.17	0.83	12.74
	G4	Day 1	138.46	37.40	1.00	4.91
	300	Day 28	1427.68	142.67	1.67	12.46
Female	G2	Day 1	502.42	60.70	3.33	6.90
	30	Day 28	452.89	44.67	2.33	16.31
	G3	Day 1	356.48	43.80	1.58	8.77
	100	Day 28	1156.48	82.07	2.25	15.11
	G4	Day 1	361.67	56.20	1.08	6.93
	300	Day 28	1330.31	120.10	1.50	17.17

<LC/MS/MS를 이용한 랫드 혈장 중 Acetylshikonin의 Method development>

SBB SCAS-BTT Bioanalysis Co.,Ltd.

Table 1. Linearity of Acetylshikonin in rat plasma (weighting factor: 1/X)

Nominal concentration (ng/mL)	Peak area			Measured concentration (ng/mL)	Accuracy (%)
	Acetylshikonin	Emodin	Ratio		
25	3785	87851	0.04308	21.47	85.87
50	9070	86274	0.10510	51.19	102.39
100	13706	57700	0.23750	114.62	114.62
500	90705	90029	1.00800	483.48	96.70
1000	179308	85607	2.09000	1004.24	100.42

$y = 0.00207x - 0.000828$ ($r = 0.9965$)

Table 2. Short-term temperature stability of Acetylshikonin in rat plasma

Analyte	Nominal concentration (ng/mL)	Classfication	Peak area	Residual ratio (%)
Acetylshikonin	25	Immediately	1930	
	50	after preparation	4872	
	100		12185	
	500		58587	
	1000		114794	
	25	1 Hour after preparation	1900	98.45
	50	on ice	4267	87.58
	100		9002	73.88
	500		48128	82.15
	1000		97972	85.35
	25	1 Hour after preparation	1163	60.26
	50	at RT	2779	57.04
	100		5364	44.02
	500		28400	48.47
	1000		61295	53.40

Table 3. Peak area variation of Acetylshikonin and Emodin in rat plasma

Nominal concentration of Acetylshikonin (ng/mL)	Analytical date	Peak area		
		Acetylshikonin	Emodin	Ratio
25	2012.10.31	3785	87851	0.04308
50		9070	86274	0.10510
100		13706	57700	0.23750
500		90705	90029	1.00800
1000		179308	85607	2.09000
25	2012.11.01	1930	45150	0.04274
50		4872	46322	0.10520
100		12185	47592	0.25600
500		58587	42734	1.37100
1000		114794	44246	2.59400

<LC/MS/MS를 이용한 비결견 혈장 중 Acetylshikonin의 Method development>

SBB SCAS-BTT Bioanalysis Co.,Ltd.

Table 1. Linearity of Acetylshikonin derivative in rat plasma after derivatization with 2M 2-mercaptoethanol (weighting: 1/X)

Nominal concentration	Peak area			Measured concentration	Accuracy
(ng/mL)	Acetylshikonin derivative	Emodin	Ratio	(ng/mL)	(%)
10	3757	72928	0.05151	9.922	92.69
25	7962	68431	0.1164	26.02	103.66
50	15694	80760	0.1943	45.38	91.87
100	32386	70635	0.4585	111.0	113.75
500	128276	66652	1.925	474.9	98.03
1,000	221848	75334	2.945	728.2	75.21[a]
2,000	346257	75620	4.579	1,134	58.58[a]

$y = 0.00390x + 0.015$ $r = 0.9977$

[a] Except for this sample, other samples were used to construct the calibration curve.

Table 2. Effect of 2-mercaptoethanol in peak area of Acetylshikonin derivative and Emodin

Molar concentration of 2-Mercaptoethanol	Nominal concentration of Acetylshikonin	Peak area	
		Acetylshikonin derivative	Emodin
10 M	1,000	25104	25837
		28928	25725
	2,000	48062	25674
		45589	31187
5 M	1,000	143969	63434
		127722	52028
	2,000	197762	58008
		205534	57933
2 M	1,000	362132	79752
		319852	71608
	2,000	556366	85200
		491808	86753
1 M	1,000	341503	78712
		312832	82893
	2,000	656551	92368
		608382	96256
0.5 M	1,000	718404	81549
		617721	75537
	2,000	978929	77516
		929305	83786

Table 3. Linearity of Acetylshikonin derivative in rat plasma after derivatization with 0.5M 2-mercaptoethanol (weighting: 1/X)

Nominal concentration	Peak area			Measured concentration	Accuracy
(ng/mL)	Acetylshikonin derivative	Emodin	Ratio	(ng/mL)	(%)
10	7609	76100	0.09999	8.108	81.08
25	16559	72708	0.2277	27.63	110.53
50	28978	76553	0.3785	50.68	101.36
100	58018	76236	0.7610	109.1	109.14
500	242630	74671	3.249	489.4	97.89
1,000	379363	77767	4.878	738.4	73.84[a]
2,000	468266	55313	8.466	1,287	64.34[a]

$y = 0.00654x + 0.046$ $r = 0.9984$

[a] Except for this sample, other samples were used to construct the calibration curve.

Table 4. Effect of organic solvent in extraction of Acetylshikonin derivative and Emodin

Classification	Peak area		Peak area ratio
	Acetylshikonin derivative	Emodin	
Ethylacetate	85596	275010	0.3112
	50486	255934	0.1973
Tert-butyl methyl ether	76408	191828	0.3983
	73886	177099	0.4172
Hexane	81531	68674	1.187
	84576	76208	1.110
Cyclohexane	114914	83326	1.379
	109772	89353	1.229

<LC/MS/MS를 이용한 랫드 혈장 중 Acetylshikonin의 검량선 확인 시험>

SBB SCAS-BTT Bioanalysis Co.,Ltd.

Table 1. System suitability for the determination of Acetylshikonin in rat plasma

Analytical date	Classification		No. 1	No. 2	No. 3	No. 4	No. 5	Mean ± SD	Precision (%)
Nov, 07. 2012	Peak area ratio		0.06312	0.06308	0.05415	0.05333	0.05140	0.05702 ± 0.00564	9.90
	Retention time (min)	Acetylshikonin	1.33	1.32	1.32	1.32	1.33	1.32 ± 0.01	0.41
		Emodin	1.25	1.26	1.26	1.26	1.26	1.26 ± 0.00	0.36

Peak area ratio = Peak area of reference standard / Peak area of internal reference standard
Precision (%) = Standard deviation (SD) / Mean × 100

Table 2. Calibration curve (weighting: 1/X) for the determination of Acetylshikonin in rat plasma

Analytical date	Nominal concentration (ng/mL)	Peak area			Measured concentration (ng/mL)	Accuracy (%)
		Acetylshikonin	Emodin	Ratio		
Nov, 07. 2012	Blank	0	0	0	-	-
	Zero	0	73469	0	-	-
	10	458	74444	0.006153	8.855	88.55
	25	1395	80467	0.01733	19.48	77.91[a]
	50	4338	88799	0.04886	49.43	98.86
	100	9331	75344	0.1238	120.7	120.68[a]
	500	53858	90113	0.5977	570.9	114.18
	1,000	86272	79250	1.089	1,037	103.73
	2,000	160646	80741	1.990	1,893	94.67
y = 0.00105x - 0.00317			r = 0.9974			

Accuracy (%) = Mean of the measured concentration / Nominal concentration × 100
- : Not calculated
[a] This sample was not satisfied with the accuracy criteria. Except for this sample, other samples were used to construct the calibration curve.

Table 3. Quality control for the determination of Acetylshikonin in rat plasma

Analytical date	Sample name	Nominal concentration (ng/mL)	Peak area			Measured concentration (ng/mL)	Accuracy (%)
			Acetylshikonin	Emodin	Ratio		
Nov, 07. 2012	QL1	30	1851	84713	0.02186	23.78	79.25
	QM1	500	54521	80225	0.6796	648.7	129.75
	QH1	1,500	134189	83681	1.604	1,527	101.78
	QL2	30	2792	77356	0.03610	37.31	124.36
	QM2	500	55599	73238	0.7591	724.3	144.86
	QH2	1,500	129924	78070	1.664	1,584	105.62

Accuracy (%) = Mean of the measured concentration / Nominal concentration × 100

Table 4. Concentration of Acetylshikonin in rat male plasma of individual test sample

Group / Dose (mg/kg)	Time (hr) / Animal ID	Final concentration (ng/mL)					
		0	0.5	1	2	4	8
G3 / 10	1201	N.D.	22.48	25.57	19.28	19.43	12.73
	1202	N.D.	30.93	29.32	28.07	BQL	BQL
	Mean	-	26.71	27.45	23.68	19.43	12.73
	SD	-	5.98	2.65	6.22	-	-
G3 / 1,000	1301	N.D.	2,878	1,952	1,073	748.6	652.1
	1302	N.D.	2,137	1,875	859.4	575.4	405.8
	Mean	-	2,508	1,914	966.2	662.0	529.0
	SD	-	524	54	151.0	122.5	174.2

N.D. : Not detected

BQL : Below Quantification Limit (10 ng/mL)

- : Not calculated

<LC/MS/MS를 이용한 랫드 혈장 중 Acetylshikonin의 검량선 확인 시험>

SBB SCAS-BTT Bioanalysis Co.,Ltd.

Table 1. System suitability for the determination of Acetylshikonin derivative in dog plasma

Analytical date	Classification		No. 1	No. 2	No. 3	No. 4	No. 5	Mean ± SD	Precision (%)
Nov, 13. 2012	Peak area ratio		0.1533	0.1595	0.1578	0.1524	0.1414	0.1529 ± 0.0071	4.63
	Retention time (min)	RS	1.31	1.33	1.32	1.33	1.32	1.32 ± 0.01	0.63
		IS	1.23	1.23	1.22	1.23	1.23	1.23 ± 0.00	0.36

Peak area ratio = Peak area of reference standard / Peak area of internal reference standard

Precision (%) = Standard deviation (SD) / Mean × 100

RS: Acetylshikonin derivative

IS: Emodin

Table 2. Calibration curve (weighting: 1/X) for the determination of Acetylshikonin derivative in dog plasma

Analytical date	Nominal concentration (ng/mL)	Peak area			Measured concentration (ng/mL)	Accuracy (%)
		Acetylshikonin derivative	Emodin	Ratio		
Nov, 13. 2012	Blank	0	0	0	-	-
	Zero	0	155309	0	-	-
	2	2934	138820	0.02114	1.913	95.67
	5	7819	151299	0.05168	4.545	90.90
	10	16892	135994	0.1242	10.79	107.95
	25	46460	150692	0.3083	26.66	106.63
	50	79587	135189	0.5887	50.82	101.63
	100	167192	148395	1.127	97.17	97.17
	200	330478	142365	2.321	200.1	100.05
	500	615650	142471	4.321	372.4	74.48[a]
y = 0.0116x + -0.00107			r = 0.9995			

Accuracy was calcurated from Analyst 1.5.2 software program.

- : Not calculated

[a] This sample was not satisfied with the accuracy criteria. Except for this sample, other samples were used to construct the calibration curve.

Table 3. Quality control for the determination of Acetylshikonin derivative in dog plasma

Analytical date	Sample name	Nominal concentration (ng/mL)	Peak area			Measured concentration (ng/mL)	Accuracy (%)
			Acetylshikonin derivative	Emodin	Ratio		
Nov, 13. 2012	QL1	2	2938	142707	0.02059	1.866	93.31
	QM1	6	9556	135452	0.07055	6.171	102.85
	QH1	400	526793	120023	4.389	378.3	94.57
	QL2	2	2328	119293	0.01952	1.774	88.69
	QM2	6	8485	126057	0.06731	5.892	98.20
	QH2	400	463888	185192	2.505	215.9	53.98

Accuracy was calcurated from Analyst 1.5.2 software program.

Table 4. Concentration of Acetylshikonin in dog male plasma of individual test sample

Group / Dose (mg/kg)	Time (hr) / Animal ID	Final concentration (ng/mL)								
		0	0.25	0.5	1	2	4	6	10	24
G3 / 10	1101	N.D.	N.D.	6.175	6.567	4.531	5.122	3.123	BQL	BQL
	1102	N.D.	3.804	3.271	2.917	5.223	6.178	5.314	BQL	BQL
	Mean	-	3.804	4.723	4.742	4.877	5.650	4.219	-	-
	SD	-	-	2.053	2.581	0.489	0.747	1.549	-	-
G3 / 1,000	1201	N.D.	11.66	29.21	22.08	11.34	8.261	5.557	3.491	4.409
	1202	N.D.	22.04	23.43	26.57	35.40	15.79	9.370	4.142	3.793
	Mean	-	16.85	26.32	24.33	23.37	12.03	7.464	3.817	4.101
	SD	-	7.34	4.09	3.17	17.01	5.32	2.696	0.460	0.436

N.D. : Not detected
BQL : Below Quantification Limit (2 ng/mL)
- : Not calculated

<LC/MS/MS를 이용한 랫드 및 비글견 혈장중 Acetylshikonin의 분석법 개발>

Inhibitor	Concentration (M) in plasma	Residual ratio (%)
Phenymethysulfony fluoride	0.01	89.1
	0.1	89.3
	1	96.4
Dichlorvos	0.01	95.2
	0.1	98.1
	1	102.6
Thenoyltrifluoroacetone (TTFE)	0.01	102.3
	0.1	95.3
	1	95.9
Acetylcholine (Ach)	0.01	95.8
	0.1	92.4
	1	94.9
Bis(4-nitoriphenyl)-phosphate (BNPP)	0.01	92.8
	0.1	96.5
	1	71.8
Paraoxon	0.01	97.3
	0.1	99.7
	1	101.2
Eserine	0.01	100.7
	0.1	100.5
	1	67.6
Sodium fluoride (NaF)	0.01	97.8
	0.1	98.5
	1	137.4

Table 2. Results of esterase inhibition in beagle plasma

Inhibitor	Concentration (M) in plasma	Residual ratio (%)
Phenymethysulfony fluoride	0.01	90.1
	0.1	99.2
	1	93.9
Dichlorvos	0.01	88.1
	0.1	78.9
	1	86.5
Thenoyltrifluoroacetone (TTFE)	0.01	89.8
	0.1	90.4
	1	87.2
Acetylcholine (Ach)	0.01	96.7
	0.1	100.7
	1	84.8
Bis(4-nitoriphenyl)-phosphate (BNPP)	0.01	73.8
	0.1	24.0
	1	45.3
Paraoxon	0.01	59.3
	0.1	89.6
	1	102.6
Eserine	0.01	74.2
	0.1	90.5
	1	89.1
Sodium fluoride (NaF)	0.01	85.3
	0.1	89.1
	1	107.9

Table 3. Selectivity of acetylshikonin in rat plasma

Analyte	Sex	Lot No.	Peak area of blank sample	Peak area of LLOQ	Interference peak area ratio* (%)
Acetylshikonin	male	RMP130201001	0	13562	0.0
		RMP130201002	0	13700	0.0
		RMP130201003	0	14928	0.0
	female	RFP130201001	0	14953	0.0
		RFP130201002	0	13014	0.0
		RFP130201003	0	14274	0.0
I.S.	male	RMP130201001	0	216707	0.0
		RMP130201002	0	270993	0.0
		RMP130201003	0	231111	0.0
	female	RFP130201001	0	333279	0.0
		RFP130201002	0	309708	0.0
		RFP130201003	0	249937	0.0

* Interference peak area ratio (%) =
Peak area of interference / Peak area of acetylshikonin and I.S. in LLOQ sample × 100
I.S.: Internal standard (Emodin)

Table 4. Selectivity of acetylshikonin in beagle plasma

Analyte	Sex	Lot No.	Peak area of blank sample	Peak area of LLOQ	Interference peak area ratio* (%)
Acetylshikonin	male	DMP130326001	0	13591	0.0
		DMP130326002	0	12533	0.0
		DMP130326003	0	11346	0.0
	female	DFP130326001	0	11894	0.0
		DFP130326002	0	13390	0.0
		DFP130326003	0	10954	0.0
I.S.	male	DMP130326001	0	193332	0.0
		DMP130326002	0	180358	0.0
		DMP130326003	0	176868	0.0
	female	DFP130326001	0	209673	0.0
		DFP130326002	0	207743	0.0
		DFP130326003	0	180722	0.0

* Interference peak area ratio (%) =
Peak area of interference / Peak area of acetylshikonin and I.S. in LLOQ sample × 100
I.S.: Internal standard (Emodin)

Table 5. Matrix effect of acetylshikonin in rat plasma

Analyte	Nominal concentration (ng/mL)	Sex	Lot No.	Determined concentration (ng/mL)	Mean ± SD (ng/mL)	Accuracy (%)	Precision (%)
Acetylshikonin	5.0	male	RMP130201001	4.74	4.11 ± 0.66	82.1	16.1
			RMP130201002	3.89			
			RMP130201003	4.89			
		female	RFP130201001	3.48			
			RFP130201002	3.28			
			RFP130201003	4.35			

Accuracy (%) = (Determined concentration / Theoretical concentration) × 100
Precision (%) = (Standard deviation (SD) / Mean) × 100

Table 6. Matrix effect of acetylshikonin in beagle plasma

Analyte	Nominal concentration (ng/mL)	Sex	Lot No.	Determined concentration (ng/mL)	Mean ± SD (ng/mL)	Accuracy (%)	Precision (%)
Acetylshikonin	5.0	male	DMP130326001	4.86	4.44 ± 0.35	88.9	8.0
			DMP130326002	4.80			
			DMP130326003	4.43			
		female	DFP130326001	3.93			
			DFP130326002	4.45			
			DFP130326003	4.19			

Accuracy (%) = (Determined concentration / Theoretical concentration) × 100
Precision (%) = (Standard deviation (SD) / Mean) × 100

Table 7. Within-run precision and accuracy on the determination of acetylshikonin in rat plasma

Nominal concentration (ng/mL)	Analytical date	Determined concentration (ng/mL)	Within-run Precision and Accuracy		
			Mean ± SD (ng/mL)	Accuracy (%)	Precision (%)
QC-LLOQ 5	May. 10, 2013	4.37 4.20 4.10 4.23 4.54	4.29 ± 0.17	85.8	4.0
QC-L 15	May. 10, 2013	13.8 14.0 14.8 11.6 14.9	13.8 ± 1.3	92.1	9.6
QC-M 300	May. 10, 2013	277 327 348 340 330	324 ± 28	108.1	8.6
QC-H 750	May. 10, 2013	679 873 607 797 633	718 ± 113	95.7	15.8

Accuracy (%) = (Mean of the measured concentration / Nominal concentration) × 100
Precision (%) = (Standard deviation (SD) / Mean) × 100

Table 8. Within-run precision and accuracy on the determination of acetylshikonin in beagle plasma

Nominal concentration (ng/mL)	Analytical date	Determined concentration (ng/mL)	Within-run Precision and Accuracy		
			Mean ± SD (ng/mL)	Accuracy (%)	Precision (%)
QC-LLOQ 5	May. 10, 2013	5.97 5.37 5.18 5.05 5.51	5.42 ± 0.36	108.3	6.6
QC-L 15	May. 10, 2013	13.1 13.0 13.9 13.4 14.1	13.5 ± 0.5	90.0	3.6
QC-M 300	May. 10, 2013	294 267 256 265 273	271 ± 14	90.3	5.3
QC-H 750	May. 10, 2013	655 681 649 639 686	662 ± 21	88.3	3.1

Accuracy (%) = (Mean of the measured concentration / Nominal concentration) × 100
Precision (%) = (Standard deviation (SD) / Mean) × 100

Table 9. Stability of acetylshikonin in rat plasma

Nominal concentration (ng/mL)	Analytical date	Classification	Determined concentration (ng/mL)	Mean (ng/mL)	Accuracy (%)
15.0	May. 23, 2013	Control	13.8 14.3 15.2	14.4	96.2
	Jun. 20, 2013	Deep freezer 20 days	23.4 22.1 22.7	22.7	151.6
	May. 24, 2013	Freeze-thaw 1 time	18.0 13.5 15.6	15.7	104.7
300	May. 23, 2013	Control	310 263 224	266	88.6
	Jun. 20, 2013	Deep freezer 20 days	422 417 445	428	142.7
	May. 24, 2013	Freeze-thaw 1 time	416 362 419	399	133.0
750	May. 23, 2013	Control	662 776 718	719	95.8
	Jun. 20, 2013	Deep freezer 20 days	1090 967 896	984	131.2
	May. 24, 2013	Freeze-thaw 1 time	635 771 885	764	101.8

Accuracy (%) = (Mean of the measured concentration / Nominal concentration) × 100
Precision (%) = (Standard deviation (SD) / Mean) × 100

Table 10. Stability of acetylshikonin in beagle plasma

Nominal concentration (ng/mL)	Analytical date	Classification	Determined concentration (ng/mL)	Mean (ng/mL)	Accuracy (%)
15.0	May. 23, 2013	Control	14.9 10.6 14.6	13.4	89.1
	Jun. 20, 2013	Deep freezer 28 days	10.2 12.4 10.8	11.1	74.2
	May. 24, 2013	Freeze-thaw 1 time	12.9 11.2 13.8	12.6	84.2
300	May. 23, 2013	Control	238 305 293	279	92.9
	Jun. 20, 2013	Deep freezer 28 days	224 250 211	228	76.1
	May. 24, 2013	Freeze-thaw 1 time	309 290 268	289	96.3
750	May. 23, 2013	Control	558 619 719	632	84.3
	Jun. 20, 2013	Deep freezer 28 days	640 539 554	578	77.0
	May. 24, 2013	Freeze-thaw 1 time	524 623 660	602	80.3

Accuracy (%) = (Mean of the measured concentration / Nominal concentration) × 100
Precision (%) = (Standard deviation (SD) / Mean) × 100

<α-iso-cubebenol의 마우스를 이용한 소핵시험>

Table 1. Clinical Signs

Group		Dose (mg/kg)	Administration route	No. of animals	Clinical signs	Days post dosing		
						0		1
						post dosing	2 hours post dosing	
Negative control	Dimethyl sulfoxide	0	P.O.	3	NAD	3	3	3
Test substance	α-iso-cubebenol	109	P.O.	3	NAD	3	3	3
		219	P.O.	3	NAD	3	3	3
		437	P.O.	3	NAD	3	3	3
Positive control	Mitomycin C (MMC)	2	I.P.	3	NAD	3	3	3

P.O. : Per Os

I.P. : Intraperitoneal injection

NAD : No Abnormalities Detected

Table 2. Body Weights

Group		Dose (mg/kg)	Hours after dosing	Animal ID	Days post dosing	
					0	1
Negative control	Dimethyl sulfoxide	0	24	1101	36.1	36.0
				1102	34.3	34.0
				1103	34.2	33.9
				Mean	34.9	34.6
				S.D.	1.1	1.2
				N	3	3
Test substance	α-iso-cubebenol	109	24	1201	35.3	33.8
				1202	34.7	34.9
				1203	33.7	33.9
				Mean	34.6	34.2
				S.D.	0.8	0.6
				N	3	3
		219	24	1301	35.1	34.6
				1302	34.7	34.0
				1303	33.4	33.5
				Mean	34.4	34.0
				S.D.	0.9	0.6
				N	3	3
		437	24	1401	35.0	35.2
				1402	34.8	34.3
				1403	33.2	32.5
				Mean	34.3	34.0
				S.D.	1.0	1.4
				N	3	3
Positive control	Mitomycin C (MMC)	2	24	1501	35.0	34.0
				1502	34.9	35.1
				1503	32.9	32.7
				Mean	34.2	33.9
				S.D.	1.2	1.2
				N	3	3

S.D. : Standard deviation

N : The number of animals

Table 3. Results

Groups		Dose (mg/kg)	Administration route	Hours post dosing	Animal ID	Counted PCE : NCE	PCE/(PCE+NCE)	MNPCE/ PCE
Negative control	Dimethyl sulfoxide	0	P.O.	24	1101	193 / 307	0.386	0 / 2000
					1102	102 / 398	0.204	0 / 2000
					1103	171 / 329	0.342	0 / 2000
					Total	-	-	0 / 6000
					Mean±S.D.	-	0.311 ± 0.095	0.0 ± 0.000
Test substance	α-iso-cubebenol	109	P.O.	24	1201	143 / 357	0.286	0 / 2000
					1202	134 / 366	0.268	0 / 2000
					1203	142 / 358	0.284	0 / 2000
					Total	-	-	0 / 6000
					Mean±S.D.	-	0.279 ± 0.010	0.0 ± 0.000
		219	P.O.	24	1301	186 / 314	0.372	0 / 2000
					1302	134 / 366	0.268	1 / 2000
					1303	160 / 340	0.320	0 / 2000
					Total	-	-	1 / 6000
					Mean±S.D.	-	0.320 ± 0.052	0.3 ± 0.577
		437	P.O.	24	1401	136 / 364	0.272	1 / 2000
					1402	112 / 388	0.224	1 / 2000
					1403	141 / 359	0.282	0 / 2000
					Total	-	-	2 / 6000
					Mean±S.D.	-	0.259 ± 0.031	0.7 ± 0.577
Positive control	Mitomycin C (MMC)	2	I.P.	24	1501	119 / 381	0.238	95 / 2000
					1502	142 / 358	0.284	85 / 2000
					1503	138 / 362	0.276	81 / 2000
					Total	-	-	261† / 6000
					Mean±S.D.	-	0.266 ± 0.025	87.0 ± 7.211

P.O. : Per Os
I.P. : Intraperitoneal injection
MNPCE : Micronucleated polychromatic erythrocyte
PCE : Polychromatic erythrocyte
NCE : Normochromatic erythrocyte
S.D. : Standard deviation
0.5% CMC-Na solution : 0.5% Carboxymethylcellulose Sodium salt solution
Significant difference compared to the negative control using the criteria of Kastenbaum-Bowmant : †$p<0.05$

Table 4. Historical Control Data

Historical control values of micronucleated polychromatic erythrocytes(MNPCE)

Group	Dose (mg/kg)	n	MNPCE/2000PCE Mean±S.D.	Range(MNPCE/2000PCE) MIN	MAX
Negative control	0	105	0.6 ± 0.55	0	2.0
Positive control	2	105	131.6 ± 31.36	53.2	210.0

Historical control values of ratio of polychromatic erythrocytes(PCE) to total erythrocytes

Group	Dose (mg/kg)	n	PCE/NCE+PCE Mean±S.D.	Range(PCE/NCE+PCE) MIN	MAX
Negative control	0	105	0.376 ± 0.040	0.276	0.476
Positive control	2	105	0.342 ± 0.045	0.229	0.456

Negative control : Including water for injection, olive oil, corn oil, 0.5% methyl cellulose 1,500cP, 0.5% CMC-Na, DMSO, Saline *etc.*

Positive control : Mitomycin C (2 mg/kg, I.P., single administration)

The above historical control values were obtained from the data pooled from June 20, 2008 to Oct. 12, 2011.

The range was calculated by the control limit from Mean ± 2.5S.D.

<α-iso-cubebenol의 세균을 이용한 복귀돌연변이시험>

Table 1. The Number of Revertant Colonies per Plate in Absence of Metabolic Activation (Dose Range Finding Study)

Strain	Test item	Dose level (μg/plate)	Individual revertant	Mean
TA98	Dimethyl sulfoxide	0	17 , 14	16
	α-iso-cubebenol	4.88	20 , 16	18
		19.5	20 , 13	17
		78.1	16 , 13	15
		313†	11* , 19*	15
		1,250†	9* , 9*	9
		5,000†	6* , 8*	7
	2-Nitrofluorene (2-NF)	5.0	585 , 712	649
TA100	Dimethyl sulfoxide	0	87 , 69	78
	α-iso-cubebenol	4.88	71 , 71	71
		19.5	62* , 63*	63
		78.1	0* , 0*	0
		313†	0* , 0*	0
		1,250†	0* , 0*	0
		5,000†	0* , 0*	0
	Sodium azide (SA)	1.5	571 , 632	602
TA1535	Dimethyl sulfoxide	0	11 , 9	10
	α-iso-cubebenol	4.88	9 , 8	9
		19.5	6* , 3*	5
		78.1	0* , 0*	0
		313†	0* , 0*	0
		1,250†	0* , 0*	0
		5,000†	0* , 0*	0
	Sodium azide (SA)	1.5	519 , 528	524
TA1537	Dimethyl sulfoxide	0	6 , 5	6
	α-iso-cubebenol	4.88	5 , 5	5
		19.5	1* , 0*	1
		78.1	0* , 0*	0
		313†	0* , 0*	0
		1,250†	0* , 0*	0
		5,000†	0* , 0*	0
	9-Aminoacridine (9-AA)	80.0	352 , 482	417
WP2*uvrA* (pKM101)	Dimethyl sulfoxide	0	96 , 101	99
	α-iso-cubebenol	4.88	105 , 122	114
		19.5	124 , 118	121
		78.1	119 , 99	109
		313†	98 , 86	92
		1,250†	95 , 72	84
		5,000†	78 , 72	75
	2-(2-furyl)-3-(5-nitro-2-furyl)acrylamide (AF2)	0.005	729 , 649	689

*: Indicated growth inhibition

†: Deposition

Table 2. The Number of Revertant Colonies per Plate in Presence of Metabolic Activation
(Dose Range Finding Study)

Strain	Test item	Dose level (μg/plate)	Individual revertant	Mean
TA98	Dimethyl sulfoxide	0	29 , 23	26
	α-iso-cubebenol	4.88	16 , 25	21
		19.5	27 , 33	30
		78.1	25 , 30	28
		313†	14* , 29*	22
		1,250†	22* , 19*	21
		5,000†	18* , 17*	18
	2-Aminoanthracene (2-AA)	1.0	133 , 142	138
TA100	Dimethyl sulfoxide	0	81 , 92	87
	α-iso-cubebenol	4.88	92 , 83	88
		19.5	78 , 97	88
		78.1	63 , 84	74
		313†	54* , 38*	46
		1,250†	30* , 13*	22
		5,000†	1* , 1*	1
	2-Aminoanthracene (2-AA)	2.0	355 , 452	404
TA1535	Dimethyl sulfoxide	0	11 , 10	11
	α-iso-cubebenol	4.88	12 , 8	10
		19.5	9 , 7	8
		78.1	9 , 6	8
		313†	6* , 8*	7
		1,250†	3* , 0*	2
		5,000†	0* , 0*	0
	2-Aminoanthracene (2-AA)	3.0	128 , 109	119
TA1537	Dimethyl sulfoxide	0	11 , 10	11
	α-iso-cubebenol	4.88	11 , 7	9
		19.5	10 , 9	10
		78.1	13 , 8	11
		313†	0* , 0*	0
		1,250†	0* , 0*	0
		5,000†	0* , 0*	0
	2-Aminoanthracene (2-AA)	3.0	120 , 134	127
WP2*uvrA* (pKM101)	Dimethyl sulfoxide	0	137 , 139	138
	α-iso-cubebenol	4.88	103 , 115	109
		19.5	130 , 159	145
		78.1	133 , 144	139
		313†	137 , 135	136
		1,250†	119 , 128	124
		5,000†	95 , 81	88
	2-Aminoanthracene (2-AA)	2.0	408 , 412	410

*: Indicated growth inhibition

†: Deposition

Table 3. The Number of Revertant Colonies per Plate in Absence of Metabolic Activation (Main Study)

Strain	Test item	Dose level (μg/plate)	Individual revertant colony counts	Mean	S.D.
TA98	Dimethyl sulfoxide	0	15 , 20 , 13	16	4
	α-iso-cubebenol	9.77	15 , 22 , 17	18	4
		19.5	20 , 12 , 12	15	5
		39.1	13 , 13 , 12	13	1
		78.1	15 , 13 , 15	14	1
		156	14* , 11* , 14*	13	2
		313†	10* , 12* , 14*	12	2
	2-Nitrofluorene (2-NF)	5.0	584 , 465 , 536	528	60
TA100	Dimethyl sulfoxide	0	61 , 83 , 62	69	12
	α-iso-cubebenol	0.610	65 , 70 , 70	68	3
		1.22	65 , 72 , 63	67	5
		2.44	59 , 68 , 50	59	9
		4.88	45 , 63 , 54	54	9
		9.77	78 , 66 , 66	70	7
		19.5	48* , 43* , 47*	46	3
	Sodium azide (SA)	1.5	574 , 470 , 451	498	66
TA1535	Dimethyl sulfoxide	0	9 , 13 , 8	10	3
	α-iso-cubebenol	0.610	10 , 8 , 8	9	1
		1.22	12 , 8 , 7	9	3
		2.44	6 , 6 , 9	7	2
		4.88	10 , 8 , 7	8	2
		9.77	11 , 13 , 7	10	3
		19.5	7* , 8* , 6*	7	1
	Sodium azide (SA)	1.5	443 , 471 , 508	474	33
TA1537	Dimethyl sulfoxide	0	5 , 6 , 5	5	1
	α-iso-cubebenol	0.610	8 , 5 , 9	7	2
		1.22	3 , 4 , 4	4	1
		2.44	7 , 6 , 4	6	2
		4.88	4 , 4 , 5	4	1
		9.77	3 , 8 , 7	6	3
		19.5	2* , 2* , 2*	2	0
	9-Aminoacridine (9-AA)	80.0	506 , 578 , 510	531	40
WP2*uvrA* (pKM101)	Dimethyl sulfoxide	0	66 , 91 , 80	79	13
	α-iso-cubebenol	313†	89 , 90 , 88	89	1
		625†	86 , 54 , 64	68	16
		1,250†	66 , 62 , 62	63	2
		2,500†	67 , 63 , 56	62	6
		5,000†	65 , 65 , 57	62	5
	2-(2-furyl)-3-(5-nitro-2-furyl)acrylamide (AF2)	0.005	698 , 621 , 513	611	93

S.D.: Standard Deviation

*: Indicated growth inhibition

†: Deposition

Table 4. The Number of Revertant Colonies per Plate in Presence of Metabolic Activation (Main Study)

Strain	Test item	Dose level (μg/plate)	Individual revertant colony counts	Mean	S.D.
TA98	Dimethyl sulfoxide	0	19 , 23 , 23	22	2
	α-iso-cubebenol	9.77	29 , 28 , 25	27	2
		19.5	18 , 18 , 27	21	5
		39.1	30 , 19 , 28	26	6
		78.1	18 , 16 , 25	20	5
		156	10* , 18* , 18*	15	5
		313†	15* , 19* , 14*	16	3
	2-Aminoanthracene (2-AA)	1.0	246 , 176 , 217	213	35
TA100	Dimethyl sulfoxide	0	63 , 70 , 77	70	7
	α-iso-cubebenol	9.77	76 , 80 , 71	76	5
		19.5	93 , 76 , 79	83	9
		39.1	72 , 83 , 73	76	6
		78.1	70 , 89 , 65	75	13
		156	32* , 26* , 38*	32	6
		313†	25* , 36* , 41*	34	8
	2-Aminoanthracene (2-AA)	2.0	501 , 361 , 339	400	88
TA1535	Dimethyl sulfoxide	0	8 , 7 , 9	8	1
	α-iso-cubebenol	9.77	11 , 9 , 7	9	2
		19.5	7 , 6 , 6	6	1
		39.1	6 , 12 , 9	9	3
		78.1	7 , 10 , 11	9	2
		156	4* , 5* , 5*	5	1
		313†	4* , 7* , 4*	5	2
	2-Aminoanthracene (2-AA)	3.0	110 , 93 , 115	106	12
TA1537	Dimethyl sulfoxide	0	12 , 8 , 9	10	2
	α-iso-cubebenol	9.77	13 , 10 , 10	11	2
		19.5	15 , 13 , 10	13	3
		39.1	18 , 17 , 10	15	4
		78.1	13 , 12 , 12	12	1
		156	6* , 8* , 6*	7	1
		313†	11* , 0* , 0*	4	6
	2-Aminoanthracene (2-AA)	3.0	175 , 149 , 135	153	20
WP2*uvrA* (pKM101)	Dimethyl sulfoxide	0	120 , 115 , 105	113	8
	α-iso-cubebenol	313†	114 , 124 , 122	120	5
		625†	115 , 103 , 100	106	8
		1,250†	107 , 108 , 97	104	6
		2,500†	127 , 69 , 83	93	30
		5,000†	90 , 80 , 76	82	7
	2-Aminoanthracene (2-AA)	2.0	426 , 548 , 488	487	61

S.D.: Standard Deviation

*: Indicated growth inhibition

†: Deposition

Table 5. Historical Control Data

Historical negative control values of revertant colonies

Strain	S9 mix	N	Mean ± S.D.	Range	
				Lower	Upper
TA100	-	112	81.4 ± 12.5	52.9	110.0
	+	112	92.8 ± 12.7	57.1	128.4
TA1535	-	112	10.3 ± 2.4	4.2	16.5
	+	112	9.8 ± 2.5	2.1	17.6
WP2*uvrA* (pKM101)	-	112	125.0 ± 19.5	72.0	177.9
	+	112	149.4 ± 18.9	97.0	201.8
TA98	-	112	15.5 ± 4.0	6.5	24.5
	+	112	22.0 ± 5.3	9.0	35.0
TA1537	-	112	6.0 ± 1.9	1.0	11.0
	+	112	10.8 ± 3.0	2.6	19.0

Historical positive control values of revertant colonies

Strain	S9 mix	Positive control	Dose (μg/plate)	N	Mean ± S.D.	Range	
						Lower	Upper
TA100	-	SA	1.5	112	436.8 ± 74.7	253.6	619.9
	+	2-AA	2.0	110	396.7 ± 133.2	73.7	719.8
TA1535	-	SA	1.5	112	440.9 ± 83.2	277.4	604.5
	+	2-AA	3.0	112	144.7 ± 38.6	54.4	235.0
WP2*uvrA* (pKM101)	-	AF2	0.005	110	977.6 ± 220.4	487.8	1467.3
	+	2-AA	2.0	112	416.6 ± 85.9	187.1	646.1
TA98	-	2-NF	5.0	112	485.7 ± 103.6	236.1	735.3
	+	2-AA	1.0	110	229.9 ± 71.9	69.8	390.1
TA1537	-	9-AA	80.0	112	316.6 ± 111.9	81.9	551.3
	+	2-AA	3.0	110	162.1 ± 48.4	54.9	269.2

Negative control : Water for injection, Dimethyl sulfoxide, Acetone, 0.5% methyl cellulose 1,500cP, 0.5% carboxymethylcellulose sodium salt solution

SA : Sodium azide

2-AA : 2-Aminoanthracene

AF2 : 2-(2-furyl)-3-(5-nitro-2-furyl)acrylamide

2-NF : 2-Nitrofluorene

9-AA : 9-Aminoacridine

The above historical control values were obtained from the data pooled from Oct. 8, 2010 to Sep. 24, 2011.

The range was calculated by the control limit of X derived from $\overline{X}$-$\overline{R}$-$\overline{Rs}$ value.

<α-iso-cubebenol의 포유류 배양세포를 이용한 염색체이상시험>

Table 1. Summary of Growth Inhibition Study

Test substance	Dose (μg/mL)	S9 mix	Trt-Rec Time (hr)	Growth of cells (OD) (Mean±S.D.)	Growth rate (%)
Dimethyl sulfoxide	0	-	6-18	0.947 ± 0.061	100
α-iso-cubebenol	5	-	6-18	0.920 ± 0.023	97.1
	10	-	6-18	0.833 ± 0.081	88.0
	50	-	6-18	0.112 ± 0.027	11.8
	100	-	6-18	0.083 ± 0.002	8.77
	250	-	6-18	0.084 ± 0.001	8.87
	500	-	6-18	0.080 ± 0.003	8.45
	1,000	-	6-18	0.078 ± 0.003	8.24
	2,500	-	6-18	0.068 ± 0.002	7.18
	5,000	-	6-18	0.065 ± 0.002	6.86
Dimethyl sulfoxide	0	+	6-18	0.874 ± 0.066	100
α-iso-cubebenol	5	+	6-18	0.883 ± 0.051	101
	10	+	6-18	0.928 ± 0.038	106
	50	+	6-18	0.881 ± 0.064	101
	100	+	6-18	0.837 ± 0.050	95.8
	250	+	6-18	0.086 ± 0.007	9.84
	500	+	6-18	0.080 ± 0.002	9.15
	1,000†	+	6-18	0.077 ± 0.002	8.81
	2,500†	+	6-18	0.072 ± 0.006	8.24
	5,000†	+	6-18	0.071 ± 0.008	8.12
Dimethyl sulfoxide	0	-	24-0	0.998 ± 0.069	100
α-iso-cubebenol	5	-	24-0	0.881 ± 0.119	88.3
	10	-	24-0	0.883 ± 0.067	88.5
	50	-	24-0	0.090 ± 0.006	9.02
	100	-	24-0	0.091 ± 0.008	9.12
	250	-	24-0	0.084 ± 0.002	8.42
	500	-	24-0	0.086 ± 0.004	8.62
	1,000	-	24-0	0.083 ± 0.003	8.32
	2,500	-	24-0	0.080 ± 0.004	8.02
	5,000	-	24-0	0.079 ± 0.006	7.92

Trt-Rec time : Treatment-Recovery times

S.D.:Standard deviation

† : Deposition

Table 2. Summary of Main Study

Test substance	Dose (μg/mL)	S9 mix	Trt-Rec Time (hr)	No. of cell analyzed	Number of cells with structural aberrations						gap (%)	Number of cells with numerical aberrations		
					ctb	csb	cte	cse	frg	total (%)		end	pol	total (%)
Dimethyl sulfoxide	0	-	6-18	100	0	0	0	0	0	0 (0.0)	0 (0.0)	0	1	1 (0.5)
				100	0	0	0	0	0			0	0	
α-iso-cubebenol	1.88	-	6-18	not observed										
	3.75	-	6-18	not observed										
	7.50	-	6-18	100	0	0	0	0	0	0 (0.0)	1 (0.5)	0	0	0 (0.0)
				100	0	0	0	0	0			0	0	
	15.0	-	6-18	100	0	0	0	0	0	0 (0.0)	0 (0.0)	0	0	0 (0.0)
				100	0	0	0	0	0			0	0	
	30.0	-	6-18	100	0	0	1	0	0	1 (0.5)	0 (0.0)	0	0	0 (0.0)
				100	0	0	0	0	0			0	0	
MMC	0.05	-	6-18	100	5	0	9	1	0	31* (15.5)	0 (0.0)	0	0	0 (0.0)
				100	4	0	17	0	0			0	0	
Dimethyl sulfoxide	0	+	6-18	100	0	0	0	0	0	0 (0.0)	0 (0.0)	0	0	0 (0.0)
				100	0	0	0	0	0			0	0	
α-iso-cubebenol	21.3	+	6-18	100	0	0	0	0	0	0 (0.0)	0 (0.0)	0	0	0 (0.0)
				100	0	0	0	0	0			0	0	
	42.5	+	6-18	100	0	0	0	0	0	0 (0.0)	0 (0.0)	0	0	0 (0.0)
				100	0	0	0	0	0			0	0	
	85.0	+	6-18	100	0	0	0	0	0	0 (0.0)	0 (0.0)	0	0	0 (0.0)
				100	0	0	0	0	0			0	0	
	170	+	6-18	toxic										
B[a]P	20	+	6-18	100	5	0	18	0	0	41* (20.5)	0 (0.0)	0	1	1 (0.5)
				100	3	0	21	1	0			0	0	
Dimethyl sulfoxide	0	-	24-0	100	0	0	1	0	0	1 (0.5)	0 (0.0)	0	0	0 (0.0)
				100	0	0	0	0	0			0	0	
α-iso-cubebenol	1.75	-	24-0	not observed										
	3.50	-	24-0	not observed										
	7.00	-	24-0	100	0	0	0	0	0	0 (0.0)	0 (0.0)	0	0	0 (0.0)
				100	0	0	0	0	0			0	0	
	14.0	-	24-0	100	0	0	0	0	0	0 (0.0)	0 (0.0)	0	0	0 (0.0)
				100	0	0	0	0	0			0	0	
	28.0	-	24-0	100	0	0	0	0	0	0 (0.0)	0 (0.0)	0	0	0 (0.0)
				100	0	0	0	0	0			0	0	
MMC	0.05	-	24-0	100	3	0	15	0	0	32* (16.0)	0 (0.0)	0	0	0 (0.0)
				100	4	1	12	1	0			0	0	

Aberration; gap: chromatid and chromosome gap, ctb: chromatid break, cte: chromatid exchange, csb: chromosome break, cse: chromosome exchange,frg: fragmentation, end: endoreduplication, polpolyploid

MMC: Mitomycin C, B[a]P: Benzo[a]pyrene

Trt-Rec time : Treatment-Recovery times

Significant difference from negative control by fisher's exact test : * p<0.05

Table 3. Historical Control Data

Historical control values of structural aberrations

Group	S9 mix	Time of exposure (hr)	N	Structural aberration cells without gap (%) (Mean±S.D.)			Range (%)	
							MIN	MAX
Negative	-	6+18	103	0.1	±	0.3	0	<5
	+	6+18	103	0.2	±	0.4	0	<5
	-	24+0	92	0.2	±	0.3	0	<5
Positive	-	6+18[a)]	103	18.8	±	5.4	<10	35*
	+	6+18[b)]	103	20.2	±	5.3	<10	36*
	-	24+0[a)]	92	19.2	±	5.4	<10	35*

Historical control values of numerical acerrations

Group	S9 mix	Time of exposure (hr)	N	Numerical aberration cells (%) (Mean±S.D.)			Range (%)	
							MIN	MAX
Negative	-	6+18	103	0.2	±	0.3	0	<5
	+	6+18	103	0.1	±	0.2	0	<5
	-	24+0	92	0	±	0.1	0	<5

Negative control : Water for injection, Dimethyl sulfoxide, Acetone, 0.5% methyl cellulose 1,500cP, 0.5% carboxymethylcellulose sodium salt, Tetrahydrofuran *etc*.

a : Mitomycin C (0.05 μg/mL)

b : Benzo[a]pyrene (20 μg/mL)

N : The total number of chromosome aberration test

The above historical control values were obtained from the data pooled from Sep. 14, 2010 to Oct. 14, 2011.

*: The range was calculated by the control limit from Mean + 3S.D.

<α-iso-cubebenol의 Sprague-Dawley 랫드를 이용한 단회 경구투여 독성시험>

Table 1. Summary of Mortality

Sex	Group / Dose (mg/kg)	No. of animals	Days after dosing															Mortality
			0	1	2	3	4	5	6	7	8	9	10	11	12	13	14	
Male	G1 0	5	0	0	0	0	0	0	0	0	0	0	0	0	0	0	0	0/5
	G2 1,500	5	0	0	0	0	0	0	0	0	0	0	0	0	0	0	0	0/5
	G3 2,000	5	0	0	0	0	0	0	0	0	0	0	0	0	0	0	0	0/5
Female	G1 0	5	0	0	0	0	0	0	0	0	0	0	0	0	0	0	0	0/5
	G2 1,500	5	0	0	0	0	0	0	0	0	0	0	0	0	0	0	0	0/5
	G3 2,000	5	0	0	0	0	0	0	0	0	0	0	0	0	0	0	0	0/5

Table 2. Summary of Clinical Signs.

Sex	Group / Dose (mg/kg)	No. of animals	Clinical sign	Hours (Day 0) after dosing				
				0.5	1	2	4	6
Male	G1 0	5	NOA	5	5	5	5	5
	G2 1,500	5	NOA Salivation Mucous stool	4 1	5	5	4 1	3 2
	G3 2,000	5	NOA Salivation Mucous stool Soiled perineal region Abnormal gait	2 3	5	5	1 4	2 3 2 1
Female	G1 0	5	NOA	5	5	5	5	5
	G2 1,500	5	NOA Salivation Mucous stool	3 2	5	5	5	1 4
	G3 2,000	5	NOA Salivation Mucous stool Soiled perineal region	3 2	5	5	3 2	3 1 1

Sex	Group / Dose (mg/kg)	No. of animals	Clinical sign	Days after dosing													
				1	2	3	4	5	6	7	8	9	10	11	12	13	14
Male	G1 0	5	NOA	5	5	5	5	5	5	5	5	5	5	5	5	5	5
	G2 1,500	5	NOA Mucous stool	5	5	5	5	5	5	5	5	5	5	5	5	5	5
	G3 2,000	5	NOA Mucous stool	5	5	5	5	5	5	5	5	5	5	5	5	5	5
Female	G1 0	5	NOA	5	5	5	5	5	5	5	5	5	5	5	5	5	5
	G2 1,500	5	NOA Mucous stool	5	5	5	5	5	5	5	5	5	5	5	5	5	5
	G3 2,000	5	NOA Mucous stool Soiled perineal region	1 4 3	5	5	5	5	5	5	5	5	5	5	5	5	5

NOA: No Observable Abnormality

Table 3. Mean Body Weights

(g)

Sex	Group / Dose (mg/kg)		Days after dosing 0	1	3	7	14	Gain 0 ~ 14
Male	G1	Mean	156.8	177.9	200.5	236.6	300.4	143.7
	0	S.D.	3.7	5.5	5.1	5.8	6.4	6.4
		N	5	5	5	5	5	5
	G2	Mean	157.8	172.9	195.8	229.5	290.0	132.2
	1,500	S.D.	3.2	4.2	4.1	6.9	10.9	8.4
		N	5	5	5	5	5	5
	G3	Mean	156.4	169.7	195.2	232.6	298.0	141.6
	2,000	S.D.	2.8	6.2	6.1	3.9	11.6	13.0
		N	5	5	5	5	5	5
Female	G1	Mean	137.8	155.3	173.5	185.3	209.4	71.5
	0	S.D.	6.6	7.6	8.6	14.1	22.4	19.3
		N	5	5	5	5	5	5
	G2	Mean	137.9	153.1	171.3	189.9	216.6	78.7
	1,500	S.D.	4.4	6.8	7.8	16.9	28.8	25.4
		N	5	5	5	5	5	5
	G3	Mean	138.6	150.9	171.7	187.9	210.4	71.8
	2,000	S.D.	6.0	3.6	9.8	9.0	10.3	8.8
		N	5	5	5	5	5	5

Table 4. Summary of Necropsy Findings

Sex	Male			Female		
Group /	G1	G2	G3	G1	G2	G3
Dose (mg/kg)	0	1,500	2,000	0	1,500	2,000
No. of animals	5	5	5	5	5	5
Unremarkable findings	5	5	5	5	5	5
No. of examined	5	5	5	5	5	5

External surface and all organs in body cavity were unremarkable.

<α-iso-cubebenol의 토끼를 이용한 피부자극시험>

Table 1. Clinical Signs

Test group	Animal ID	Day			
		0	1	2	3
G1 Test substance	1101	-	-	-	-
	1102	-	-	-	-
	1103	-	-	-	-
	1104	-	-	-	-
	1105	-	-	-	-
	1106	-	-	-	-

-: No Observable Abnormality

Table 2. Body Weights

(kg)

Test group	Animal ID	Day		Gain
		0	3	
G1 Test substance	1101	2.13	2.23	0.10
	1102	2.12	2.21	0.09
	1103	2.23	2.36	0.13
	1104	2.05	2.16	0.11
	1105	2.15	2.25	0.10
	1106	2.26	2.36	0.10
	Mean	2.16	2.26	0.11
	S.D.	0.08	0.08	0.01
	No. of animals	6	6	6

Table 3. Skin Irritation Scores

Applied area	Animal ID	Score of erythema and eschar/edema					
		Intervals (hours)					
		24		(48)		72	
		Intact	Abraded	Intact	Abraded	Intact	Abraded
100% Test substance	1101	3 / 0	3 / 0	(2 / 0)	(2 / 0)	2 / 0	2 / 0
	1102	3 / 0	3 / 0	(2 / 0)	(2 / 0)	2 / 0	2 / 0
	1103	3 / 0	3 / 0	(2 / 0)	(2 / 0)	2 / 0	2 / 0
	1104	3 / 0	3 / 0	(2 / 0)	(2 / 0)	2 / 0	2 / 0
	1105	3 / 0	3 / 0	(2 / 0)	(2 / 0)	2 / 0	2 / 0
	1106	3 / 0	3 / 0	(2 / 0)	(2 / 0)	2 / 0	2 / 0
	Total score	18	18	(12)	(12)	12	12
	Mean score	6.0		(4.0)		4.0	
	P.I.I.[a]	2.5					
Only patch	1101	0 / 0	0 / 0	(0 / 0)	(0 / 0)	0 / 0	0 / 0
	1102	0 / 0	0 / 0	(0 / 0)	(0 / 0)	0 / 0	0 / 0
	1103	0 / 0	0 / 0	(0 / 0)	(0 / 0)	0 / 0	0 / 0
	1104	0 / 0	0 / 0	(0 / 0)	(0 / 0)	0 / 0	0 / 0
	1105	0 / 0	0 / 0	(0 / 0)	(0 / 0)	0 / 0	0 / 0
	1106	0 / 0	0 / 0	(0 / 0)	(0 / 0)	0 / 0	0 / 0
	Total score	0	0	(0)	(0)	0	0
	Mean score	0.0		(0.0)		0.0	
	P.I.I.[a]	0.0					

hours : Observation after application

a: P.I.I. (primary skin irritation index) = $\frac{\text{Summation mean score of 24 and 72 hours}}{\text{Intervals (2)} \times \text{Test site (2)}}$

( ) = Total values not used for calculation of P.I.I.

<α-iso-cubebenol의 토끼를 이용한 안점막자극시험>

Table 1. Summary of Clinical Signs

Test group	Clinical signs	Day							
		0	1	2	3	4	5	6	7
G1 Unwashed	No. of animals	6	6	6	6	6	6	6	6
	NOA	6	6	6	6	6	6	6	6
G2 Washed	No. of animals	3	3	3	3	3	3	3	3
	NOA	3	3	3	3	3	3	3	3

NOA : No Observable Abnormality

Table 2. Mean Body Weights

(kg)

Test group		Day		Gain
		0	7	
G1 Unwashed	Mean	2.13	2.35	0.22
	S.D.	0.06	0.06	0.03
	No. of animals	6	6	6
G2 Washed	Mean	2.19	2.41	0.22
	S.D.	0.06	0.05	0.03
	No. of animals	3	3	3

Table 3. Summary of Eye Irritation Scores.

Test group (Conc.)	No. of animals	M.I.O.I Intervals (Day)					I.A.O.I
		1	2	3	4	7	
G1 Unwashed (100%)	6	0	0	0	0	0	0
G2 Washed (100%)	3	0	0	0	0	0	0

Day : Observation after application

M.I.O.I.: Mean Index of Ocular Irritation

I.A.O.I.: Index of Acute Ocular Iritaiton (The maximum value of M.I.O.I. during the observation time)

<LC/MS/MS법을 이용한 랫드 및 비글견 혈장중 α-isocubebenol 분석법 개발 및 검증>

Table 1 Calibration curve of α-isocubebenol-NPA in rat plasma over the calibration range of 10 to 2,000 ng/mL

Nominal concentration (ng/mL)	Peak area			Measured concentration (ng/mL)	Accuracy (%)
	Alpha-isocubebenol-NPA	Mefenamic acid	Ratio		
Blank	0	12969	-	-	-
Zero	489	424,575	0.001153	-	-
10	8,643	350,241	0.02468	10.0	100.2
20	18,514	365,302	0.05068	19.9	99.4
50	43,114	353,788	0.1219	46.9	93.7
100	87,514	279,793	0.3128	119	119.3
200	141,658	274,239	0.5165	197	98.3
500	389,541	339,840	1.146	435	87.1
1,000	725,413	278,002	2.609	990	99.0
2,000	1,849,181	340,202	5.436	2060	103.1
y = 0.0264x -0.00173		r = 0.9980			

- Not calculated.

Table 2 Calibration curve of α-isocubebenol-NPA in beagle plasma over the calibration range of 10 to 2,000 ng/mL

Nominal concentration (ng/mL)	Peak area			Measured concentration (ng/mL)	Accuracy (%)
	Alpha-isocubebenol-NPA	Mefenamic acid	Ratio		
Blank	481	3504	0.1372	-	-
Zero	332	914,993	0.0003630	-	-
10	5637	883,003	0.006383	11.4	114.5
20	10830	922,412	0.01174	21.2	105.9
50	24376	919,000	0.02652	48.0	96.1
100	48826	860,071	0.05677	103	103.0
200	87215	913,790	0.09544	173	86.6
500	236361	916,464	0.2579	468	93.7
1,000	465654	891,948	0.5221	948	94.8
2,000	1028125	887,012	1.159	2110	105.3
y =0.0055x -0.00083		r = 0.9980			

- Not calculated.

Table 3 Accuracy and precision of α-isocubebenol-NPA in rat plasma as a within run

Nominal concentration (ng/mL)	Measured concentration (ng/mL)	Within-run reproducibility		
		Mean ± SD (ng/mL)	Accuracy (%)	Precision (%)
10	8.17	10.63 ± 1.91	106.3	17.9
	11.5			
	10.0			
	10.2			
	13.3			
30	30.9	29.44 ± 3.15	98.1	10.7
	25.1			
	33.6			
	28.3			
	29.3			
250	321	336.6 ± 49.1	134.6	14.6
	277			
	406			
	362			
	317			
1500	1890	2370 ± 413	158	17.4
	2510			
	2220			
	2860			

Accuracy (%) = (Mean of measured concentration / Nominal concentration) × 100.
Precision (%) = (Standard deviation (SD) / Mean) × 100.

Table 4 Accuracy and precision of α-isocubebenol-NPA in beagle plasma as a within run

Nominal concentration (ng/mL)	Measured concentration (ng/mL)	Within-run reproducibility		
		Mean ± SD (ng/mL)	Accuracy (%)	Precision (%)
10	9.51	10.46 ± 1.40	104.6	13.4
	11.8			
	12.10			
	9.9			
	8.99			
30	25.2	23.64 ± 1.44	78.8	6.1
	23.3			
	22.5			
	25.1			
	22.1			
250	427	416.4 ± 28.7	166.6	6.9
	462			
	403			
	397.0			
	393			
1500	10400	12360 ± 1193	824	9.7
	12400			
	12900			
	13600			
	12500			

Accuracy (%) = (Mean of measured concentration / Nominal concentration) × 100.
Precision (%) = (Standard deviation (SD) / Mean) × 100.

<EC-18의 랫드를 이용한 13주 반복 경구투여 독성시험>

Table 1. Summary of Clinical Signs

Sex: Male

Group / Dose (mg/kg/day)	No. of animals	Clinical sign	No. of animals affected	Days 1 ~ 91 - observed during the days
G1 0	10	No observable abnormality	10	Days 1 ~ 91
G2 500	10	No observable abnormality	10	Days 1 ~ 91
G3 1,000	10	No observable abnormality	10	Days 1 ~ 91
G4 2,000	10	No observable abnormality	9	Days 1 ~ 91
		No observable abnormality	1	Days 1 ~ 88
		Hemorrhage (toe, right hindlimb)		Day 89
		Crust formation (toe, right hindlimb)		Days 90 ~ 91

Sex: Female

Group / Dose (mg/kg/day)	No. of animals	Clinical sign	No. of animals affected	Days 1 ~ 91 - observed during the days
G1 0	10	No observable abnormality	10	Days 1 ~ 91
G2 500	10	No observable abnormality	10	Days 1 ~ 91
G3 1,000	10	No observable abnormality	10	Days 1 ~ 91
G4 2,000	10	No observable abnormality	10	Days 1 ~ 91

Table 2. Summary of Mean Body Weights

Sex: Male (g)

Group / Dose (mg/kg/day)		Week 0	1	2	3	4	5	6
G1	Mean	201.2	262.0	316.9	361.7	401.8	432.3	459.2
0	S.D.	4.2	9.5	17.0	27.3	34.8	40.5	45.9
	N	10	10	10	10	10	10	10
G2	Mean	201.1	265.4	322.8	372.9	414.3	444.9	469.6
500	S.D.	4.9	7.7	11.0	15.6	19.8	26.9	31.0
	N	10	10	10	10	10	10	10
G3	Mean	201.6	265.6	319.2	364.2	403.2	436.6	463.7
1,000	S.D.	4.8	10.7	24.4	34.6	43.0	46.7	51.7
	N	10	10	10	10	10	10	10
G4	Mean	201.2	266.5	328.7	376.4	419.1	453.9	480.6
2,000	S.D.	5.2	8.6	17.2	26.4	32.4	34.1	36.5
	N	10	10	10	10	10	10	10

Group / Dose (mg/kg/day)		Week 7	8	9	10	11	12	13
G1	Mean	485.0	504.8	522.4	538.1	550.5	568.5	574.2
0	S.D.	51.2	56.4	60.4	62.7	65.4	69.3	73.7
	N	10	10	10	10	10	10	10
G2	Mean	494.8	517.6	537.0	548.2	564.5	578.9	589.5
500	S.D.	36.1	38.8	42.5	44.6	49.0	52.9	54.8
	N	10	10	10	10	10	10	10
G3	Mean	490.3	516.8	537.0	554.6	568.2	581.1	588.5
1,000	S.D.	52.8	56.3	57.9	58.4	61.5	64.0	65.1
	N	10	10	10	10	10	10	10
G4	Mean	511.7	534.9	555.3	572.8	589.7	604.2	608.3
2,000	S.D.	38.6	40.2	43.3	41.4	44.4	47.7	55.6
	N	10	10	10	10	10	10	10

Table 2. (Continued)

Sex: Female (g)

Group / Dose (mg/kg/day)		Week 0	1	2	3	4	5	6
G1	Mean	156.1	181.0	199.7	218.4	230.5	246.3	257.0
0	S.D.	5.2	10.3	11.3	11.1	11.4	17.0	19.7
	N	10	10	10	10	10	10	10
G2	Mean	154.9	178.5	203.8	216.8	230.8	246.5	259.2
500	S.D.	7.5	7.5	12.8	15.3	17.4	16.5	20.6
	N	10	10	10	10	10	10	10
G3	Mean	155.9	181.8	202.2	221.0	236.4	252.1	264.6
1,000	S.D.	9.1	11.0	10.7	16.0	18.7	16.1	18.0
	N	10	10	10	10	10	10	10
G4	Mean	154.8	181.5	202.5	219.3	232.6	251.5	263.0
2,000	S.D.	10.6	11.3	16.4	20.4	21.4	24.8	27.7
	N	10	10	10	10	10	10	10

Group / Dose (mg/kg/day)		Week 7	8	9	10	11	12	13
G1	Mean	269.8	280.1	289.2	296.9	301.7	304.0	302.9
0	S.D.	21.4	22.4	26.6	31.3	29.1	29.1	33.7
	N	10	10	10	10	10	10	10
G2	Mean	265.7	276.8	287.0	294.7	296.5	301.7	304.0
500	S.D.	19.9	23.4	22.0	23.6	25.6	31.1	31.1
	N	10	10	10	10	10	10	10
G3	Mean	273.0	282.0	292.6	302.2	304.4	309.2	312.3
1,000	S.D.	19.0	21.7	21.4	22.6	20.8	23.1	21.1
	N	10	10	10	10	10	10	10
G4	Mean	270.8	279.0	292.0	298.6	300.8	305.2	310.0
2,000	S.D.	30.8	31.2	29.3	31.5	34.7	35.7	34.6
	N	10	10	10	10	10	10	10

Table 3. Summary of Mean Food Consumption

Sex: Male (g/day)

Group / Dose (mg/kg/day)		Week 0	1	2	3	4	5	6
G1	Mean	26.6	27.1	29.8	30.0	30.3	30.2	29.4
0	S.D.	1.3	1.4	2.3	3.5	3.7	3.8	3.4
	N	10	10	10	10	10	10	10
G2	Mean	26.9	27.4	30.0	30.5	30.2	29.8	29.2
500	S.D.	1.7	1.1	1.7	2.2	2.0	2.7	2.8
	N	10	10	10	10	10	10	10
G3	Mean	26.9	27.5	29.5	29.1	28.8	29.2	28.7
1,000	S.D.	1.6	1.9	3.7	4.5	3.9	3.5	3.5
	N	10	10	10	10	10	10	10
G4	Mean	26.7	27.2	31.1	31.6	31.5	31.3	30.6
2,000	S.D.	2.9	2.0	3.0	3.8	4.2	3.5	3.9
	N	10	10	10	10	10	10	10

Group / Dose (mg/kg/day)		Week 7	8	9	10	11	12	13
G1	Mean	29.1	28.3	27.3	26.9	26.0	26.3	24.9
0	S.D.	2.9	3.5	3.5	2.7	2.4	2.7	2.6
	N	10	10	10	10	10	10	10
G2	Mean	29.3	28.9	28.3	27.5	26.5	26.2	25.0
500	S.D.	2.8	2.9	2.8	3.4	3.9	3.9	4.2
	N	10	10	10	10	10	10	10
G3	Mean	29.0	29.0	28.6	28.2	27.0	26.3	24.9
1,000	S.D.	3.1	3.2	2.5	2.3	2.7	2.6	2.7
	N	10	10	10	10	10	10	10
G4	Mean	30.9	30.0	29.6	28.8	28.2	27.6	25.4
2,000	S.D.	3.8	3.1	3.3	3.5	3.2	3.4	3.7
	N	10	10	10	10	10	10	10

Table 3. (Continued)

Sex: Female (g/day)

Group / Dose (mg/kg/day)		Week 0	1	2	3	4	5	6
G1	Mean	20.1	18.1	19.1	19.3	19.2	19.6	19.8
0	S.D.	2.4	1.3	1.4	1.2	1.1	1.8	1.7
	N	10	10	10	10	10	10	10
G2	Mean	20.1	18.8	20.0	19.7	20.3	20.9	20.7
500	S.D.	3.7	1.2	2.0	1.9	1.9	2.0	2.6
	N	10	10	10	10	10	10	10
G3	Mean	20.1	18.8	19.0	19.5	20.1	20.1	19.9
1,000	S.D.	2.8	1.7	1.3	2.2	1.8	1.5	1.6
	N	10	10	10	10	10	10	10
G4	Mean	19.1	19.0	19.9	20.0	20.2	21.2	20.7
2,000	S.D.	2.8	1.8	2.7	3.3	3.0	3.8	3.8
	N	10	10	10	10	10	10	10

Group / Dose (mg/kg/day)		Week 7	8	9	10	11	12	13
G1	Mean	19.5	19.2	19.1	18.6	17.5	16.8	15.1
0	S.D.	1.7	1.7	1.8	1.4	0.9	1.6	1.5
	N	10	10	10	10	10	10	10
G2	Mean	20.3	20.3	20.2	19.7	18.2	18.5	16.8
500	S.D.	2.0	1.8	1.8	1.9	1.6	2.4	2.3
	N	10	10	10	10	10	10	10
G3	Mean	19.2	19.1	18.8	18.8	17.4	17.5	15.8
1,000	S.D.	1.6	1.8	1.8	1.6	1.4	1.7	1.4
	N	10	10	10	10	10	10	10
G4	Mean	20.2	20.0	20.3	19.6	18.3	18.5	17.5 *
2,000	S.D.	3.2	3.0	2.6	2.5	2.5	2.3	2.2
	N	10	10	10	10	10	10	10

Significantly different from control by Dunnett's t-test: * $p<0.05$.

<EC-18의 비글견을 이용한 4주 반복 경구투여 독성시험 및 2주 회복시험>

Table 1. Summary of Clinical Signs

Ses	Group /Dose (mg/kg/day)	Animal ID	Dosing for 4-week			Recovery for 2-week
			Diarrhea	Grayish stool	Soft stool	Abnormal findings
Male	G1 0	1101	0	0	0	
		1102	0	0	3	
		1103	0	0	3	
		1104	1	0	2	0
		1105	0	0	0	0
	G2 500	1201	0	0	0	
		1202	0	2	0	
		1203	0	0	0	
	G3 1,000	1301	0	3	0	
		1302	0	3	2	
		1303	0	2	0	
	G4 2,000	1401	0	6	3	
		1402	1	16	3	
		1403	0	7	1	
		1404	9	24	9	0
		1405	0	4	1	0
Female	G1 0	2101	0	0	0	
		2102	0	0	2	
		2103	1	0	2	
		2104	0	0	0	0
		2105	2	0	7	0
	G2 500	2201	1	1	5	
		2202	0	0	0	
		2203	0	2	0	
	G3 1,000	2301	1	7	3	
		2302	1	4	6	
		2303	0	4	0	
	G4 2,000	2401	0	1	1	
		2402	0	7	1	
		2403	5	19	13	
		2404	1	16	0	0
		2405	8	23	13	0

Values are total number of days with findings.

Table 2. Mean Body Weights

Sex	Group /Dose (mg/kg/day)		Week of dosing (kg)					Week of recovery (kg)	
			0	1	2	3	4	5	6
Male	G1 0	Mean	6.58	6.70	6.89	7.05	7.10	7.53	7.66
		S.D.	0.29	0.37	0.40	0.45	0.46	0.31	0.22
		N	5	5	5	5	5	2	2
	G2 500	Mean	6.45	6.65	7.00	7.23	7.33		
		S.D.	0.33	0.28	0.30	0.24	0.29		
		N	3	3	3	3	3		
	G3 1,000	Mean	6.60	6.82	7.03	7.22	7.32		
		S.D.	0.17	0.19	0.22	0.33	0.29		
		N	3	3	3	3	3		
	G4 2,000	Mean	6.53	6.69	6.89	7.02	7.14	7.52	7.68
		S.D.	0.38	0.42	0.46	0.52	0.54	0.69	0.60
		N	5	5	5	5	5	2	2
Female	G1 0	Mean	5.99	6.10	6.19	6.38	6.40	6.56	6.74
		S.D.	0.27	0.27	0.31	0.37	0.34	0.59	0.61
		N	5	5	5	5	5	2	2
	G2 500	Mean	5.95	6.14	6.22	6.38	6.48		
		S.D.	0.45	0.48	0.59	0.60	0.54		
		N	3	3	3	3	3		
	G3 1,000	Mean	5.94	6.10	6.14	6.46	6.49		
		S.D.	0.52	0.61	0.64	0.61	0.70		
		N	3	3	3	3	3		
	G4 2,000	Mean	5.98	6.16	6.29	6.49	6.61	6.56	6.73
		S.D.	0.21	0.28	0.34	0.33	0.30	0.37	0.39
		N	5	5	5	5	5	2	2

Table 3. Mean Food Consumptions

Sex	Group /Dose (mg/kg/day)		Week of dosing (g/day)					Week of recovery (g/day)	
			0	1	2	3	4	5	6
Male	G1 0	Mean	250	205	242	238	250	250	250
		S.D.	0	41	18	27	0	0	0
		N	5	5	5	5	5	2	2
	G2 500	Mean	234	247	227	250	250		
		S.D.	28	6	40	0	0		
		N	3	3	3	3	3		
	G3 1,000	Mean	250	231	225	231	250		
		S.D.	0	17	22	32	0		
		N	3	3	3	3	3		
	G4 2,000	Mean	250	232	247	250	250	183	250
		S.D.	0	31	7	0	0	95	0
		N	5	5	5	5	5	2	2
Female	G1 0	Mean	201	221	242	237	250	250	250
		S.D.	87	41	19	19	0	0	0
		N	5	5	5	5	5	2	2
	G2 500	Mean	250	227	250	250	250		
		S.D.	0	39	0	0	0		
		N	3	3	3	3	3		
	G3 1,000	Mean	250	202	218	233	250		
		S.D.	0	27	33	29	0		
		N	3	3	3	3	3		
	G4 2,000	Mean	240	195	232	231	250	250	225
		S.D.	22	52	25	27	0	0	36
		N	5	5	5	5	5	2	2

<EC-18의 비글견을 이용한 13주 반복 경구투여 독성시험, 4주 회복시험 및 독성동태시험>

Table 1. Summary of Clinical Signs

Sex	Group /Dose (mg/kg/day)	Animal ID	Dosing for 13-week						Recovery for 4-week
			Diarrhea	Grayish stool	Mucous stool	Soft stool	Mucous stool	Vomiting	Abnormal findings
Male	G1 0	1101	0	0	0	0	0	0	
		1102	0	0	0	0	0	0	
		1103	0	0	0	0	0	0	
		1104	10	0	0	24	0	0	0
		1105	3	0	0	21	0	0	0
	G2 500	1201	0	14	0	8	0	0	
		1202	0	41	2	0	2	0	
		1203	1	6	0	1	0	0	
	G3 1,000	1301	0	31	0	1	0	0	
		1302	0	25	0	9	0	2	
		1303	1	83	0	33	0	0	
	G4 2,000	1401	0	49	0	13	0	0	
		1402	0	70	0	18	0	0	
		1403	3	70	0	33	0	0	
		1404	0	76	0	36	0	0	0
		1405	0	49	0	20	0	0	0
Female	G1 0	2101	0	0	0	5	0	0	
		2102	0	0	0	0	0	0	
		2103	0	0	0	0	0	0	
		2104	0	0	0	0	0	0	0
		2105	0	0	0	0	0	0	0
	G2 500	2201	0	1	0	0	0	0	
		2202	0	8	0	0	0	0	
		2203	0	4	0	3	0	0	
	G3 1,000	2301	0	42	0	2	0	0	
		2302	1	19	0	9	0	0	
		2303	2	67	0	10	0	0	
	G4 2,000	2401	1	73	0	27	0	3	
		2402	1	66	0	7	0	1	
		2403	0	35	0	11	0	0	
		2404	0	78	0	17	0	0	0
		2405	0	50	0	26	0	0	0

Values are total number of days with findings.

Table. 2. Mean Body Weights

Sex : Male

Group /Dose (mg/kg/day)		Week of dosing (kg)								
		0	1	2	3	4	5	6	7	8
G1	Mean	8.00	8.17	8.32	8.45	8.53	8.60	8.62	8.70	8.77
0	S.D.	0.39	0.42	0.46	0.58	0.62	0.65	0.67	0.72	0.80
	N	5	5	5	5	5	5	5	5	5
G2	Mean	7.99	8.22	8.42	8.57	8.72	8.77	8.79	8.91	8.86
500	S.D.	0.66	0.67	0.66	0.55	0.52	0.42	0.41	0.35	0.33
	N	3	3	3	3	3	3	3	3	3
G3	Mean	8.05	8.32	8.55	8.76	8.89	9.05	9.13	9.28	9.35
1,000	S.D.	0.37	0.31	0.29	0.24	0.25	0.16	0.18	0.15	0.12
	N	3	3	3	3	3	3	3	3	3
G4	Mean	8.07	8.28	8.52	8.69	8.90	9.05	9.15	9.26	9.32
2,000	S.D.	0.36	0.31	0.33	0.31	0.25	0.31	0.28	0.34	0.31
	N	5	5	5	5	5	5	5	5	5

Group /Dose (mg/kg/day)		Week of dosing (kg)					Week of recovery (kg)			
		9	10	11	12	13	14	15	16	17
G1	Mean	8.79	8.86	8.92	9.00	8.98	8.73	8.93	8.93	9.03
0	S.D.	0.83	0.88	0.92	1.00	0.95	0.64	0.77	0.80	0.83
	N	5	5	5	5	5	2	2	2	2
G2	Mean	8.89	8.85	8.89	8.91	8.87				
500	S.D.	0.34	0.33	0.32	0.31	0.31				
	N	3	3	3	3	3				
G3	Mean	9.45	9.55	9.69	9.72	9.74				
1,000	S.D.	0.12	0.07	0.01	0.06	0.10				
	N	3	3	3	3	3				
G4	Mean	9.45	9.53	9.67	9.84	9.84	10.08	10.16	10.25	10.29
2,000	S.D.	0.47	0.44	0.47	0.45	0.47	0.64	0.71	0.83	0.73
	N	5	5	5	5	5	2	2	2	2

Table 2. (Continued).

Sex: Female

Group /Dose (mg/kg/day)		Week of dosing (kg)								
		0	1	2	3	4	5	6	7	8
G1	Mean	7.00	7.16	7.31	7.44	7.54	7.65	7.68	7.78	7.90
0	S.D.	0.59	0.63	0.63	0.66	0.68	0.69	0.75	0.80	0.83
	N	5	5	5	5	5	5	5	5	5
G2	Mean	7.03	7.14	7.41	7.47	7.63	7.70	7.76	7.85	7.96
500	S.D.	0.63	0.73	0.69	0.74	0.69	0.70	0.72	0.68	0.58
	N	3	3	3	3	3	3	3	3	3
G3	Mean	7.02	7.18	7.37	7.58	7.70	7.85	7.92	8.10	8.18
1,000	S.D.	0.56	0.77	0.75	0.77	0.82	0.95	0.96	1.02	1.15
	N	3	3	3	3	3	3	3	3	3
G4	Mean	7.03	7.25	7.46	7.65	7.84	7.95	8.10	8.21	8.40
2,000	S.D.	0.59	0.62	0.66	0.69	0.72	0.81	0.82	0.77	0.85
	N	5	5	5	5	5	5	5	5	5

Group /Dose (mg/kg/day)		Week of dosing (kg)					Week of recovery (kg)			
		9	10	11	12	13	14	15	16	17
G1	Mean	7.95	8.01	8.10	8.16	8.20	8.47	8.58	8.59	8.66
0	S.D.	0.85	0.84	0.87	0.87	0.91	1.24	1.22	1.20	1.12
	N	5	5	5	5	5	2	2	2	2
G2	Mean	8.04	8.13	8.20	8.24	8.31				
500	S.D.	0.59	0.60	0.54	0.57	0.49				
	N	3	3	3	3	3				
G3	Mean	8.26	8.38	8.52	8.64	8.69				
1,000	S.D.	1.19	1.21	1.19	1.29	1.37				
	N	3	3	3	3	3				
G4	Mean	8.45	8.59	8.74	8.87	8.88	9.66	9.76	9.96	10.08
2,000	S.D.	0.83	0.87	0.90	0.88	0.93	0.37	0.33	0.33	0.37
	N	5	5	5	5	5	2	2	2	2

Table 3. Mean Food Consumptions

Sex: Male

Group /Dose (mg/kg/day)		Week of dosing (g/day)								
		0	1	2	3	4	5	6	7	8
G1	Mean	250	250	250	250	250	250	250	250	250
0	S.D.	0	0	0	0	0	0	0	0	0
	N	5	5	5	5	5	5	5	5	5
G2	Mean	250	250	250	250	250	250	250	250	250
500	S.D.	0	0	0	0	0	0	0	0	0
	N	3	3	3	3	3	3	3	3	3
G3	Mean	250	250	250	250	250	250	250	250	250
1,000	S.D.	0	0	0	0	0	0	0	0	0
	N	3	3	3	3	3	3	3	3	3
G4	Mean	250	250	250	250	250	250	250	250	250
2,000	S.D.	0	0	0	0	0	0	0	0	0
	N	5	5	5	5	5	5	5	5	5

Group /Dose (mg/kg/day)		Week of dosing (g/day)					Week of recovery (g/day)			
		9	10	11	12	13	14	15	16	17
G1	Mean	250	250	250	250	250	250	250	250	250
0	S.D.	0	0	0	0	0	0	0	0	0
	N	5	5	5	5	5	2	2	2	2
G2	Mean	250	250	250	250	250				
500	S.D.	0	0	0	0	0				
	N	3	3	3	3	3				
G3	Mean	250	250	250	250	250				
1,000	S.D.	0	0	0	0	0				
	N	3	3	3	3	3				
G4	Mean	250	250	250	250	250	250	250	250	250
2,000	S.D.	0	0	0	0	0	0	0	0	0
	N	5	5	5	5	5	2	2	2	2

Table 3. (Continued)

Sex : Female

Group /Dose (mg/kg/day)		Week of dosing (g/day)								
		0	1	2	3	4	5	6	7	8
G1	Mean	250	250	250	250	250	250	250	250	250
0	S.D.	0	0	0	0	0	0	0	0	0
	N	5	5	5	5	5	5	5	5	5
G2	Mean	250	201	238	238	250	250	250	250	250
500	S.D.	0	84	21	21	0	0	0	0	0
	N	3	3	3	3	3	3	3	3	3
G3	Mean	250	199	250	250	250	250	250	250	250
1,000	S.D.	0	88	0	0	0	0	0	0	0
	N	3	3	3	3	3	3	3	3	3
G4	Mean	250	250	250	241	250	250	250	250	250
2,000	S.D.	0	0	0	20	0	0	0	0	0
	N	5	5	5	5	5	5	5	5	5

Group /Dose (mg/kg/day)		Week of dosing (g/day)					Week of recovery (g/day)			
		9	10	11	12	13	14	15	16	17
G1	Mean	250	250	250	250	250	250	250	250	250
0	S.D.	0	0	0	0	0	0	0	0	0
	N	5	5	5	5	5	2	2	2	2
G2	Mean	250	250	250	223	250				
500	S.D.	0	0	0	47	0				
	N	3	3	3	3	3				
G3	Mean	250	250	250	250	250				
1,000	S.D.	0	0	0	0	0				
	N	3	3	3	3	3				
G4	Mean	250	250	250	250	250	250	250	250	250
2,000	S.D.	0	0	0	0	0	0	0	0	0
	N	5	5	5	5	5	2	2	2	2

<EC-18의 단회 경구투여에 의한 랫드의 중추신경계에 미치는 영향 평가시험>

Table 1. Summary Data of Home Cage Observations

Group/ Dose (mg/kg)		Body posture (ranked, normal score; 3)					
		Time after administration (hours)					
		0	0.5	1	3	6	24
G1 0	Mean	3.0	3.0	3.0	3.0	3.0	3.0
	S.D.	0.0	0.0	0.0	0.0	0.0	0.0
	N	8	8	8	8	8	8
G2 500	Mean	3.0	3.0	3.0	3.0	3.0	3.0
	S.D.	0.0	0.0	0.0	0.0	0.0	0.0
	N	8	8	8	8	8	8
G3 1,000	Mean	3.0	3.0	3.0	3.0	3.0	3.0
	S.D.	0.0	0.0	0.0	0.0	0.0	0.0
	N	8	8	8	8	8	8
G4 2,000	Mean	3.0	3.0	3.0	3.0	3.0	3.0
	S.D.	0.0	0.0	0.0	0.0	0.0	0.0
	N	8	8	8	8	8	8

No statistically significant differences were noted in the control group (G1) and the test substance group (G2 ~ G4).

Group/ Dose (mg/kg)		Behavior (ranked, normal score; 0)					
		Time after administration (hours)					
		0	0.5	1	3	6	24
G1 0	Mean	0.0	0.0	0.0	0.0	0.0	0.0
	S.D.	0.0	0.0	0.0	0.0	0.0	0.0
	N	8	8	8	8	8	8
G2 500	Mean	0.0	0.0	0.0	0.0	0.0	0.0
	S.D.	0.0	0.0	0.0	0.0	0.0	0.0
	N	8	8	8	8	8	8
G3 1,000	Mean	0.0	0.0	0.0	0.0	0.0	0.0
	S.D.	0.0	0.0	0.0	0.0	0.0	0.0
	N	8	8	8	8	8	8
G4 2,000	Mean	0.0	0.0	0.0	0.0	0.0	0.0
	S.D.	0.0	0.0	0.0	0.0	0.0	0.0
	N	8	8	8	8	8	8

No statistically significant differences were noted in the control group (G1) and the test substance group (G2 ~ G4).

Table 1. (Continued).

Group/ Dose (mg/kg)		Ease of removal from cage (ranked, normal score; 0)					
		Time after administration (hours)					
		0	0.5	1	3	6	24
G1 0	Mean	0.0	0.0	0.0	0.0	0.0	0.0
	S.D.	0.0	0.0	0.0	0.0	0.0	0.0
	N	8	8	8	8	8	8
G2 500	Mean	0.0	0.0	0.0	0.0	0.0	0.0
	S.D.	0.0	0.0	0.0	0.0	0.0	0.0
	N	8	8	8	8	8	8
G3 1,000	Mean	0.0	0.0	0.0	0.0	0.0	0.0
	S.D.	0.0	0.0	0.0	0.0	0.0	0.0
	N	8	8	8	8	8	8
G4 2,000	Mean	0.0	0.0	0.0	0.0	0.0	0.0
	S.D.	0.0	0.0	0.0	0.0	0.0	0.0
	N	8	8	8	8	8	8

No statistically significant differences were noted in the control group (G1) and the test substance group (G2 ~ G4).

Table 2. Summary Data of Open Field Observations

Group/ Dose (mg/kg)		Number of unit areas crossed (quantitative value, /3min)					
		Time after administration (hours)					
		0	0.5	1	3	6	24
G1	Mean	73.4	26.9	7.5	2.6	2.5	5.3
0	S.D.	22.7	20.8	7.4	1.5	1.7	7.2
	N	8	8	8	8	8	8
G2	Mean	57.8	19.0	9.4	4.8	1.5	12.1
500	S.D.	20.3	20.2	5.5	4.3	0.9	24.9
	N	8	8	8	8	8	8
G3	Mean	50.3	37.6	13.3	4.1	1.6	8.3
1,000	S.D.	25.8	22.7	14.6	4.5	1.5	9.2
	N	8	8	8	8	8	8
G4	Mean	53.6	16.5	6.6	4.9	1.5	5.1
2,000	S.D.	14.4	9.6	13.5	7.1	1.4	9.4
	N	8	8	8	8	8	8

No statistically significant differences were noted in the control group (G1) and the test substance group (G2 ~ G4).

Group/ Dose (mg/kg)		Rearing counts (quantitative value, /3min)					
		Time after administration (hours)					
		0	0.5	1	3	6	24
G1	Mean	9.1	2.9	0.5	0.1	0.1	0.4
0	S.D.	2.0	5.1	0.8	0.4	0.4	1.1
	N	8	8	8	8	8	8
G2	Mean	6.6	4.1	1.8	0.8	0.0	2.4
500	S.D.	3.8	6.9	3.5	1.2	0.0	4.8
	N	8	8	8	8	8	8
G3	Mean	4.6	2.9	2.4	0.4	0.3	0.4
1,000	S.D.	3.0	2.2	1.8	0.7	0.7	0.5
	N	8	8	8	8	8	8
G4	Mean	5.9	2.3	0.8	0.3	0.3	0.4
2,000	S.D.	4.9	2.5	2.1	0.7	0.5	0.5
	N	8	8	8	8	8	8

No statistically significant differences were noted in the control group (G1) and the test substance group (G2 ~ G4).

Table 2. (Continued)

Group/ Dose (mg/kg)		Respiration rate (ranked, normal score; 0)					
		Time after administration (hours)					
		0	0.5	1	3	6	24
G1	Mean	0.0	0.0	0.0	0.0	0.0	0.0
0	S.D.	0.0	0.0	0.0	0.0	0.0	0.0
	N	8	8	8	8	8	8
G2	Mean	0.0	0.0	0.0	0.0	0.0	0.0
500	S.D.	0.0	0.0	0.0	0.0	0.0	0.0
	N	8	8	8	8	8	8
G3	Mean	0.0	0.0	0.0	0.0	0.0	0.0
1,000	S.D.	0.0	0.0	0.0	0.0	0.0	0.0
	N	8	8	8	8	8	8
G4	Mean	0.0	0.0	0.0	0.0	0.0	0.0
2,000	S.D.	0.0	0.0	0.0	0.0	0.0	0.0
	N	8	8	8	8	8	8

No statistically significant differences were noted in the control group (G1) and the test substance group (G2 ~ G4).

Group/ Dose (mg/kg)		Stereotypy (ranked, normal score; 0)					
		Time after administration (hours)					
		0	0.5	1	3	6	24
G1	Mean	0.0	0.0	0.0	0.0	0.0	0.0
0	S.D.	0.0	0.0	0.0	0.0	0.0	0.0
	N	8	8	8	8	8	8
G2	Mean	0.0	0.0	0.0	0.0	0.0	0.0
500	S.D.	0.0	0.0	0.0	0.0	0.0	0.0
	N	8	8	8	8	8	8
G3	Mean	0.0	0.0	0.0	0.0	0.0	0.0
1,000	S.D.	0.0	0.0	0.0	0.0	0.0	0.0
	N	8	8	8	8	8	8
G4	Mean	0.0	0.0	0.0	0.0	0.0	0.0
2,000	S.D.	0.0	0.0	0.0	0.0	0.0	0.0
	N	8	8	8	8	8	8

No statistically significant differences were noted in the control group (G1) and the test substance group (G2 ~ G4).

Table 2. (Continued).

Group/ Dose (mg/kg)		Unusual behavior (ranked, normal score; 0)					
		Time after administration (hours)					
		0	0.5	1	3	6	24
G1 0	Mean	0.0	0.0	0.0	0.0	0.0	0.0
	S.D.	0.0	0.0	0.0	0.0	0.0	0.0
	N	8	8	8	8	8	8
G2 500	Mean	0.0	0.0	0.0	0.0	0.0	0.0
	S.D.	0.0	0.0	0.0	0.0	0.0	0.0
	N	8	8	8	8	8	8
G3 1,000	Mean	0.0	0.0	0.0	0.0	0.0	0.0
	S.D.	0.0	0.0	0.0	0.0	0.0	0.0
	N	8	8	8	8	8	8
G4 2,000	Mean	0.0	0.0	0.0	0.0	0.0	0.0
	S.D.	0.0	0.0	0.0	0.0	0.0	0.0
	N	8	8	8	8	8	8

No statistically significant differences were noted in the control group (G1) and the test substance group (G2 ~ G4).

Group/ Dose (mg/kg)		Tremor (ranked, normal score; 0)					
		Time after administration (hours)					
		0	0.5	1	3	6	24
G1 0	Mean	0.0	0.0	0.0	0.0	0.0	0.0
	S.D.	0.0	0.0	0.0	0.0	0.0	0.0
	N	8	8	8	8	8	8
G2 500	Mean	0.0	0.0	0.0	0.0	0.0	0.0
	S.D.	0.0	0.0	0.0	0.0	0.0	0.0
	N	8	8	8	8	8	8
G3 1,000	Mean	0.0	0.0	0.0	0.0	0.0	0.0
	S.D.	0.0	0.0	0.0	0.0	0.0	0.0
	N	8	8	8	8	8	8
G4 2,000	Mean	0.0	0.0	0.0	0.0	0.0	0.0
	S.D.	0.0	0.0	0.0	0.0	0.0	0.0
	N	8	8	8	8	8	8

No statistically significant differences were noted in the control group (G1) and the test substance group (G2 ~ G4).

Table 2. (Continued).

Group/ Dose (mg/kg)		Convulsion (ranked, normal score; 0)					
		Time after administration (hours)					
		0	0.5	1	3	6	24
G1 0	Mean	0.0	0.0	0.0	0.0	0.0	0.0
	S.D.	0.0	0.0	0.0	0.0	0.0	0.0
	N	8	8	8	8	8	8
G2 500	Mean	0.0	0.0	0.0	0.0	0.0	0.0
	S.D.	0.0	0.0	0.0	0.0	0.0	0.0
	N	8	8	8	8	8	8
G3 1,000	Mean	0.0	0.0	0.0	0.0	0.0	0.0
	S.D.	0.0	0.0	0.0	0.0	0.0	0.0
	N	8	8	8	8	8	8
G4 2,000	Mean	0.0	0.0	0.0	0.0	0.0	0.0
	S.D.	0.0	0.0	0.0	0.0	0.0	0.0
	N	8	8	8	8	8	8

No statistically significant differences were noted in the control group (G1) and the test substance group (G2 ~ G4).

Group/ Dose (mg/kg)		Gait (ranked, normal score; 0)					
		Time after administration (hours)					
		0	0.5	1	3	6	24
G1 0	Mean	0.0	0.0	0.0	0.0	0.0	0.0
	S.D.	0.0	0.0	0.0	0.0	0.0	0.0
	N	8	8	8	8	8	8
G2 500	Mean	0.0	0.0	0.0	0.0	0.0	0.0
	S.D.	0.0	0.0	0.0	0.0	0.0	0.0
	N	8	8	8	8	8	8
G3 1,000	Mean	0.0	0.0	0.0	0.0	0.0	0.0
	S.D.	0.0	0.0	0.0	0.0	0.0	0.0
	N	8	8	8	8	8	8
G4 2,000	Mean	0.0	0.0	0.0	0.0	0.0	0.0
	S.D.	0.0	0.0	0.0	0.0	0.0	0.0
	N	8	8	8	8	8	8

No statistically significant differences were noted in the control group (G1) and the test substance group (G2 ~ G4).

Table 2. (Continued).

Group/ Dose (mg/kg)		Arousal level (ranked, normal score; 4)					
		Time after administration (hours)					
		0	0.5	1	3	6	24
G1 0	Mean	4.0	4.0	4.0	4.0	4.0	4.0
	S.D.	0.0	0.0	0.0	0.0	0.0	0.0
	N	8	8	8	8	8	8
G2 500	Mean	4.0	4.0	4.0	4.0	4.0	4.0
	S.D.	0.0	0.0	0.0	0.0	0.0	0.0
	N	8	8	8	8	8	8
G3 1,000	Mean	4.0	4.0	4.0	4.0	4.0	4.0
	S.D.	0.0	0.0	0.0	0.0	0.0	0.0
	N	8	8	8	8	8	8
G4 2,000	Mean	4.0	4.0	4.0	4.0	4.0	4.0
	S.D.	0.0	0.0	0.0	0.0	0.0	0.0
	N	8	8	8	8	8	8

No statistically significant differences were noted in the control group (G1) and the test substance group (G2 ~ G4).

Group/ Dose (mg/kg)		Number of fecal pellets (quantitative value, /3min)					
		Time after administration (hours)					
		0	0.5	1	3	6	24
G1 0	Mean	3.9	2.0	1.5	0.6	2.9	4.5
	S.D.	2.0	2.3	1.9	1.1	1.2	0.9
	N	8	8	8	8	8	8
G2 500	Mean	2.0	2.3	0.4	2.4	1.8	4.1
	S.D.	1.9	2.5	0.5	2.1	1.6	2.2
	N	8	8	8	8	8	8
G3 1,000	Mean	3.3	2.9	0.6	2.1	2.5	3.1
	S.D.	2.3	2.5	1.2	2.7	1.9	1.8
	N	8	8	8	8	8	8
G4 2,000	Mean	2.9	3.1	1.4	1.0	1.3	3.3
	S.D.	1.8	2.0	0.9	0.9	1.8	2.1
	N	8	8	8	8	8	8

No statistically significant differences were noted in the control group (G1) and the test substance group (G2 ~ G4).

Table 2. (Continued).

Group/ Dose (mg/kg)		Number of urine pools (quantitative value, /3min). Time after administration (hours).					
		0	0.5	1	3	6	24
G1 0	Mean	0.6	0.8	0.8	0.6	0.9	0.6
	S.D.	0.5	0.7	0.5	0.5	0.6	0.5
	N	8	8	8	8	8	8
G2 500	Mean	0.3	0.4	0.3	0.3	0.5	0.5
	S.D.	0.5	0.5	0.5	0.5	0.5	0.5
	N	8	8	8	8	8	8
G3 1,000	Mean	0.4	0.6	0.5	0.8	0.6	0.9
	S.D.	0.5	0.5	0.5	0.5	0.5	0.4
	N	8	8	8	8	8	8
G4 2,000	Mean	0.4	0.5	0.5	0.8	0.5	0.5
	S.D.	0.5	0.5	0.5	0.5	0.5	0.5
	N	8	8	8	8	8	8

No statistically significant differences were noted in the control group (G1) and the test substance group (G2 ~ G4).

Table 3. Summary Data of Hand Held Observations

Group/ Dose (mg/kg)		Fur and skin appearance (ranked, normal score; 0)					
		Time after administration (hours)					
		0	0.5	1	3	6	24
G1 0	Mean	0.0	0.0	0.0	0.0	0.0	0.0
	S.D.	0.0	0.0	0.0	0.0	0.0	0.0
	N	8	8	8	8	8	8
G2 500	Mean	0.0	0.0	0.0	0.0	0.0	0.0
	S.D.	0.0	0.0	0.0	0.0	0.0	0.0
	N	8	8	8	8	8	8
G3 1,000	Mean	0.0	0.0	0.0	0.0	0.0	0.0
	S.D.	0.0	0.0	0.0	0.0	0.0	0.0
	N	8	8	8	8	8	8
G4 2,000	Mean	0.0	0.0	0.0	0.0	0.0	0.0
	S.D.	0.0	0.0	0.0	0.0	0.0	0.0
	N	8	8	8	8	8	8

No statistically significant differences were noted in the control group (G1) and the test substance group (G2 ~ G4).

Group/ Dose (mg/kg)		Piloerection (ranked, normal score; 0)					
		Time after administration (hours)					
		0	0.5	1	3	6	24
G1 0	Mean	0.0	0.0	0.0	0.0	0.0	0.0
	S.D.	0.0	0.0	0.0	0.0	0.0	0.0
	N	8	8	8	8	8	8
G2 500	Mean	0.0	0.0	0.0	0.0	0.0	0.0
	S.D.	0.0	0.0	0.0	0.0	0.0	0.0
	N	8	8	8	8	8	8
G3 1,000	Mean	0.0	0.0	0.0	0.0	0.0	0.0
	S.D.	0.0	0.0	0.0	0.0	0.0	0.0
	N	8	8	8	8	8	8
G4 2,000	Mean	0.0	0.0	0.0	0.0	0.0	0.0
	S.D.	0.0	0.0	0.0	0.0	0.0	0.0
	N	8	8	8	8	8	8

No statistically significant differences were noted in the control group (G1) and the test substance group (G2 ~ G4).

Table 3. (Continued).

Group/ Dose (mg/kg)		Contaminated abdominal region (ranked, normal score; 0). Time after administration (hours).					
		0	0.5	1	3	6	24
G1 0	Mean	0.0	0.0	0.0	0.0	0.0	0.0
	S.D.	0.0	0.0	0.0	0.0	0.0	0.0
	N	8	8	8	8	8	8
G2 500	Mean	0.0	0.0	0.0	0.0	0.0	0.0
	S.D.	0.0	0.0	0.0	0.0	0.0	0.0
	N	8	8	8	8	8	8
G3 1,000	Mean	0.0	0.0	0.0	0.0	0.0	0.0
	S.D.	0.0	0.0	0.0	0.0	0.0	0.0
	N	8	8	8	8	8	8
G4 2,000	Mean	0.0	0.0	0.0	0.0	0.0	0.0
	S.D.	0.0	0.0	0.0	0.0	0.0	0.0
	N	8	8	8	8	8	8

No statistically significant differences were noted in the control group (G1) and the test substance group (G2 ~ G4).

Group/ Dose (mg/kg)		Lacrimation (ranked, normal score; 0). Time after administration (hours).					
		0	0.5	1	3	6	24
G1 0	Mean	0.0	0.0	0.0	0.0	0.0	0.0
	S.D.	0.0	0.0	0.0	0.0	0.0	0.0
	N	8	8	8	8	8	8
G2 500	Mean	0.0	0.0	0.0	0.0	0.0	0.0
	S.D.	0.0	0.0	0.0	0.0	0.0	0.0
	N	8	8	8	8	8	8
G3 1,000	Mean	0.0	0.0	0.0	0.0	0.0	0.0
	S.D.	0.0	0.0	0.0	0.0	0.0	0.0
	N	8	8	8	8	8	8
G4 2,000	Mean	0.0	0.0	0.0	0.0	0.0	0.0
	S.D.	0.0	0.0	0.0	0.0	0.0	0.0
	N	8	8	8	8	8	8

No statistically significant differences were noted in the control group (G1) and the test substance group (G2 ~ G4).

Table 3. (Continued).

Group/Dose (mg/kg)		Salivation (ranked, normal score; 0). Time after administration (hours).					
		0.	0.5.	1.	3.	6.	24.
G1. 0.	Mean.	0.0.	0.0.	0.0.	0.0.	0.0.	0.0.
	S.D.	0.0.	0.0.	0.0.	0.0.	0.0.	0.0.
	N.	8.	8.	8.	8.	8.	8.
G2. 500.	Mean.	0.0.	0.0.	0.0.	0.0.	0.0.	0.0.
	S.D.	0.0.	0.0.	0.0.	0.0.	0.0.	0.0.
	N.	8.	8.	8.	8.	8.	8.
G3. 1,000.	Mean.	0.0.	0.0.	0.0.	0.0.	0.0.	0.0.
	S.D.	0.0.	0.0.	0.0.	0.0.	0.0.	0.0.
	N.	8.	8.	8.	8.	8.	8.
G4. 2,000.	Mean.	0.0.	0.0.	0.0.	0.0.	0.0.	0.0.
	S.D.	0.0.	0.0.	0.0.	0.0.	0.0.	0.0.
	N.	8.	8.	8.	8.	8.	8.

No statistically significant differences were noted in the control group (G1) and the test substance group (G2 ~ G4).

Group/Dose (mg/kg)		Palpebral closure (ranked, normal score; 0). Time after administration (hours).					
		0.	0.5.	1.	3.	6.	24.
G1. 0.	Mean.	0.0.	0.0.	0.0.	0.0.	0.0.	0.0.
	S.D.	0.0.	0.0.	0.0.	0.0.	0.0.	0.0.
	N.	8.	8.	8.	8.	8.	8.
G2. 500.	Mean.	0.0.	0.0.	0.0.	0.0.	0.0.	0.0.
	S.D.	0.0.	0.0.	0.0.	0.0.	0.0.	0.0.
	N.	8.	8.	8.	8.	8.	8.
G3. 1,000.	Mean.	0.0.	0.0.	0.0.	0.0.	0.0.	0.0.
	S.D.	0.0.	0.0.	0.0.	0.0.	0.0.	0.0.
	N.	8.	8.	8.	8.	8.	8.
G4. 2,000.	Mean.	0.0.	0.0.	0.0.	0.0.	0.0.	0.0.
	S.D.	0.0.	0.0.	0.0.	0.0.	0.0.	0.0.
	N.	8.	8.	8.	8.	8.	8.

No statistically significant differences were noted in the control group (G1) and the test substance group (G2 ~ G4).

Table 3. (Continued).

Group/ Dose (mg/kg)		Pupil size (ranked, normal score; 0)					
		Time after administration (hours)					
		0	0.5	1	3	6	24
G1	Mean	0.0	0.0	0.0	0.0	0.0	0.0
0	S.D.	0.0	0.0	0.0	0.0	0.0	0.0
	N	8	8	8	8	8	8
G2	Mean	0.0	0.0	0.0	0.0	0.0	0.0
500	S.D.	0.0	0.0	0.0	0.0	0.0	0.0
	N	8	8	8	8	8	8
G3	Mean	0.0	0.0	0.0	0.0	0.0	0.0
1,000	S.D.	0.0	0.0	0.0	0.0	0.0	0.0
	N	8	8	8	8	8	8
G4	Mean	0.0	0.0	0.0	0.0	0.0	0.0
2,000	S.D.	0.0	0.0	0.0	0.0	0.0	0.0
	N	8	8	8	8	8	8

No statistically significant differences were noted in the control group (G1) and the test substance group (G2 ~ G4).

Group/ Dose (mg/kg)		Pupillary reflex (ranked, normal score; 1)					
		Time after administration (hours)					
		0	0.5	1	3	6	24
G1	Mean	1.0	1.0	1.0	1.0	1.0	1.0
0	S.D.	0.0	0.0	0.0	0.0	0.0	0.0
	N	8	8	8	8	8	8
G2	Mean	1.0	1.0	1.0	1.0	1.0	1.0
500	S.D.	0.0	0.0	0.0	0.0	0.0	0.0
	N	8	8	8	8	8	8
G3	Mean	1.0	1.0	1.0	1.0	1.0	1.0
1,000	S.D.	0.0	0.0	0.0	0.0	0.0	0.0
	N	8	8	8	8	8	8
G4	Mean	1.0	1.0	1.0	1.0	1.0	1.0
2,000	S.D.	0.0	0.0	0.0	0.0	0.0	0.0
	N	8	8	8	8	8	8

No statistically significant differences were noted in the control group (G1) and the test substance group (G2 ~ G4).

Table 3. (Continued)

Group/ Dose (mg/kg)		Muscle tone (ranked, normal score; 0)					
		Time after administration (hours)					
		0	0.5	1	3	6	24
G1 0	Mean	0.0	0.0	0.0	0.0	0.0	0.0
	S.D.	0.0	0.0	0.0	0.0	0.0	0.0
	N	8	8	8	8	8	8
G2 500	Mean	0.0	0.0	0.0	0.0	0.0	0.0
	S.D.	0.0	0.0	0.0	0.0	0.0	0.0
	N	8	8	8	8	8	8
G3 1,000	Mean	0.0	0.0	0.0	0.0	0.0	0.0
	S.D.	0.0	0.0	0.0	0.0	0.0	0.0
	N	8	8	8	8	8	8
G4 2,000	Mean	0.0	0.0	0.0	0.0	0.0	0.0
	S.D.	0.0	0.0	0.0	0.0	0.0	0.0
	N	8	8	8	8	8	8

No statistically significant differences were noted in the control group (G1) and the test substance group (G2 ~ G4).

Group/ Dose (mg/kg)		Extensor-thrust reflex (ranked, normal score; 0)					
		Time after administration (hours)					
		0	0.5	1	3	6	24
G1 0	Mean	0.0	0.0	0.0	0.0	0.0	0.0
	S.D.	0.0	0.0	0.0	0.0	0.0	0.0
	N	8	8	8	8	8	8
G2 500	Mean	0.0	0.0	0.0	0.0	0.0	0.0
	S.D.	0.0	0.0	0.0	0.0	0.0	0.0
	N	8	8	8	8	8	8
G3 1,000	Mean	0.0	0.0	0.0	0.0	0.0	0.0
	S.D.	0.0	0.0	0.0	0.0	0.0	0.0
	N	8	8	8	8	8	8
G4 2,000	Mean	0.0	0.0	0.0	0.0	0.0	0.0
	S.D.	0.0	0.0	0.0	0.0	0.0	0.0
	N	8	8	8	8	8	8

No statistically significant differences were noted in the control group (G1) and the test substance group (G2 ~ G4).

Table 4. Summary Data of Sensori-Motor Function Observations

Group/ Dose (mg/kg)		Visual response (ranked, normal score; 3)					
		Time after administration (hours)					
		0	0.5	1	3	6	24
G1 0	Mean	3.0	2.0	2.0	2.0	2.0	2.0
	S.D.	0.0	0.0	0.0	0.0	0.0	0.0
	N	8	8	8	8	8	8
G2 500	Mean	3.0	2.4	2.0	2.1	2.0	2.0
	S.D.	0.0	0.5	0.0	0.4	0.0	0.0
	N	8	8	8	8	8	8
G3 1,000	Mean	2.6	2.5	2.1	2.0	2.0	2.0
	S.D.	0.5	0.5	0.4	0.0	0.0	0.0
	N	8	8	8	8	8	8
G4 2,000	Mean	2.9	2.3	2.1	2.0	2.0	2.0
	S.D.	0.4	0.5	0.4	0.0	0.0	0.0
	N	8	8	8	8	8	8

No statistically significant differences were noted in the control group (G1) and the test substance group (G2 ~ 4).

Group/ Dose (mg/kg)		Touch response (ranked, normal score; 3)					
		Time after administration (hours)					
		0	0.5	1	3	6	24
G1 0	Mean	2.9	2.3	2.4	2.1	2.1	2.1
	S.D.	0.4	0.5	0.5	0.4	0.4	0.4
	N	8	8	8	8	8	8
G2 500	Mean	2.8	2.4	2.4	2.0	2.1	2.1
	S.D.	0.5	0.5	0.5	0.0	0.4	0.4
	N	8	8	8	8	8	8
G3 1,000	Mean	2.6	2.6	2.3	2.1	2.0	2.1
	S.D.	0.5	0.5	0.5	0.4	0.0	0.4
	N	8	8	8	8	8	8
G4 2,000	Mean	2.6	2.4	2.1	2.0	2.0	2.1
	S.D.	0.5	0.5	0.4	0.0	0.0	0.4
	N	8	8	8	8	8	8

No statistically significant differences were noted in the control group (G1) and the test substance group (G2 ~ 4).

Table 4. (Continued)

Group/ Dose (mg/kg)		Click response (ranked, normal score; 3)					
		Time after administration (hours)					
		0	0.5	1	3	6	24
G1 0	Mean	3.0	2.8	2.8	2.6	2.5	2.6
	S.D.	0.0	0.5	0.5	0.5	0.5	0.5
	N	8	8	8	8	8	8
G2 500	Mean	3.0	2.5	2.8	2.3	2.6	2.8
	S.D.	0.0	0.5	0.5	0.5	0.5	0.5
	N	8	8	8	8	8	8
G3 1,000	Mean	3.0	2.8	2.4	2.5	2.5	2.4
	S.D.	0.0	0.5	0.5	0.5	0.5	0.5
	N	8	8	8	8	8	8
G4 2,000	Mean	3.0	2.9	2.8	2.5	2.4	2.8
	S.D.	0.0	0.4	0.5	0.5	0.5	0.5
	N	8	8	8	8	8	8

No statistically significant differences were noted in the control group (G1) and the test substance group (G2 ~ G4).

Group/ Dose (mg/kg)		Tail pinch response (ranked, normal score; 3)					
		Time after administration (hours)					
		0	0.5	1	3	6	24
G1 0	Mean	3.0	3.0	3.0	2.9	2.9	3.0
	S.D.	0.0	0.0	0.0	0.4	0.4	0.0
	N	8	8	8	8	8	8
G2 500	Mean	3.0	3.0	3.0	3.0	3.0	3.0
	S.D.	0.0	0.0	0.0	0.0	0.0	0.0
	N	8	8	8	8	8	8
G3 1,000	Mean	3.0	3.0	3.0	2.9	2.6	2.9
	S.D.	0.0	0.0	0.0	0.4	0.5	0.4
	N	8	8	8	8	8	8
G4 2,000	Mean	3.0	3.1	3.1	2.9	3.0	3.1
	S.D.	0.0	0.4	0.4	0.4	0.0	0.4
	N	8	8	8	8	8	8

No statistically significant differences were noted in the control group (G1) and the test substance group (G2 ~ G4).

Table 4. (Continued)

Group/ Dose (mg/kg)		Aerial righting reflex (ranked, normal score; 0)					
		Time after administration (hours)					
		0	0.5	1	3	6	24
G1 0	Mean	0.0	0.0	0.0	0.0	0.0	0.0
	S.D.	0.0	0.0	0.0	0.0	0.0	0.0
	N	8	8	8	8	8	8
G2 500	Mean	0.0	0.0	0.0	0.0	0.0	0.0
	S.D.	0.0	0.0	0.0	0.0	0.0	0.0
	N	8	8	8	8	8	8
G3 1,000	Mean	0.0	0.0	0.0	0.0	0.0	0.0
	S.D.	0.0	0.0	0.0	0.0	0.0	0.0
	N	8	8	8	8	8	8
G4 2,000	Mean	0.0	0.0	0.0	0.0	0.0	0.0
	S.D.	0.0	0.0	0.0	0.0	0.0	0.0
	N	8	8	8	8	8	8

No statistically significant differences were noted in the control group (G1) and the test substance group (G2 ~ G4).

Group/ Dose (mg/kg)		Hindlimb landing foot splay (quantitative value, mm)					
		Time after administration (hours)					
		0	0.5	1	3	6	24
G1 0	Mean	81.61	78.32	75.71	70.53	68.26	70.44
	S.D.	10.50	5.93	5.66	6.66	10.17	12.32
	N	8	8	8	8	8	8
G2 500	Mean	72.86	77.08	68.42	65.91	59.42	55.53
	S.D.	12.70	7.44	10.45	8.54	8.76	12.74
	N	8	8	8	8	8	8
G3 1,000	Mean	83.19	79.21	77.06	69.34	66.10	68.81
	S.D.	16.69	19.49	15.75	15.01	7.72	14.44
	N	8	8	8	8	8	8
G4 2,000	Mean	74.83	72.05	67.07	64.42	62.85	59.81
	S.D.	15.75	10.96	13.36	13.71	13.48	16.26
	N	8	8	8	8	8	8

No statistically significant differences were noted in the control group (G1) and the test substance group (G2 ~ G4).

Table 4. (Continued).

Group/ Dose (mg/kg)		Forelimb grip strength (quantitative value, kgf)					
		Time after administration (hours)					
		0	0.5	1	3	6	24
G1	Mean	0.707	0.696	0.626	0.539	0.508	0.578
0	S.D.	0.106	0.119	0.103	0.104	0.121	0.087
	N	8	8	8	8	8	8
G2	Mean	0.694	0.641	0.574	0.526	0.525	0.577
500	S.D.	0.043	0.121	0.084	0.084	0.079	0.112
	N	8	8	8	8	8	8
G3	Mean	0.728	0.680	0.640	0.539	0.541	0.612
1,000	S.D.	0.045	0.093	0.049	0.080	0.064	0.063
	N	8	8	8	8	8	8
G4	Mean	0.711	0.641	0.621	0.539	0.471	0.579
2,000	S.D.	0.110	0.116	0.096	0.113	0.094	0.103
	N	8	8	8	8	8	8

No statistically significant differences were noted in the control group (G1) and the test substance group (G2 ~ G4).

Group/ Dose (mg/kg)		Hindlimb grip strength (quantitative value, kgf)					
		Time after administration (hours)					
		0	0.5	1	3	6	24
G1	Mean	0.377	0.341	0.309	0.305	0.303	0.322
0	S.D.	0.061	0.051	0.058	0.046	0.041	0.076
	N	8	8	8	8	8	8
G2	Mean	0.379	0.337	0.297	0.289	0.278	0.289
500	S.D.	0.022	0.043	0.048	0.039	0.026	0.033
	N	8	8	8	8	8	8
G3	Mean	0.346	0.320	0.301	0.314	0.305	0.331
1,000	S.D.	0.051	0.038	0.046	0.031	0.035	0.028
	N	8	8	8	8	8	8
G4	Mean	0.341	0.326	0.312	0.285	0.299	0.329
2,000	S.D.	0.040	0.043	0.036	0.049	0.043	0.050
	N	8	8	8	8	8	8

No statistically significant differences were noted in the control group (G1) and the test substance group (G2 ~ G4).

Table 5. Summary Data of Body Temperature

Group/ Dose (mg/kg)		Rectal temperature (quantitative value, °C)					
		Time after administration (hours)					
		0	0.5	1	3	6	24
G1	Mean	38.16	38.31	38.33	38.35	38.13	38.04
0	S.D.	0.37	0.38	0.38	0.38	0.32	0.39
	N	8	8	8	8	8	8
G2	Mean	38.00	38.19	38.26	38.09	38.07	38.05
500	S.D.	0.34	0.30	0.30	0.27	0.25	0.27
	N	8	8	8	8	8	8
G3	Mean	38.08	38.24	38.37	38.16	37.97	38.14
1,000	S.D.	0.49	0.49	0.45	0.28	0.34	0.50
	N	8	8	8	8	8	8
G4	Mean	38.06	38.15	38.21	38.13	37.78	37.98
2,000	S.D.	0.49	0.38	0.36	0.41	0.32	0.32
	N	8	8	8	8	8	8

No statistically significant differences were noted in the control group (G1) and the test substance group (G2 ~ G4).

<EC-18의 누드마우스에 이식된 인체 유래의 골수암 세포주 RPMI 8226에 대한 항암시험 >

Table 1. Mean Data of Tumor Volume during Observation Period

Group/ Dose (mg/kg)		Tumor volume (mm^3)									
		Time after administration (days)									
		1	5	8	12	15	19	22	26	29	33
G1	Mean	123	229	375	578	859	1369	1513	1814	2073	2368
0	S.D.	4	64	156	291	388	542	569	739	898	1009
	N	10	10	10	10	10	10	10	10	10	10
G2	Mean	123	195	316	564	742	993	1421	1734	2060	2292
125	S.D.	4	10	66	126	169	242	431	506	628	785
	N	10	10	10	10	10	10	10	10	10	10
G3	Mean	123	187	303	485	624	796	1034	1333	1593	1659
500	S.D.	3	14	91	201	247	354	435	597	709	702
	N	10	10 *	10	10	10	10 *	10	10	10	10
G4	Mean	123	204	328	556	712	825	1257	1641	1968	2081
2,000	S.D.	3	22	86	287	397	521	805	1051	1285	1361
	N	10	10	10	10	10	10	10	10	10	10
G5	Mean	123	201	324	567	770	830	963	1097	1202	1428
120	S.D.	5	9	99	122	159	191	217	222	254	386
	N	10	10	10	10	10	10 *	10	10	10	10

G1: Negative control (Olive oil), G2-G4: EC-18, G5: Gemcitabine

*: $p<0.05$, Significant difference from the negative control group (G1) by Steel's test

S.D.: Standard Deviation

N: Number of animals

Table 2. Mean Data of Tumor Weights and Tumor Growth Inhibition Rate

Group/ Dose (mg/kg)		Tumor weights (g)	IR (%)
G1	Mean	1.306	0.0
0	S.D.	0.677	
	N	10	
G2	Mean	1.563	-19.7
125	S.D.	0.775	
	N	10	
G3	Mean	1.253	4.0
500	S.D.	0.771	
	N	10	
G4	Mean	1.532	-17.3
2,000	S.D.	1.198	
	N	10	
G5	Mean	1.044	20.0
120	S.D.	0.644	
	N	10	

G1: Negative control (Olive oil), G2-G4: EC-18, G5: Gemcitabine

No statistically significant differences were noted in the test substance (G2-G4) and the positive substance groups (G5) from the negative control group (G1) ($p>0.05$, ANOVA)

S.D.: Standard Deviation

N: Number of animals

Table 3. Summary of Clinical Signs during Observation Period

Group / Dose (mg/kg)		Clinical signs															
		Time after administration (days)															
		1	2	3	4	5	6	7	8	9	10	11	12	13	14	15	16
G1	NOA	10	10	10	10	10	10	10	10	10	10	10	10	10	10	10	10
0	N	10	10	10	10	10	10	10	10	10	10	10	10	10	10	10	10
G2	NOA	10	10	10	10	10	10	10	10	10	10	10	10	10	10	10	10
125	N	10	10	10	10	10	10	10	10	10	10	10	10	10	10	10	10
G3	NOA	10	10	10	10	10	10	10	10	10	10	10	10	10	10	10	10
500	N	10	10	10	10	10	10	10	10	10	10	10	10	10	10	10	10
G4	NOA	10	10	10	10	10	10	10	10	10	10	10	10	10	10	10	10
2,000	N	10	10	10	10	10	10	10	10	10	10	10	10	10	10	10	10
G5	NOA	10	10	10	10	10	10	10	10	10	10	10	10	10	10	10	10
120	N	10	10	10	10	10	10	10	10	10	10	10	10	10	10	10	10

Group / Dose (mg/kg)		Clinical signs																
		Time after administration (days)																
		17	18	19	20	21	22	23	24	25	26	27	28	29	30	31	32	33
G1	NOA	10	10	10	10	10	10	10	10	10	10	10	10	10	10	10	10	10
0	N	10	10	10	10	10	10	10	10	10	10	10	10	10	10	10	10	10
G2	NOA	10	10	10	10	10	10	10	10	10	10	10	10	10	10	10	10	10
125	N	10	10	10	10	10	10	10	10	10	10	10	10	10	10	10	10	10
G3	NOA	10	10	10	10	10	10	10	10	10	10	10	10	10	10	10	10	10
500	N	10	10	10	10	10	10	10	10	10	10	10	10	10	10	10	10	10
G4	NOA	10	10	10	10	10	10	10	10	10	10	10	10	10	10	10	10	10
2,000	N	10	10	10	10	10	10	10	10	10	10	10	10	10	10	10	10	10
G5	NOA	10	10	10	10	10	10	10	10	10	10	10	10	10	10	10	10	10
120	N	10	10	10	10	10	10	10	10	10	10	10	10	10	10	10	10	10

G1: Negative control (Olive oil), G2-G4: EC-18, G5: Gemcitabine

NOA: No Observable Abnormality

N: Number of animals

Table 4. Mean Data of Body Weights during Observation Period

Group/ Dose (mg/kg)		Body weights (g)									
		Time after administration (days)									
		1	5	8	12	15	19	22	26	29	33
G1	Mean	24.4	24.3	24.2	24.2	24.6	24.8	24.6	24.5	24.1	24.1
0	S.D.	1.1	1.3	1.5	1.4	1.5	1.4	1.5	1.6	1.9	2.1
	N	10	10	10	10	10	10	10	10	10	10
G2	Mean	25.1	25.0	24.8	25.2	25.2	25.2	25.1	25.0	24.1	23.9
125	S.D.	1.1	1.1	1.1	1.1	1.0	1.2	1.2	1.4	1.6	1.7
	N	10	10	10	10	10	10	10	10	10	10
G3	Mean	24.6	24.7	24.7	24.7	24.7	24.9	24.6	24.9	24.5	24.4
500	S.D.	0.9	0.9	0.9	0.9	1.1	1.3	1.3	1.2	1.2	1.6
	N	10	10	10	10	10	10	10	10	10	10
G4	Mean	24.5	24.7	24.7	24.6	24.7	24.8	24.8	24.9	25.0	25.1
2,000	S.D.	0.7	0.8	0.9	0.9	0.8	0.8	0.7	0.9	0.8	1.2
	N	10	10	10	10	10	10	10	10	10	10
G5	Mean	25.0	24.9	23.3	23.8	24.8	25.1	25.4	25.5	25.8	26.0
120	S.D.	0.9	1.3	0.9	0.9	0.4	0.5	0.7	0.6	0.6	0.6
	N	10	10	10	10	10	10	10	10	10	10

G1: Negative control (Olive oil), G2-G4: EC-18, G5: Gemcitabine

No statistically significant differences were noted in the test substance (G2-G4) and the positive substance groups (G5) from the negative control group (G1) ($p>0.05$, ANOVA)

S.D.: Standard Deviation

N: Number of animals

<EC-18의 collagen으로 유발된 DBA/1J 마우스의 관절염에 대한 효능시험>

Table 1. Mean Data of Arthritic Scores

Group Dose (mg/kg)		Arthritic score Time after administration (days)										
		1	5	8	12	15	19	22	26	29	33	36
G1	Mean	0.0	0.0	0.0	0.0	0.0	0.0	0.0	0.0	0.0	0.0	0.0
0	S.E.	0.0	0.0	0.0	0.0	0.0	0.0	0.0	0.0	0.0	0.0	0.0
	N	10	10	10	10	10	10	10	10	10	10	10
G2	Mean	0.0	1.3	2.6	4.3	5.0	6.1	8.0	10.0	10.3	10.4	10.7
0	S.E.	0.0	0.3	0.4	0.6	0.7	0.6	0.7	0.7	0.7	0.5	0.4
	N	10	10 [b]	10 [b]	10 [b]	10 [b]	10 [b]	10 [b]	10 [b]	10 [b]	10 [b]	10 [b]
G3	Mean	0.0	0.7	1.7	2.5	2.7	4.3	4.9	4.8	4.9	5.8	6.2
125	S.E.	0.0	0.2	0.3	0.3	0.4	0.7	0.8	0.8	0.8	0.9	1.0
	N	10	10	10	10 [**]	10 [**]	10	10 [*]	10 [**]	10 [**]	10 [**]	10 [##]
G4	Mean	0.0	0.6	1.6	2.0	2.2	4.0	4.2	5.2	5.1	6.3	6.2
500	S.E.	0.0	0.2	0.3	0.3	0.4	0.7	1.0	1.1	1.2	1.2	1.3
	N	10	10	10 [*]	10 [**]	10 [**]	10 [*]	10 [**]	10 [**]	10 [**]	10 [**]	10
G5	Mean	0.0	0.7	1.0	1.8	2.1	3.5	4.4	5.6	6.1	6.8	7.2
2,000	S.E.	0.0	0.2	0.2	0.3	0.3	0.5	0.7	0.7	0.7	0.8	1.2
	N	10	10	10 [**]	10 [**]	10 [**]	10 [**]	10 [**]	10 [**]	10 [**]	10 [**]	10 [#]
G6	Mean	0.0	1.0	1.3	2.1	3.0	3.9	4.2	4.0	3.9	4.6	5.8
20	S.E.	0.0	0.3	0.3	0.3	0.5	0.6	0.8	0.9	0.9	0.9	0.8
	N	10	10	10 [**]	10 [**]	10 [*]	10 [*]	10 [**]	10 [**]	10 [**]	10 [**]	10 [##]
G7	Mean	0.0	0.7	1.0	1.2	1.3	2.3	2.4	2.6	2.2	3.8	3.9
2.5	S.E.	0.0	0.2	0.3	0.3	0.4	0.5	0.5	0.5	0.4	0.6	0.5
	N	10	10	10 [**]	10 [**]	10 [**]	10 [**]	10 [**]	10 [**]	10 [**]	10 [**]	10 [##]

G1: Normal control (Olive oil), G2: Negative control (Olive oil), G3-G5: EC-18, G6: Remicade

G7: Methotrexate

[b] $p<0.01$, Significant differences between the normal control group (G1) and the negative control group (G2) by Aspin-Welch t-test.

[*] $p<0.05$, Significant differences from the negative control group (G2) by Dunnett's t-test.

[**] $p<0.01$, Significant differences from the negative control group (G2) by Dunnett's t-test.

[#] $p<0.05$, Significant difference from the negative control group (G2) by Dunnett's t-test.

[##] $p<0.01$, Significant difference from the negative control group (G2) by Dunnett's t-test.

S.E.: Standard Error

N: Number of animals/group

Table 2. Mean Data of Paw Thicknesses

Group Dose (mg/kg)		Paw thickness (mm) Time after administration (days)										
		1	5	8	12	15	19	22	26	29	33	36
G1	Mean	1.90	1.97	1.98	2.01	1.98	2.00	2.04	2.04	1.96	2.05	2.02
0	S.E.	0.0	0.0	0.0	0.0	0.0	0.0	0.0	0.0	0.0	0.0	0.0
	N	10	10	10	10	10	10	10	10	10	10	10
G2	Mean	1.96	2.04	2.08	2.51	2.38	2.50	2.64	2.68	2.40	2.55	2.54
0	S.E.	0.0	0.1	0.1	0.1	0.1	0.1	0.1	0.1	0.1	0.1	0.1
	N	10	10	10	10 [b]	10 [a]	10 [b]	10 [b]	10 [b]	10 [b]	10 [b]	10 [b]
G3	Mean	1.93	1.98	2.15	2.36	2.25	2.52	2.54	2.45	2.18	2.37	2.34
125	S.E.	0.0	0.0	0.1	0.1	0.1	0.1	0.1	0.1	0.1	0.1	0.1
	N	10	10	10	10	10	10	10	10	10	10	10
G4	Mean	1.92	2.04	2.21	2.28	2.24	2.42	2.46	2.48	2.20	2.37	2.37
500	S.E.	0.0	0.0	0.1	0.1	0.1	0.1	0.1	0.1	0.1	0.1	0.1
	N	10	10	10	10	10	10	10	10	10	10	10
G5	Mean	1.96	1.97	2.08	2.15	2.11	2.29	2.40	2.60	2.45	2.58	2.57
2,000	S.E.	0.0	0.0	0.1	0.1	0.1	0.1	0.1	0.1	0.1	0.1	0.1
	N	10	10	10	10	10	10	10	10	10	10	10
G6	Mean	1.92	2.05	2.09	2.28	2.45	2.52	2.56	2.55	2.32	2.47	2.51
20	S.E.	0.0	0.1	0.1	0.1	0.2	0.1	0.1	0.1	0.1	0.1	0.1
	N	10	10	10	10	10	10	10	10	10	10	10
G7	Mean	1.97	2.03	2.13	2.22	2.17	2.30	2.39	2.36	2.31	2.40	2.44
2.5	S.E.	0.0	0.0	0.1	0.1	0.1	0.1	0.1	0.1	0.1	0.1	0.1
	N	10	10	10	10	10	10	10	10	10	10	10

G1: Normal control (Olive oil), G2: Negative control (Olive oil), G3-G5: EC-18, G6: Remicade

G7: Methotrexate

[a] $p<0.05$, Significant differences between the normal control group (G1) and the negative control group (G2) by Aspin-Welch t-test.

[b] $p<0.01$, Significant differences between the normal control group (G1) and the negative control group (G2) by Aspin-Welch t-test.

No statistically significant differences were noted in the test substance, the positive substance 1 and 2 groups (G3-G7) from the negative control group (G2) ($p>0.05$, ANOVA).

S.E.: Standard Error

N: Number of animals/group

Table 3. Mean Data of Serum IL-6 and Anti-CII IgG Concentrations

Group Dose (mg/kg)		Concentrations	
		IL-6 (pg/mL)	Anti-CII IgG (U/L)
G1	Mean	0.101	0.048
0	S.E.	0.005	0.001
	N	10	10
G2	Mean	0.425	0.969
0	S.E.	0.059	0.108
	N	10 [b]	10 [b]
G3	Mean	0.323	0.862
125	S.E.	0.044	0.088
	N	10	10
G4	Mean	0.243	1.010
500	S.E.	0.046	0.103
	N	10 *	10
G5	Mean	0.263	0.947
2,000	S.E.	0.043	0.073
	N	10 *	10
G6	Mean	0.270	0.892
20	S.E.	0.051	0.100
	N	10 *	10
G7	Mean	0.222	0.950
2.5	S.E.	0.024	0.120
	N	9 **	9

G1: Normal control (Olive oil), G2: Negative control (Olive oil), G3-G5: EC-18, G6: Remicade

G7: Methotrexate

[b] $p<0.01$, Significant differences between the normal control group (G1) and the negative control group (G2) by Aspin-Welch t-test.

* $p<0.05$, Significant differences from the negative control group (G2) by Dunnett's t-test.

** $p<0.01$, Significant differences from the negative control group (G2) by Dunnett's t-test.

S.E.: Standard Error

N: Number of animals/group

Table 4. Mean Data of Histopathological Arthritic Scores

Group Dose (mg/kg)		Histopathological arthritis score
G1	Mean	0.0
0	S.E.	0.0
	N	10
G2	Mean	6.6
0	S.E.	0.4
	N	10 [b]
G3	Mean	5.0
125	S.E.	0.8
	N	10
G4	Mean	4.3
500	S.E.	0.8
	N	10
G5	Mean	5.7
2,000	S.E.	0.4
	N	10
G6	Mean	4.6
20	S.E.	0.8
	N	10
G7	Mean	3.6
2.5	S.E.	0.9
	N	10

G1: Normal control (Olive oil), G2: Negative control (Olive oil), G3-G5: EC-18, G6: Remicade

G7: Methotrexate

[b] $p<0.01$, Significant differences between the normal control group (G1) and the negative control group (G2) by Aspin-Welch t-test.

No statistically significant differences were noted in the test substance, the positive substance 1 and 2 groups (G3-G7) from the negative control group (G2) ($p>0.05$, ANOVA).

S.E.: Standard Error

N: Number of animals/group

Table 5. Summary of Clinical Signs

Group Dose (mg/kg)		Clinical signs: Time after administration (days) 1	2	3	4	5	6	7	8	9	10	11	12	13	14	15
G1	NOA	10	10	10	10	10	10	10	10	10	10	10	10	10	10	10
0	N	10	10	10	10	10	10	10	10	10	10	10	10	10	10	10
G2	NOA	10	10	10	10	10	10	10	10	10	10	10	10	10	10	10
0	N	10	10	10	10	10	10	10	10	10	10	10	10	10	10	10
G3	NOA	10	10	10	10	10	10	10	10	10	10	10	10	10	10	10
125	N	10	10	10	10	10	10	10	10	10	10	10	10	10	10	10
G4	NOA	10	10	10	10	10	10	10	10	10	10	10	10	10	10	10
500	N	10	10	10	10	10	10	10	10	10	10	10	10	10	10	10
G5	NOA	10	10	10	10	10	10	10	10	10	10	10	10	10	10	10
2,000	N	10	10	10	10	10	10	10	10	10	10	10	10	10	10	10
G6	NOA	10	10	10	10	10	10	10	10	10	10	10	10	10	10	10
20	N	10	10	10	10	10	10	10	10	10	10	10	10	10	10	10
G7	NOA	10	10	10	10	10	10	10	10	10	10	10	10	10	10	10
2.5	N	10	10	10	10	10	10	10	10	10	10	10	10	10	10	10

Group Dose (mg/kg)		Clinical signs: Time after administration (days) 16	17	18	19	20	21	22	23	24	25	26	27	28	29	30
G1	NOA	10	10	10	10	10	10	10	10	10	10	10	10	10	10	10
0	N	10	10	10	10	10	10	10	10	10	10	10	10	10	10	10
G2	NOA	10	10	10	10	10	10	10	10	10	10	10	10	10	10	10
0	N	10	10	10	10	10	10	10	10	10	10	10	10	10	10	10
G3	NOA	10	10	10	10	10	10	10	10	10	10	10	10	10	10	10
125	N	10	10	10	10	10	10	10	10	10	10	10	10	10	10	10
G4	NOA	10	10	10	10	10	10	10	10	10	10	10	10	10	10	10
500	N	10	10	10	10	10	10	10	10	10	10	10	10	10	10	10
G5	NOA	10	10	10	10	10	10	10	10	10	10	10	10	10	10	10
2,000	N	10	10	10	10	10	10	10	10	10	10	10	10	10	10	10
G6	NOA	10	10	10	10	10	10	10	10	10	10	10	10	10	10	10
20	N	10	10	10	10	10	10	10	10	10	10	10	10	10	10	10
G7	NOA	10	10	10	10	10	10	10	10	10	10	10	10	10	10	10
2.5	N	10	10	10	10	10	10	10	10	10	10	10	10	10	10	10

G1: Normal control (Olive oil), G2: Negative control (Olive oil), G3-G5: EC-18, G6: Remicade

G7: Methotrexate

NOA: No Observable Abnormality

N: Number of animals/Group

Table 5. (Continued)

Group Dose (mg/kg)		Clinical signs: Time after administration (days) 31	32	33	34	35	36
G1	NOA	10	10	10	10	10	10
0	N	10	10	10	10	10	10
G2	NOA	10	10	10	10	10	10
0	N	10	10	10	10	10	10
G3	NOA	10	10	10	10	10	10
125	N	10	10	10	10	10	10
G4	NOA	10	10	10	10	10	10
500	N	10	10	10	10	10	10
G5	NOA	10	10	10	10	10	10
2,000	N	10	10	10	10	10	10
G6	NOA	10	10	10	10	10	10
20	N	10	10	10	10	10	10
G7	NOA	10	10	10	10	10	10
2.5	N	10	10	10	10	10	10

G1: Normal control (Olive oil), G2: Negative control (Olive oil), G3-G5: EC-18, G6: Remicade

G7: Methotrexate

NOA: No Observable Abnormality

N: Number of animals/Group

<EC-18의 랫드를 이용한 경구투여 배태자 발생독성시험>

Table 1. Summary of Clinical Signs

Signs	Group	G1	G2	G3	G4
	Dose (mg/kg)	0	500	1,000	2,000
	No. of dams	21	22	21	20
No abnormalities detected		20	22	21	20
Abnormalities detected		1			
- Mass, left axillary		1			

Dosing period : Gestation day 7~17.

Table 2. Summary of Body Weights of Dams

Group/ Dose (mg/kg)		Gestation day (g)													
		0	3	7	8	9	10	11	12	13	14	15	16	17	20
G1	Mean	233.5	256.5	279.4	284.5	289.2	296.6	303.4	311.1	316.4	324.5	333.1	344.0	355.0	397.7
0	S.D.	21.9	25.2	25.6	25.3	24.6	26.2	26.5	25.7	26.9	28.6	30.1	28.8	31.3	35.7
	N	21	21	21	21	21	21	21	21	21	21	21	21	21	21
G2	Mean	233.4	254.8	275.6	279.9	285.5	292.9	299.9	305.8	311.7	318.5	326.2	336.0	348.1	393.2
500	S.D.	19.8	22.1	20.7	21.3	21.6	22.7	22.6	24.0	25.2	24.7	26.9	28.2	29.5	35.8
	N	22	22	22	22	22	22	22	22	22	22	22	22	22	22
G3	Mean	232.1	255.2	278.5	280.4	286.5	292.7	299.9	305.4	312.6	318.3	326.5	335.8	346.8	387.1
1,000	S.D.	18.8	20.9	21.0	21.1	19.7	21.0	21.3	21.6	22.6	24.0	24.3	26.3	28.5	36.4
	N	21	21	21	21	21	21	21	21	21	21	21	21	21	21
G4	Mean	233.5	256.5	276.1	278.1	284.2	291.3	298.5	304.5	312.6	318.6	326.1	336.2	349.8	395.4
2,000	S.D.	19.2	21.0	19.8	19.6	20.2	20.8	22.2	23.3	23.6	22.2	24.3	26.1	28.1	33.9
	N	20	20	20	20	20	20	20	20	20	20	20	20	20	20

Dosing period : Gestation day 7~17.

Table 3. Summary of Food Consumption

Group/ Dose (mg/kg)		Gestation day (g)					
		1	4	8	11	15	18
G1	Mean	21.6	28.3	25.4	26.9	29.0	30.8
0	S.D.	5.4	3.5	3.7	3.8	3.7	4.0
	N	21	21	21	21	21	21
G2	Mean	20.9	27.2	23.8	26.0	26.4	28.7
500	S.D.	4.5	3.4	3.4	3.9	4.0	4.1
	N	22	22	22	22	22	22
G3	Mean	22.5	27.4	23.2	26.8	27.0	28.2
1,000	S.D.	4.0	2.9	3.9	3.9	4.5	4.8
	N	21	21	21	21	21	21
G4	Mean	21.3	26.2	23.1	26.0	27.2	29.9
2,000	S.D.	4.1	3.3	3.1	3.4	2.9	3.9
	N	20	20	20	20	20	20

Dosing period : Gestation day 7~17.

Table 4-1. Summary of Absolute Organ Weights

(Unit: g)

Group/ Dose (mg/kg)		B.W.	Brain	Pituitary	Heart	Liver	Spleen	Kidneys		Adrenals		Ovaries		Gravid uterus
								Lt.	Rt.	Lt.	Rt.	Lt.	Rt.	
G1	Mean	397.7	1.90	0.0163	1.03	14.94	0.71	1.02	1.04	0.0358	0.0334	0.0702	0.0753	77.12
0	S.D.	35.7	0.07	0.0019	0.11	2.10	0.14	0.11	0.11	0.0050	0.0039	0.0144	0.0198	22.44
	N	21	21	21	21	21	21	21	21	21	21	21	21	21
G2	Mean	393.2	1.93	0.0163	1.01	14.96	0.69	0.98	1.00	0.0357	0.0343	0.0708	0.0689	78.11
500	S.D.	35.8	0.06	0.0023	0.08	1.75	0.10	0.11	0.10	0.0047	0.0040	0.0166	0.0151	18.97
	N	22	22	22	22	22	22	22	22	22	22	22	22	22
G3	Mean	387.1	1.91	0.0148	1.00	14.43	0.70	0.96	0.99	0.0332	0.0307	0.0697	0.0700	74.27
1,000	S.D.	36.4	0.07	0.0021	0.10	1.90	0.09	0.10	0.10	0.0050	0.0037	0.0167	0.0156	30.28
	N	21	21	21	21	21	21	21	21	21	21	21	21	21
G4	Mean	395.4	1.89	0.0161	1.01	14.81	0.66	1.00	1.00	0.0357	0.0328	0.0681	0.0729	80.10
2,000	S.D.	33.9	0.07	0.0028	0.09	2.12	0.09	0.10	0.11	0.0042	0.0037	0.0149	0.0128	22.27
	N	20	20	20	20	20	20	20	20	20	20	20	20	20

Table 4-2. Summary of Relative Organ Weights

(Unit: g/ 100 g body weight)

Group/ Dose (mg/kg)		Correct B.W. (g)	Brain	Pituitary	Heart	Liver	Spleen	Kidneys		Adrenals		Ovaries		Gravid uterus
								Lt.	Rt.	Lt.	Rt.	Lt.	Rt.	
G1	Mean	320.6	0.60	0.0051	0.32	4.66	0.22	0.32	0.32	0.0112	0.0105	0.0222	0.0235	24.46
0	S.D.	34.4	0.06	0.0008	0.02	0.39	0.05	0.02	0.02	0.0017	0.0015	0.0052	0.0059	7.77
	N	21	21	21	21	21	21	21	21	21	21	21	21	21
G2	Mean	315.1	0.62	0.0052	0.32	4.74	0.22	0.31	0.32	0.0114	0.0110	0.0226	0.0220	24.86
500	S.D.	26.1	0.04	0.0007	0.01	0.31	0.04	0.03	0.02	0.0018	0.0015	0.0056	0.0051	6.11
	N	22	22	22	22	22	22	22	22	22	22	22	22	22
G3	Mean	312.9	0.62	0.0047	0.32	4.61	0.22	0.31	0.32	0.0107	0.0098	0.0224	0.0226	24.15
1,000	S.D.	28.5	0.06	0.0005	0.03	0.45	0.02	0.02	0.02	0.0016	0.0010	0.0055	0.0056	10.21
	N	21	21	21	21	21	21	21	21	21	21	21	21	21
G4	Mean	315.3	0.60	0.0051	0.32	4.69	0.21	0.32	0.32	0.0114	0.0105	0.0215	0.0231	25.57
2,000	S.D.	25.5	0.05	0.0007	0.02	0.46	0.02	0.02	0.02	0.0017	0.0015	0.0039	0.0039	7.55
	N	20	20	20	20	20	20	20	20	20	20	20	20	20

Correct B.W. = Body weight in gestation day 20 - Weight of gravid uterus.

Table 5. Summary of Necropsy Findings

	Group	G1	G2	G3	G4
Organ / Findings	Dose (mg/kg)	0	500	1,000	2,000
	No. of examined	21	22	21	20
	Remarkable findings	1	0	1	0
Subcutaneous tissue					
	-Mass, left axillary	1			
Uterus					
	-Cyst, cervix, dark red			1	

Table 6. Summary of Caesarean Section Data

Group/ Dose (mg/kg)		No. of corpora lutea			No. of implantation			Implantation rate (%)	No. of embryo-fetal death			Embryo-fetal mortality (%)	No. of live fetuses			Sex ratio
		Lt.	Rt.	Total	Lt.	Rt.	Total		Resorption		Dead fetuses		Sex		Total	
									Early	Late			Male	Female		
G1	Mean	8.7	8.8	17.5	7.5	6.8	14.3	82.8	1.2	0.0	0.1	9.6	5.8	7.1	13.0	0.8
0	S.D.	2.7	3.3	3.3	2.6	3.1	3.8	20.6	1.1	0.2	0.4	11.0	2.6	3.3	3.8	-
	N	21	21	21	21	21	21	21	21	21	21	21	21	21	21	21
G2	Mean	8.5	8.5	17.0	7.2	6.9	14.1	84.1	0.8	0.0	0.0	5.9	6.8	6.5	13.3	1.0
500	S.D.	2.6	2.6	3.2	2.1	2.9	2.8	16.5	0.8	0.0	0.0	5.9	2.0	2.2	2.7	-
	N	22	22	22	22	22	22	22	22	22	22	22	22	22	22	22
G3	Mean	8.2	8.2	16.5	6.7	6.5	13.2	79.8	0.8	0.0	0.0	10.2	5.8	7.3	13.1	0.8
1,000	S.D.	2.8	2.8	3.8	3.1	2.9	4.8	28.5	1.1	0.0	0.0	22.1	2.3	2.9	4.1	-
	N	21	21	21	21	21	21	21	21	21	21	21	20	20	20	20
G4	Mean	8.0	9.0	16.9	6.9	7.4	14.3	85.7	0.6	0.1	0.0	4.4	6.9	6.7	13.6	1.0
2,000	S.D.	2.0	2.3	2.7	2.4	2.7	3.3	19.5	0.9	0.2	0.0	7.2	2.2	2.9	3.3	-
	N	20	20	20	20	20	20	20	20	20	20	20	20	20	20	20

Implantation rate (%) = (No. of implantation / No. of corpora lutea) × 100.
Embryo-fetal mortality (%) = (No. of resorption and dead fetuses / No. of implantation) × 100.
Sex ratio = No. of live male fetuses / No. of live female fetuses.

Table 7. Summary of Fetus Body Weights and Placenta Weights

Group/ Dose (mg/kg)		Body weights (g)		Placenta weights (g)	
		Male	Female	Male	Female
G1	Mean	4.08	3.88	0.45	0.45
0	S.D.	0.79	0.73	0.05	0.06
	N	20	21	20	21
G2	Mean	4.01	3.77	0.47	0.46
500	S.D.	0.61	0.59	0.05	0.04
	N	22	22	22	22
G3	Mean	4.16	3.72	0.48	0.43
1,000	S.D.	0.95	1.22	0.12	0.11
	N	20	20	20	20
G4	Mean	4.08	3.84	0.46	0.45
2,000	S.D.	0.99	0.91	0.04	0.04
	N	20	20	20	20

Table 8. Summary of External Findings of Fetuses and Placentas

Group/ Dose (mg/kg)	No. of dams	No. of fetuses	Fetuses	Placenta
			Supernumerary hindlimb	Enlargement
G1	21	272	0	0
0		Incidence (%)	0.00	0.00
G2	22	293	0	0
500		Incidence (%)	0.00	0.00
G3	20	261	1	1
1,000		Incidence (%)	0.38	0.38
G4	20	272	0	0
2,000		Incidence (%)	0.00	0.00

Incidence (%) = (No. of Fetuses or Placentas with external abnormalies / No. of Fetuses) × 100.

Table 10. Summary of Skeletal Findings of Fetuses

Group/ Dose (mg/kg)	Animal ID	No. of fetuses	Variation				
			Cervical vertabra	Thoracic centrum	Rib		
			Cervical rib	Dumbell shape	13th rib short	Wavy rib	Lumbar rib (14th rib)
G1	21	130	0	2	2	1	4
0		Incidence (%)	0.00	1.54	1.54	0.77	3.08
G2	22	142	1	5	1	1	7
500		Incidence (%)	0.70	3.52	0.70	0.70	4.93
G3	20	125	0	4	0	0	5
1,000		Incidence (%)	0.00	3.20	0.00	0.00	4.00
G4	20	132	0	1	1	0	5
2,000		Incidence (%)	0.00	0.76	0.76	0.00	3.79

Incidence (%) = (No. of Fetuses with skeletal abnormalies / No. of Fetuses) x 100.

Table 11. Summary of Ossification Status of Fetuses

Group/ Dose (mg/kg)		No. of fetuses	OSSB	Pairs of rib	Sternebra	Sacro-caudal vertebra	Forelimbs		Hindlimbs	
							Mc	Pp	Mt	Pp
G1	Mean	6.2	2.0	13.0	5.8	8.1	7.9	4.9	9.0	2.0
0	S.D.	2.0	0.0	0.1	0.3	1.2	0.2	2.7	0.8	2.7
	N	21	21	21	21	21	21	21	21	21
G2	Mean	6.5	2.0	13.0	5.8	7.9	8.0	4.5	9.0	2.2
500	S.D.	1.3	0.0	0.0	0.3	1.0	0.0	2.3	0.7	2.5
	N	22	22	22	22	22	22	22	22	22
G3	Mean	6.3	2.0	13.1	5.9	8.4	7.9	5.3	9.0	2.9
1,000	S.D.	2.0	0.0	0.2	0.2	1.6	0.3	3.2	0.9	2.9
	N	20	20	20	20	20	20	20	20	20
G4	Mean	6.6	2.0	13.0	5.9	8.2	8.0	5.7	9.1	2.6
2,000	S.D.	1.7	0.0	0.0	0.2	1.9	0.1	2.9	0.9	2.4
	N	20	20	20	20	20	20	20	20	20

OSSB: ossified step of supraoccipital bone. N: No. of animals (dams).

Mc: metacarpal, Pp: proximal phalanx, Mt: metatarsal.

<EC-18의 랫드를 이용한 경구투여 수태능 및 초기배 발생독성시험>

Table 1. Summary of Clinical Signs

Sex: Male

	Group	G1	G2	G3	G4
Signs	Dose (mg/kg/day)	0	500	1,000	2,000
	No. of animals	22	22	22	22
Abnormalities detected		0	0	0	0

Sex: Female

	Group	G1	G2	G3	G4
Signs	Dose (mg/kg/day)	0	500	1,000	2,000
	No. of animals	22	22	22	22
Abnormalities detected		1	1	0	1
	-Loss of fur, left forelimb and hindlimb	1	0	0	0
	-Loss of fur, right forelimb	0	1	0	1

Table 2. Summary of Body Weights

Sex : Male

Group/ Dose (mg/kg/day)		Day (g)																		
		0	3	7	10	14	17	21	24	28	31	35	38	42	45	49	52	56	59	61/62 †
G1	Mean	266.4	295.3	329.1	352.6	378.2	398.0	423.8	441.6	461.6	468.7	487.4	499.8	515.8	523.8	538.4	548.4	559.0	566.6	571.2
0	S.D.	8.6	9.8	12.9	15.4	18.4	19.8	21.4	22.9	26.8	27.6	29.2	31.4	32.3	32.1	34.6	34.2	36.5	36.1	37.9
	N	22	22	22	22	22	22	22	22	22	22	22	22	22	22	22	22	22	22	22
G2	Mean	265.2	293.3	325.0	346.8	371.3	388.2	414.3	430.3	450.5	457.8	477.2	489.6	504.9	514.6	521.3	536.1	547.6	554.1	557.5
500	S.D.	9.7	12.1	16.6	20.3	23.6	26.2	30.8	31.2	33.4	34.0	37.2	39.0	40.4	42.5	42.6	44.7	45.9	48.4	46.1
	N	22	22	22	22	22	22	22	22	22	22	22	22	22	22	22	22	22	22	22
G3	Mean	265.4	294.1	326.3	347.0	373.2	389.7	413.6	429.9	448.7	457.7	475.2	486.5	502.5	511.5	520.3	531.2	542.0	548.8	554.0
1,000	S.D.	8.7	10.9	13.0	16.2	20.4	22.6	24.3	26.4	27.5	29.4	29.9	32.1	34.6	35.4	37.3	39.3	41.2	42.1	42.4
	N	22	22	22	22	22	22	22	22	22	22	22	22	22	22	22	22	22	22	22
G4	Mean	265.3	293.5	326.5	349.5	375.0	392.0	415.9	433.8	454.0	461.8	481.7	493.4	510.1	519.1	531.3	539.9	546.5	553.7	558.8
2,000	S.D.	9.3	9.7	13.6	16.9	20.5	21.7	23.8	25.1	26.9	27.8	30.1	30.8	31.8	31.9	31.4	32.2	34.7	34.8	35.8
	N	22	22	22	22	22	22	22	22	22	22	22	22	22	22	22	22	22	22	22

† : Body weights of 12 animals per group were recorded on Day 62.

Table 2. (Continued)

Sex : Female

Group/ Dose (mg/kg/day)		Pre-mating day (g)					Gestation day (g)					
		0	3	7	10	14	0	3	7	10	13	15
G1	Mean	204.8	216.5	227.9	234.5	241.7	251.9	275.4	296.0	312.6	332.8	347.3
0	S.D.	6.7	6.9	8.2	10.4	10.4	10.5	10.3	12.1	14.7	16.8	18.5
	N	22	22	22	22	22	21	21	21	21	21	21
G2	Mean	203.5	216.9	230.1	239.6	247.0	257.1	278.9	304.6	324.1	339.4	356.3
500	S.D.	7.8	8.4	10.0	12.2	13.9	15.5	15.8	18.6	25.4	24.0	25.9
	N	22	22	22	22	22	22	22	22	22	22	22
G3	Mean	205.5	215.6	227.7	237.9	245.3	252.4	274.3	296.1	311.0	332.0	344.7
1,000	S.D.	6.0	7.9	9.6	11.8	13.0	11.3	14.7	16.9	17.0	20.5	21.0
	N	22	22	22	22	22	22	22	22	22	22	22
G4	Mean	205.0	217.2	229.7	240.4	249.2	257.1	277.5	299.0	316.1	336.1	350.9
2,000	S.D.	6.5	7.7	10.2	13.2	16.3	17.9	19.7	23.1	24.9	26.4	27.6
	N	22	22	22	22	22	21	21	21	21	21	21

Table 3. Summary of Food Consumptions

Sex : Male

Group/ Dose (mg/kg/day)		Day (g/day)							
		0	7	14	21	28	42	49	56
G1	Mean	31.0	30.7	30.0	31.3	30.6	28.0	30.0	28.4
0	S.D.	2.2	2.6	2.4	3.2	3.3	2.4	2.7	2.1
	N	22	22	22	22	22	22	22	22
G2	Mean	30.2	30.7	29.0	30.1	29.4	28.5	27.7	28.2
500	S.D.	2.7	3.6	3.9	4.1	3.5	3.9	3.9	3.7
	N	22	22	22	22	22	22	22	22
G3	Mean	30.2	30.4	30.0	29.6	30.0	27.8	28.0	28.9
1,000	S.D.	2.8	3.1	3.8	2.8	3.0	2.7	3.3	3.2
	N	22	22	22	22	22	22	22	22
G4	Mean	30.9	29.7	29.1	29.0	30.0	27.9	29.0	27.4
2,000	S.D.	3.9	3.0	4.5	3.6	3.9	3.1	3.1	4.5
	N	22	22	22	22	22	22	22	22

Table 3. (Continued)

Sex : Female

Group / Dose (mg/kg/day)		Pre-mating day (g/day)			Gestation day (g/day)		
		0	7	14	0	7	15
G1	Mean	21.1	21.0	20.9	25.2	29.0	33.6
0	S.D.	2.9	3.2	3.5	3.3	3.5	4.0
	N	22	22	22	21	21	21
G2	Mean	19.9	21.3	22.0	24.7	29.9	33.6
500	S.D.	3.9	2.6	4.0	4.0	4.6	5.1
	N	22	22	22	22	22	22
G3	Mean	20.8	20.0	22.0	24.6	28.7	31.7
1000	S.D.	3.1	3.2	3.6	4.4	4.5	5.0
	N	22	22	22	22	22	22
G4	Mean	20.6	20.6	22.5	23.4	27.8	33.0
2,000	S.D.	2.4	2.6	3.4	2.9	3.3	3.3
	N	22	22	22	21	21	21

Table 5. Summary of Reproductive Function Test

(Caesarean at gestation day 15)

Group/ Dose (mg/kg/day)	No. of females cohabitated with males	No. of females with males mated	No. of females pregnant	Mating index (%)	Male fertility index (%)	Female fertility index (%)		Mating period (day)	No. of C.L.	No. of Imp.	No. of Res.	Imp. Rate (%)	Embryo mortality (%)
G1	22	21	21	95.5	100.0	100.0	Mean	2.7	18.9	15.6	0.7	84.4	4.2
0				(21 / 22)	(21 / 21)	(21 / 21)	S.D.	1.5	4.3	2.9	0.8	14.5	5.0
							N	21	21	21	21	21	21
G2	22	22	22	100.0	100.0	100.0	Mean	2.2	19.3	15.1	0.6	80.7	4.2
500				(22 / 22)	(22 / 22)	(22 / 22)	S.D.	1.0	3.9	2.1	0.8	15.9	5.5
							N	22	22	22	22	22	22
G3	22	22	22	100.0	100.0	100.0	Mean	1.7	18.9	15.8	1.1	85.1	7.2
1,000				(22 / 22)	(22 / 22)	(22 / 22)	S.D.	0.9	3.3	1.8	1.4	10.7	8.6
							N	22	22	22	22	22	22
G3	22	21	21	95.5	100.0	100.0	Mean	1.8	18.7	15.1	0.7	82.7	4.7
2,000				(21 / 22)	(21 / 21)	(21 / 21)	S.D.	0.8	4.2	2.8	1.0	17.9	6.3
							N	21	21	21	21	21	21

C.L.: Corpus luteum, Imp.: Implantation, Res.: Resorption.

Mating index (%) = (No. of confirmed mating / No. of females cohabitated with males) × 100.

Male fertility index (%) = (No. of males impregnating a female / No. of males mated) × 100.

Female fertility index (%) = (No. of females pregnant / No. of females mated) × 100.

Implantation rate (%) = (No. of implantation / No. of corpus luteum) × 100.

Embryo mortality (%) = (No. of reabsorption / No. of implantation) × 100.

Table 6. Summary of Absolute and Relative Organ Weights

Sex : Male (Unit : g)

Group/ Dose (mg/kg/day)	Animal ID	B.W.	Brain	Pituitary	Heart	Liver	Spleen	Kidneys		Adrenals		Testis		Epididymis	
								Lt.	Rt.	Lt.	Rt.	Lt.	Rt.	Lt.	Rt.
G1	Mean	571.2	2.10	0.0135	1.63	20.84	0.86	1.89	1.86	0.0318	0.0308	1.82	1.82	0.70	0.73
0	S.D.	37.9	0.05	0.0014	0.15	2.48	0.13	0.15	0.17	0.0049	0.0042	0.17	0.17	0.06	0.05
	N	22	22	22	22	22	22	22	22	22	22	22	22	22	22
G2	Mean	557.5	2.12	0.0132	1.60	20.22	0.84	1.77	1.74	0.0313	0.0286	1.80	1.86	0.69	0.72
500	S.D.	46.1	0.11	0.0020	0.16	3.19	0.21	0.19	0.18	0.0054	0.0043	0.25	0.19	0.11	0.06
	N	22	22	22	22	22	22	22	22	22	22	22	22	22	22
G3	Mean	554.0	2.13	0.0128	1.65	20.36	0.89	1.81	1.78	0.0304	0.0289	1.83	1.84	0.70	0.72
1,000	S.D.	42.4	0.07	0.0019	0.16	2.90	0.15	0.25	0.24	0.0058	0.0059	0.15	0.13	0.06	0.06
	N	22	22	22	22	22	22	22	22	22	22	22	22	22	22
G4	Mean	558.8	2.13	0.0133	1.62	19.75	0.86	1.78	1.75	0.0305	0.0272	1.79	1.79	0.68	0.71
2,000	S.D.	35.8	0.07	0.0014	0.12	2.05	0.15	0.13	0.12	0.0050	0.0049	0.15	0.15	0.05	0.06
	N	22	22	22	22	22	22	22	22	22	22	22	22	22	22

(g/ 100 g body weight)

Group/ Dose (mg/kg/day)	Animal ID	B.W. (g)	Brain	Pituitary	Heart	Liver	Spleen	Kidneys		Adrenals		Testis		Epididymis	
								Lt.	Rt.	Lt.	Rt.	Lt.	Rt.	Lt.	Rt.
G1	Mean	571.2	0.37	0.0024	0.29	3.64	0.15	0.33	0.33	0.0056	0.0054	0.32	0.32	0.12	0.13
0	S.D.	37.9	0.02	0.0003	0.03	0.29	0.02	0.03	0.03	0.0010	0.0008	0.04	0.04	0.02	0.01
	N	22	22	22	22	22	22	22	22	22	22	22	22	22	22
G2	Mean	557.5	0.38	0.0024	0.29	3.61	0.15	0.32	0.31	0.0056	0.0051	0.32	0.33	0.12	0.13
500	S.D.	46.1	0.03	0.0003	0.02	0.34	0.03	0.02	0.02	0.0008	0.0006	0.05	0.04	0.02	0.02
	N	22	22	22	22	22	22	22	22	22	22	22	22	22	22
G3	Mean	554.0	0.39	0.0023	0.30	3.67	0.16	0.33	0.32	0.0055	0.0052	0.33	0.33	0.13	0.13
1,000	S.D.	42.4	0.03	0.0003	0.03	0.41	0.02	0.03	0.03	0.0010	0.0010	0.03	0.03	0.01	0.01
	N	22	22	22	22	22	22	22	22	22	22	22	22	22	22
G4	Mean	558.8	0.38	0.0024	0.29	3.53	0.16	0.32	0.31	0.0055	0.0049	0.32	0.32	0.12	0.13
2,000	S.D.	35.8	0.03	0.0002	0.02	0.26	0.03	0.02	0.02	0.0009	0.0008	0.03	0.03	0.01	0.01
	N	22	22	22	22	22	22	22	22	22	22	22	22	22	22

Table 1 System suitability for the determination of gomisin J in rat plasma

Analytical date	Classification		No. 1	No. 2	No. 3	No. 4	No. 5	Mean ± SD	Precision (%)
Apr. 18, 2013	Peak area ratio		0.02557	0.02185	0.02462	0.02283	0.02408	0.02379 ± 0.00147	6.17
	Retention time (min)	Gomisin J	1.39	1.38	1.38	1.39	1.38	1.38 ± 0.01	0.40
		IS	2.04	2.05	2.05	2.04	2.05	2.05 ± 0.01	0.27

Peak area ratio = Peak area of reference standard / Peak area of internal reference standard.
Precision (%) = (Standard deviation (SD) / Mean) × 100.
IS: Internal standard, glimepiride

Table 2 System suitability for the determination of gomisin in beagle dog plasma

Analytical date	Classification		No. 1	No. 2	No. 3	No. 4	No. 5	Mean ± SD	Precision (%)
Apr. 17, 2013	Peak area ratio		0.01933	0.01983	0.02021	0.02028	0.01750	0.01943 ± 0.00114	5.88
	Retention time (min)	Gomisin J	1.40	1.39	1.39	1.37	1.38	1.39 ± 0.01	0.82
		IS	2.05	2.05	2.06	2.04	2.05	2.05 ± 0.01	0.34

Peak area ratio = Peak area of reference standard / Peak area of internal reference standard.
Precision (%) = (Standard deviation (SD) / Mean) × 100.
IS: Internal standard, glimepiride

Table 3 Carryover effect for the determination of gomisin J in rat plasma
[Analytical date: Apr. 18, 2013]

Analyte	No.	Peak area of blank sample	Peak area of LLOQ	Peak area ratio (%)
Gomisin J	1	0	4261	0
	2	0		0
	3	0		0
IS	1	0	161710	0
	2	0		0
	3	0		0

Peak area ratio (%) = (Peak area of blank sample / Peak area of LLOQ sample) × 100.
IS: Internal standard, glimepiride

Table 4 Carryover effect for the determination of gomisin J in beagle dog plasma
[Analytical date: Apr. 17, 2013]

Analyte	No.	Peak area of blank sample	Peak area of LLOQ	Peak area ratio (%)
Gomisin J	1	0	4548	0
	2	0		0
	3	0		0
IS	1	0	189245	0
	2	0		0
	3	0		0

Peak area ratio (%) = (Peak area of blank sample / Peak area of LLOQ sample) × 100.
IS: Internal standard, glimepiride

Table 5 Calibration curve (weighting factor: 1/X) for the determination of gomisin J in rat plasma

Analytical date	Nominal concentration (ng/mL)	Peak area			Measured concentration (ng/mL)	Accuracy (%)
		Gomisin J	IS	Ratio		
Apr. 18, 2013	Blank	0	0	0	-	-
	Zero	0	213475	0	-	-
	2	4261	161710	0.02635	2.154	107.7
	5	9815	161473	0.06078	4.843	96.9
	10	19062	161432	0.1181	9.318	93.2
	20	41547	165535	0.2510	19.70	98.5
	50	109440	159672	0.6854	53.62	107.2
	100	191078	157346	1.214	94.94	94.9
	500	1122037	170761	6.571	513.3	102.7
	1,000	2075890	163915	12.66	989.2	98.9
y = 0.0128x-0.00123			r = 0.9997			

Accuracy was calculated using Analyst 1.4.2 software program.

- : Not calculated.

IS: Internal standard, glimepiride

Table 6 Calibration curve (weighting factor: 1/X) for the determination of gomisin J in beagle dog plasma

Analytical date	Nominal concentration (ng/mL)	Peak area			Measured concentration (ng/mL)	Accuracy (%)
		Gomisin J	IS	Ratio		
Apr. 17, 2013	Blank	0	0	0	-	-
	Zero	0	209560	0	-	-
	2	4548	189245	0.02403	2.142	107.1
	5	10248	205346	0.04991	4.659	93.2
	10	20047	209930	0.09549	9.094	90.9
	20	41987	193233	0.2173	20.94	104.7
	50	90250	172008	0.5247	50.85	101.7
	100	212472	197801	1.074	104.3	104.3
	500	976067	195540	4.992	485.5	97.1
	1,000	2090738	201463	10.38	1010	101.0
y = 0.0103x+0.00202			r = 0.9997			

Accuracy was calculated using Analyst 1.4.2 software program.

- : Not calculated.

IS: Internal standard, glimepiride

Table 7 Reproducibility for the determination of gomisin J in rat plasma

Analytical data	Nominal concentration (ng/mL)	Measured concentration (ng/mL)	Intra reproducibility		
			Mean ± SD (ng/mL)	Accuracy (%)	Precision (%)
Apr. 18, 2013	2	1.901	2.035 ± 0.113	101.7	5.5
		2.184			
		2.081			
		2.062			
		1.946			
	6	6.030	5.609 ± 0.294	93.5	5.2
		5.627			
		5.665			
		5.509			
		5.215			
	80	80.92	74.25 ± 4.91	92.8	6.6
		71.60			
		67.79			
		75.92			
		75.00			
	800	762.6	751.8 ± 20.1	94.0	2.7
		744.7			
		754.0			
		722.2			
		775.7			

Accuracy (%) = (Mean of the measured concentration / Nominal concentration) × 100.
Precision (%) = (Standard deviation (SD) / Mean) × 100.

Table 8 Reproducibility for the determination of gomisin J in beagle dog plasma

Analytical data	Nominal concentration (ng/mL)	Measured concentration (ng/mL)	Intra reproducibility		
			Mean ± SD (ng/mL)	Accuracy (%)	Precision (%)
Apr. 17, 2013	2	1.893	1.695 ± 0.114	84.8	6.7
		1.664			
		1.640			
		1.676			
		1.602			
	6	6.773	6.213 ± 0.909	103.5	14.6
		6.503			
		4.624			
		6.819			
		6.345			
	80	87.09	82.93 ± 2.48	103.7	3.0
		81.43			
		82.13			
		80.84			
		83.16			
	800	859.5	817.0 ± 32.2	102.1	3.9
		842.5			
		802.8			
		785.0			
		795.3			

Accuracy (%) = (Mean of the measured concentration / Nominal concentration) × 100.
Precision (%) = (Standard deviation (SD) / Mean) × 100.

<LC/MS/MS를 이용한 랫드 혈장 중 Gomisin J의 분석법 Validation >

Table 1. System suitability for the determination of Gomisin J in rat plasma

Analytical date	Classification		No. 1	No. 2	No. 3	No. 4	No. 5	Mean ± SD	Precision (%)
Sep. 25, 2013	Peak area ratio		0.04007	0.03813	0.04437	0.04121	0.04214	0.04118 ± 0.00233	5.6
(Reinjection†)	Retention time (min)	Gomisin J	1.55	1.55	1.53	1.51	1.52	1.53 ± 0.02	1.2
		Glimepiride	2.16	2.15	2.15	2.15	2.15	2.15 ± 0.00	0.2
Sep. 25, 2013	Peak area ratio		0.04894	0.04506	0.04451	0.04567	0.04527	0.04589 ± 0.00176	3.8
	Retention time (min)	Gomisin J	1.52	1.54	1.52	1.53	1.52	1.53 ± 0.01	0.6
		Glimepiride	2.15	2.15	2.15	2.15	2.15	2.15 ± 0.00	0.0
Sep. 26, 2013	Peak area ratio		0.04591	0.03840	0.04587	0.04721	0.04497	0.04447 ± 0.00349	7.8
	Retention time (min)	Gomisin J	1.51	1.49	1.53	1.53	1.51	1.51 ± 0.02	1.1
		Glimepiride	2.14	2.14	2.15	2.14	2.14	2.14 ± 0.00	0.2
Sep. 27, 2013	Peak area ratio		0.04041	0.03896	0.03924	0.03793	0.03106	0.03752 ± 0.00372	9.9
	Retention time (min)	Gomisin J	1.52	1.51	1.51	1.52	1.50	1.51 ± 0.01	0.6
		Glimepiride	2.15	2.14	2.14	2.15	2.14	2.14 ± 0.01	0.3
Oct. 29, 2013	Peak area ratio		0.007071	0.007033	0.007321	0.007174	0.007044	0.007129 ± 0.000121	1.7
(Reinjection††)	Retention time (min)	Gomisin J	1.53	1.51	1.51	1.51	1.50	1.51 ± 0.01	0.7
		Glimepiride	2.12	2.11	2.11	2.11	2.11	2.11 ± 0.00	0.2
Oct. 29, 2013	Peak area ratio		0.04724	0.04888	0.04853	0.04836	0.04934	0.04847 ± 0.00078	1.6
	Retention time (min)	Gomisin J	1.52	1.51	1.52	1.52	1.52	1.52 ± 0.00	0.3
		Glimepiride	2.14	2.13	2.13	2.14	2.14	2.14 ± 0.01	0.3
Oct. 30, 2013	Peak area ratio		0.04903	0.04860	0.05104	0.05177	0.04852	0.04979 ± 0.00151	3.0
	Retention time (min)	Gomisin J	1.53	1.52	1.52	1.54	1.53	1.53 ± 0.01	0.5
		Glimepiride	2.14	2.14	2.13	2.14	2.13	2.14 ± 0.01	0.3
Oct. 31, 2013	Peak area ratio		0.03632	0.03816	0.04106	0.04130	0.03797	0.03896 ± 0.00215	5.5
	Retention time (min)	Gomisin J	1.54	1.53	1.51	1.51	1.52	1.52 ± 0.01	0.9
		Glimepiride	2.13	2.13	2.13	2.13	2.13	2.13 ± 0.00	0.0
Nov. 01, 2013	Peak area ratio		0.05909	0.06130	0.06315	0.06780	0.06358	0.06298 ± 0.00322	5.1
	Retention time (min)	Gomisin J	1.54	1.52	1.53	1.52	1.53	1.53 ± 0.01	0.5
		Glimepiride	2.13	2.12	2.13	2.13	2.13	2.13 ± 0.00	0.2

Peak area ratio = Peak area of reference standard / Peak area of internal reference standard.

Precision (%) = (Standard deviation (SD) / Mean) × 100.

Reinjection†: The analytical batch was re-injected after re-optimization of MS conditions because the results of intra reprosucibility did not meet the acceptance criteria on Sep. 24, 2013.

Reinjection††: The analytical batch was re-injected because the analytical run was stopped by setting error of LC vials on Oct. 28, 2013.

Table 2. Carryover effect for the determination of Gomisin J in rat plasma [Analytical date: Sep. 25, 2013 (re-injection)]

Analyte	No.	Peak area of blank sample	Peak area of LLOQ	Carryover effect (%)
Gomisin J	1	0	3783	0.00
	2	0		0.00
	3	0		0.00
Glimepiride	1	0	82016	0.00
	2	0		0.00
	3	0		0.00

Carryover effect (%) = (Peak area of blank sample / Peak area of LLOQ sample) × 100.

Table 3. Selectivity for the determination of Gomisin J in rat plasma
[Analytical date: Sep. 25, 2013]

Analyte	No.	Peak area of blank sample	Peak area of LLOQ	Selectivity (%)
Gomisin J	1	0	3665	0.00
	2	0		0.00
	3	0		0.00
	4	0		0.00
	5	0		0.00
	6	0		0.00
Glimepiride	1	0	79500	0.00
	2	0		0.00
	3	0		0.00
	4	0		0.00
	5	0		0.00
	6	0		0.00

Sectivity (%) = (Peak area of blank sample / Peak area of LLOQ sample) × 100.

Table 4-1. Matrix effect for the determination of Gomisin J in rat plasma
[Analytical date: Sep. 25, 2013]

Analyte	Nominal concentration (ng/mL)	Classification		Peak area	IS peak area	Peak are ratio	Matrix effect (%)
Gomisin J	6	Control		39612	986483	0.04015	-
				37711	978875	0.03852	-
				35966	979144	0.03673	-
				37972	977339	0.03885	-
				38775	980244	0.03956	-
				37757	986989	0.03825	-
		Mean				0.03868	-
		Test	Lot No.: RMP130621015	22647	899946	0.02516	65.1
			Lot No.: RMP130621016	22764	889457	0.02559	66.2
			Lot No.: RMP130621017	21782	886778	0.02456	63.5
			Lot No.: RFP130621017	22356	886264	0.02522	65.2
			Lot No.: RFP130621018	22279	899156	0.02478	64.1
			Lot No.: RFP130621019	22489	895118	0.02512	65.0
		Mean				0.02507	64.8
		SD					0.9
		Precision (%)					1.4
	800	Control		4212914	872438	4.829	-
				4331961	929170	4.662	-
				4633679	969637	4.779	-
				4583435	983367	4.661	-
				4425344	971490	4.555	-
				3256386	926123	3.516	-
		Mean				4.500	-
		Test	Lot No.: RMP130621015	2952331	892160	3.309	73.5
			Lot No.: RMP130621016	2930661	877746	3.339	74.2
			Lot No.: RMP130621017	3079887	891308	3.455	76.8
			Lot No.: RFP130621017	2946184	889593	3.312	73.6
			Lot No.: RFP130621018	3048528	902501	3.378	75.1
			Lot No.: RFP130621019	3279499	910287	3.603	80.1
		Mean					75.5
		SD					2.5
		Precision (%)					3.3

Matrix effect (%) = (Peak area of individual test sample / Mean peak area of control sample) × 100.

Precision (%) = (Standard deviation (SD) / Mean) × 100.

Table 4-2. Matrix effect for the determination of Glimepiride (IS) in rat plasma
[Analytical date: Sep. 25, 2013]

Analyte	Nominal concentration† (ng/mL)	Classification	IS peak area	Peak area	Peak are ratio	Matrix effect (%)
Glimepiride	60	Control	872438	4212914	0.2071	-
			929170	4331961	0.2145	-
			969637	4633679	0.2093	-
			983367	4583435	0.2145	-
			971490	4425344	0.2195	-
			926123	3256386	0.2844	
		Mean			0.2249	-
			892160	2952331	0.3022	134.4
			877746	2930661	0.2995	133.2
			891308	3079887	0.2894	128.7
			889593	2946184	0.3019	134.3
			902501	3048528	0.2960	131.6
			910287	3279499	0.2776	123.4
		Mean			0.2944	130.9
		SD				4.2
		Precision (%)				3.2

Matrix effect (%) = (Peak area of individual test sample / Mean peak area of control sample) × 100.

Precision (%) = (Standard deviation (SD) / Mean) × 100.

Table 5-1. Recovery for the determination of Gomisin J in rat plasma
[Analytical date: Sep. 26, 2013]

Nominal concentration (ng/mL)	Classification	No.	Peak area	IS peak area	Peak area ratio	Mean of peak area ratio	Recovery (%)	Precision (%)
6	Control	1	27604	987655	0.02795	0.02349	48.9	12.7
		2	20125	958288	0.02100			
		3	20827	968154	0.02151			
	Test	1	11405	954140	0.01195	0.01148		
		2	12123	997777	0.01215			
		3	10028	969212	0.01035			
80	Control	1	273584	986928	0.27721	0.28671	63.1	
		2	277372	966213	0.28707			
		3	284981	963239	0.29586			
	Test	1	177382	965577	0.18371	0.18098		
		2	171541	968661	0.17709			
		3	178369	979346	0.18213			
800	Control	1	2794114	956747	2.92043	3.05602	57.6	
		2	2995346	949086	3.15603			
		3	2925448	946257	3.09160			
	Test	1	1749444	957304	1.82747	1.75914		
		2	1659847	938467	1.76868			
		3	1619227	963090	1.68128			

Recovery (%) = (Mean peak area of test sample / Mean peak area of control sample) × 100.

Precision (%) = (Standard deviation (SD) of recovery for each concentration / Mean of recovery for each concentration) × 100.

Table 5-2. Recovery for the determination of Glimepride (IS) in rat plasma
[Analytical date: Sep. 26, 2013]

Nominal concentration (ng/mL)	Classification	No.	IS peak area	Peak area	Peak area ratio	Mean of peak area ratio	Recovery (%)
60	Control - QM	1	986928	273584	3.607	3.490	7.2
		2	966213	277372	3.483		
		3	963239	284981	3.380		
	Test - QM	1	73079	311583	0.2345	0.2498	
		2	78110	306188	0.2551		
		3	81613	314211	0.2597		

Recovery (%) = (Mean peak area of test sample / Mean peak area of control sample) × 100.

Table 6. Calibration curves (weighting: 1/X) for the determination of Gomisin J in rat plasma

Analytical date	Nominal concentration (ng/mL)	Peak area			Measured concentration (ng/mL)	Accuracy (%)
		Gomisin J	Glimepiride	Ratio		
Sep. 25, 2013	Blank	0	0	-	-	-
(Reinjection†)	Zero	0	83122	0.000	-	-
	2	3783	82016	0.04612	2.113	105.7
	5	9849	83964	0.1173	4.785	95.7
	10	20527	84782	0.2421	9.470	94.7
	20	46899	85028	0.5516	21.09	105.4
	50	105026	82573	1.272	48.13	96.3
	100	223094	84002	2.656	100.1	100.1
	500	1183031	85409	13.85	520.4	104.1
	1000	2181080	83497	26.12	981.0	98.1
y = 0.0266x-0.0102		r = 0.9996				
Sep. 25, 2013	Blank	0	0	-	-	-
	Zero	0	85008	0.000	-	-
	2	3407	79754	0.04272	2.031	101.6
	5	10324	80147	0.1288	5.299	106.0
	10	18815	78541	0.2396	9.503	95.0
	20	38217	77955	0.4902	19.02	95.1
	50	102114	75838	1.346	51.52	103.0
	100	212343	81940	2.591	98.78	98.8
	500	1000751	75346	13.28	504.6	100.9
	1000	2010834	76644	26.24	996.3	99.6
y = 0.0263x-0.0108		r = 0.9999				
Sep. 26, 2013	Blank	0	0	-	-	-
	Zero	0	76832	0.000	-	-
	2	3453	73362	0.04707	2.108	105.4
	5	8827	78586	0.1123	4.583	91.7
	10	18138	73984	0.2452	9.621	96.2
	20	37898	74457	0.5090	19.63	98.1
	50	99062	74222	1.335	50.94	101.9
	100	204127	72317	2.823	107.4	107.4
	500	991494	75208	13.18	500.3	100.1
	1000	1917485	73301	26.16	992.4	99.2
y = 0.0264x-0.00852		r = 0.9998				

Accuracy was calcurated from Analyst 1.4.2 software program.

Reinjection†: The analytical batch was re-injected after re-optimization of MS conditions because the results of intra reprosucibility did not meet the acceptance criteria on Sep. 24, 2013.

Table 6. (Continued)

Analytical date	Nominal concentration (ng/mL)	Peak area			Measured concentration (ng/mL)	Accuracy (%)
		Gomisin J	Glimepiride	Ratio		
Sep. 27, 2013	Blank	0	0	-	-	-
	Zero	0	88824	0.000	-	-
	2	2435	86055	0.02830	2.027	101.3
	5	8175	85550	0.09555	5.031	100.6
	10	16640	81238	0.2048	9.913	99.1
	20	36012	84661	0.4254	19.76	98.8
	50	92498	80938	1.143	51.81	103.6
	100	176860	82303	2.149	96.76	96.8
	500	933571	84335	11.07	495.3	99.1
	1000	1868728	83009	22.51	1,006	100.6
y = 0.0224x-0.0171		r = 0.9999				
Oct. 29, 2013	Blank	0	0	-	-	-
	Zero	0	153650	0.000	-	-
	2	7777	143897	0.05405	1.881	94.0
	5	16544	140041	0.1181	4.410	88.2
	10	40339	143622	0.2809	10.83	108.3
	20	70693	142244	0.4970	19.36	96.8
	50	196225	145655	1.347	52.91	105.8
	100	380791	133484	2.853	112.3	112.3
	500	1631811	139881	11.67	460.1	92.0
	1000	3827409	147270	25.99	1025	102.5
y = 0.0253x+0.00638		r = 0.9982				
Oct. 30, 2013	Blank	0	0	-	-	-
	Zero	0	185564	0.000	-	-
	2	7357	149566	0.04919	1.914	95.7
	5	20579	153859	0.1338	5.292	105.8
	10	41211	156997	0.2625	10.44	104.4
	20	75416	159374	0.4732	18.86	94.3
	50	219677	185638	1.183	47.23	94.5
	100	408567	155170	2.633	105.2	105.2
	500	2053939	162804	12.62	504.0	100.8
	1000	4026853	161847	24.88	994.1	99.4
y = 0.0250x+0.00130		r = 0.9998				

Accuracy was calcurated from Analyst 1.4.2 software program.

Table 6. (Continued)

Analytical date	Nominal concentration (ng/mL)	Peak area			Measured concentration (ng/mL)	Accuracy (%)
		Gomisin J	Glimepiride	Ratio		
Oct. 31, 2013	Blank	0	0	-	-	-
	Zero	0	198808	0.000	-	-
	2	7414	204398	0.03627	2.166	108.3
	5	18709	205317	0.09112	4.900	98.0
	10	43639	211482	0.2063	10.64	106.4
	20	82480	217219	0.3797	19.29	96.4
	50	190311	192632	0.9880	49.60	99.2
	100	391303	204231	1.916	95.86	95.9
	500	1949471	214576	9.085	453.2	90.6
	1000	4109811	194934	21.08	1,051	105.1
y = 0.0201x-0.00718		r = 0.9978				
Nov. 01, 2013	Blank	0	0	-	-	-
	Zero	0	177627	0.000	-	-
	2	10787	169559	0.06362	2.396	119.8
	5	23440	180715	0.1297	4.538	90.8
	10	55571	169352	0.3281	10.97	109.7
	20	116822	192538	0.6067	20.00	100.0
	50	254191	179721	1.414	46.17	92.3
	100	453272	161924	2.799	91.05	91.1
	500	2382596	171112	13.92	451.6	90.3
	1000	5317476	162580	32.71	1,060	106.0
y = 0.0309x-0.0103		r = 0.9970				

Accuracy was calcurated from Analyst 1.4.2 software program.

Table 7. Reproducibility for the determination of Gomisin J in rat plasma

Nominal concentration (ng/mL)	Analytical date	Measured concentration (ng/mL)	Intra reproducibility			Inter reproducibility		
			Mean ± SD (ng/mL)	Accuracy (%)	Precision (%)	Mean ± SD (ng/mL)	Accuracy (%)	Precision (%)
2	Sep. 25, 2013	1.955	1.987 ± 0.117	99.4	5.9	1.980 ± 0.177	99.0	8.9
	(Reinjection†)	1.809						
		1.991						
		2.102						
		2.079						
	Sep. 25, 2013	1.920	1.853 ± 0.126	92.7	6.8			
		1.814						
		1.734						
		2.040						
		1.759						
	Sep. 26, 2013	1.783	1.862 ± 0.074	93.1	4.0			
		1.839						
		1.812						
		1.963						
		1.914						
	Sep. 27, 2013	2.151	2.282 ± 0.074	114.1	3.2			
		2.330						
		2.307						
		2.301						
		2.321						
	Oct. 30, 2013	1.998	1.915 ± 0.112	95.7	5.9			
		1.975						
		1.827						
		2.011						
		1.763						

Accuracy (%) = (Mean of the measured concentration / Nominal concentration) × 100.
Precision (%) = (Standard deviation (SD) / Mean) × 100.
Reinjection†: The analytical batch was re-injected after re-optimization of MS conditions because the results of intra reprosucibility did not meet the acceptance criteria on Sep. 24, 2013.

Table 7. (Continued)

Nominal concentration (ng/mL)	Analytical date	Measured concentration (ng/mL)	Intra reproducibility			Inter reproducibility		
			Mean ± SD (ng/mL)	Accuracy (%)	Precision (%)	Mean ± SD (ng/mL)	Accuracy (%)	Precision (%)
6	Sep. 25, 2013	5.826	5.853 ± 0.110	97.6	1.9	5.650 ± 0.292	94.2	5.2
	(Reinjection†)	5.999						
		5.931						
		5.728						
		5.782						
	Sep. 25, 2013	5.224	5.440 ± 0.284	90.7	5.2			
		5.294						
		5.238						
		5.887						
		5.557						
	Sep. 26, 2013	5.049	5.324 ± 0.212	88.7	4.0			
		5.546						
		5.170						
		5.357						
		5.497						
	Sep. 27, 2013	6.017	6.034 ± 0.130	100.6	2.2			
		5.840						
		6.021						
		6.196						
		6.095						
	Oct. 30, 2013	5.899	5.602 ± 0.377	93.4	6.7			
		5.422						
		6.017						
		5.076						
		5.594						

Accuracy (%) = (Mean of the measured concentration / Nominal concentration) × 100.
Precision (%) = (Standard deviation (SD) / Mean) × 100.
Reinjection†: The analytical batch was re-injected after re-optimization of MS conditions because the results of intra reprosucibility did not meet the acceptance criteria on Sep. 24, 2013.

Table 7. (Continued)

Nominal concentration (ng/mL)	Analytical date	Measured concentration (ng/mL)	Intra reproducibility			Inter reproducibility		
			Mean ± SD (ng/mL)	Accuracy (%)	Precision (%)	Mean ± SD (ng/mL)	Accuracy (%)	Precision (%)
800	Sep. 25, 2013 (Reinjection†)	706.6	728.6 ± 29.5	91.1	4.1	749.5 ± 33.3	93.7	4.4
		709.5						
		731.1						
		717.3						
		778.7						
	Sep. 25, 2013	680.6	702.1 ± 29.3	87.8	4.2			
		711.9						
		712.9						
		665.5						
		739.8						
	Sep. 26, 2013	787.3	775.7 ± 33.7	97.0	4.3			
		819.1						
		772.8						
		774.0						
		725.5						
	Sep. 27, 2013	783.7	761.3 ± 26.4	95.2	3.5			
		771.8						
		777.9						
		718.1						
		754.9						
	Oct. 30, 2013	810.9	779.9 ± 32.1	97.5	4.1			
		762.7						
		812.9						
		738.0						
		775.1						

Accuracy (%) = (Mean of the measured concentration / Nominal concentration) × 100.

Precision (%) = (Standard deviation (SD) / Mean) × 100.

Reinjection†: The analytical batch was re-injected after re-optimization of MS conditions because the results of intra reprosucibility did not meet the acceptance criteria on Sep. 24, 2013.

Table 7. (Continued)

Nominal concentration (ng/mL)	Analytical date	Measured concentration (ng/mL)	Intra reproducibility			Inter reproducibility		
			Mean ± SD (ng/mL)	Accuracy (%)	Precision (%)	Mean ± SD (ng/mL)	Accuracy (%)	Precision (%)
80	Sep. 25, 2013 (Reinjection†)	69.10	69.68 ± 1.72	87.1	2.5	73.73 ± 4.21	92.2	5.7
		70.82						
		67.71						
		72.02						
		68.74						
	Sep. 25, 2013	68.29	68.66 ± 0.22	85.8	0.3			
		68.62						
		68.82						
		68.74						
		68.82						
	Sep. 26, 2013	77.12	76.35 ± 1.5525	95.4	2.0			
		75.68						
		77.47						
		77.55						
		73.92						
	Sep. 27, 2013	77.00	77.51 ± 1.83	96.9	2.4			
		75.06						
		78.64						
		76.99						
		79.87						
	Oct. 30, 2013	74.57	76.48 ± 4.88	95.6	6.4			
		84.22						
		74.27						
		77.83						
		71.50						

Accuracy (%) = (Mean of the measured concentration / Nominal concentration) × 100.

Precision (%) = (Standard deviation (SD) / Mean) × 100.

Reinjection†: The analytical batch was re-injected after re-optimization of MS conditions because the results of intra reprosucibility did not meet the acceptance criteria on Sep. 24, 2013.

Table 8. Dilution reproducibility for the determination of Gomisin J in rat plasma
[Analytical date: Sep. 25, 2013]

Analyte	Nominal concentration (ng/mL)	Dilution factor	No.	Measured concentration (ng/mL)	Mean ± SD (ng/mL)	Accuracy (%)	Precision (%)
Gomisin J	1,500	2	1	1,455	1,459 ± 41	97.2	2.8
			2	1,418			
			3	1,528			
			4	1,450			
			5	1,442			

Accuracy (%) = (Mean of the calculated concentration / Nominal concentration) × 100.

Precision (%) = (Standard deviation (SD) / Mean) × 100.

Table 9. Stability for the determination of Gomisin J in rat plasma

Nominal concentration (ng/mL)	Analytical date	Classification	Measured concentration (ng/mL)	Mean ± SD (ng/mL)	Accuracy (%)	Precision (%)
6	Sep. 25, 2013 (Reinjection†)	Control	5.826	5.853 ± 0.110	97.6	1.9
			5.999			
			5.931			
			5.728			
			5.782			
	Nov. 01, 2013	Room temperature	6.006	6.144 ± 0.879	102.4	14.3
			7.084			
		4 hrs	5.343			
	Oct. 29, 2013	Deep freezer	5.137	5.330 ± 0.372	88.8	7.0
		35 days	5.094			
			5.758			
	Nov. 01, 2013	Deep freezer	6.006	6.144 ± 0.879	102.4	14.3
		38 days	7.084			
			5.343			
	Oct. 30, 2013	Freeze-thaw	5.332	5.551 ± 0.190	92.5	3.4
		5 cycles	5.662			
			5.659			
	Oct. 31, 2013	Processed sample in autosampler (10°C)	6.893	6.751 ± 0.317	112.5	4.7
			6.524			
		27.5 hrs	7.102			
			6.324			
			6.911			

Accuracy (%) = (Mean of the measured concentration / Nominal concentration) × 100.

Precision (%) = (Standard deviation (SD) / Mean) × 100.

Reinjection†: The analytical batch was re-injected after re-optimization of MS conditions because the results of intra reprosucibility did not meet the acceptance criteria on Sep. 24, 2013.

Table 9. (Continued)

Nominal concentration (ng/mL)	Analytical date	Classification	Measured concentration (ng/mL)	Mean ± SD (ng/mL)	Accuracy (%)	Precision (%)
800	Sep. 25, 2013 (Reinjection†)	Control	706.6	728.6 ± 29.5	91.1	4.1
			709.5			
			731.1			
			717.3			
			778.7			
	Nov. 01, 2013	Room temperature 4 hrs	721.9	748.8 ± 57.0	93.6	7.6
			814.2			
			710.2			
	Oct. 29, 2013	Deep freezer 35 days	794.5	763.0 ± 27.5	95.4	3.6
			744.4			
			750.0			
	Nov. 01, 2013	Deep freezer 38 days	721.9	748.8 ± 57.0	93.6	7.6
			814.2			
			710.2			
	Oct. 30, 2013	Freeze-thaw 5 cycles	779.3	791.9 ± 26.1	99.0	3.3
			821.9			
			774.6			
	Oct. 31, 2013	Processed sample in autosampler (10°C) 27.5 hrs	935.4	915.1 ± 21.3	114.4	2.3
			911.7			
			928.6			
			880.5			
			919.2			

Accuracy (%) = (Mean of the measured concentration / Nominal concentration) × 100.

Precision (%) = (Standard deviation (SD) / Mean) × 100.

Reinjection†: The analytical batch was re-injected after re-optimization of MS conditions because the results of intra reprosucibility did not meet the acceptance criteria on Sep. 24, 2013.

Table 10. Stability of Gomisin J in the stock and working solutions

Analytical date	Nominal concentration (ng/mL)	Preparation date	Classification	Peak area ratio	Mean ± SD	Precision (%)	Residual ratio (%)
Oct. 29, 2013	200,000	Oct. 28, 2013	Control	0.009221	0.008794 ± 0.000816	9.3	-
				0.009308			
				0.007854			
		Oct. 28, 2013	Room temperature	0.009383	0.008822 ± 0.000900	10.2	100.3
				0.007784			
			6 hrs	0.009298			
		Sep. 24, 2013	Refrigerator	0.007804	0.007920 ± 0.001145	14.5	90.1
			34 days	0.009119			
				0.006838			
	10	Oct. 28, 2013	Control	0.009221	0.008794 ± 0.000816	9.3	-
				0.009308			
				0.007854			
		Oct. 28, 2013	Room temperature	0.009315	0.008878 ± 0.000525	5.9	101.0
				0.009024			
			6 hrs	0.008296			
		Sep. 24, 2013	Refrigerator	0.008571	0.008115 ± 0.000426	5.3	92.3
			34 days	0.007726			
				0.008049			

The stock and working solutions of Gomisin J were dissolved in methanol.

Precision (%) = (Standard deviation (SD) / Mean) × 100.

Residual ratio (%) = (Mean peak area ratio of sample after storage / Mean peak area ratio of sample immediately after preparation) × 100.

Table 11 Stability of IS (Glimepride) in the stock and working solutions

Analytical date	Nominal concentration (ng/mL)	Preparation date	Classification	Glimepiride peak area	Gomisin J peak area	Peak area ratio (IS/RS)	Mean ± SD	Precision (%)	Residual ratio (%)
Oct. 29, 2013	200,000	Oct. 28, 2013	Control	1826443	16841	108.5	114.4 ± 11.2	9.8	-
				1711997	15936	107.4			
				1735509	13631	127.3			
		Oct. 28, 2013	Room temperature 6 hrs	1887939	17478	108.0	118.8 ± 10.4	8.8	103.8
				1783035	14924	119.5			
				1799084	13968	128.8			
		Sep. 24, 2013	Refrigerator 34 days	1822268	14648	124.4	131.2 ± 6.1	4.6	114.7
				1701417	12795	133.0			
				1715778	12606	136.1			
	300	Oct. 28, 2013	Control	1826443	16841	108.5	114.4 ± 11.2	9.8	-
				1711997	15936	107.4			
				1735509	13631	127.3			
		Oct. 28, 2013	Room temperature 6 hrs	1720546	16539	104.0	108.0 ± 12.4	11.5	94.4
				1708882	14018	121.9			
				1684468	17182	98.04			
		Sep. 24, 2013	Refrigerator 34 days	1453601	15884	91.51	97.87 ± 12.47	12.7	85.5
				1412634	12587	112.2			
				1405765	15645	89.85			

The stock and working solutions of Glimepiride were dissolved in methanol.

Precision (%) = (Standard deviation (SD) / Mean) × 100.

Residual ratio (%) = (Mean peak area ratio of sample after storage / Mean peak area ratio of sample immediately after preparation) × 100.

<LC/MS/MS를 이용한 랫드 및 비글 혈장 중 Gomisin J의 분석법 개발을 위한 타당성 시험>

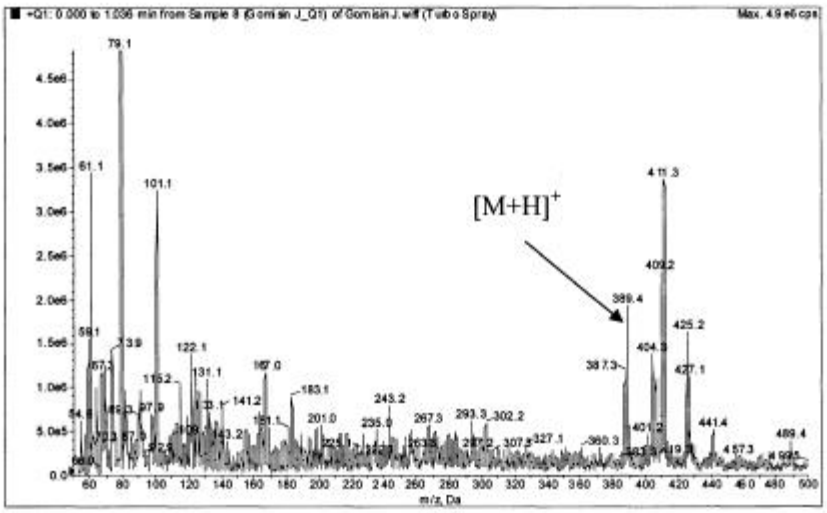

Figure 1. Q1 full scan spectrum of gomisin J (M.W. =388.46)

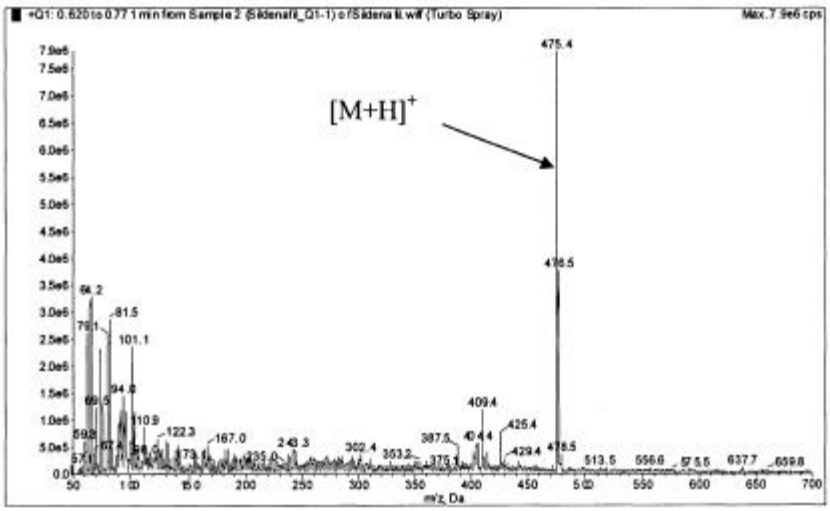

Figure 2. Q1 full scan spectrum of sildenafil (IS, M.W. =474.58)

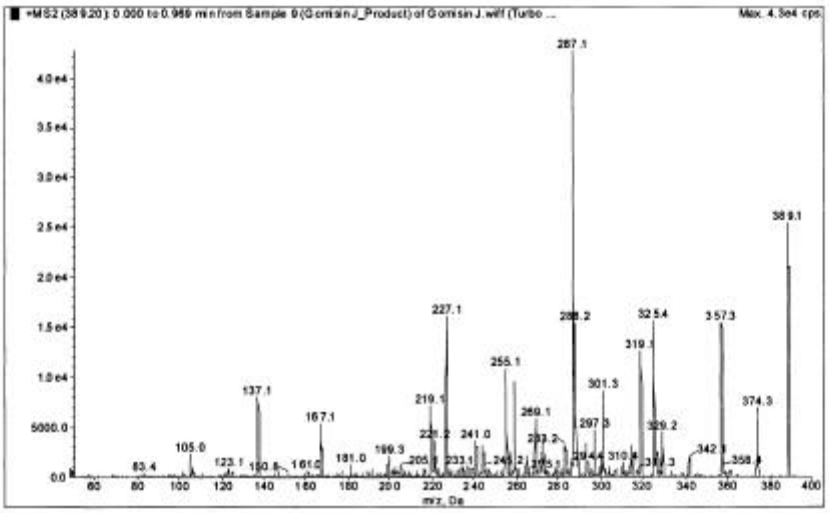

Figure 3. Product ion scan spectrum from *m/z* 389 of gomisin J

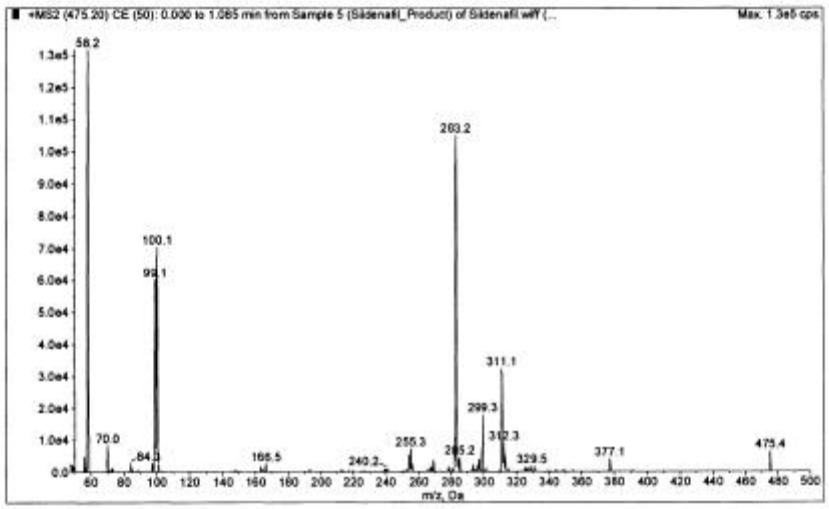

(A)

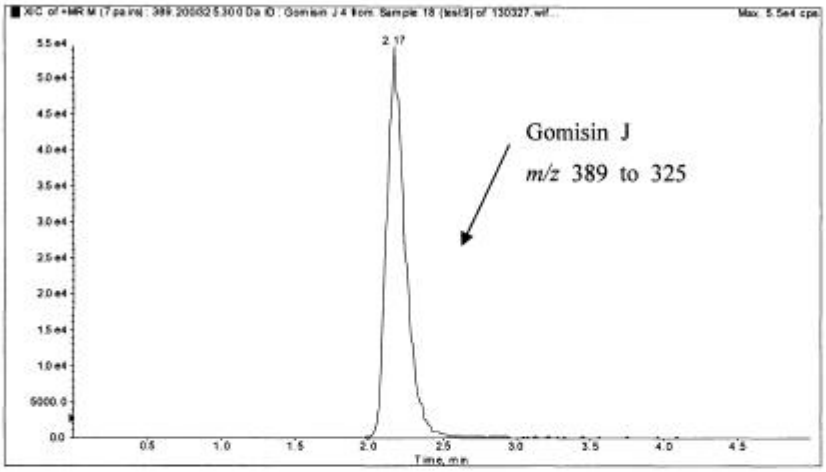
2.17
Gomisin J
m/z 389 to 325
Time, min

(B)

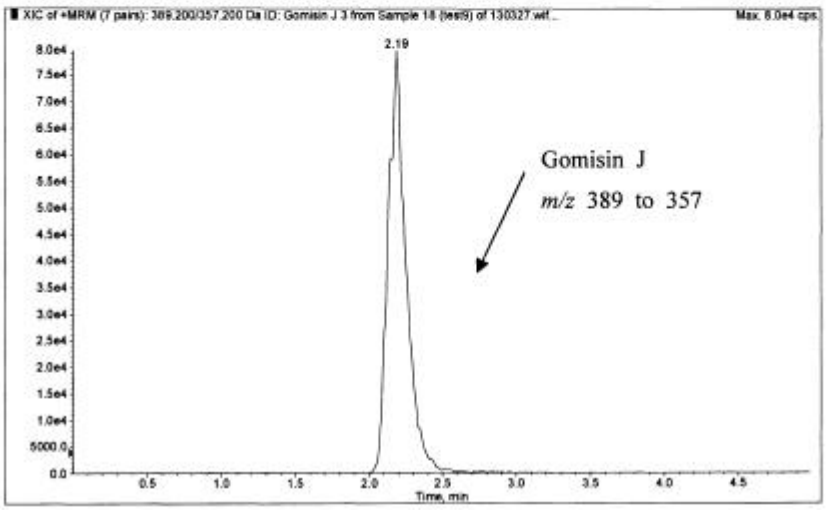
2.19
Gomisin J
m/z 389 to 357
Time, min

(C)

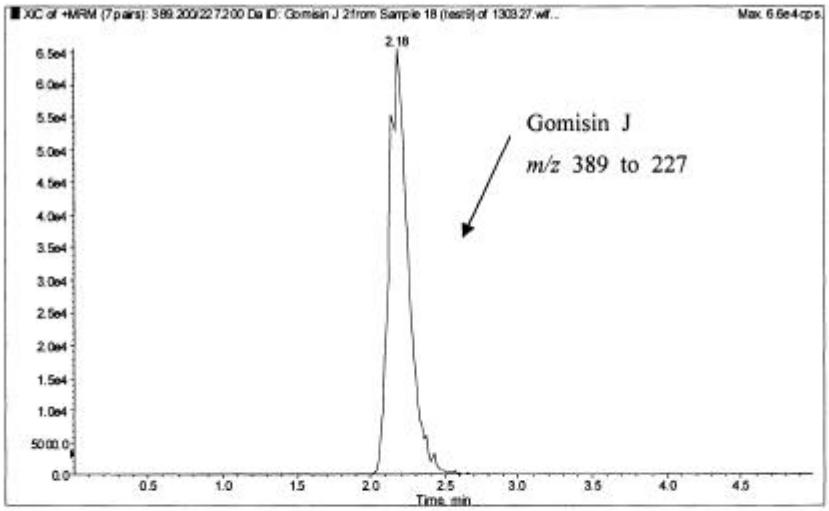

(D)

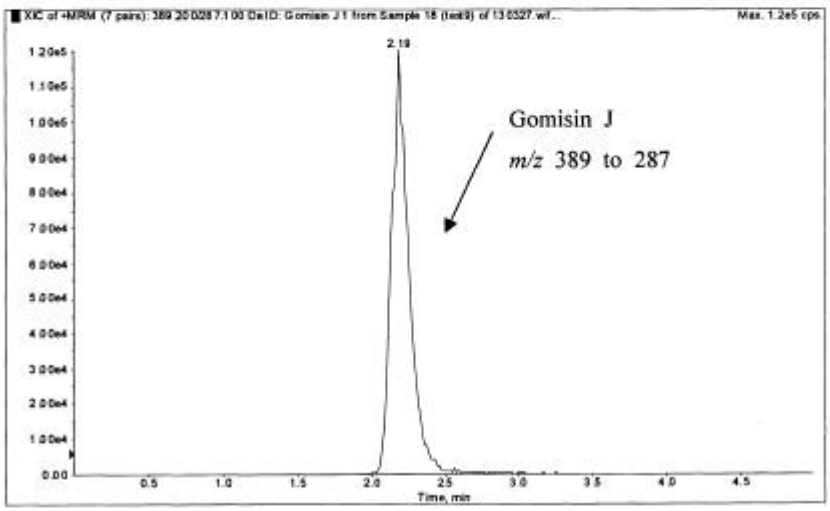

Figure 5. Chromatograms of gomisin J in the working solution (500 ng/mL, 10 μL injection) (Continued)

(A)

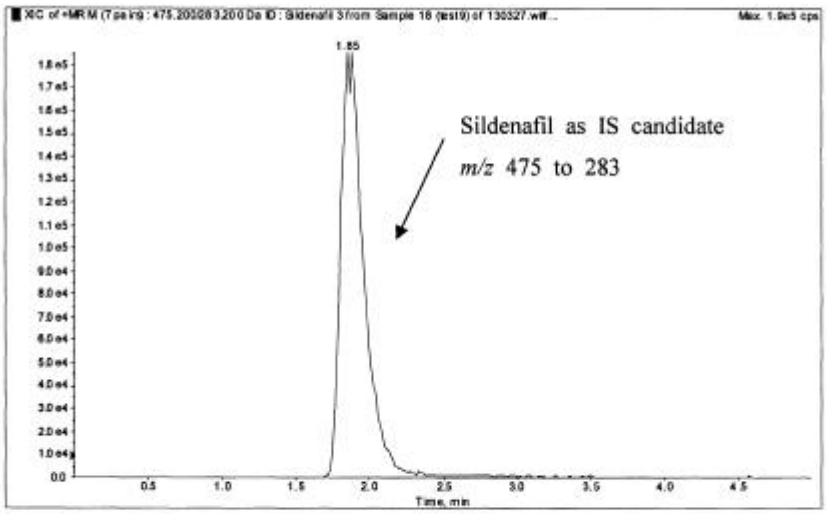

(B)

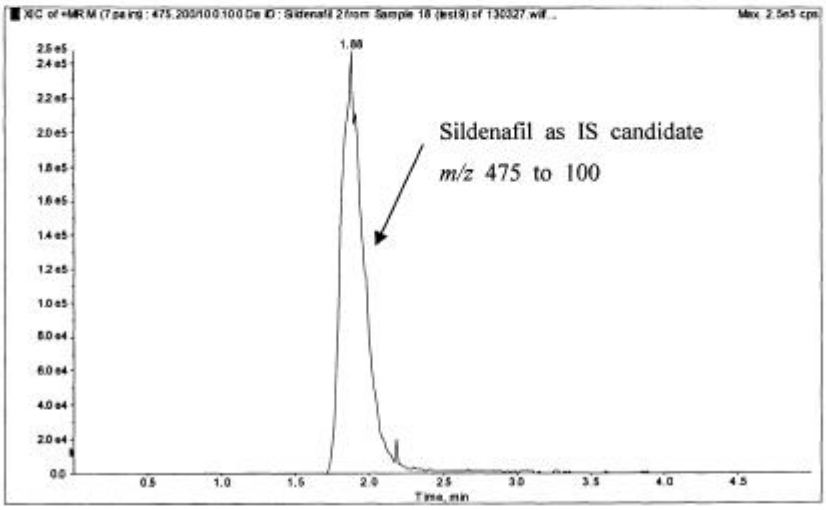

Figure 6. Chromatograms of sildenafil as IS candidate in the working solution (500 ng/mL, 10 μL injection)

(C)

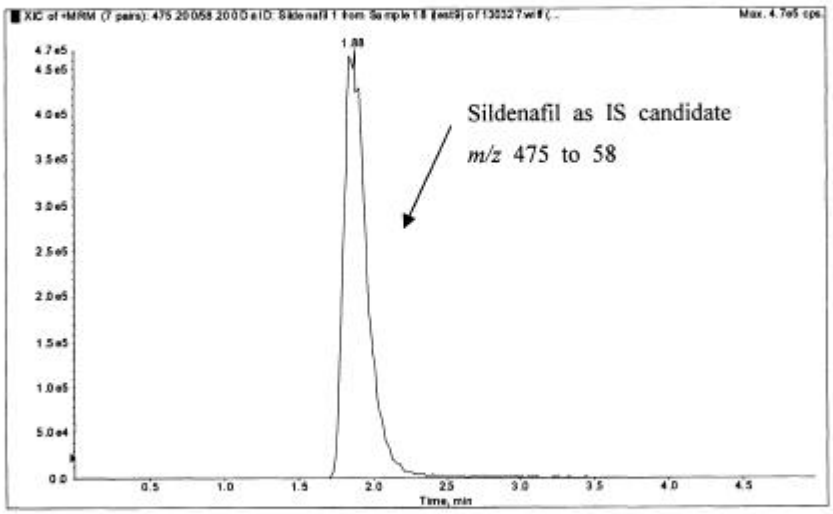

Figure 6. Chromatograms of sildenafil as IS candidate in the working solution (500 ng/mL, 10 µL injection) (Continued)

(A)

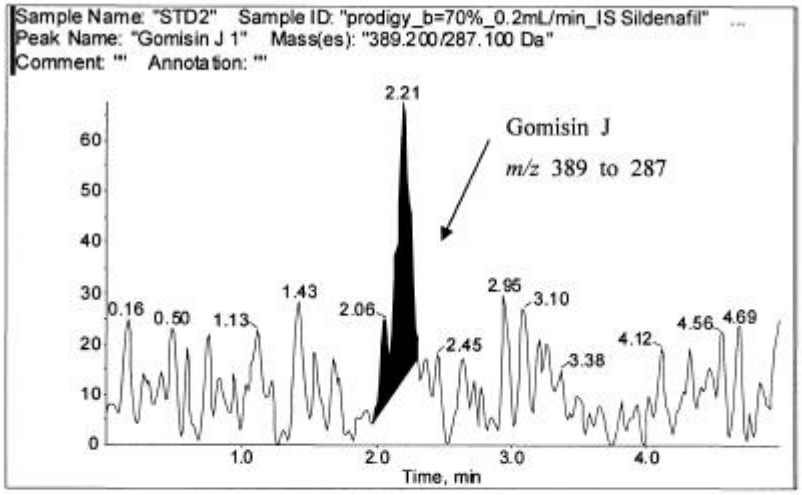

(B)

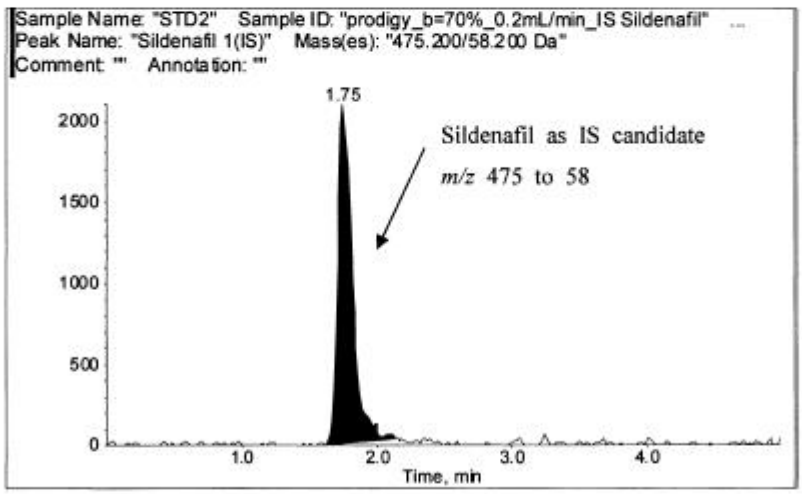

Figure 7. Chromatograms of gomisin J and sildenafil in the working solution
Gomisin J: 0.25 ng/mL, 10 μL injection (2.5 pg on column)
Sildenafil: 2.5 ng/mL, 10 μL injection (25 pg on column)

주 의

1. 이 보고서는 농림축산식품부에서 시행한 질환 동물 모델을 이용한 농업바이오 분야의 CRO 구축사업의 연구보고서입니다.

2. 이 보고서 내용을 발표할 때에는 반드시 농림축산식품부에서 시행한 질환 동물 모델을 이용한 농업바이오 분야의 CRO 구축사업의 연구결과임을 밝혀야 합니다.

3. 국가과학기술 기밀유지에 필요한 내용은 대외적으로 발표 또는 공개하여서는 아니 됩니다.